Minimally Invasive Clinical Monitoring and Data Transference in Cardiac Patients

A thesis submitted in accordance with the conditions governing candidates for the degree of Philosophiae Doctor in Cardiff University

by

Emma Louise Baczkowski

May 2022

Cardiff School of Pharmacy and Pharmaceutical Sciences

Cardiff University

ACKNOWLEDGMENTS

ABSTRACT

'Wet' electrodes used in electrocardiography (ECG), are applied to the surface of the skin to record cardiac activity. Over time, water-based electrolytic gels between the electrodes and skin dehydrate, reducing signal quality. Microneedle-electrodes negate the need for conductive gels and potentially improve signal fidelity by circumventing the stratum corneum and contacting the underlying conductive epidermal layers. This thesis aimed to assess the wearability and functionality of microneedle-electrodes in cardiac signal acquisition.

Epoxy, 500µm-length microneedles were applied to excised skin models to assess insertion performance. Increasing downward application force increased microneedle penetration efficiency from 79%±8.20 (5N) to 87%±13.32 (15N). The microneedle application technique also had an impact on penetration efficiency, with impact insertion (93%±5.75) proving more effective than manual downward force (71%±22.01).

Metallised versions of the epoxy microneedles were integrated into a commercial electrode and compared to conventional wet electrodes in human volunteers. Wet electrodes recorded higher quality signals than microneedle-electrodes in healthy human participants (1.6dB difference between the electrode types). This clinical data informed the development of an in vitro laboratory skin model to assess the influence of microneedle-electrode parameters on a simulated ECG signal. Increasing microneedle length from 500µm (25.2dB±3.25) to 600µm (24.3dB±2.31) did not result in a sustained improvement in signal quality (p>0.05).

Bespoke second-generation microneedle-electrodes were manufactured allowing an improved signal quality to be maintained over the recording period (17.3dB±2.11 compared to 15.0dB±1.97 for wet electrodes; p>0.05) in the laboratory model. Human participant studies assessed their wearability and functionality. At rest, the metallised epoxy (23.2dB±5.79) and bespoke (22.5dB±7.57) microneedle-electrode performance was comparable to wet electrodes (24.9dB±6.44) (p>0.05). Under active conditions, the signal-to-noise ratio declined for all electrodes and ECG traces highlighted increased motion artifacts. Participants preferred wet electrodes and highlighted seven key wearability themes. Further optimisation of microneedle-electrodes for ECG monitoring is therefore, warranted.

RESEARCH DISSEMINATION

Conference presentation(s)

- Baczkowski, EL., Bocchino, A., O'Sullivan, M., O'Mahony, C., Mukhopadyay, S., Sutton, N., Coulman, SA. and Birchall, JC. 2020. Polymeric microneedle-based 'dry' electrodes for wearable cardiac monitoring. *UKICRS Virtual Symposium*. Online, 14 October, 2020.

- Baczkowski, EL., Bocchino, A., O'Sullivan, M., O'Mahony, C., Mukhopadyay, S., Sutton, N., Coulman, SA. and Birchall, JC. 2020. Polymeric microneedle-based 'dry' electrodes for wearable cardiac monitoring. *Microneedles 2020: The 6th International Conference on Microneedles.* Online, 10-11 November, 2020.

- Baczkowski, EL., Bocchino, A., O'Sullivan, M., O'Mahony, C., Mukhopadyay, S., Sutton, N., Coulman, SA. and Birchall, JC. 2021. Polymeric microneedle-based 'dry' electrodes for wearable cardiac monitoring. 2021. *Controlled Release Society Virtual Annual Meeting (YoungSciVision).* Online, 25-29 July 2021.

Conference poster(s)

- Baczkowski, EL., Bocchino, A., O'Sullivan, M., O'Mahony, C., Mukhopadyay, S., Sutton, N., Coulman, SA. and Birchall, JC. 2020. Polymeric microneedle-based 'dry' electrodes for wearable cardiac monitoring. *UKICRS Virtual Symposium*. Online, 14 October, 2020.

Cardiff School of Pharmacy postgraduate research day

- Baczkowski, EL., Bocchino, A., O'Sullivan, M., O'Mahony, C., Mukhopadyay, S., Sutton, N., Coulman, SA. and Birchall, JC. 2019. Minimally invasive clinical monitoring and data transference. *Cardiff School of Pharmacy and Pharmaceutical Sciences Postgraduate Research Day.* Wales; Cardiff, 1 May, 2019 (poster).

- Baczkowski, EL., Bocchino, A., O'Sullivan, M., O'Mahony, C., Mukhopadyay, S., Sutton, N., Coulman, SA. and Birchall, JC. 2021. Polymeric microneedle-based 'dry' electrodes for wearable cardiac monitoring. *Cardiff School of Pharmacy and Pharmaceutical Sciences Postgraduate Research Day.* Wales; Cardiff, 14 April, 2021 (presentation).

Webinar(s)

- Baczkowski, EL., Bocchino, A., O'Sullivan, M., O'Mahony, C., Mukhopadyay, S., Sutton, N., Mehta, S., Coulman, SA. and Birchall, JC. 2020. Minimally invasive clinical monitoring and data transference. *CALIN Series 2* [Webinar]. 4 August 2020.

Note: references highlighted in blue were selected for oral presentation prizes.

TABLE OF CONTENTS

Page number

LIST OF FIGURES

LIST OF TABLES

LIST OF ABBREVIATIONS

Abbreviation	
A&E	Accident and emergency
AC	Alternating current
ACS	Acute coronary syndrome
AECG	Ambulatory electrocardiography
AF	Atrial fibrillation
Ag/AgCl	Silver/silver chloride
AI	Artificial intelligence
ATPase	Adenosine triphosphatase
AWG	Arbitrary waveform generator
AV	Atrioventricular
BMI	Body mass index
BNC	Bayonet Neill-Concelman
bpm	Beats per minute
BW	Baseline wander
Ca^{2+}	Calcium ion(s)
CALIN	Celtic Advanced Life Science Innovation Network
Cl^-	Chloride ion(s)
CVD	Cardiovascular disease
DC	Direct current
DSP	Digital signal processing
ECG	Electrocardiography / Electrocardiogram
EEG	Electroencephalography / Electroencephalogram
ELR	Event loop recorder(s)
EMG	Electromyography / Electromyogram
ESC	European Society of Cardiology
FDA	Food and Drug Administration
FFT	Fast Fourier Transform
GUI	Graphical user interface
H&E	Haematoxylin and eosin
HF	Heart failure
HR	Heart rate
HRV	Heart rate variability
Hz	Hertz
ICM	Implantable cardiac monitor
IoT	Internet of things

K^+	Potassium ion(s)
$k\Omega$	Kiloohm
KOH	Potassium hydroxide
MCOT	Mobile cardiac outpatient telemetry
MHRA	Medicines and Healthcare products Regulatory Agency
MI	Myocardial infarction
MN	Microneedle
ms	Millisecond(s)
mV	Millivolt(s)
Na^+	Sodium ion(s)
NBF	Neutral buffered formalin
NFC	Near-field communication
NHS	National Health Service
NICE	National Institute for Health and Care Excellence
NSTEMI	Non-ST elevated myocardial infarction
OCT	Optical coherence tomography
PAF	Paroxysmal atrial fibrillation
PBS	Phosphate buffered saline
PDMS	Polydimethylsiloxane
PEDOT	Poly(3,4-ethylenedioxythiophene)
PEM	Patch electrode monitors
PIN	Personal Identification Number
PLI	Powerline interference
RF	Radio frequency
SA	Sinoatrial
SC	Stratum corneum
SCST	Society for Cardiological Science and Technology
SEM	Scanning electron microscopy
SME	Small and medium sized enterprise
SNR	Signal to noise ratio
STEMI	ST elevated myocardial infarction
TEWL	Transepidermal water loss
Ti/Au	Titanium/gold
UK	United Kingdom
UV	Ultraviolet
μV	Microvolt(s)
VE	Viable epidermis

LIST OF EQUIPMENT

Equipment	Manufacturer, Country
Adhesive carbon tabs (25mm)	Agar Scientific, UK
Adhesive epoxy (C12400)	Farnell Element, UK
Aluminium specimen stubs (25mm)	Agar Scientific, UK
AmScope stereo microscope	AmScope, USA
Antex ER30 soldering iron	Farnell Element, UK
Antex electronics soldering iron stand	RS Components, UK
BD Microlance stainless steel needle (26G)	Fisher Scientific, UK
Bespoke electrode applicator	Maddison Product Design Ltd, UK
Conductive fabric (stretch)	Kitronik Ltd, UK
Cryotome FSE	Fisher Scientific, UK
Cyton biosensing board (8-channels)	OpenBCI, USA
Digital Eyecam Plus	Brunel Microscopes, UK
Disposable biopsy punch (8.0mm)	Fisher Scientific, UK
E0S 70D digital DSLR camera body	Canon, UK
Duracell ULTRA power alkaline AA batteries	RS Components, UK
EF-S 18-135mm F/3.5-5.6 IS USM lens	Canon, UK
EMG/ECG snap electrode cables	OpenBCI, USA
Epoxy, solid microneedles	Tyndall National Institute, Ireland
E4980A/AL precision LCR meter	Keysight, UK
Falcon conical centrifuge tubes (50mL)	Fisher Scientific, UK
FEI XL30 environmental scanning electron microscope (ESEM) with a field emission gun (FEG)	Philips, USA
Fisherbrand™ disposable base molds	Fisher Scientific, UK
Fisherbrand™ qualitative filter papers (240mm)	Fisher Scientific, UK
Fisherbrand™ sheet compressed cork	Fisher Scientific, UK
Fluke industrial 115 true RMS multimeter	Fluke Corporation, UK
Hair trimmer, Contura Wella Professionals HS61	Contura, Germany
MBO 0.7mm wire lead free solder	RS Components, UK
Menzel Gläser cover glasses (20x50mm)	Fisher Scientific, UK
MX35 premier+ microtome blade (34º/80mm)	Fisher Scientific, UK
Olympus BX50 Microscope	Olympus, UK
Optical coherence tomography system	VivoSight, UK
2239 Red Dot adult ECG monitoring electrodes	3M, UK
RS pro test leads	RS Components

RS BNC 50Ω plug to alligator clip coaxial cable	RS Components, UK
RS PRO male to male BNC coaxial cable, 50Ω	RS Components, UK
RS PRO crocodile clip, nickel-plated iron contact	RS Components, UK
RS PRO PCB circuit board holder	RS Components, UK
RS PRO AA battery holder, coil spring contact	RS Components, UK
RS PRO die cast aluminium enclosure	RS Components, UK
Sauter Digital Force Gauge (FH100)	Sauter GmbH, Germany
SC500 sputter coater	Bio-Rad, USA
Snipe nose pliers with cutter (160mm)	Knipex, UK
Soldering iron cleaning sponge	RS Components, UK
Stemi 508 Stereo microscope	Zeiss, Germany
SuperFrost^{TM} plus adhesion slides	Fisher Scientific, UK
Surgical steel blade disposable scalpels	Swann-Morton Ltd., UK
TBS1072B-EDU oscilloscope, 70MHz	Tektronix, UK
TE connectivity UPW50 resistors (100kΩ and 100Ω)	RS Components, UK
Universal stripping tool, cable stripper (135mm)	Knipex, UK
Waveform generator, 20MHz, 1-channel (33511B)	Keysight, UK
Wi-Fi shield	OpenBCI, USA

LIST OF REAGENTS

Equipment	Manufacturer, Country
Dulbecco's Modified Eagle's Medium (DMEM)	Fisher Scientific, UK
Ethanol absolute laboratory grade (99%)	Fisher Scientific, UK
Histomount mounting solution	Fisher Scientific, UK
Hydrochloric acid (0.1M)	Fisher Scientific, UK
Methylene blue	Fisher Scientific, UK
Neutral buffered formalin (10%)	Sigma-Aldrich, UK
Optimal cutting temperature compound	Fisher Scientific, UK
Penicillin-Streptomycin (10,000U/mL), Gibco®	Life Technologies, UK
Phosphate buffered saline (pH 7.4)	Sigma-Aldrich, UK
Scott's tap water substitute concentrate	Sigma-Aldrich, UK
Shandon Harris Haematoxylin	Fisher Scientific, UK
Shandon Eosin Y Cytoplasmic Counterstain	Fisher Scientific, UK

CHAPTER 1

GENERAL INTRODUCTION

1.1 Electrocardiography

Many organs within the human body, including the brain (Moruzzi and Magoun 1949), heart (Lewis 1912) and muscle (Feinstein 1946) produce measurable electrical signals known as biopotentials (Tatarenko 1975). The term biopotential refers to the electrical potential generated from the electrochemical activity of excitable cells which are found along neurons, and over the surface of muscle cells (Hille 2001). These cells exhibit a resting potential resulting from differences in ion concentration on either side of the membrane. When cells are appropriately stimulated, an action potential is generated (Hodgkin and Huxley 1939; Curtis 1949). As the human body is considered a volume conductor, impulses arising from changes in ion concentrations are propagated towards the surface of the skin where they are detected (Reilly and Lee 2010). Electrocardiography (ECG), electroencephalography (EEG) and electromyography (EMG) are examples used in clinical practice to record the electrical activity of the heart (NICE 2014), brain (NICE 2012) and muscle (NICE 2020b) respectively. This postgraduate research will focus on the recording of cardiac activity, therefore only the ECG will be discussed.

1.1.1 Principles of the electrocardiogram and the electricity of the heart

Since its introduction, the ECG has become an essential component in the evaluation and diagnosis of cardiovascular conditions through the provision of valuable information regarding the electrical activity of the heart. The human ECG is considered one of the more familiar electrograms however, to interpret results, an understanding of the electrical events that underpin the cardiac cycle is required. The main function of the heart is to pump blood to both the pulmonary and systemic circulation. The heart is therefore required to beat in a synchronized manner through the contraction (systole) and relaxation (diastole) of cardiac muscles. The muscular tissue of the heart, termed the myocardium, contains a group of specialised cells, named pacemaker cells which involuntarily generate electrical impulses (Kohlhardt et al. 1976; Qin et al. 1994). This ability to spontaneously generate an impulse

without requiring external stimuli is termed automaticity. Whilst pacemaker cells are considered the endogenic source of electrical impulses, the autonomic nervous system can influence the rate at which impulses are generated (Robinson et al. 1966). The parasympathetic nervous system can decrease heart rate (HR), whilst the sympathetic nervous system can increase HR (Federici et al. 1985; Olshansky et al. 2008). The sympathetic nervous system can also affect AV conduction speed, force of contraction and auto-rhythmicity (Federici et al. 1985; Olshansky et al. 2008).

Myocardial activity is influenced by the movement of three key ions, namely sodium (Na^+) (Weidmann 1955), calcium (Ca^{2+}) (Gibbons and Fozzard 1975) and potassium (K^+) (Barry and Nerbonne 1996). At rest, a charge differential exists between the interior and exterior of myocytes. This resting potential of -90mV is maintained through the action of the Na^+/K^+ adenosine triphosphatase (ATPase) pump which controls the intra- and extracellular concentration of Na^+ and K^+ (Levick 2010; Huszar and Wesley 2017). Due to the impermeability of the myocyte membrane, ions are only capable of moving in and out of cells through channels. Once an impulse is generated by pacemaker cells located in the sinoatrial (SA) node, the interior of the right and left atrial myocytes become positive as Ca^{2+} enters, resulting in depolarisation. This depolarisation causes the right and left atria to contract simultaneously. The wave of depolarisation is propagated until the atrioventricular (AV) node is encountered. Depolarisation subsequently continues, but at a slower pace, allowing both atria to relax and fill with blood. The wave of depolarisation continues to the ventricular conduction system, travelling at a more rapid pace due to the movement of Na^+. Subsequently, myocytes return to their original polarised state through the removal of K^+. Ion movement and the subsequent mechanical response of the myocardium is documented on the ECG (Huszar and Wesley 2017; Pocock and Richards 2018).

A single heartbeat, or complete cardiac cycle of systole and diastole, is represented on the ECG by three key deflections (Figure 1.1) which are labelled alphabetically as P, QRS and T (Einthoven 1895). The frequency, morphology and amplitude of each wave, interval and segment are also documented. Assuming no conduction abnormalities are present, the first wave noted on an ECG is small deflection termed the P wave, which is positive in most leads (Levick 2010; Prutkin 2019). This wave corresponds to atrial depolarisation and is typically <0.12s in duration with an amplitude of <0.25mV (Prutkin 2019). Subsequently the large mass of ventricular muscle rapidly depolarises resulting in ventricular systole. This is represented by a set of deflections termed the QRS complex. As the name suggests, this complex consists of the Q, R and S waves which occur in rapid succession lasting between 0.06 to 0.10s (Prutkin 2019). Ventricular repolarisation follows, resulting ventricular diastole. Since ventricular repolarisation is slower than depolarisation, a broad, asymmetrical deflection known as the T

wave can be observed. With respect to atrial repolarisation, there is no discernible wave corresponding to this event which occurs during ventricular depolarisation. In comparison to the ventricles, atrial muscle mass is smaller, and repolarisation is therefore masked by the much larger generated QRS complex. In addition to the P, QRS and T waves, a U wave can sometimes be observed. The precise cause of this wave is uncertain; however, it is thought that it may be from the late repolarisation of the mid-myocardial M cells (Hopenfeld and Ashikaga 2010). This wave typically measures <0.2mV in amplitude and is clearly separate from the T wave (Prutkin 2019). Intervals including the PR, ST, QT and RR are also important during ECG interpretation. As the name suggests, the PR interval is measured from the beginning of the P wave to the first part of the QRS complex which may be either the Q or R wave (Figure 1.1) (Prutkin 2019). This interval corresponds to the time taken for atrial depolarisation and conduction through the AV node and His-Purkinje system. The length of the PR interval is typically 0.12 to 0.20s, however it can change with HR, for instance at slower HRs, the interval is longer (Prineas et al. 2010; Huszar and Wesley 2017).
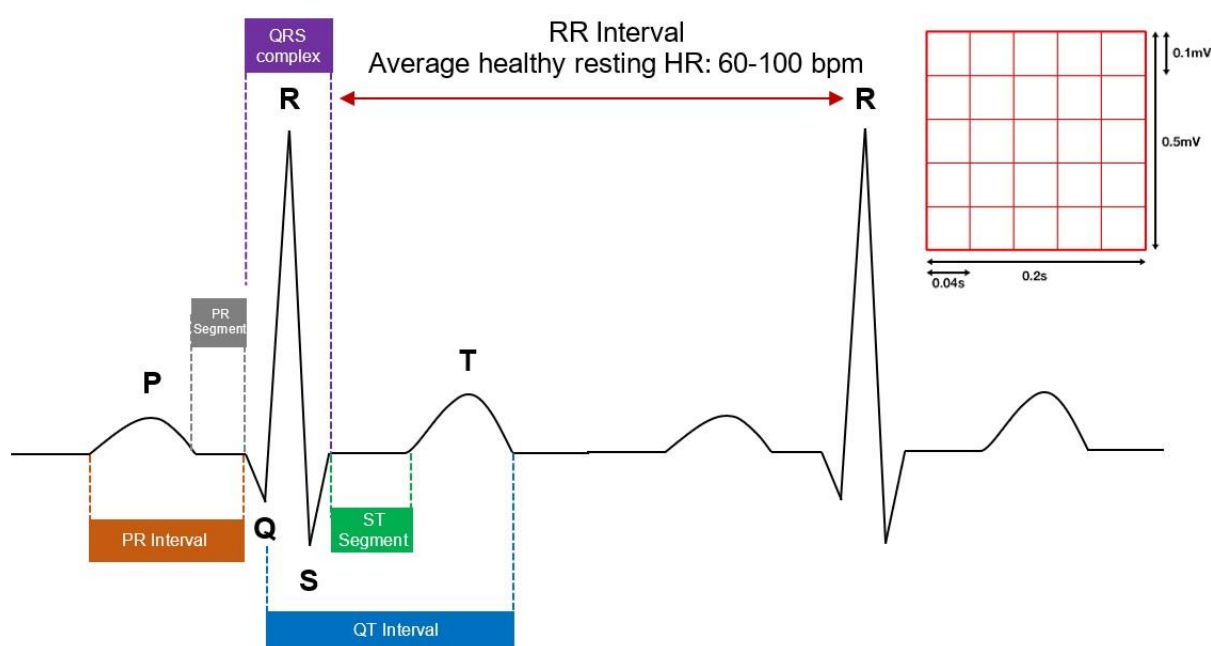
Figure 1.1: Labelled ECG trace identifying P, QRS and T waves. PR interval, PR segment, ST segment and QT interval are also highlighted. Example of the graph paper used to record cardiac activity is also shown. Vertical axis measures wave amplitude, whilst the horizontal axis measures time. When recording a standard electrocardiogram, the paper speed is 25 mm/s. Authors own image.

The ST segment is measured from the end of the QRS complex to the beginning of the subsequent T wave. It is considered a time of electrocardiographic silence as it occurs after ventricular depolarisation and before repolarisation. This segment can be considered a separate waveform as elevation or depression of this segment can be indicative of

ischaemia/infarction. The QT interval contains the QRS complex, ST segment and T wave hence it is a measure of ventricular repolarisation (Stroobandt et al. 2016; Huszar and Wesley 2017). The length of the interval varies with HR, for example at increased HR's it is shorter (Huszar and Wesley 2017). Several methods have been used to correct the QT interval, however Bazett's formula is widely used to correct the QT interval based on HR and is abbreviated to QTc (Bazett 1920). This method can be inaccurate at the extremes of HR. QT generally increases with age and tends to be longer in women, than men with the upper normal QTc in men measuring approximately $\leq$440ms in duration, whilst in women this is approximately $\leq$450 to 460ms (Prineas et al. 2010; Isbister and Page 2013; Prutkin 2019). Finally, the RR interval. This is measured from one point on the QRS complex, typically the R wave, to the corresponding point on the next cardiac cycle. This interval can be used to calculate the HR which, for a healthy resting adult is between 60 to 100 beats per minute (bpm) (Huszar and Wesley 2017). A HR below 60bpm is considered bradycardic, whilst above 100bpm is tachycardic (Stroobandt et al. 2016; Huszar and Wesley 2017).

1.1.2 Types of electrocardiography

There are three main types of ECG namely resting, exercise and ambulatory (Madias 2019; Chareonthaitawee and Askew 2020; Reeder et al. 2021). The type of ECG conducted will depend upon the patient's symptoms and the cardiovascular condition suspected. The resting 12-lead ECG is a simple, quick, and painless test where the patient is typically lying in the supine position (Crawford and Doherty 2013). Any changes in position must be clearly annotated on the ECG trace (Campbell et al. 2017). Data is typically recorded over 10 seconds and during this test movement is discouraged as this can introduce artifacts into the recording (Crawford and Doherty 2012). This type of ECG can be used in various healthcare settings to detect abnormalities including bundle branch blocks which can manifest as traces with a widened QRS complex and evidence of acute coronary syndrome (ACS) such as an ST-segment elevated myocardial infarction (STEMI) (Ponikowski et al. 2016; Stroobandt et al. 2016; Ibanez et al. 2018). Additionally, a resting ECG can also be used preoperatively to assess known cardiovascular disease (CVD), detect undiagnosed cardiovascular conditions and to provide a baseline standard against which to measure changes postoperatively.

An exercise ECG is a form of ECG used to establish a diagnosis and prognosis of coronary heart disease (Pelliccia et al. 2021). Typically performed using either a motor-driven treadmill or stationary cycle ergometer, the exercise ECG focuses on the presence or absence of ischaemic changes alongside any induced arrhythmias. Whilst the treadmill is the preferred method, cycle ergometry can be used in patients where weight bearing is problematic or for frailer individuals (Chareonthaitawee and Askew 2020; Pelliccia et al. 2021). Each method is associated with its own advantages and disadvantages. For instance, ECG data acquired with

cycle ergometry are clearer due to reduced upper body motion (Chareonthaitawee and Askew 2020). However, patients who are not routine cyclists may tire with respect to their quadricep muscles before achieving the desired cardiovascular effort. For most clinical indications, exercise ECGs require a protocol which progresses from low intensity through to a higher intensity until either a predetermined end point is achieved, or symptoms develop that prevent the test from continuing (Chareonthaitawee and Askew 2020). The optimal duration of an exercise test is one that continues until the patient feels they cannot exercise further. Prior to the start of the procedure, a resting 12-lead ECG should be conducted and subsequently reviewed to establish any test contraindications. A resting ECG can be recorded from patients in both the supine position and whilst standing, as the patient's position can influence certain ECG parameters such as the QRS complex and T wave (Baevsky et al. 2007; Campbell et al. 2017; Roccia et al. 2021). ECGs obtained during the test are compared with the resting ECG conducted when the patient was standing, whilst ECGs obtained during the recovery period should be compared with the resting ECG in the same position (Pelliccia et al. 2021). With respect to the test's conclusion, the decision to stop can be patient, protocol or provider determined. For instance, patient-determined endpoints include significant symptoms such as light-headedness or limiting chest pain. Provider-determined endpoints however may involve ECG changes such as marked ST depression. Protocol determined endpoints conversely are endpoints which have been defined, however in most circumstances the test continues until a patient has reached their maximum capability, or another clinically related endpoint. After a cool-down period, whilst the patient remains on the treadmill or bicycle, further ECGs should be recorded until the patient's HR falls below 100bpm or the ECG waveform returns to normal (Chareonthaitawee and Askew 2020).

Compared to the 10-second snapshot provided by the standard ECG; ambulatory monitoring provides a view of cardiac activity over extended periods of time. This allows for the detection of spontaneous and often variable conduction abnormalities and arrhythmias (Poblete et al. 1978; Boudoulas et al. 1979). Several professional guidelines such as the European Society of Cardiology (ESC) recommend ambulatory ECG (AECG) monitoring for patients experiencing symptoms including unexplained and recurrent palpitations, unexplained syncope, or episodic dizziness (Crawford et al. 1999; Kirchhof et al. 2016; Steinberg et al. 2017; Hindricks et al. 2021). Several AECG monitoring methods exist and can be used for short periods of time of up to 48 hours, or for as long as months to years. The initial choice of AECG monitoring depends upon symptom frequency and severity. For patients experiencing daily, or near daily symptoms, continuous ECG monitoring is considered the most practical. Holter monitoring, named after Norman J. Holter, is the current method of AECG monitoring and involves a small, battery-operated device which records cardiac data

from electrodes attached to the patient's chest (Holter and Generelli 1949; Holter 1961; Madias 2019). Following 24 to 48 hours of recording, current monitors must be returned for analysis by a healthcare professional and therefore do not provide real-time information regarding a patient's symptoms. For patients experiencing symptoms on a weekly or monthly basis, an event or loop monitor is preferred, of which several types exist. Firstly, post event monitoring devices which are typically small, and lightweight are placed on a patient's chest at the onset symptoms. Data is stored for a specific amount of time after the recording has begun. Secondly, event and loop recorders. These devices continuously record for a specified period. They do not, however, save the data until they are triggered by the patient. Thirdly, auto-triggered event recorders which are considered more advanced devices as they have an auto-detect feature allowing them to capture asymptomatic arrhythmias based upon detection algorithms (Reiffel et al. 2005; Madias 2019). A further form of AECG monitoring is mobile cardiac outpatient telemetry (MCOT). This form is useful for patients who experience less frequent symptoms, for example weekly to monthly, where a comprehensive assessment of all cardiac activity is required. Compared with loop recorders, MCOT has been shown to detect more arrhythmias. For instance, Rothman et al. 2006 compared an MCOT system with a patient activated external loop recorder for symptoms suggestive of a cardiac arrhythmia e.g., syncope, presyncope or palpitations. This randomised controlled trial demonstrated that MCOT (88%) provided a significantly higher diagnostic yield than the standard loop recorder (75%). Monitors used in MCOT can be worn for up to 30 days where a 3-lead sensor transfers data to a portable monitoring device which subsequently transfers data to a monitoring centre for further analysis. The device can be activated automatically or by the patient, should they experience symptoms. Finally, implantable cardiac monitors (ICM) can be used for AECG. They are rarely the preferred initial choice as these devices involve a simple, yet invasive procedure (Madias 2019). Implantation is generally performed in an outpatient setting and devices are subcutaneously inserted using a local anaesthetic in the left pectoral region (Madias 2019; NICE 2020a). In patients with potentially deleterious symptoms occurring infrequently, whose previous assessments with both Holter and event monitoring have proved inconclusive, ICM can prove extremely useful. The duration of use for ICMs can range between two to four years depending upon manufacturer and battery longevity (Madias 2019).

1.1.3 Clinical significance of electrocardiography

The ECG is a non-invasive clinical tool, fundamental in the diagnosis of many cardiovascular conditions. Information provided by this simple, yet valuable test has substantial clinical implications. Any deviations from what is considered normal may be indicative of a cardiac pathology.

ACS is an overarching term which, based upon ECG appearance, encompasses a range of conditions including STEMI and non-ST elevated myocardial infarction (NSTEMI) (Figure 1.2). This syndrome is associated with a set of signs and symptoms produced as a result of decreased blood flow to the coronary arteries. ACS is considered a medical emergency requiring a prompt and accurate diagnosis. In addition to measuring the degree of cardiomyocyte injury using the biomarker troponin, ECG remains one of the primary tests used to diagnose and distinguish between a STEMI and NSTEMI. Guidelines produced by the ESC recommend a 12-lead ECG ideally at first contact with paramedics or within 10 minutes of a patient presenting to accident and emergency (A&E) with symptoms suggestive of a myocardial infarction (MI) (NICE 2014; Roffi et al. 2015; Ibanez et al. 2018; Collet et al. 2021). The use of ECG alongside the biomarker troponin contributes to a rapid diagnosis and therefore, rapid intervention which improves the overall prognosis.

Low likelihood   **High likelihood**

Presentation

ECG

Troponin   –   +   ++

Diagnosis | Non-cardiac | UA * | Other Cardiac | NSTEMI * | STEMI *

* NSTEMI: non-ST elevated myocardial infarction
STEMI: ST elevated myocardial infarction
UA: unstable angina
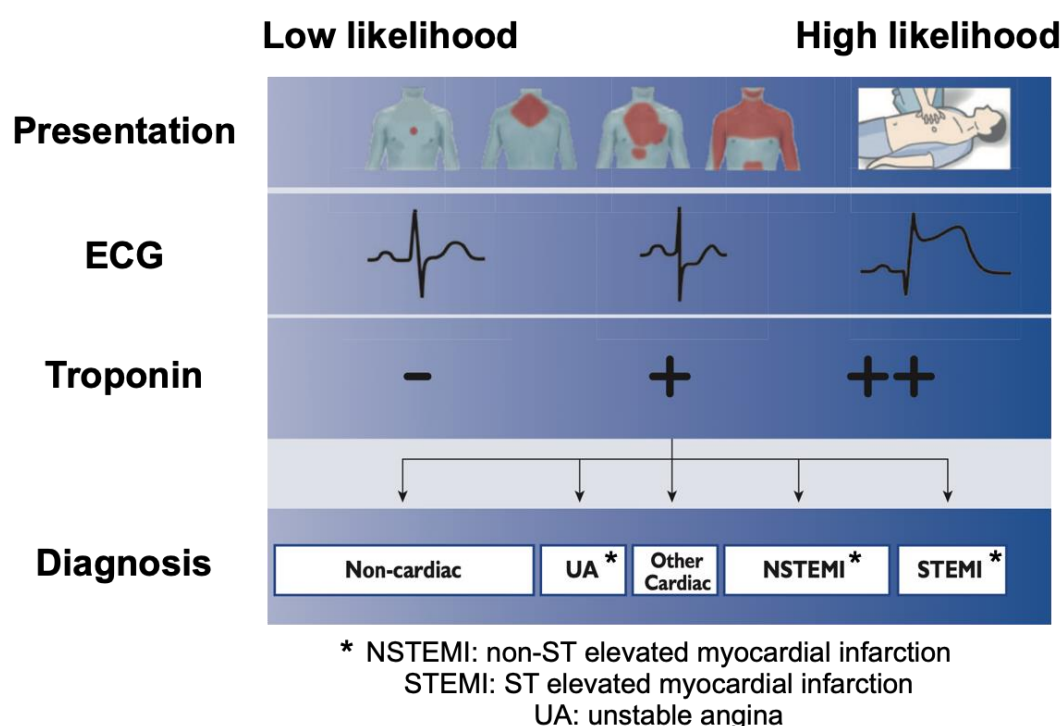
Figure 1.2: Initial assessment of patients presenting with suspected acute coronary syndrome. When presenting to accident and emergency the initial assessment is based upon patient symptoms, 12-lead ECG, and cardiac troponin. Image adapted from Roffi et al. (2015).

Atrial fibrillation (AF) is a form of arrhythmia which remains one of the major causes of stroke, sudden death, and cardiovascular morbidity (Kirchhof et al. 2016; Hindricks et al. 2021). In the coming years, the number of patients diagnosed with this arrythmia is predicted to rise. This increase can be attributed to improved detection, alongside increasing age and conditions which pre-dispose patients to AF (Kishore et al. 2014; Sanna et al. 2014; Schnabel et al. 2015). Rhythm documentation using an ECG is required for a diagnosis. A typical pattern of

AF involves irregular RR intervals with no discernible, distinct P waves (Kirchhof et al. 2016; Hindricks et al. 2021). Evidence suggests that prolonged ECG monitoring can help enhance the detection of undiagnosed AF for example 72-hour monitoring post stroke (Rizos et al. 2012; Grond et al. 2013) or for even longer periods (Gladstone et al. 2014; Sanna et al. 2014). Paroxysmal AF (PAF) is a form of AF which is often missed due to its intermittent nature. Repeated ECG monitoring can increase the detection of asymptomatic PAF. Various patient-operated devices and AECG patch devices have been validated for the detection of this arrythmia (Kaleschke et al. 2009; Barrett et al. 2014; Tieleman et al. 2014). Following a diagnosis, ECG monitoring can also be undertaken to inform patient management regarding symptom changes, development of new symptoms and monitoring the effects of prescribed therapeutics (Kirchhof et al. 2016; Hindricks et al. 2021). In addition to AF, ECG can be used to detect other abnormal cardiac rhythms. A resting 12-lead ECG is recommended by the ESC in all patients who are evaluated for ventricular arrhythmias such as long QT, Brugada syndrome and Torsades de Pointes. Arrhythmias such as Torsades can be drug induced and are frequently observed with antiarrhythmics mainly class I and III. This form of arrhythmia is characterised by rapid, irregular QRS complexes and is associated with a prolonged QT interval. In addition to a resting 12-lead ECG, exercise ECGs are commonly used, particularly for the detection of silent ischaemia in patients suspected of having underlying coronary heart disease (Zipes et al. 2006). Additionally, AECG can also be used when there is a requirement to clarify the diagnosis by detecting and monitoring changes in the QT interval, ST segment and T waves (Zipes et al. 2006).

Heart failure (HF) is a chronic, progressive clinical syndrome characterised by symptoms including breathlessness, ankle swelling and fatigue (Ponikowski et al. 2016). A comprehensive assessment of patients presenting with symptoms suggestive of HF is undertaken, considering medical history and physical examination (Ponikowski et al. 2016). When used alongside a myriad of additional tests, a resting ECG can prove useful to determine HR, heart rhythm, QRS morphology and duration. The ECG may reveal abnormalities including AF, repolarisation abnormalities or left-ventricular hypertrophy. In patients presenting with a normal ECG, HF is unlikely, therefore the routine use of an ECG is recommended mainly to rule out HF (Ponikowski et al. 2016). ECG is used in both acute and chronic HF, and should the condition be diagnosed, the information gleaned from an ECG can be used to plan and subsequently monitor a patient's treatment.

Due to its versatility and inexpensive nature, the immediate information produced by an ECG helps rapidly diagnose problems relating to myocardial ischaemia, infarction, electrolyte disturbances, hypertrophy and more. In addition to the aforementioned benefits, and its use

for more than a century, the ECG can be considered an essential clinical test in the diagnosis of numerous cardiovascular conditions.

1.1.4 Recording a standard 12-lead electrocardiogram

Since the introduction of the first ECG by Willem Einthoven in the early 1900s, this clinical procedure has become indispensable. The clinically accepted 12-lead system is the preferred method when diagnosing and monitoring cardiovascular conditions as the majority of recommended diagnostic ECG criteria have been derived and validated using this system (Ibanez et al. 2018). Due to the broad applicability of the standard ECG, accurate recording and precise interpretation are crucial.

1.1.4.1 Lead system for a standard 12-lead electrocardiogram

As the name suggests, the 12-lead ECG provides twelve different views of the heart following the application of ten electrodes to specific locations on the body. With respect to ECG, the term lead can have two definitions. It can either refer to the physical wired connection between the electrodes and recording equipment or, represent differences in electrical potentials measured between two points. The latter explanation is important as each 'lead' records a different view of the heart that can be used to provide information regarding its structure and function (Huszar and Wesley 2017). The standard leads used during the 12-lead ECG can be subdivided into two groups. The extremity leads, commonly termed the limb leads, record electrical potentials transmitted onto the frontal plane (Crawford and Doherty 2013; Houghton 2019). These six leads can be further subdivided into three bipolar leads (I, II and III) and three unipolar leads (aAVR, aVL and aVF). Each bipolar lead measures the potential difference between two electrodes where one is of positive polarity and the other negative (Houghton 2019; Prutkin 2019). The right arm is always negative, and the left leg is always positive, however, the left arm varies depending upon whether an ECG is being recorded in lead I or II. As shown by Einthoven's triangle in Figure 1.3, lead I measures the potential difference between the negative right arm and positive left arm. Conversely, lead II measures the potential difference between the negative right arm and positive left leg. Lead II lies close to the cardiac axis, closely resembling the direction of depolarisation as it travels from the upper right atrium to the larger, lower left ventricle (Huszar and Wesley 2017; Houghton 2019; Prutkin 2019). Furthermore, lead II is considered one of the most useful leads in the detection of cardiac arrhythmias (Houghton 2019). Lastly, lead III measures the potential difference between the negative left arm and positive left leg. Provided there are no conduction abnormalities, ECG traces from the three bipolar limb leads will generally produce positive P and T waves, with a predominantly positive QRS complex with some small negative deflections. The combination of leads I, II and III is commonly referred to as the Einthoven triangle. Comparatively, the unipolar limb leads measure the cardiac voltage at one site

relative to a central point which has approximately zero potential. The three leads aVR, aVL and aVF record potentials in the right arm, left arm and left leg respectively whilst the right leg electrodes functions as a ground.
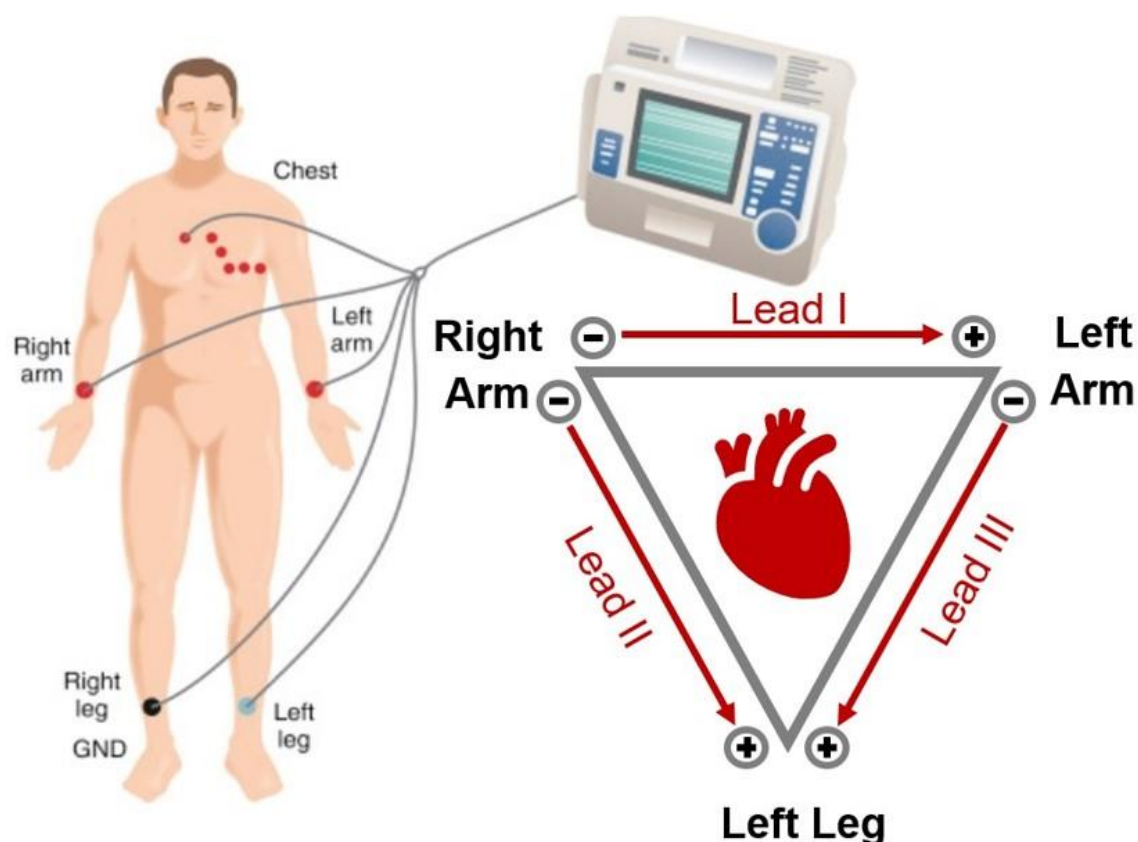
Figure 1.3: Electrode positions in a 12-lead ECG and Einthoven's triangle. Image shows three bipolar leads (I, II and III) and provides a view of electrical potential between positive (+) and negative (-) electrodes. Lead I is obtained by attaching the negative electrode to the right arm and the positive electrode to the left arm. Lead II is possible by attaching the negative electrode to the right arm and the positive electrode to the left leg. Lead III is obtained by attaching the negative electrode to the left arm, the positive electrode to the left leg. Image adapted from Huszar and Wesley (2017).

The six chest leads, also termed precordial leads, are also unipolar. They again represent the differences in voltage between the central terminal and electrodes placed at specific positions on the chest (Figure 1.3). In comparison with the extremity leads, the chest leads record electrical potentials transmitted onto the horizontal plane. Misplacement of these chest leads can lead to considerable diagnostic confusion. The leads are designed so that if a wave of depolarisation spreads towards the positive pole of that lead, a positive deflection is seen. A negative deflection can be observed if the wave of depolarisation travels towards the negative polar of the lead. The combination of extremity and chest leads provide a three-dimensional description of cardiac electrical activity which is important for ECG interpretation and analysis. The placement of these leads is crucial as 12-lead ECG misplacement such as placing the

electrodes in the reverse order can result in diagnostic errors (Finlay et al. 2010; DiLibero et al. 2016; Giannetta et al. 2020). Despite the large number of publications within the scientific literature documenting the correct positioning of the 12-lead ECG on the body, studies such as Giannetta et al. (2020) have highlighted that further education is required to ensure that 12-lead ECG misplacement, mistaken interpretation and misdiagnosis do not happen (Funk et al. 2017).

1.1.4.2   The silver/silver chloride wet electrode

Biopotentials created as a result of ion movement during the cardiac cycle can be detected at the surface of the skin (Ha et al. 2014; Zhang and Hoshino 2019). A link, however, is required to bridge the gap between the biopotentials within the body and external recording equipment. ECG signal acquisition, therefore, involves the use of electrodes. These devices are typically affixed to the outermost layer of skin and transduce surface biopotentials into electrical signals (Grimnes and Martinsen 2014). The stud electrode is an example of one type of electrode used during cardiac signal acquisition (Figure 1.4).
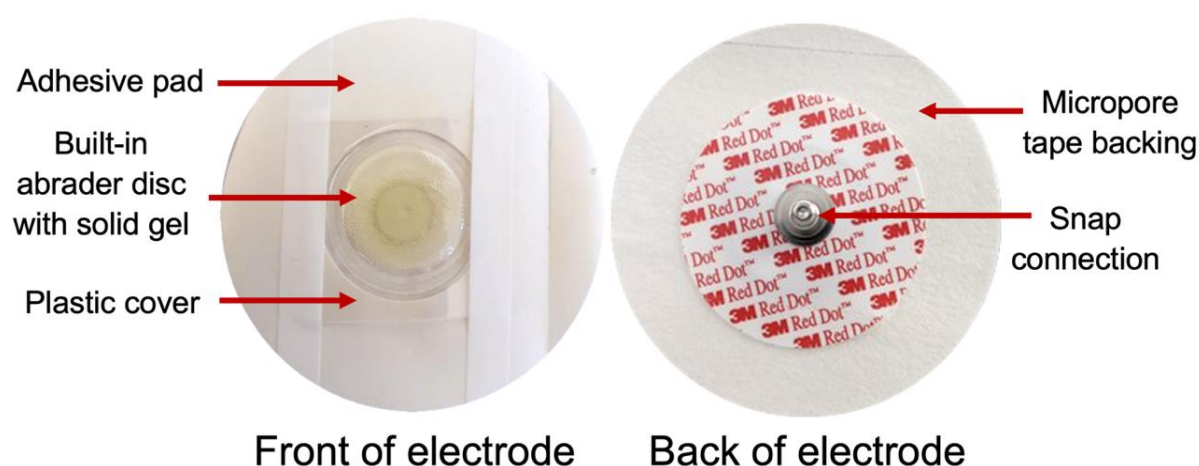
Figure 1.4: Pre-gelled adult cardiac monitoring electrode. Labelled image of the front and back of a 3M Red Dot 2239 single-use cardiac monitoring electrode. Authors own image.

These electrodes are assembled with a sensing element covered with an electrolytic gel containing free ions such as Na^+ and chloride (Cl^-). These gels form a conductive path between the electrode and surface of the skin. At the interface between the sensing element and electrolytic gel, a reversible REDOX reaction occurs. A similar exchange occurs between the body and gel, however the situation at each interface is more complex involving resistive elements of both the skin and electrode (Crawford and Doherty 2012). Additional components of the electrode include an adhesive patch to allow for secure attachment to the body, and a snap connection to attach to ECG recording equipment. Currently, single use, disposable,

solid gel electrodes are the preferred method for recording ECGs (Campbell et al. 2017; NHS 2018).

During the manufacture of these class II devices, ECG monitoring electrodes must meet or exceed the performance safety and labelling requirements set out in the American National Standard ANSI/AAMI EC:12:2000/(R)2015 for disposable ECG electrodes when used for diagnostic ECGs or ECG monitoring (AAMI 2005). As monitoring electrodes record the electrical activity of the heart, their electrical performance is important. Currently, no European standards exist for pre-gelled ECG electrodes, however the Association for the Advancements of Medical Instrumentation (AAMI) and the American National Standards Institute (ASNI) produced guidance regarding impedance and offset voltage recovery time following defibrillation (AAMI 2005). In addition to electrical performance, ECG electrodes are required to be biocompatible however biocompatibility can depend upon the duration that the electrode remains attached to the skin. If an electrode contains an electrolytic gel with a high concentration of Cl^-, this may not irritate the skin if applied for 5-10 minutes (Crawford and Doherty 2012,2013). However, if left attached for a longer period of time, this may result in skin reactions. The materials used in the electrolytic gel are regulated to reduce the likelihood of allergic reactions and irritation. Depending on the desired indication, care must be taken to select a suitable electrode.

Most ECG electrodes have a shelf-life of approximately 2 years if they remain unopened. The manufacturer is required to indicate the shelf-life of their electrodes highlighting how long the electrodes are expected to remain in a useable, high-quality condition. Upon opening, the shelf-life reduces to 30 days as electrodes containing electrolytic gels are prone to drying out (NHS 2018; 3M 2021). The electrolytic gels used in ECG can be aqueous, cream-based, liquid, or solid (NHS 2018). Solid gels are less prone to drying out, however it is recommended that once opened, the electrodes remain stored in the original packaging and a new expiry documented. Several methods have been investigated to address this notable limitation, for instance a continuous supply of electrolytic solution to the skin to keep it moist and maintain a low skin-electrode impedance (Alba et al. 2010; Fong and Chung 2015). Alba and colleagues proposed a hydrogel swollen with a sodium chloride solution embedded on a metal cup electrode. The hydrogel acted as a sponge maintaining skin moisture for a certain period of time (Alba et al. 2010). Alternatively, electrodes containing reservoirs have been proposed some of which contain long tips capable of dispensing the solution (Mota et al. 2013; Weder et al. 2015; Hua et al. 2019). These suggested electrodes are bulky and the presence of stiff tips against the body can make them uncomfortable to wear. Xing et al. (2018) fabricated micro-seepage EEG electrodes with flexible and elastic tips. Whilst the electrodes demonstrated low impedance, they were complex and difficult to

fabricate. Xing and colleagues however found that these electrodes were only suitable for short-term recordings due to the formation of salt crystals at the electrode/scalp interface (Xing et al. 2018). In addition to electrolytic gels, ECG electrodes are required to securely attach to the skin for the desired duration of use. An ECG electrode required for a short, 10-second resting ECG would be less adhesive than electrodes used for longer-term monitoring.

1.1.4.3 Skin preparation prior to electrode application

The quality of an ECG trace can be influenced by several factors including the type of electrode, lead positioning and the immediate environment. The presence of the outermost epidermal layer, the stratum corneum (SC), also poses a challenge as it is a considerable barrier to the recording of high-quality diagnostic ECGs (Tobin 2006; Crawford and Doherty 2012). During an ECG recording, a phenomenon termed skin-impedance is often encountered. The human body is a known electrical conductor; however, the body can resist the flow of electricity to some extent. The majority of the body's electrical resistance is at skin level, namely the SC (Grimnes and Martinsen 2014). At a higher impedance, increased levels of interference are observed due to an increased incidence of alternating current (AC). This therefore produces ECG traces of poor quality (Yamamoto and Yamamoto 1976; Davis-Smith 2000). To reduce the effect of the SC, electrolytic gels are beneficial. These gels facilitate signal transduction by hydrating the skin thereby reducing the effects of skin impedance and enhancing trace quality. In addition to electrolytic gels, the skin underneath the electrode can be primed and this is an important step during the ECG recording procedure. It is assumed that new electrode designs can solve the problem of skin impedance, often resulting in skin preparation being overlooked. An increase in skin impedance occurs for multiple reasons including the accumulation of dry, dead skin cells, dirt, grease, and the presence of excess hair. A dry and calloused area of skin may have a resistance greater than 100kΩ due to the increased presence of dry and dead SC cells acting as a layer of electrical insulation (Fish and Geddes 2009). The cells of the SC are rigid and dry, with a reduced capacity to bind with water, hence contributing to increased impedance (Björklund et al. 2013; Grimnes and Martinsen 2014). Whilst skin preparation adds time to the recording procedure, a high-quality trace is typically obtained on the first attempt. In general, skin preparation techniques are poorly defined throughout the literature and can vary between healthcare settings and practitioners. The most effective method demonstrating a reduction in skin impedance involves abrasion (Medina et al. 1989; Oster 2005). This method is achieved by gently rubbing the surface of the skin with disposable dry gauze wipes, or disposable ultrafine grade sandpaper to remove loose, dry portions of the outer epidermis (Crawford and Doherty 2012; Campbell et al. 2017). When performed lightly, there is little chance of irritation, however the surface of the skin should appear pink and not visibly red. A further benefit of this technique

involves the removal of some oils and skin debris. This may, therefore, reduce electrode motion artifacts as the electrode adheres closer to the skin.

For certain patients', removal of hair in the areas under the electrodes is recommended (Campbell et al. 2017). It is impractical to part and flatten the hair as this can form a barrier between the skin and electrode. The presence of hair also reduces the adhesion of electrodes, potentially increasing the degree of motion artifact in the resulting ECG trace. Subsequently, if hair is not removed, the contact and subsequent penetration of electrolytes into the skin is reduced. Razor blades are not recommended to remove hair due to the risk of infection and injury (Crawford and Doherty 2012). Furthermore, for patients with oily skin or those who have recently applied skin lotions, it may be necessary to cleanse the skin using a mild soap solution. In some instances, alcohol-based cleansers may be required. Care, however, should be taken, and time must be permitted to allow the alcohol to evaporate prior to electrode application as this can dehydrate the SC thereby increasing impedance (Carim and Hawkinson 1982; Oster 2005). For these reasons, alcohols are not routinely employed as a standard skin preparation technique. It is recommended that following skin preparation and electrode application, the electrode should be allowed a short stabilisation period before recording.

1.1.4.4   Accuracy of the 12-lead electrocardiogram

It must be noted that whilst the 12-lead ECG is a quick and cost-effective diagnostic step, inaccuracies can arise for several reasons, for instance, non-modifiable patient factors including biological sex, race, and body habitus (Crawford and Doherty 2012). It can also result from practitioner factors such as poor skin preparation and incorrect placement of electrodes (Finlay et al. 2010). By adhering to guidelines and standardised procedures, these inaccuracies can be limited however, some remain. The 12-lead ECG provides data over a limited period of time which equates to approximately 10 seconds. Anything which occurs before or after this period is not recorded. Therefore, in patients complaining of frequent palpitations, it is common to record an ECG which is interpreted as normal. Subsequent further tests would have to be conducted before a conclusive diagnosis can be made.

The ECG is prone to false positive and negative results due to the limited sensitivity and specificity in different disease states (Prutkin 2019). False positives occur when the data indicates the presence of a disease or structural change when there is not. Conversely, a false negative suggests that the data is normal despite the presence of disease or structural changes. For instance, a patient's symptoms may indicate ischaemia whilst the ECG may be considered normal. Despite the 12-lead ECG providing twelve different views of the heart, electrical blind spots remain (Sgarbossa et al. 2001; Green et al. 2007). Furthermore, the

definition of 'normal' and reference values concerning voltages and timings of ECG parameters are based upon limited cohorts of patients from the earlier days of ECG. It is now known that variations relating to gender, ethnicity and body habitus exist (Hancock et al. 2009). In addition to the aforementioned variations, day-to-day variability also exists. HR is one of the most variable factors, followed by the QT interval (Huszar and Wesley 2017). When comparing successive ECGs, minor changes in waveforms and voltages can be observed.

An ECG should always be interpreted by an experienced practitioner as studies confirm that intra-observer variability is satisfactory (Campbell et al. 2017; Ajmal and Marcus 2021). However, inter-observer variability is less so, as practitioners may not always agree in their interpretation. Standardised algorithms can be used to analyse ECGs however, whilst improvements in computerised recordings of ECGs have been made, it is evident that over-reading and confirmation by a clinician is required (Willems et al. 1991; Salerno et al. 2003b,a).

1.2 Wearable devices in cardiovascular care

Wearable biosensors, also termed 'wearables' refer to small electronic devices or computers with wireless communications that are incorporated into gadgets, accessories or clothing. Devices include smartwatches and patches which can be used to collect and subsequently process a plethora of health data including physiological signals, HR, skin temperature, amongst others (Pierleoni et al. 2019; Xiao et al. 2020; Zhang 2020; Zhang et al. 2021). The field of cardiology has an established history of using wearable medical devices to help determine the cause of symptoms such as palpitations and syncope. Several diagnoses can be made using a resting, 12-lead ECG, however some abnormalities are intermittent and could be absent when the patient is assessed in an outpatient setting (Zimetbaum and Goldman 2010). The clinical requirement to monitor outpatients has resulted in the development of several AECG recording devices which are available for use in the short-term through to long-term. The choice of device is guided by several factors including indication and frequency of symptoms.

1.2.1 Continuous monitoring devices

Continuous monitoring devices record every heartbeat during the recording period and store this data to memory (Kennedy 2013). This provides a complete picture of electrical events helping assess factors such as arrhythmia burden, HR profile or rate control (Steinberg et al. 2017). Due to the substantial amounts of data collected during the monitoring period, the duration in which continuous recording devices are used is short. Whilst the patient is assessed for a greater period of time in comparison to the 10 second resting, 12-lead ECG, recording cardiac electrical activity for up to 7 days can make these devices less suitable for patients with symptoms which occur less than weekly (Zimetbaum and Goldman 2010). Whilst

continuous monitoring provides comprehensive data regarding a patient's health status, data collected by various devices must be evaluated by a physiologist which requires time and expertise despite automation. Furthermore, clinicians and other members of the healthcare team have additional clinical commitments and will therefore be unable to monitor every second of data recorded by the device.

1.2.1.1　Holter monitors

Remote cardiac telemetry was developed to allow for the monitoring of patients with suspected cardiac arrhythmias whilst they are at home conducting their typical daily activities. It was first introduced in the 1940s by Norman J. Holter. The first, original Holter involved an 85-pound backpack which could record a single ECG lead over several hours (Holter and Generelli 1949; Holter 1961). Since the introduction of the first commercially available device in the early 1960s, Holter monitors are a powerful tool in patient assessment (Kohno et al. 2017). Events which would be difficult to capture using the 12-lead ECG or bedside monitoring, can be captured, and analysed (Khalil et al. 2017). These devices use wet electrodes to capture cardiac signals which are subsequently transmitted to a recording device which is typically worn around the neck using a lanyard or can be attached to a belt (Figure 1.5).
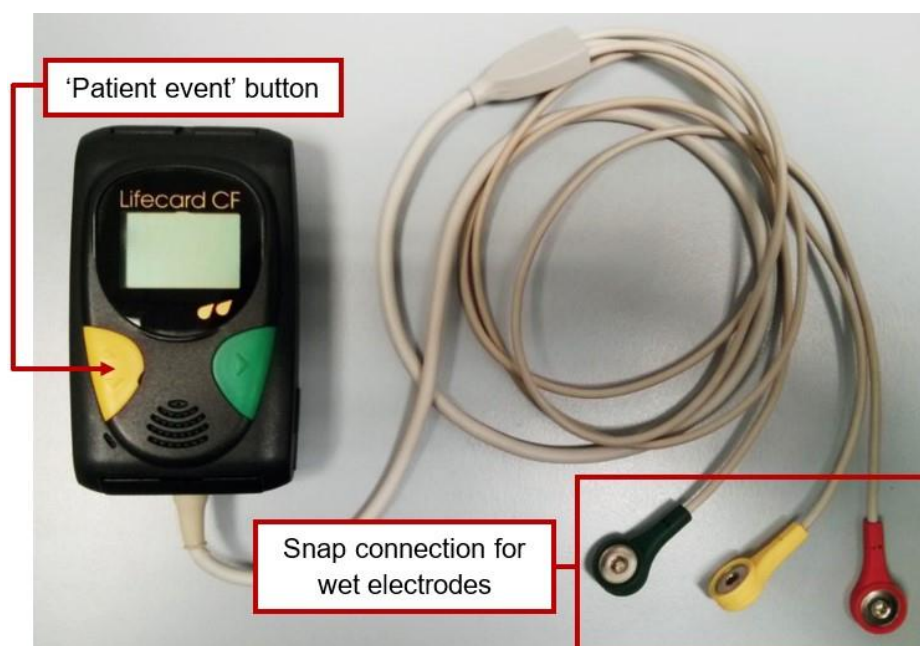
Figure 1.5: Example of a typical 3-electrode Holter monitor. Monitor shown is the 3-channel, 3-electrode Lifecard CF which is a small, battery-powered device capable of recording up to 7 days of continuous cardiac activity. Image adapted from Sampson (2019).

Early devices were limited in terms of the data that could be captured. This has since been addressed, to some degree, where modern devices record digital data to memory cards allowing for the recording of multiple channels over a longer timeframe (Kennedy 2013). Using multiple recording channels allows for the comparison of ECG leads which proves useful when

assessing waveforms and excluding artifacts (Bennett 2013). Within the National Health Service (NHS), Holter monitors are typically fitted to patients in the cardiology department. However, during the COVID-19 pandemic some health boards have provided patients with instructions to allow them to fit the devices themselves. Monitors used by the NHS are capable of recording two or three channels for up to 7 days, however durations of 24 or 48 hours are more common (Steinberg et al. 2017). Upon completion of the recording, patients return their monitor to the relevant cardiology department. The digital data is then analysed where a range of values including minimum, maximum and mean HR are calculated (Khalil et al. 2017). Despite the wide availability, low-cost and widespread acceptance by clinicians, Holter monitors are associated with several limitations (Steinberg et al. 2017; Sampson 2019). The short duration of monitoring can result in low diagnostic yields for infrequent events; therefore, a negative result does not necessarily exclude the presence of disease (Zimetbaum and Goldman 2010). Diagnosis depends upon correlating symptoms with ECG findings. When the device is recording, patients are asked to press the 'patient event' button on the Holter (Figure 1.9) when they experience symptoms and maintain a diary of their symptoms to increase the correlation between detected rhythm abnormalities and symptoms (Zimetbaum and Goldman 2010). Compliance with this requirement is poor making it difficult to interpret the significance of results (Bennett 2013). Furthermore, data analysis does not take place until the patient has returned the monitor. This leads to a delay in the identification of important events and a subsequent diagnosis (Steinberg et al. 2017). Due to the volume of Holter monitors which are analysed by NHS organisations, this delay could extend to several weeks.

1.2.1.2   Patch electrode monitors

Emerging technologies are addressing the shortcomings associated with wet electrodes and ambulatory devices such as the Holter monitor. Whilst the Holter remains the most used continuous monitoring device, the use of patch electrode monitors (PEM) is becoming more widespread. Devices such as the Zio® XT Patch (iRhythm Technologies, USA), BodyGuardian® (Preventice Solutions Group, USA) and SEEQ™ MCT (Corventis Inc, USA) are beginning to reshape the field of AECG monitoring (Turakhia et al. 2013; Cheung et al. 2014; Engel et al. 2015; Castelletti et al. 2018). PEMs are single-use AECG recorders which continuously record cardiac activity over 7 to 14 days (Sampson 2019). These self-contained adherent units are typically worn on the upper left pectoral region and contain electrodes, a microelectronic circuit with recorder, memory storage and an internal battery embedded in a relatively flexible material (Turakhia et al. 2013; Fung et al. 2015). Within the UK, the Zio® XT Patch (Figure 1.5) is the most used PEM.
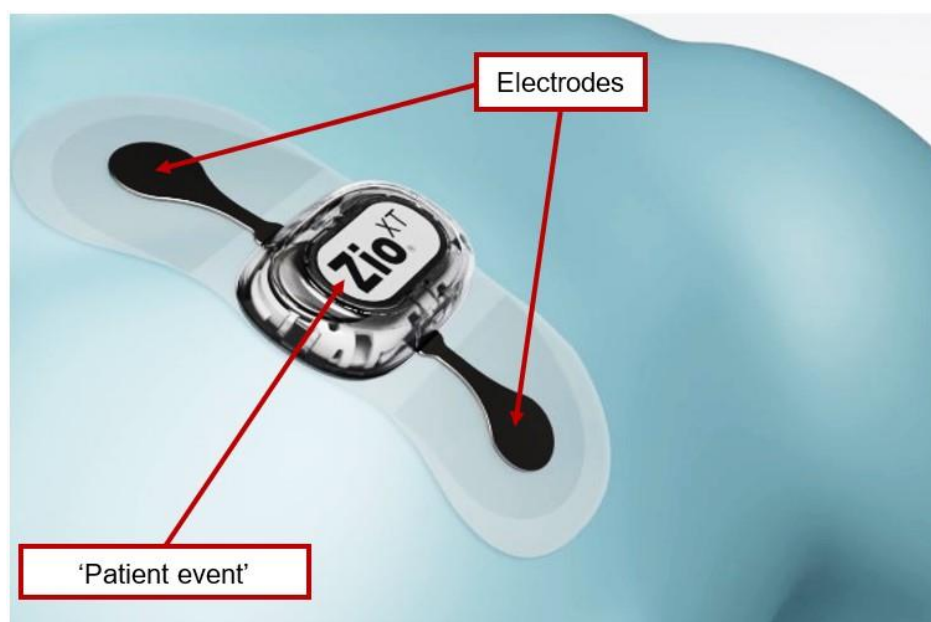
Figure 1.6: Zio® XT patch produced by iRhythm Technologies (USA). The leadless Zio® XT patch can continuously record cardiac activity and be worn for up to 14 days. Image adapted from iRhythm (2019).

This leadless device is water resistant and provides 14 days of continuous ECG recording (Turakhia et al. 2013). Similarly, to the Holter monitor, patients highlight symptoms by deploying a button on the device. Patients are encouraged to detail the nature of the symptom, time at which the symptom occurred and what activity they were performing using a diary or smartphone application. In a study conducted by Barrett et al. (2014), almost twice as many arrythmias were detected in patients fitted with a Zio® patch compared to those with a 24-hour Holter monitor. A key objective in the development of novel acquisition systems is the construction of a device that causes the least amount of aggravation for the patient and ease of use for the clinician. The ease of application of these PEM have resulted in high study completion rates (Shinbane et al. 2013; Fung et al. 2015), suggesting a high acceptance rate, which could translate into improved compliance when compared to other devices (Barrett et al. 2014; Halcox et al. 2017). The main advantages of this type of device are that they are simple to use, leadless, water resistant and unobtrusive. Despite these advantages, devices such as the Zio® XT are not available in most NHS trusts. The primary reason behind this could be related to cost. The National Institute for Health and Care Excellence (NICE) estimated that the device, inclusive of analysis and report, costs between £265 to £310 per patient (NICE 2020c). By comparison, an NHS Holter monitor, which is reusable, costs approximately £1600, with an estimated cost of £118.60 per patient for fitting and analysis of data (Sampson 2019). The cost stated by Sampson (2019) was determined using guidance from NICE published in 2017. Recently updated NICE guidelines have stated that whilst more evidence is required, the technology is likely to be cost-neutral or cost saving when compared

with the 24-hour Holter monitoring (NICE 2020c). Whilst recent guidance is positive in terms of costing, devices must be returned to the company, via mail, at the end of the monitoring period to extract the raw data and generate a report (Fung et al. 2015). Therefore, there is a delay between device submission and the availability of a summary report. This could take days before a cardiologist or electrophysiologist is able to review the report and provide a diagnosis based on the clinical data. The time taken for this processing period may not be of concern for patients with suspected conditions that are considered relatively benign or assessing rate control in response to therapy, but the turnaround time may be too long for those patients with more severe conditions.

1.2.2 Intermittent monitoring devices

Intermittent recorders are used for longer monitoring periods of up to 4 weeks for external devices and between 3 to 4 years for implantable devices (Kennedy 2013). Unlike the aforementioned devices, intermittent recorders do not capture every heartbeat. Whilst this makes then unsuitable for rate control assessment, they are however more effective at aiding diagnoses when symptoms or events are infrequent (Zimetbaum and Goldman 2010).

1.2.2.1 Event recorders

Event recorders are typically handheld devices capable of capturing a single lead ECG over several minutes (Kohno et al. 2017). These devices typically only store data when activated by the patient. To trigger the device the patient presses a button on the device whilst holding it against the chest. The recorded data can be downloaded to the monitoring centre allowing for near real-time monitoring. Whilst event recorders are unassuming with no wires attached to the chest, the lack of constant monitoring can be viewed as a limitation as the initiation of the arrhythmia can provide information about the arrhythmic mechanism (Zimetbaum and Goldman 2010). Capturing brief symptomatic episodes can prove challenging as the device must be placed against the chest. Furthermore, asymptomatic events will not be recorded (Kohno et al. 2017). These devices are of limited value in the evaluation of syncope, as the unconscious individual will be unable to activate the recorder (Ruwald and Zareba 2013).

1.2.2.2 Loop recorders

Loop recorders can either be external or internal. An implantable loop recorder (ILR), also known as an insertable cardiac monitor, is a small device which is implanted subcutaneously to the left of the sternum. For patients who require prolonged monitoring, an ILR is an effective alternative to external monitors. Whilst several devices are available, Medtronic's Reveal LINQ^{TM} is the most widely known and studied (Pürerfellner et al. 2015; Mittal et al. 2016). The latest device is the Reveal LINQ^{TM} which, as shown in Figure 1.6, looks similar to a USB and

is recommended as an option to help detect AF following a cryptogenic stroke, including transient ischaemic attacks (NICE 2020a).
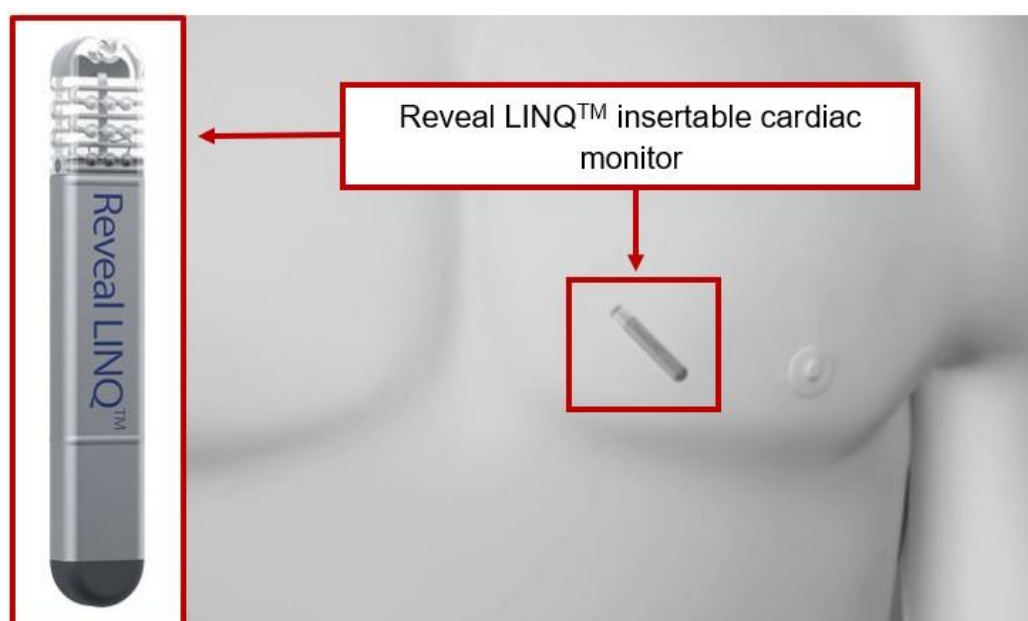
Figure 1.7: Reveal LINQ™ system manufactured by Medtronic. Image shows the anatomical location where the Reveal LINQ™ monitor is subcutaneously inserted. Magnified image of the Reveal LINQ™ is also shown. Image adapted from Medtronic (2020).

Once inserted, the device can detect abnormal heart rhythms for up to 3 years. Recordings can either be triggered by programmable detection software or by the patient using a handheld activator. Data can be downloaded in the pacing department or using the MyCareLink™ monitor which sits at the patient's bedside. Data is downloaded wirelessly before being transmitted to the local monitoring centre (Medtronic 2020). Clinicians are then able to access this information and contact the patient if required. Diagnostic yields are generally improved with the use of ILRs due to their ability to monitor for longer durations. Steinburg and colleagues estimated a yield of 80-90% for palpitations and 15-20% for cryptogenic strokes. NICE (2020) evaluated the cost-effectiveness of the device and concluded that the Reveal LINQ™ is likely to be a cost-effective use of NHS resources, provided that it is used following non-invasive ECG and no other cause for the stroke has been identified. Whilst ILRs provide an unobtrusive way of monitoring patients, the main concern is the invasive nature of the device. The CRYSTAL-AF trial was a randomised prospective study with the aim of evaluating a novel approach to the long-term monitoring for the detection of AF in patients with cryptogenic stroke (Sanna et al. 2014). Patients were either assigned to the standard arrhythmia monitoring or implantation of the Reveal XT. During the study, 2.4% of patients had the ILR removed due to infection or pocket erosion (Sanna et al. 2014). A systematic

review conducted by Solbiati in 2017 found that ILR infections or complications were rare but recognised under-reporting of these events (Gunda et al. 2015; Solbiati et al. 2017).

By comparison, external event loop recorders (ELR) are similar to the Holter monitors as they involve the application of wet electrodes to the chest and a monitor is either carried around the neck or can be attached to the belt (Khalil et al. 2017). This direct attachment of electrodes allows for the continuous monitoring of cardiac activity. The data, however, is only stored to memory when the patient activates the device, or abnormal rhythms are detected automatically. Older devices relied on patient activation and were not equipped with software to detect arrhythmias. In this case, asymptomatic or disabling events were not captured (Kennedy 2013). When 24-hour Holter monitoring, patient-activated ELRs and auto-ELRs were compared by Reiffel et al. (2005), it was determined that the percentage diagnostic yield was greatest for ELRs with auto-triggering (36%) and lowest for Holter monitoring (6.2%) (Reiffel et al. 2005). All ELRs can store several minutes of data in the short-term memory loop. The device is also able to record data immediately before and after an event which is beneficial when evaluating the nature of the suspected arrhythmia (Steinberg et al. 2017). Notable shortcomings of ELRs include a dependence upon patient data transmission (Zimetbaum and Goldman 2010). A study conducted by Gula et al. (2004) reported that test transmission was successfully performed by 84.5% of patients. However, only 58.9% of patients were successful at recording and transmitting a symptomatic event (Gula et al. 2004). In addition, ELRs have limited memory, therefore timely transmission to the relevant monitoring centre is important. To operate and subsequently download data from the devices, a degree of technological ability is required. This may prove problematic when AF is reported to be more common in individuals aged 65 years and older (Zulkifly et al. 2018). Newer ELRs combine features of the Holter monitor and within the UK, the Novacor R. Test is the best-known example (Figure 1.8). The most recent device is the R Test Evolution 4 which is waterproof and capable of extending the monitoring period from 24 to 48 hours through to 32 days (Novacor 2018; Sampson 2019). The advantage of this device over other ELRs is that patients are not required to transmit their data via the telephone.
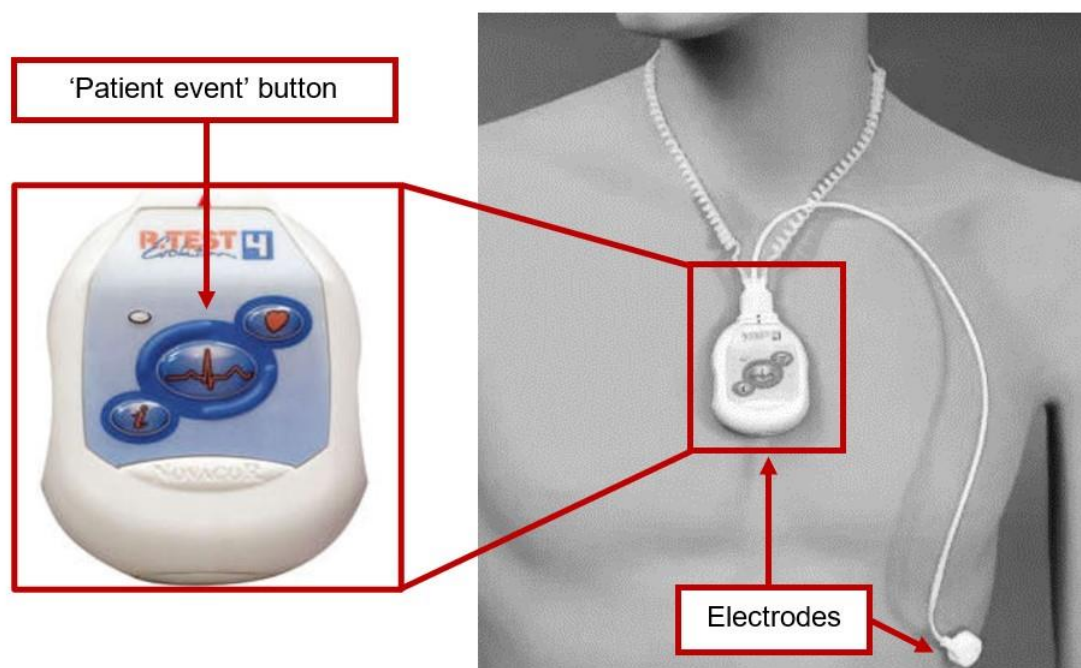
Figure 1.8: R Test Evolution 4 event loop recorder is a reusable device capable of extending the traditional monitoring duration of 24 hours through to 32 days. Image adapted from Novacor (2018).

1.2.3 Patient-led monitoring devices

The aforementioned devices all record data which requires interpretation by a clinician and until recently, AECG monitoring was exclusively conducted by healthcare providers. Recently, consumers are now able to record their own ECG using small devices which communicate with smartphone technology. This technology is affordable, easy to use and provides consumers/patients with the ability to take responsibility for the monitoring of their own health. Several devices are available; however, the Kardia™ Mobile and Apple watch are the most relevant devices within the UK.

1.2.3.1 Kardia™ Mobile

Currently, the most popular of the smartphone ECG technologies is Kardia™ Mobile and its associated Kardia™ app (AliveCor®, USA). This Food and Drug Administration (FDA) approved, handheld device is approximately the size of a credit card and currently costs £99 (AliveCor 2020). To use the device, users place their index and middle fingers on each of the stainless electrode housed within the device as shown in Figure 1.9 (Halcox et al. 2017). The detector pad subsequently sends data using ultrasound to the user's smartphone or tablet.
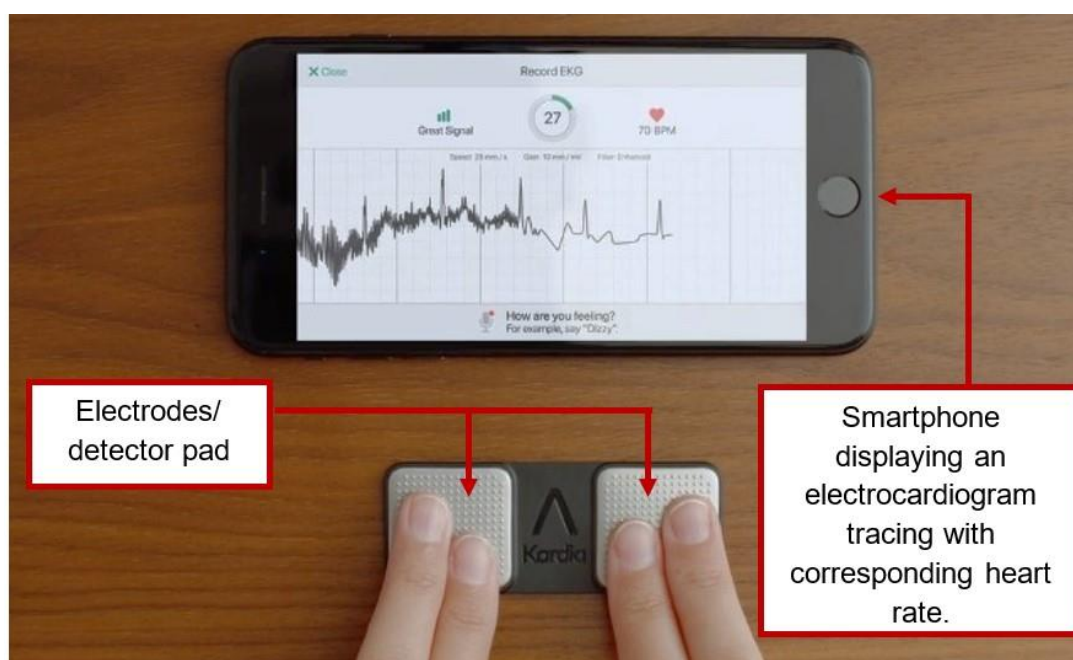
Figure 1.9: Kardia^{TM} Mobile. Image shows a user applying both their index and middle finger on the detector pad. An electrocardiogram tracing is subsequently shown on the compatible smartphone. Image adapted from AliveCor (2020).

The smartphone Kardia^{TM} application is capable of basic arrhythmia recognition and categorises each recording as normal sinus rhythm, probable AF, or unclassified. The device has proven efficacy in clinical trials at identifying AF with a sensitivity and specificity of 96.6% and 94.1% respectively (William et al. 2018; Wegner et al. 2020). It must be noted, however that this was after unclassified results where the device cannot interpret the data was excluded. Whilst this device allows patients to monitor their own ECG, the device is associated with several limitations. Cardiac data are transmitted as sound signals. If the user's smartphone or tablet is too far from the detector pad, or if there is ambient noise, the recording may be unsuccessful. Whilst detection of AF has been proven (Halcox et al. 2017), the detection of atrial flutter has proven problematic and may be misdiagnosed due to regular R-R intervals. As stated previously Kardia^{TM} Mobile records cardiac activity in lead I. P wave amplitude is often low in this lead which can make interpretation difficult. A possible solution would be recording cardiac activity in lead II which provides a clear view of the P wave (Rajakariar et al. 2018). In a study conducted by Rajakariar and colleagues, a modified lead II trace was obtained from patients with known atrial flutter. A lead II ECG was generated using Kardia^{TM} Mobile by holding the panel in the right hand and placing the opposite electrode onto the left leg (AliveCor 2018; Rajakariar et al. 2018). Whilst this repositioning can be hard to achieve good contact with the electrodes and necessitates the removal of clothing, an improvement in the diagnosis of atrial flutter was observed (Rajakariar et al. 2018; Sampson 2019). Therefore, this new position could be used in those patients who are considered high risk.

1.2.3.2   Apple Watch

The Apple Watch Series 6 was released by Apple in September of 2020. Although this device is in its early stages, the watch enables consumers to record their cardiac activity. In terms of design, the watch has an electrode built into the back of the device with another electrode in the small control wheel located on the side of the device, termed the digital crown (Figure 1.10).

Figure 1.10: Apple Watch Series 4. To record cardiac activity user, place their finger on the digital crown as highlighted in the Figure. Image adapted from Sampson (2019).

Similarly, to Kardia™ Mobile, a dedicated app is used to instigate recordings. The watch is capable of monitoring HR, which is the frequency of the heartbeats over time, however this parameter does not provide information about the pattern of beats. The single-lead ECG recorded by the watch provides information about the relative spacing of those beats and uses a similar process of arrhythmia analysis as with Kardia™ Mobile, where traces are categorised as normal, AF or unclassified. In the Apple Heart Study, it was found that 34% of participants who received an arrhythmia notification were later found to have AF (Perez et al. 2019). This study involved Series 1 to 3 of the Apple Watch which relied on optical sensors to detect irregular pulse rates in addition to a proprietary algorithm to identify arrhythmias (Perez et al. 2019). In an internal study conducted by Apple, using 588 subjects, it was demonstrated that the ECG application algorithm classification achieved a 98.3% sensitivity and 99.6% specificity with an unclassified rate of 6% (Apple 2020). By comparison, Seshadri et al. (2020) assessed the accuracy of the Apple Watch Series 4 in the detection of AF in a group of patients who frequently cycle between AF and normal sinus rhythm. In comparison to the 6% reported by Apple, Seshadri and colleagues reported an inconclusive rate of 31% (Apple 2020; Seshadri

et al. 2020). The popularity of Apple products and convenience of the design suggests that this watch will become widely used in the future.

1.3 Data transference as a clinical platform

Advancements in sensor technology, microelectronics and telecommunication have contributed to the development of remote health monitoring systems (Majumder et al. 2017). These wearable and wireless systems have both diagnostic and monitoring capabilities and can collect real time physiological and biochemical data enabling remote patient surveillance (Wang et al. 2018b). Data captured by sensors requires a two-stage communication process (Figure 1.11).
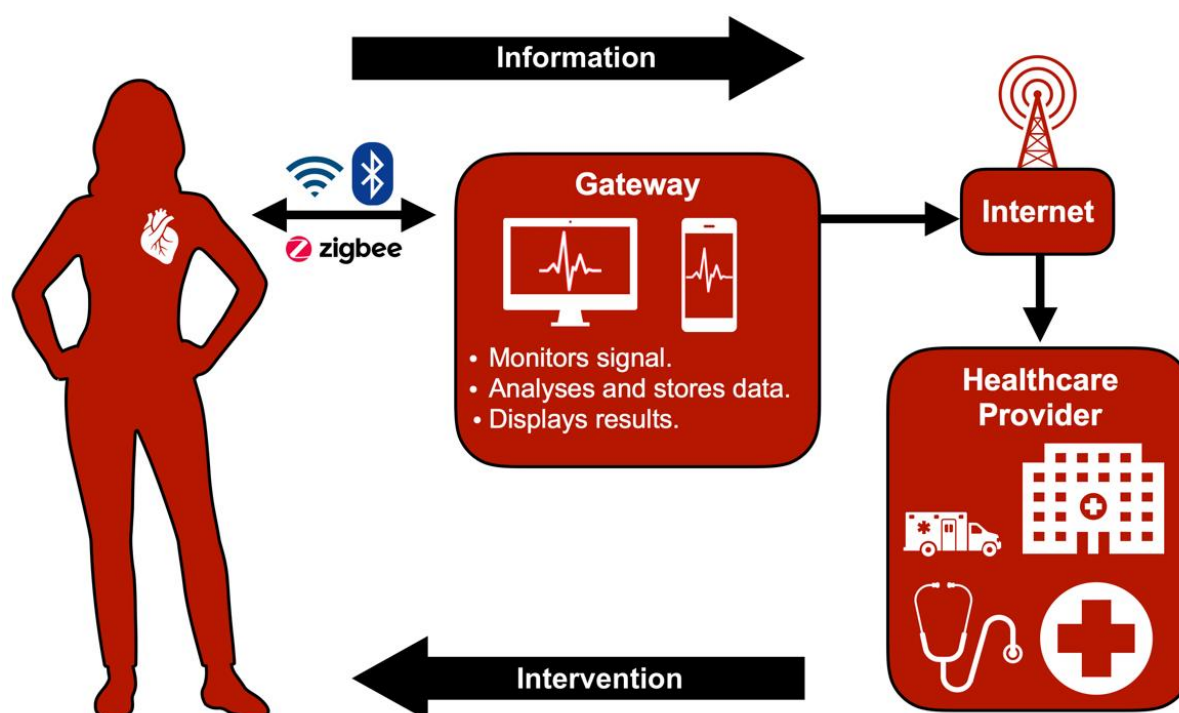
Figure 1.11: Data transference process for clinical purposes. Diagrammatic illustration of the data transference process associated with remote health monitoring systems. Authors own image.

Data is firstly transmitted via short-range communication to a gateway such as a smartphone which is responsible for processing and displaying data (Majumder et al. 2017). Popular methods of short-range communication include Wi-Fi, Bluetooth, and ZigBee. Wi-Fi is considered unsuitable for long-term monitoring systems as a result of its high-power consumption (Lee et al. 2007). Bluetooth and ZigBee are forms of radio-wave technology used for communicating over short distances. They are preferred due to their low cost and low power wireless connectivity which is important for extending battery life (Lee et al. 2007). Following this, data can be transmitted via the internet or cellular communication networks to a server located in a healthcare facility (Majumder et al. 2017). In the case of a medical

emergency, an alert can be relayed to the emergency services using this technology, notifying the need for immediate medical assistance as well as informing family members or caregivers.

The rapid expansion of AECG and remote monitoring technologies provides clinicians with obvious advantages including increased, comprehensive data which is available in real time. It does however, present concerns regarding device accuracy, clinical validity, and data privacy (Majumder et al. 2017; Bayoumy et al. 2021). Despite surging consumer interest in wearable devices and remote monitoring, the technology is in its infancy and large, well-designed clinical trials are required to establish and demonstrate the accuracy and validity of remote wearables in cardiovascular disease prevention, diagnosis, and management.

1.4 Anatomy and physiology of human skin

Skin is the largest organ of the body and accounts for approximately 15% of total adult body weight (Burns and Rook 2010). This complex membrane performs many roles important for sustaining life. In addition to protection, skin is important for thermoregulation, hydration, and aids in cushioning mechanical impacts (Burns and Rook 2010). It is therefore, required to be flexible enough to enable movement, whilst being strong enough to resist damage. Skin can be broadly divided into three layers, with each layer possessing different functions and appendages (Figure 1.12).
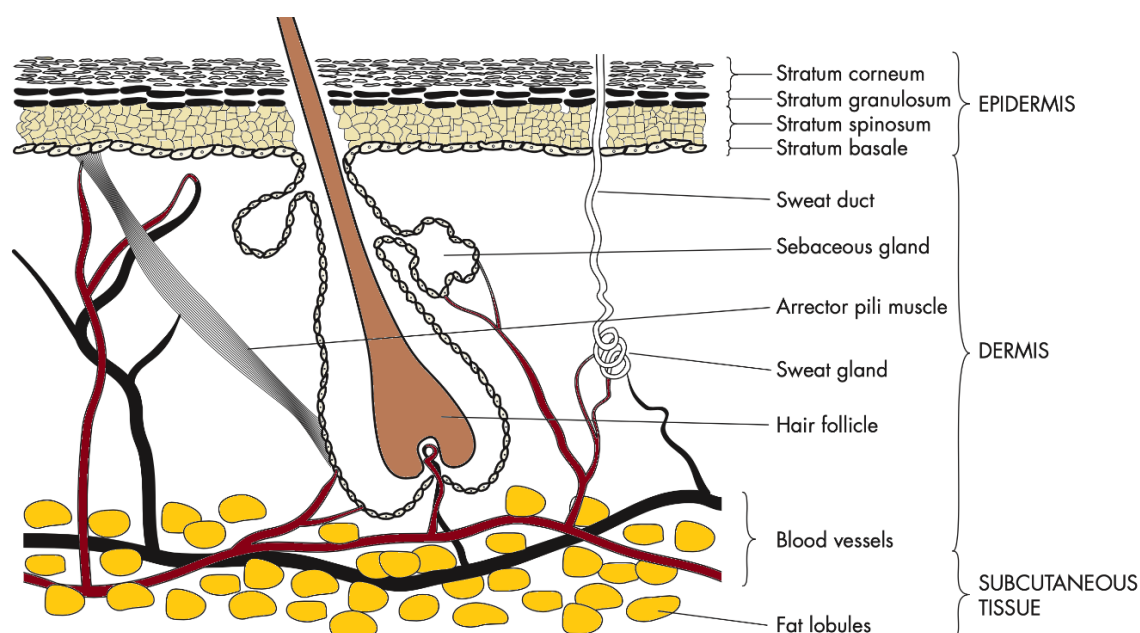
Figure 1.12: Diagrammatic, cross-sectional image of human skin highlighting the three main layers - epidermis, dermis and hypodermis/subcutaneous tissue. Image adapted from Benson and Watkinson (2012).

1.4.1 Epidermis

The epidermis is the outermost layer of skin containing layers of terminally differentiated stratified squamous epithelium (Burns and Rook 2010; Arda et al. 2014). The major cell type, accounting for 95% of the epidermis, is the keratinocyte. Other cell types forming the remaining 5% include the pigment producing melanocytes, Merkel cells which are sensitive to mechanical stimuli and Langerhans cells which have an immune function (Fore 2006). Epidermal tissue remains in a state of constant turnover whereby keratinocytes migrate upwards from the epidermal basement membrane towards the skin's surface where they eventually slough off. The transition of these cells forms four well defined layers, each representing a specific stage of keratinocyte maturation. The stratum corneum (SC) is the most superficial layer of the epidermis and is often described as having a 'brick and mortar' structure (Elias 1983; Elias 1988). Flat, enucleated keratinocytes termed corneocytes are analogous with 'bricks' which are embedded in a 'mortar' of specialised lipids, composed of ceramides, fatty acids and cholesterols (Elias 1983; Elias 1988; Prausnitz and Langer 2008; Bariya et al. 2012). Whilst corneocytes provide protection, the lipid matrix is important for the barrier's hydrophobic nature (Fore 2006).

SC thickness varies according to anatomical location but is maintained by desquamation and cellular replacement from underlying layers (Gambichler et al. 2006). Keratinocyte generation begins in the stratum basale which is a proliferating layer primarily composed of basal keratinocyte stem cells (Gawkrodger and Arden-Jones 2017). Due to constant cellular proliferation, keratinocytes are pushed upwards into the stratum spinosum where they begin to accumulate lipid and protein deposits (Fore 2006). As they transition into the stratum granulosum, keratinocytes flatten, lose their nuclei and release lipids into the intracellular space (Gawkrodger and Arden-Jones 2017). On areas of thick skin such as the palms of the hands and soles of the feet, keratinocytes transition through the stratum lucidum before moving to the SC. The entire maturation process in humans takes approximately 1 month but can be expedited in diseased states (Houben et al. 2007).

1.4.2 Dermis

Subdivided into two regions, papillary and reticular, the dermis is a connective tissue layer that lies beneath the epidermis (Bariya et al. 2012; Arda et al. 2014). In humans, the dermis measures an average of 1.5-3mm in thickness, however this can vary depending upon anatomical location and biological sex, ranging from 0.6mm on the eyelids, to 3mm on the palms of the hands (Arda et al. 2014). Protrusions termed dermal papillae extend upwards into the epidermis aiding the adhesion between layers and providing nourishment to the epidermis due to its avascular nature (Fore 2006).

The dermis is a fibrous tissue which contains two principal types of protein fibre. Collagen and elastin afford the dermis with a mechanical function and provide tensile strength, flexibility, and elasticity (Burns and Rook 2010). The uppermost papillary dermis contains a perpendicular arrangement of thin collagen and elastin fibres (Burns and Rook 2010). The underlying reticular layer, however, forms the principal part of the dermis and comprises of densely packed collagen with elastin fibres that run parallel to the skin's surface (Silver et al. 2003; Anderson et al. 2018). In addition to collagen and elastin, various appendages are present which contribute to the skin's homeostatic function. Eccrine sweat glands and hair follicles lie within the dermis and are responsible for aiding thermoregulation (Romanovsky 2014). The dermis also contains sensory nerves for touch, pressure, pain, and temperature as well as sebaceous glands which release sebum onto the skin's surface maintaining hydration (Fluhr et al. 2003; Burns and Rook 2010).

1.4.3 Hypodermis

The hypodermis, also termed the subcutaneous layer, is a layer of adipose tissue which lies beneath the dermis (Tobin 2006). Primary functions of this innermost layer include insulation, energy reserves and cushioning trauma (Arda et al. 2014). Embedded within this skin layer are larger lymphatic and blood vessels.

1.4.4 Biomechanical properties of human skin

The biomechanical properties of skin are of great importance as they contribute to the skin's health and structural integrity. Human skin is a complex tissue which possesses unique biomechanical properties which are influenced by variety of factors including age, anatomical location, and level of hydration (Brown 1973; Wu et al. 2006; Groves et al. 2013). With respect to the development of transdermal drug delivery and diagnostic systems understanding the skin's mechanical response under an applied load is important for the design and optimisation of these devices.

The mechanical properties of human skin have been extensively studied through uniaxial and biaxial (Annaidh et al. 2012; Kalra et al. 2016), indentation tests (Pailler-Mattei et al. 2008), suction (Jemec et al. 2001; Kalra et al. 2016) and torsion tests (Sanders 1973; Kalra et al. 2016). In addition to these tests, the skin has been imaged using numerous imaging techniques such as optical elastography (Liang and Boppart 2010) and magnetic resonance imaging (An et al. 2017). Human skin is often described as anisotropic, viscoelastic, and non-linear (Brown 1973; Groves et al. 2013). The anisotropic nature of skin was first recognised by Karl Langer in the 19th century and refers to the mechanical behaviour of skin which varies according to direction. Resulting from the skin's viscoelasticity, it undergoes a phenomenon termed pre-conditioning. Under cyclical loads, the relationship between stress and strain

constantly alters until a steady state has been achieved (Liu and Yeung 2008). The dermis is the largest contributor to the skin's overall mechanical properties and allows the skin to endure large deformations. Collagen is the main source of structural support due to its high tensile strength, whilst elastin is responsible for the skin's ability to recoil. The non-linear response of the dermis under an applied load can be divided into three phases, each relating to collagen and elastin (Brown 1973). When the skin is relaxed, collagen fibres are randomly arranged. During the initial loading phase, a large displacement is observed at a relatively low force as fibres re-orientate towards the load. Characterised by increasing stiffness, fibres progressively align themselves directly underneath the load during phase two. Finally, the extension of fibres produces an almost linear third phase where the overall mechanical response becomes dependent upon collagen (Brown 1973).

In addition to the dermis, the 'brick and mortar' structure of the SC results in a stiff mechanical barrier. However, the mechanical response, particularly elasticity, of this layer varies with hydration, humidity, and temperature (Wu et al. 2006). As the skin ages, the network of collagen and elastin degenerates resulting in a decline in biomechanical properties (Cua et al. 1990; Smalls et al. 2006).

1.5 Microneedle array devices

1.5.1 Microneedles and how they function

Microneedles (MN) are minimally invasive devices that consist of single, or multiple micron-sized needles which range in height from approximately 50µm to 1000µm (Mikszta et al. 2002; Gill et al. 2008). These devices are capable of penetrating through the SC and into underlying skin layers, mainly the viable epidermis (VE) (Henry et al. 1998; Davis et al. 2004; Donnelly et al. 2010). Originally conceptualised and patented in the 1970's, MNs were considered a novel approach to transdermal drug delivery (Gerstel and Place 1976). It was not until the late 1990's when advancements in the microfabrication industry made the manufacture of MNs possible (Henry et al. 1998). Henry et al. (1998) realised the first MN device and demonstrated Calcein permeability in excised human skin following MN application. With the growth in engineering capabilities, MNs have now been fabricated in a range of geometries, in a variety of materials, using several fabrication methods (Griss et al. 2002; McAllister et al. 2003; Park et al. 2005; O'Mahony et al. 2016).

1.5.2 Microneedle categories

Regarding drug delivery, MNs are generally classified into four categories (Figure 1.13). Solid MNs are typically fabricated using silicon or metal and can be pressed into the skin and withdrawn. Subsequently, a topical formulation (cream, ointment, or gel) can be applied whereby the therapeutic diffuses through the newly created channels (McAllister et al. 2003;

Wu et al. 2010). These solid MNs can also be coated with a formulation containing an encapsulated therapeutic which, when inserted, allows for drug dissolution within the skin (Gill and Prausnitz 2007). Dissolvable or biodegradable MNs are used for controlled release as they contain a therapeutic embedded within a matrix. Materials used in their fabrication include biodegradable polymers which can be used for sustained release (Park et al. 2005), or water-soluble substances for rapid release (Martin et al. 2012). Similarly, to hypodermic needles, hollow MNs contain individual bores whereby a drug solution can be directly injected into the skin (Wang et al. 2006). MNs have been fabricated using several materials including silicon, stainless steel, glass, and sugar (Martin et al. 2012; O'Mahony et al. 2016). With an understanding of skin anatomy, MNs can be designed to avoid puncturing blood vessels or innervating nerve endings located in underlying skin layers. MN insertion has been reported as effortless, blood free and minimally painful (Kaushik et al. 2001; Haq et al. 2009; Birchall et al. 2011). Haq et al. (2009) determined that MNs caused significantly less pain than a hypodermic needle whilst Kaushik et al. (2001) found no difference in pain caused by 150µm silicon MNs and a MN free silicon wafer. With the numerous options available in terms of MN type, material, and fabrication methods, MNs can be optimised to suit a number of desired applications including the development of minimally invasive sensing and diagnostic systems.
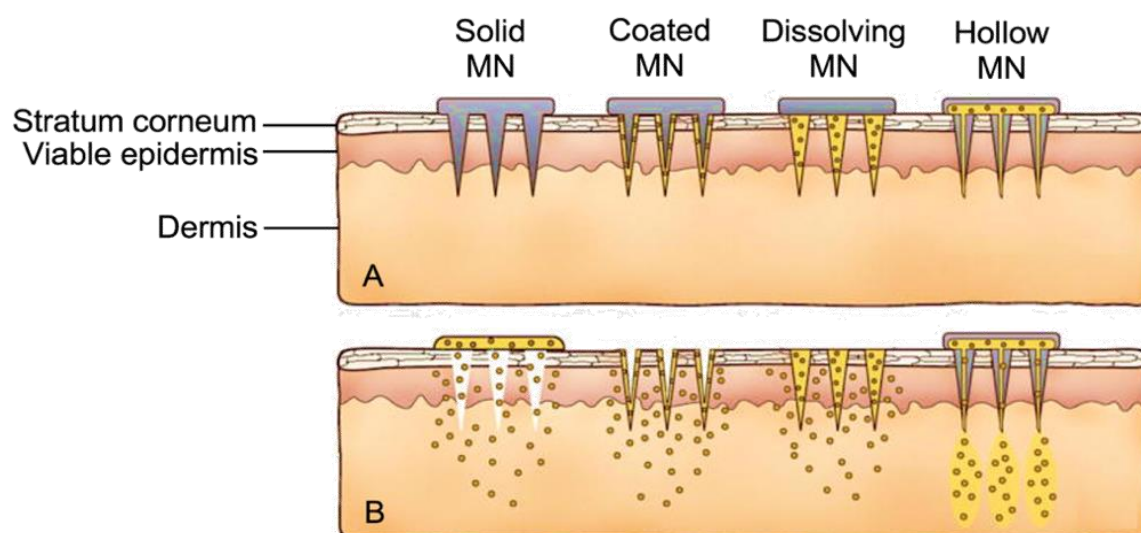
Figure 1.13: Types of microneedle and drug delivery methods to skin. Image displays the four distinct types of microneedle (A) and the methods of drug delivery to the skin (B). Image adapted from Kim et al. (2012).

1.5.3 Applications of microneedles

MNs were initially developed to enhance the penetration and transportation of therapeutics through skin thereby overcoming the limitations of conventional transdermal drug delivery methods. Over the years, MNs have become more versatile, and their applications have expanded beyond their initial use and are now utilised in several fields including cosmetics

(Mohammed et al. 2014), cancer therapy (Bhatnagar et al. 2018), ocular delivery (Singh et al. 2017) and diagnostics (Bollella et al. 2019).

1.5.3.1 Transdermal sensing and diagnostics

Conductive MN 'dry' electrodes (Figure 1.14) also termed, spikes (Griss et al. 2000), microtips (Hsu et al. 2014) and microstructures (Zhou et al. 2017) have been used to detect and record physiological signals including ECG, EEG and EMG when applied to skin (Forvi et al. 2012; O'Mahony et al. 2016; O'Sullivan et al. 2019).
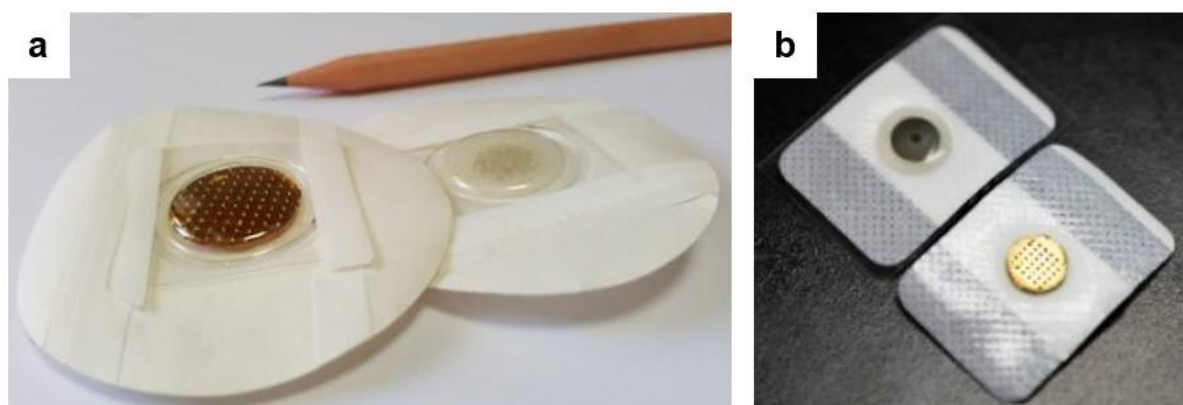
Figure 1.14: Microneedle electrode prototypes alongside wet electrodes. Images adapted from O'Mahony et al. (2016) (**a**) and Chen et al. (2016) (**b**).

'Dry' electrodes do not require an electrolytic gel and are based upon capacitive detection rather than an electrochemical electrode-electrolyte interface (Gruetzmann et al. 2007; O'Mahony et al. 2016). MN electrodes have been manufactured from materials such as silicon or polymers through various techniques including wet-etching (O'Mahony et al. 2016), thermal drawing (Ren et al. 2016) and magnetisation-induced self-assembly (Chen et al. 2016). Following fabrication, non-conductive MNs are coated with a conductive metal layer such as silver/silver chloride (Ag/AgCl) (Griss et al. 2000; Liu et al. 2018) or titanium/gold (Ti/Au) (Chen et al. 2016; Ren et al. 2016). These novel bioelectrodes have attracted increasing amounts of attention for longer term monitoring as MNs can penetrate the electrically insulated SC directly contacting the conductive epidermal layers below (Griss et al. 2000; Griss et al. 2001; Griss et al. 2002). Additionally, they do not require an electrolytic gel or any form of skin preparation. When compared with standard wet electrodes, Griss and colleagues demonstrated a reduction in the electrode-skin-electrode impedance when using Ag/AgCl coated silicon electrodes. Whilst these electrodes could record physiological signals, it was documented that approximately 5% of all dry electrodes used were found to have fractured spikes following removal. Confirmation of skin penetration was not investigated (Griss et al. 2001). A study conducted by Wang et al. (2011) used silicon-based MN electrodes which pierced through the

SC, without stimulating pain receptors in the dermis. The MN electrode's impedance and ability to record EEG signals was investigated alongside a commercially available wet electrode. Despite the absence of skin preparation and the application of an electrolytic gel, MN electrodes resulted in lower impedance values than the wet electrode as well as recording comparative EEG signals to the wet electrodes. Many MN based physiological sensors proposed in the literature are comprised of solid MNs (Griss et al. 2002; Matteucci et al. 2007; Wang et al. 2013; Ren et al. 2016), with some publications focusing on hollow MNs (Yu et al. 2009; Strambini et al. 2015; Ribet et al. 2018). Solid MNs can be considered the simplest form and were used in most of the early research for both drug delivery and sensing (Henry et al. 1998; Griss et al. 2000). For instance, O'Mahony et al. (2013) fabricated solid, silicon based MNs using a potassium hydroxide (KOH) wet etching technique as described by Wilke and Morrissey (2007). These ultrasharp MNs were used by Forvi et al. (2012) to record physiological signals. In this study gold-coated, solid MN electrodes produced comparable performances to wet electrodes under static conditions. In 2016, O'Mahony and colleagues replicated these solid, silicon MNs in polymeric materials and subsequently demonstrated their capability in recording biopotentials, namely ECGs. Alternatively, hollow MNs have also been used to record physiological signals (Matteucci et al. 2007; Yu et al. 2009). For instance, Yu et al. (2009) proposed a novel bioelectrode consisting of hollow MNs containing a reservoir of sodium chloride solution in place of conventional electrolytic gels. This novel electrode, when compared to an electrode consisting of no MNs, resulted in improved ECG signals.

Over the years, the ability of silicon based MNs in successfully puncturing skin, and in recording physiological signals have been demonstrated (Henry et al. 1998; Griss et al. 2000; O'Mahony et al. 2012; Narayanan and Raghavan 2017). The continued use of silicon could be driven by its ability to be shaped with microscopic precision into complex structures. Silicon, however, is brittle (Runyan and Bean 1990; Davis et al. 2004; Forvi et al. 2012; O'Mahony 2014). Whilst several studies have investigated the failure mechanisms of silicon MNs, this fragility is not suitable for longer term monitoring devices as MNs may break during insertion or on movement. Fractured needles could reside within the skin and become a safety and infection risk. Arrays have since been fabricated using a range of materials. For sensing and diagnostics, widely used alternatives to silicon include metals and polymers (Miller et al. 2014; O'Mahony et al. 2016; Rajabi et al. 2016; Ren et al. 2018; O'Sullivan et al. 2019). Ceramics, carbohydrates, and glass have been used to fabricate MNs, however they are largely used for drug delivery applications (Wang et al. 2006; Martin et al. 2012; Cai et al. 2014). Stainless steel was the first metal used in MN production with titanium as an alternative (Verbaan et al. 2007; Niinomi and Nakai 2011; Larrañeta et al. 2016). In the medical field, metals have been used for decades with examples including stainless steel hypodermic needles or titanium

implants. Compared to silicon, these materials have suitable mechanical strength to avoid fracturing during insertion. In addition to their conductivity, metals such as steel, titanium and gold are biocompatible. Biocompatibility is an important safety consideration when developing MN devices. As devices could remain in contact with skin for prolonged periods, they must be able to exist in harmony with surrounding tissue without inducing local or systemic responses in the body.

Whilst this postgraduate research focuses on ECG signal acquisition, MNs have also been utilised in the field of diabetes. Hollow MNs have largely been employed in this area of research to continuously sample the interstitial fluid found within skin to monitor glucose (Nicholas et al. 2018). Traditional glucose monitoring is performed by the patient using capillary blood extracted via finger pricking a number of times a day. As MNs can reach the dermis, MNs can be used to sample and extract dermal fluids which are considered more reflective of systemic levels of key analytes. It is for this reason, that glucose monitoring has been extensively researched and has shown that continuously monitoring glucose improves glycaemic control in type I diabetics (Tamborlane et al. 2008; Mayer-Davis et al. 2017). The first-generation glucose biosensor was proposed by Clark and Lyons. This biosensor adopted an electrochemical approach using the enzyme glucose oxidase. Decreases in the measured oxygen concentration was proportional to the concentration of glucose (Clark and Lyons 1962). Since then, a plethora of glucose sensors with and without MNs have been investigated. In addition to diabetes, monitoring pH (Mirza et al. 2017) and analytes including lactate (Bollella et al. 2019) and glucose (Ribet et al. 2018) could be utilised in other areas such as sports science.

1.5.3.2 Transdermal drug delivery

With the primary focus of this postgraduate research centring around the use of MNs as transdermal sensors, the transdermal drug delivery capability of MNs will not be discussed in detail. However, as MNs were initially developed as a way of improving the transdermal delivery the capability of MNs in delivering therapeutics to the skin has been studied extensively. Therapeutics agents have been administered to either act locally within the skin or for systemic effect once absorbed into the bloodstream.

Over the years, a variety of therapeutics have been delivered to the skin using MNs. including proteins (Li et al. 2009), nanoparticles (Coulman et al. 2009) and small molecule drugs (Sivamani et al. 2005). Insulin represents the most widely investigated biopharmaceutical which is almost entirely delivered via hypodermic injection. Reductions in blood-glucose levels have been reported in human and animal subjects following the application of solid MNs prior to the application of a formulation containing insulin (Martanto

et al. 2004; Wu et al. 2010). Additional biopharmaceuticals including desmopressin (Fukushima et al. 2011) and human growth hormone (Burton et al. 2011) have been delivered via MNs to animal models. Furthermore, the skin contains several immunocompetent cells and therefore, is an attractive target for vaccine delivery. In vivo animal studies have suggested that influenza vaccines delivered using dry coated MNs produce a comparable or superior immune response compared to vaccines administered via the intramuscular route (Pearton et al. 2010; Koutsonanos et al. 2012; Rouphael et al. 2017). In addition to influenza, the human papilloma virus (Corbett et al. 2010) and herpes simplex virus (Chen et al. 2010) amongst others have been delivered to various animal models using coated MNs.

1.5.3.3 Patient compliance and safety of microneedle application

Whilst MNs are accompanied with several advantages, they are associated with mild side effects including localised erythema and skin irritation (Martanto et al. 2004; Nordquist et al. 2007; Gupta et al. 2009). These reactions are usually transient and resolve within a few hours. It is important to remember that whilst MNs can measure between 50 to 1000µm in length, they are needles which can constitute a sharps hazard with the possibility of blood contamination and transmission. Their facile application and pain-free nature may further enhance this risk where accidental puncture could go unnoticed as bleeding has not generally been associated with their use particularly with MNs up to 1mm in length (Martanto et al. 2004; Alarcon et al. 2007; Gill et al. 2008). For MNs greater than 1mm, small droplets of blood at the site of microneedle insertion have been observed (Laurent et al. 2007; Gill et al. 2008). Martin et al. (2017) investigated the ability of MNs to puncture nitrile and latex gloves approximately 100µm in thickness as gloves would be considered appropriate personal protective equipment. Whilst the level of risk of MN penetration is dependent upon several factors, MNs measuring 800µm in length resulted in a punctured glove. It must be noted that clear variations in skin penetration will exist between MN devices and variability between individuals and age will which influence the skin's elasticity. In terms of physiological signal monitoring, standard wet electrodes are associated with some degree of irritation, however the electrode is non-invasive. Utilising a MN-based electrode therefore introduces a degree of risk and minimal invasion. MN lengths could be reduced to improve safety; however, the length of the needles used depend on the application of interest.

A concern regarding the use of MNs in biomedical applications relates to microbial contamination and infection. Microbes may be able to travel through microchannels either through MN insertion into skin or could be transferred from the environment following MN removal (Donnelly et al. 2009). An in vivo study conducted by Li et al. (2010) investigated the flux of a Staphylococcus aureus solution through conduits following the application of 70-80µm

length MNs. It was shown that MN application did not result in increased white cell counts, leukocytes, and neutrophils in blood. Comparatively, the damage following the insertion of 1500µm length MNs enabled the transport of microbes through the skin resulting in the increased presence of immune cells within blood (Li et al. 2010)

The ability of the skin to reseal following MN treatment is important to reduce infection. It has been demonstrated that the length of skin-resealing time relates to MN density, length, and width of the needle base. Gupta et al. (2011) demonstrated that skin sealed 35% quicker when using shorter (500µm) rather than longer (750µm) MNs. In addition, needle density also played an important role in the rate of skin-resealing. Skin resealed approximately six times faster when using an array with 10 MNs as opposed to an array with 50 MNs. Moreover, MNs which were wider were shown to prolong the length of time that the skin takes to reseal (Gupta et al. 2011).

1.5.3.4 Approved microneedle devices

Several products using microneedles have been approved for both medical and cosmetic purposes. The first microneedle-approved product was the Dermaroller®, which is now sold around the world. This cylindrical roller contains solid, metal MNs which measure between 0.2-2.5mm in length. The shorter length MNs are designed for patient use to help improve skin texture, whilst the longer MNs are used by clinicians to treat scars (Afra et al. 2019). In terms of therapeutic delivery, Soluvia® is a pre-filled microinjection system that consists of a hollow MN measuring 1.5mm long. Manufactured by Sanofi Pasteur, Soluvia® is now marketed worldwide to vaccinate against influenza (Levin et al. 2016). A further example is the MicronJet® which is an FDA cleared device consisting of a row of hollow, silicon MNs. The MicronJet® has been used for the intradermal delivery of the influenza vaccine amongst others (Levin et al. 2014). Most recently, Zosano Pharma submitted a new drug application to the FDA for Qtrypta which contains zolmitriptan and would be used for the acute treatment of migraines (Tepper et al. 2019).

1.6 Project rationale

In 2019, CVD accounted for approximately 163,888 deaths in the UK and a third of all deaths globally (Murray et al. 2020; BHF 2021). With growing populations and increased life expectancy these numbers can be expected to rise. In the diagnosis and monitoring of cardiovascular conditions ECGs are an essential element. The use of wet electrodes in the acquisition of cardiac signals have several limitations. Whilst the use of electrolytic gels aid in signal conduction, it has been reported that they dry out. Most wet electrodes have a shelf-life of approximately 2 years if they remain unopened, however this reduces to 30 days once removed from packaging (3M 2021). Whilst partial abrasion of the SC aids in improved contact

between the skin and electrode, the process of skin preparation could be uncomfortable for patients and coupled with this breach in the skin's barrier, application of electrolytic gels could result in irritation. Furthermore, as the skin in is a constant state of turnover, the abraded layer will be replaced over time. These disadvantages, render the use of wet electrodes unsuitable for prolonged monitoring.

Wearable devices can capture real-time information regarding parameters such as temperature, and various physiological signals, therefore providing an overview of a patient's health status over time. Medically, devices which are both wearable and wireless offer advantages including remote monitoring, where patients can be monitored at home rather than in healthcare facilities over a longer period of time. In addition to other novel electrodes and monitoring systems, MNs are a promising alternative to wet electrodes. They painlessly penetrate the SC, contacting underlying epidermal layers negating the need for skin abrasion and gel application. Due to the conductivity of the VE and dermis, there is the potential to improve signal fidelity. Several publications have demonstrated the capability of wearable MN systems in monitoring glucose (Barrett et al., 2015), ECG (Lozano and Stoeber 2021), EEG (Arai et al. 2015) and EMG (Forvi et al. 2012). Whilst functionality is a crucial element in the development of a monitoring system, wearability is of equal importance. Many published MN systems are composed of stiff, non-conformable materials which are plagued by motion artifacts resulting from poor contact between the sensor and skin. Both wearability and functionality aspects of these systems are poorly defined within the literature and require further investigation to improve the success of MN electrodes in longer-term monitoring applications.

This postgraduate research will exploit complementary expertise in human skin model development and assessment of MN performance (Cardiff University), sensing and diagnostic technologies, as well as MN fabrication (Tyndall National Institute) and data management/transfer (SymlConnect Ltd). Through collaborative working, this postgraduate research aims to use ECG signal acquisition to assess and explore the wearability and functionality aspects of MNs for long-term patient monitoring.

1.7 Aims and objectives of the thesis

The overarching aim of this project is to use ECG signal acquisition to assess the functionality and wearability of polymeric MN electrodes for the longer-term monitoring of cardiac patients. The specific thesis objectives are to:

- Characterise the geometry of solid, epoxy 500µm length MNs and assess their insertion performance in piercing established ex vivo human and porcine skin models under

increasing downward application force, changing application method and when compared to alternative microneedle arrays.

- Quantitatively and qualitatively compare the performance of an initial prototype epoxy MN electrode with a commercially available adult ECG monitoring wet electrode when simultaneously recording cardiac signals in a lead II configuration from healthy adult volunteers under resting conditions.

- Develop and optimise a suitable ex vivo laboratory model for simulated ECG whereby a cardiac waveform is generated by a waveform generator and acquired through an adapted ex vivo porcine skin model using different electrode technologies.

- Record simulated cardiac waveforms through the developed laboratory model using different electrode technologies to assess the effects of MN length, application duration and design on electrode performance.

- Compare the performance of an optimised bespoke MN electrode prototype with the initial MN electrode and commercially available adult ECG monitoring wet electrode when simultaneously recording cardiac signals in a lead II configuration from healthy adult volunteers at rest and during activity immediately following electrode application to skin and after 6 hours of wear.

- Develop and administer a preliminary questionnaire to capture volunteer demographics and user perception of sensations, usability, and wearability of the bespoke MN electrode, initial MN electrode and current gold standard wet electrode immediately following electrode application to skin and after 24 hours of wear.

- Provide our collaborating small and medium sized enterprise (SME), SymlConnect Ltd., with real-world ECG data, to develop a robust data transference solution and end-user interface.

CHAPTER 2

CHARACTERISATION OF POLYMERIC MICRONEEDLES

2.1 Introduction

2.1.1 Analytical techniques used to assess microneedle insertion

Within the last decade the use of MN electrodes for physiological signal monitoring has been explored (Ventrelli et al. 2015). The proposed benefit of using MNs for signal monitoring is the ability to painlessly penetrate the SC and directly contact the underlying epidermis thereby reducing the electrode-skin impedance (Forvi et al. 2012). As needle insertion is potentially important for signal acquisition, the ability of MNs used in these electrodes to penetrate the skin must be investigated. Laboratory methods including dyes, electrical impedance and transepidermal water loss (TEWL) are frequently used to confirm disruption of the skin barrier following MN application (Haq et al. 2009; Gomaa et al. 2010; Forvi et al. 2012; Lutton et al. 2015). However, these methods are unable to provide information regarding MN penetration depth. Histology and optical coherence tomography (OCT) have been employed to overcome this challenge and further characterise MN insertion in skin (Coulman et al. 2011; Cheung et al. 2014; Lutton et al. 2015).

2.1.1.1 En face staining methods

Numerous coloured dyes including trypan blue (Gomaa et al. 2010; Kochhar et al. 2013), methylene blue (Kalluri et al. 2011; Moronkeji et al. 2017) and gentian violet (Gill et al. 2008; Arya et al. 2017) have been used to visually confirm MN penetration en face. Breaches in the lipophilic SC following MN application allow dyes to penetrate underlying aqueous regions of the VE and dermis, which surround the microchannel. Park et al. (2005) briefly applied trypan blue to human cadaver skin following the application of polymer microneedles, whilst Birchall et al. (2005) applied methylene blue to MN treated skin in vivo. Gill et al. (2007) randomly

selected three MN insertion sites on each human volunteer and stained with 2% gentian violet to validate MN puncture.

Whilst dyes confirm breaches in the SC, they do not indicate depth of penetration. Furthermore, the SC may not truly be pierced, only indented. Pooling of dye within indentations could result in false positive results. When using dyes, the duration of staining varies within the literature. Durations range from 1 minute to 2 hours for methylene blue (Kalluri et al. 2011; Stahl et al. 2012) and 5 minutes to 1 hour for trypan blue (Gomaa et al. 2010; Kochhar et al. 2013; van der Maaden et al. 2014). If staining durations are too short, noticeable microchannels may not be observed as the dye has not had enough time to stain. Conversely, if the application of the dye is prolonged, more than the microchannel could be stained potentially hindering channel identification. Generally, staining can be used for rapid confirmation of MN penetration, however additional analytical methods should be used to corroborate the results and obtain further microchannel information such as dimensions.

2.1.1.2 Optical coherence tomography (OCT)

OCT is a non-invasive, non-destructive imaging technique that has often been likened to ultrasound. OCT uses infrared laser light to create detailed images of skin by mapping changes in reflected light as a function of depth (Fercher 2010). This imaging technique can provide both quantitative and qualitative analysis of biological tissues and is used in clinical practice in the fields of ophthalmology and dermatology. It can, however, provide real-time information regarding the morphological changes in skin following the application of MNs. In comparison to other imaging techniques such as confocal microscopy, OCT can visualise depths of up to 2mm, which is beneficial in terms of assessing the depth of MN penetration.

Coulman et al. (2011) used OCT to visualise MN penetration in vivo. Using OCT allowed for the analysis of epidermal and dermal disruptions that remained following the removal of MNs and conventional hypodermic needles. Coulman and colleagues demonstrated the capability of this imaging technique in assessing MN insertion and determined that MNs were less invasive than histology previously suggested (Coulman et al. 2011). In addition to skin-related research, OCT has been used to image MN penetration into other tissues including the sclera (Park et al. 2014; Thakur et al. 2014). Moreover, this technique can provide useful information regarding the recovery of skin following MN removal and the dissolution of soluble MNs in-situ (Donnelly et al. 2010b; Pattani et al. 2012; Tsai et al. 2016).

2.1.1.3 Histological sectioning and staining

Histology is routinely used when analysing MN insertion to firstly observe the structure and organisation of skin and secondly, identify the presence of microchannels. Typically, the MN

treated section of skin is excised from the bulk sample and fixed in a suitable media such as neutral buffered formalin (NBF) to preserve tissue components and minimise tissue breakdown (Choi et al. 2006; Lutton et al. 2015). Upon fixing, the tissue is snap frozen using dry ice or liquid nitrogen and subsequently stored at -80°C (Lutton et al. 2015). When required for analysis, the sample is then embedded in a suitable media and sectioned into slices of approximately 6-12μm in thickness using a cryostat. These sections can be analysed further by applying a routine histological stain to obtain a detailed view of the tissue. The sections are typically stained using haematoxylin which is a basic dye that stains the nuclei of cells purple/blue. Sections are subsequently counterstained using eosin which is an acidic dye that stains basic structures such as the cytoplasm pink (Fischer et al. 2008).

The process of histological cryosectioning and staining is associated with several limitations. The technique is laborious and destructive. Excision of the skin using a biopsy punch and mechanical damage exerted during sectioning can generate artifacts as well as altering the sample in terms of tissue hydration and tension. It can prove difficult to identify MN induced microchannels within the skin due to the irregularity of this biological tissue. Moreover, Coulman et al. (2011) recognised that analysing microchannel dimensions using histology can result in the overestimation of measurements.

2.1.1.4 Electrical impedance

Electrical impedance is a non-invasive technique used by several groups to assess MN insertion (Davis et al. 2004; Roxhed et al. 2007; Gupta et al. 2011; Forvi et al. 2012). In this context, and as stated by Lutton et al. (2015), impedance is the phase dependent resistance of the skin to the flow of AC. The electrical resistance of skin is predominantly associated with the SC. Any breach in this electrically insulated layer results in a decrease in impedance, therefore making this technique useful in assessing MN insertion. The process involves an active electrode measuring impedance at the site of MN penetration, whilst a reference electrode is placed within the vicinity to complete the electrical circuit.

Gupta et al. (2011) used electrical impedance spectroscopy to investigate the effects of MN geometry and occlusion on the resealing kinetics of skin in healthy adult human volunteers. Unlike other publications, impedance values were normalised with respect to a corresponding 26G hypodermic needle which acted as positive control. The authors commented that 350μm length MNs failed to penetrate the skin due to insignificant drops in skin impedance, suggesting that this method may not be sensitive enough to detect small changes in impedance. Conversely, Forvi et al. (2012) simultaneously measured skin reaction force and electrical impedance during the application of 300μm length, silicon MNs into ex vivo human skin samples. A decrease in electrical impedance was observed when the MN

array encountered skin and a further decrease was noted when the MN pierced the skin. Whilst Forvi and colleagues demonstrated the ability of these MNs in recording physiological signals, no further method of MN insertion analysis was conducted.

2.1.1.5 Transepidermal water loss (TEWL)

TEWL refers to the amount of water that passively evaporates from the surface of the skin. TEWL monitoring is non-invasive and has been used to characterise the skin's barrier function and provide information regarding the effects of MN insertion (Gomaa et al. 2010; Yan et al. 2010; Kalluri et al. 2011; Liu et al. 2014). In healthy skin, TEWL is proportional to the level of hydration, however disruption within the barrier results in increased water loss from the surface of the skin (Bal et al. 2008; Gomaa et al. 2010). Numerous studies have documented increased TEWL from baseline values following the application of MNs both in vitro and in vivo (Bal et al. 2008; Yan et al. 2010; Kalluri et al. 2011; Liu et al. 2014). Gomaa et al. (2010) monitored TEWL to observe changes in the barrier function of human skin following the insertion of MN arrays. The authors noted a correlation between the number of stained microchannels and measured TEWL values 1 hour post MN application. The authors concluded that TEWL values loosely corresponded to the number of microchannels produced following the application of MN arrays.

TEWL is not without its limitations. Whilst TEWL provides information about MN puncture, the technique provides no information regarding microchannel dimensions. It is also well recognised that TEWL values vary between research laboratories (Kottner et al. 2013; Liu et al. 2014). This may be due to differences between experimental protocols, skin samples and equipment used. Additionally, TEWL studies are highly sensitive to the hydration status of skin and therefore with changing atmospheric conditions such as temperature and humidity TEWL values will vary.

2.1.2 Aims and objectives of the chapter

This chapter addressed the aim of characterising the geometry and insertion performance of solid, epoxy MN arrays prior to their fabrication into electrodes. The objectives were to:

- Visualise and characterise the geometry of solid, epoxy MNs using scanning electron microscopy and stereomicroscopy.
- Assess the suitability of ex vivo porcine skin as an alternative to ex vivo human skin using OCT imaging and histology.
- Compare the penetration efficiency of solid, epoxy MNs with alternative MNs that have been manufactured with different geometries and using different materials when manually inserted into ex vivo human and porcine skin models.
- Investigate how application force effects the penetration of solid, epoxy MNs when inserted into ex vivo human and porcine skin.
- Assess how application technique effects the penetration of solid, epoxy MNs when inserted into ex vivo human and porcine skin.

2.2 Materials

Details of equipment and reagents used in the studies described below are listed in the equipment and reagents tables. Data processing was conducted using Microsoft Excel version 16.46 (Microsoft Corporation, USA) and MATLAB 2018a (The MathWorks Inc., Natick, MA). Image processing was conducted using ImageJ software (NIH, USA) and Microsoft PowerPoint version 16.37 (Microsoft Corporation, USA). Scanning electron micrographs were captured using microscope control software (FEI, USA).

2.3 Methods

2.3.1 Epoxy microneedle fabrication

Epoxy MNs were fabricated and supplied by collaborators at Tyndall National Institute, Cork, Ireland. Silicon MN arrays were initially fabricated using a KOH wet-etching technique as described by Wilke and Morrissey 2007. To summarise, standard photolithography tools were used to pattern square oxide/nitride masks on boron doped, <100> mono-crystalline silicon wafers. A need shape was formed when this patterned silicon wafer was etched in a 29% w/v KOH solution. The subsequent MN measured 500µm in length and was comprised of eight {2 6 3} planes, a base of {2 1 2} planes and an aspect ratio of 3:2. As stated by O'Mahony et al. (2016), to reproduce these silicon MNs in polymeric materials, polydimethylsiloxane (PDMS) molds of a master silicon template were fabricated. A 10:1 ratio of elastomer to curing agent was used mixed, degassed and poured over the MN master template. The elastomer was cured at 100˚C for 60 seconds and peeled from the master once cool. Polymeric MN wafers were fabricated by spreading a fixed mass of biocompatible epoxy over PDMS molds. Molds were subsequently degassed on a vacuum table at room temperature, overnight. Following this, the epoxy was cured in an oven at 90˚C for 1 hour. A schematic of this process is shown in Figure 2.1. Once fabricated, wafers were packaged and dispatched to Cardiff School of Pharmacy and Pharmaceutical Sciences.
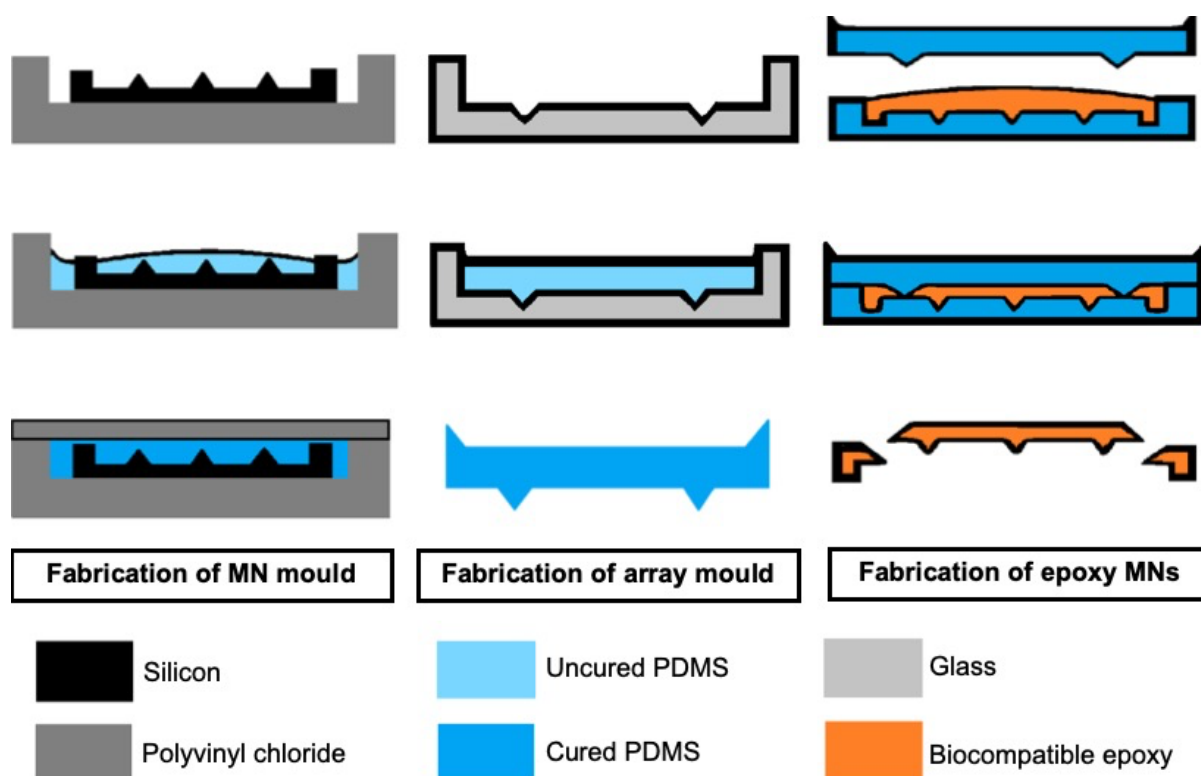
Figure 2.1: Diagrammatic representation demonstrating the steps required to fabricate epoxy microneedle arrays using a silicon master template. Image adapted from O'Mahony et al. (2016).

2.3.2 Imaging of epoxy microneedles

2.3.2.1 Stereomicroscopy

Solid, uncoated epoxy MN arrays used in this thesis were imaged using stereomicroscopy both before and after insertion into skin explants. Digital images were captured using an AmScope stereomicroscope and Digital Eyecam Plus. Images were processed using the software program ImageJ to assess the morphology of MNs.

2.3.2.2 Scanning electron microscopy

Scanning electron microscopy (SEM) is an imaging technique that scans a focused beam of electrons over the surface of a prepared sample to produce highly magnified images. The ease of use and analytical capabilities of SEM make it a useful technique to examine the morphology and dimensions of MNs. For SEM observations, a circular adhesive carbon tab was placed onto an aluminium specimen stub measuring 25mm in diameter. An epoxy MN array was mounted on to the stub and secured into place. The mounted sample was placed within a sputter coater under a low-pressure (0.04 torr) argon atmosphere to remove residual substances. MN arrays were coated with a 20-30nm thick layer of 10% palladium and 90% gold to improve surface conductivity and increase the generation of secondary electrons, which improves the signal to noise ratio (SNR). MN arrays before and after insertion into ex

vivo human and porcine skin explants were observed in an environmental scanning electron microscope operating at 10kV. Images were captured using a microscope control software and dimensions (Figure 2.2) were measured using ImageJ.
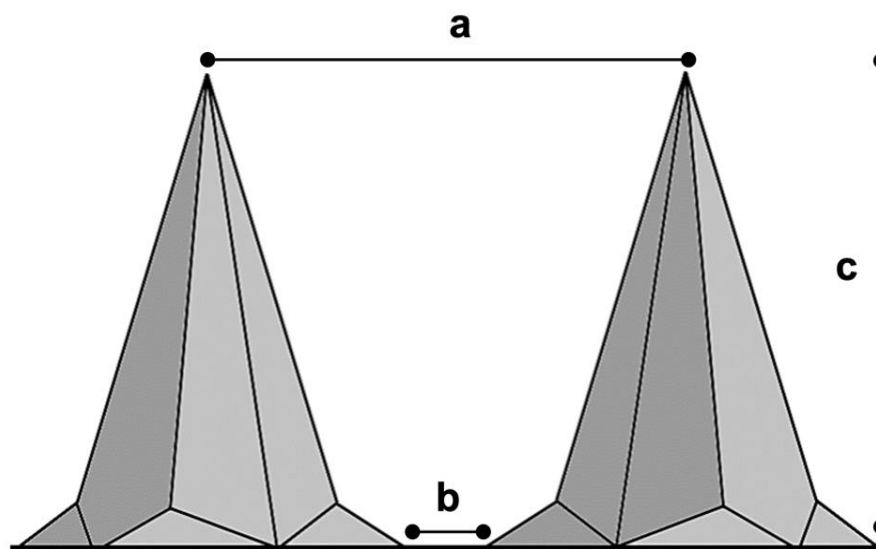
Figure 2.2: Microneedle parameters using scanning electron microscopy. Dimensions measured include tip interspacing (**a**), base interspacing (**b**) and length (**c**). Authors own image.

2.3.3 Preparation of skin explants

2.3.3.1 Excised human skin

Human skin samples were obtained from patients undergoing mastectomy or breast reduction surgery with informed consent and ethical committee approval (South-East Wales Ethics Committee Ref 08/WSR03/55). Following surgery, excised skin was transported to Cardiff School of Pharmacy and Pharmaceutical Sciences at approximately 4°C in Dulbecco's Modified Eagle's Medium supplemented with 1% penicillin/streptomycin (100IU/mL), as described by Ng et al. (2009). Samples used in these studies were frozen upon arrival and defrosted prior to use. In a laminar flow hood, located in a containment II laboratory, the defrosted sample was placed on a piece of foil covered cork with dermis/subcutaneous fat facing upwards. Subcutaneous fat was separated from the dermis using blunt dissection to yield full thickness skin (Figure 2.3a). Skin was stretched and pinned to two layers of compressed cork (Figure 2.3b).
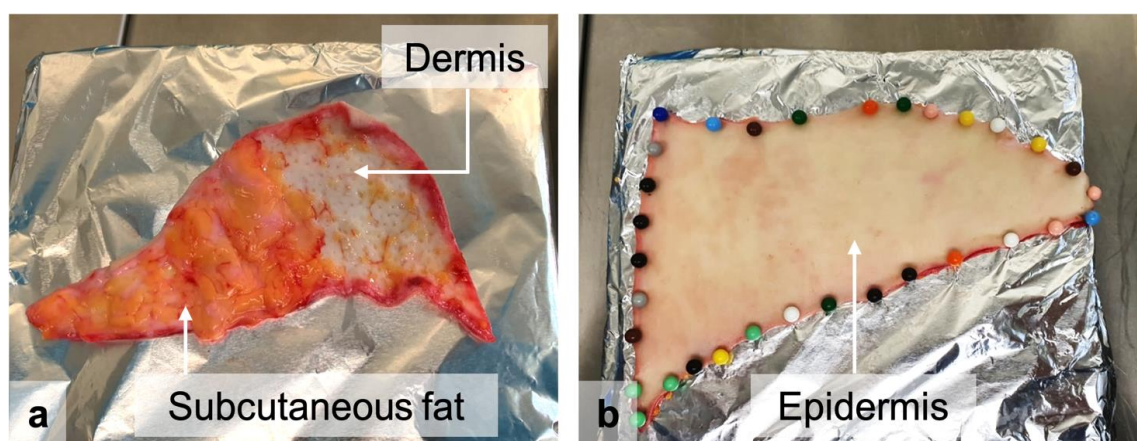
Figure 2.3: Ex vivo human skin preparation. Defrosted ex vivo human breast skin from a 59-year-old female donor. The left side of the image shows an area subjected to blunt dissection i.e., subcutaneous fat removal from the dermis (**a**). Excised human breast skin tensioned, using pins, to two layers of compressed cork covered in a layer of foil (**b**). Authors own image.

2.3.3.2 Excised porcine skin

Porcine ears (not steam cleaned) shown in Figure 2.4a were obtained from NS James Butchers of Raglan and transported to Cardiff School of Pharmacy and Pharmaceutical Sciences. Upon arrival, samples were either used immediately or individually wrapped in foil and frozen at -20°C for use later. Once defrosted, the ear was gently washed with lukewarm tap water to remove residue from the tissue. The ear was subsequently placed on a layer of compressed cork covered in two layers of foil and patted dry. Using a scalpel, the skin was separated from the cartilage on the dorsal side of the ear using blunt dissection. The full thickness skin explant was placed on a new layer of foil (Figure 2.4b) and hair was removed from the surface of the skin using electric clippers. The skin was stretched and pinned to two layers of compressed cork (Figure 2.4c).
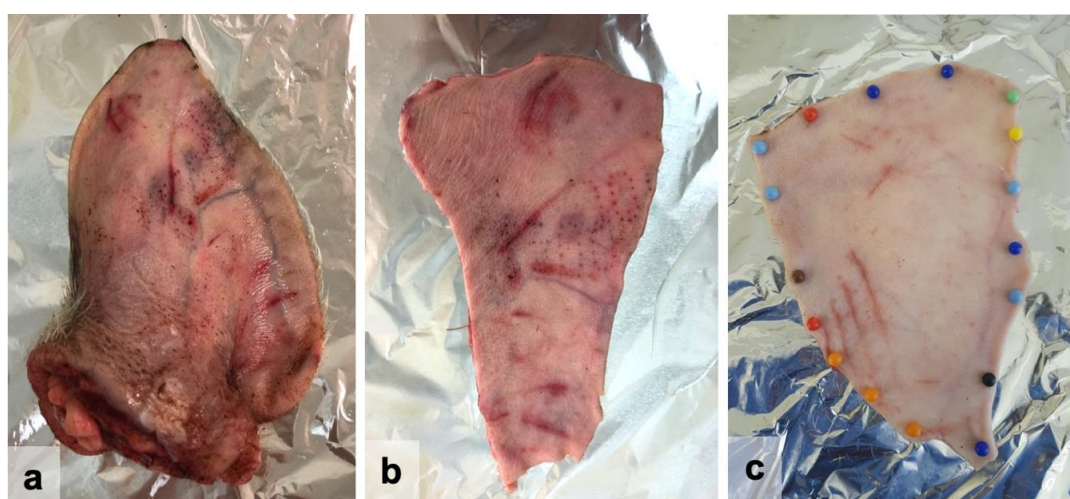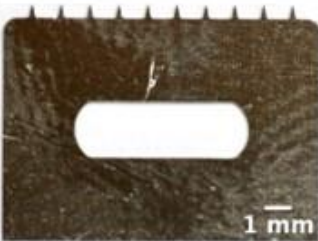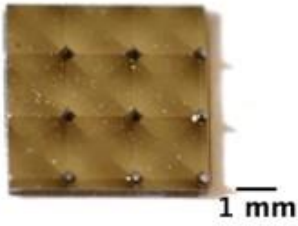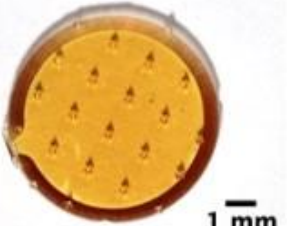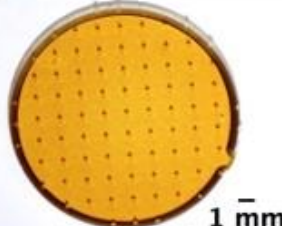
Figure 2.4: Ex vivo porcine skin preparation. Defrosted, non-steamed and intact porcine ear on a layer of foil after gently washing with lukewarm tap water **(a)**. Full thickness porcine skin separated from the cartilage on the dorsal side of the ear prior to hair removal **(b)**. Porcine skin following hair removal and pinned to two layers of compressed cork covered in a layer of foil (**c**). Authors own images.

2.3.4 Microneedle insertion into skin explants

2.3.4.1 Effect of changing parameters on microneedle penetration

To assess the effects of changing MN parameters on penetration, four different MN arrays were manually pressed into excised skin specimens by the operator (force not measured) and held in place for 60 seconds. MNs used in this study (Table 2.1) measured approximately 500µm in length but varied in geometry, composition and the number of needles per array.

Table 2.1: Table to compare the four types of microneedles manually inserted into ex vivo human and porcine skin. Microneedle arrays included solid, epoxy, microneedle arrays measuring 18mm and 9mm in diameter, solid, silicon, microneedles and solid, steel microneedles. All microneedles measured 500µm in length. Authors own images.

Microneedle parameter				
Material	Needle length	No of needles per array	Composition	Image
Steel	500µm	10	In plane	1 mm
Silicon	500µm	9	Out of plane	1 mm
Epoxy (9mm)	500µm	22	Out of plane	1 mm
Epoxy (18mm)	500µm	85	Out of plane	1 mm

For this study, two epoxy MN arrays measuring 18mm and 9mm were first inserted. The second MN array was fabricated from silicon using a KOH wet-etching technique as described by Wilke and Morrissey (2007). The final type of MN was manufactured from medical grade stainless steel by wire electrical discharge machining and were ready-electropolished as described by Arikat (2019).

2.3.4.2 Effect of downward application force on microneedle penetration

To assess the effect of increasing the downward application force on the penetration of epoxy MNs, arrays measuring 18mm in diameter were affixed to an FH100 handheld digital force gauge which measured application loads with an accuracy of 0.5% and resolution of 0.05N. MN arrays were subsequently pressed into the prepared skin explants at 5N, 10N and 15N by the operator. Arrays were held in placed for 60 seconds. Force-time data was recorded using AFH-FAST data transfer software to allow the operator to control and assess application force. The average application forces over the array and individual MNs were calculated once the target force was reached.

2.3.4.3 Effect of application method on microneedle penetration

To assess the effect of changing application methods on MN penetration, three different techniques were used. Firstly, epoxy MN arrays measuring 18mm in diameter were pressed into skin explants using a digital force gauge until a target force of 15N was achieved. A second method used manual insertion of a MN array by the operator at an approximate force of 15N followed by gentle agitation for 60 seconds. A final MN, attached to a digital force gauge, was manually inserted at a greater velocity i.e., impact insertion by quickly pressing down on the skin (although not accurately measured) until a target force of 15N was achieved. The force-time data software was used as an approximate guide of velocity.

2.3.5 Analysis of microneedle insertion into skin explants

2.3.5.1 Optical coherence tomography (OCT)

OCT is a non-invasive imaging system which gathers real-time data as a series of images in the x-y plane and can produce 2D and 3D images for analysis. In this study, a multi-beam swept-source frequency domain VivoSight^{TM} OCT with a resolution of 4.5µm/pixel was used to image skin explants following MN application. Prior to insertion, the area of skin selected for MN treatment was visually inspected and imaged using a hand-held probe connected to the OCT system. The orientation of the sample and probe was marked on the skin to ensure the same area was imaged following MN application. Scans containing 500 frames were acquired using a scan area of 6x2mm (width x length). Image depth varied between 1-2mm,

depending upon the tissue. Following acquisition, frames were further analysed using ImageJ to identify the presence of, and measure channel width and length.

2.3.5.2 Histological analysis of microneedle insertion

Following imaging with OCT, 1mL of 2%w/v methylene blue dye was applied to the test site to stain for the presence of microchannels. After 10 minutes, excess dye was removed from the skin's surface using ethanol. The number of visible microchannels were counted, and skin puncture was calculated as a percentage of the total number of MNs on the applied array. Biopsies of MN treated skin were subsequently taken using an 8mm disposable biopsy punch. Each biopsy was immersed in 20mL of 10% NBF and stored at 4°C to fix. Following 24 hours, NBF was removed, and each biopsy was immersed in phosphate buffered saline (PBS) for 90 minutes. The fixed skin biopsies were then immersed in optimal cutting temperature compound at room temperature and subsequently snap frozen using dry ice. Sections, measuring 10µm in thickness, were obtained using a cryostat. Skin sections were collected on adhesive microscope slides and stored at -80°C until required for analysis. Selected slides were immersed in PBS for 5 minutes to remove the optimal cutting temperature compound. Sections were subsequently stained with filtered Harris' Haematoxylin for 3 to 4 minutes before rinsing with deionised water for 1 minute to remove any unbound haematoxylin. Sections were decolourised using 1%v/v acid alcohol (1%v/v hydrochloric acid in 70%v/v ethanol/deionised water) followed by immersion in deionised water for 1 minute. Sections were then 'blued' for 1 minute using Scott's tap water substitute which has an alkaline pH and changes the haematoxylin-stained nuclei from a reddish colour to blue. The sections were then dipped in the cytoplasmic counterstain Eosin Y and immediately rinsed using deionised water until the water ran clear. The staining process is summarised in Table 2.2.

Table 2.2: Haematoxylin and Eosin staining method for 10µm sections of human and porcine skin explants.

Step	Station	Reagent	Time (mins:sec)	Time critical
1	Compound removal	PBS	2:30	No
2	Compound removal	PBS	2:30	No
3	Stain	Filtered Haematoxylin	3:00 – 4:00	Yes
4	Stain	Filtered Haematoxylin	3:00 – 4:00	Yes
5	Wash	Deionised water	1:00	No
6	Regression	1% acid/alcohol	1 dip	Yes
7	Wash	Deionised water	1:00	No
8	Blue	Scott's tap water	1:00	No
9	Stain	0.5% Eosin Y	1 dip	Yes
10	Wash	Deionised water	Until water runs clear	Yes

2.4 Results

2.4.1 Geometry of epoxy microneedles prior to insertion

A selection of stereomicroscope and SEM images of epoxy MNs prior to insertion are shown in Figure 2.5.
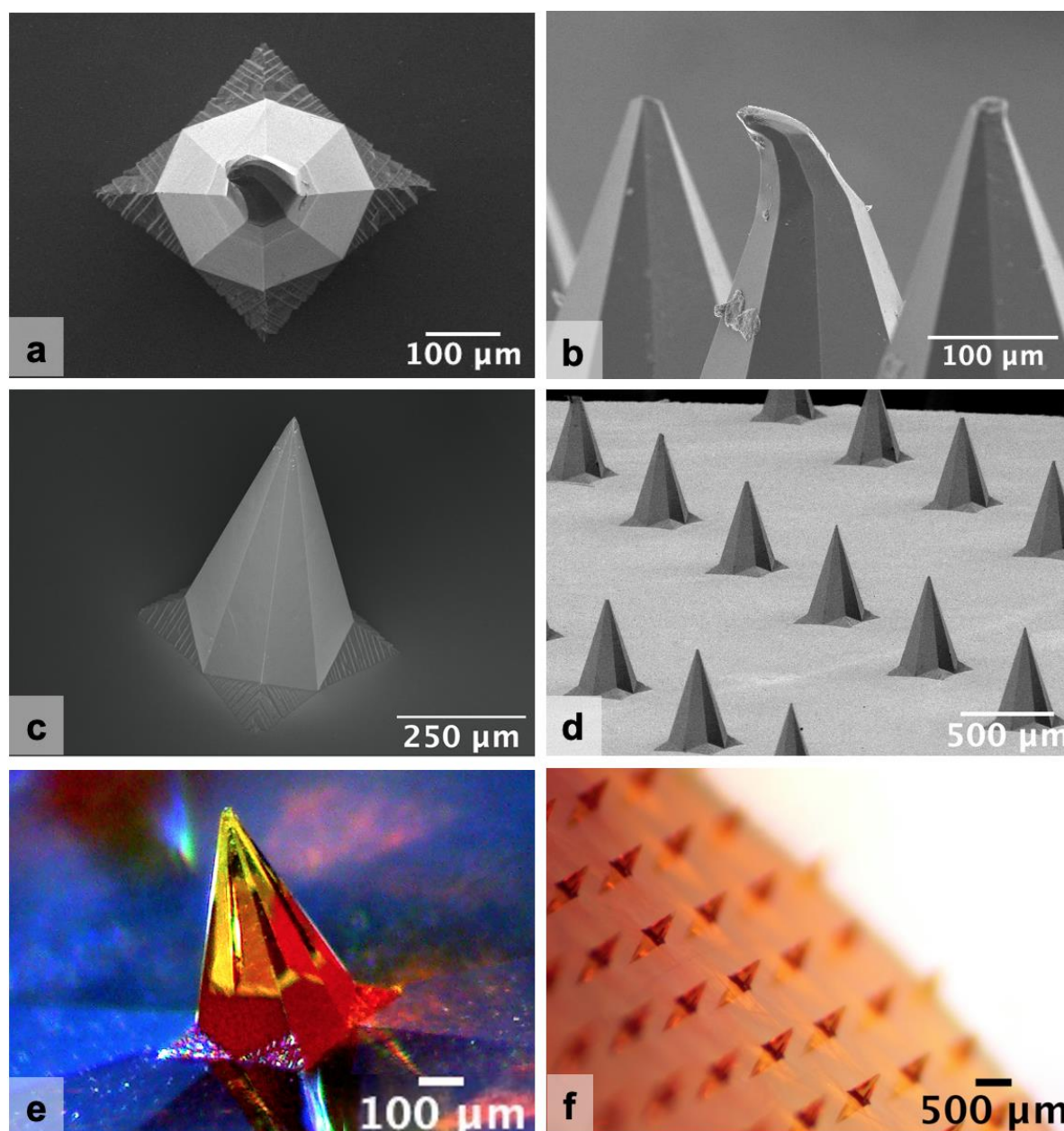
Figure 2.5: Stereomicroscope images and scanning electron micrographs of 500µm epoxy microneedles in an array measuring 18mm in diameter. SEM images of microneedles subjected to damage at 250x magnification/working distance of 13.7mm **(a)** and 500x magnification/working distance of 25.8mm **(b)**. Scanning electron micrographs of undamaged microneedles at 100x magnification and working distance of 9.9mm **(c)** and 100x magnification and working distance of 80.21mm **(d)**. Stereomicroscope images of a single microneedle **(e)** and microneedle array **(f)** prior to insertion.

Each individual out of plane MN comprised of eight smooth planes to form a pyramidal structure. Imaging revealed that MNs from the first batch of wafers were damaged. MN tip diameter ranged from 21.5µm to 64.4µm. As shown by Figure 2.5a-b, the tips of some MNs were bent. Following improved handling and packaging procedures, subsequent wafers were not subject to the same defects.

Using SEM images and the software programme Fiji, quantitative values for parameters known to affect MN insertion were calculated (Table 2.3). In general, needle length varied across the array however the mean MN length measured 471µm ±14.51. Tip and base interspacing remained relatively consistent at 1.71mm ±0.06 and 1.20mm ±0.04 respectively. With each array measuring 18mm in diameter, the average number of MN per array was 85 ±1.

Table 2.3: Summary of the physical features of uncoated, solid, epoxy microneedle arrays prior to insertion into skin explants. Data presented as the mean ±SD (*n=10*).

Microneedle parameter	Diameter of microneedle array	
	18mm	**9mm**
Number of microneedles per array	85 ±1	22 ±3
Microneedle length (µm)	471 ±14.51	476 ±24.26
Tip interspacing (mm)	1.71 ±0.06	1.64 ±0.01
Base interspacing (mm)	1.20 ±0.04	1.15 ±0.02

2.4.2 Ex vivo skin models used for transdermal testing

To provide reference values for the structure of ex vivo human and porcine skin, OCT was used to capture images of intact samples. Both skin types were treated in a similar manner. For storage, both human and porcine skin were frozen and stored at -20°C. Samples were allowed to thaw prior to use. During preparation notable differences were observed. Compared to human skin, which was surgically excised from the breast, porcine skin was manually removed from the dorsal side of a non-steam cleaned ear. Due to the differences in anatomical location, ex vivo human breast skin required the removal of subcutaneous fat, whilst this was not required for the porcine ear. Following preparation, cross-section images demonstrating the structure of ex vivo human and porcine skin were captured and are shown in Figure 2.6.
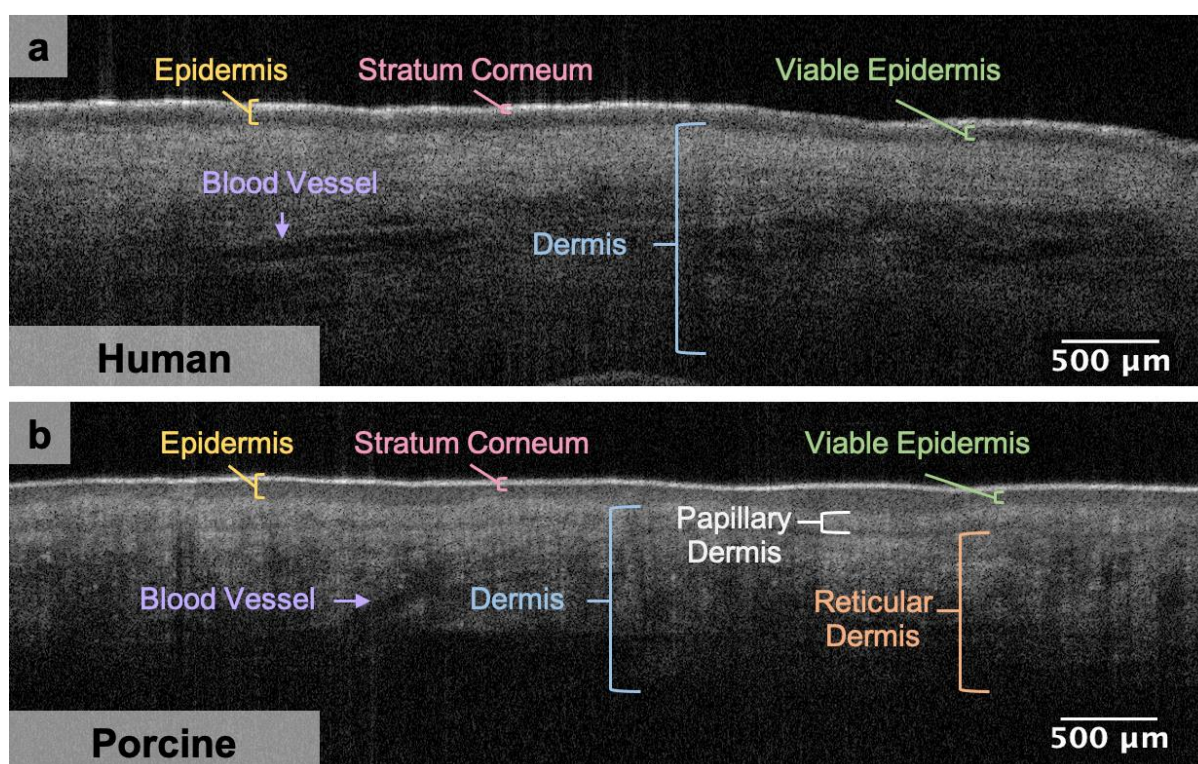
Figure 2.6: Cross-sectional image comparing the structure of excised human (**a**) and porcine (**b**) skin. Scans contained 500 frames and were acquired using a scan area of 6x2mm (width x length). Images were analysed using Fiji. Sub-surface anatomical features within skin are highlighted within the Figure.

Before analysing MN penetration, it is important to recognise the morphology of untreated excised human and porcine skin. For both skin types the epidermis consisted of a well-defined, grey line which corresponded to the SC. A slightly darker section below corresponded to the VE. In human skin (Figure 2.6a), the dermis was not as well defined by the image. The two dermal regions, however, were identifiable in ex vivo porcine skin. The uppermost papillary dermis and the underlying reticular dermis are shown in Figure 2.6b. Using Fiji, the thickness of the SC and epidermis in both skin types were measured and are shown in Table 2.4. Mean epidermal thickness in human breast skin and from the dorsal side of a pig ear were 96µm ± 13.58 and 134µm ± 18.77 respectively. SC thickness for human and porcine skin were comparable, measuring 28µm ± 3.64 and 24µm ± 3.90.

Table 2.4: Epidermal measurements comparing the thickness of the stratum corneum and full epidermis between ex vivo human (**a**) and porcine (**b**) skin. Data presented as the mean ±SD (*n=6*).

Thickness (µm)	Type of skin explant	
	Human	Porcine
Stratum corneum	28 ± 3.64	24 ± 3.90
Total epidermis	96 ± 13.58	134 ± 18.77

Following OCT imaging, biopsies were taken from each skin type and further analysed histologically. Using a cryotome, 10µm skin sections were generated and subsequently stained with haematoxylin and eosin (H&E). As shown by Figure 2.7 haematoxylin staining can be observed in both skin types, predominantly within the viable epidermis. As the SC consists of anucleated cells no haematoxylin staining was observed. Other structures appeared to take on different shades and combinations of these colours. As the dermis predominantly consists of two major protein fibres, collagen and elastin, most of the cytoplasm in both skin types was rendered pink.
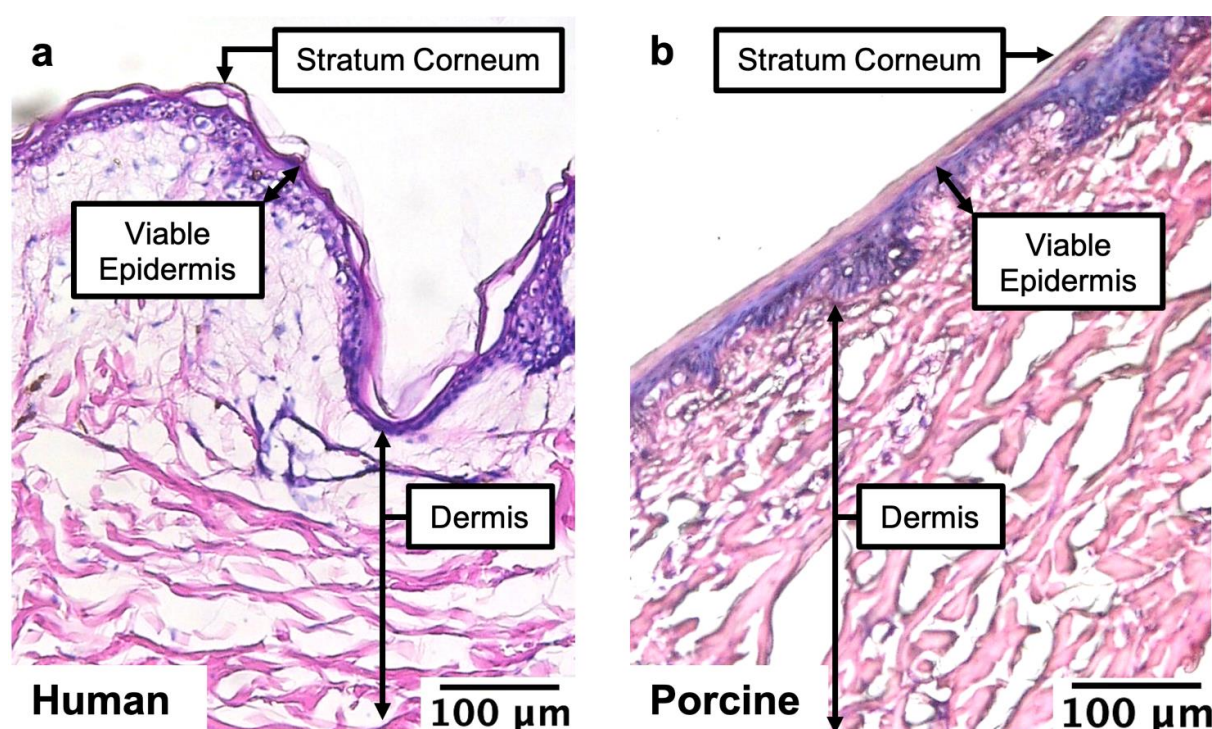
Figure 2.7: Excised human (**a**) and porcine (**b**) skin stained with haematoxylin and eosin. Sections, measuring 10µm in thickness, were generated using a Cryotome FSE. Sections were subsequently stained with Harris' Haematoxylin and counterstained with Eosin Y.

2.4.3 Effect of changing microneedle parameters on penetration

In total, four different MN arrays were applied to ex vivo human and porcine skin. Steel arrays contained ten MNs that were each designed to be 500µm ±50 in length and 200µm in width (Arikat 2019). Silicon arrays contained a maximum of nine MNs per array and were fabricated to measure approximately 500µm in length (O'Mahony 2014). Polymeric MN arrays measuring 18mm in diameter contained an average of 85 ±1, whilst 9mm arrays contained 22 ±3. Following MN application to skin specimens' methylene blue was applied to stain for microchannels. The staining results for each MN type in both skin types is shown in Figure 2.8. As shown in the images, the use of ethanol on porcine skin did not remove methylene

blue as effectively as human skin and left a non-specific background stain. Despite this, each MN array appeared to pierce both skin types due to the presence of identifiable blue dots.
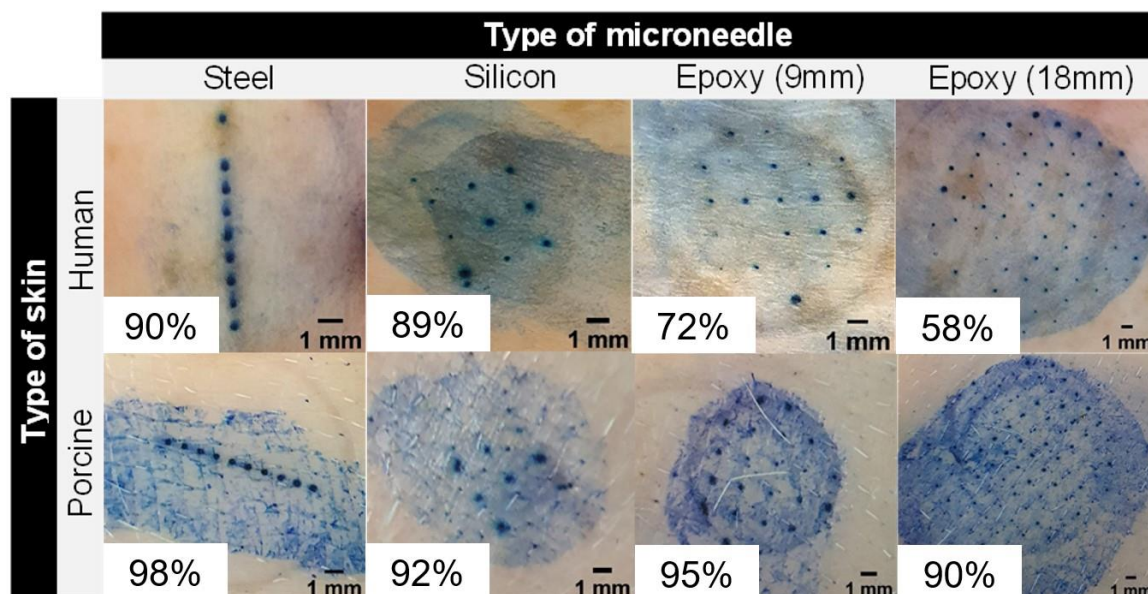
Figure 2.8: Methylene blue staining of skin following the manual application of four different microneedle arrays. En-face images of excised human and porcine skin treated with uncoated, solid, 500µm steel, silicon and epoxy microneedle arrays. Epoxy microneedle arrays measuring 9mm and 18mm in diameter were included. Skin was stained with 2%w/v methylene blue solution for ten minutes following array removal. Breast skin from two female donors aged 83 and 60 years old. Mean percentage puncture efficiency is shown in the bottom left of each image (*n=6*).

Mean puncture efficiency was determined by identifying the number of visually identifiable channels following staining and comparing them to the number of MNs per array. This measure was used to determine the number of needles which pierced the skin for each type of MN in each skin type. Mean puncture efficiency results are shown in Figure 2.9. Steel MNs resulted in the highest puncture efficiency in human and porcine skin whilst 18mm epoxy MNs resulted in the lowest puncture efficiency overall. By contrast, 9mm arrays, which were the same shape and length epoxy MNs, resulted in a greater puncture efficiency of 72% in human and 95% in porcine skin. Arrays consisting of silicon MNs, which were the same shape and length as the epoxy MNs, were comparable in terms of puncture efficiency in both skin types. As shown in Figure 2.9, 100% penetration was not observed, however puncture efficiency appeared less variable when arrays were inserted into porcine skin than human skin.
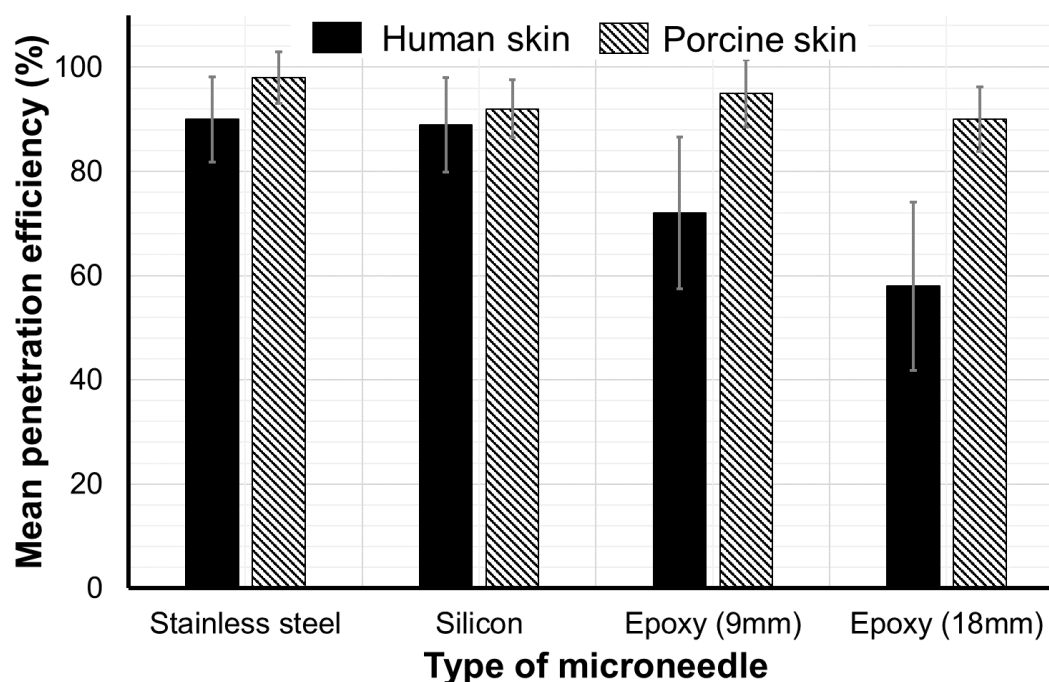
Figure 2.9: Mean puncture efficiency following microneedle application to ex vivo skin. Puncture efficiency of 500µm length steel, silicon and epoxy arrays inserted into ex vivo human and porcine skin. Epoxy arrays measured 9mm and 18mm in diameter. Breast skin from two female donors aged 83 and 60 years old. A total of two porcine ears were used during this study. Data presented as the mean ±SD (*n=6*).

OCT imaging and histological analysis were conducted to corroborate staining results and confirm MN penetration. Figure 2.10 displays a selection of cross-sectional images of ex vivo human and porcine skin following MN application. Microchannels were visible, demonstrating that each array was capable of piercing through the SC. OCT imaging showed that steel MNs produced the most discernible microchannels which extended into the dermis in both ex vivo human and porcine skin. By comparison, silicon and epoxy MNs were capable of reaching the VE in both skin types. Histology further confirmed that all MN arrays pierced the skin as parts of the VE were stained blue, with clear disruption in the SC. H&E staining of the sections was poor with a lack of clearly defined nuclei which indicated reduced haematoxylin staining. Eosin, conversely, overstained the tissue resulting in an intense pink appearance. Whilst Figure 2.10 demonstrates poor H&E staining, microchannels were again identified for all MN types.
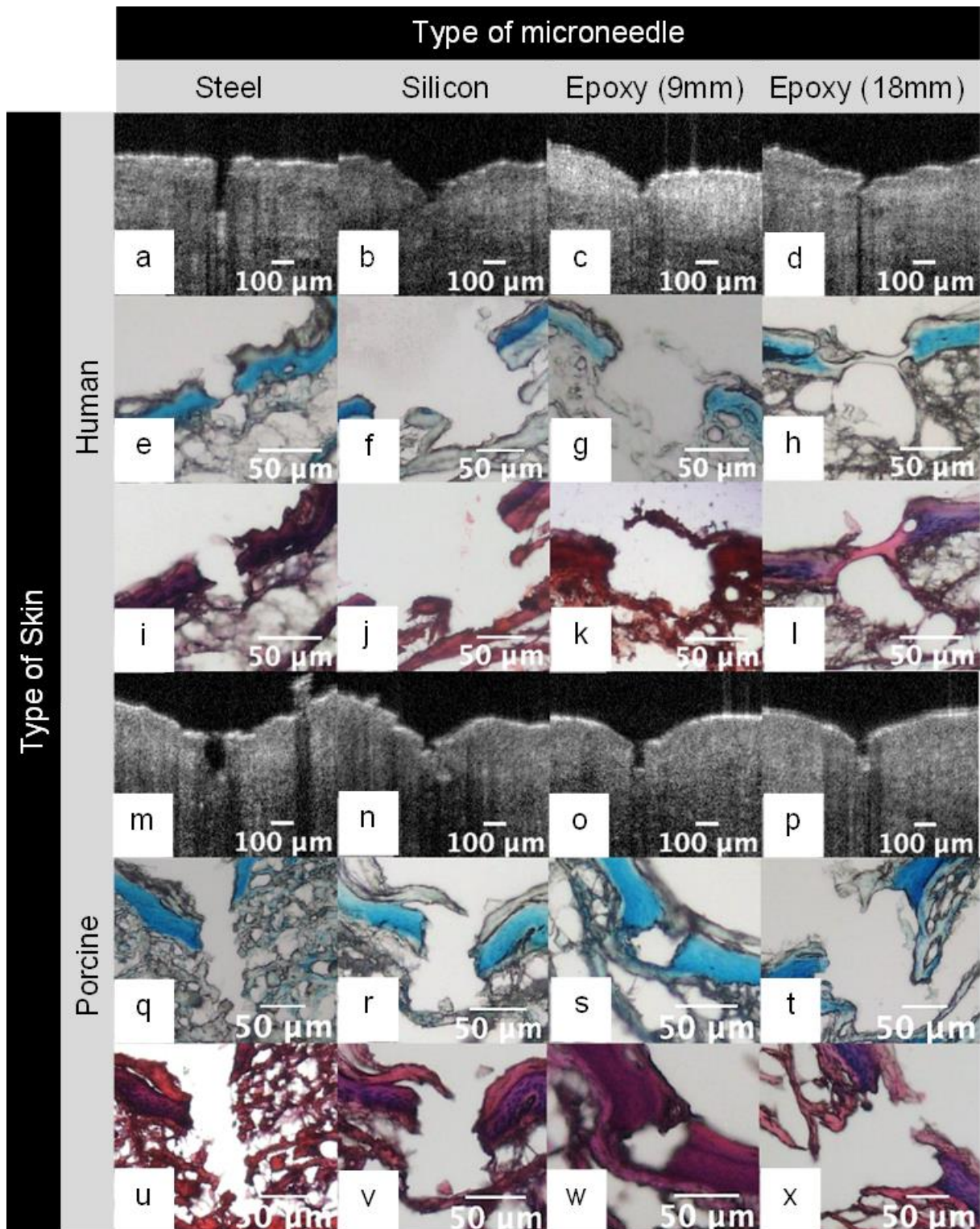
Figure 2.10: OCT and histological images of skin puncture following microneedle application. Individual OCT sub-surface images of excised human (a-d) and porcine (m-p) skin treated with uncoated, solid, 500µm length steel, silicon and epoxy arrays. Images of 10µm sections of methylene blue stained microchannels created in human (e-h) and porcine (q-t) skin. Haematoxylin and eosin stained, 10µm sections of microneedle treated human (i-l) and porcine (u-x) skin. Breast skin from two female donors aged 83 and 60 years old. A total of two porcine ears were used during this study

OCT imaging revealed an intact dermis, whilst considerable sized tears were identified in the dermis following sectioning. Therefore, to measure channel dimensions, OCT images were analysed using Fiji. Figure 2.11 displays the mean microchannel dimensions for each type of MN inserted in both skin types. Whilst application force was not measured steel MN arrays produced the deepest channels in both skin types overall, followed by silicon MNs. Epoxy MNs resulted in the smallest channels overall. Of the two epoxy MNs, 9mm arrays resulted in deeper microchannels than those created by 18mm diameter arrays. As shown by Figure 2.11, channels created in porcine skin were deeper than those created in human skin using the same type of MN.

Channel width was also measured. Mean microchannel width for steel, silicon and epoxy MNs inserted into both skin types are also shown in Figure 2.11. Unlike depth, minimal changes in channel width were observed and overall, values were comparable between MN arrays.
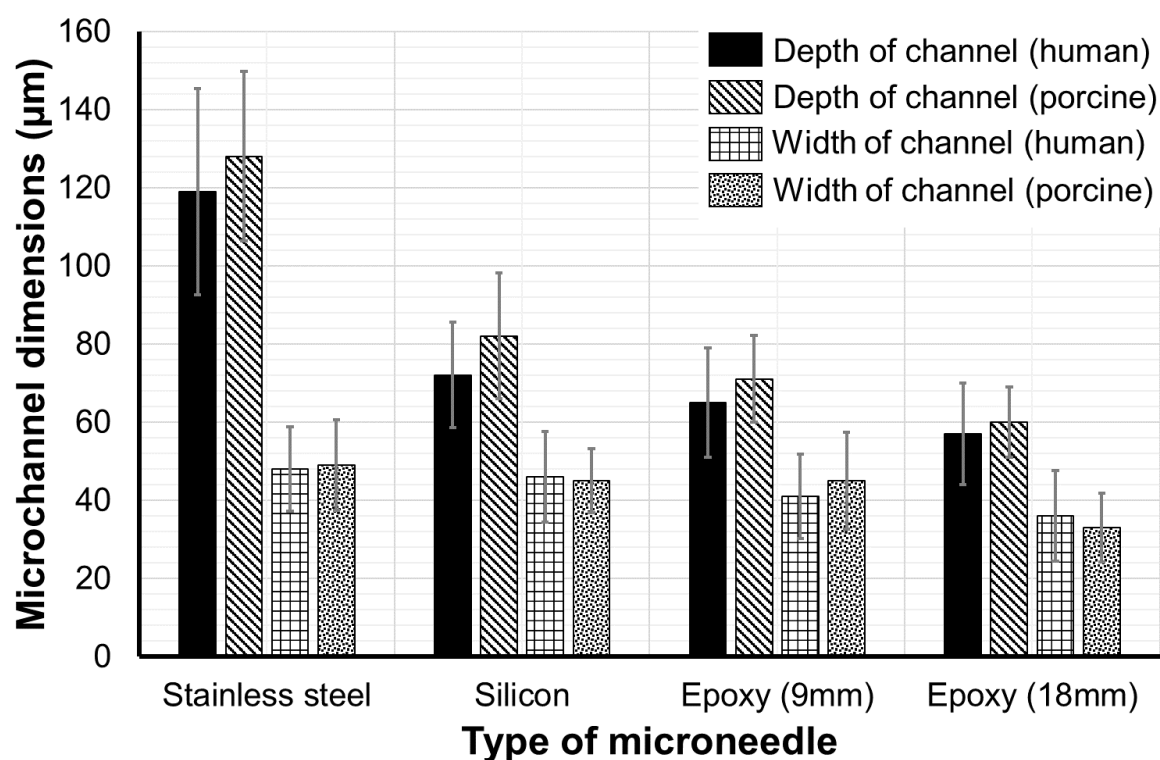
Figure 2.11: Mean microchannel dimensions identified following the manual application of microneedles to ex vivo skin specimens. Uncoated, solid, 500µm steel, silicon and epoxy microneedle arrays (9mm and 18mm in diameter) were applied to excised human and porcine skin. Microchannels were identified using OCT and measured using Fiji. Breast skin from two female donors aged 83 and 60 years old. A total of two porcine ears were used during this study. Data presented as the mean ±SD (*n=6*).

2.4.4 Effect of downward application force on microneedle penetration

Epoxy MNs containing an average of 85 ±1 needles per array were inserted into ex vivo human and porcine skin using three downward application forces. Overall, application forces over an 18mm array measured 5.3N ±0.17, 10.4N ±0.16 and 15.4N ±0.11 when pressed into human skin. For porcine skin, mean application force measured 5.4N ±0.17, 10.3N ±0.16, and 15.31N ±0.14 for the same sized array. This force data showed that manual application by a single operator, was relatively reproducible, with comparable recorded forces between applications at all target application forces and with both skin types.

A selection of images of methylene blue stained skin following MN application at the three respective forces are shown in Figure 2.12. The use of ethanol did not remove the dye from porcine skin as effectively as human skin, but MN arrays appeared to pierce both skin types at each application due to the presence of clear blue dots.
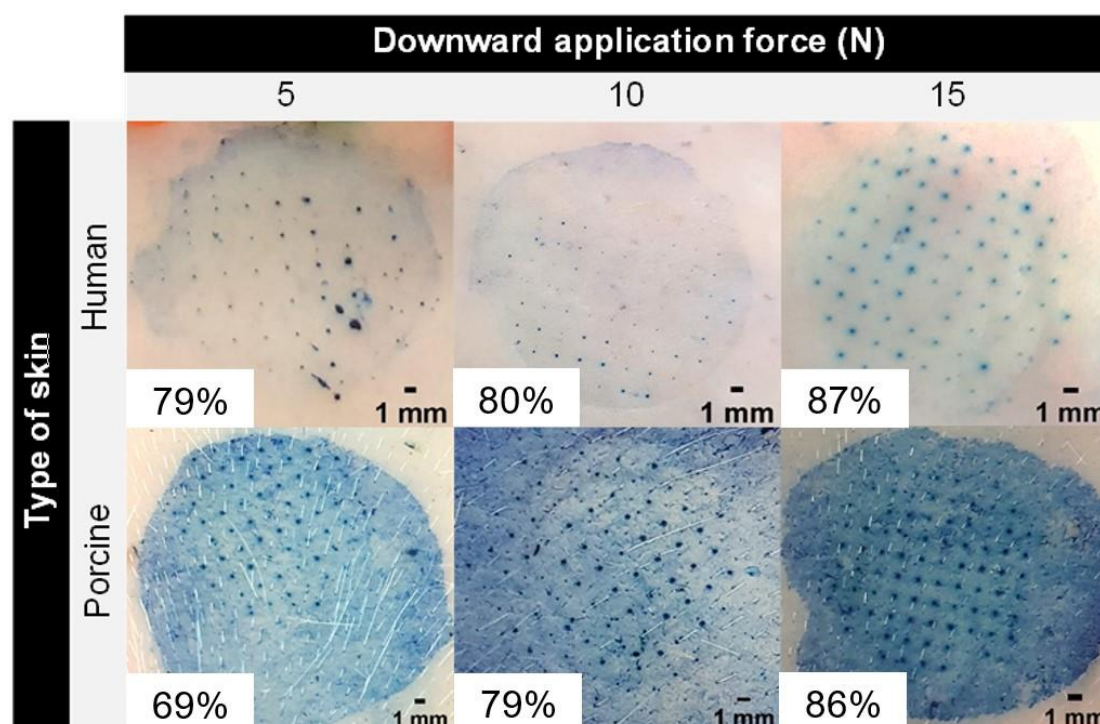
Figure 2.12: Methylene blue staining following the removal of microneedles which were pressed into ex vivo human and porcine skin at three forces. Selection of en face images of human and porcine skin explants treated with solid, uncoated, polymeric, 500µm length microneedles. Microneedles were applied by one operator using a handheld digital force gauge at 5N, 10N and 15N. Breast skin from two female donors aged 59 and 52 years old. A total of two porcine ears were used during this study. Percentage puncture efficiency is shown in the bottom left of each image. Puncture efficiency presented as the mean of *n=6* experiments.

Figure 2.13 displays the penetration efficiency for MNs inserted into human and porcine skin explants at 5N, 10N and 15N. Generally, the mean penetration efficiency was comparable at each force in both skin types. An approximate 10% reduction in penetration efficiency was observed when arrays were applied to porcine skin at 5N. Overall, as the downward

application force increased, mean penetration efficiency also increased. Skin puncture was greatest when MNs were pressed into skin at 15N. As the number of potential microchannels varied with each application reproducible penetration was not achieved and 100% penetration was not observed at any force.
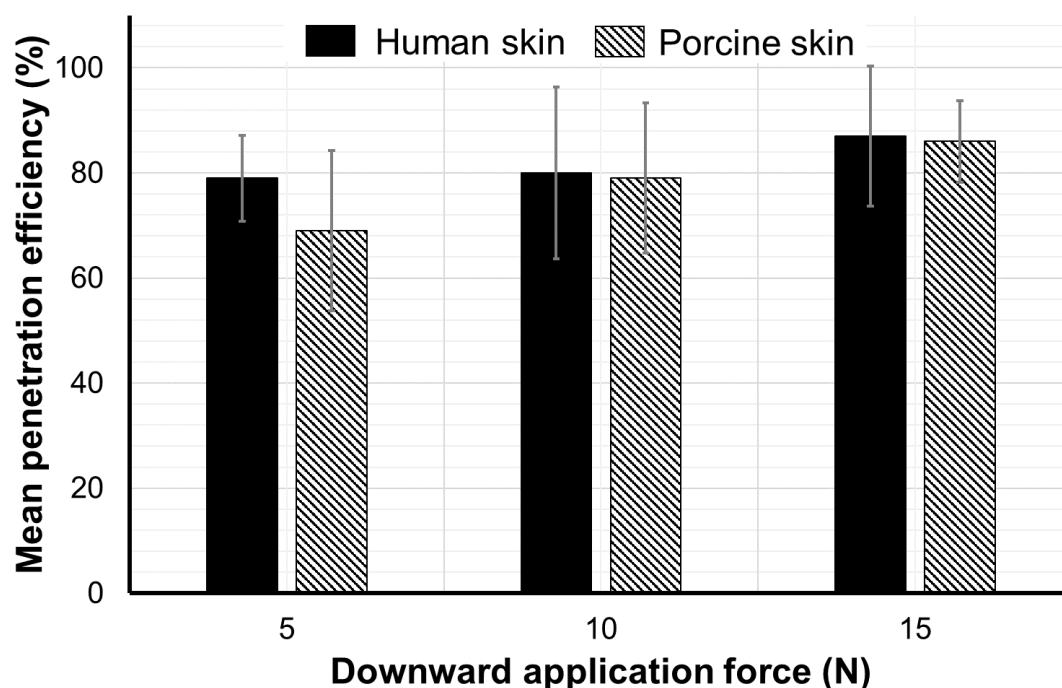
Figure 2.13: Mean penetration efficiency of microneedles applied to skin specimens at three forces. Penetration efficiency of excised human and porcine skin treated with uncoated, epoxy, solid, 500µm length microneedles. Arrays were applied manually using a handheld digital force gauge at 5N, 10N, 15N and held in placed for 60 seconds. Breast skin from two female donors aged 83 and 60 years old. A total of two porcine ears were used during this study. Data presented as the mean ±SD (*n=6*).

Figure 2.14 displays a selection of cross-section images of human and porcine skin following MN insertion at three application forces. OCT imaging and histology revealed microchannels at each application force in both human and porcine skin, confirming MN penetration. Overall, microchannels resulting from a 5N downward application force were not as easily identified than those created at 10N and 15N. In general, an increased number of indentations and minor disruption in the epidermis was observed, rather than discreet distinguishable channels at the lowest force of 5N.
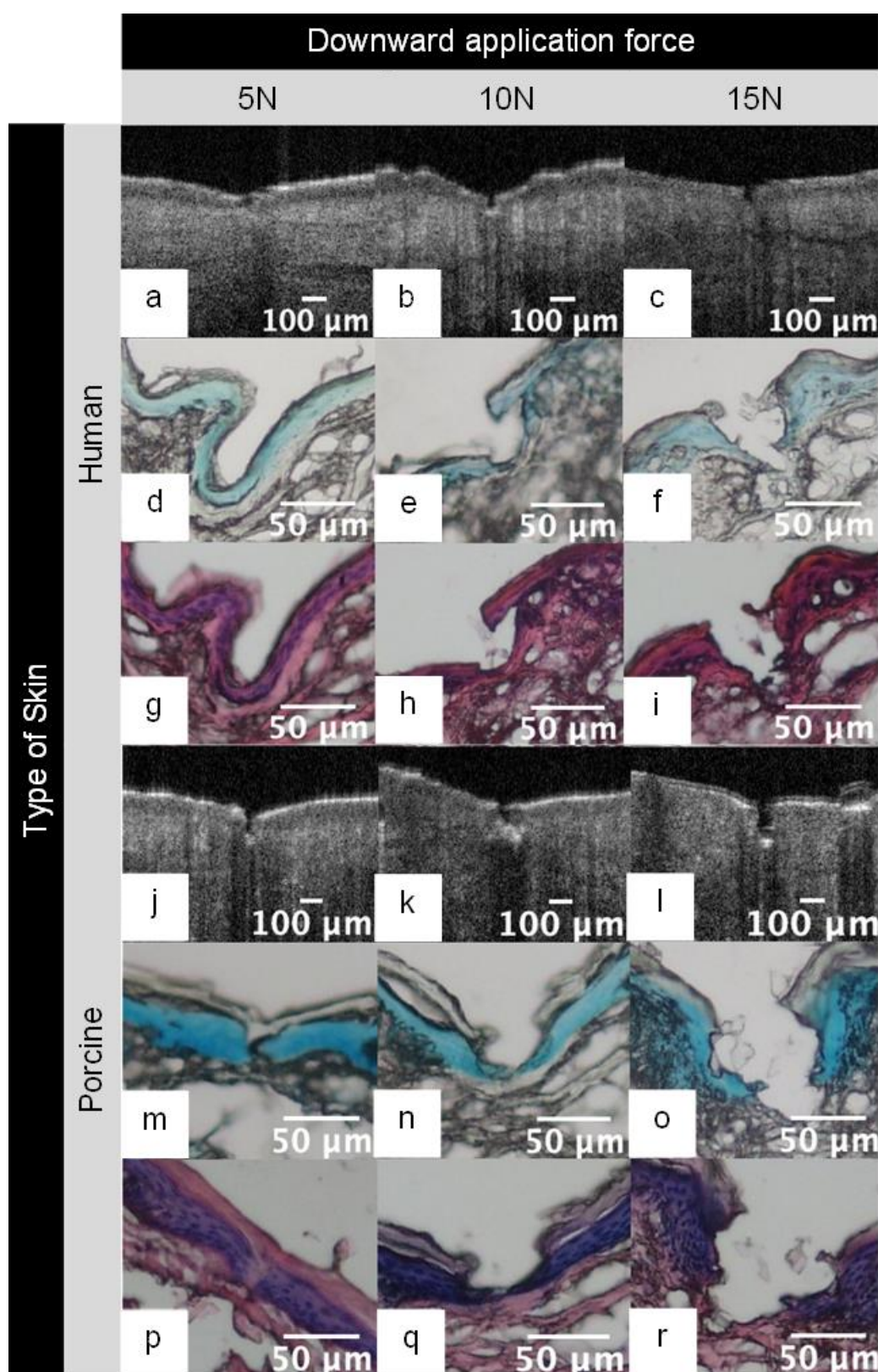
Figure 2.14: OCT and histological images of skin puncture following microneedle application over a range of forces. Individual OCT sub-surface images of excised human (a-c) and porcine (j-l) skin treated with uncoated, solid, 500µm epoxy arrays. Images of 10µm sections of methylene blue stained microchannels created in human (d-f and porcine (m-o) skin. Haematoxylin and eosin stained, 10µm sections of microneedle treated human (g-i) and porcine (p-r) skin. Breast skin from two female donors aged 83 and 60 years old. A total of two porcine ears were used during this study.

Figure 2.15 displays the mean microchannel dimensions for each application force in ex vivo human and porcine skin. Microchannel depth was comparable at each force, however as shown by Figure 2.15 as the downward application force increased, the mean depth of channel increased. Figure 2.15 demonstrates that minimal changes in microchannel width were observed. Overall, as pressing force increased, microchannel width remained comparable.
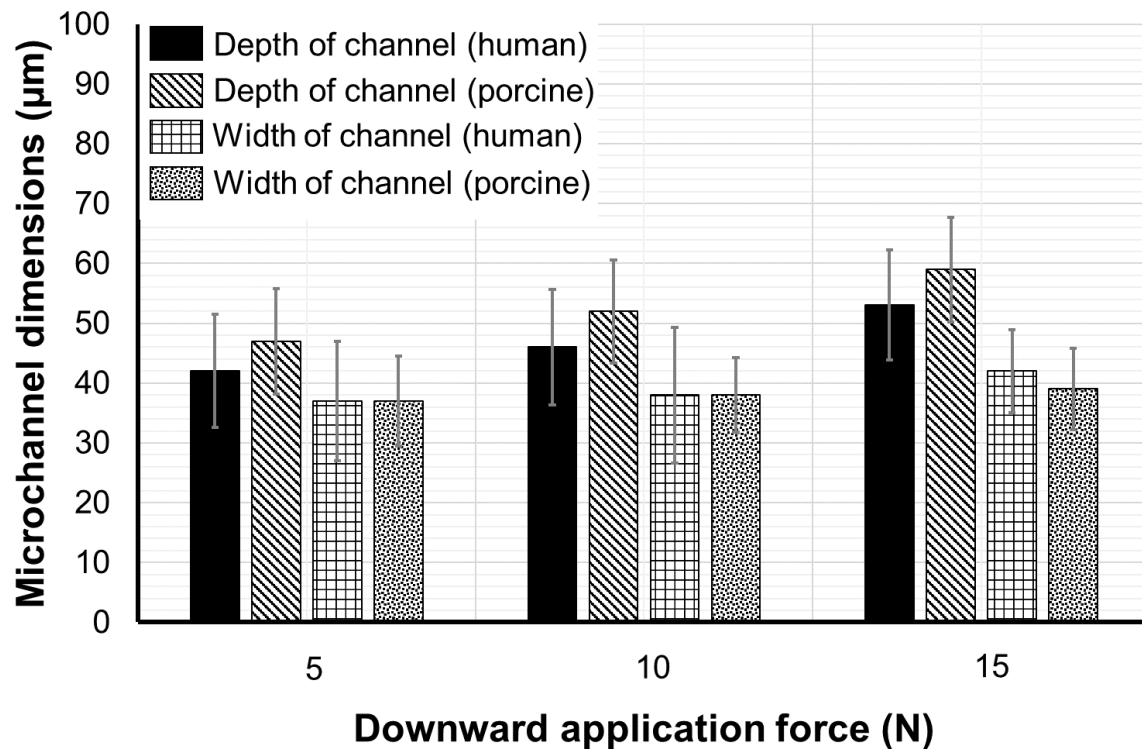
Figure 2.15: Mean microchannel dimensions identified following the manual application of microneedles to ex vivo skin specimens at three forces. Uncoated, epoxy, solid, 500µm length microneedles were applied to ex vivo human and porcine skin manually using a handheld digital force gauge at 5N, 10N, 15N. Microchannels were identified using OCT scans and measured using Fiji. Breast skin from two female donors aged 59 and 52 years. A total of two porcine ears were used during this study. Data presented as the mean ±SD (*n=6*).

2.4.5 Effect of changing application method on microneedle penetration

Epoxy MNs were inserted into excised human and porcine skin using three application methods. MNs were either pressed into skin using a downward force measuring approximately 15N, at a greater velocity (impact insertion) or manually inserted and gently agitated over 60 seconds. Figure 2.16 displays a selection of en face images of methylene blue stained skin explants treated with each application method. As shown by Figure 2.16, MNs appeared to pierce both ex vivo human and porcine skin using each application technique due to the presence of identifiable blue dots
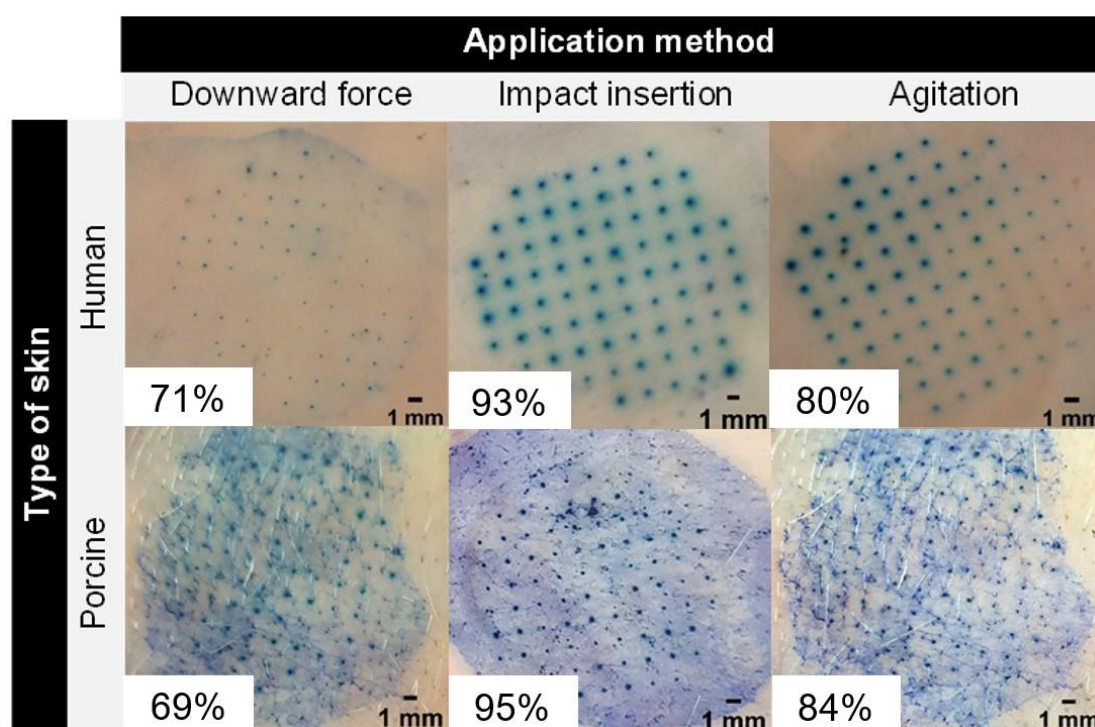
Figure 2.16: Methylene blue staining following the removal of microneedles which were applied to skin specimens using three methods. En face images of excised human and porcine skin treated with solid, uncoated, epoxy 500μm length microneedles. Microneedles were applied using compression, impaction and agitation. Breast skin from two female donors aged 52 and 60 years old. A total of two porcine ears were used during this study. Percentage penetration efficiency is shown in the bottom left of each image. Penetration efficiency presented as the mean of $n=6$ experiments.

In addition to Figure 2.16, penetration efficiency for each of the application methods used is also shown in Figure 2.17. Overall, pressing MNs into skin using a downwards force resulted in the overall lowest mean penetration efficiency whilst impact insertion resulted in the greatest penetration efficiency. When compared to pressing force and agitation, MNs inserted using impact insertion resulted in more reproducible skin puncture. In general, and similarly to the studies discussed previously, the number of potential microchannels varied with each application and 100% MN penetration was not observed in either skin type. However, impact insertion did improve the efficiency of penetration and reduced variability.
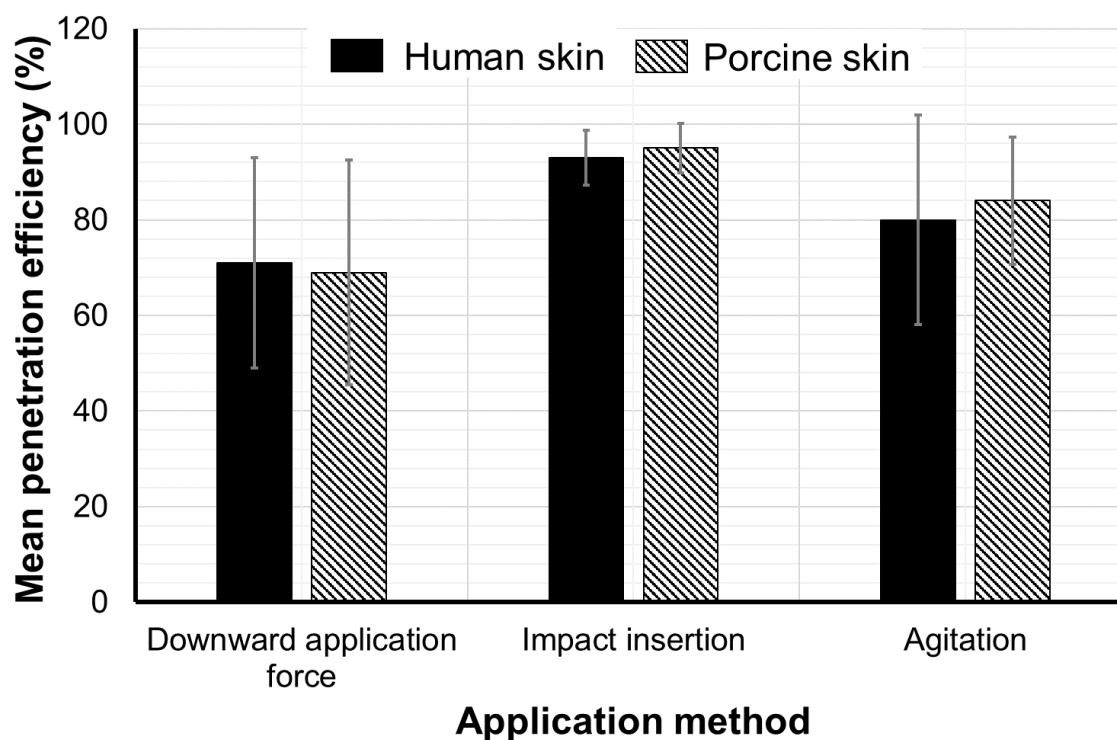
Figure 2.17: Mean penetration efficiency of microneedles applied to skin explants using three methods. Penetration efficiency of excised human and porcine skin samples treated with uncoated, epoxy, solid, 500µm length microneedles. Arrays were applied manually using pressing force, impact insertion and agitation. Breast skin from two female donors aged 52 and 60 years. A total of two porcine ears were used during this study. Data presented as the mean ±SD (*n=6*).

Figure 2.18 displays a selection of cross-section, sub-surface images of ex vivo human and porcine skin following the insertion of MNs using three application methods. Despite the non-uniformity of skin, sub-surface microchannels were visible both with OCT and following each method of application. Epoxy MNs physically disrupted the SC and reaching the VE for the three application methods. Figure 2.18 also demonstrates that the H&E staining of skin sections was poor. The epidermis, however, was distinguished from the dermis and microchannels were again identified for all application methods.
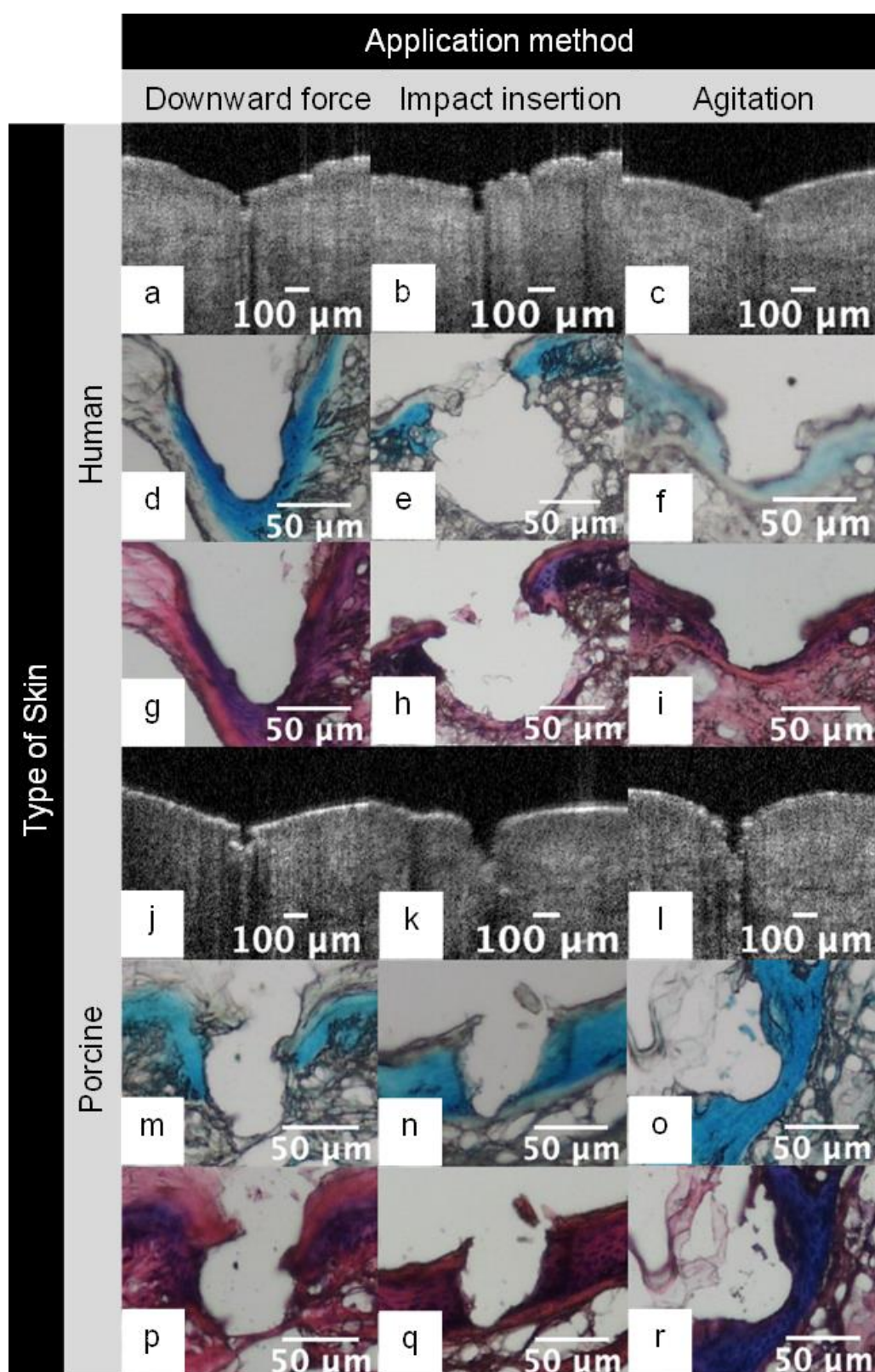
Figure 2.18: OCT and histological images of skin puncture following microneedle application using three methods. Individual OCT sub-surface images of excised human (a-c) and porcine (j-l) skin treated with uncoated, solid, 500µm epoxy microneedles. Images of 10µm sections of methylene blue stained microchannels created in human (d-f) and porcine (m-o) skin. Haematoxylin and eosin stained, 10µm sections of human (g-i) and porcine (p-r) skin. Microneedles were applied by one operator using pressing force, impact insertion and agitation. (*n=6* using porcine skin and breast skin from two female donors aged 52 and 60 years). A total of two porcine ears were used during this study.

Figure 2.19 displays the mean depth and width of microchannels observed in both skin types for each of the application methods. Applying MNs by impact insertion resulted in the greatest depth microchannels measuring approximately 57µm in human skin and 63µm in porcine. The microchannel width remained consistent between application methods and in general, microchannels were slightly larger in diameter in porcine skin, than those measured in human skin.
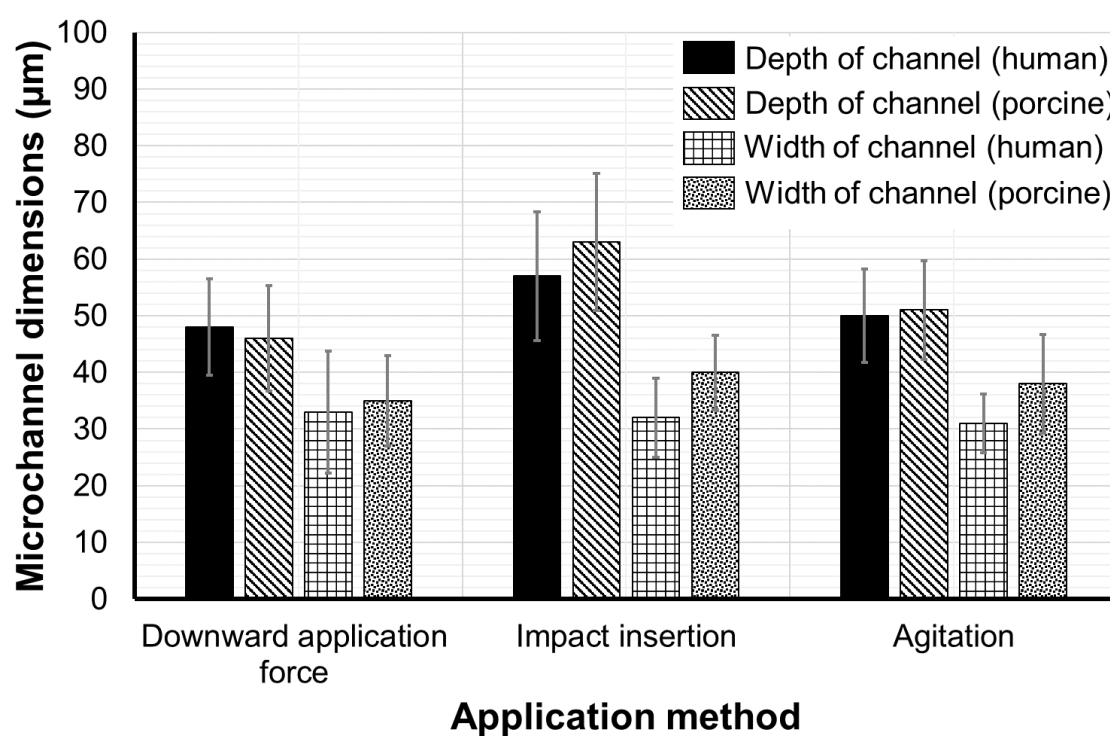
Figure 2.19: Mean microchannel dimensions identified following the manual application of microneedles to ex vivo skin specimens using three methods. Uncoated, epoxy, solid, 500µm length microneedles were applied to ex vivo human and porcine skin using pressing force, impact insertion and agitation. Microchannels were identified using OCT and measured using Fiji. Breast skin from two female donors aged 52 and 60 years. A total of two porcine ears were used during this study. Data presented as the mean ±SD (*n=6*).

2.4.6 Geometry of epoxy microneedles post insertion

MNs are exposed to a range of stress during insertion, which can be unpredictable due to the non-uniformity of the skin. These stresses could result in bending, buckling and base-plate fracture. Uncoated, solid, epoxy MN arrays were re-imaged following insertion into ex vivo human and porcine skin. Stereo- and scanning electron microscopy were used to determine any changes to the epoxy MNs structure following skin insertion. Whilst mechanical failure tests were not conducted, an increased number of MN tips had blunted (Figure 2.20a) or bent (Figure 2.20b) when compared to the intact images shown prior to insertion (Figure 2.5). No cases of MN fracture were observed in the images acquired.
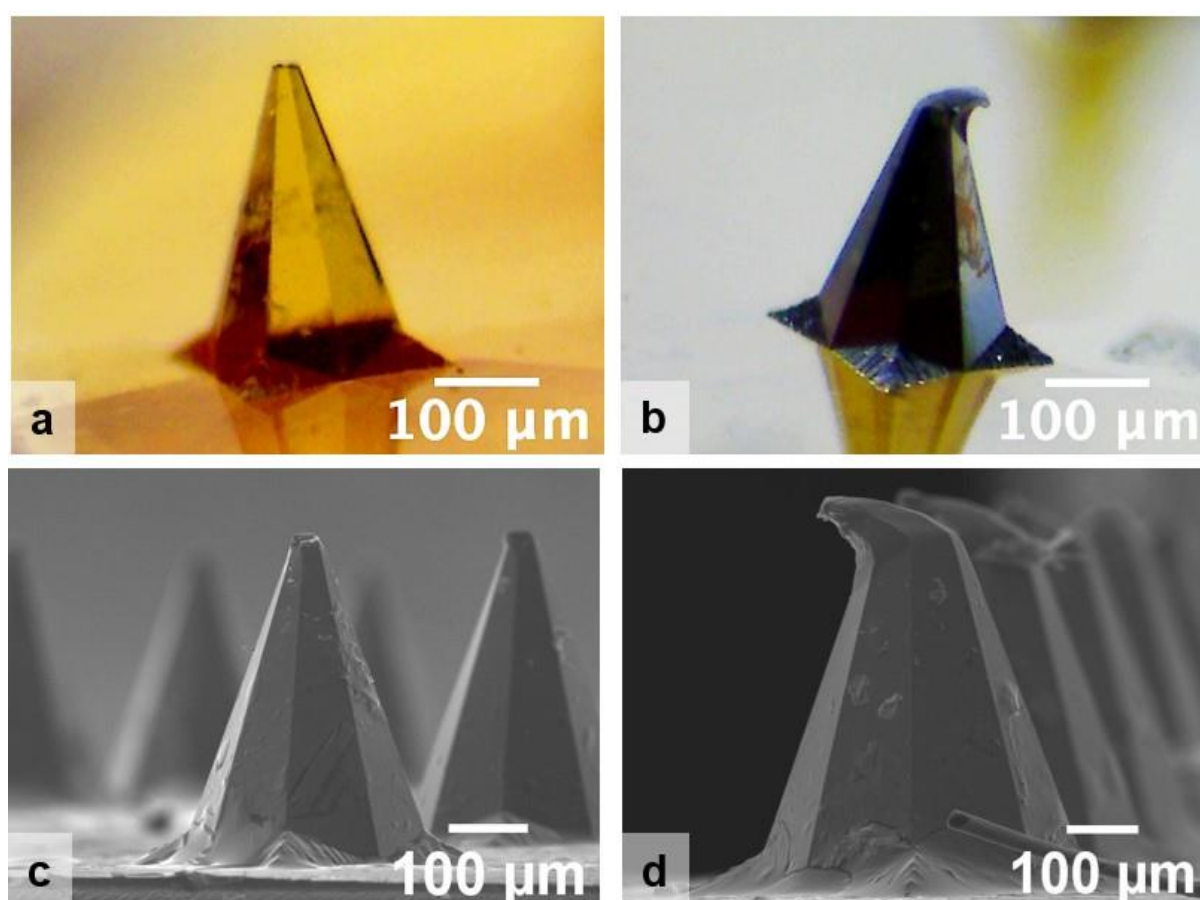
Figure 2.20: Uncoated, solid, epoxy microneedles post insertion into human and porcine skin explants (*n=10*). Stereomicroscope images of single microneedles post insertion which had blunted (**a**) or bent (**b**) at x4 magnification. Scanning electron micrographs of microneedles post insertion which had blunted (**c**) (250x magnification and working distance of 18.4mm) or bent (**d**) (350x magnification and working distance of 20.0mm).

2.5 Discussion

2.5.1 Influence of microneedle geometry and materials on skin insertion

A comparison of the insertion performance of four different arrays in skin explants from human and porcine sources revealed comparable mean penetration efficiency for both steel and silicon MNs. However, steel MNs produced deeper channels in both human and porcine skin. The MN design is crucial for effective skin penetration, which is important in sensing as MNs need to contact conductive skin layers to aid the acquisition of high-fidelity recordings. Whilst this chapter focused on MN characterisation and insertion performance, future chapters focus on the sensing capabilities of MN electrodes. Despite steel and silicon MNs resulting in a greater insertion performance, the 18mm diameter epoxy MN array was of interest as their diameter was comparable in size to the gel-soaked foam pad on a commercially available wet electrode. When interpreting the results, there are various considerations, as MN insertion is influenced by several factors (Davis et al. 2004; Gill et al. 2008; Gittard et al. 2013; Römgens et al. 2014; Loizidou et al. 2016). In the present study, epoxy arrays with a greater needle density produced a lower penetration efficiency compared to epoxy, steel and silicon arrays with less MNs. These arrays were manually inserted into skin in a comparable manner to other publications (Gill et al. 2008; Peng et al. 2021). Whilst application force and velocity were not measured or controlled, variability would exist if devices were manually deployed by clinical users. Microchannel depth was also reduced for more densely populated arrays when compared to the smaller array consisting of 22 MNs. This is consistent with other publications and is of interest as a greater needle density might compromise needle puncture due to differences in pressures at the MN tips, thereby resulting in different piercing properties (Verbaan et al. 2008; Gomaa et al. 2010; Yan et al. 2010; Larrañeta et al. 2014). Larger arrays make it more difficult to apply uniform forces across the whole array and may reduce the intimate contact between the array and the undulating skin surface, which could impact on the electrode-skin interface and the subsequent signal recorded.

MN parameters including length, interspacing, needle density and material (Prausnitz 2017), application velocity (Jeong et al. 2017) and skin type will influence MN penetration. Tip and base interspacing of epoxy MNs measured approximately 1.71mm and 1.20mm. If MNs are in close proximity, the 'bed-of-nails' effect may be observed (Makvandi et al. 2021b). Whilst the effect of needle pitch was not investigated, if needle density is high or needle pitch is reduced, there may be insufficient pressure per needle for skin puncture to occur (Yan et al. 2010). This effect has been evidenced by Gomaa et al. (2010). Compared with arrays consisting of 196 MNs/cm^2, TEWL was reduced for 361 MNs/cm^2 arrays when inserted into ex vivo human skin (Gomaa et al. 2010). Contrariwise, a recent study by Ramöller et al. (2020)

demonstrated no significant difference between the insertion efficiency of low- and high-density hydrogel-forming MN arrays into both artificial and ex vivo skin models at a force of 32N. However, this study did also demonstrate that low-density MN arrays resulted in better insertion when compared with high-density arrays at lower forces of 10N and 20N. It has been acknowledged that the number of MNs per array and the insertion method influence the 'bed of nails' which can be reduced by increasing MN spacing or using an applicator (Widera et al. 2006; Verbaan et al. 2008; Larrañeta et al. 2014; Li et al. 2021).

A further parameter not investigated was needle length, however, as may be expected, publications have shown that longer MNs penetrate deeper into the skin (Gill et al. 2008; Sasaki 2017). MNs used in electrodes range from approximately 200µm (Resnik et al. 2015) to 700 µm (Chen et al. 2018) in length. MNs used in this chapter measured 500µm which is similar to other publications (O'Mahony et al. 2016; O'Sullivan et al. 2019) and can be considered an appropriate length for a minimally invasive device, as 700µm MNs do not appear to cause pain (Gill et al. 2008). During MN insertion, the skin first indents due to its elasticity. Following sufficient pressure, MN penetration occurs. The effect of skin deformation is overcome by using longer MNs thereby increasing the efficiency of skin puncture (Prausnitz 2017). Regarding MN electrodes, needle length may play a role in the quality of the acquired signal. Viable skin contains approximately 70 to 80% water (Blank 1952; Johnsen et al. 2009; Grimnes and Martinsen 2014). Whilst the hydration of the SC can be influenced by several factors, this layer has less water than viable skin and a higher electrical resistance (Blank 1952; Blank et al. 1984; Pliquett et al. 1995; Alonso et al. 1996; Johnsen et al. 2009). Resnik et al. (2015) demonstrated a significant reduction in skin impedance using MNs. Therefore, MN length could be optimised to capture the highest quality signal whilst ensuring the needles do not cause significant pain by stimulating pain receptors in the epidermis and dermis. This point could be addressed in future studies.

Due to the brittle nature of silicon MNs, it has been reported that they could fracture and subsequently embed in skin (O'Mahony 2014). Imaging demonstrated that fractures were not observed for silicon MNs. Concerns, however, have been raised over its biocompatibility (Runyan and Bean 1990; Braybrook 1997). Steel microneedles can be used as an alternative due to their advantages of simple and cost-effective manufacture, biocompatibility and reliable skin puncture (González-González et al. 2011; Pearton et al. 2012). Their ability to conduct an electrical signal could make them a useful material in the fabrication of MN electrodes. Polymers have also been used in the MN field for both drug delivery (Machekposhti et al. 2017; Lim et al. 2021) and sensing (Srivastava et al. 2015; Caliò et al. 2016). Several groups have used biocompatible polymeric MNs during electrode fabrication (Chen et al. 2013; Barrett et al. 2015; Caliò et al. 2016; O'Mahony et al. 2016; Stavrinidis et al. 2016). Using a

biocompatible epoxy can be considered cost-effective, particularly when considering scale up (O'Mahony 2014; O'Mahony et al. 2016) but polymer MNs typically have a lower Young's Modulus compared to other materials such as silicon (O'Mahony et al. 2016). Post-insertion imaging of MNs used in this study revealed that MN tips had remained intact, blunt or bent indicating an area of weakness in the MN structure. Maintaining needle integrity during insertion is likely to be crucial in overcoming the skin barrier and recording high quality signals. It is important that MNs do not fracture with upon insertion. The force of insertion has been reported in previous literature as approximately 10N (Sharma et al. 2017), however, no fractured or broken MNs were observed in any of the studies conducted in this chapter where forces higher than 10N were used.

2.5.2 Influence of application method on microneedle skin insertion

When investigating the effects of application force on MN penetration, this study determined that pressing epoxy MN arrays in skin explants using a downward force of 15N produced the greatest overall mean penetration efficiency in both ex vivo human (87%) and porcine skin (86%). This study also demonstrated that increased application force resulted in increased microchannel depth which agrees with other publications including Donnelly et al. (2010a) and Gittard et al. (2013). Identifying a suitable application force for needle penetration is important for MN electrodes as they need to pierce the SC and contact the underlying conductive layers to facilitate the acquisition of high-quality recordings. There are, however, several considerations when interpreting these results. In the context of the published literature, several studies have shown successful MN penetration over a range of forces, with a force of 10N being classified as moderate thumb pressure (Sharma et al. 2017). The maximum pressing force of 15N used in this study is higher than other research groups (Davis et al. 2004; Wei-Ze et al. 2010; O'Mahony et al. 2013; Resnik et al. 2015; Xenikakis et al. 2021) although, publications including Verbaan et al. (2007) and Donnelly et al. (2010a) applied MN arrays at application forces of 50N and 16.4N respectively. In this Chapter, the force has been discussed in terms of force per array, as was the case in publications by Donnelly et al. (2010a), Larrañeta et al. (2014) and Lhernould et al. (2015). In comparison, other publications discuss force per individual needle (Park et al. 2010; Wang et al. 2015; Yu et al. 2021). This measure is useful at explaining penetration results for instance, Park et al. (2010) demonstrated that when a 100 MN array was pressed into porcine skin at 5N, this corresponded to 0.05N per needle. In the present study, epoxy arrays contained an average of 85 MNs per array. When inserted at 5N this would result in approximately 0.06N per needle, compared to 0.18N when inserted at 15N. The increased application force per needle resulted in greater MN penetration. However, the effects of this increased application force on sensations, such as pain, could not be assessed as MNs were applied to ex vivo skin.

Regarding MN insertion and pain in human subjects, Gill et al. (2008) concluded that pain depended primarily on the force of MN tip insertion and depth to which the MN tip extends into the skin. Several methods could be used to decrease application force. For instance, arrays with fewer MNs receive more force per needle which is known to facilitate insertion at lower array application forces (Makvandi et al. 2021a). For MN electrodes however, a balance must exist between the optimal number of MNs to avoid pain and discomfort without jeopardising signal quality. A further method to reduce application force is to reduce to needle tip radius (Davis et al. 2004; Roxhed et al. 2007; Römgens et al. 2014). The tip diameter of epoxy MNs fabricated by Tyndall National Institute, and used in this chapter measure 1-2µm, which is less sharp than their silicon counterparts (O'Mahony et al. 2016). This tip diameter is lower than those by Römgens et al. (2014) who fabricated MNs with tip diameters ranging from 5µm to 37µm and concluded that sharper MNs pierced the skin at lower forces.

The way arrays are applied to skin can influence the degree of skin puncture. Downward application that is perpendicular to the skin surface, or pressing force, is not the only method of MN application. Throughout the literature, many groups have investigated MN application using impact insertion (Verbaan et al. 2008; Leone et al. 2018). When 'pressing force' was compared against impact insertion and manual agitation in this chapter, impact insertion resulted in the greatest mean penetration efficiency and the deepest microchannels overall. Reproducible puncture is likely to contribute to consistent MN electrode performance during signal acquisition and so an applicator capable of controlling velocity or impact energy is highly desirable. In this study, force-time data software on a hand-held digital force gauge was used as guide to indicate that epoxy MNs were being manually inserted at a greater velocity. It must be noted that impact insertion resulted in improved penetration compared to downward application at minimal velocity (pressing) or downward application followed by agitation but, the maximum force that MNs were exposed to during the impact insertion was also increased from approximately 15N to 20.3N ±5.34. This is likely to have contributed to the increased penetration and channel depth. Furthermore, as MN arrays were manually inserted, application velocity was not consistent between applications with it taking an average of 2.5s ±1.09 to reach the maximum force. The force gauge did provide some control though when pressing the MNs into skin at 15N, however there is some variability due to operator hand movement. Whilst simple downward MN application could be performed manually (Edens et al. 2015; Vrdoljak et al. 2016), the method of impact insertion within this chapter was not accurately performed. Therefore, further work is required to develop and use an applicator to apply MNs at a pre-determined velocity or impact energy (van der Maaden et al. 2014; Leone et al. 2018). Compared to manual MN application, e.g., the pressing force of the thumb, an impact applicator, or an applicator able to control the downward force and insertion velocity

can ensure improved reproducibility of MN skin puncture, independent of the user (Norman et al. 2014; van der Maaden et al. 2014). For instance, Leone et al. (2018) developed a digitally controlled applicator to insert MNs into skin whereby a set of MN arrays with varying parameters were inserted into ex vivo human abdominal skin using impact insertion or downward pressing force. When inserting MNs using impact application, penetration efficiency reached approximately 100%, whilst pressing MNs into skin reached 80%. The published applicator was capable of delivering a chosen impact velocity and pressing force with high reproducibility, although the angle of the applicator also influenced the impact velocity.

2.5.3 Influence of the analytical techniques used to evaluate microneedle penetration

Effective evaluation of skin penetration with MNs requires an understanding of the strengths and limitations of the data that is produced by different analytical techniques. Insertion studies discussed in this chapter needed to confirm that MNs pierced the SC and contacted the VE where there is a higher water content and the potential for improved cardiac signal acquisition (Grimnes and Martinsen 2014). After MN removal from skin explants, methylene blue was used to stain for microchannels (Pearton et al. 2012; Moronkeji et al. 2017; Arikat 2019) and was left on MN treated skin for a maximum of 10 minutes. Whilst staining duration was not optimised in this chapter, other publications have demonstrated that 10 minutes is suitable duration to stain for microchannels although some studies have used staining times up to 30 minutes (Haq et al. 2009; Pearton et al. 2012; Arikat 2019). The presence of blue dots in an array pattern suggests that epoxy MNs were capable of penetrating both human and porcine skin which is consistent with other publications using similar MNs (O'Mahony 2014; O'Mahony et al. 2016). The number of microchannels varied with each application, and as expected 100% penetration was not observed (O'Mahony et al. 2016). Staining can provide rapid confirmation of MN insertion; however, the method is associated with multiple limitations. The SC may not be pierced, and the dye could pool within indentations resulting in a false positive (Lutton et al. 2015). This technique also highlights the existence of potential microchannels, but it does not provide information regarding their dimensions.

OCT imaging and histological techniques were therefore used to corroborate methylene blue staining and have been used by multiple groups to assess MN penetration (Donnelly et al. 2010a; Enfield et al. 2010; Coulman et al. 2011). To assess microchannel dimensions, the imaging techniques used throughout this thesis were dependent upon the removal of MNs from skin explants. For instance, OCT imaging was conducted immediately following MN removal and captured sub-surface images of microchannels in real-time. Scans of human skin demonstrated some discernible microchannels, particularly at a downward application force of 15N and following impact insertion. When used as electrodes, MNs would remain in place

during signal acquisition. OCT imaging, however, was unable to capture in situ images of MNs as the arrays were not transparent and resulted in 'noisy' scans. Therefore, MN penetration depth could have been greater due to the resealing ability of skin following array removal. Images captured using OCT and histology demonstrated that microneedles appeared to reach the epidermis in both skin types, however an increasing number of channels in porcine skin reached the dermis. For porcine skin, efforts were made to remove hair using electrical clippers, yet when compared to human skin, OCT imaging revealed a much greater density of hair follicles. Following imaging with OCT, 10μm sections were generated using a cryotome (Roxhed et al. 2007; Chu and Prausnitz 2011; Larrañeta et al. 2014) and H&E staining was used to observe the structure and organisation of skin layers. Therefore, histological analysis was conducted as an additional method to confirm skin puncture. Despite optimising the process for both skin types, overall, the H&E staining of skin in this chapter was poor. Haematoxylin did not produce clear cellular nuclei and so whilst the stain used was in-date, haematoxylin may have been oxidised to hematein which is further degraded into non-staining products, thereby losing its potency (Davis 2012). Section thickness can also range between 6-12μm (Lutton et al. 2015). The 10μm thick sections generated may have been too thin resulting in the poor staining ((NSH) 2001; Fischer et al. 2008). Conversely, whilst a 0.5% eosin concentration was used to counterstain, this may have been too concentrated giving rise to an intense pink appearance even after rinsing with water. The method of H&E staining used in this chapter requires further optimisation and could include automated staining devices to improve results. Despite the inadequate staining, discernible microchannels were present, but not in all cases. The lowest application force of 5N was the least invasive. As channels were smaller, locating the site of MN penetration was more difficult to identify using this method. Excision of the skin during biopsy and the mechanical insults exerted when sectioning could result in tension changes within the sample and may have impeded microchannel identification (Chu and Prausnitz 2011; Lutton et al. 2015).

Coulman et al. (2011) recognised that analysing microchannel dimensions using histology can overestimate measurements. This error could be compounded by the inaccuracies due to skin retraction when microneedles are removed from the skin prior to staining (Donnelly et al. 2010a; Loizidou et al. 2015). This was highlighted by comparing histological images of microchannels captured in a previous study, with OCT images of channels produced using the same MNs (Birchall et al. 2005). Therefore, to reduce the risk of overestimating microchannel dimensions OCT images were used to provide an indication of the depth and width of microchannels. As expected, penetration depth was greatest for an application force of 15N when using an impact-insertion application method. In most cases, microchannel depth was greater in porcine skin than human skin. Differences in porcine skin

properties at different anatomical locations have been discussed in several publications, for instance, Moronkeji et al. (2017) found that abdominal tissue is typically thinner than back tissue. Whilst handling porcine skin explants, the skin also seemed considerably stiffer than human skin in some cases, indicating a difference in biomechanical properties and potentially contributing to the increased depth of penetration.

2.5.4 Influence of the skin models used to evaluate microneedle penetration

For MN electrodes, understanding the biological organisation of the skin and its mechanical and electrical properties can inform the development and optimisation of novel electrodes. MN insertion studies were initially conducted using an ex vivo human skin model where skin was obtained from mastectomies or breast reduction surgery. Testing MN arrays on skin from the chest is important with respect to MN electrode development as this is the anatomical site where they would be applied. For instance, Holter monitors and patch-based monitors such as the Zio-XT® are placed on the chest to capture cardiac signals (Barrett et al. 2014). Factors including age, biological sex, region of the body and condition of the skin are likely to influence MN penetration (Fore 2006; Li et al. 2006; Kottner et al. 2013; Tsugita et al. 2013; Firooz et al. 2017; Maiti et al. 2020). Explants used for MN insertion studies were from donors aged 50 years and older. Age is an important consideration when selecting an excised human skin specimen for MN testing as age can influence the thickness of skin (Li et al. 2006; Vashi et al. 2016). Whilst this was not investigated, as the skin ages, changes in structure and function occur. For instance, the epidermis and dermis become thinner, whilst the time taken for skin to turnover increases (Gambichler et al. 2006; Blair et al. 2020). Blood flow within the skin decreases and a reduction in elasticity is observed due to changes in the structure of elastic fibres (Fore 2006). These alterations make ageing skin increasingly prone to injury and impacts upon all aspects of wound healing (Ashcroft et al. 2002; Makrantonaki and Zouboulis 2008; Zouboulis and Makrantonaki 2011). During MN application, the skin first indents due to the elasticity of skin. Following sufficient pressure, MN penetration occurs (Davis et al. 2004). When using older human skin samples, the reduced elasticity and thickness of skin could potentially result in increased MN penetration when compared to younger human skin specimens. Quinn et al. (2018), for example, applied hydrogel-forming MN arrays to participants aged over 65 years where breaches in the SC were determined using OCT. Quinn and colleagues found that insertion depths were similar when compared to a group aged between 20 and 30 years. However, using TEWL, it was determined that the time taken for skin to recover following MN application occurred at a slower rate in the older subjects (Quinn et al. 2018).

Whilst testing MN devices in vivo is ideal, the use of ex vivo human skin is considered the next appropriate model for transdermal testing. Due to reductions in surgical procedures which occurred during this postgraduate research, availability of ex vivo human skin was limited, and an alternative was sought. Several animal models including pig, mouse and rat have served as a substitute for human skin in many fields, including MNs (Kim et al. 2012; Jung et al. 2013; Rampton et al. 2013; Sheu et al. 2014; Moronkeji et al. 2017; Arikat et al. 2020). Several publications have highlighted the use of ex vivo porcine skin as an alternative from an anatomical, physiological and cellular component perspective than synthetic skin substitutes (Jacobi et al. 2007; Abd et al. 2016; Ranamukhaarachchi et al. 2016; Moronkeji et al. 2017). OCT imaging and histological analysis revealed that anatomically, human and porcine skin explants were comparable. Following this finding, insertion studies were repeated using porcine skin. Within the literature, several studies have used porcine skin to test MN arrays (Lavker et al. 1991; Avon and Wood 2005; Cheung et al. 2014; Larrañeta et al. 2014; Loizidou et al. 2016; Moronkeji et al. 2017). Using OCT scans, thickness of the SC and epidermis in both ex vivo human breast skin and porcine skin from the dorsal side of the ear were comparable to values quoted in the literature. For instance, whilst epidermal thickness varies with location, total epidermis in porcine skin can vary from approximately 30 to 140µm in thickness in comparison to the 50-120µm in humans (Meyer et al. 1978; Kong and Bhargava 2011; Tfaili et al. 2012; Debeer et al. 2013). Whilst studies such as Tfaili et al. (2012) and Debeer et al. (2013) used alternative methods to measure porcine skin to those used in this chapter, it was found that SC thickness in pigs can range from 20-26µm which is comparable to what is observed in humans and similar to the results in this chapter (Summerfield et al. 2015). Whilst similarities in measurements, hair sparseness and blood supply have been observed, mechanical differences exist between porcine and human skin (Ranamukhaarachchi et al. 2015). Distinct regional differences in composition and morphology have been observed, particularly regarding epidermal and dermal thickness as well as the amount of collagen and elastin within each tissue (Turner et al. 2014). Appreciating these regional differences is important to avoid misinterpretation of results. In this chapter, skin from the dorsal side of the pig ear was used for MN experimentation. It has however been shown by publications such as Turner et al. (2014) that rostral and mid-back regions are the closest in terms of thickness to human skin. Currently, the location of porcine skin used is not well defined and tissues from different anatomical regions are used. The literature shows that the most common sites used include the ear and abdomen. When assessing MN geometry, application force and method on skin puncture, it was observed that microchannels created in porcine skin were deeper than those in human skin, in the majority of cases. When comparing the ex vivo skin models, similarities in data trends observed from studies conducted using porcine skin were applicable to human skin studies. Therefore, whilst ex vivo human and

porcine skin are not representative of in vivo conditions, porcine skin can be considered a suitable model in the absence of human skin explants.

For storage, skin specimens are typically frozen to prevent biological decomposition and structural changes, whilst preserving mechanical properties (Foutz et al. 1992; Mansoor et al. 2015; Barbero and Frasch 2016). Prior to use, samples are allowed to thaw. Several publications have investigated the effect of storage conditions on skin, but with contradictory results (Foutz et al. 1992; Mansoor et al. 2015; Ranamukhaarachchi et al. 2016). Mansoor et al. (2015) demonstrated that freezing porcine skin resulted in increased diffusivity of doxorubicin. The authors suggest that this was likely the result of ice crystal formation during the freezing process (Mansoor et al. 2015). The formation of crystals could subsequently lead to structural damage and potential changes in the mechanical properties of skin (Mansoor et al. 2015). Mechanical properties of skin impact how MN arrays are applied to the surface of the skin. Similarly, to the studies conducted in this chapter, the majority of MN insertion tests have been conducted using freshly, frozen and thawed human and porcine skin explants, amongst other animal models (Yang and Zahn 2004; Khanna et al. 2010; Mansoor et al. 2013; Olatunji et al. 2013). Ranamukhaarachchi et al. 2016 compared the mechanical properties of human and porcine skin before and after freezing. The authors demonstrated mechanical changes relating to decreasing stiffness and increasing energy required to break the SC (Ranamukhaarachchi et al. 2016). The findings suggest that in the absence of fresh ex vivo human skin, using fresh porcine skin explants at higher humidity conditions may provide a more suitable skin model for MN testing.

Further considerations regarding the model relate to the excision of skin from its natural environment. Once removed from the body, skin undergoes further biomechanical changes, particularly relating to tension and hydration. Both ex vivo skin models used during this, and subsequent chapters were tensioned using pins which is a method described in other publications (Ng et al. 2009; Martin et al. 2012; Zhao et al. 2017). As discussed previously, skin first indents when MNs are applied to the surface of the skin. Puncture only occurs once sufficient pressure has been applied. If inappropriately tensioned, the skin could fold around the needle tip and resist penetration. As they hydration and tension of each sample was neither measured, nor compared to in vivo conditions, this could have influenced the penetration efficiency observed in this chapter. Moreover, the thickness of the hypodermis, particularly in human skin, varied between specimens, therefore the subcutaneous fat was removed. As porcine skin from dorsal side of the ear was used, little to no subcutaneous fat was observed. The subsequent full thickness samples were placed on a double layer of compressed cork which were present to simulate the mechanical properties of underlying tissue (Martin et al. 2012). Many studies have used several materials to mimic the mechanical

properties of underlying skin layers, for instance soft sponge (Yan et al. 2010), clay (Kochhar et al. 2013) and gelatine gel (Moronkeji et al. 2017). Kochhar et al. (2013) compared the extent of MN penetration with substrate stiffness. It was determined that harder substrates resulted in the overestimation in the depth of MN penetration. In comparison to steel or clay, cork can be considered a relatively soft substrate. However, this does not mimic in vivo conditions, particularly the variability in the thickness of subcutaneous fat at different anatomical locations which could impact the ECG.

2.5.5 Limitations and further work

Studies conducted during Chapter 2 were subject to a number of limitations. MNs were manually applied to skin using a handheld digital force gauge which controlled pressing force, but not insertion velocity. A material testing machine similar to Davies et al. (2004), Donnelly et al. (2010) and Gittard et al. (2013) could be used in further studies to assess the effects of application speed on MN penetration over a wider range of forces. The use of a testing machine would also remove variability introduced by the operator. Alternatively, the digital force gauge could be attached to a manual test stand which could be used to control compression forces. Whilst controlling these variables is important when analysing data, when devices are used by patients and consumers, variability is likely to occur. Manual application of devices provides some insight into the variability of epoxy MN performance. Furthermore, to reliably assess the effects of velocity/impact energy on MN insertion, further studies could focus on the development and testing of an applicator which could apply MNs at a consistent speed and force (Singh et al. 2011; Prausnitz 2017). A simple patch applicator would aid untrained patients or their care providers when applying a MN device.

Due to limitations in the availability of ex vivo human skin, porcine skin was investigated and subsequently included in the study as a suitable alternative. Whilst porcine skin was anatomically similar to human, differences in MN penetration and microchannel dimensions were observed between the skin types. Whilst the use of skin explants in general is not truly representative of the environment in which these MNs would be applied, these models provide insight into how MNs would perform under certain conditions. Furthermore, only two samples of ex vivo human and porcine skin were used for each study. Whilst this allows for some sample variability, a small sample size (*n=6*) was used. Studies could be repeated using specimens from different donors of varying age to improve the validity of results. Finally, fresh, frozen skin explants were used in this chapter. Simple cryopreservation techniques such as freezing at -20˚C are the most widely used however, it has been shown that freezing results in the formation of ice crystals (Karlsson and Toner 1996) and changes in the skin's mechanical characteristics (Babu et al. 2003; Nielsen et al. 2011). For instance, Nielson and

colleagues demonstrated that storing human skin samples at -80°C for 3 weeks prior to use resulted in an overestimation of penetration rate and total penetration. It would be desirable to conduct further studies in vivo to assess MN performance in its target population. Whilst the literature provides conflicting evidence the freezing process could have contributed to the increased differences in MN penetration and microchannel dimensions.

2.6 Conclusion

This chapter aimed to characterise the geometry of epoxy MNs and understand their insertion performance in both ex vivo human and porcine skin models. SEM imaging revealed that each individual, out of plane MN was comprised of eight smooth planes forming a pyramidal structure and measured approximately 471µm in length (n=10). Epoxy MN arrays measuring 18mm in diameter were of interest in this chapter, as they are of similar diameter to the gel-soaked foam pad of a commercially available ECG monitoring wet electrode. This MN array was compared with alternative MNs which were manufactured with different geometries or using different materials. Overall, four different MN arrays measuring 500µm in length were manually inserted into skin explants. Compared with steel, silicon and 9mm epoxy arrays, the larger 18mm epoxy MN array resulted in the lowest overall penetration efficiency in human skin (58%). Repeating studies in porcine skin, highlighted comparable mean penetration efficiency between the arrays. When assessing the effect of downward application force on MN penetration, it was determined that as the force increased from 5N to 15N, penetration efficiency and channel depth increased. Pressing the 18mm epoxy MN arrays into human and porcine skin explants at 15N resulted in the greatest overall penetration efficiency of 87% and 86% respectively. Unlike depth, microchannel width was comparable at each force. Epoxy MNs were also inserted into skin explants using three application methods. Impact insertion resulted in the highest overall penetration in both human (93%) and porcine (95%) skin. Pressing MNs into skin at force of 15N resulted in the lowest penetration in human (71%) and porcine (69%) skin. Methylene blue, OCT imaging and histology provided en face and sub-surface confirmation of MN penetration in all studies.

Piercing the electrically insulated SC could be important in the acquisition of high-fidelity cardiac signals. Parameters including application force, method and geometry all influenced the extent of penetration. Further work is now required to develop a MN electrode and assess how MN parameters could influence the quality of recorded cardiac signals.

CHAPTER 3

IN VIVO COMPARISON OF ELECTRODE TECHNOLOGIES

3.1 Introduction

The previous chapter aimed to characterise MN insertion in both ex vivo human and porcine skin. Findings highlighted how differences in application force, method and needle geometry could influence insertion, which is an important aspect of MN-based sensors. This chapter will explore how epoxy MNs, introduced in Chapter 2, could be fabricated into an electrode capable of cardiac signal acquisition. This initial design will then be compared against the current gold standard wet electrode in a human volunteer study.

3.1.1 Types of ambulatory monitoring electrodes

Compared to the 10-second snapshot captured by the 12-lead ECG, AECG provides a view of cardiac data over extended periods of time (Madias 2019). The most common application of AECG monitoring is the outpatient diagnosis and assessment of cardiovascular arrhythmias including atrial fibrillation (AF) and atrial flutter. These arrhythmias are considered prothrombotic with consequences including sudden death and stroke (Kirchhof et al. 2016). Therefore, early detection and prompt intervention could prevent life-threatening consequences. Routine ambulatory monitoring of these conditions is generally conducted over 24 to 48 hours using Holter monitors (Kirchhof et al. 2016; Sutton et al. 2018; Madias 2019). However, the bulkiness and inconvenience of the device can reduce patient compliance and therefore, diagnostic effectiveness (Fung et al. 2015). Whilst the Holter is the current standard, the technology relating to cardiovascular disease detection is rapidly evolving.

3.1.1.1 Wet electrodes

Physiological signal monitoring generally involves the use of single-use, surface electrodes (NHS 2018). Holter monitors capture cardiac signals when electrodes are applied to the surface of the skin at specific locations. Ag/AgCl (silver/silver chloride) wet electrodes are the current gold standard due to their superior performance for very low to high frequency biopotential recordings (Grimnes and Martinsen 2014). These non-polarisable electrodes create a stable environment for use in physiological signal monitoring and are associated with a high SNR (Tallgren et al. 2005). These electrodes are generally composed of silver and use an electrolytic gel containing free ions as a means of conducting the signal between the skin and the electrode (Crawford and Doherty 2012). The main drawbacks regarding wet electrodes are their longevity and comfort. The reliance on the 'wet' component of the electrode poses numerous challenges, particularly for those patients who require a longer duration of ambulatory monitoring. The clinical impact of gel dehydration could result in misinterpretation, misdiagnosis and substandard patient experiences (Searle and Kirkup 2000; Ferree et al. 2001; Albulbul 2016). To improve signal quality and reduce the effect of skin impedance, ultra-fine grade sandpaper or disposable dry gauze wipes are used to partially abrade the outermost layer of skin (Tam and Webster 1977; Medina et al. 1989). However, as epidermal tissue remains in a state of constant turnover, the abraded layer is replaced over time (Houben et al. 2007). This breach in the skin's barrier coupled with the application of an electrolytic gel can result in irritation and cause patient discomfort. Although cases are rare, there have been concerns regarding the effect that the repeated application of wet electrodes has upon the skin, namely contact dermatitis (Uter and Schwanitz 1996; Avenel-audran et al. 2003).

3.1.1.2 Dry electrodes

Dry electrodes can be considered an alternative to wet electrodes as they do not require a bridging electrolytic gel, but rather they use mechanical force to push the electrode against the skin (Taheri et al. 1994). Numerous dry electrode designs are cited in the literature for ECG (Gruetzmann et al. 2007; Wang et al. 2011; Meziane et al. 2013; Chen et al. 2014). Whilst this electrode alternative offers several advantages, including rapid setup, user convenience, comfort due to the eradication of conductive gels and skin preparation, they are yet to achieve acceptance for medical use (Li et al. 2018). Dry electrodes are more sensitive to movement than wet electrodes immediately following their application (Searle and Kirkup 2000). However, after a short stabilisation time, allowing perspiration to fill the space between the skin and electrode, they have been reported to have less noise than the standard wet

electrode (Searle and Kirkup 2000). Numerous metals have been used as dry electrodes including stainless steel due to its availability, price and electrical performance (Bergey et al. 1971; De Luca et al. 1979). Whilst many studies have showcased promising results using metals, these materials are rigid and unable to conform to skin resulting in a loss of contact and subsequent charging effects (Gruetzmann et al. 2007). To address this issue, researchers have developed flexible or soft electrodes composed of rubber (Chen et al. 2014) or fabric (Mestrovic et al. 2007; An and Stylios 2018) which can conform to the body (Gruetzmann et al. 2007; Gargiulo et al. 2008). Gruetzmann and colleagues used a foam electrode which displayed excellent stability with increased resistance to motion artifacts when compared with the wet Ag/AgCl electrode (Gruetzmann et al. 2007).

3.1.1.3 Microneedle electrodes

MN electrodes are being explored as another promising alternative to address some of the challenges posed by wet electrodes. The SC is largely composed of dead skin cells and is therefore highly resistive. This increased resistance can greatly degrade signal quality. As MNs can circumvent the electrically insulated SC, they can access underlying epidermal layers which have a higher electrical conductivity, comparable to that of an electrolyte (Griss et al. 2001). This negates the need for conductive gels and removes the requirement for skin abrasion. Additionally, contacting the more conductive skin layers provides the potential to improve signal fidelity. Furthermore, the length of MNs can be optimised to avoid stimulating nerve endings found within skin. Forvi and colleagues assessed the use of MN-based dry electrodes when recording physiological signals in healthy volunteers (Forvi et al. 2012). Whilst the sample size was small, in the short-term the silicon MN electrode arrays demonstrated performances comparable to that of the wet electrodes under static conditions.

Whilst advancements allow for the production of several novel monitoring electrodes and devices, the testing of these systems for clinical purposes remains challenging. There are a lack of unified performance methods or models for testing novel devices. Furthermore, long-term studies regarding hygiene, comfort and safety of this technology for ECG purposes is limited.

3.1.2 Sources of artifacts in the electrocardiogram

During signal acquisition, various artifacts are often merged with cardiac data (Van Alsté and Schilder 1985; Friesen et al. 1990; Singh and Tiwari 2006; Kher 2019; Xie et al. 2020). Artifacts are a common problem when recording biopotential data. They can be defined as unwanted electrical signals, not of cardiac origin. Multiple types exist, but all can interfere with, and

reduce the diagnostic quality of ECG traces. Distortion of the true cardiac signal could result in misdiagnosis and mismanagement (Chase and Brady 2000). Chase and Brady (2000) highlighted that upon interpretation, ECG artifacts resulted in false pathological changes such as ischaemic disease and arrhythmias. Some of these artifacts occur at similar frequencies as components within the ECG waveform such as the P and T waves (Figure 3.1).
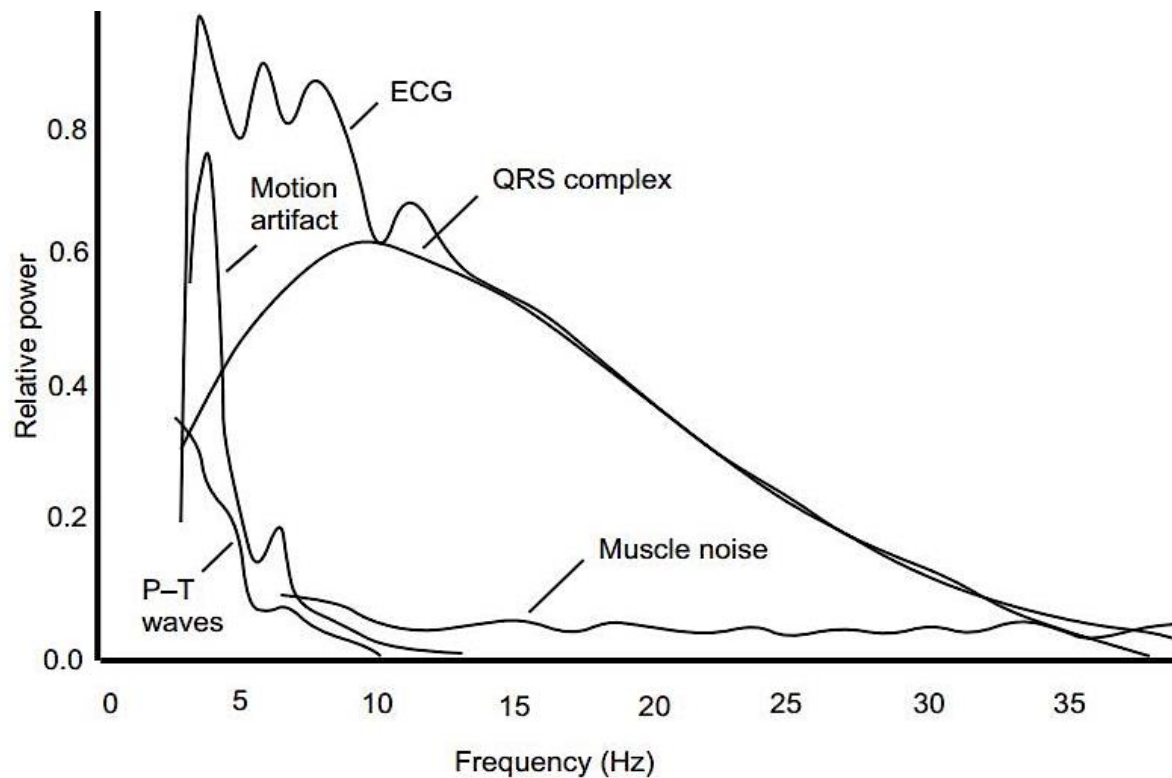
Figure 3.1: Relative power spectra of P/T waves, QRS complex, EMG noise and motion artifacts. Power spectra is based upon an average of 150 beats. Image has been adapted from Afonso 1993.

This creates obstacles for clinicians when making a diagnosis (Sareen et al. 2018). Whilst the acquisition of cardiac data can be problematic, signal processing is not without its own unique set of challenges. Signal processing typically involves a series of steps which aim to remove or reduce artifacts to allow for confident ECG interpretation. Following data collection, cardiac signals are pre-processed to improve the quality of the raw signal and remove several artifacts. Within the literature, artifacts can be classified into five main groups, namely baseline wander (BW), powerline interference (PLI), muscle contraction (EMG noise), electrode motion artifacts and electrode contact noise (Zywietz and Willems 1987; Willigenburg et al. 2012; Grimnes and Martinsen 2014; Serhani et al. 2020). Depending upon the type of artifact, methods used to address them can vary.

3.1.2.1 Baseline wander (BW)

A common artifact observed in patients, particularly with respiratory conditions, such as chronic obstructive pulmonary disease or during hyperventilation is termed respiratory swing, or BW. Chest wall movement results in electrode and lead movement as well as stretching of the skin. BW also termed baseline drift is a low frequency artifact where the x-axis of the signal appears to 'wander' or migrate up and down rather than follow a straight line (Gupta et al. 2015; Kher 2019). This results in the entire signal shifting from its normal baseline as shown in Figure 3.2.
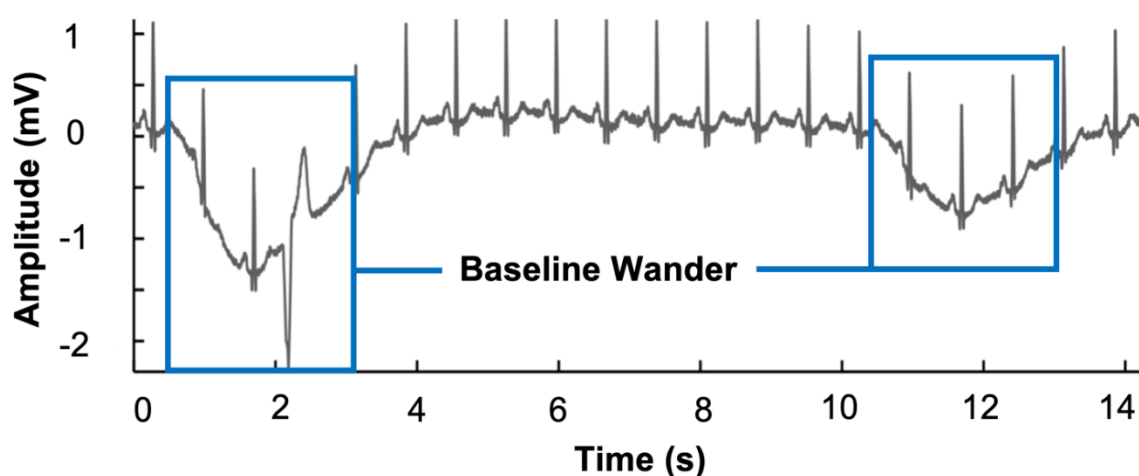
Figure 3.2: Electrocardiogram corrupted with baseline wander. Artifact removal is necessary when diagnosing changes in the ST segment. Areas of baseline wander are highlighted within the Figure by the blue boxes. Image adapted from Lenis et al. (2017).

BW can hinder the detection of certain components of the ECG, particularly the ST segment. Elevation or depression of the ST segment is an important marker when managing ACS (NICE 2014; Ibanez et al. 2018). Minor baseline fluctuations can have a substantial effect on the resultant diagnosis as it may lead to STEMI patients being classified as NSTEMI or vice versa. This, therefore, has a considerable effect on the therapeutic approach taken. BW typically results from patient movement, respiration and electrically charged electrodes (Gupta et al. 2015). This artifact occurs at approximately 0.5Hz, however increased movement, for example during a stress test, increases the frequency content of BW (Sörnmo and Laguna 2005; Kher 2019). Cardiac stress tests aim to measure cardiac response to exercise, and study coronary circulation in comparison to resting conditions (Kharabsheh et al. 2006; Pelliccia et al. 2021). This test should be stopped, if, among other criteria, significant ST changes appear on the resultant ECG trace (Pelliccia et al. 2021). Assessing ST segment changes can prove

challenging if the baseline is not constant (Froning et al. 1988; Lenis et al. 2017). Removal of BW is a standard processing step in many devices or post-processing algorithms (Serhani et al. 2020). A straightforward approach to remove BW is through the design and implementation of a high-pass filter. This type of filter is especially useful at removing low-frequency components (Blanco-Velasco et al. 2008). High-pass filters pass signals with a frequency that is higher than a defined cut-off point, whilst attenuating signals with frequencies below the cut-off point (Huelsman 2003; Isaksen et al. 2017). This cut-off frequency should be determined to reduce distortion of the ECG, particularly the ST segment. Guidance provided by the Society for Cardiological Science and Technology (SCST) states that the lower frequency cut-off should be no higher than 0.67Hz in 'auto' mode, which refers to 'computer processed' signals. The most frequent cut-off frequency observed in the literature was 0.5Hz (Kligfield et al. 2007; Censi et al. 2009; Venkatachalam et al. 2011; Buendía-Fuentes et al. 2012). In 'manual' mode, however, where the ECG is expressed in real-time without a delay, the lower frequency cut-off should be reduced to 0.05Hz to avoid ST segmented distortion (Campbell et al. 2017). Implementation of a filter with a 0.05Hz cut-off results in better reproduction of ST segments whilst also reducing direct current (DC) voltages, which occur around 0Hz. The trade-off however, when using this lower cut-off is increased baseline drift.

3.1.2.2 Powerline interference and electrical artifact

Environments where cardiac signals are captured can easily become contaminated by electrical artifacts. In the clinical setting, surrounding areas can include various machines including ventilators and personal electronic equipment (Venkatachalam et al. 2011). Other departments may also be in close proximity to where the ECG is being recorded. Large electromagnetic fields, for example from the radiography department, can result in high levels of electrical artifact being recorded (Venkatachalam et al. 2011). These problems either cause electrical artifact in the form of electrical field coupling, or magnetic induction. When the mains supply and/or mains cable between the wall socket and the electrocardiograph come into close proximity with an electrical field, electrical field coupling results (Venkatachalam et al. 2011). If this field interacts with the patient, ECG leads and/or electrocardiograph a stored charge is formed. This stored charge, termed capacitance, can flow to ground through the mains cable and not contaminate the ECG. Alternatively, this charge can flow to an ECG lead, through the electrode and skin creating interference before being grounded by the patient. This form of artifact typically appears as spikes in the baseline which are equally spaced and of similar amplitude as shown in Figure 3.3 (Kher 2019).
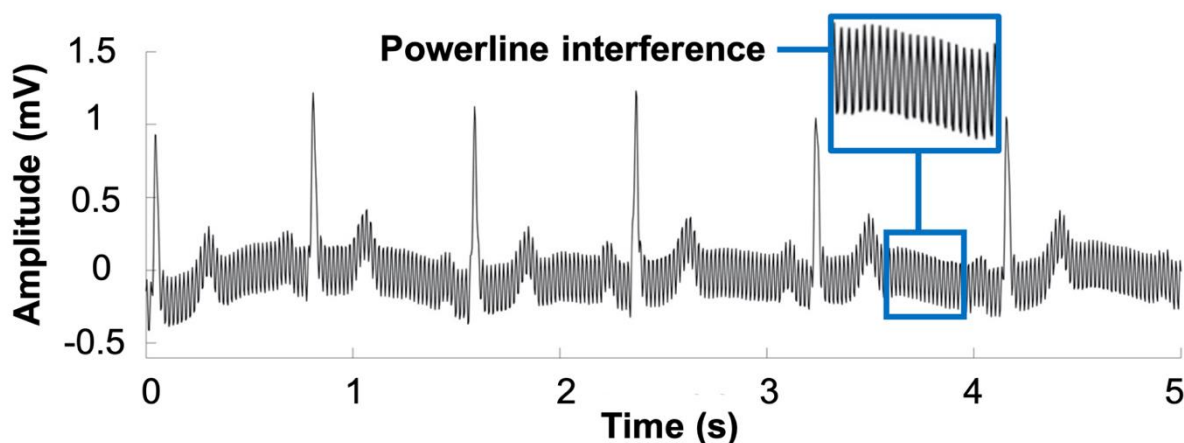
Figure 3.3: Electrocardiogram corrupted with powerline interference. As shown, the artifact completely superimposes the low frequency P wave. Area of interference is highlighted by the blue box. Authors own image. Data captured from a 26-year-old male. For improved visualisation only 5 seconds of data shown.

Fifty spikes per second are observed when recording ECGs in the UK and Europe whilst sixty spikes per second are observed in the USA and parts of Asia. This corresponds to the frequency of mains power supply, which is 50Hz in the UK and Europe, and 60Hz in the USA and parts of Asia. Occasionally, harmonics of these frequencies are observed. PLI and subsequent harmonics can distort the ECG significantly making interpretation and analysis challenging as spurious waveforms are introduced into the trace. An electrocardiograph is generally powered by mains electricity. As the machine will be connected to patients, the equipment is grounded. If the electrocardiograph is the only machine connected to the patient and assuming that the earth system is functioning, with no other problems such as damaged cables, no electrical artifacts should be observed in the resultant ECG trace. If the patient however is connected to other devices also powered by a mains supply, for instance an infusion pump, all connected machines will be earthed via the mains supply through sockets. Electrical artifacts tend to occur when different earth impedances exist between each piece of electrical equipment. If a machine, such as a ventilator, is attached to an earth at a higher impedance than the electrocardiograph, trace current will flow from the ventilator, through the patient, into the ECG leads and finally the electrocardiograph where it is grounded. Electrical devices can leak small currents to ground. If this leakage is less than the level of earth leakage protection, they can go unnoticed. However, if a patient is connected to the ECG recording equipment when a fault occurs this can have considerable health implications. If the current is of sufficient magnitude, an electrical shock can occur which could prove fatal, therefore, ground loop problems have important safety implications. In addition to ground loop problems,

poorly maintained ECG lead cables for instance, roughly handled, over-stretched or caught within the wheels of the ECG machine, will result in internal broken wires. This can subsequently act as an antenna when an electrode is attached as it is no longer in good contact with the corresponding lead. This results in the induction of high electrical potentials in the lead as a result of the surrounding environment. As discussed previously, this electrical noise occurs at 50Hz in the UK and has a bandwidth of less than 1Hz. This frequency is very different to that of the ECG; therefore, it can be removed. Whilst it is desirable, to rectify the cause, PLI is always a problem during physiological signal recordings. To reduce this form of electrical artifact, shielded ECG leads can be used, where the shield is grounded at the ECG machine. Techniques such as using common mode rejection filtering in the amplifiers, raising the input impedance of the amplifiers and reducing the skin-electrode impedance can reduce the level of electrical interference (Crawford and Doherty 2012). Furthermore, many ECG machines contain internal filters which can remove PLI without distorting the ECG. A notch filter, also termed a band-stop filter, is a filter which has a very narrow bandwidth and can reject a single, or very small band of frequencies. All filters introduce distortion in the resulting output signal however, it has been reported that notch filters do not cause appreciable distortion to human ECG signals (Bock et al. 2000; Gruetzmann et al. 2007; Beck et al. 2009; Vale-Cardoso and Guimarães 2010) however differing opinions exist within the literature (Levkov et al. 2005).

3.1.2.3 Electromyographic noise (EMG)

EMG is a diagnostic procedure which evaluates the health of muscles and the nerves that control them. Whilst this is an important clinical test which helps diagnose neuromuscular abnormalities, the presence of muscle noise can overwhelm cardiac signals (Sadikoglu et al. 2017). Myographic noise is a form of physiological artifact which occurs when muscles contract within the vicinity of the electrodes. The presence of this type of artifact represents a major problem in many ECG applications particularly during exercise tests and ambulatory ECGs. Compared with the electrical signals produced by cardiac muscle, skeletal muscle, when contracted, produces signals which are much larger in amplitude and therefore can obscure low amplitude waveforms (Limaye and Deshmukh 2016). EMG noise typically appears as spikes within the baseline which occur at irregular intervals and amplitudes as shown in Figure 3.4. As shown by the Figure, when both ECG and EMG are captured, the PQRS and T waves are not easily discernible.
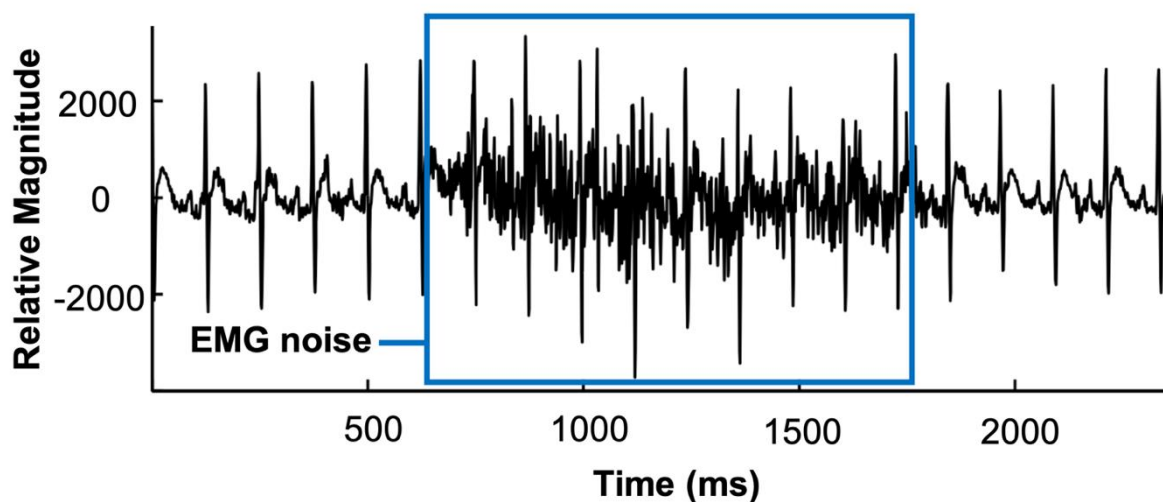
Figure 3.4: Electrocardiogram corrupted with muscle noise. As shown, electromyographic noise can overwhelm cardiac signals, particularly low amplitude waveforms such as the P wave. An area of muscle contraction is highlighted by the blue box. Image adapted from Raphisak et al. (2004).

This form of artifact is typically intermittent i.e., whilst the patient moves. Alternatively, this artifact can be continuous in certain patient groups for instance individuals with an uncontrollable tremor or neurological condition such as Parkinson's Disease (Pérez-Riera et al. 2018). This myographic noise is known to cause changes in the ECG which can mimic dangerous arrhythmias (Srikureja et al. 2000). Upon relaxation of the muscle, the artifact stops or partially reduces. It is, therefore, imperative that a patient relaxes during an ECG recording in an attempt to remove or reduce this artifact. In certain circumstances, this may not be possible for instance in a patient who may have a tremor due to an underlying condition or cannot fully relax their muscles. In comparison to the BW and PLI, muscle noise cannot be removed using filters as the spectral content of muscle activity overlaps with that of the ECG waves (PQRST) (Tereshchenko and Josephson 2015). As the heartbeat is a repetitive signal, techniques can be used to reduce the effects of muscle noise in a similar manner to the processing of evoked potentials. As EMG is a high-frequency artifact, a moving average filter could be applied to the data. Whilst this would remove, or at least reduce EMG noise from the cardiac signals, there is still a need to develop methods to reduce the influence of muscle noise on the ECG trace (Sörnmo and Laguna 2005; Kher 2019).

3.1.2.4 Motion artifact

Whilst Ag/AgCl electrodes are the current electrode of choice during ECG monitoring, the largest concern when using this type of electrode is the noise associated with motion artifact. Motion artifact is an overarching term which incorporates myographic noise, but also artifacts

resulting from electrode movement and vibrations from the surrounding environment. Electrode motion artifacts are particularly bothersome during AECG monitoring as their morphology and frequency are unpredictable. This form of motion artifact is predominantly caused by the stretching of skin underneath the electrodes which alters the skin's impedance (Tam and Webster 1977; Odman and Oberg 1982; Cömert and Hyttinen 2015). Within an ECG trace, deformation of skin results in an electrical potential of several millivolts (mV) presenting on the subsequent ECG trace as large amplitude waveforms which could be misinterpreted as QRS complexes (Figure 3.5).
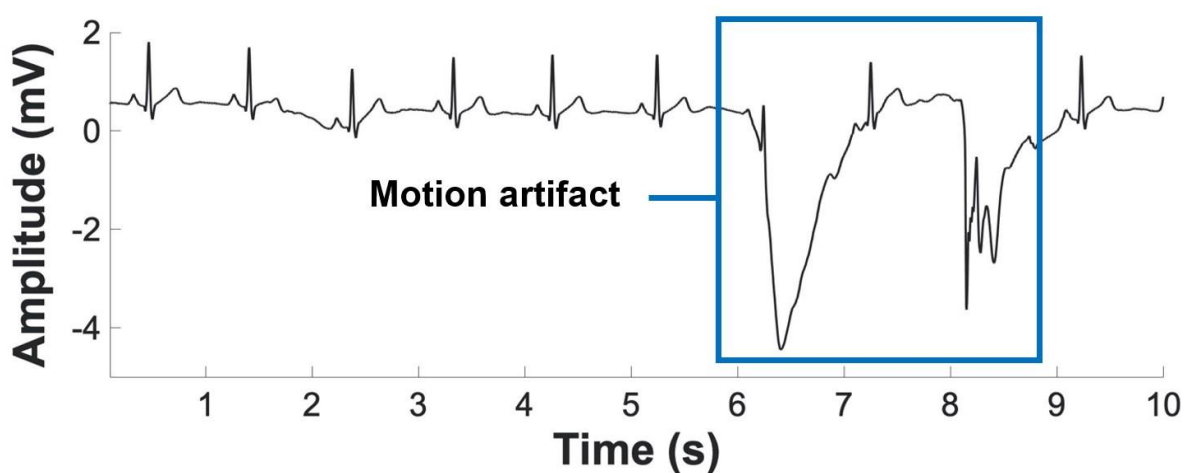
Figure 3.5: Electrocardiogram affected by electrode motion artifact. An area of motion artifact is highlighted by the blue box. Authors own image. Data captured from a 26-year-old male. For improved visualisation only 10 seconds of data shown.

With respect to AECG monitoring, electrode motion artifacts constitute the main source of falsely detected heartbeats (Kher 2019). Motion artifacts can also transpire when changes occur between boundaries such as the electrode-electrolyte interface and the electrolyte-skin interface (Hamilton et al. 2000). New electrode designs have aided a reduction in this form of motion artifact, however the presence of excess sweat, poor skin preparation techniques, application of body lotions and poor adhesive quality can result in movement of the electrode and hence contribute to electrode charges at the electrolyte-skin interface (Crawford and Doherty 2012). Performing chest compressions or trying to record cardiac data whilst travelling in an ambulance can result in motion artifact. Vibrations from the environment can also be captured alongside cardiac activity (Crawford and Doherty 2012).

3.1.3 Comparing electrode performance in human volunteers

When comparing device performance numerous research groups test wearables in human volunteers (Chen et al. 2016; Chlaihawi et al. 2018; Dong et al. 2021). Following signal acquisition several approaches can be used to evaluate the data. Nearly all publications evaluating wearables perform qualitative visual comparisons (Chlaihawi et al. 2018). This involves plotting traces recorded from each device on the same Figure. Key ECG characteristics (PQRST) are routinely annotated on the traces demonstrating the ability of devices in recording physiological signals. From these traces, basic assessments such as HR and heart rate variability (HRV) (Mahdiani et al. 2015; Burma et al. 2021) can be conducted. When data are recorded under dynamic conditions e.g., walking or arm swinging, visual trace comparisons can highlight specific artifacts such motion (Chlaihawi et al. 2018; Zahed et al. 2020). Artifacts such as PLI can also be visually observed in traces and through Fast Fourier Transform (FFT) which converts signals from the time domain to the frequency domain. Specific frequencies and magnitudes of ECG spectral components/artifacts can also be obtained (Prasad and Parthasarathy 2018; Fink et al. 2021).

Qualitative data, however, is often difficult to compare between novel devices and the standard wet electrode. Following signal acquisition several methods can be used to quantitatively evaluate device performance. Publications including Wu et al. (2018), O'Sullivan et al. (2019) and Dong et al. (2021) collected SNR as an indicator of signal quality and used it to compare device performance. SNR estimates signal quality by comparing the level of a desired signal to the level of background noise. Specific SNR equations vary however, they are all defined as a ratio of signal power to noise power and expressed in decibels (dB).

Skin-electrode impedance is a further method of assessing electrode performance. This technique evaluates the contact between electrodes and skin. High or unstable impedances are often associated with poor quality traces. O'Mahony et al. (2016) investigated the effects of contact force on skin-electrode impedance using compression bandages on a single human volunteer. As contact force increased, skin-electrode impedance declined. When comparing wet and MN electrodes O'Mahony and colleagues found that the use of two/three bandage layers significantly improved the mean SNR of MN electrodes. The authors concluded that the improved SNR observed with increasing application force was the result of a decrease in the skin-electrode impedance which occurred when skin-electrode contact improved. Alternative methods include peak-to-peak signal amplitude and correlation which can be used to compare electrode performance (Chlaihawi et al. 2018).

3.1.4 Aims and objectives of the chapter

This chapter aimed to compare the functionality of an initial MN electrode prototype with a commercially available adult ECG monitoring wet electrode when recording cardiac signals from healthy adult volunteers at rest. The objectives were to:

- To use metallised epoxy MNs, supplied by Tyndall National Institute, to fabricate MN electrodes capable of capturing cardiac signals.
- To design a study, construct all the necessary documentation and gain the ethical approvals required to record cardiac activity using an initial MN electrode prototype and commercially available wet electrode in healthy adult volunteers.
- To develop a quantitative method of calculating the SNR of acquired cardiac signals in MATLAB using pilot study data.
- To simultaneously record cardiac signals using wet and MN electrodes from ten volunteers under resting conditions and use the data:
  - To design and implement digital filters, using MATLAB, to reduce the effects of artifacts in the recorded ECG traces.
  - To quantitatively compare and assess the performance of MN electrodes with commercially available wet electrodes by calculating the SNR of recorded ECG traces.
  - To visually assess and compare ECG traces captured using MN electrodes and commercially available wet electrodes.
- To capture images of the volunteers' skin to assess the effects of both MN and wet electrodes.

3.2 Materials

Details of equipment and reagents used in the studies described below are listed in the equipment and reagents tables. Cardiac data was acquired using the OpenBCI GUI version 5.0.6 (OpenBCI, USA). Data processing was conducted using Microsoft Excel version 16.46 (Microsoft Corporation, USA) and MATLAB 2018a (The MathWorks Inc., Natick, MA). Image processing was conducted using ImageJ software (NIH, USA) and Microsoft PowerPoint version 16.37 (Microsoft Corporation, USA).

3.3 Methods

3.3.1 Epoxy microneedle electrode fabrication

Epoxy MN arrays (Figure 3.6a) were fabricated by a collaborator, Tyndall National Institute, using the method described in Chapter 2. For the polymer MNs to conduct a signal, a 20nm titanium adhesion layer, followed by a 200nm layer of gold was coated on both sides of the MN wafer (Figure 3.6b) by our collaborators, using a metal evaporator (O'Mahony et al. 2016).
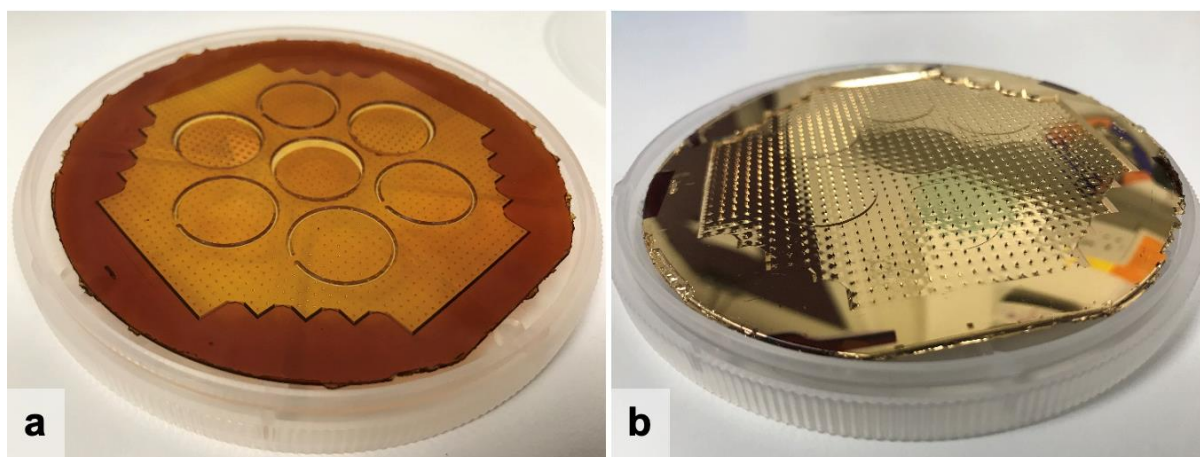
Figure 3.6: Epoxy microneedle wafer before (**a**) and after (**b**) metallisation. Each wafer contained seven individual microneedle arrays measuring 18mm in diameter. Microneedles measured approximately 500μm in length.

To create a wearable MN electrode, the gel-soaked foam pads were carefully removed from commercially available adult ECG monitoring wet electrodes using a scalpel. Equal amounts of part 'A' and part 'B' of the conductive adhesive epoxy were mixed thoroughly for 2 minutes and applied to the electrode, as demonstrated in Figure 3.7d. Individual metallised MN arrays were then detached from the wafer and affixed to the centre of the electrodes. A wooden rod was used to gently press down on the arrays to avoid damaging the gold coating. The manufactured MN electrodes were left at room temperature for a minimum of 4 hours to cure. Following this, electrode continuity was assessed using a digital multimeter. An audible beep

indicated that a complete path for current to flow was present. Electrodes which passed the continuity test were deemed capable of conducting and were subsequently used in the clinical study. Resistance between the snap on conductor and surface of the MN were crudely measured using a digital multimeter for 10 seconds and the mean value was calculated. For storage purposes MN electrodes were protected by the plastic cover that formed part of the initial wet electrode. To allow for a comparison between wet electrodes, the diameter of the MN array was chosen to be equal to that of the 18mm foam pad (Figure 3.7). As MNs were in direct contact with skin, they were sterilised using 70% v/v ethanol before electrode fabrication.
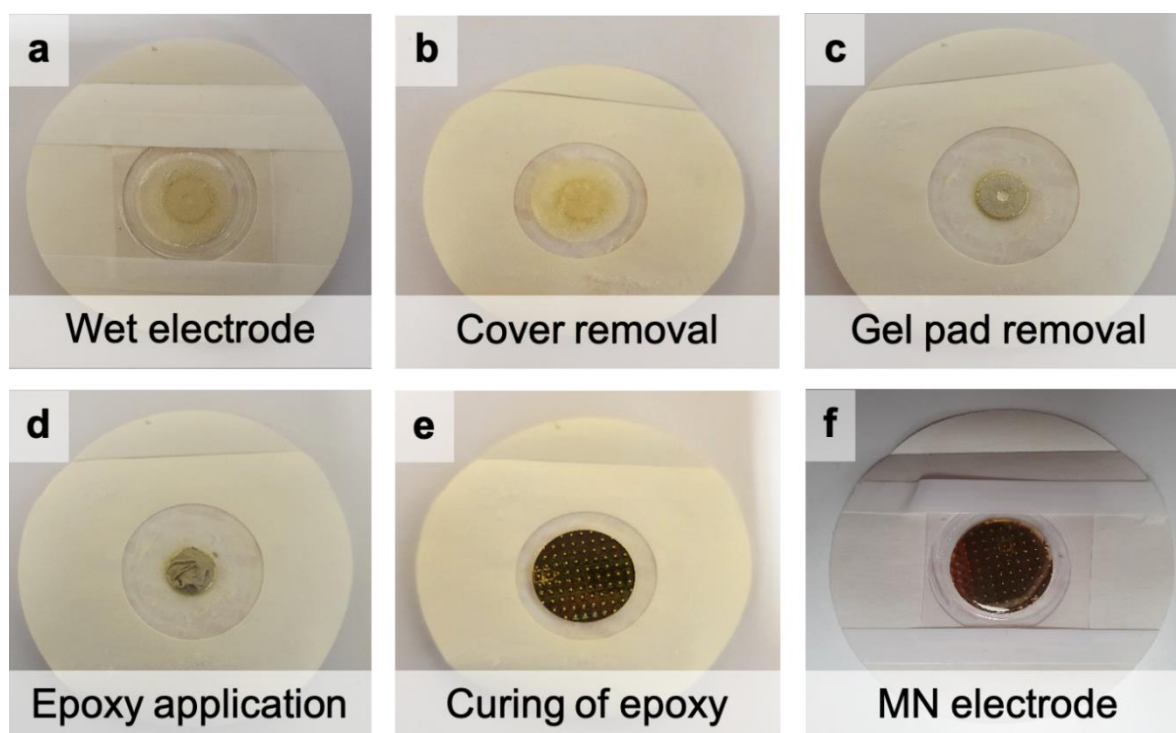
Figure 3.7: Process of microneedle electrode fabrication. The protective cover of a wet ECG electrode (**a**) was removed (**b**), followed by the removal of the electrolytic gel-soaked foam pad (**c**). Conductive adhesive epoxy was applied to the electrode (**d**) and individual microneedle arrays were applied and left to cure (**e**). The initial protective cover was replaced to protect the microneedles from damage whilst in storage.

3.3.2 Ethics application and study development

The study discussed below was approved by Cardiff School of Pharmacy and Pharmaceutical Sciences Ethics Committee Ref: A1819-15 (Appendix I).

3.3.2.1 Eligibility and recruitment

Study volunteers were aged 18 years and older, with no known cardiac history or allergy to any of the materials used. Recruitment occurred via word of mouth, through existing contacts and/or recruitment email (Appendix II). Prospective volunteers were provided with a consent

form (Appendix III) and participant information sheet (Appendix IV) and given 72 hours to decide whether they wished to be involved.

3.3.2.2 Pilot study

Prior to the main study, a pilot was conducted using three healthy, adult volunteers. Informed consent was acquired prior to data collection. All recordings were conducted in private consultation rooms at Cardiff School of Pharmacy and Pharmaceutical Sciences. The participant was placed in a semi-recumbent position at an approximate 45⁰ angle. Wet electrodes were placed in the positions shown in Figure 3.8. Each single-use MN and wet electrode were connected to a separate channel on an OpenBCI Cyton biosensing board. In total, 3 minutes of cardiac data were recorded from each participant and transferred wirelessly using Bluetooth. Cardiac data was captured using a sampling frequency of 250Hz, at a maximum gain of x24, in a lead II configuration. This study was conducted to develop and optimise the ECG recording procedure and management of data.
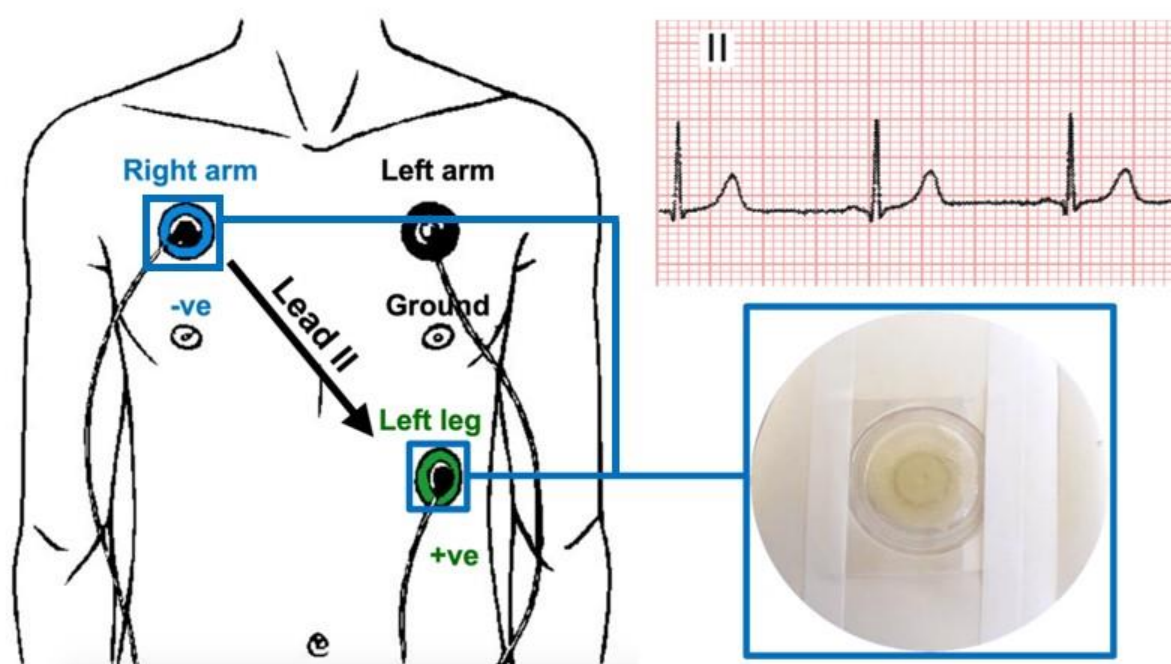
Figure 3.8: Positioning of wet electrodes on the torso of volunteers. Electrodes were placed to achieve a lead II configuration which measures the potential difference between the right arm and left leg. Electrodes were applied below the right (negative) and left (ground) clavicle as well as left of the umbilicus (positive). An example of a lead II ECG is shown. Image adapted from Goldberger et al. 2018.

3.3.2.3 Main study protocol

All cardiac data recordings were conducted in a private consultation room at Cardiff School of Pharmacy and Pharmaceutical Sciences. Before data collection informed consent was obtained. On the day of recording, participants were placed in a semi-recumbent position at

an approximate 45° angle to minimise movement. Both unmodified, commercial wet electrodes and epoxy MN electrodes were applied to the torso of each volunteer (Figure 3.9) and held in place by a simple adhesive.
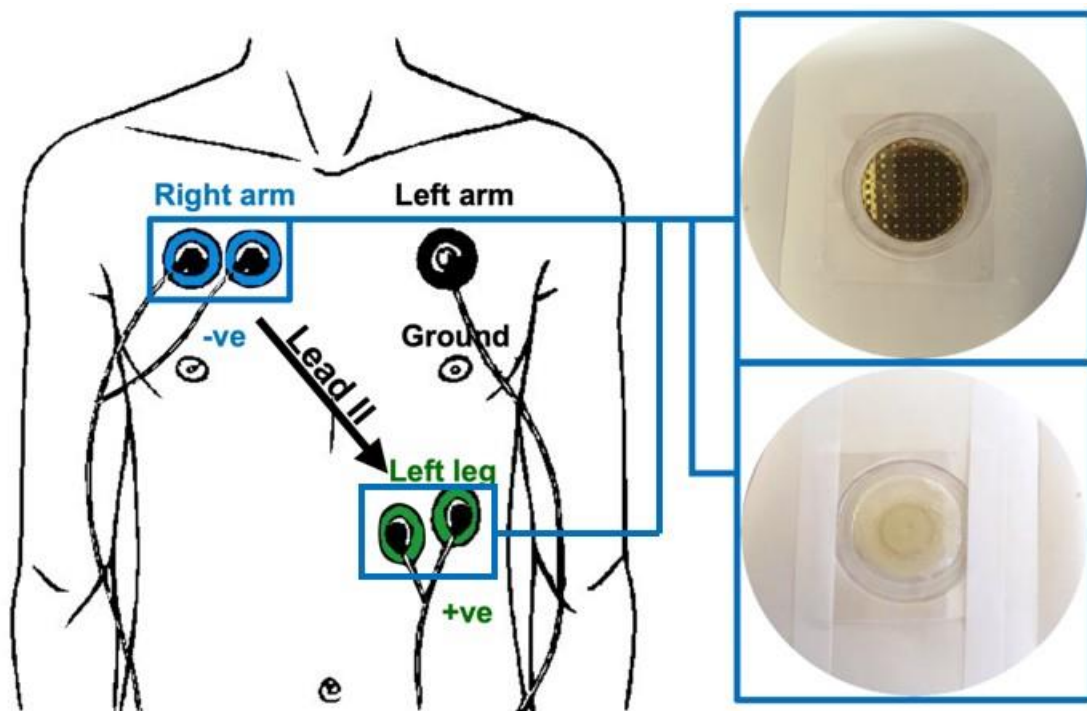
Figure 3.9: Positioning of wet and microneedle electrodes on the torso of volunteers. Electrodes were applied to achieve a lead II configuration which measures the potential difference between the right arm and left leg. Below the right collarbone, one wet electrode and one microneedle electrode were placed. A single wet electrode was applied beneath the left collarbone. On the lower abdomen a single wet electrode and microneedle electrode was applied. Data was simultaneously acquired from each type of electrode.

A wet and MN electrode was placed underneath the right clavicle whilst a single wet electrode was placed beneath the left clavicle. Care was taken not to apply these electrodes directly to the bony area. An additional wet and MN electrode was placed left of the umbilicus. Before signal acquisition, volunteers were asked to press firmly down on the centre of each electrode for 10 seconds. This was taken to ensure that all electrodes were in good contact with skin. Each single-use electrode was connected to a separate channel on a biosensing board (Figure 3.10). No external methods of skin preparation were conducted such as abrasive wipes or hair removal, however the wet electrodes used contained a gel-soaked abrader disc. Data were captured using the same communication methods, sampling frequency and gain as the pilot study. In total, three recordings were captured, each lasting 60 seconds. Following electrode removal, images were taken of the volunteers' skin to observe the effects of the adhesive, gel-

soaked pads and MNs on human skin. Images captured the area of skin directly contacting the electrodes and did not contain any identifying features.
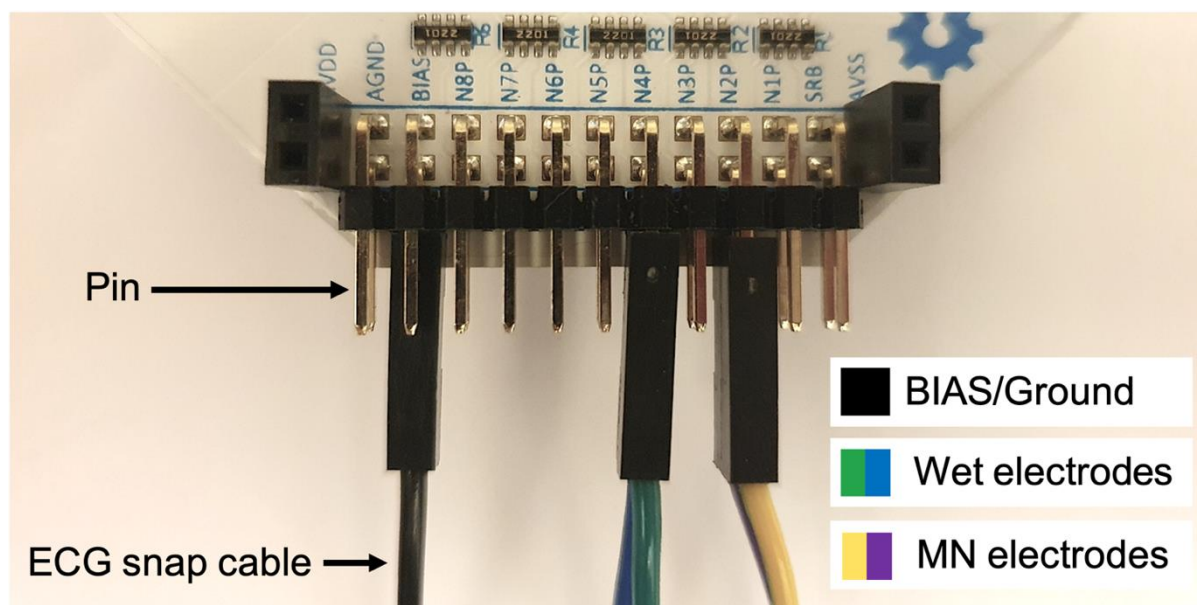
Figure 3.10: Connection of snap cables to the Cyton biosensing board. Black lead is connected to the BIAS pin which acts as the ground. Green/blue leads are connected to the N4P and N4N pins which act as the positive and negative for the wet electrodes. Yellow/purple leads are connected to the N2P and N2N which act as the positive and negative for the microneedle electrodes.

3.3.2.4 Clinical review of recorded traces

Whilst the interpretation and physiological impact of the traces were not investigated, data collected in this study could have clinical implications. For ethical reasons, a consultant cardiologist and electrophysiologist, Dr Peter O'Callaghan, was contacted and subsequently agreed to review the ECG traces within 28 days of recording. As Dr O'Callaghan reviewed the data from a clinical perspective, only the traces recorded with the conventional and clinically established wet electrode were reviewed. ECG traces produced from MN electrodes were not clinically interpreted as they were novel, and not clinically approved. Participants were only contacted if a potential problem was identified. Depending upon the problem identified, participants would be instructed with respect to the appropriate action to take.

3.3.3 Quantitative comparisons of electrode performance

All recorded data was anonymised using a numerical identifier to maintain subject confidentiality. The anonymised data was stored in its unprocessed state on an encrypted external hard drive to further protect the confidentiality of data. Methods of data management and analysis were developed and optimised using pilot study data in MATLAB.

3.3.3.1 Magnitude of powerline interference

The susceptibility of electrodes to PLI was assessed by plotting the FFT of signals using MATLAB (Appendix V). The frequency and magnitude of PLI captured alongside cardiac activity was determined by obtaining the peak amplitude of the signal occurring at approximately 50Hz.

3.3.3.2 Calculating signal-to-noise ratio

To quantitatively compare the performance of each electrode, MATLAB code was developed using pilot data. The specific steps taken will be discussed in more detail below as results informed the development of the SNR calculation. Data were filtered with a digital high-pass filter with cut-off frequency of 0.5Hz to remove BW and DC offset. FFT of the resultant signals were plotted to identify the most prevalent PLI frequencies.

To isolate the signal, a digital lowpass filter with 40Hz cut-off frequency was designed in MATLAB and applied to the data. Signal power was subsequently determined by taking the maximum and minimum values of the ECG which were found within the QRS complex of filtered signals. As the maximum and minimum values varied with each heartbeat, six QRS complexes were selected. Throughout the 60 second trace, an overall mean maximum and minimum were calculated. To isolate noise, a second digital high-pass filter with a cut-off frequency of 40Hz was designed and applied to the data. Noise power was determined by calculating the standard deviation of the noise and multiplying this by four to have a 95% confidence interval.

During signal acquisition, three 60 second recordings were captured from each volunteer. SNR was calculated for each 60 second recording and was subsequently averaged to provide a mean SNR for each volunteer. In addition, an overall mean was also taken to produce a single SNR for each type of electrode. The equations used to calculate SNR are shown in Figure 3.11.

$$\text{Signal power } (V_{pp}) = \text{maximum (QRS)} - \text{minimum (QRS)}$$
$$\text{Noise power} = 4 * \text{standard deviation (noise)}$$
$$SNR(dB) = 20\log_{10} * (\text{signal power / noise power})$$

Figure 3.11: Equations used to calculate the signal to noise ratio of cardiac signals recorded by both electrode designs. Signal power was calculated by subtracting the minimum component of the QRS complex from the maximum. Noise was isolated using a digital high-pass filter.

3.3.4 Qualitative comparisons of electrode performance

To qualitatively compare electrode performance, visual comparisons were made. Using MATLAB, raw cardiac data was imported into the workspace. Data were initially managed using the code documented in Appendix V. A 0.5Hz high-pass filter designed using MATLAB was applied offline to remove BW and DC offset. To limit the effects of DSP a notch filter was not applied to the data. Traces were plotted using code similar to that provided in Appendix V. For visual comparisons, only the first 5 seconds of data was plotted to allow for improved visualisation of trace characteristics e.g., PQRST and clear identification of the traces recorded by each electrode.

3.3.5 Statistical analysis

To determine statistical significance of mean SNR data, a 2-sample independent t-test was calculated using the statistical software package SPSS. Significance was defined as $p < 0.05$.

3.4 Results

3.4.1 Polymeric microneedle electrode fabrication

To create a simple, wearable MN electrode prototype, commercially available wet electrodes were adapted to incorporate metallised MN arrays (Figure 3.12). Continuity was used to test if a complete path for current flow was present in the newly created MN electrodes. All fabricated MN electrodes resulted in an audible bleep and therefore passed the continuity test. Electrode resistance was also measured. Resistance values were variable therefore a mean was taken over the course of 30 seconds. The mean resistance of microneedle electrodes was 1.72Ω ±0.35 (*n=10*).
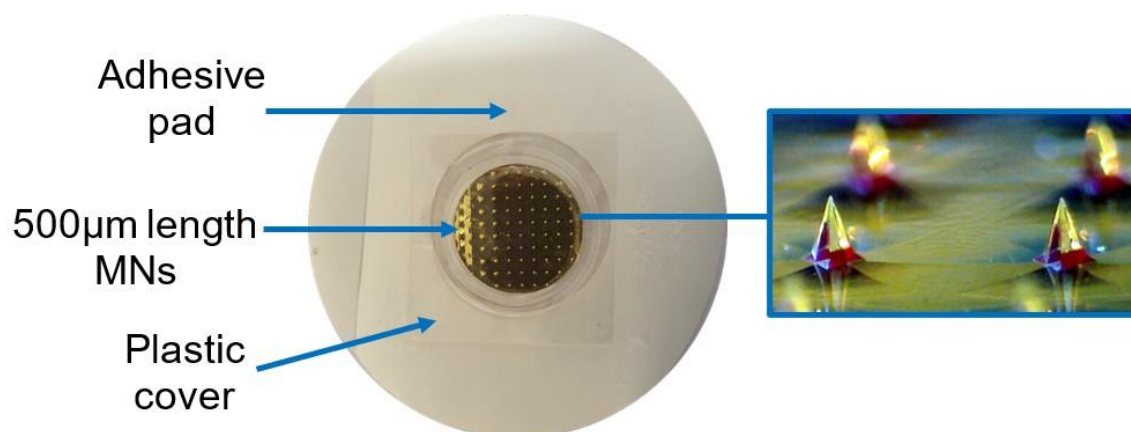
Figure 3.12: Microneedle electrode adapted from a wet electrode. Gold-coated array measuring 18mm in diameter and containing 500μm length microneedles was adhered to a 3M Red Dot 2239 pre-gelled adult ECG monitoring electrode. Stereomicroscope image demonstrates a magnified view of individual metallised microneedles.

3.4.2 Pilot study and data management

3.4.2.1 Initial management of cardiac data

A pilot study was conducted to develop a procedure for ECG recording and method of data management prior to subsequent electrode comparisons. Following informed consent, cardiac data was recorded from three human volunteers using wet electrodes. In total, 3 minutes of cardiac data was recorded from each volunteer using a biosensing board. Data was communicated at a 250Hz sample rate over Bluetooth to the GUI. Raw, numerical data were imported and managed using MATLAB (Figure 3.13).
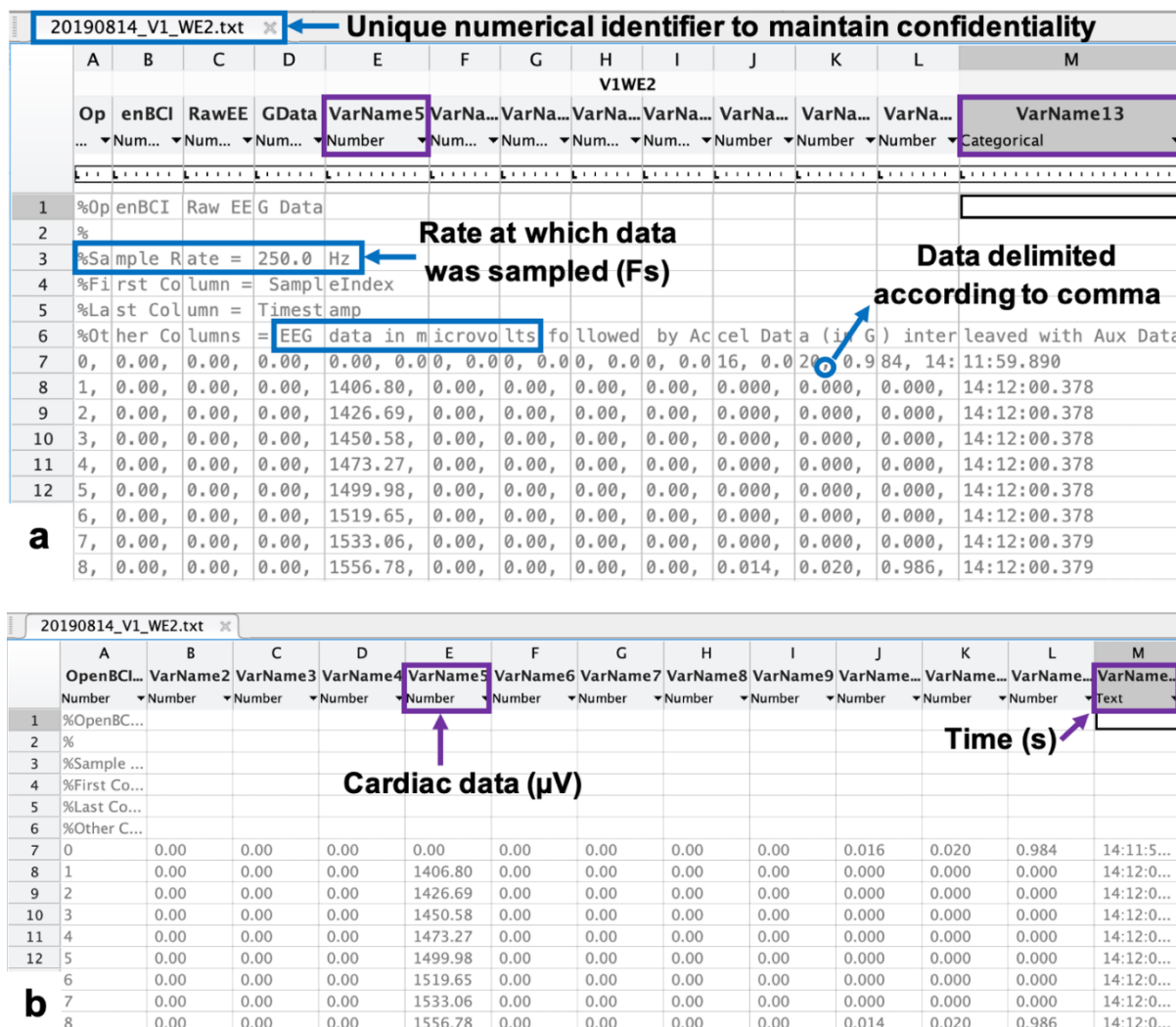
Figure 3.13: Computer screenshots of raw numerical cardiac data imported into MATLAB. Data initially imported where columns appear to overlap (**a**). Data subsequently delimited according to commas and the output type changed from table to column vectors (**b**). Screenshot displays fifteen rows only and purple boxes highlight the data to be imported.

Figure 3.13a displays a screenshot of the raw, numerical cardiac data initially imported into MATLAB. Data were displayed as thirteen columns whilst the number of rows was dependent upon the length of recording. The format of data in Figure 3.13a was problematic when importing the data of interest as some values extended into neighbouring columns. To address this issue, the data was delimited using commas to separate the data points and the result is shown in Figure 3.13b. The output type of the data was changed from table to column vectors for ease of further manipulation. Once imported into the workspace, vectors were assigned names for ease of identification. Rows one to six were removed as they did not contain numerical data, only text information (Figure 3.13a). These rows and the renaming of variables were carried out using the code documented in Figure 3.14. As the biosensing board was originally developed for EEG recordings which are smaller in voltage than cardiac signals, the

data was in the form of microvolts (µV) (Figure 3.13a). Whilst cardiac signals generally only measure a few millivolts or less, the data was converted from µV to mV (Figure 3.14).

```matlab
%% Renaming variables, removal of unnecessary rows and data conversion

WE = VarName5(7:end,:);
%VarName5 renamed as WE (wet electrode) and rows 1-6 have been removed.

Time = VarName13(7:end,:);
%VarName13 renamed as Time and rows 1-6 have been removed.

WE = WE/1000;
%Converts the data from µV to mV.

%% Recreating time domain

Fs = 2.5e2;
%When transferring data over Bluetooth, Cyton board samples data at 250Hz.

Num_secs = size(Time,1)/Fs;
%Divide the number of measurements by the sample rate for the total number of seconds.

T = linspace(0,Num_secs,size(Time,1));
%Linear array from 0 to the total number of seconds taken divided into the number of measurements.

T(1:5)
%View what the data looks like.

T=T.';
%Transpose the data from rows to a column.
```

Figure 3.14: MATLAB code user for the initial management of data recorded from volunteers. Code developed in MATLAB to help prepare the data for subsequent analytical steps. Text in black corresponds to the code, whilst text in green is an explanation of the step.

The data corresponding to time was imported into the workspace in the form of 'datetime'. This format refers to data which is divided into hours, minutes and seconds. Initially, the format of this data was changed to numerical data using the import tool, however when opened in the workspace the expression 'NaN' was observed which stands for 'Not a Number' and represents values which are not real. This prevented a graphical representation of cardiac activity from being created. To overcome this challenge, the time domain was recreated into a numerical format using the code shown in Figure 3.14. As the sample rate and number of measurements were known, the total number of seconds could be calculated. A linear array with equally spaced vectors was created from zero through the total number of seconds taken during and subsequently divided into the number of measurements made. This resulted in the creation of numerical data which could be plotted. An ECG trace was subsequently created (Figure 3.15a) using the code documented in Figure 3.15b. Fonts, styles and size documented in the Figure 3.15b could be adjusted to suit the desired ECG trace.
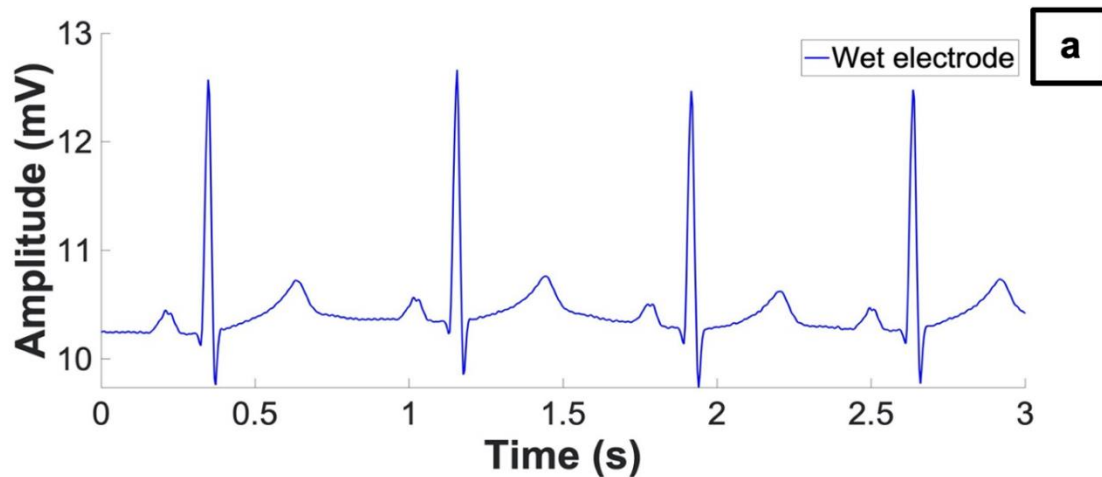
```
%% Plotting the initial data                                        b

figure
%Creates a new figure.

plot(T,WE,'LineWidth',1,'color',[0 0 1])
%Plots wet electrode with time.
%Seconds (x-axis) and amplitude in mV(y-axis).

box off
%Removes the box from the plot.

ylabel('Amplitude (mV)','FontSize',40,'FontWeight','bold')
%Labels y axis with size 40 and bold font.

xlabel('Time (s)','FontSize',40,'FontWeight','bold');
%Labels x axis with size 40 and bold font.

set(gca,'FontSize',30);
%Sets size of axes to 30.

legend('Wet electrode');
%Creates a legend which describes the plotted data.
%Write the legend in the order in which you plotted the data.
```

Figure 3.15: ECG trace and code required to plot the trace. Code written in MATLAB to plot cardiac data (**a**). Text in black corresponds to the code, whilst text in green is an explanation of the step. Graphical plot, using the aforementioned code, of unfilteers, cardiac data (y-axis) over time (x-axis) recording using a commercially available wet electrode from a 25-year-old male volunteer (**b**). For improved visibility, only 3 seconds of cardiac data shown.

3.4.2.2 Digital filter design and implementation

Problems associated with ECG interpretation relate to the presence of unwanted artifacts. When plotting cardiac data acquired from pilot study volunteers, the two key artifacts observed were BW and PLI. EMG noise and motion artifact were not observed in large quantities as this study was conducted whilst the participant was at rest. In practice, most cardiac monitors select appropriate filters depending upon the situation, however as a battery-operated biosensing board was used to record cardiac signals, digital filters were created using MATLAB and implemented offline.

3.4.2.2.1 Baseline wander

In digital signal processing (DSP) filters play an important role by separating signals which have been combined or restoring signals which have been distorted. BW was one type of artifact encountered when analysing pilot data. Whilst BW was not apparent in all recordings, Figure 3.16 shows a segment of unfiltered, cardiac data recorded from one participant where BW was evident. The regularly occurring waveforms do not follow a straight line, instead the baseline undulates and is slowly wandering upwards as demonstrated by the arrow.
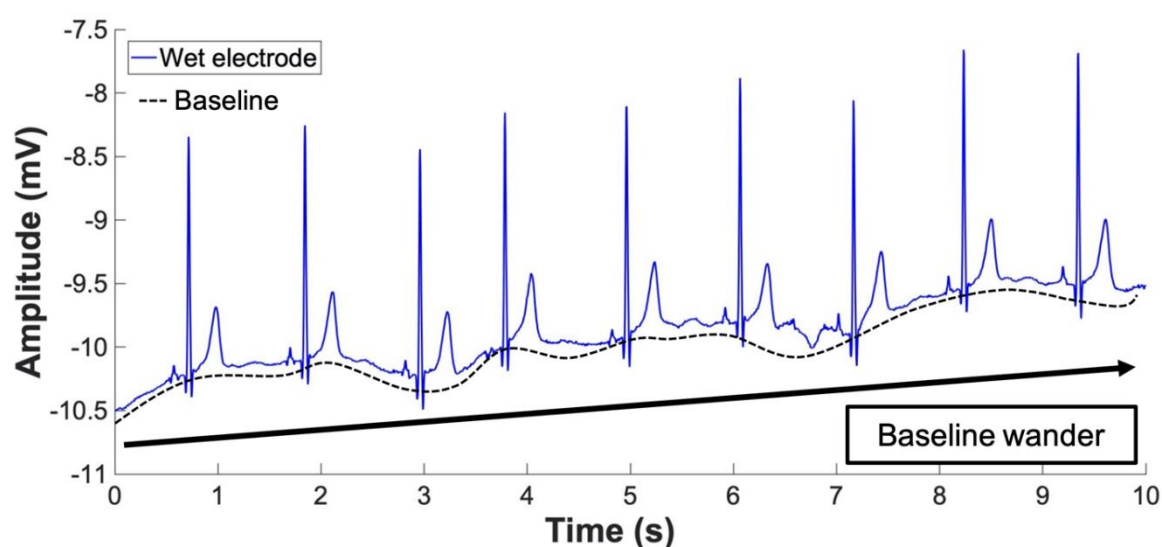
Figure 3.16: ECG trace demonstrating a wandering baseline. Unfiltered data recorded from a 26-year-old male using commercially available wet electrodes. Cardiac signals were recorded using a sample frequency of 250Hz and a gain of x24. For improved visibility, only 10 seconds of cardiac data shown.

Varying degrees of offsets were observed in the data. In Figure 3.15a the baseline occurs at approximately 10mV, whilst the baseline fluctuates around -10mV in Figure 3.16. The presence of such artifacts will have a considerable effect when analysing future ECG recordings in terms of calculating SNR. A simple approach to remove offset is through the application of a digital high-pass filter. This filter allows higher frequencies to pass, whilst rejecting lower frequencies after a defined cut-off point. This cut-off frequency should be optimised to avoid distorting ECG components.

Using MATLAB, high-pass filters were developed to explore the effect of the cut-off frequencies on pilot study data. The magnitude of response of each filter is shown in Figure 3.17. The two cut-off frequencies used to develop the filters were 0.5Hz (Figure 3.17a) and 0.05Hz (Figure 3.17b). Guidance provided by SCST recommends that the lower frequency cut-off should be no higher than 0.67Hz in 'auto' mode, however a value of 0.5Hz is widely

used within the literature. Furthermore, SCST recommends that in manual model, 0.05Hz should be used to avoid ST segment disruption.
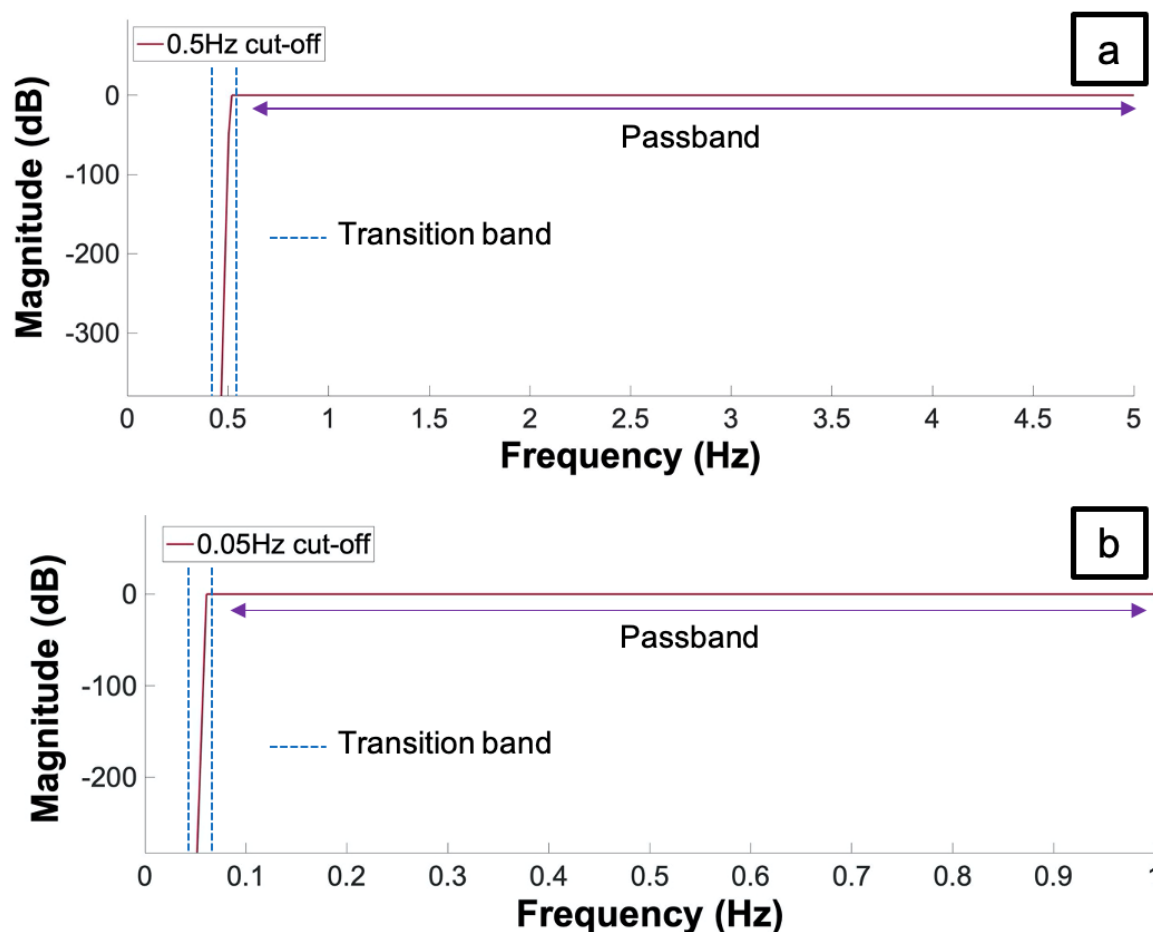
Figure 3.17: Magnitude response of two high-pass filters design in MATLAB. High-pass filters were designed with either a 0.5Hz (**a**) or 0.05Hz (**b**) cut-off frequency using the filter designer application in MATLAB. Zoom has been applied for improved visualisation.

High-pass filters were applied to the same data set and the effects of each cut-off frequency are shown in Figure 3.18. Following the application of 0.5Hz and 0.05Hz high-pass filters, BW was reduced in both instances and the baseline now appears straighter than the original, unfiltered trace (Figure 3.16). Furthermore, the offset of approximately -10mV has also been reduced, with each trace now fluctuating around a baseline of zero. Whilst it is not as noticeable in Figure 3.18a, Figure 3.18b does demonstrate that a slight wandering baseline is still present. As BW occurs at approximately 0.5Hz it is therefore still present when using a cut-off frequency of 0.05Hz. Using a cut-off frequency of 0.5Hz reduced BW more so than 0.05Hz as evidenced by Figure 3.18, however some ST segment changes were noted.
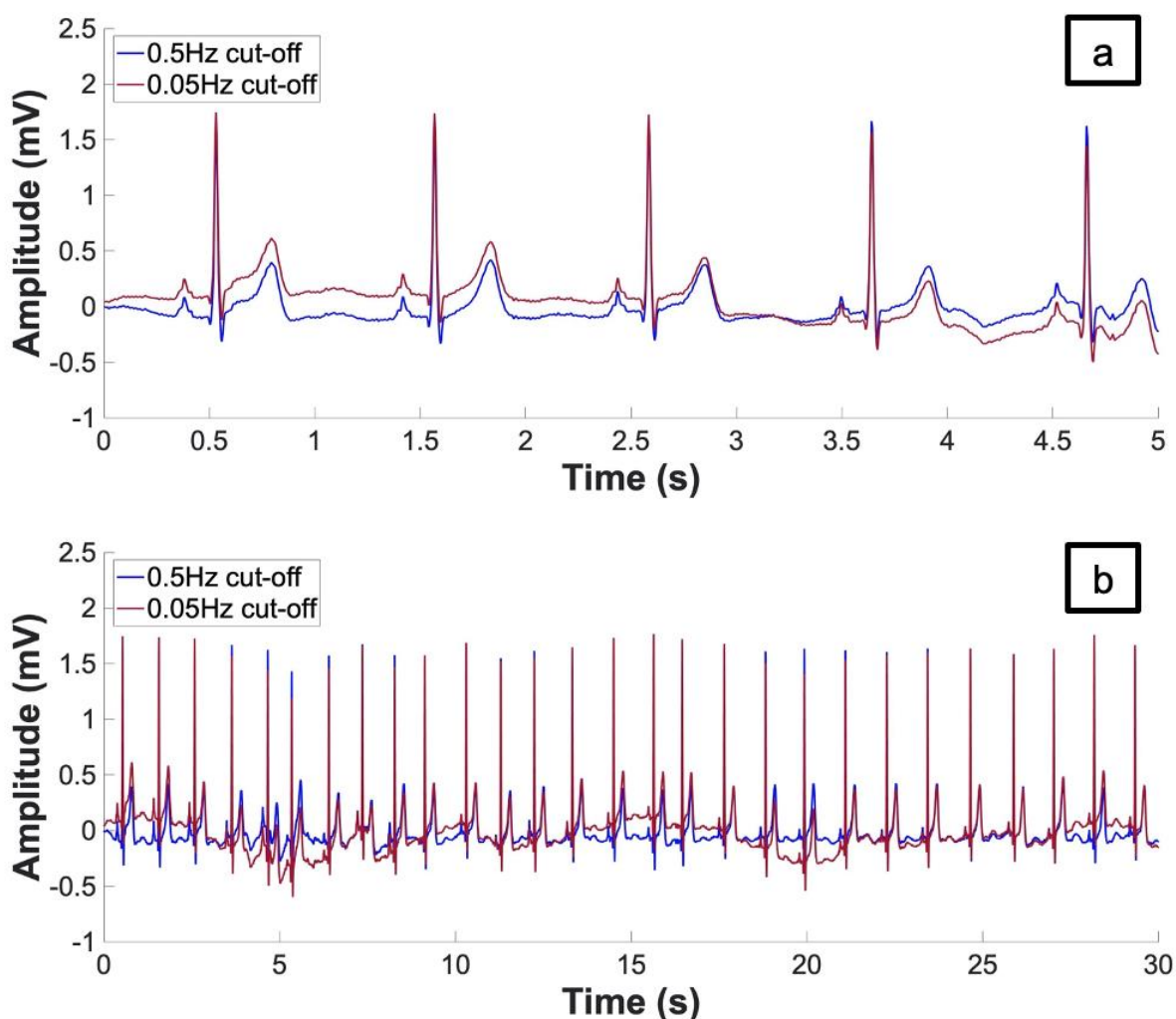
Figure 3.18: ECG traces following application of two high-pass filters. ECG trace showing 5 seconds of cardiac signals following application of two high-pass filters with 0.5Hz and 0.05Hz cut-off frequencies (**a**). ECG trace showing 30 seconds of cardiac signals following application of two high-pass filters with 0.5Hz and 0.05Hz cut-off frequencies (**a**). Data recorded from a 26-year-old male using commercially available wet electrodes.

3.4.2.2.2 Powerline interference

As previously stated, PLI was a second artifact encountered when recording cardiac signals from adult volunteers. To remove this frequency from recordings, an IIR Butterworth band-stop filter was designed in MATLAB (Figure 3.19). A notch filter, also termed a band-stop filter, has a very narrow bandwidth and rejects a single, or very small band of frequencies making them very useful at removing just powerline noise, and no other components of the ECG. The bandwidth of a notch filter can be adjusted to suit the desired application. To remove PLI for ECG traces, the filter shown in Figure 3.19 was designed with a bandwidth of 49.5 to 50.5Hz and a central frequency of 50Hz.
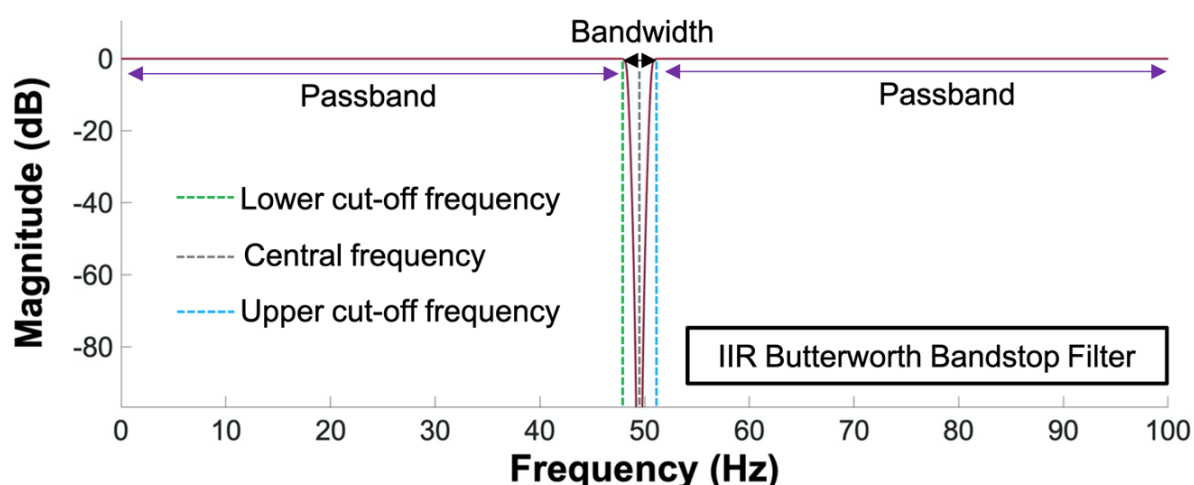
Figure 3.19: Magnitude response of digital IIR Butterworth Bandstop filter. Attenuated frequency is set at 50Hz in order remove AC powerline interference from recorded cardiac signals.

Whilst recording cardiac signals from the three participants during the pilot study, it was clear that the magnitude of PLI at 50Hz varied. Figure 3.20a shows an unprocessed ECG trace recorded using commercially available wet electrodes from a female volunteer aged 28 years. It appeared that in addition to cardiac activity, PLI was also acquired due to the presence of oscillations in the baseline. QRS complexes were clearly identifiable in the trace, however P and T waves were slightly obscured by the spurious waveforms. To determine the frequency of noise causing the artifact, Fourier analysis was conducted which converted the whole signal from its original time domain to a representation in the frequency domain. Figure 3.20b shows a discernible peak around 50Hz, confirming the presence of PLI. No harmonic frequencies were observed in any of the pilot recordings.
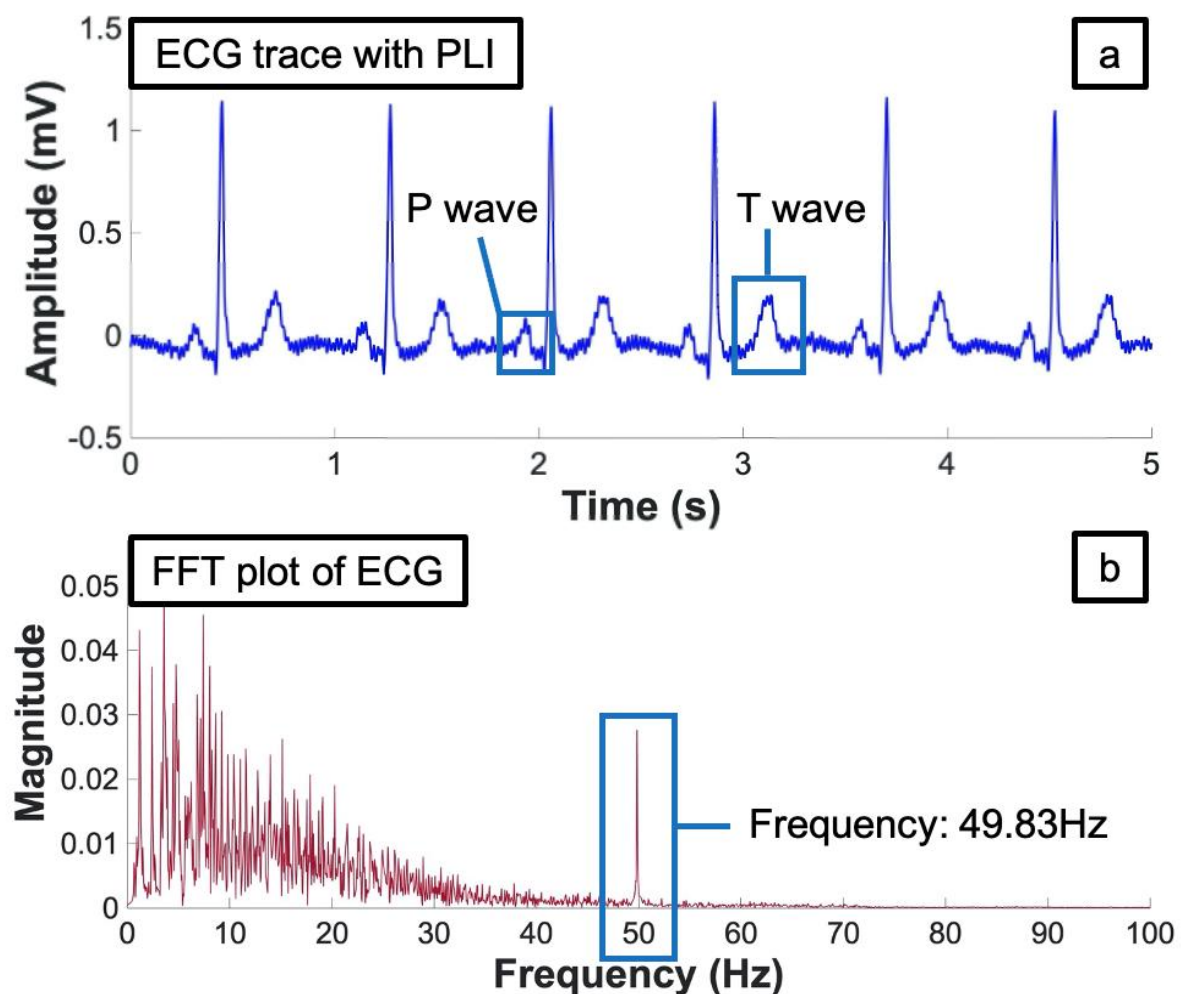
Figure 3.20: Noisy trace and frequency plot of cardiac signals. ECG trace recorded from a 28-year-old female prior to the application of a digital notch filter (**a**). FFT plot showing the frequency domain of the cardiac signals acquired over 60 seconds where a clear peak is highlighted by the blue box (**b**). Data were filtered using a high-pass filter with a cut-off frequency of 0.67Hz to remove BW and adjust the baseline to zero. For improved visualisation, only 5 seconds of cardiac data shown.

ECG signals are often corrupted by PLI which is the frequency from the mains power supply and the traces recorded in this pilot study were no exception. Therefore, it was necessary to remove PLI using the digital notch filter shown in Figure 3.19 which was designed in MATLAB using the filter designer application. The subsequent filtered signal is shown in Figure 3.21a where the signal appears smoother with discernible P/T waves. Figure 3.21b demonstrates the FFT plot of the cardiac signal following the removal of PLI. As highlighted in the Figure, the magnitude of peak originally observed at 49.83Hz has reduced and was no longer identifiable.
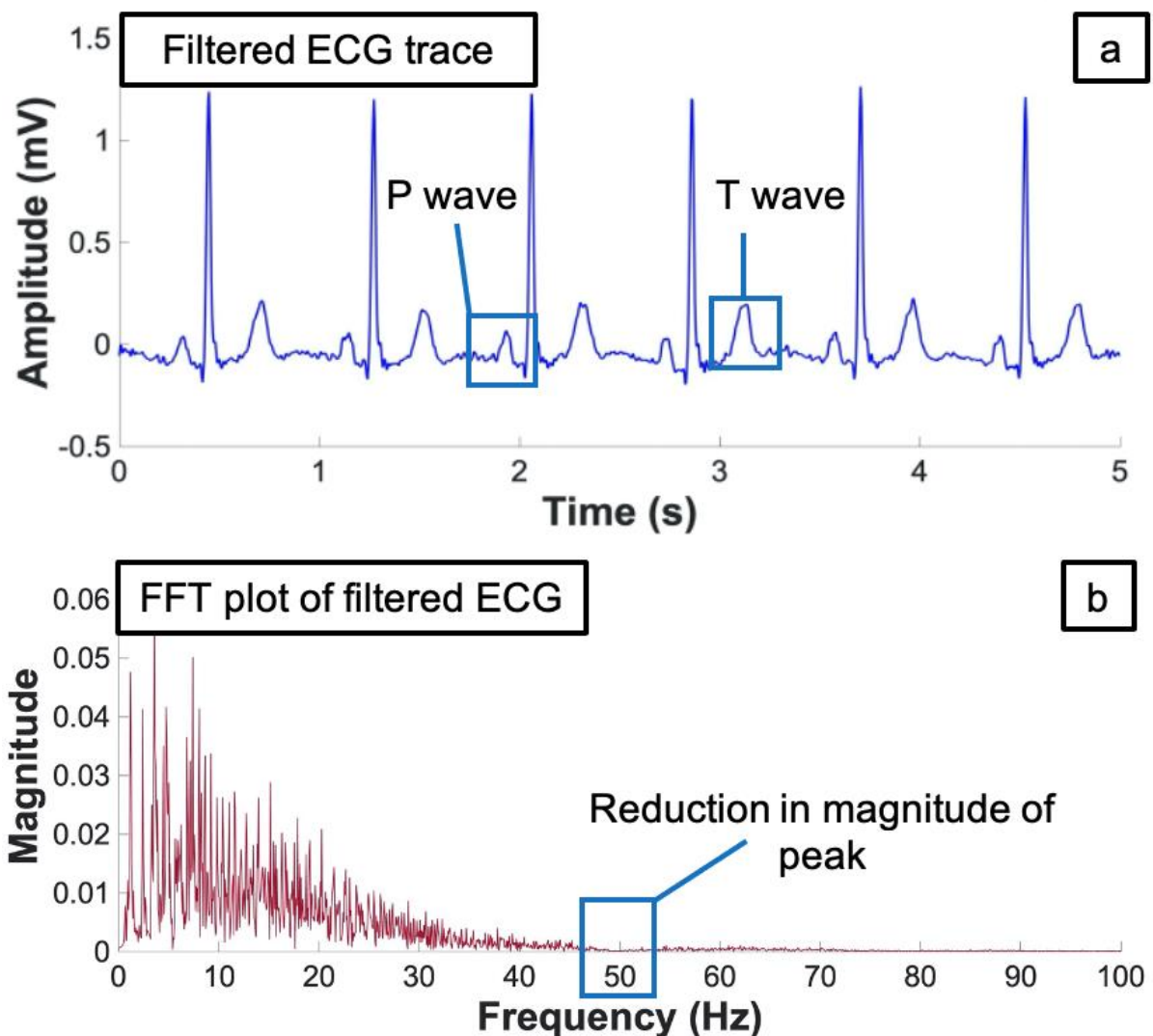
Figure 3.21: Trace and frequency plot of filtered cardiac signals. ECG trace recorded from a 28-year-old female following the application of a digital notch filter (**a**). FFT plot showing the frequency domain of the cardiac signals acquired over one minute where a reduction in the peak is highlighted by the blue box (**b**). Data were also filtered using a high-pass filter with a cut-off frequency of 0.67Hz to remove baseline wander and adjust the baseline to zero. For improved visualisation, only 5 seconds of cardiac data shown.

3.4.2.3 Signal to noise ratio calculation of pilot study data

3.4.2.3.1 Noise frequency isolation

The first step in calculating SNR was to identify the frequency at which noise occurred. To identify and determine this frequency in the acquired ECG traces, signals were converted from the time domain to the frequency domain using FFT. An example FFT plot was shown previously in Figure 3.20b, where a clear peak was observed at 49.83Hz. This peak is most likely the result of PLI as it occurs in a larger magnitude than neighbouring frequencies and is close to the fundamental frequency of mains electricity. During the pilot study, three, 60

second recordings were captured from each volunteer. By plotting the FFT of each recording, the overall mean frequency of PLI was determined to be 49.89Hz ±0.06. Mean noise frequencies for each volunteer who participated in the pilot study are shown in Table 3.1.

Table 3.1: Frequency of powerline interference from pilot study data. Frequencies (Hz) of powerline interference was determined by plotting the Fast Fourier Transform of each 1-minute recording acquired using wet electrodes from each of three healthy participants. The mean noise frequency for all three volunteers was 49.89Hz ±0.06. Data presented as the mean ±SD (*n=3*).

	Volunteer number		
	1	**2**	**3**
Frequency of PLI (Hz)	49.95 ±0.01	49.82 ±0.01	49.89 ±0.01

3.4.2.3.2 Cardiac signal and noise isolation

The next step involved separating the cardiac signal from noise. Data was firstly filtered using the high-pass filter shown in Figure 3.17a to remove BW. Following this, a lowpass filter was designed and implemented in MATLAB to isolate the signal. Figure 3.22 shows the code and subsequent effects of implementing a lowpass filter with a 40Hz cut-off frequency on cardiac data.
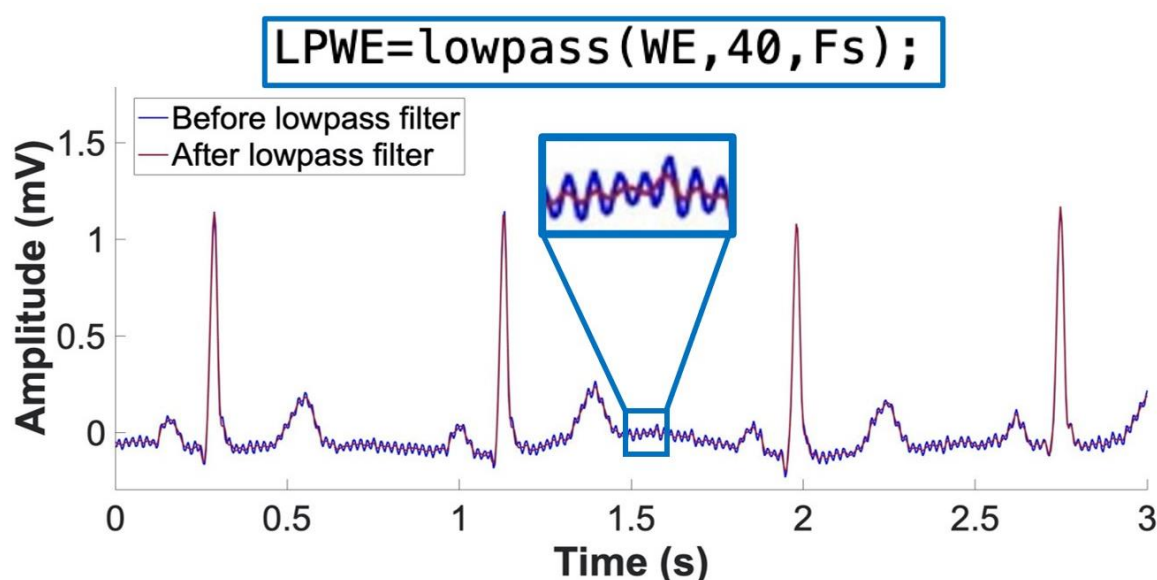
Figure 3.22: Effect of a digital lowpass filter on cardiac data. A digital lowpass filter was implemented using MATLAB with a 40Hz cut-off frequency to isolate the signal. Data prior to filtering is shown in blue, whilst filtered data is shown in red. The code used to execute the filter is also shown. Data was initially filtered with high-pass filter with a 0.5Hz cut-off frequency to remove BW. For improved visualisation, only 3 seconds of cardiac data is shown.

For real-world ECG traces, it is challenging to remove 100% of noise. Traces following application of the filter were of higher fidelity as this type of filter rejected frequencies above 40Hz. The subsequent trace contained less spurious waves in the baseline as PLI was removed.

To isolate noise, the original cardiac data was again filtered using the high-pass filter shown in Figure 3.17a to remove BW. A second high-pass filter was designed in MATLAB also with a 40Hz cut-off frequency. This filter was designed to pass frequencies above 40Hz and upon implementation the inverse of Figure 3.22 was observed. As shown by Figure 3.23, only noise was present as the filter had rejected frequencies below 40Hz and therefore the signal had been attenuated.
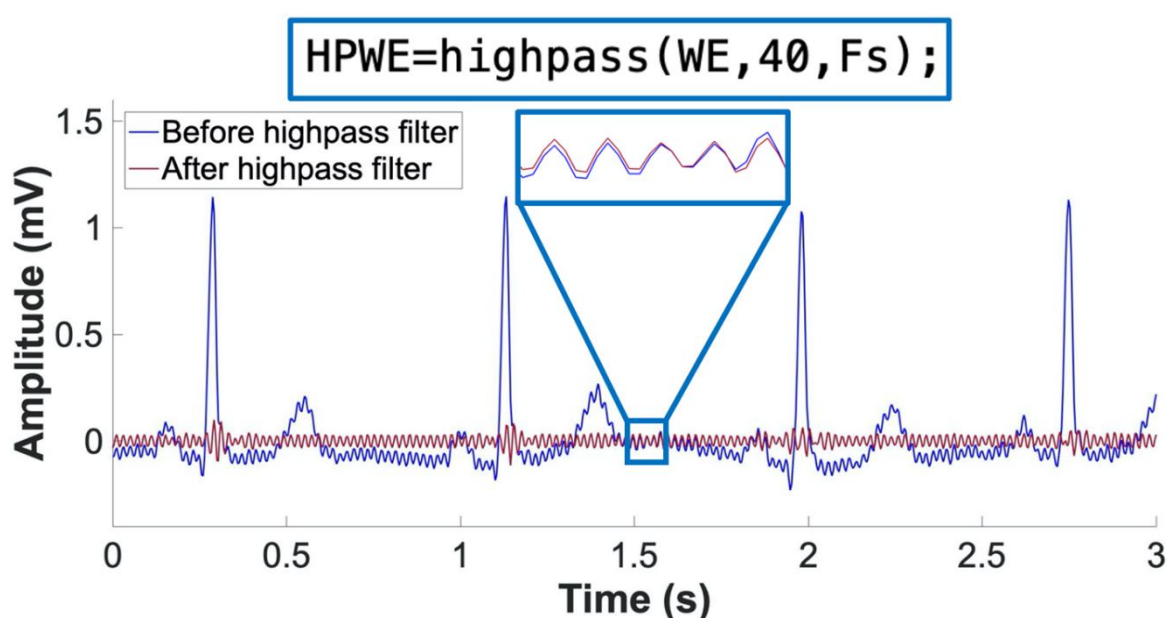
Figure 3.23: Effect of a digital high-pass filter on cardiac data. A digital high-pass filter was implemented using MATLAB with a 40Hz cut-off frequency to isolate noise. Data prior to filtering is shown in blue, whilst filtered data is shown in red. The code used to execute the filter is also shown. Data was initially filtered with high-pass filter with a 0.5Hz cut-off frequency to remove BW. For improved visualisation, only 3 seconds of cardiac data is shown.

Having isolated both signal and noise (Figure 3.24), their respective powers were calculated. Within ECG traces, maximum and minimum values were typically found within the QRS complex (Figure 3.24). Prior to the lowpass filter, cardiac data had been filtered with the high-pass filter shown in Figure 3.17a to aid in the removal of BW and DC offset which could affect maximum and minimum values. To calculate signal power, the minimum value of the QRS complex was subtracted from the maximum as shown by the equation in Figure 3.11. As

maximum and minimum values varied with each heartbeat, six QRS complexes were selected throughout the 60 second trace which equated to one waveform every ten seconds. Mean values were manually determined and used to calculate signal power. To calculate noise power, the standard deviation of isolated noise was calculated and subsequently multiplied by four to achieve a 95% confidence interval.
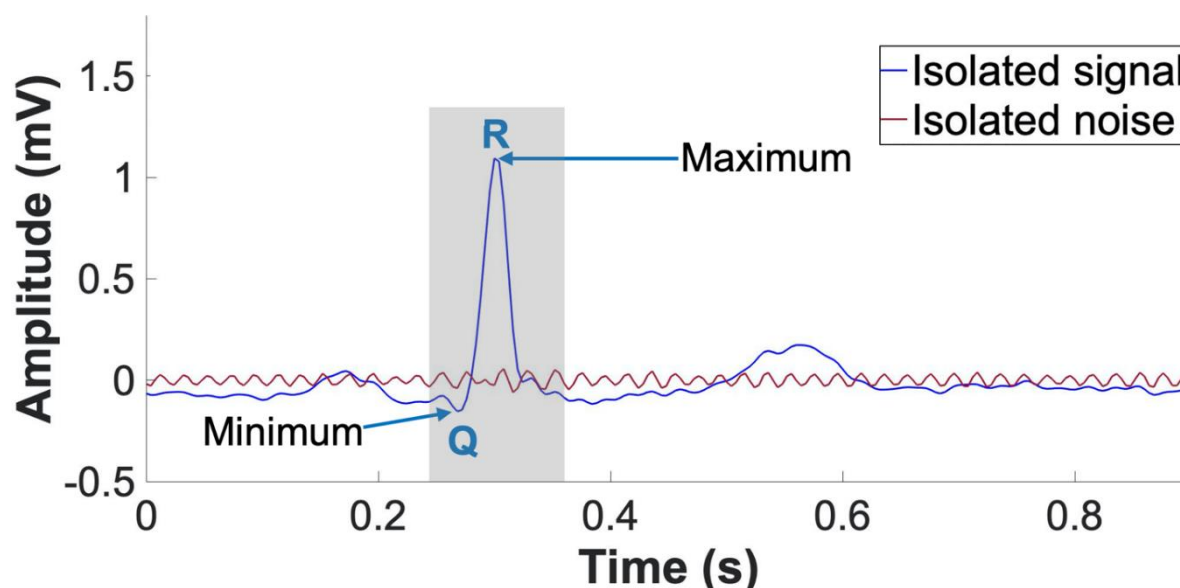
Figure 3.24: Isolated cardiac signal and noise. Isolated signal is shown in blue whilst isolated noise is shown in red. Both were isolated using a digital lowpass and high-pass filter respectively. QRS complex is highlighted in grey. Within this complex, maximum and minimum areas are highlighted. For improved visualisation, a single ECG waveform is shown.

Using the equation shown in Figure 3.11, the SNR of each 60 second recording was calculated and averaged. Mean SNR values for each volunteer are shown in Figure 3.25. ECG traces recorded from volunteers one, two and three resulted in SNR values of 26.7dB ±0.15, 22.2dB ±0.05 and 33.0dB ±0.21 respectively. Traces from volunteer three (Figure 3.25c) produced the highest SNR whilst traces from volunteer two (Figure 3.25b) resulted in the lowest SNR. Wet electrodes resulted in an overall mean SNR of 27.3dB ±5.39 for the three volunteers. Figure 3.25 also displays 5 seconds of cardiac activity for each volunteer to provide a visual comparison. As shown by Figure 3.25, ECG waveforms including relevant P, QRS and T waves, were clearly identified for each volunteer.
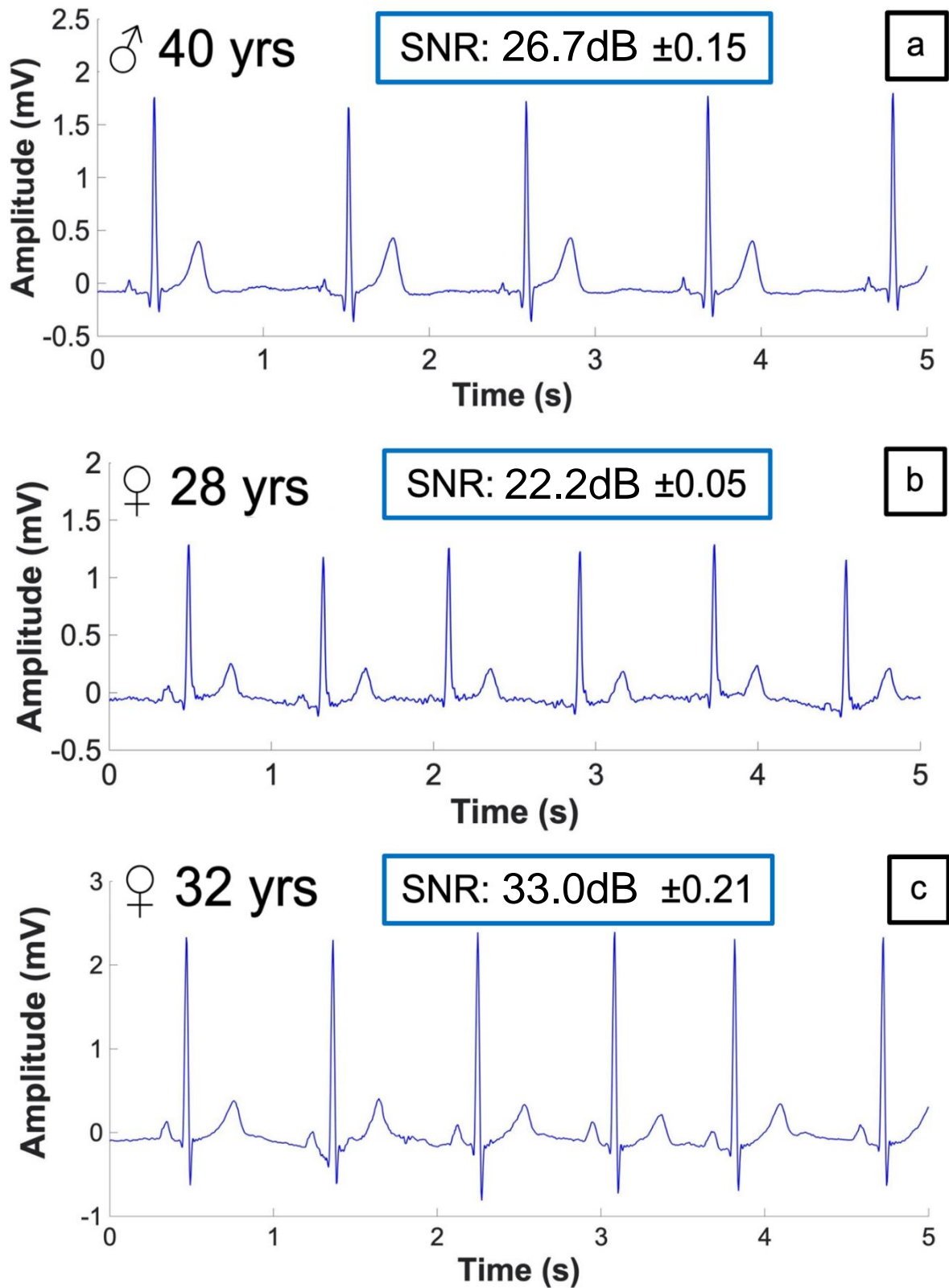
Figure 3.25: ECG traces recorded using wet electrodes from three healthy adult volunteers. Pilot data was acquired using wet electrodes placed in a lead II configuration from volunteer one (**a**), two (**b**) and three (**c**). Data filtered with both a high-pass and notch filter. For improved visualisation, only 5 seconds of data shown.

3.4.3 Electrode comparison study

3.4.3.1 Volunteer demographics

Table 3.2 displays the biological sex and age of recruited volunteers. In total, ten subjects were included in the present study. Equal numbers of males (n=5) and females (n=5) were recruited with all subjects completing the study in its entirety. Demographic data regarding biological sex and age were captured for each participant. Volunteers ranged from 21 to 25 years old. The largest percentage of volunteers were aged 21, whilst the mean age was 22.8 years ±1.81.

Table 3.2: Demographics of recruited volunteers. Volunteer demographics were captured after completion of signal acquisition.

Demographics		Numbers (n=)	Percentage (%)
Biological sex	Male	5	50
	Female	5	50
Age (years)	21	4	40
	22	1	10
	23	1	10
	24	1	10
	25	3	30

3.4.3.2 Signal to noise ratio of cardiac signals at rest

Individual SNR values were calculated using each type of electrode for each volunteer. Furthermore, mean SNR was calculated for both electrode types to determine the overall performance. Figure 3.26 shows a SNR comparison between wet and MN electrodes in the ten healthy adult volunteers. The overall mean SNR for each electrode type is also highlighted. As shown by Figure 3.26, intra- and inter-variability in SNR values were observed. Analysing the data, a little more closely revealed instances where MN electrodes recorded signals of higher fidelity when compared to wet electrodes. For instance, when recording cardiac activity from volunteer one, MN electrodes resulted in an SNR of 32.8dB ±0.21, in comparison to 28.0dB ±0.16 for the wet electrodes. Contrariwise, cases were observed where wet electrodes resulted in a higher quality signal. A large variation between the data for wet and MN electrodes was observed in volunteer two. Wet electrodes resulted in an SNR of 31.5dB ±0.12,

in comparison to the lower value of 19.5dB ±0.45 for MN electrodes. For volunteers six, seven and nine, SNR values for both types of electrodes were comparable.
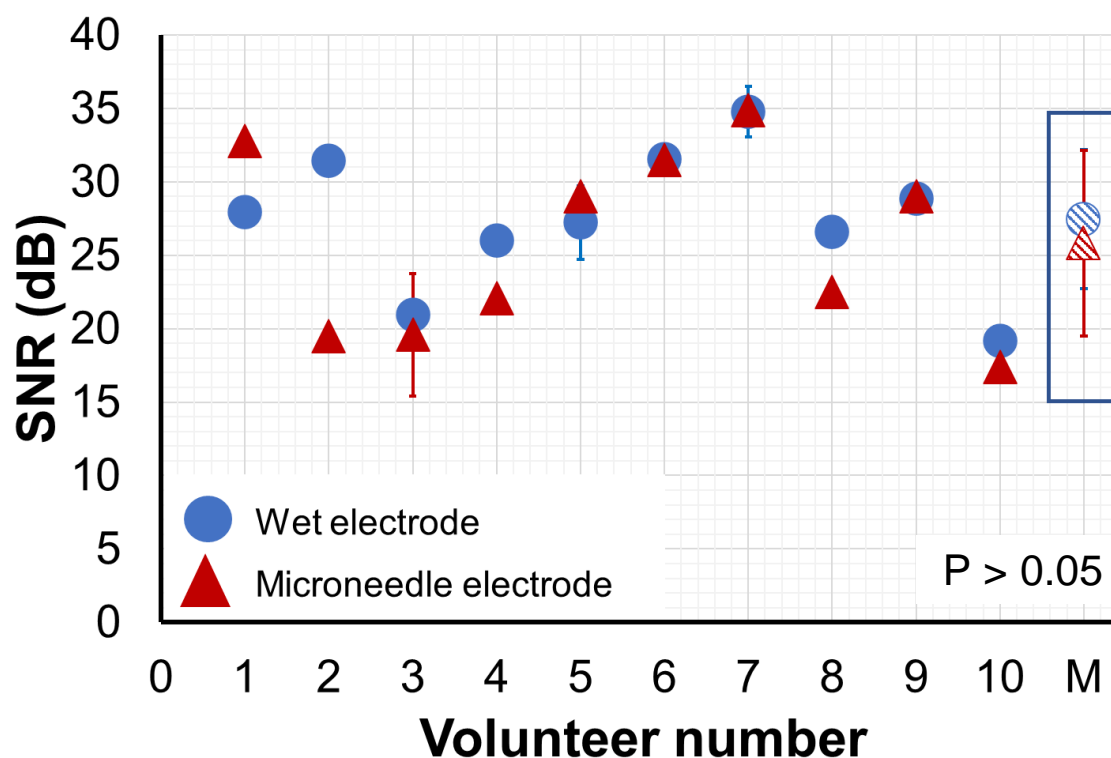
Figure 3.26: Signal to noise ratio comparison between wet and microneedle electrodes in human volunteers. Results calculated for each of the ten adult volunteers. Wet electrodes represented by blue circles and microneedle electrodes represented by red triangles. Mean signal to noise ratio values for wet and microneedle electrode are highlighted by the blue box. For each volunteer data presented as the mean ±SD (*n=3*). For the overall average data presented as the mean ±SD *(n=10).*

Overall numerical SNR data are shown in Table 3.3. Wet electrodes resulted in a mean SNR of 27.5dB ±4.74 in comparison to the slightly lower value of 25.8dB ±6.31 for MN electrodes. In general, MN electrodes were associated with greater variability as indicated by standard deviations, than wet electrodes. Out of the ten volunteers, MN electrodes resulted in both the highest (34.9dB ±0.20) and lowest (17.4dB ±0.21) SNR. The differences in SNR between wet and MN electrodes were statistically insignificant (p =0.52).

Table 3.3: Signal to noise ratio comparison between wet and microneedle electrodes in human volunteers. Signal to noise ratio results and overall average calculated for each of the ten adult volunteers. For each volunteer data presented as the mean ±SD (*n=3*). For the overall average data presented as the mean ±SD *(n=10).*

Volunteer number	Signal-to-noise ratio (dB)	
	Wet electrode	Microneedle electrode
1	28.0 ±0.16	32.8 ±0.21
2	31.5 ±0.12	19.5 ±0.45
3	20.9 ±0.48	19.6 ±4.19
4	26.0 ±0.68	22.1 ±0.35
5	27.2 ±2.5	29.0 ±0.15
6	31.6 ±0.19	31.5 ±0.28
7	34.8 ±1.73	34.9 ±0.20
8	26.6 ±0.78	22.5 ±0.20
9	28.9 ±0.48	29.1 ±0.13
10	19.2 ±0.11	17.4 ±0.21
Overall mean	27.5 ±4.74	25.8 ±6.31

3.4.3.3 Signal to noise ratio of cardiac signals between biological sexes

Biological sex was equally represented with the recruitment of five males and five females who were similar in age. To determine if any differences existed in electrode performance between the sexes, mean SNR values were determined for each electrode type. SNR values comparing electrode technologies in both males and females, including the overall mean, are shown in Figure 3.27. MN data are displayed using the red triangles and data for wet electrodes are shown by the blue circles. Whilst the sample size was small for both sexes (n=5), overall, wet electrodes recorded signals of higher fidelity in both males (27.6dB ±7.02) and females (27.3dB ±1.12). By comparison, MN electrodes resulted in a clear reduction in SNR for males (24.6dB ±8.01) however, the performance in females was similar to that of the wet electrodes (27.1dB ±4.64). As indicated by the standard deviation values, the performance of both types of electrodes in males was more variable than the performance in females. When comparing the electrode performance between males and females, no statistical significance was found for wet electrodes (p=0.939) or MN electrodes (p=0.559). Furthermore, no

statistical difference was observed when comparing the performance of wet electrodes with MN electrodes in males (p=0.544) or females (p=0.913).
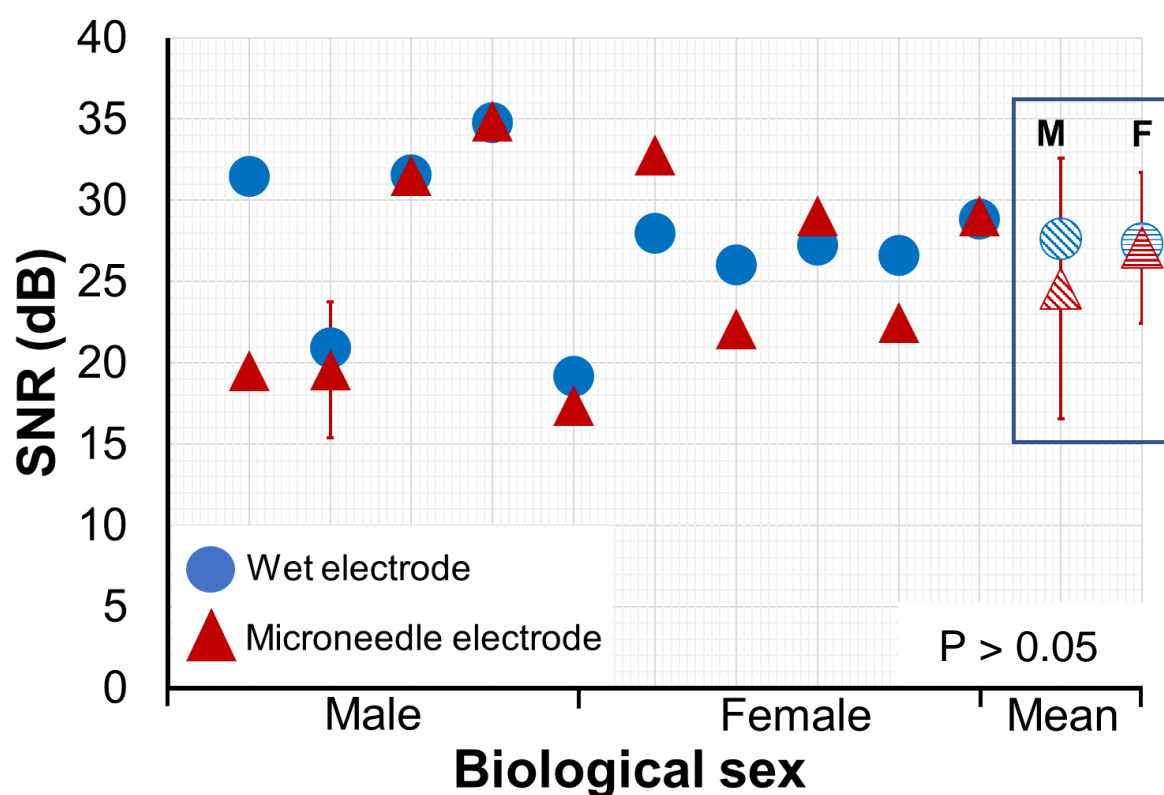
Figure 3.27: Signal to noise ratio comparison between wet and microneedle electrodes between the sexes. Results calculated for each of the five males and females. Wet electrodes represented by blue circles and microneedle electrodes represented by red triangles. Overall mean signal to noise ratio for wet and microneedle electrodes is highlighted by the blue box. For each volunteer data presented as the mean ±SD (*n=3*). For the overall average for each electrode in each sex data presented as the mean ±SD *(n=5)*.

3.4.3.4 Magnitude of powerline interference in cardiac signals

The frequency domain of cardiac signals recorded using both electrode types was plotted using FFT. Table 3.4 displays the magnitude of PLI at a mean frequency of 49.93Hz ±0.05. PLI is routinely captured alongside cardiac signals during ECG. As shown by Table 3.4, the cardiac recordings in this study were no different. The magnitude of PLI was present in variable amounts. Overall, MN electrodes were more susceptible to PLI and more variable (30.4µV ±36.58) compared to wet electrodes (12.4µV ±16.31).

Table 3.4: Magnitude of powerline interference between electrode types in human volunteers. Powerline interference results and overall average calculated for each of the ten adult volunteers. For each volunteer data presented as the mean ±SD (*n=3*). For the overall average data presented as the mean ±SD *(n=10).*

Volunteer number	Magnitude of 50Hz powerline interference (µV)	
	Wet electrode	Microneedle electrode
1	26.8 ±2.99	3.1 ±1.42
2	4.9 ±0.23	73.7 ±8.96
3	18.5 ±1.73	94.0 ±1.82
4	14.2 ±1.09	28.4 ±1.95
5	0.8 ±0.52	2.8 ±0.29
6	4.0 ±0.78	5.0 ±1.33
7	1.5 ±0.38	5.1 ±0.90
8	1.6 ±0.37	13.0 ±2.40
9	0.6 ±0.06	1.6 ±0.14
10	51.2 ±0.32	77.2 ±1.6
Overall mean	12.4 ±16.31	30.4 ±36.58

3.4.3.5 Visual comparison of traces

Whilst SNR allows for quantitative conclusions between electrode performance, in practice, this is not available to clinicians. Therefore, qualitative visual comparisons of traces were undertaken to support SNR results. In addition to providing visual comparisons, these traces were used to determine important parameters including HR and durations of relevant waves, segments, and intervals, all of which provides information regarding the clinical picture of a patient.

Based on SNR, a selection of traces were chosen to demonstrate differences in performance between electrodes and volunteers. Whilst Figure 3.28 displays traces from three volunteers, the overall analysis was based upon the traces acquired from all ten volunteers, which are shown in Appendix VI. Figure 3.28a illustrates a 5 second segment of cardiac activity acquired from volunteer one, a healthy 21-year-old female. Data shown in Figure 3.28a was filtered offline in MATLAB using a high-pass filter with a 0.5Hz cut-off to remove BW and DC offset. A digital notch filter was not applied to the data to remove PLI to show the ECG waveforms with minimal DSP. Figure 3.28a was included to demonstrate a trace where MN electrodes acquired higher fidelity signals than the wet electrode. Cardiac data acquired using

wet electrodes resulted in the presence of more spurious waves within the baseline than MN electrodes, indicating the increased presence of PLI. Figure 3.28b shows a further 5 second segment of cardiac activity acquired from volunteer two, a healthy 25-year-old male. Similarly, to Figure 3.28a, data were filtered using a high-pass filter with a 0.5Hz cut-off to remove BW and DC offset. A digital notch filter was not applied to the data. Figure 3.28b was subsequently included to show the reverse of Figure 3.28a. It is demonstrably clear that the commercially available wet electrodes, shown in blue, recorded a signal of higher fidelity than MN electrodes due to reduced spurious waves in the baseline. In this instance, the use of MN electrodes resulted in a 'noisier' trace which contained a mean of 93.0µV ±29.97 of 50Hz PLI (WE noise: 4.8 V ±0.23). Whilst Figure 3.28a and Figure 3.28b shown traces where one of the electrodes outperformed the other, Figure 3.28c was included to show an example where signal fidelity was visually comparable between both types of electrodes. SNR values were 31.6dB ±0.19 for wet electrodes and 31.5dB ±0.28 for MN electrodes. Figure 3.28c was recorded from volunteer six, a healthy 23-year-old male. Data again was filtered with a 0.5Hz high-pass filter and PLI was not removed using a notch filter. Whilst varying degrees of noise can be observed in each trace, the typical cardiac signatures of the P wave, QRS complex and T wave are clearly visible. In all ECG traces visually assessed, volunteers were found to be within normal sinus rhythm due to the cardiac waveform occurring at regular and appropriate intervals. This demonstrates the ability of 'dry' MN electrodes to adequately sense and record cardiac signals.
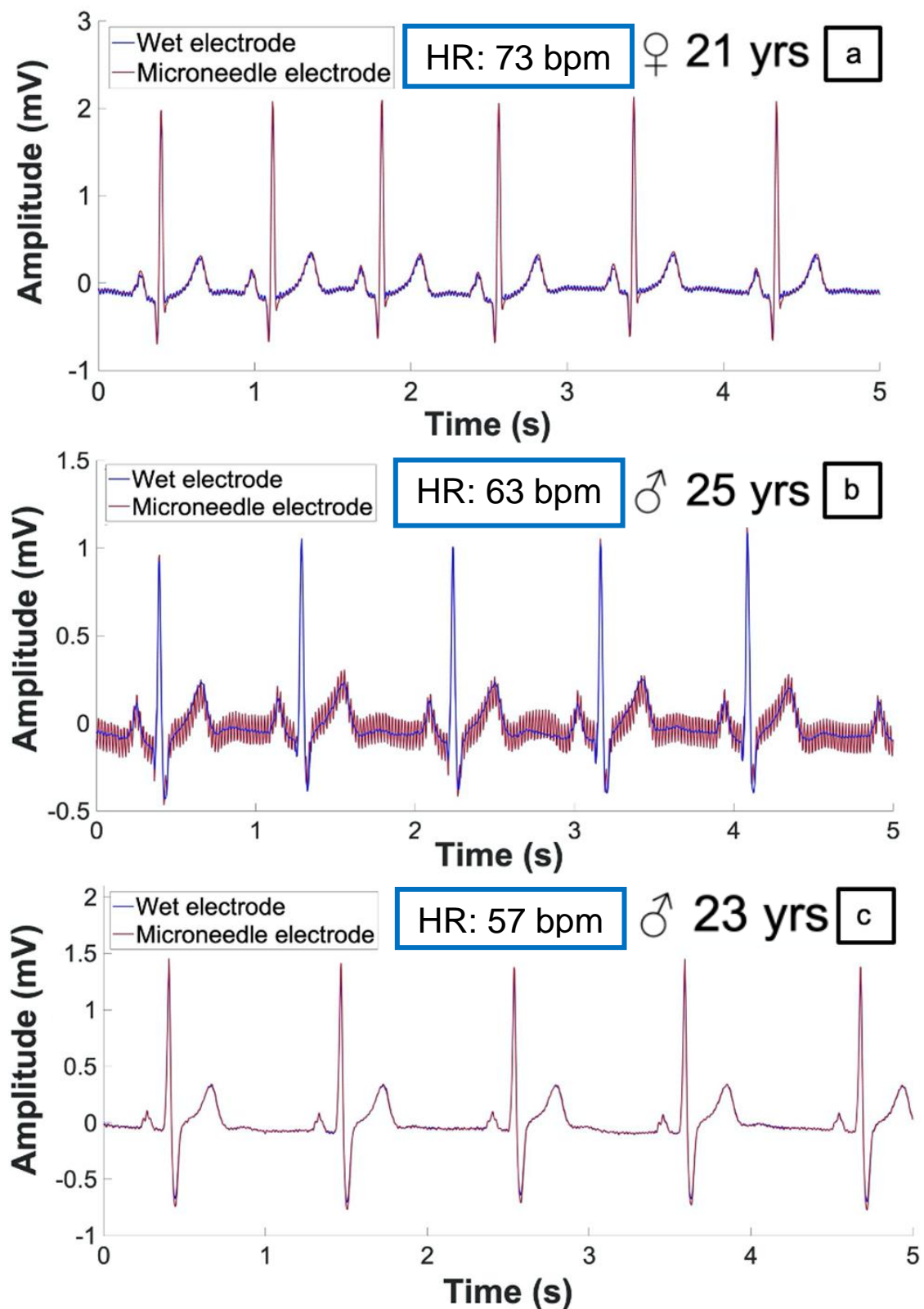
Figure 3.28: Segments of cardiac activity recorded using wet and microneedle electrodes. Traces from volunteer one (**a**), two (**b**) and six (**c**) to highlight the recording differences between both electrodes. Data filtered with a high-pass filter to adjust the baseline. Traces recorded by microneedle electrodes are shown in red and wet electrodes in blue. For improved visualisation only 5 seconds of data shown.

3.4.3.5 Effects of electrode technologies on human skin

Several participants reported that the initial application of MN electrodes was accompanied by minor discomfort, particularly beneath the right collarbone. This discomfort was reported to subside within a few minutes. No bleeding, or spots of blood were observed at any time during the application of MN electrodes. Images of the participant's skin were captured immediately following the removal of both types of electrodes. A selection of images acquired from volunteers one, two and six are shown in Figure 3.29. A well-defined skin erythema in the shape of a circular array was observed at the site of the MN electrode. Additionally, indentations highlighting where each individual needle was placed was also visible. Whilst no follow up images were captured, this skin erythema was transient and started to fade soon after the removal of the electrodes. Skin erythema was observed following the removal of the wet electrode, however, appeared less than that of the MN electrodes. Transient circular markings due to the adhesive pad were apparent.
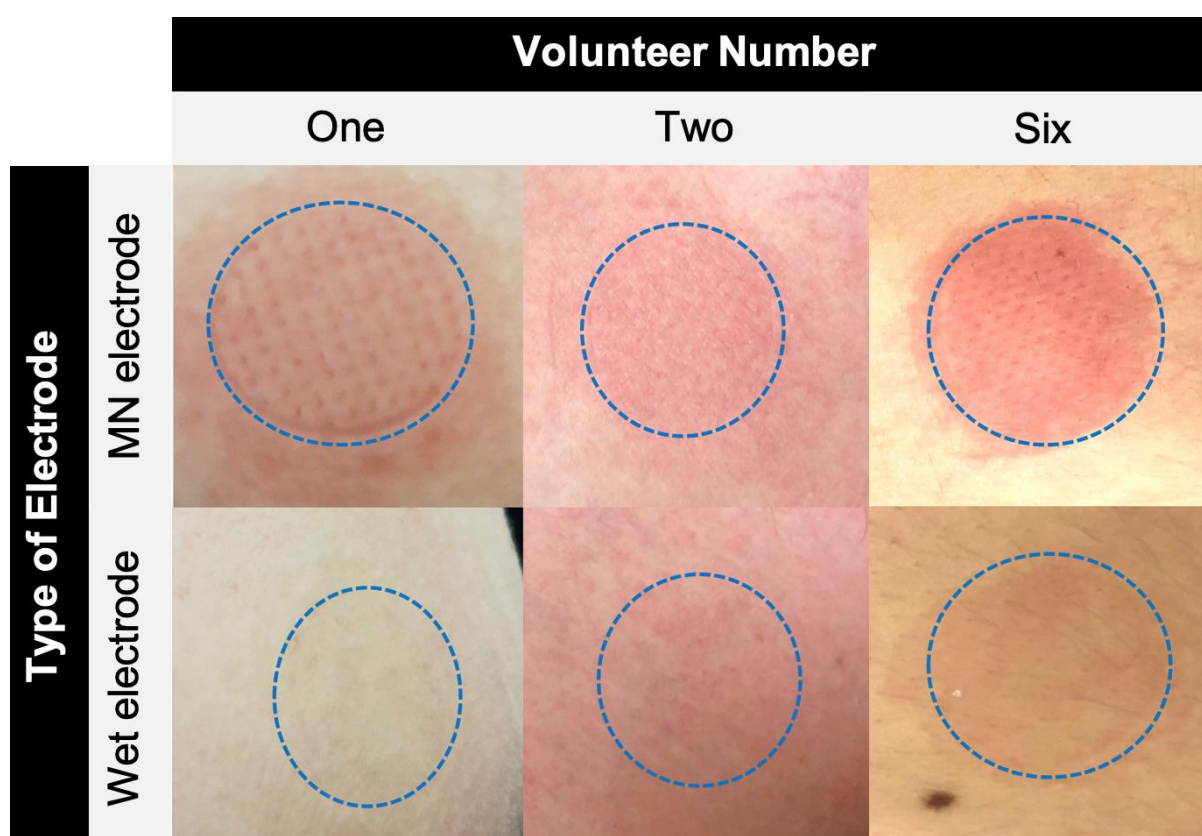
Figure 3.29: Images of skin following the removal of microneedle and wet electrodes. Images shown are of volunteers one, two and six's skin (underneath the right clavicle) immediately following the removal of both types of electrodes. The blue dashed line highlights the area of the electrode in direct contact with the skin.

3.4.4 Post insertion microneedle-electrode imaging

Following removal from each volunteer, MN arrays were imaged using stereomicroscopy and SEM to identify changes to the MN structure and coating following skin insertion and signal acquisition. Figure 3.30 displays a selection of images of the coated MNs post-insertion and are representative of all the images acquired. The Ti/Au coating applied to enable the epoxy MNs to conduct a signal remained intact following insertion and removal from skin. However, cracks in the coating appeared at the needle tip (Figure 3.30b) which was consistent with other acquired images. As shown by Figure 3.30a-b, potential biological remnants were also observed, attached to the needle tip. SEM images demonstrated that a number of MN tips had blunted, which is consistent with previous images shown in Chapter 2. Overall, no instances of MN fracture were observed in any of the images acquired.
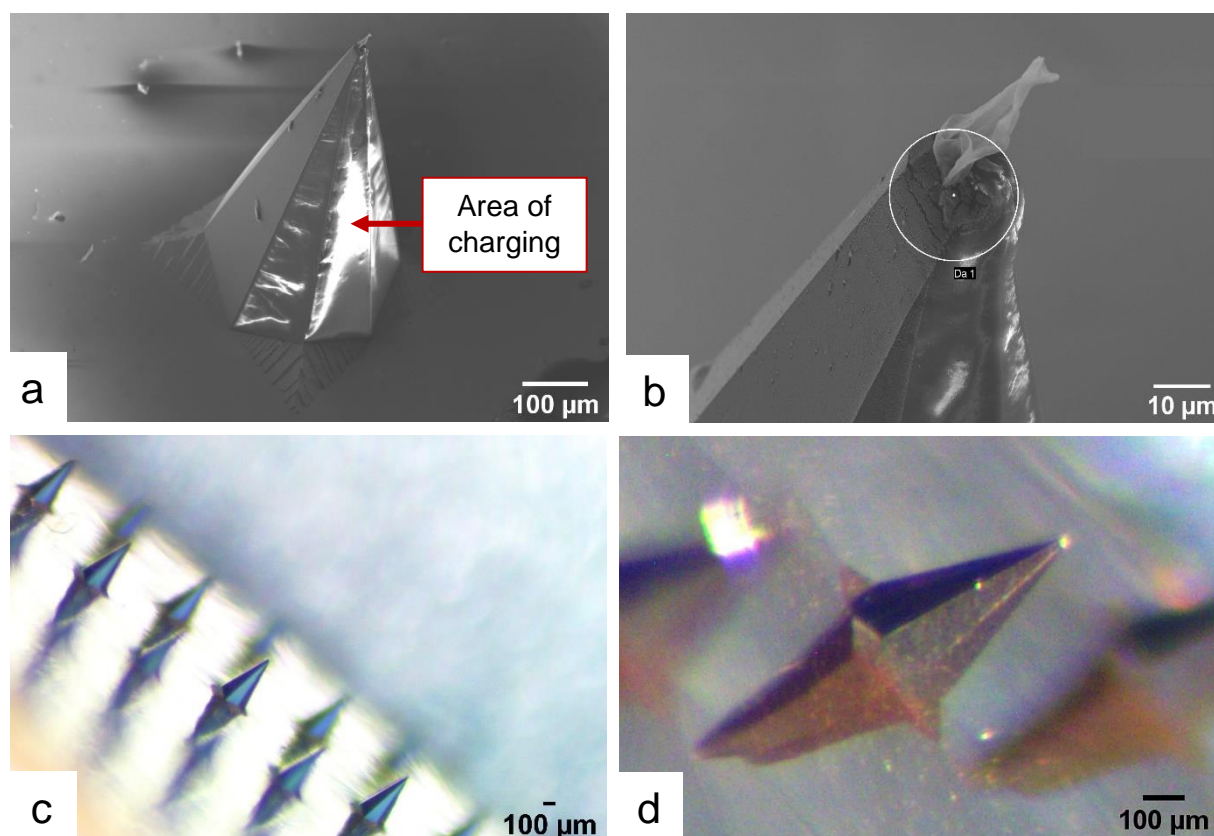
Figure 3.30: Gold-coated, solid, epoxy microneedles post insertion into in vivo human skin (beneath right clavicle) following cardiac signal acquisition. Scanning electron micrographs post insertion of a single microneedle (**a**) (100x magnification and working distance of 5.1mm) and corresponding needle tip measuring 23.45µm (**b**) (1.00K x magnification and working distance of 4.8mm). Stereomicroscope images of part of a microneedle array (**c**) and a single microneedle (**d**).

3.5 Discussion

3.5.1 Influence of electrode design

In Chapter 2, epoxy MNs were characterised and their ability to puncture both ex vivo human and porcine skin models under a variety of conditions was assessed. Whilst their skin puncture was demonstrated, the FDA approved, non-conducting polymer used to fabricate the MNs was not able to conduct a signal. To address this challenge, our collaborators, Tyndall National Institute, coated both sides of the MN wafers using a metal evaporator (O'Mahony et al. 2012; O'Mahony et al. 2016). A 20nm layer of titanium was first coated on the wafers to act as an adhesion layer. This layer subsequently allowed for a 200nm layer of gold to be coated on to the wafers to allow the MNs to conduct a signal. Gold, however, is known to bio-foul which is detrimental to device performance (Saraf et al. 2015; Daggumati et al. 2015). The length of time that the MN arrays were in direct contact with skin was minimal, therefore, the effects of the body on the MN electrodes was not assessed. Furthermore, recording durations used throughout this study were not representative of the durations used for AECG monitoring in practice. Whilst there is a lack of information with respect to the biofouling of MN electrodes for physiological signal monitoring, Chinnadayyala and colleagues recently developed a gold MN sensor for continuous glucose monitoring (Chinnadayyala et al. 2021). MN sensors were packaged into a biocompatible Nafion membrane to prevent electrode biofouling (Chinnadayyala et al. 2021). In vivo, the 550µm length MN sensor exhibited good stability over 7 days. Functional activity, however, was lost after this period and was attributed to electrode biofouling. Despite the potential issue of biofouling, a 'wearable' MN electrode prototype was developed using a commercially available wet electrode. Removal of the plastic covering did prove problematic at first as the scalpel routinely sliced through the remainder of the electrode. It was discovered that using a blunter scalpel resulted in improved removal of the plastic covering. Additionally, removing wet electrodes from their sealed packaging 24 hours earlier also aided removal, as the adhesive connecting the plastic cover to the electrode had time to dry out. The gel-soaked foam pad was also removed to access the sensing element which was subsequently coated in a conductive epoxy as a way of adhering the coated array to the electrode. This allowed signals to flow from the MN through to the connected leads.

It was acknowledged by O'Mahony et al. (2016) that polymers could reduce MN electrode fabrication costs which is important when considering scale up, but conductive coating materials are then required, as employed in this study. Many publications exploring the potential of MN electrodes in physiological signal monitoring use methods of applying a conductive coating. Griss et al. (2001) recorded low amplitude EEG signals using Ag/AgCl

coated MNs. Similarly, to O'Mahony et al. (2016), Ren et al. (2016) coated polymeric MNs with titanium and gold. More recently, Satti et al. (2020) captured cardiac signals using parylene coated MN arrays. An additional way of reducing cost could be locating and trialling an alternative polymer which is both biocompatible and conductive. This would remove the additional step of coating MNs with titanium or gold. Promising conductive polymeric candidates for biomedical applications include poly(3,4-ethylenedioxythiophene) (PEDOT) and polypyrrole (Kaur et al. 2015). Whilst conductive polymers have several advantages, tailoring them to possess suitable mechanical properties, electrical conductivity and acceptable biocompatibility remains challenging. For instance, Chen et al. (2013) investigated the electrochemical performance of MN based dry electrodes which were coated with electropolymerized PEDOT. These electrodes were able to successfully capture biopotentials in both humans and rats (Chen et al. 2013b).

The MN electrode fabrication described in this chapter was initially used by collaborators based at Tyndall National Institute. Several of their published studies have demonstrated the capability of these electrodes in recording ECGs, EMGs and EEGs over short durations (Forvi et al. 2012; O'Mahony et al. 2016; O'Sullivan et al. 2019). In 2012, O'Mahony and colleagues demonstrated the design, fabrication, and implementation of a MN-based electrode in the recording of cardiac and muscle signals. Visually, the ECG traces were comparable with standard wet electrodes, however no quantitative analysis was conducted (O'Mahony et al. 2012). Similarly, to O'Mahony et al. (2012), Forvi and colleagues also demonstrated the capability of these MN-based dry electrodes when recording physiological signals however, again no quantitative calculations were performed (Forvi et al. 2012). This Chapter provides data to corroborate and augment the published data as it has also demonstrated the capability of MN electrodes in recording cardiac activity in healthy volunteers. Mean SNR values calculated during this study were similar those published by Tyndall using the same MN and wet electrodes. Furthermore, publications such as O'Mahony et al. (2016) were used to help develop a method of quantitatively analysing ECG traces. The process of calculating SNR however differs to the aforementioned publications, particularly regarding the use of filters to isolate the signal and noise.

A notable limitation of the study is inconsistent electrode application. MN devices were applied to the volunteer by one individual that was familiar with the technique. Each electrode was applied by the researcher for consistency and volunteers were asked to press down firmly on the electrodes for 10 seconds. Application force was neither measured nor kept constant, therefore in some instances, the MNs may not have pierced the skin, or the depth of MN penetration may have varied. Alternatively, MNs may have punctured the skin but they may

have been expelled if the volunteer shifted their position despite being asked to remain still whilst cardiac signals were acquired. Furthermore, the location of the connection to the snap cables was directly above the MN array. This may have resulted in the leads pulling MNs out of skin. Other designs of ambulatory ECG monitoring electrodes, such as the Ambu® Blue Sensor, have the snap connection located away from the conductive gel pad (Ambu 2013). This could be adapted in future MN electrode designs. Furthermore, future devices could include a built-in applicator which would apply MNs at a consistent force/velocity. Potential ineffective contact of the MNs with the conductive viable epidermal layers may have resulted in the increased acquisition of noise for the dry MN electrode. O'Mahony and colleagues assessed this element of electrode performance by changing contact force (O'Mahony et al. 2016). As the applied force per array increased from 0.18N to 0.55N, the SNR for MN electrodes improved compared to standard wet electrodes. SNR values quoted by O'Mahony, and colleagues ranged from 26.0dB to 30.3dB.

To reduce the impact of the SC and improve contact, skin abrasion is often conducted prior to the application of conventional ECG monitoring electrodes (Campbell et al. 2017) which also contain electrolytic gels to hydrate the skin and reduce impedance. MN electrodes in contrast, can be characterised as a dry electrode as they do not contain electrolytic gels. Instead, they circumvent the SC and directly contact viable skin layers which are considered comparable to an electrolyte (Griss et al. 2000; Griss et al. 2001; Griss et al. 2002; Grimnes and Martinsen 2014). Many studies have examined the performance of dry electrodes (non-MN) which have traditionally been shown to provide a poorer signal when compared to wet electrodes. Very few have directly compared dry electrodes with wet electrodes. Searle and Kirkup (2000) compared three types of electrodes wet, dry and insulating. The data in this Chapter compared dry MN electrodes and wet electrodes containing electrolytic gels, which was comparable to Searle and Kirkup (2000). In the context of Searle and Kirkup (2000), the dry electrode referred to an inert metal with no electrolytic gel at the interface between the skin and electrode which differs from our 'dry' MN electrode. The authors used an oscillating mechanical device, the amount of artifact associated with the wet electrode resulted in little variation over 15 minutes. In comparison, the dry electrode resulted in greater artifact than the wet electrode initially, but lower artifact than the wet electrode following completion of the test. It is suggested by Searle and Kirkup (2000) that this occurred due to the accumulation of perspiration. Following placement of dry electrodes, the skin starts to secrete sweat which aids in electrical conduction due to the presence of ions (Neuman 2000; Wang et al. 2011; Fayyaz Shahandashti et al. 2019). This, however, may take time to occur and account for a degree of stabilisation time. For wet electrodes, this stabilisation refers to the time taken for

the electrolytic gel to diffuse into the skin which aids in signal conduction (Ruffini et al. 2006). During the comparison study presented in this Chapter, no specific time was dedicated to allow the electrodes to settle or stabilise. Following application of both types of electrodes, volunteers pressed firmly down to ensure adequate adhesion between the electrode and skin. Whilst this would have allowed a degree of stabilisation, a specific duration was not stipulated. Multiple publications involving the use of both wet and MN electrodes for physiological signal monitoring do not explicitly state a duration allowing the electrodes to acclimate following their application (Forvi et al. 2012; O'Mahony et al. 2012; Chen et al. 2016; O'Mahony et al. 2016; Wang et al. 2017; Ren et al. 2018; O'Sullivan et al. 2019). A total duration of 3 minutes was recorded, this may not have been enough time for electrodes to settle and for sweat to build up beneath the electrodes. Future studies could set a stabilisation time following electrode application to skin and investigate the performance of both electrode types over time.

Compared to Searle and Kirkup, Griss et al. (2000) designed a dry 'spiked' electrode which could pierce the SC. This early MN-based electrode was coated with Ag/AgCl and resulted in reduced electrical impedance and shorter application times when compared to the conventional wet electrodes (Griss et al. 2000). It was noted that approximately 5% of all spiked electrodes used suffered from needle fracture following removal. Whilst electrical impedance of both electrode types was not investigated in this chapter, unlike Griss et al. (2000), no fracture or breakage of MNs were observed during the baseline comparison study. Furthermore, whilst the use of Ag/AgCl has been proposed as a dry electrode interface material, with excellent results (Griss et al. 2001; Dias et al. 2010), AgCl has been shown to be toxic with an associated infection risk as it dissolves in skin (Ferree et al. 2001; Dias et al. 2010). Another investigation by Wang and colleagues assessed the impedance and ability of MN silicon-based electrodes to record EEG signals when compared to a commercial electrode. The dry MN electrode resulted in lower impedance values than the commercial electrode in the absence of skin preparation and electrolytic gels (Wang et al. 2011). It was determined that the novel dry electrode provided comparable results to the commercial electrode (Wang et al. 2011).

3.5.2 Influence of biological sex

In the present study participants ranged from 21 to 25 years old. Whilst this age range was narrow and not representative of the population requiring AECG monitoring, focusing on individuals who are under 30 years does help minimise the effects of age as arrythmias like AF, are generally more common in the older population (Molander et al. 2003). Furthermore, the researcher was not experienced in analysing traces containing potential anomalies.

Similar healthy volunteer studies conducted by O'Mahony et al. (2016), Chen et al. (2016) and Satti et al. (2020) recruited a similar aged cohort. In total, ten volunteers took part in the study with an equal distribution of females to males. Whilst the sample size was small, recruited volunteers were comparable in terms of age and biological sex. Equal numbers of males and females were recruited to determine if physiology resulted in differences in electrode performance as it is known that meaningful differences in measured ECG parameters exist between males and females (Moss 2010). For instance, during adolescence the resting heart rate is faster in females than males in addition to a longer QT interval, potentially the result of female hormones (Rautaharju et al. 1992). For males, the amplitude and duration of the QRS complex becomes larger than females as a result of male hormones and the associated increase in cardiac mass (Moss 2010). Provided no cardiovascular disease or complications occur, these differences remain between the sexes through adulthood (Moss 2010). There were no statistically significant differences in terms of electrode performance between the sexes in our study. For future studies, an increased sample size would be required alongside the recruitment of a more heterogeneous group of subjects to increase the generalisability of the results. Demographics of particular interest would be body habitus through the measurement of body mass index (BMI) and ethnicity. Both of these parameters are known to influence measured parameters of the ECG but can also result in a variety of ECG abnormalities (Alpert et al. 2001; Fraley et al. 2005; Macfarlane et al. 2014; Santhanakrishnan et al. 2016).

3.5.3 Effects of electrodes on human skin

When developing transdermal monitoring systems an important factor to consider is the effect that the device has on the skin. Following electrode removal, images of the underlying skin were captured to assess signs of irritation. Transient erythema was observed for both electrode types at all locations, however the erythema was visually more intense following the removal of MN electrodes. The non-invasive wet electrode resulted in faint erythema in addition to anecdotal reports of generalised itching. Whilst the erythema was not as intense as in MN electrodes, in practice, the process of conventional electrode application involves an irritating skin preparation to improve the quality of the trace. Skin preparation is conducted to reduce artifacts introduced by the SC (Tam and Webster 1977; Medina et al. 1989; Philips 2008; Campbell et al. 2017). These artifacts are particularly troublesome as they are often difficult to remove using filters and artifact amplitudes are often larger than cardiac signals (Ödman and Åke Öberg 1982). Methods of skin preparation include shaving or cutting excess hair to improve contact between the electrode and skin (Philips 2008; Crawford and Doherty 2012). Skin is typically cleaned with soap and water, or a non-alcoholic wipe to improve

electrical flow (Philips 2008; Crawford and Doherty 2012). Following this, abrasive fine sandpaper is used to remove part of the SC to also aid electrical flow and help reduce motion artifact (Tam and Webster 1977; Medina et al. 1989; Philips 2008; Crawford and Doherty 2012). Tam and Webster (1977), demonstrated that skin abrasion, using abrasive strokes with sandpaper, prior to the application of electrodes improved the quality of biopotential recording by minimising the skin impedance and motion artifacts. Medina et al. (1989) also showed a reduction in skin resistance and artifact with just one stroke of fine sandpaper. Whilst wet electrodes resulted in visibly less redness in our study, the process of skin abrasion that would commonly be used in clinical practice with this electrode would result in irritation (Tam and Webster 1977). Furthermore, applying electrodes which contain conductive gels could irritate the skin further. Abrasive methods of skin preparation for conventional electrodes may therefore produce greater irritation than MN electrodes. Whilst the wet electrodes contained a built-in, gel-soaked abrader disc, the use of external skin preparation techniques, including abrasive wipes and hair removal, were deliberately excluded in the current in vivo study to compare the performance of the two electrode types when applied directly to skin

MN electrodes are minimally invasive. Whilst no methods were used to measure the extent of erythema for example using a chromameter as conducted in Bal et al. (2008), gross visual comparisons indicated that the MN electrode resulted in increased erythema compared to the conventional electrode. As demonstrated in Chapter 2, these epoxy MNs could pierce the skin and breaching the skin's barrier is likely to induce a degree of irritation and inflammation, as evidenced by the captured images. Moreover, indentations (impressions in the skin due to micro-features) were observed for all subjects, in all anatomical locations. Whilst indentations confirmed MN contact with skin, the extent varied with anatomical location and volunteer. Inconsistency in MN application force could explain the differences in erythema observed between volunteers as increased application force is likely to have resulted in MNs being inserted deeper within the skin thus potentially resulting in increased inflammatory response. Furthermore, as no method was used to confirm MN insertion, for instance application of a methylene blue dye (Moronkeji et al. 2017) or OCT imaging (Coulman et al. 2011), it cannot be confirmed that the MN electrodes had pierced the skin. The materials used in MN electrode fabrication could have also contributed to the skin erythema. MNs were comprised of an FDA approved epoxy coated with a 200nm layer of gold for conductivity. Gold-coated MNs have been used by several groups for the sensing of various molecules within interstitial fluid (Barrett et al. 2015; Bollella et al. 2019; Madden et al. 2020) and during physiological signal monitoring (Chen et al. 2013a; Ren et al. 2018; Satti et al. 2020). Whilst gold is a biocompatible material which is known to be inert and does not routinely result in skin

reactions (Nimi et al. 2011), three volunteers stated they had a history of eczema. This common skin condition is associated with unpredictable flare-ups of skin inflammation thereby potentially contributing to the increased erythema observed in these volunteers (Asher et al. 2006).

Subjective data including anecdotal information regarding electrode-induced pain or sensations reported by volunteers was also gathered during the study. Upon application of the non-invasive wet electrodes to the skin, no volunteer reported any immediate signs of discomfort or pain. During the short period, volunteers stated that the electrodes were noticeable alongside other common forms of irritation including minor redness and generalised itching which is consistent with other publications (Taheri et al. 1994; Oster 2005; Rood and Sparks 2006; Ruffini et al. 2006). Following the application of MN electrodes to the required anatomical locations, six subjects reported some minor discomfort regarding the MN electrode placed underneath the right clavicle (RA). Compared to the lower abdomen, MN application just underneath the right clavicle may have resulted in increased discomfort due to the pressure of underlying bone or may have impacted more on pain receptors. MNs used throughout this postgraduate research measured approximately 500μm in length which was considered to be a suitable length considering that Gill and colleagues reported that the insertion of 700μm length MNs to the volar forearm of volunteers did not appear to cause pain (Gill et al. 2008). However, as application force was not controlled the volunteers who reported minor discomfort may have experienced greater MN penetration due to an increased application force as witnessed in Chapter 2 and the published literature (Donnelly et al. 2010; Gittard et al. 2013; Cheung et al. 2014).

Once applied to the skin, volunteers who reported initial minor discomfort indicated that this subsided shortly after, during the ECG recording and while they were at rest. During signal acquisition, all volunteers stated that whilst both types of electrodes were not painful, they were noticeable. A further consideration with respect to volunteer discomfort could be explained by the number of MNs per array. Arrays were deliberately fabricated to be 18mm in diameter to be directly comparable to the diameter of the gel-soaked pad in wet electrodes. As shown in Chapter 2, these arrays contained approximately 85 MNs. Gill et al. (2008) demonstrated that whilst length had the greatest influence on pain, the number of MNs also affected the level of pain. A 10-fold increase in the number of MNs increased pain by over 2-fold. Whilst it would be beneficial in terms of pain and discomfort to reduce the number of MNs per array, the fidelity of the recorded signal may suffer as there would be a reduced surface area with fewer MNs in contact with the skin. A balance is therefore required between needle density, penetration and performance versus pain.

A key requirement when developing wearable technology is the construction of a device that causes the least amount of irritation. Whilst anecdotal information was captured, future studies could include a pain scoring system such as the visual analogue scale used by Kaushik et al. (2001) and Gill et al (2008). Furthermore, questionnaires could be included in future studies to ascertain enhanced information regarding perceived sensations.

3.6 Conclusion

Chapter 3 compared the ability of two electrode designs to record cardiac activity in healthy adult volunteers. An ethics application was submitted to and approved by the Cardiff School of Pharmacy Ethics Committee. A pilot study was conducted and used to develop a quantitative method of ECG analysis using SNR to measure signal quality. Epoxy MNs, introduced and tested in Chapter 2, were successfully incorporated into MN electrodes by adapting a commercially available wet electrode. Both MN and conventional wet electrodes were used to record 3 minutes of cardiac activity from ten volunteers at rest. Quantitative SNR data revealed that electrodes were comparable in their performance however, a 1.7dB difference existed between the designs with conventional electrodes recording signals with a greater SNR. However, the clinical impact of these signals was not assessed, and the effect of this 1.7dB difference on the clinical interpretation of ECG traces has yet to be determined. Accompanying qualitative visual comparisons of the traces indicated that both electrodes were successful at capturing cardiac signals. However, there were differences in the magnitude of PLI, with MN electrodes recording signals with a greater quantity of noise. Whilst this initial comparative study highlighted the promise of the MN design, limitations were identified. Further work is now required to refine the design, improve the consistency of application, and ensure MNs are retained within the skin. Although this study calculated SNR and PLI in addition to visual comparisons, a study investigating the electrode-skin impedance is essential to further characterise the electrodes. Furthermore, whilst the use of human volunteers is clearly beneficial to the testing of novel ECG devices, this does involve applying uncertified electronics to participants. A suitable laboratory skin model would enable optimisation of MN parameters and design for improved electrode performance prior to in vivo evaluation.

CHAPTER 4

EX VIVO SKIN MODEL DEVELOPMENT FOR SIMULATED CARDIAC MEASUREMENTS

4.1 Introduction

In vivo human data captured in the previous chapter will inform the development of a model whereby 'artificial' cardiac signals are generated through skin explants and acquired using various electrode technologies.

4.1.1 Experimental models with potential for testing transdermal sensors

4.1.1.1 In vivo human models

Medical research has an extensive history of using human volunteers to test the effects of new interventions. Several publications investigating the performance of novel physiological sensors such as MNs (Ren et al. 2017), textiles (Tsukada et al. 2019) and electronic 'tattoos' (Wang et al. 2018b) use volunteers as a means of evaluating electrode performance. For transdermal sensors, the use of human volunteers offers a plethora of physiological signals which can be monitored including EEG, EMG and ECG (Forvi et al. 2012; Ren et al. 2017). These recorded signals would be 'real' as opposed to simulated, and the clinical implications of these signals can be assessed. Yu et al. (2009), Forvi et al. (2012), Srivastava et al. (2015), and Ren et al. (2017) are all examples where human volunteers were recruited to test novel MN electrodes. Small studies such as these can glean useful information regarding device performance and wearability. Following device development and testing in healthy participants, at risk individuals can be recruited to assess device functionality in target populations. For instance, larger studies such as REHEARSE-AF recruited at-risk patients over a 12-month period to evaluate the ability of an AliveCor Kardia™ monitor to screen for AF (Halcox et al. 2017). Evaluating new cardiac sensors in their target patient groups offers volunteers with opportunities to provide feedback regarding device wearability. User feedback

aids the development of devices which are suitable for both patient and practitioner. Studies such as Bolourchi et al. (2020) demonstrated comparable performance between the Holter monitor and ZIO patch =with patients often preferring the ZIO patch over the Holter monitor due to the lack of wires and the ability to shower. Halcox et al. (2017) and Hermans et al. (2021) demonstrated that patients found the AliveCor device easy to use and more convenient without any restrictions on activities. This device is now available for sale allowing the public to take control and monitor their cardiac health. Furthermore, in vivo human studies allow researchers to investigate and observe the local effects of the device upon the skin, which is important when examining adverse effects such as irritation.

4.1.1.2 In vivo animal models

Similarly, to human volunteers, the use of animals for scientific purposes is a longstanding practice in biological research and medicine. Regarding physiological signals, mice, rats, rabbits, guineapigs, and dogs are some of the most frequently used animal species in experimental cardiac electrophysiology. These animals show similarities in cardiac ion channels with the human myocardium (Eckardt et al. 2002; Gralinski 2003; Stubhan et al. 2008; Konopelski and Ufnal 2016). Furthermore, the use of smaller animals allows for increased sample sizes and more treatment groups, however they are less representative of human skin. Comparisons between mice and humans have been investigated in terms of cardiac electrophysiology (Kaese and Verheule 2012) and mice have become a popular model in the research of cardiac arrhythmias (Kaese et al. 2013). Results of murine studies should be transferred to humans with caution as murine electrophysiology, particularly ion currents underpinning the action potential, differs from humans (Kaese et al. 2013). Rats have also become a suitable model when investigating cardiac performance under physiological conditions (Konopelski and Ufnal 2016). ECG using live rats is an important investigational tool in cardiovascular research, however, the interpretation of ECG parameters can prove challenging. The use of sedation could influence ECG parameters as several anaesthetics are known to cause ECG changes (Zorniak et al. 2010; Konopelski and Ufnal 2016). Whilst the majority of research conducted in rats relates to the monitoring of ECG parameters whilst under the influence of various therapeutics (Milliez et al. 2005; Hamdy and Brocks 2009; Mackiewicz et al. 2014) their use in the testing of wearables is limited. ECG recordings are also feasible in larger animals including goats (Kant et al. 2010). Although, the use of larger animals could incur higher costs if significant sample sizes are required.

4.1.1.3 Excised human skin

Human skin explants are considered an appropriate substitute for in vivo MN testing. Ex vivo human skin models typically use excised skin obtained from routine surgeries such as

mastectomy (Ng et al. 2009), breast reduction (Ng et al. 2009) or abdominoplasty (Ranamukhaarachchi et al. 2016). The excised human skin Trowell-type organ culture model described by Ng et al. (2009), has been employed in multiple research areas include immunology (Ng et al. 2009), transdermal drug delivery (Davies et al. 2017) and wound repair (Danso et al. 2015). In addition to being a valuable laboratory tool, ex vivo human skin could help bridge the gap between animal models and real-world clinical situations as it is architecturally more representative of the tissue than synthetic models or animal studies. The model, however, is not without limitations. Following excision from its natural environment, the cells of human skin can remain viable for up to 72 hours with appropriate handling and culture conditions (Ng et al. 2009). This short window of viability limits the range and duration of experiments it can be used for. The irregularity of surgical procedures and considerable sample variability results in tissue which is not frequently available and varies in sample size, age and condition. Regarding cardiac monitoring, the structure of ex vivo human skin is more representative of the in vivo environment, however unlike human volunteers or in vivo animal models, the skin has been severed from the source of physiological signals, therefore assessing electrode performance in terms of cardiac signal acquisition could prove problematic as an artificial signal source would be required.

4.1.1.4 Excised animal skin

Skin penetration studies are an important part of assessing MN devices. Therefore, choice of model is important. In vivo human studies or ex vivo human skin explants would be the ideal in assessing transdermal sensors. However, human skin explants which are of suitable size and quality are not readily accessible or are limited in availability. Ex vivo animal models are used as alternatives to in vivo and ex vivo human skin in the testing of MN systems (Gittard et al. 2013; Moga et al. 2013). The most relevant ex vivo animal model used for transdermal testing is considered to be the pig (Ranamukhaarachchi et al. 2016). Ex vivo porcine skin is easy to obtain and has been shown to be comparable to human tissue in terms of structure, histological and biochemical properties (Schmook et al. 2001; Jacobi et al. 2007; Debeer et al. 2013). Many published studies have demonstrated that the thickness of the SC and VE in porcine skin is similar to humans (Sandby-Møller et al. 2003; Jacobi et al. 2007). In terms of biomechanical properties, porcine skin has a similar dermal collagen fibre arrangement and SC composition (Ranamukhaarachchi et al. 2016). Ranamukhaarachchi and colleagues compared the mechanical similarity and assessed the impact of freezing on the mechanical properties of human and porcine skin explants. In conclusion fresh ex vivo porcine skin at high humidity conditions might present a more suitable skin model in the absence of fresh human skin explants. Regarding ECG wearables, Wang and colleagues used porcine skin to investigate the underlying mechanisms of how cardiac signals were captured using their

carbon nanotube-PDMS based wearable device (Wang et al. 2020). The authors subsequently recorded cardiac signals using their wearable device in nine healthy volunteers aged between 18 and 20 years (Wang et al. 2020). Similarly, to ex vivo human skin, ex vivo animal skin would have been severed from the source of physiological signals.

4.1.1.5 Electrode-skin impedance and electrical equivalent models

Surface electrodes act as an interface and convert ionic currents flowing within the body to electrical currents flowing within recording equipment. Electrical properties of this electrode-skin interface depend on the type of electrode and contact area (Chlaihawi et al. 2018). To assess the electrical properties of this interface, an important parameter, termed impedance, is used. Broadly speaking, impedance is the amount of resistance that a component offers to current flow within a circuit, at a specific frequency (Grimnes and Martinsen 2014). Generally, a large and unstable electrode-skin impedance can result in signal distortion (Li et al. 2017). Therefore, a high-quality connection between the skin and electrode is required to acquire high fidelity signals. Several groups have used impedance to assess this connection between electrodes and skin (Wu et al. 2018; Shahandashti et al. 2019; Zahed et al. 2020; Dong et al. 2021; Ullas Pradhan et al. 2021). Wet electrodes are considered the current gold standard electrode in clinical practice due to their reliability, low impedance and high SNR (NHS 2018). Limitations including preparation time and gel dehydration have encouraged efforts in the development of dry electrodes. Whilst this type of electrode offers advantages including quick setup, user friendliness and cleanliness due to the elimination of conductive gels, dry electrodes generally result in a high electrode-skin impedance (Searle and Kirkup 2000; Li et al. 2017; Chlaihawi et al. 2018). Compared to a few kΩ for wet electrodes, dry electrode impedance is frequently several hundreds of kΩ or higher (Kitoko et al. 2011; Li et al. 2017). Moreover, dry electrodes, in particular rigid electrodes cannot conform to the irregular nature of the skin's surface, resulting in an unstable electrode-skin interface which subsequently affects signal quality (Kitoko et al. 2011; Chen et al. 2014; Fatoorechi et al. 2015). Efforts have been made to develop dry electrodes which are flexible and conformable (Lee et al. 2014; Chlaihawi et al. 2018; Stephen et al. 2018; Wang et al. 2018b). Whilst these newer electrodes still exhibit a larger impedance compared to wet electrodes, they have been shown to have improved performance during movement due to better conformal contact (Chlaihawi et al. 2018). With respect to human skin, the dermis, is considered to have a higher electrical conductivity, comparable to that of an electrolyte (Griss et al. 2001). Conversely, the outermost layer of the epidermis, the SC, is considered to be an area of increased electrical resistance due to its composition of dead cells. MN electrodes reduce the contact impedance by penetrating through the electrically insulated SC and directly contacting conductive layers of skin. Electrically, the contact between the MN electrode and skin is typically described by the

equivalent circuit model shown in Figure 4.1. In principle, the impedance of MN electrodes is lower than that of wet electrodes.
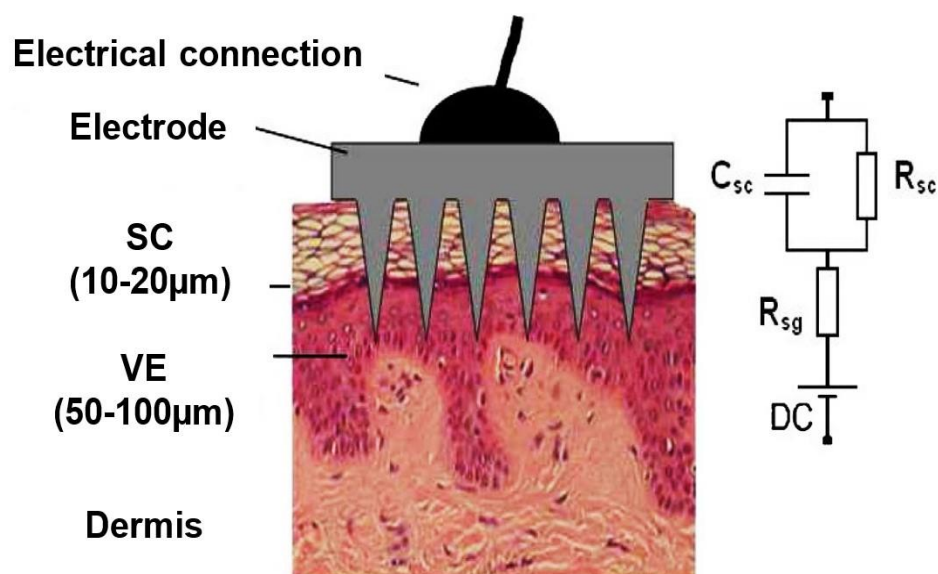
Figure 4.1: Circuit equivalent model alongside a cross-sectional view of the interface between the microneedle electrode and skin. At a metal-electrolyte interface a charge distribution occurs. A potential called the half-cell DC potential is generated as a result of the charge layer and is modelled by a **DC** voltage source. The resistance (R_{sg}) models the electrical properties of the conductive layers of skin. Contact impedance can be modelled as a parallel combination of the interface capacitance (C_{sc}) and the charge transfer resistance (R_{sc}). Image adapted from Pini et al. (2012).

Regarding a potential model for clinical data simulations, an electrical equivalent model of the electrode-skin interface could be developed to remove the dependence on, and variability of biological tissue (O'Sullivan et al. 2019). O'Sullivan and colleagues conducted impedance testing using three types of electrodes on healthy adult volunteers. This testing helped develop simplified passive impedance models of the electrodes which were subsequently incorporated into a simulation framework (O'Sullivan et al. 2019). The authors used EEG signals obtained from a database of clinically acquired neonatal EEG at the Irish Centre for Foetal and Neonatal Translational Research. For ECG simulation, the resource PhysioNet could be used (Goldberger et al. 2000). These digital recordings of physiological signals were collected from both healthy subjects and patients with a variety of conditions with major public health implications including congestive heart failure and AF (Goldberger et al. 2000). Whilst the use of such a model overcomes the variable nature of tissue, the presence of the biological tissue and how it responds to an applied load is important for the design and optimisation of novel transdermal sensors.

Whilst the models discussed above have their own unique benefits and limitations, a model which combines the in vivo environment with a suitable source of physiological signals is required to test the effects of changing MN parameters on electrode performance.

4.1.2 Aims and objectives of the chapter

This chapter aimed to develop and assess the suitability of a laboratory model whereby simulated cardiac signals are generated and acquired through ex-vivo porcine skin using different electrode technologies. This chapter then aims to use the developed model to assess the effects of changing parameters on MN electrode performance. The objectives were to:

- To integrate a method of signal generation and acquisition to an ex vivo porcine skin model that has been established and validated in the laboratory at Cardiff School of Pharmacy and Pharmaceutical Sciences (Ng et al. 2009).

- To fabricate and test a resistor divider to use within the laboratory model as a suitable method of simulating the low voltages of real-world cardiac signals.

- To record simulated cardiac signals at four locations on the model and calculate signal loss using Pearson's Correlation coefficient and signal quality using SNR.

- To assess the susceptibility of wet, MN and dry disc electrodes to PLI by plotting the FFT of recorded simulated cardiac signals.

- To assess the performance of wet electrodes and the initial MN electrode prototype by recording simulated signals through ex vivo porcine skin over 6 hours.

- To assess how needle length can affect electrode performance by recording simulated signals through ex vivo porcine skin using 500µm and 600µm length epoxy MN electrodes.

- To develop a bespoke MN electrode and assess how device design can affect electrode performance by recording simulated signals through ex vivo porcine skin using wet electrodes, initial MN prototype electrodes and bespoke MN electrodes.

- To determine the electrode-skin impedance of wet, MN and disc electrodes in human volunteers over a range of frequencies.

- To assess the dehydration of conductive gels by measuring how the weight of electrolytic gel-soaked foam pads from a commercially available wet electrode changes over 48 hours.

4.2 Materials

Details of equipment and reagents used in the studies described below are listed in the equipment and reagents tables. Simulated cardiac data was acquired using the OpenBCI GUI version 5.0.6 (OpenBCI, USA). Data processing was conducted using Microsoft Excel version 16.46 (Microsoft Corporation, USA) and MATLAB 2018a (The MathWorks Inc., Natick, MA). Image processing was conducted using ImageJ software (NIH, USA) and Microsoft PowerPoint version 16.37 (Microsoft Corporation, USA).

4.3 Methods

4.3.1 Simulation framework overview

The method outlined below is an overview of the simulation process. Throughout its progress results have informed the development of the model which will be discussed in further detail in section 4.4. Figure 4.2 displays the model highlighting the stages involved in signal generation and acquisition.
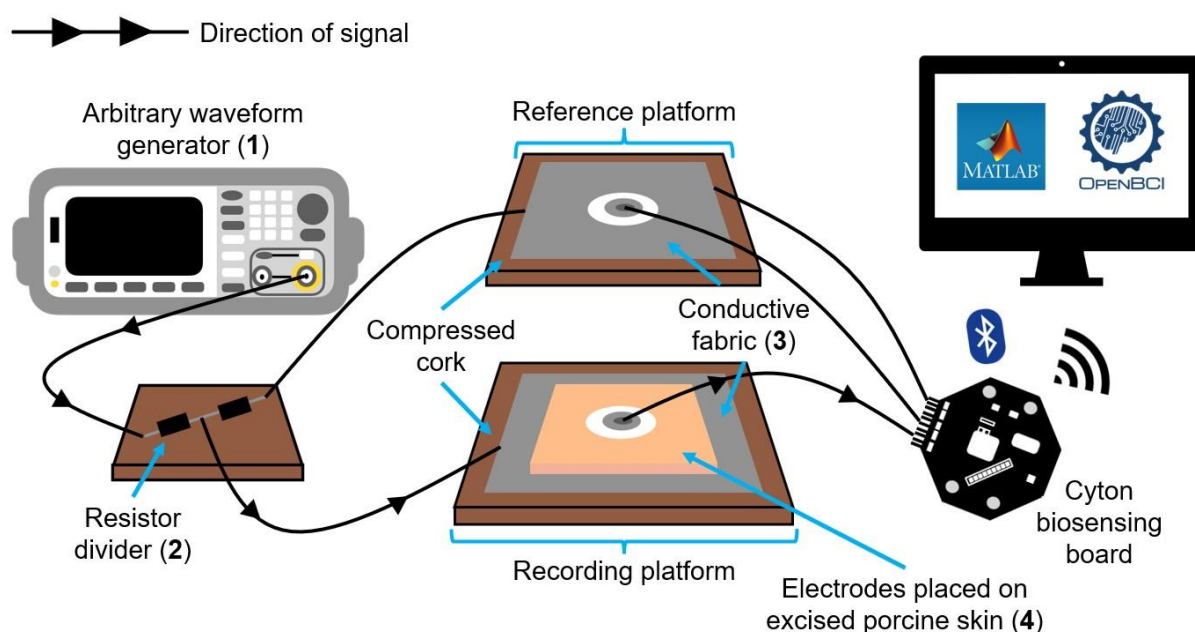
Figure 4.2: Diagrammatic representation of the experimental setup used for data simulations. Simulated cardiac signals were generated using a waveform generator which emitted signals at a sample rate of 500Sa/s and amplitude of 1.37Vpp. Signals were reduced to mV using a resistor divider and conducted through the recording platform. Signals were then recorded through prepared ex vivo porcine skin using three electrode types connected to a Cyton biosensing board which transferred data to computer software using Wi-Fi. Numbers shown in brackets represent the specific locations where signals were recorded from to account for signal loss resulting from model setup, biosensing board and electrode types.

An arbitrary waveform generator (AWG) contained software which included a pre-programmed cardiac waveform containing the ECG characteristics of a healthy individual. The waveform was emitted from the AWG at a sample rate of 500Sa/s, peak-to-peak amplitude of

1.37Vpp with no DC offset. Using a 50Ω BNC plug-alligator clip coaxial cable, the AWG was connected to a resistor divider to simulate the low voltages of cardiac signals. The resistor divider comprised a 100kΩ wire-wound resistor soldered in series, using lead-free solder, to a 100Ω wire-wound resistor. Scaled signals were subsequently conducted, using crocodile clips, through the recording platform. This platform contained two layers of compressed cork covered with a layer of stretch, conductive fabric with a resistance of <5Ω/sq. Porcine skin explants were prepared using the method described in Chapter 2. Prepared explants were pinned to the conductive fabric covering the two layers of compressed cork. Figure 4.3 displays the three types of electrodes used in the acquisition of simulated cardiac signals.

Wet electrode   **Microneedle electrode**   **Disc electrode**

+ve control   Electrode of interest   -ve control
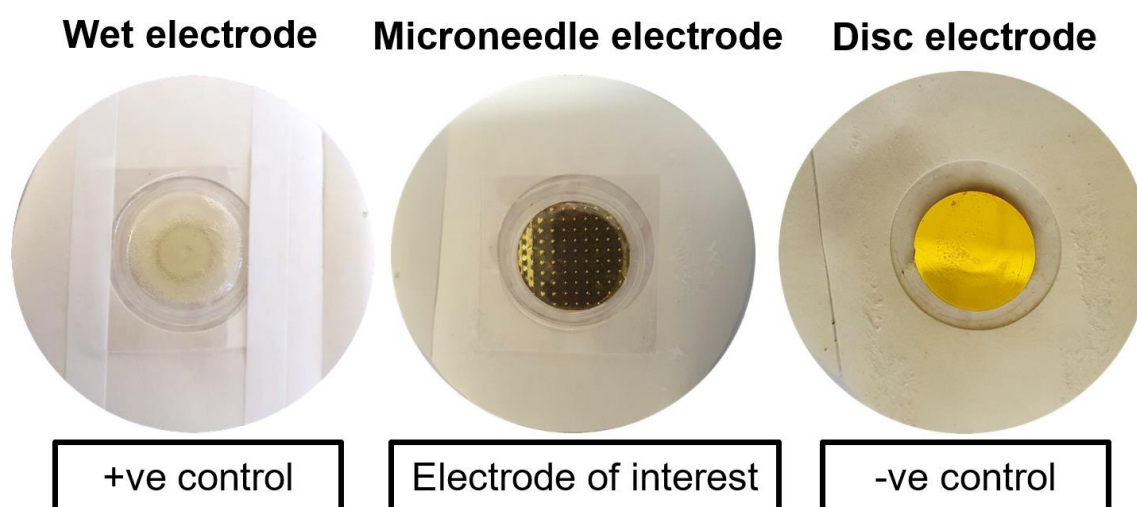
Figure 4.3: Types of electrodes used for simulated cardiac signal acquisition. 3M Red Dot 2239 pre-gelled adult ECG monitoring electrode acted as the positive control (**a**). Epoxy microneedle electrode was the electrode of interest and consisted of 500µm length microneedles coated with titanium and gold (**b**). Epoxy dry, disc electrode acted as the negative control due to the absence of microneedles (**c**). Authors own images.

Wet electrodes are the current gold standard therefore, they were included as a positive control (Figure 4.3a). Epoxy, MN electrodes were the electrode of interest (Figure 4.3b) whilst epoxy 'blank' disc electrodes were included as the negative control as this type of electrode did not contain MNs (Figure 4.3c). Epoxy MN and blank electrodes were fabricated using the method stated in Chapter 3. Electrodes were manually applied to tensioned skin samples however application force was not controlled. Each electrode was connected to a separate channel on an OpenBCI 8-channel Cyton biosensing board with a 32-bit processor. A Wi-Fi shield, currently in beta testing mode, was attached to the board to allow for increased sample rates and data transfer over Wi-Fi. During signal acquisition, 30 second recordings were acquired, in triplicate, using a sample rate of 500Hz and transferred via Wi-Fi to the OpenBCI GUI software. To account for signal losses due to model configuration, the biosensing board and the three types of electrodes, simulated signals were recorded simultaneously from specific locations within the model. Location 1 recorded signals directly from the AWG using

an oscilloscope to determine if the cardiac waveform was emitted as programmed. The remaining locations were recorded simultaneously using five channels on the biosensing board. Recording the output of the resistor divider (location 2) demonstrated the accuracy of waveform recreation within the mV range. Following this, signals were recorded from the conductive fabric (location 3). This location allowed for losses to be calculated from the use of a 15cm length piece of stretch, conductive fabric. Location 4 was the final stage and recorded the respective outputs of each of the three electrode types through prepared ex vivo porcine skin.

4.3.2 Assessing changing parameters using simulated electrocardiography

4.3.2.1 Effect of microneedle electrode performance over time

To assess the performance of MN electrodes over time, simulated ECG was conducted using the aforementioned method. Epoxy, 500µm length MN electrodes were manually applied to the surface of excised porcine skin in addition to a wet electrode. Each electrode was connected to a separate channel on a Cyton biosensing board using snap connectors. A Wi-Fi shield was attached to the board to allow for increased sampling rates. Cardiac waveforms were recorded simultaneously from both types of electrodes immediately following application (0hrs) and at designated time intervals (0.5hrs, 1hr, 2hrs, 4hrs and 6hrs). At each time point, three, 30-second recordings were acquired using a sample rate of 500Hz and gain of x24. Data were transferred over Wi-Fi to the OpenBCI GUI and subsequently analysed.

4.3.2.2 Effect of changing microneedle length on electrode performance

To assess the effects of changing MN length, 18mm arrays were fabricated by our collaborators, Tyndall National Institute, with needles measuring either 500µm or 600µm in length. Using the same method of waveform generation and acquisition as detailed above, signals were recorded through ex vivo porcine skin using wet electrodes and two length MN electrodes. During signal acquisition three, 30-second recordings were acquired using a sample rate of 500Hz and gain of x24.

4.3.2.3 Effect of changing electrode design on performance

A bespoke electrode design was manufactured by Maddison Product Design Ltd (West Sussex, UK). Metallised MN arrays measuring 18mm in diameter and containing 500µm length needles were affixed to the design using the conductive, adhesive epoxy as described in Chapter 3. Using the same methods of generation and acquisition as detailed above, cardiac waveforms were recorded through ex vivo porcine skin using three types of electrodes. Wet electrodes, initial MN electrodes and bespoke MN electrodes (Figure 4.4) were used to

compare the effects of design on electrode performance. In total, three, 30-second recordings were acquired using a sample rate of 500Hz and gain of x24.
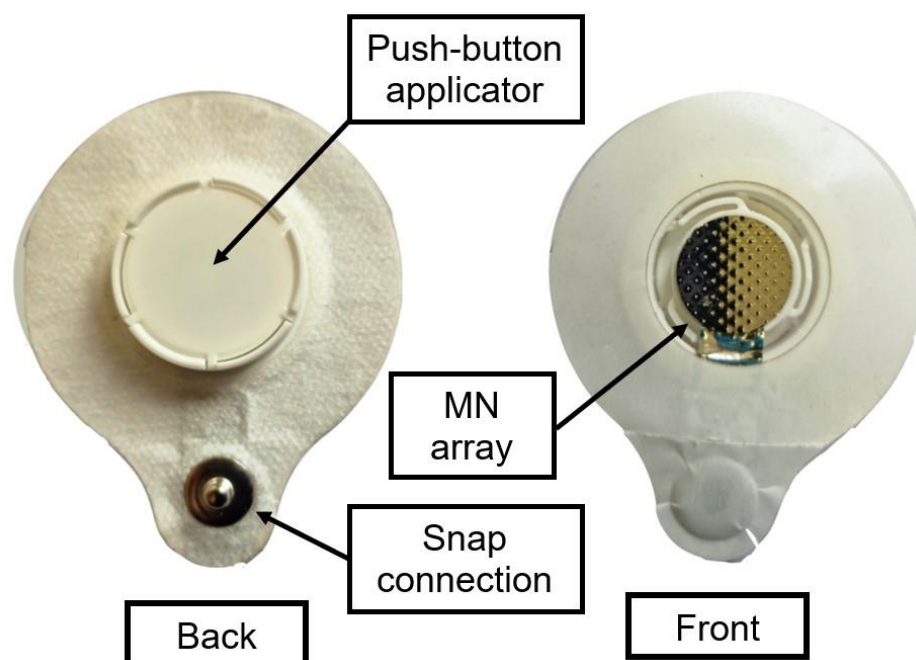
Figure 4.4: Front and back of a bespoke microneedle electrode with push-button applicator. Design fabricated by Maddison Product Design and features a push button applicator which applies a pressing force of approximately 15N. An audible click can be heard when the device is deployed. Authors own images.

4.3.3 Analysis of microneedle penetration

OCT imaging was conducted using the method described in Chapter 2. To summarise, 500 frame scans were captured following the removal of each electrode from skin explants. Scans had an area measuring 6x2mm (width x length), whilst image depth varied between 1-2mm, depending upon the tissue. Following OCT imaging, 1mL of 2%w/v methylene blue dye was applied to the area of skin in contact with the electrode. After 10 minutes, a pipette was used to remove excess dye from the skin explant. Subsequently, 70% ethanol was applied to the surface of the skin to further remove any remaining methylene blue and aid the identification of microchannels.

4.3.4 Data processing and analysis

MATLAB was used to process and subsequently analyse the recorded simulated signals. Recorded data were stored in its unprocessed state and imported into the MATLAB workspace when required for analysis. As stated in the previous chapter, the Cyton board was originally developed for EEG recordings. Due to the low voltages of EEG signals, the board stores data in the form of µV. Therefore, the simulated data were first converted to mV as ECG traces are typically measured in this range. Simulated signals were filtered using a 0.5Hz digital high-

pass filter to remove artifacts such as offset. For each 30 second recording, six individual waveforms were selected for further analysis. Similarly, to the method described by O'Sullivan et al. (2019), the amplitudes of the selected signals were normalised using z-score normalisation (Appendix VIII). SNR and Pearson's Correlation Coefficient were calculated with respect to the original signal used by the AWG for simulation using MATLAB functions (Appendix VIII). SNR and coefficients were calculated both before and after filtering using a 50Hz digital notch filter. Mean and standard deviation values for correlation and SNR were calculated.

4.3.5 Characterisation of electrode technologies

4.3.5.1 Electrolytic gel dehydration

An electrode weight loss study was conducted whereby 3M Red Dot 2239 pre-gelled adult ECG monitoring electrodes (n=5) were removed from their sealed packaging. Using a scalpel, the conductive gel-soaked foam pads were removed and subsequently placed in weighing boats of known weight. Electrodes were either covered with the original adhesive component or left uncovered. The boats were re-weighed at designated time intervals (0, 1, 2, 4, 6, 24 and 48 hours) alongside the temperature and humidity of the surrounding environment. The weight of the boat was subtracted from the results to yield the weight of the gel pad over time. All gel pads were imaged before and after the study using stereomicroscopy and digital images were captured. MN and disc electrodes were also weighed to act as controls.

4.3.5.2 Electrode susceptibility to powerline interference

To assess the susceptibility of MN electrodes to PLI, simulated cardiac signals, as described in section 4.3.1, were recorded using the three types of electrodes shown in Figure 4.3. During signal acquisition, three recordings were acquired from each type of electrode with each recording lasting 30 seconds in duration. Within the UK PLI generally occurs at a frequency of 50Hz. Using MATLAB, the frequency and magnitude of PLI was determined by plotting the FFT and obtaining the peak amplitude of the signal occurring at approximately 50Hz. Mean and standard deviation noise values for each type of electrode were determined.

4.3.5.3 Electrode-skin impedance

Impedance measurements were conducted on a single, healthy adult volunteer by the postgraduate researcher whilst visiting collaborators at Tyndall National Institute. The study was approved by the Clinical Research Ethics Committee of the Cork Teaching Hospital (Ref: ECM 4 (I) 10/01/17 & ECM 3 (j) 29/03/19). A precision LCR meter with a frequency range of 20Hz to 2MHz and basic accuracy of ±0.05% was used to setup the frequency sweep and measure the impedance response (Keysight 2014). Prior to electrode application, the device

was calibrated using a resistor of known value to determine if the machine was stable and capable of detecting pre-determined resistances. A four-point probe bioimpedance measurement setup was used to remove the impedance of the machine and cables. The cables were subsequently taped in position to the table to reduce movement which could affect measurements. Wet, MN and disc electrodes were used within this impedance study (Figure 4.3). As shown in Figure 4.5, pairs of electrodes were attached to the volar forearm, spaced 3cm apart (centre to centre), and allowed to equilibrate for 5 minutes. No skin preparation of any kind, including washing, shaving or abrading were conducted prior to electrode attachment. Following equilibration, the LCR meter injected an AC signal through one electrode and subsequently recorded the signal at the second electrode. A total of three, 10 second frequency sweeps were conducted sequentially using each electrode type. Wet electrodes were applied first, followed by dry disc electrodes and MN electrodes. Following the removal of the MN electrodes, a further wet electrode was reapplied. To allow comparisons between various electrode technologies, the gel-soaked foam pad on the wet electrode, MN array and Ti/Au coated disc all measured 18mm in diameter.
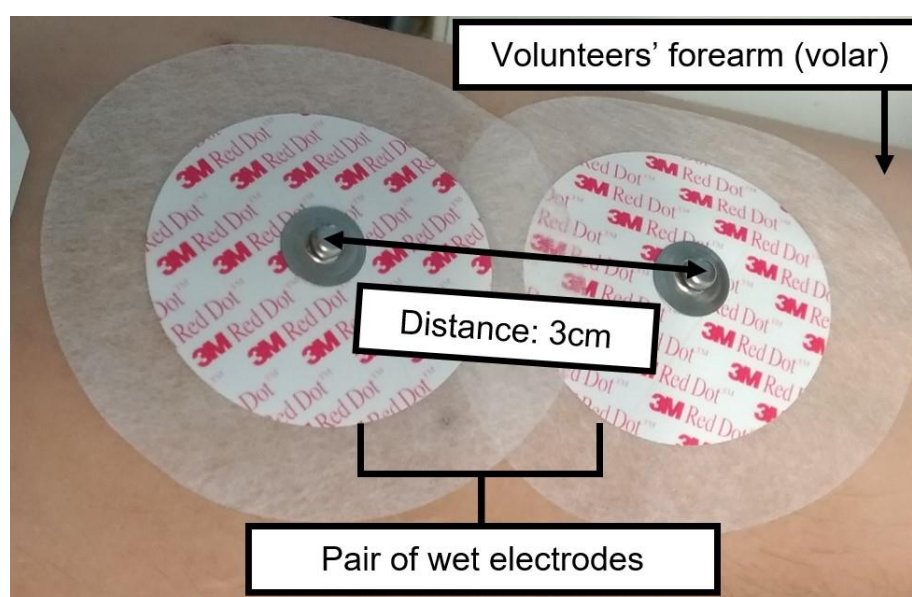
Figure 4.5: Pair of wet electrodes used for impedance recording. Electrodes were applied to the volunteers' volar forearm where the distance between the centre of the electrodes measured 3cm. Authors own image.

4.3.6 Statistical analysis

An independent samples t-test or one way ANOVA were used to calculate statistical significance using the statistical software package SPSS when considered appropriate. Significance was defined as $p < 0.05$.

4.4 Results

4.4.1 Development of an ex vivo model for simulated electrocardiography

4.4.1.1 Signal generation

The main focus of this chapter was the development of a suitable laboratory model to allow for the future testing of MN parameters on electrode performance. However, the first step in model development was identifying a suitable cardiac waveform, and a method of generating this waveform further. An AWG was used as this device contained software which included a pre-programmed cardiac waveform and could emit this waveform further. The pre-programmed cardiac waveform (Figure 4.6) consisted of 450 data points, 0V DC offset and an R wave with a peak amplitude of 1V. Initially, one complete waveform lasted 1.8 seconds when emitted at a sample rate of 250Sa/s. However, the sample could be adjusted to alter the duration of the waveform.
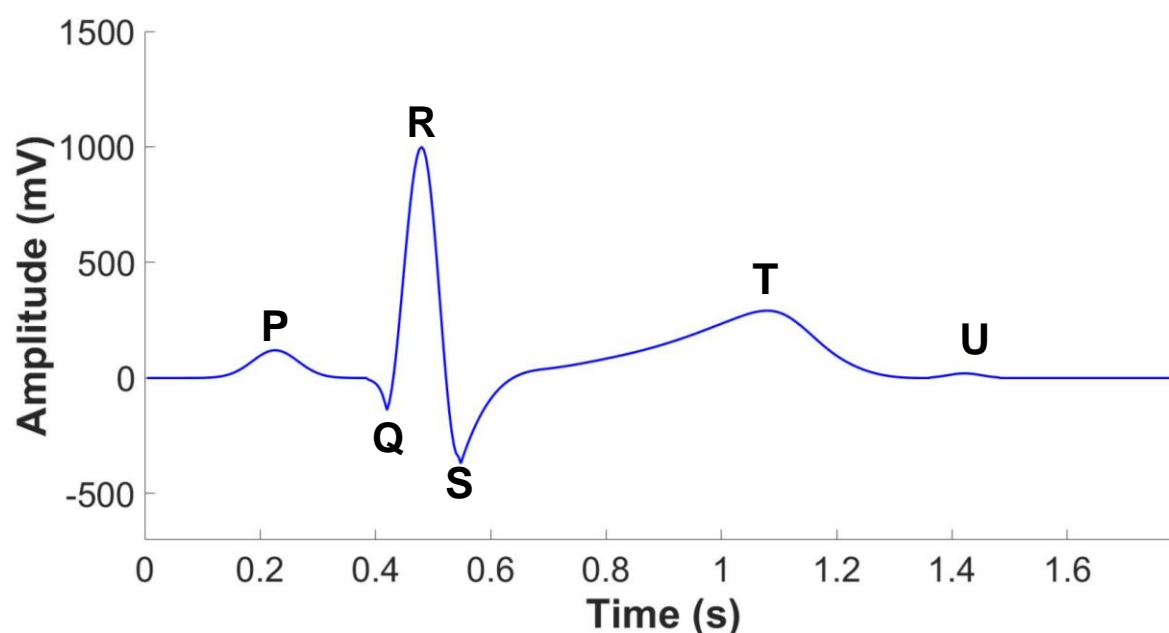
Figure 4.6: Unaltered, raw pre-programmed cardiac waveform which contained the necessary waves (highlighted), segments and intervals. Waveform consisted of 450 data points and an R wave with a peak amplitude of 1V.

To ensure that the AWG emitted the waveform as programmed, it was connected to an oscilloscope. Simulated waveforms were emitted at a sample rate of 500Sa/s resulting in the emission of 500 data points every second. The emitted waveform was also set to include an R peak amplitude of 1V from the baseline. However, as shown by Figure 4.7a, the oscilloscope displayed waveforms with R peaks measuring approximately 2V, which was double the expected value. Upon further investigation, the doubled output resulted from an impedance mismatch between the AWG and oscilloscope. As the oscilloscope used was unable to change

its input impedance to a 50Ω termination, a 50Ω feed through terminator was included to overcome this problem. Following incorporation of the feed through termination, the oscilloscope subsequently displayed the simulated waveform with an R peak of 1V (Figure 4.7b). This demonstrated that the feedthrough terminator addressed the impedance mismatch between the two instruments and confirmed that the AWG emitted the signal as instructed.
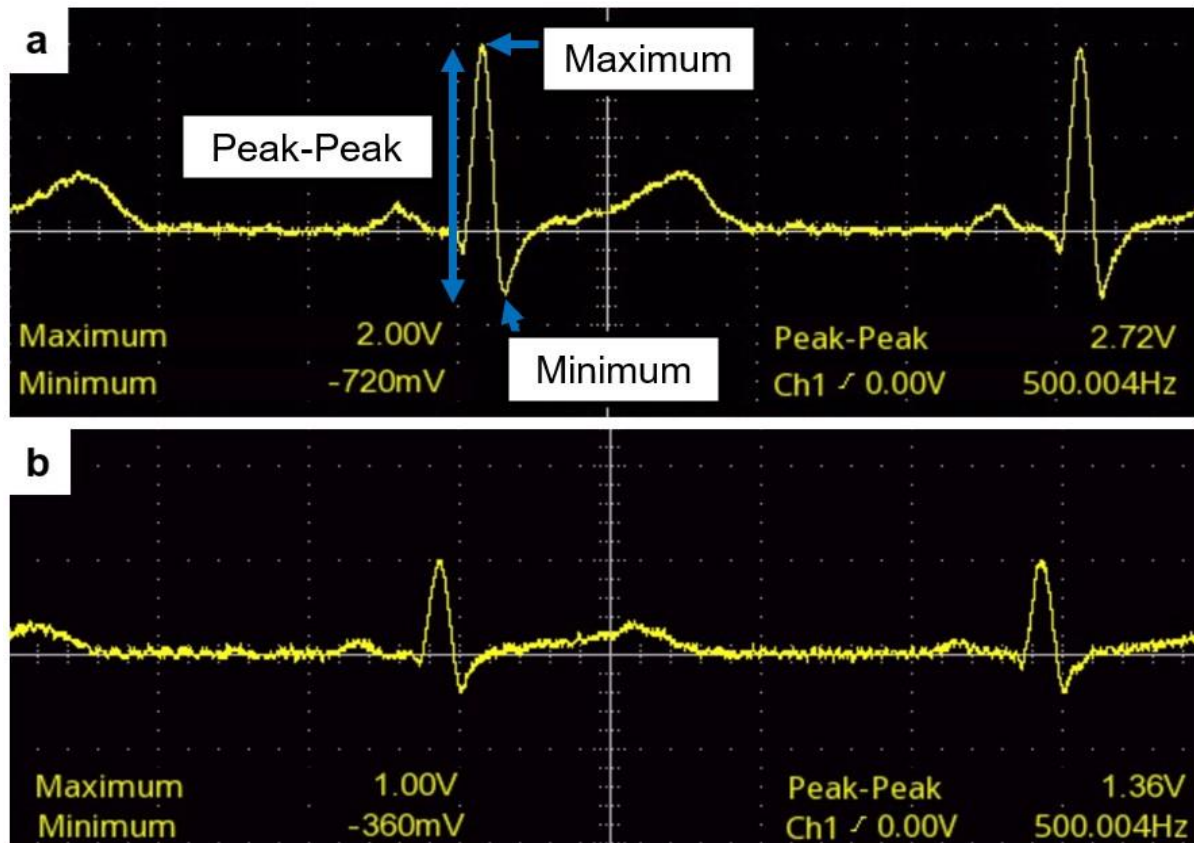
Figure 4.7: Output of the arbitrary waveform generator on an oscilloscope. This step was undertaken to confirm the output of the waveform generator when connected to an oscilloscope without (**a**) and with (**b**) the inclusion of a 50Ω feedthrough terminator.

4.4.1.2 Simulating a healthy adult resting heart rate

Having identified a suitable waveform and method of generation, simulation of a HR which was reflective of a healthy resting adult was necessary. Cardiac data captured from healthy volunteers during Chapter 3 was used to inform the simulation of a resting HR. HR refers to the number of times the heart beats per minute and is abbreviated to bpm. For healthy adults, a normal resting HR ranges from 60 to 100bpm (Huszar and Wesley 2017). To replicate this within the model, the rate at which the simulated waveform was emitted from the AWG was optimised. Simulated signals were emitted from the AWG and recorded over 30 seconds using an OpenBCI Cyton biosensing board. Using MATLAB, data were converted from µV to mV and exposed to a digital high-pass filter with a 0.5Hz cut-off frequency. HR was determined by identifying the number of R peaks, in complete waveforms, over 30 seconds. This figure

was subsequently doubled to achieve the bpm. Regarding the emission of cardiac waveforms from the AWG, sample rate referred to the number of data points emitted per second. Initially, 250Sa/s was selected to match the 250Hz sampling frequency of the biosensing board. At this rate, one complete heartbeat lasted 1.8 seconds (Figure 4.8a) and an average HR of 33bpm was achieved (Figure 4.8b). This HR can be considered bradycardic and is outside of the normal range. Therefore, an increased sample rate was required to increase the HR.
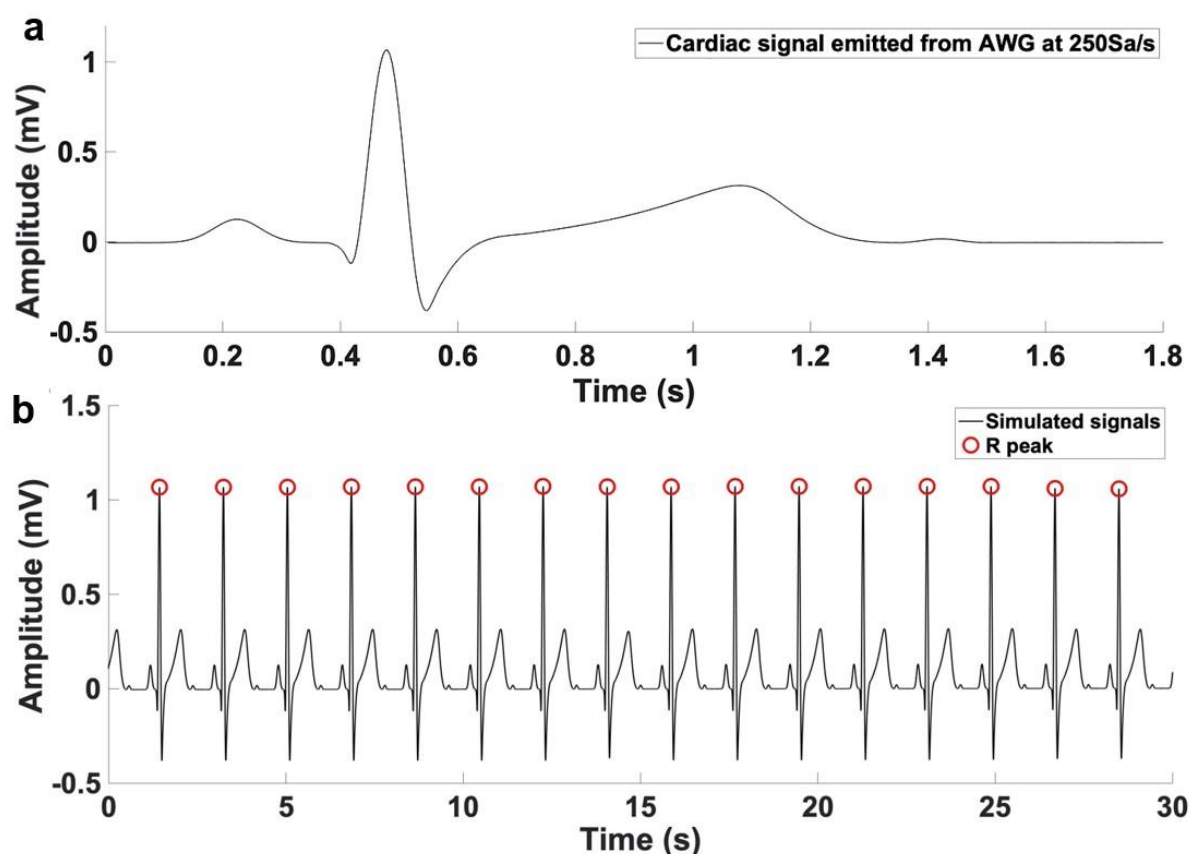
Figure 4.8: Simulated heartbeat when emitted from the waveform generator at 250Sa/s. Individual simulated waveform (**a**) and waveforms recorded over 30 seconds (**b**). Red circles highlight the R peaks which were used to calculate bpm. Data filtered with a digital high-pass and notch filter.

The biosensing board used to capture simulated waveforms had a fixed sampling frequency of 250Hz when transferring data via Bluetooth. Increasing the AWG's sample rate to 500Sa/s was attempted. However, due to the mismatch in sample rates between the AWG and biosensing board, incomplete waveforms were acquired. To overcome this challenge, a Wi-Fi shield was obtained and attached to the Cyton board. This add-on component allowed for data transfer over Wi-Fi, thus enabling increased sample rates. Simulated cardiac waveforms were subsequently emitted from the AWG at 500Sa/s and recorded at 500Hz using a UDPx3 protocol resulting in one complete waveform lasting 0.9 seconds (Figure 4.9a). As expected, doubling the sample rate from 250Sa/s to 500Sa/s resulted in a HR of 66bpm (Figure 4.9b) which is within range and therefore, was used in subsequent studies.
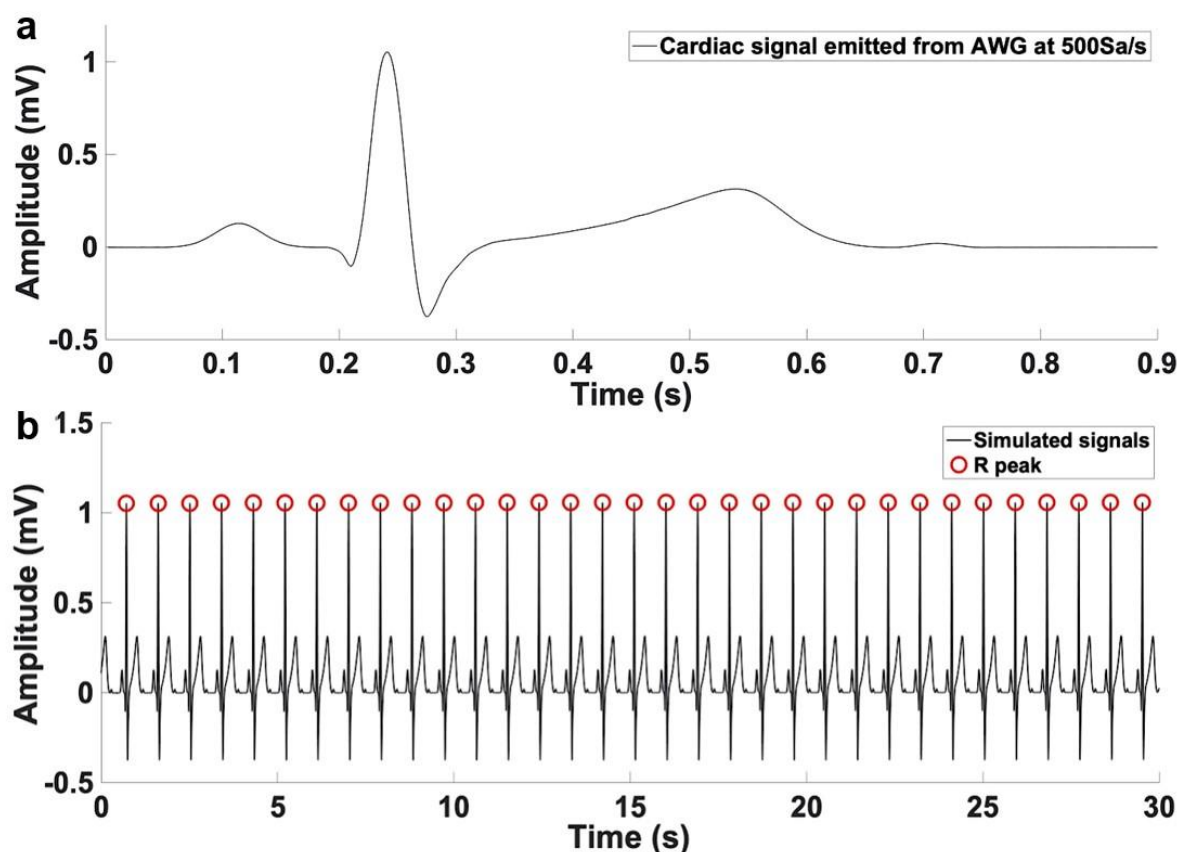
Figure 4.9: Simulated heartbeat when emitted from the waveform generator at 500Sa/s. Individual simulated waveform (**a**) and waveforms recorded over 30 seconds (**b**). Red circles highlight the R peaks which were used to calculate bpm. Data filtered with a digital high-pass and notch filter.

4.4.1.3 Simulating low voltage cardiac signals

Real-world cardiac signals are low in amplitude measuring only a few mV or less. Therefore, cardiac data captured during Chapter 3 was also used to optimise low voltage cardiac waveforms. As shown by Figure 4.6, the initial waveform had a maximum R peak of 1V. For the simulated signal to be more representative of human data, the various waves (PQRST) need to be within the mV range. The lowest programmable amplitude using the AWG was 1mV. However, this was the lower limit of the machine and therefore noise from the generator could have impacted signal quality. To address this problem, a resistor divider, shown in Figure 4.10, was used. This simple circuit comprised two resistors and could reduce voltages to a fraction of the input. Using the equation and calculation shown in Figure 4.10, resistor values were determined as 100kΩ for resistor one (R_1) and 100Ω for resistor two (R_2).

$$\mathbf{Vout = Vin} \times \left(\frac{\mathbf{R2}}{\mathbf{R1 + R2}}\right)$$

Let: $Vin = 1V, R1 = 100,000\Omega$ and $R2 = 100\Omega$

$$\mathbf{Vout} = 1 \times \left(\frac{100}{100,000 + 100}\right)$$

$$\mathbf{Vout} = 1 \times (0.000999)$$

$$\therefore \mathbf{Vout} = 0.000999V \approx 0.999mV$$
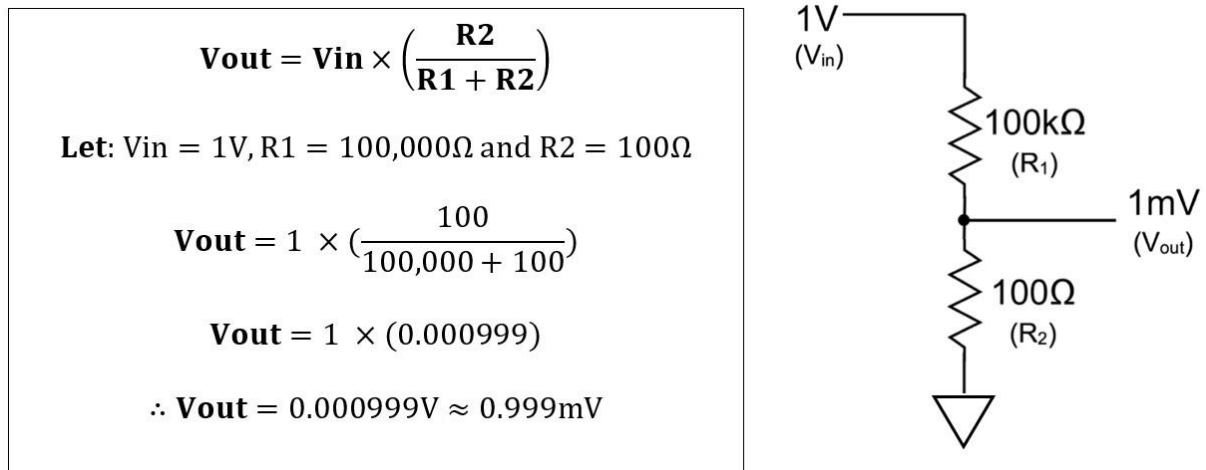
Figure 4.10: Resistor divider calculation and corresponding circuit which scaled the waveform from V to mV. The resistor closest to the input voltage (V_{in}) is resistor one (R_1) and the resistor closest to the ground is resistor two (R_2). Resistor values were calculated using the equation which states that the output voltage (V_{out}) is directly proportional to the V_{in} and the ratio between R_1 and R_2.

with a quoted nominal voltage of 1.5V. A digital multimeter was used to quickly determine the voltage after R_1. The measured voltage was approximately 1.5mV demonstrating that the divider was capable of reducing V to mV. The resistor divider was subsequently connected to the AWG by means of a 50Ω BNC plug-alligator clip coaxial cable. Simulated signals were again recorded using the biosensing board over 30 seconds using multiple amplification settings, also termed gain. Signals were recorded with, and without a feedthrough terminator to determine if a similar impedance mismatch existed between the AWG and biosensing board. As shown by Figure 4.11, the resistor divider could reduce the cardiac waveform from V to mV. The incorporation of a feedthrough terminator produced an R wave measuring approximately 1mV from the baseline, when recording at a maximum gain of x24 (Figure 4.11a). The amplitude of other relevant waves (PQRST) was reduced, to produce a simulated waveform which was more representative of a human ECG. Upon removal of the terminator the maximum R wave peak amplitude doubled to 2.17mV at a gain of x24, whilst a gain of x12 resulted in a peak of 1mV (Figure 4.11b).
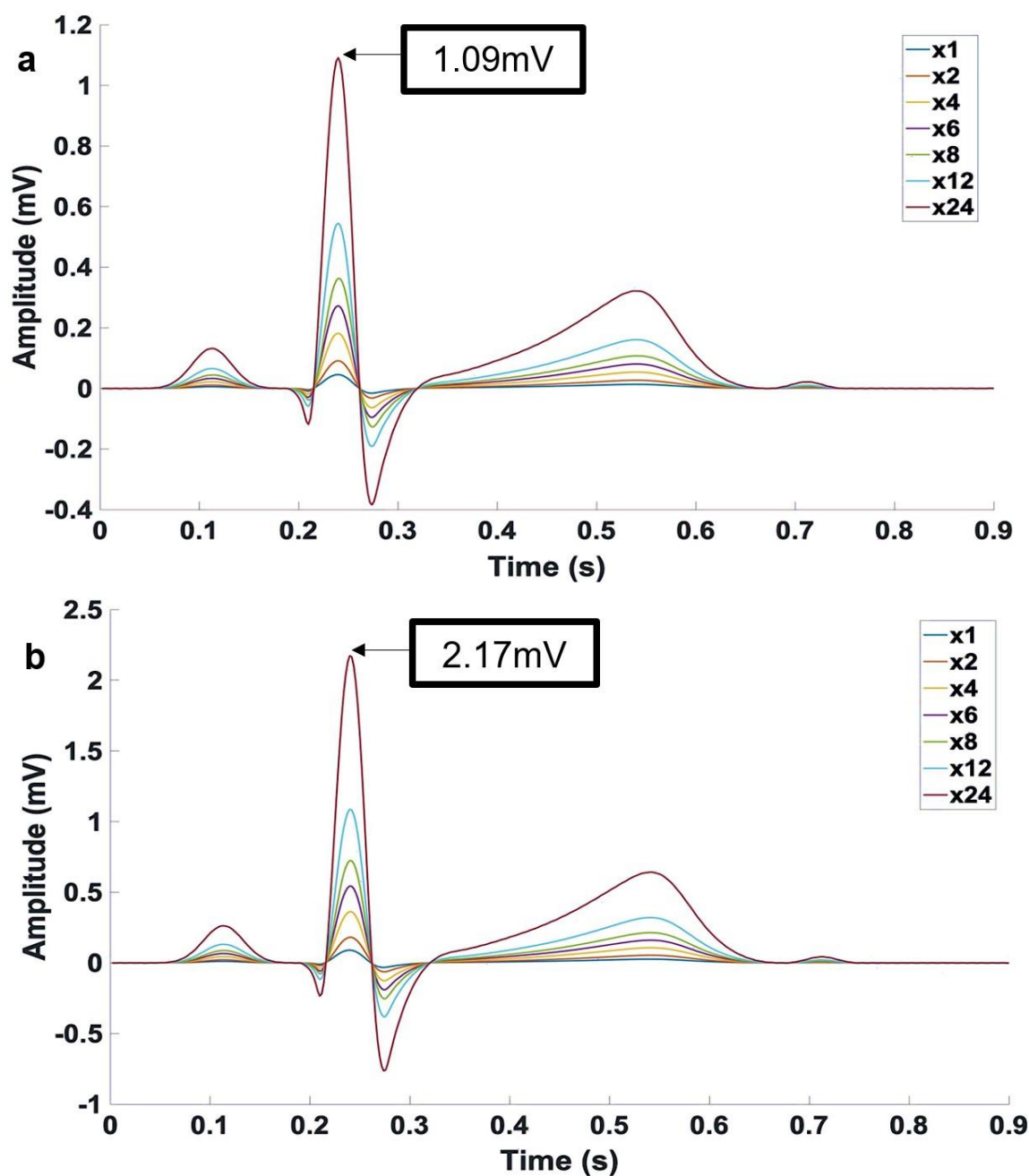
Figure 4.11: Individual cardiac waveform recorded using multiple gains. Simulated waveforms were emitted from the waveform generator at 500Sa/s and recorded with (**a**) and without (**b**) a feedthrough terminator. Gains used were x1, x2, x4, x6, x8, x12 and x24. Data processed using a digital notch and high-pass filter.

The decision to include the feedthrough terminator within the model was based on a comparison with the pilot study data recorded from three healthy adult volunteers, as discussed in Chapter 3. Figure 4.12 displays a single cardiac waveform captured from a 28-year-old female using wet electrodes at a gain of x24. With a mean R wave peak amplitude of 1.31mV ± 0.46 obtained across recordings from the three participants, the feedthrough terminator was incorporated into the model.
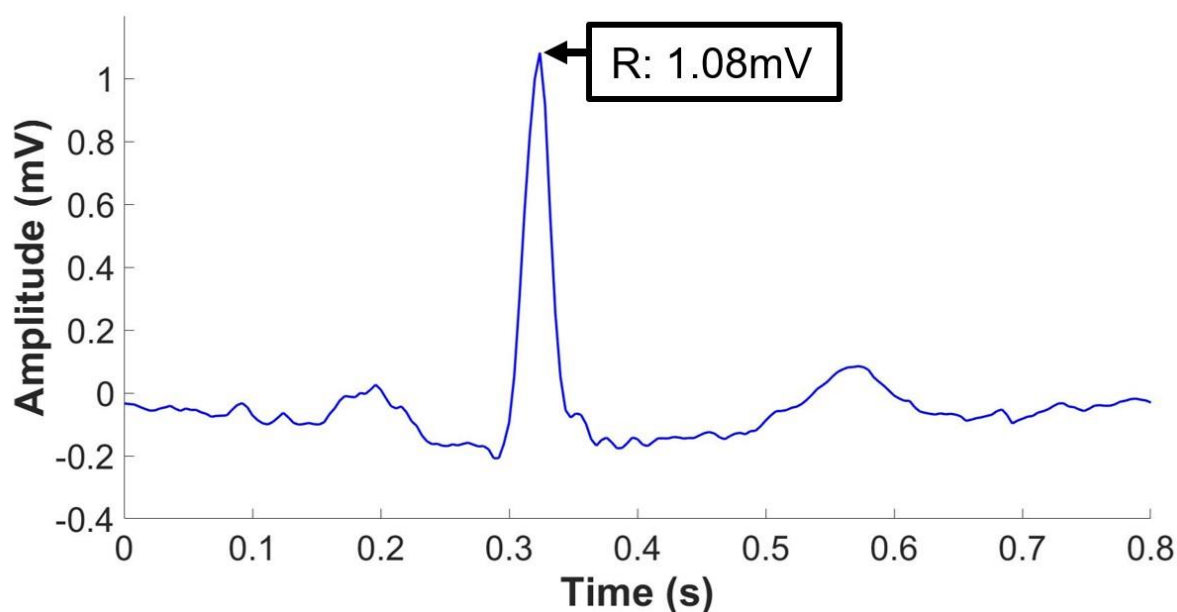
Figure 4.12: Example of a single cardiac waveform recorded from a healthy adult volunteer. Data recorded from a 28-year-old female using commercially available wet electrodes. Cardiac signals were recorded using a sample frequency of 250Hz and a gain of x24. Data filtered using a digital notch and 0.5Hz high-pass filter.

Following waveform optimisation, the durations and amplitude of necessary waves, segments and intervals were subsequently compared with ECG traces acquired from healthy adult volunteers and values quoted within the literature (Table 4.1). Whilst these values can vary between patients, lead configuration and cardiovascular condition, the durations and amplitudes of each wave, segment and interval were similar when compared between the simulated waveform, clinical ECG traces and the values quoted within the literature (Goldberger et al. 2017; Huszar and Wesley 2017; Prutkin 2019). The similarities in cardiac characteristics between the simulated signal, clinical traces and the literature led to the selection of a sample rate of 500Sa/s for all future simulation studies.

Table 4.1: Comparing amplitudes and durations of ECG waves, segments and intervals. Table compares the relevant cardiac waveform characteristics between the simulated cardiac waveform when emitted at 500Sa/s, real world cardiac signals captured from healthy adult volunteers and values quoted within literature sources. Clinical data acquired from volunteers is presented as the mean ±SD *(n=10).* Quoted literature resources from Goldberger et al. (2017), Huszar and Wesley (2017); Prutkin (2019).

ECG component	Simulated		Real world		Literature	
	Amplitude (mV)	Duration (s)	Amplitude (mV)	Duration (s)	Amplitude (mV)	Duration (s)
P wave	0.12	0.1	0.18 ±0.03	0.12 ±0.05	0.05-0.25	0.08-0.12
PR interval	■	0.15	■	0.14 ±0.01	■	0.12-0.20
PR segment	0	0.05	0	0.05 ±0.01	0	0.02-0.10
R wave	1.06	■	1.59 ±0.51	■	0.2-1.5	■
QRS complex	■	0.12	■	0.06 ±0.01	■	0.06-0.12
T wave	0.32	0.32	0.47 ±0.13	0.23 ±0.03	<1	0.10-0.32
QT interval	■	0.46	■	0.38 ±0.02	■	≤0.46*
ST segment	0	0.15	0	0.13 ±0.01	0	≤0.20*
Resting HR (bpm)	■	66	■	66.4 ±7.44	■	66-100

When the tabulated data shown in Table 4.1 is displayed graphically, the simulated cardiac waveform (Figure 4.13a) is comparable to a healthy human ECG trace (Figure 4.13b). All the necessary waves (PQRST) were present and were similar in both duration and amplitude.
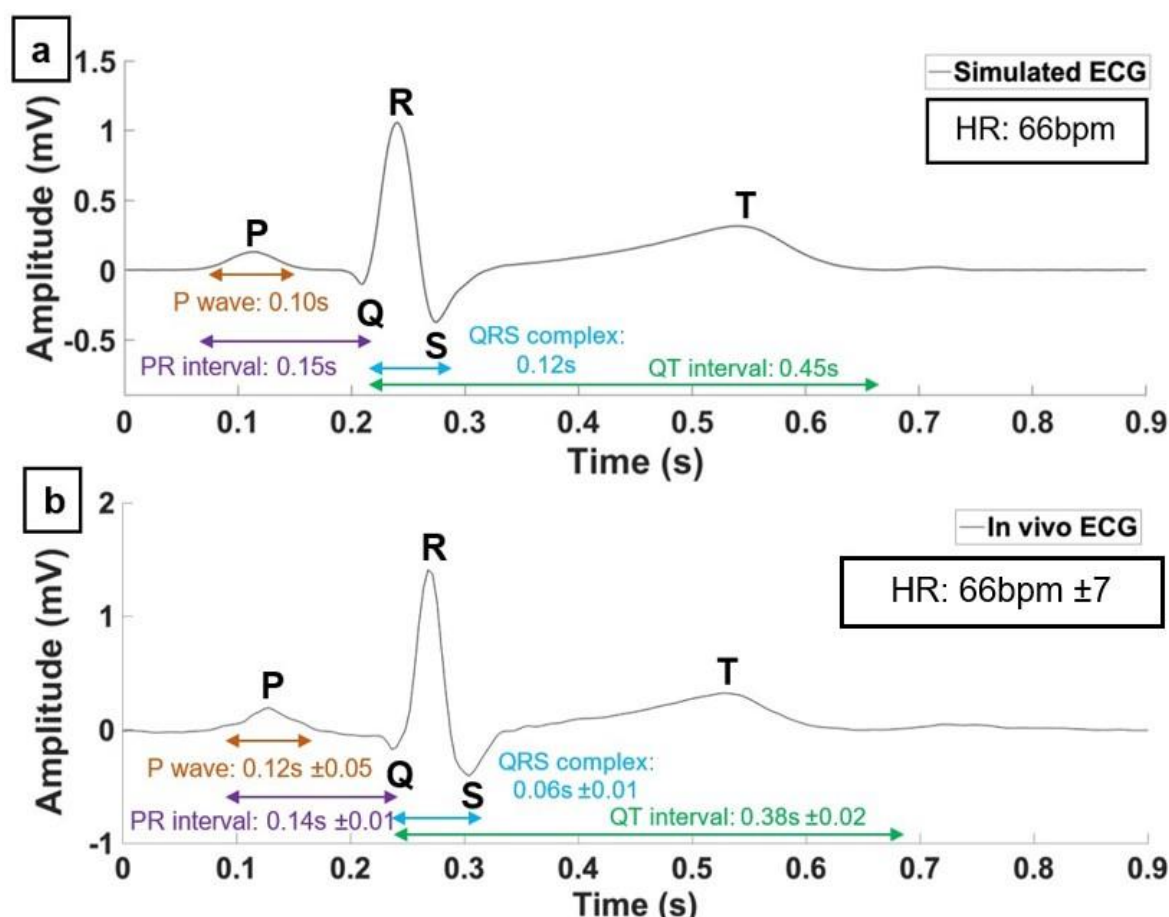
Figure 4.13: Comparisons between a simulated and real-world cardiac waveform. Simulated waveform (**a**) emitted from the waveform generator. Cardiac waveform acquired from a healthy adult volunteer whilst at rest using a lead II configuration (**b**).

4.4.1.5 Model optimisation to reduce magnitude of powerline interference

Overall, the magnitude of PLI recorded alongside signals at different locations on the model varied. Signal were recorded over 30 seconds, in triplicate, directly from the resistor divider, conductive fabric and through ex vivo porcine skin using wet electrodes. FFT was used to determine the magnitude of PLI at 50Hz. Figure 4.14 shows that as signals progressed from the resistor divider to recording equipment, the magnitude of PLI increased. The AWG was not included within this study as it was directly connected to the mains power supply and emitted the signal in volts, therefore an increased magnitude of PLI would be expected.

Mains electricity is supplied at a given voltage and frequency. Within the UK it is supplied at a voltage of 230V and a frequency of 50Hz. Study results revealed that the frequency of PLI averaged 49.9Hz ± 0.07. Several interventions were made during model construction to reduce the effects of PLI on the simulated waveform. Signals

were re-recorded over 30 seconds, in triplicate, at each location following the interventions and results are shown in Figure 4.14.
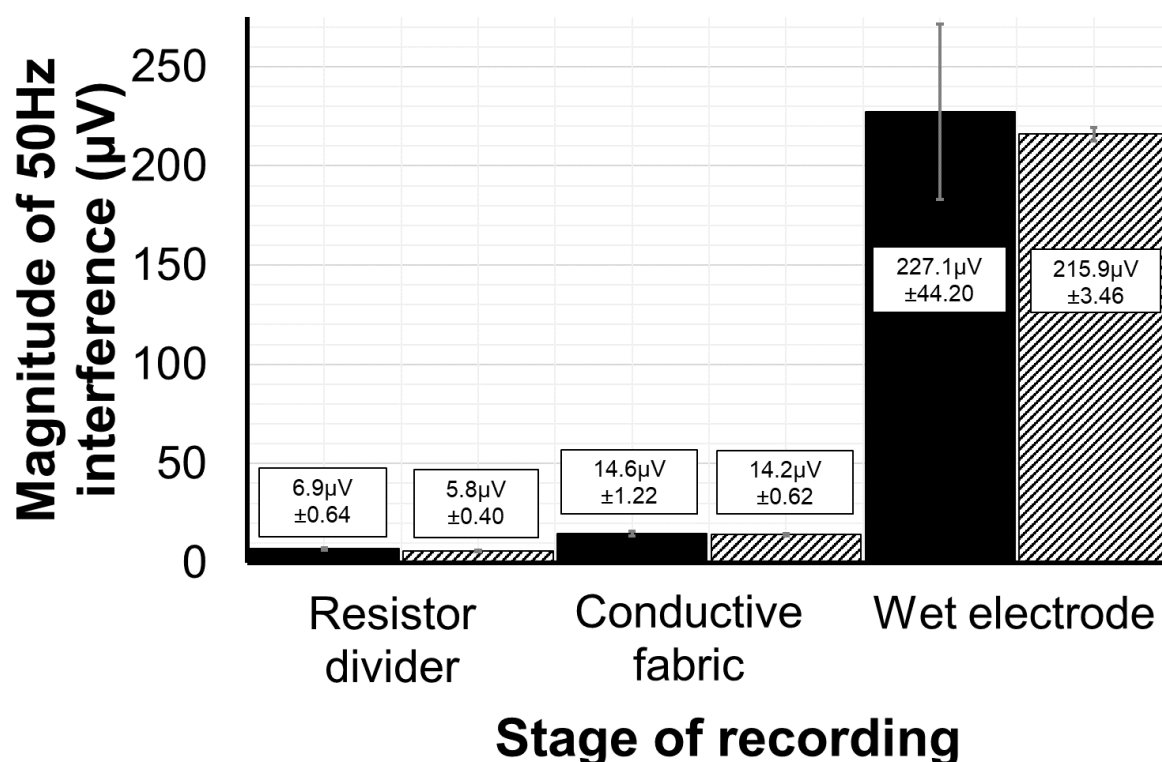
Figure 4.14: Magnitude of 50Hz powerline interference throughout the ex vivo model with and without interventions. Powerline interference was determined by plotting the Fast Fourier Transform of recorded signals at each stage and obtaining the magnitude of the peak occurring at 50Hz. Data presented as the mean ±SD (*n=3*).

When connected to the AWG, the resistor divider was initially left exposed to the surrounding environment. Signals captured at this location resulted in 6.9µV ± 0.64 of PLI. When encased in a layer of foil, the magnitude of PLI decreased to 5.8µV ± 0.40. Due to the slight reduction in PLI, this intervention was kept. Stretch conductive fabric with a surface resistivity of <5Ω/sq. was originally included to bridge the gap between the electronics and ex vivo porcine skin. Signals recorded directly from this type of fabric contained 14.6µV ± 1.22 of PLI. An alternative fabric without stretch and lower surface resistivity of <1Ω/sq. was sourced. Signals recorded using this fabric contained 14.2µV ± 0.62 of PLI. Whilst the non-stretch conductive fabric resulted in a comparable level of PLI, stretch fabric was more suitable when preparing and incorporating ex vivo porcine skin in the model. Compared to the previous locations, the initial acquisition of signals through excised porcine skin using wet electrodes resulted in a greater magnitude of PLI measuring 227.1µV ± 44.20 and was more variable. Both the reference and recording platforms were subsequently placed within shielded aluminium enclosures. Whilst a small reduction in the magnitude of PLI was observed, the aluminium enclosures were incorporated within the model and used for future studies. Despite the interventions, PLI was

still present within the recorded simulated signals. Therefore, similarly to Chapter 3, a digital notch filter was applied offline to all subsequent data.

4.4.2 Assessing the functionality of an ex vivo model for simulated electrocardiography

Following optimisation of the laboratory model, simulation studies determined model functionality and its potential for investigating MN electrode performance. Signals were recorded at four locations to account for signal loss resulting from model setup, electrode type and acquisition equipment. Signals were recorded directly from the AWG (location 1), resistor divider (location 2), conductive fabric (location 3) and through porcine skin explants using three types of electrodes (location 4). Except for location 1, signals were captured from each location simultaneously (recording from each location at the same time) and sequentially (recording from each location individually).

4.4.2.1 Signal correlation of simulated cardiac signals

Figure 4.15 shows the correlation of signals recorded simultaneously from each model location before and after the application of a digital notch filter. Pearson correlation coefficient measured the relationship between recorded signals and the original signal used for simulation. Correlation returned values between -1 and +1, where a value of +1 indicates a strong correlation.

Data showed that as signals progressed from the AWG to individual electrodes, correlation declined. Upon removal of PLI using a digital filter, signal correlation improved. Recording signals directly from the AWG resulted in a near perfect signal recreation before filtering and achieved a correlation of 0.999 ±0.00. Whilst signal correlation was comparable between locations 2 and 3, a decline in correlation was observed when signals were recorded through excised porcine skin using wet, MN and disc electrodes. Overall, the dry, disc electrode resulted in the lowest initial correlation. Upon removal of PLI, signal correlation was comparable between all three electrodes.
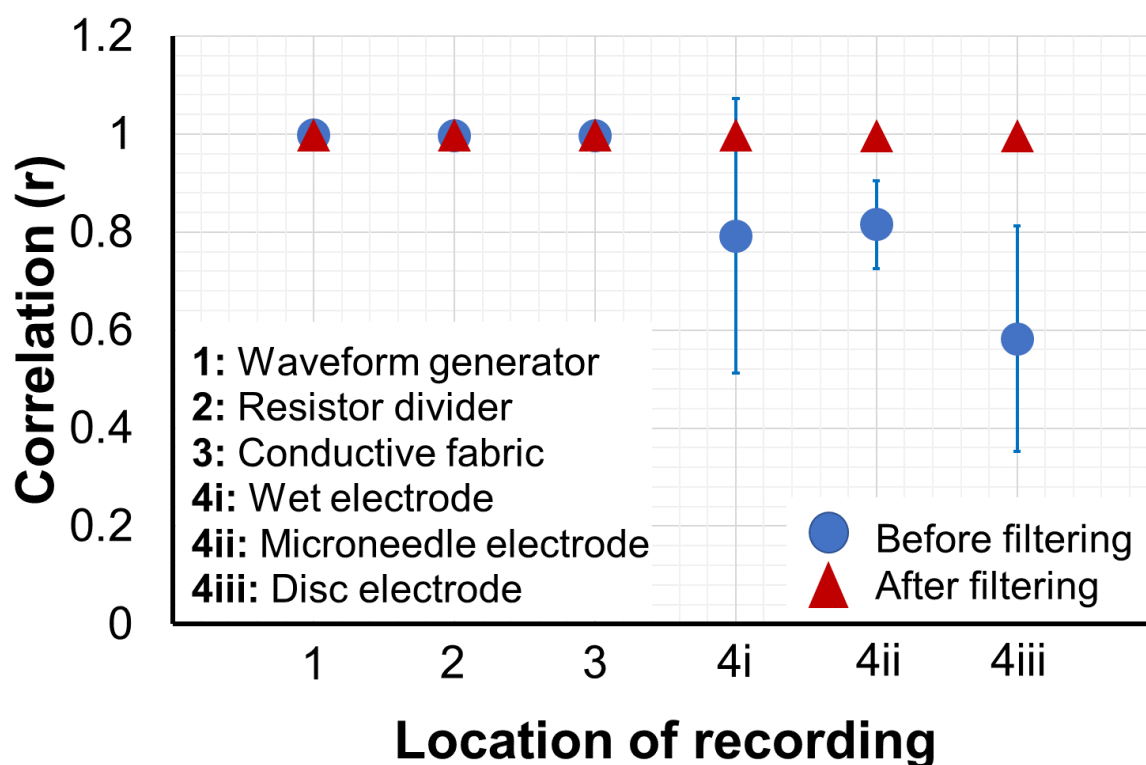
Figure 4.15: Correlation of recorded simulated signals recorded <u>simultaneously</u>. Signals were recorded from the waveform generator (location 1), resistor divider (location 2), conductive fabric (location 3) and through porcine skin using wet (location 4i), microneedle (location 4ii) and disc (location 4iii) electrodes. Pearson correlation coefficient was calculated with respect to the original signal used by the waveform generator for simulation. Data presented as the mean ±SD (*n=3*).

When applying electrodes to skin samples, the distance between electrodes was approximately 1cm. However, due to variability in the size of porcine skin explants used throughout the study and the limited size of the recording platform, due to aluminum enclosures, in some instances maintaining the 1cm distance between electrodes proved challenging. It was unknown whether the proximity impacted the performance of the neighboring electrode. Therefore, a further study was conducted whereby simulated signals were recorded from each location sequentially. Figure 4.16 shows the correlation of signals recorded individually from each model location before and after the application of a digital notch filter. Recording signals from locations 1, 2 and 3 resulted in a near perfect signal recreation. Similarly, to Figure 4.15, a decline in correlation was observed when signals were recorded through excised porcine skin using wet, MN and disc electrodes. Again, the dry, disc electrode resulted in the lowest out of the three electrodes. Correlation improved following the application of a digital notch filter. After filtering correlation was comparable between all three electrodes.
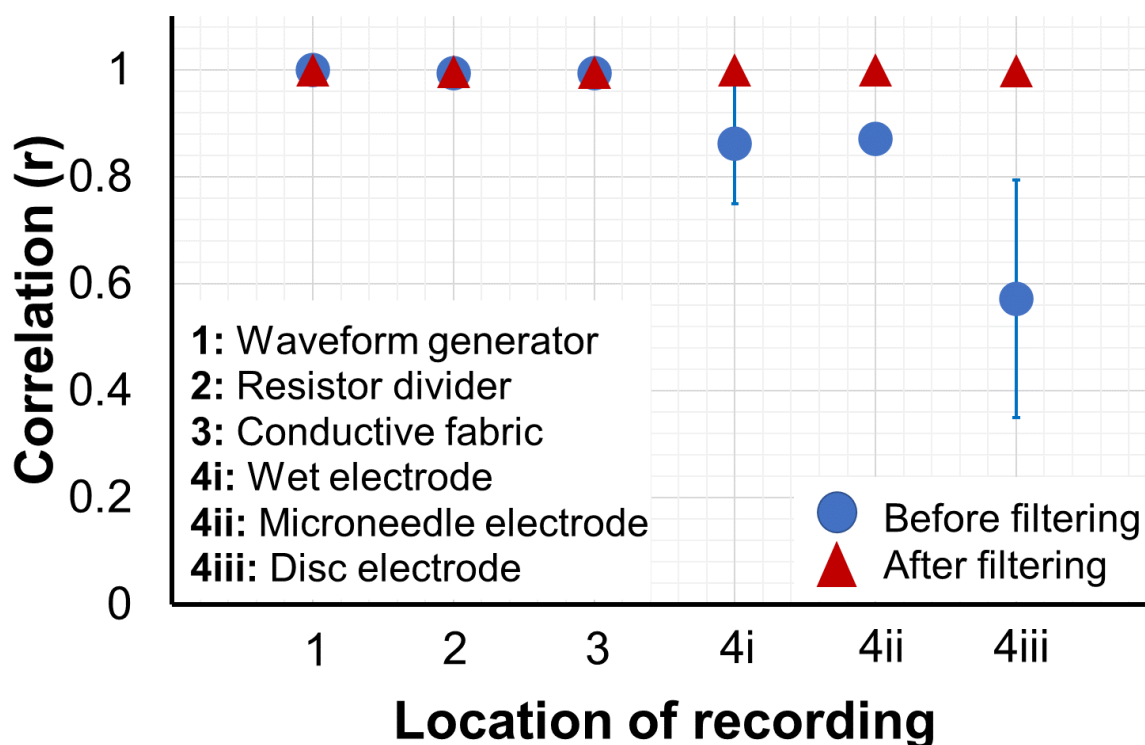
Figure 4.16: Correlation of recorded simulated signals recorded <u>sequentially.</u> Signals were recorded from the waveform generator (location 1), resistor divider (location 2), conductive fabric (location 3) and through porcine skin using wet (location 4i), microneedle (location 4ii) and disc (location 4iii) electrodes. Pearson correlation coefficient was calculated with respect to the original signal used by the waveform generator for simulation. Data presented as the mean ±SD (*n=3*).

4.4.2.2 Signal to noise ratio of simulated cardiac signals

In addition to correlation, SNR was calculated and used as a measure of signal quality. Figure 4.17 shows the SNR of signals recorded simultaneously from each model location before and after the application of a digital notch filter. Similarly, to signal correlation, signal quality decreased as signals progressed from the AWG to individual electrodes. Signals recorded from the AWG resulted in an SNR of 29.4dB ±2.4 which improved to 31.7dB ±1.0 upon filtering. SNR was comparable for signals recorded from locations 2 and 3. Simulated signals recorded using wet electrodes had a higher initial SNR than MN electrodes. Disc electrodes recorded signals with the lowest overall quality. The resultant signals were corrupted with noise and PQRST waves were unidentifiable. Following filtering signal quality improved for the three electrodes, however signals were of lower quality than those recorded from the AWG (location 1).
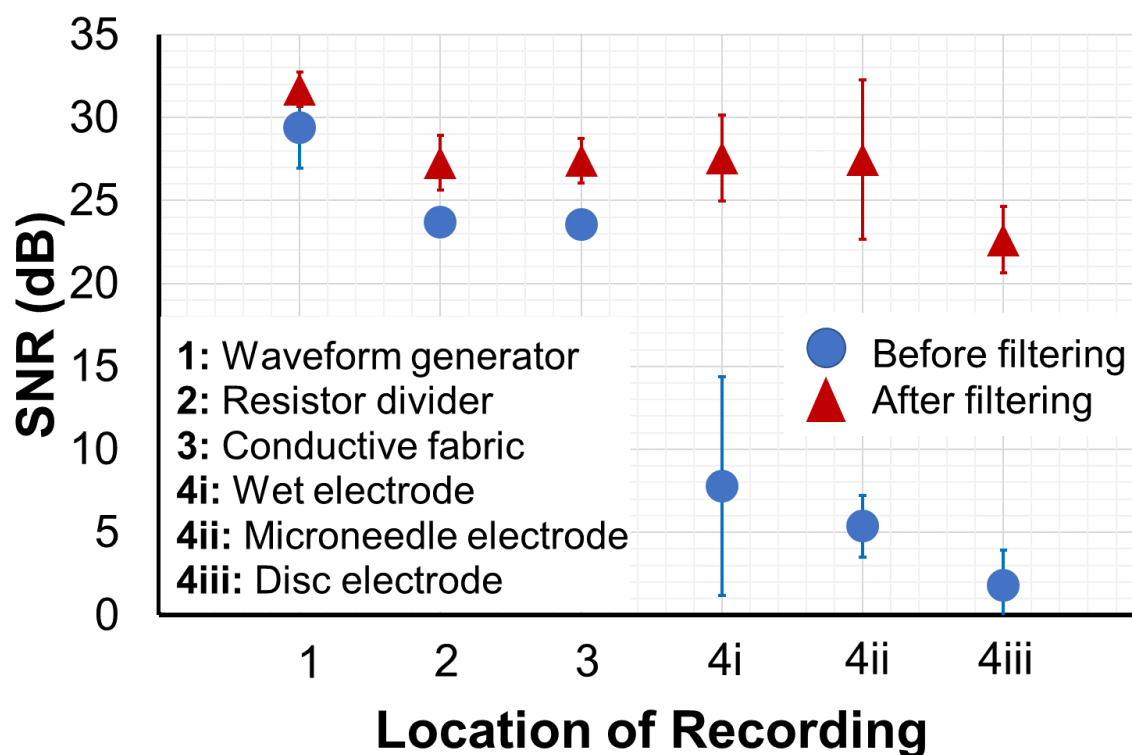
Figure 4.17: Signal to noise ratio of recorded simulated signals recorded <u>simultaneously</u>. Signals were recorded from the waveform generator (location 1), resistor divider (location 2), conductive fabric (location 3) and through porcine skin using wet (location 4i), microneedle (location 4ii) and disc (location 4iii) electrodes. Pearson correlation coefficient was calculated with respect to the original signal used by the waveform generator for simulation. Data presented as the mean ±SD (*n=3*).

Figure 4.18 shows the SNR of signals recorded sequentially from each model location before and after the application of a digital notch filter. Comparably to Figure 4.16, signal quality decreased as signals progressed from the AWG to individual electrodes. Recording signals directly from the AWG (location 1) resulted in the highest fidelity signals overall. Regarding the three electrodes, the dry disc electrodes again captured signals with the lowest SNR initially and following filtering. SNR improved for all electrodes upon filtering. No statistical difference ($p>0.05$) was observed when comparing SNR means between sequential and simultaneous recordings for each stage of the model. Therefore, simultaneous recordings could be used in subsequent studies as signals would be directly comparable.
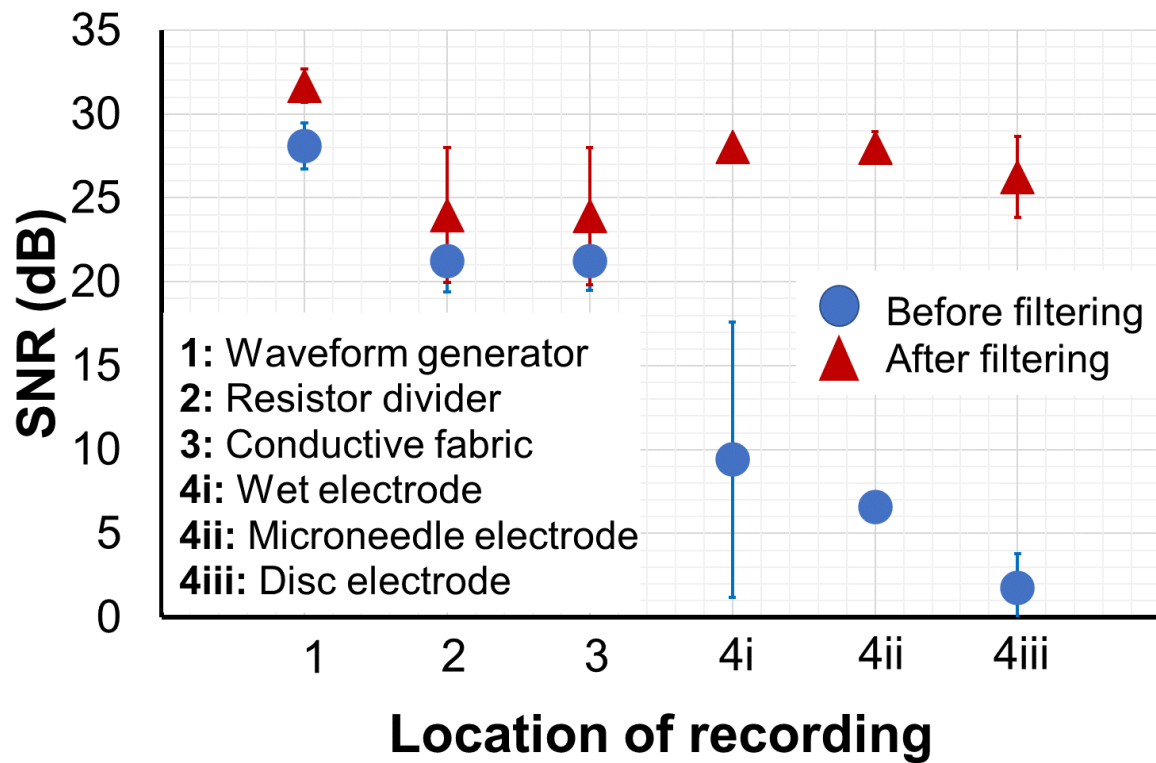
Figure 4.18: Signal to noise ratio of recorded simulated signals recorded <u>sequentially</u>. Signals were recorded from the waveform generator (location 1), resistor divider (location 2), conductive fabric (location 3) and through porcine skin using wet (location 4i), microneedle (location 4ii) and disc (location 4iii) electrodes. Pearson correlation coefficient was calculated with respect to the original signal used by the waveform generator for simulation. Data presented as the mean ±SD (*n=3*).

4.4.3 Effect of microneedle length on electrode performance

Figure 4.19 displays both the individual and mean SNR values for each type of electrode used. Wet, 500μm and 600μm MN electrodes resulted in mean SNR values of 24.0dB ±2.84, 25.2dB ±3.25 and 24.3dB ±2.31 respectively. Overall, performance was comparable between the three electrodes. No statistical significance was observed ($p>0.05$) when comparing the means using a one-way ANOVA.
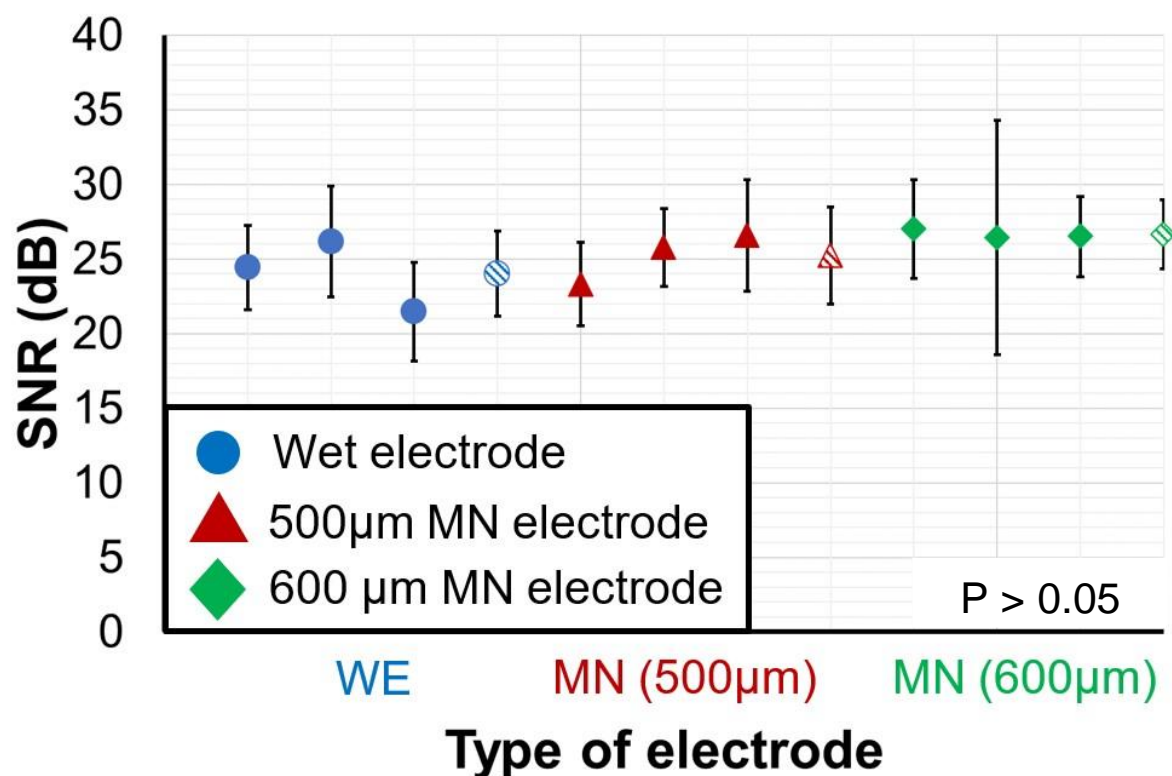
Figure 4.19: Scatter plot of the signal to noise ratio (dB) of simulated signals recorded using three electrodes. Simulated signals were recorded simultaneously through ex vivo porcine skin using 500μm and 600μm length epoxy microneedles electrodes. Commercially available wet electrodes were used as a positive control. Mean signal to noise ratio for each electrode is highlighted by the patterned shapes. Data presented as the mean ±SD (*n=3*).

Figure 4.20 displays en face and sub-surface images of skin treated with wet and MN electrodes. Staining with methylene blue visualised microchannels, due to the presence of identifiable blue dots, indicating that both the 500μm and 600μm length MNs pierced the skin. No penetration was observed with the control. Percentage penetration for 500μm and 600μm length MNs were 89% ±15.92 and 92% ±14.47 respectively. As shown by Figure 4.20, OCT imaging subsequently corroborated MN penetration through the presence of clear channels extending into the VE and dermis.
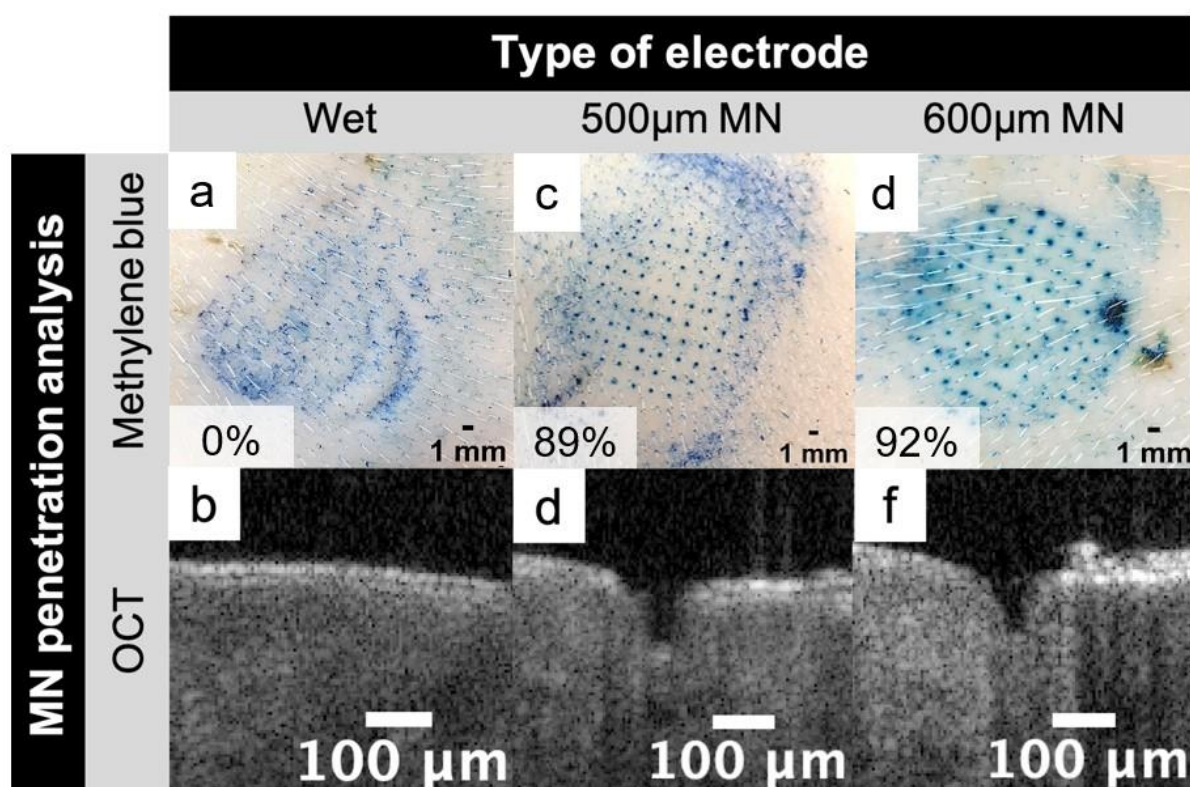
Figure 4.20: En face and sub-surface images of excised porcine skin treated with three electrodes. Porcine skin was stained with 2%w/v methylene blue and imaged with optical coherence tomography following the removal of wet electrodes (**a-b**), 500µm length microneedle electrodes (**c-d**) and 600µm length microneedle electrodes (**e-f**) to confirm penetration. Commercially available wet electrode was included as the positive control. Percentage penetration efficiency is highlighted within the Figure.

OCT images acquired during this study were used to measure both microchannel depth and width to determine if increased MN length affected channel dimensions. Figure 4.21 displays the mean microchannel dimensions for 500µm and 600µm length MN electrodes following their removal from ex vivo porcine skin. Despite the manual application of MN electrodes, both microchannel depth and width were comparable between the two needle lengths. Compared with the dimensions shown in Chapter 2, channel dimensions shown in Figure 4.21 exceeded those determined for a downward application force of 15N (Figure 2.16) suggesting that a greater force was used to insert these MN electrodes in porcine skin.

CHAPTER 4
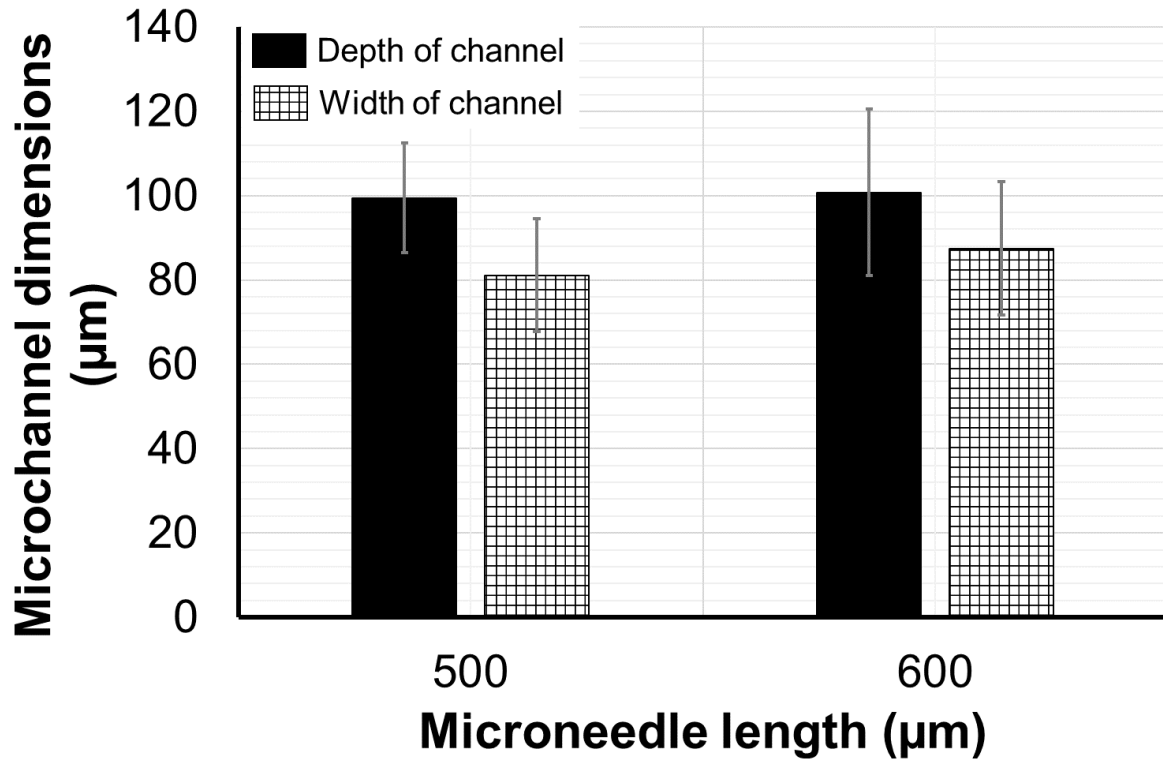
Figure 4.21: Mean microchannel dimensions identified following the manual application of microneedle electrodes. Metallised, epoxy microneedle electrodes measuring either 500μm or 600μm in length were manually applied to ex vivo porcine skin whereby they subsequently recorded simulated cardiac signals. Microchannels were identified using OCT and measured using Fiji. Data presented as the mean ±SD (*n=3*).

4.4.4 Effect of duration on electrode performance

SNR values for MN and wet electrodes over 6 hours are shown in Figure 4.22. Over this duration SNR ranged from 26 to 30dB for MN electrodes and 24 to 28dB for wet electrodes. Figure 4.22 shows that whilst SNR fluctuated within the first 2 hours, wet and MN electrode performance was comparable overall. By 4 hours both electrode types recorded signals of similar SNR measuring 27.7dB ±1.95 and 27.8dB ±2.74 for wet and MN electrodes respectively. No statistical significance ($p > 0.05$) was observed when comparing the electrode types at each time point using an independent t-test.
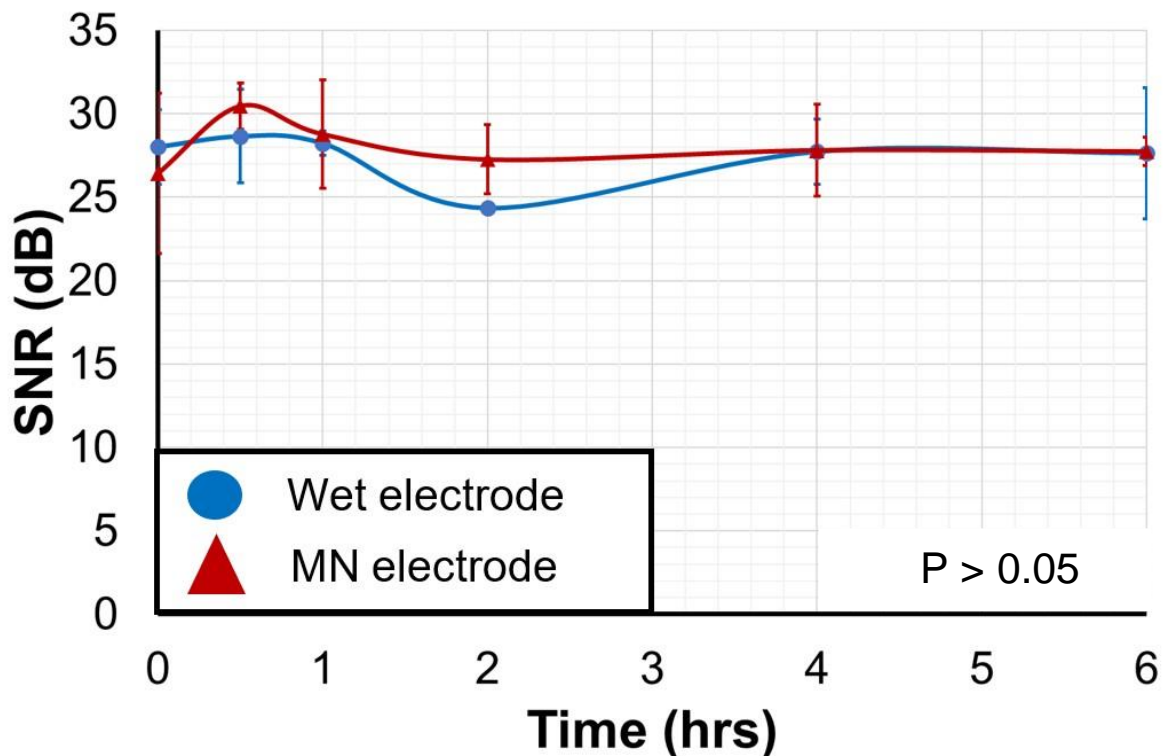
Figure 4.22: Signal to noise ratio (dB) of simulated signals recorded over 6 hours. Simulated signals were recorded simultaneously through ex vivo porcine skin using 500μm epoxy microneedle electrodes and commercially available wet electrodes. Data presented as the mean ±SD (*n=3*).

Figure 4.23 displays a selection of en face and sub-surface images confirming MN penetration. Following the removal of the MN arrays after 6 hours, microchannels were visible following the application of methylene blue (Figure 4.22c) whilst OCT imaging demonstrated clear sub-surface disruption in the epidermis (Figure 4.22d). No microchannels were observed following the removal of the wet electrode using staining and as shown by Figure 4.22b, no disruption in the epidermis was observed.
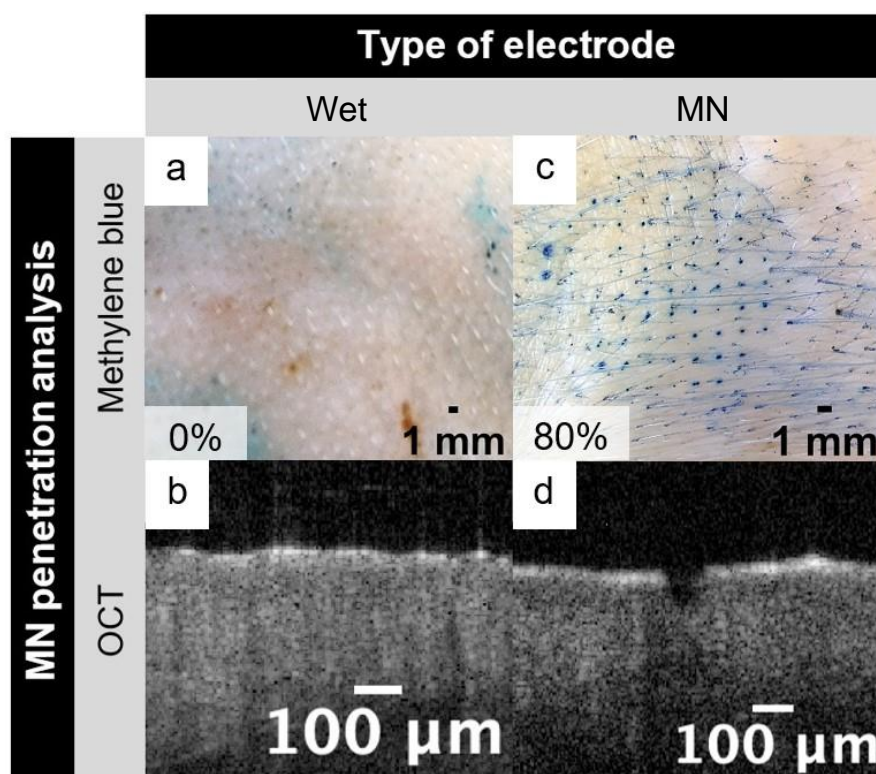
Figure 4.23: En face and sub-surface images of excised porcine skin treated with electrodes after 6 hours. Porcine skin was stained with 2%w/v methylene blue and imaged with optical coherence tomography following the removal of wet electrodes (**a-b**) and 500µm length microneedle electrodes (**c-d**). Commercially available wet electrodes were included as the positive control.

4.4.5 Effect of design on electrode performance

In response to the limitations highlighted in Chapter 3 regarding the MN electrode design, a bespoke device was designed and fabricated. Figure 4.24 displays the SNR of simulated signals recorded using the three electrode designs. Patterned shapes indicate the overall mean SNR for wet electrodes, original MN electrode and bespoke design which measured 15.0dB ±1.97, 15.5dB ±2.14 and 17.3dB ±2.11 respectively. SNR values for each repeat are also shown in the Figure. Whilst the bespoke electrode resulted in the greatest overall mean, numerically, the standard deviation demonstrates that SNR values were similar between the designs. When conducting a one-way ANOVA, no statistical difference ($p > 0.05$) was observed between the designs demonstrating that both MN electrodes were at least comparable to the wet electrodes. Compared to the SNR values quoted elsewhere in this chapter, values shown in Figure 4.24 are lower.
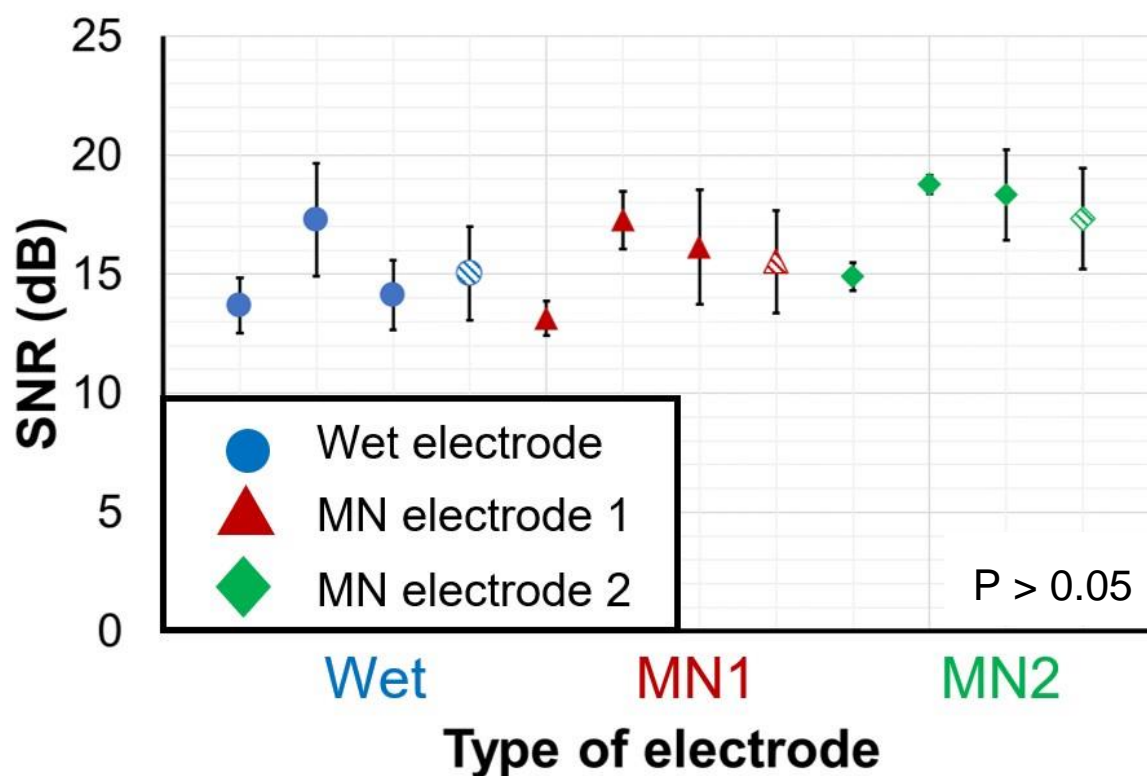
Figure 4.24: Signal to noise ratio values (dB) of simulated signals recorded using three electrode designs. Simulated signals were recorded simultaneously through ex vivo porcine skin using wet electrodes, original microneedle electrode (MN1) and bespoke microneedle electrode (MN2). Mean signal to noise ratio for each electrode is highlighted by the patterned shapes. Data presented as the mean ±SD (*n=3*).

Figure 4.25 shows a variety of en-face and sub-surface images of porcine skin treated with the three electrode designs. Microchannels were visible following the removal of both the original MN design (Figure 4.25c) and bespoke design (Figure 4.25e) when stained with methylene blue. OCT imaging further confirmed sub-surface penetration for both MN electrode designs. The original MN design resulted in a higher percentage penetration of 74% compared to the 67% achieved by the bespoke design. Unlike the MN devices and as shown by Figure 4.25a-b the application of wet electrodes did not result in a breached SC.
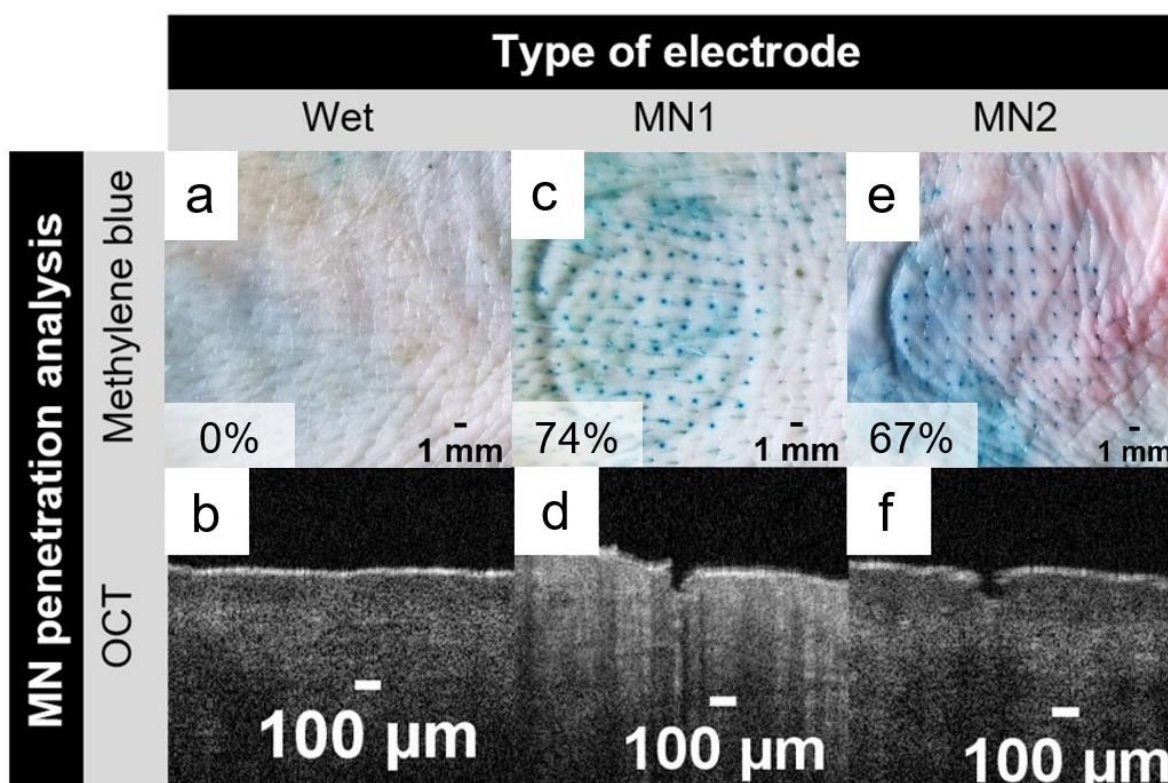
Figure 4.25: En face and sub-surface images of excised porcine skin treated with three electrode designs. Porcine skin was stained with 2%w/v methylene blue and imaged with optical coherence tomography following the removal of wet electrodes (**a-b**), original microneedle electrodes (**c-d**) and bespoke microneedle electrodes (**e-f**).

OCT images were again used to measure microchannel dimensions to determine if MN electrode design affected channel dimensions. Figure 4.26 shows the mean microchannel width and depth for both the original MN electrode prototype (MN1) and bespoke electrode (MN2) fabricated by Maddison Product Design. Whilst Figure 4.26 shows that MN2 produced deeper and wider channels, standard deviation indicates that overall, channel depth and width were comparable between the two designs. Again, channel dimensions observed in this study exceeded those measured for a downward application force of 15N (Figure 2.16) in Chapter 2, suggesting that a greater force was used to insert these MN electrodes in porcine skin.
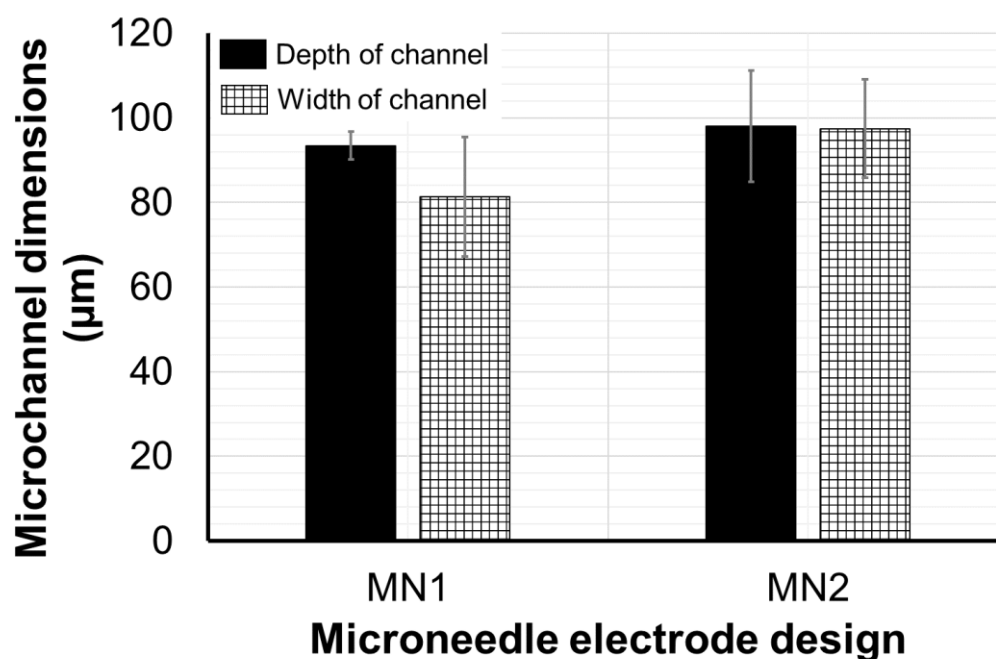
Figure 4.26: Mean microchannel dimensions identified following the manual application of two microneedle electrode designs. The initial microneedle electrode prototype (MN1) and bespoke microneedle electrode (MN2) fabricated by Maddison Product Design were manually applied to ex vivo porcine skin whereby they recorded simulated cardiac signals. Microchannels were identified using OCT and measured using Fiji. Data presented as the mean ±SD (*n=3*).

4.4.6 Characterisation of electrode technologies

4.4.6.1 Electrode-skin impedance

Figure 4.27 shows the electrode-skin impedance for wet, disc and MN electrodes over four frequencies (0.1kHz, 1kHz, 10kHz and 100kHz). All electrodes were applied to the same area on the volunteer's volar forearm. Wet electrodes were applied first and subsequently removed after impedance measurements. Dry disc electrodes were then applied, followed by MN electrodes. Within this study, two sizes of dry disc and MN electrodes (9mm and 18mm) were used to investigate the effects of diameter on electrode-skin impedance. Furthermore, to assess impedance following a breach in the skin's barrier, a further set of wet electrodes were applied after the removal of MN electrodes.
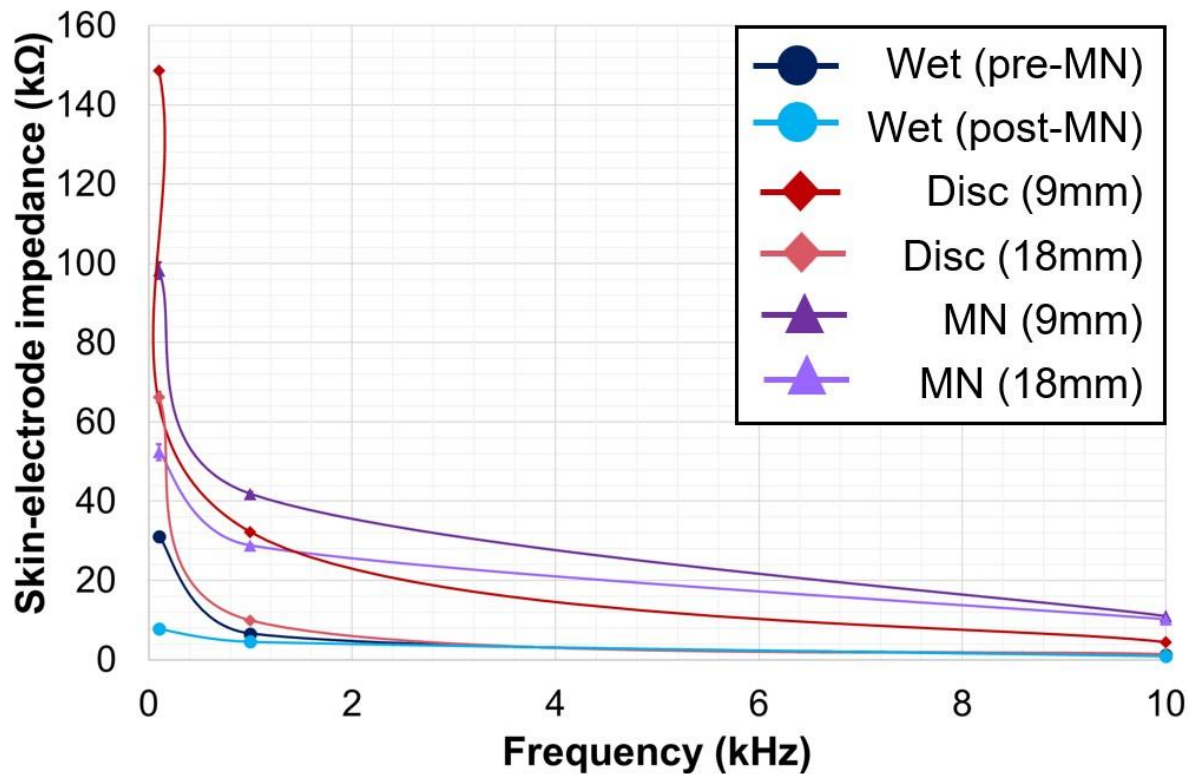
Figure 4.27: Electrode-skin impedance of electrode technologies at 0.1kHz, 1kHz and 10kHz. Order of electrode application: wet (before microneedles), disc (9mm), disc (18mm), microneedles (9mm), microneedles (18mm) and wet (after microneedles). Data is presented as the mean ±SD (*n=1*).

Overall, wet electrodes resulted in the lowest electrode-skin impedance for each of the four frequencies both before and after MN application. At 0.1kHz, wet electrodes applied prior to MNs resulted in an electrode-skin impedance of 31.0kΩ ± 0.50. When wet electrodes were re-applied after MN removal, a reduced impedance of 7.9kΩ ±0.21 was achieved for the same frequency. Dry disc electrodes measuring 18mm in diameter resulted in an electrode-skin impedance of 66.2kΩ ±1.28 at 0.1kHz. By comparison, 18mm MN electrodes resulted in a lower electrode-skin impedance of 52.4kΩ ±1.99 at the same frequency. When the electrode size was reduced to 9mm, the electrode-skin impedance for both the disc and MN electrodes increased to 148.6kΩ ±0.35 and 98.18kΩ ±2.07 respectively at a frequency of 0.1kHz. Interestingly, disc electrodes measuring 18mm in diameter achieved a lower electrode-skin impedance at all four frequencies when compared to a MN electrode measuring 9mm in diameter. Whilst values varied between type and size, it is evident from Figure 4.18 that as the frequency increased from 0.1kHz to 100kHz, the electrode-skin impedance decreased for each of the electrodes used.

4.4.6.2 Electrolytic gel dehydration

Electrolytic gels within conventional electrodes play an important role in the acquisition of high-fidelity physiological signals. A drawback, however, is the potential dehydration of these gels. This study, therefore measured the weight of conductive pads over 48 hours as an indicator of dehydration. MN and disc electrodes were used as controls. Wet electrodes used in this study were single use and were supplied pre-gelled with a built-in abrader disc, which is present to improve trace quality. The pre-gelled discs, when removed from the electrode, measured 18mm in diameter and weighed 0.49g ± 0.03. At designated time intervals, the discs were weighed, and the percentage weight calculated (Figure 4.28).
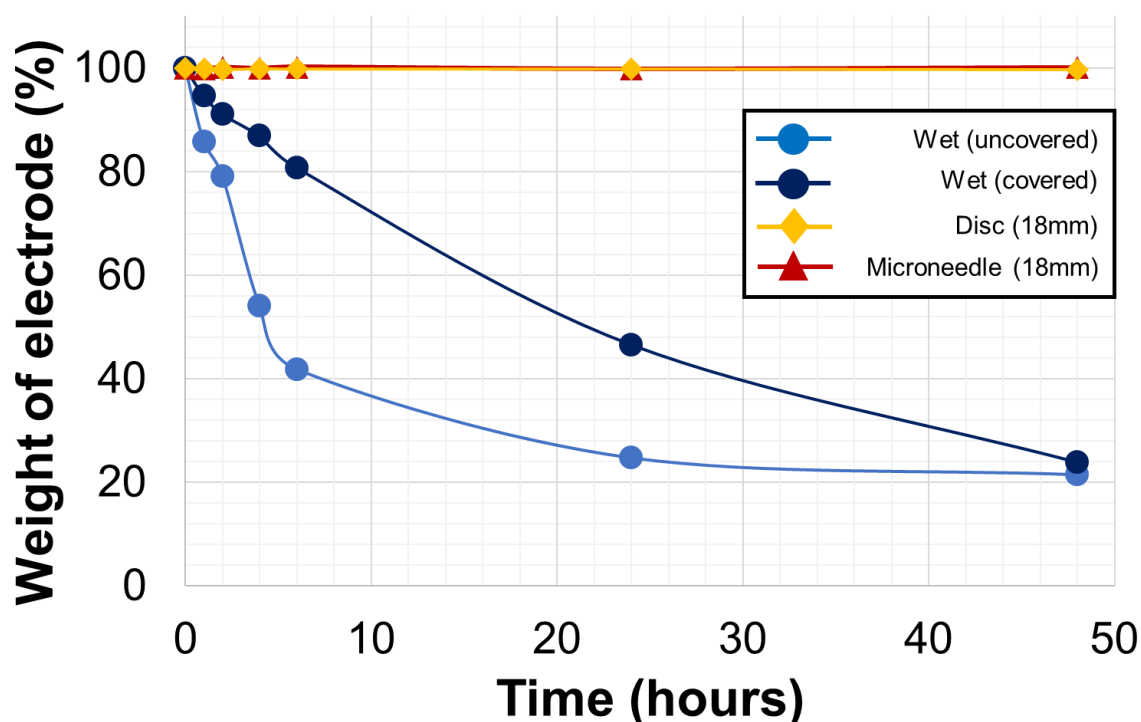
Figure 4.28: Percentage weight loss of covered and uncovered wet electrodes over 48 hours. Microneedle and dry disc electrodes were used as controls. Data presented as the mean ±SD (*n=9*).

Both the uncovered and covered pre-gelled discs resulted in weight loss over time. In comparison, the covered discs showed a more gradual decline in weight loss than the uncovered discs. Following a 48-hour period, both uncovered and covered electrodes reached similar end points. Mean percentage weight loss for uncovered and covered electrodes was 78% and 76% respectively. Throughout the study, temperature and relative humidity were monitored. Over the two days, mean temperature measured 19.9°C ±1.08, whilst relative humidity measured 41% ±5.20. Pre-gelled discs were imaged at the start of the study and following its conclusion. Figure 4.29 displays an example of pre-gelled discs, MN and disc arrays at 0 hours and 48 hours. Whilst this Figure shows a single example, it is representative of all discs that were evaluated. Compared to the pre-gelled disc at the beginning of the study,

the disc at 48 hours appeared notably 'dryer'. No changes in appearance were observed for the MN or disc arrays.
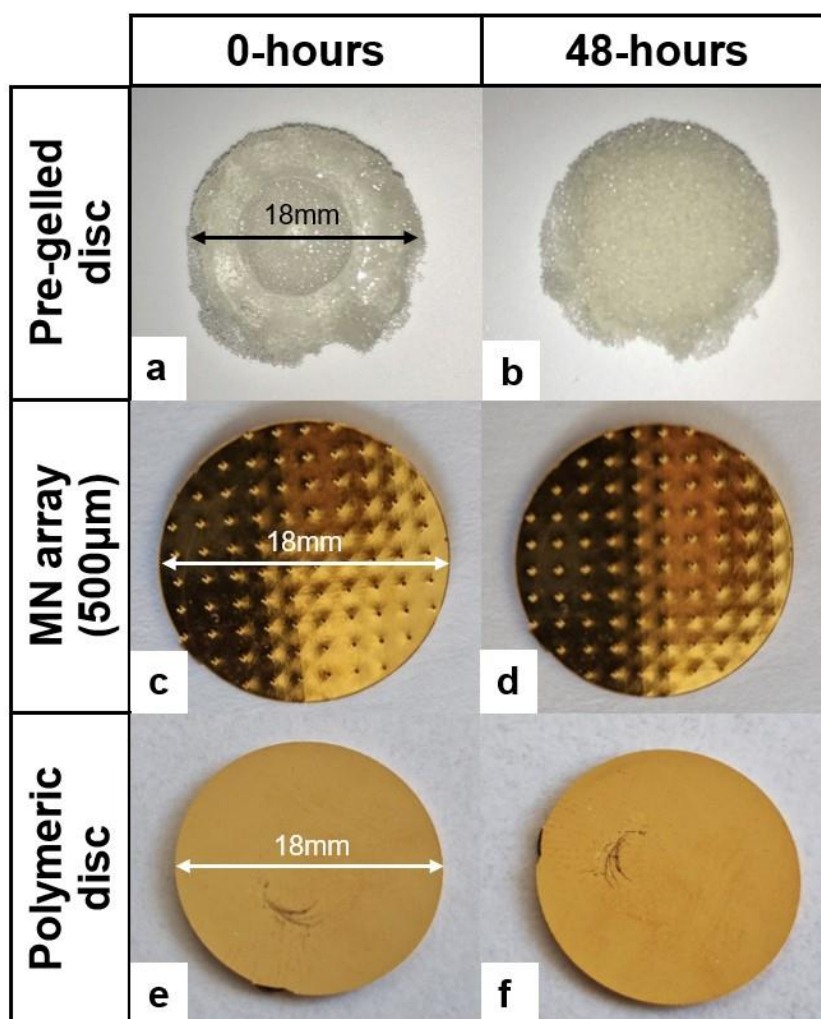
Figure 4.29: Comparison between pre-gelled discs, microneedle and disc arrays at 0 and 48 hours. Pre-gelled discs from 3M Red Dot 2239 ECG monitoring electrodes at 0 hours (**a**) and 48 hours (**b**). Epoxy, microneedle arrays at 0 hours (**c**) and 48 hours (**d**). Epoxy, disc arrays without microneedles at 0 hours (**e**) and 48 hours (**f**). The diameter of the pre-gelled discs and microneedle/disc arrays measured 18mm in diameter.

4.4.6.3 Electrode susceptibility to powerline interference

To characterise the electrodes further and assess their susceptibility to PLI, the FFT of simulated cardiac signals recorded using wet, MN and disc electrodes through ex vivo porcine skin were plotted. Figure 4.28 displays the mean magnitude of 50Hz PLI from simulated signals that were recorded from each type of electrode. As shown in Figure 4.30, wet and MNs were comparable in terms of PLI susceptible measuring 5.3µV ± 4.72 and 5.5µV ± 0.75 respectively. Dry, disc epoxy electrodes were the most sensitive to PLI recording a mean of 14.7µV ±7.31. The increased standard deviation shows that this electrode type was the most

variable. This result does demonstrate that MN-based electrodes can reduce the susceptibility to PLI.
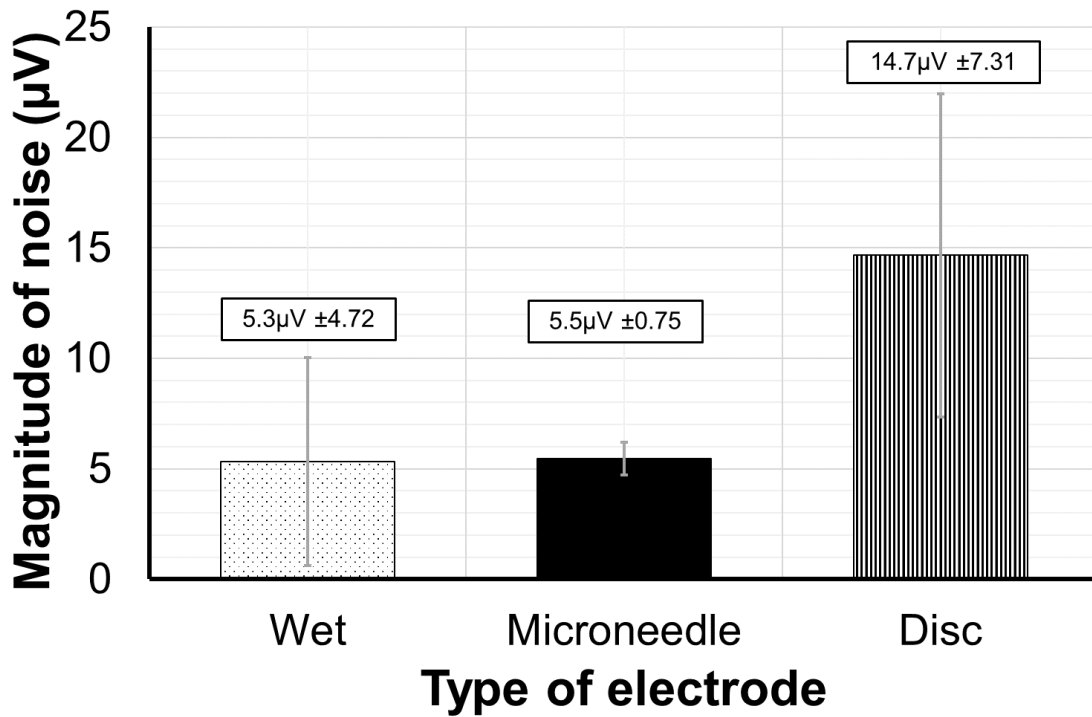
Figure 4.30: Magnitude of powerline interference from three types of electrodes. Simulated cardiac signals were recorded through porcine skin using Red Dot 2239 pre-gelled adult ECG monitoring electrodes, epoxy microneedle and disc electrodes. Magnitude of powerline interference was determined by plotting the Fast Fourier Transform of recorded signals. Data is presented as the mean ±SD (*n=9*).

4.5 Discussion

4.5.1 Development of an ex vivo laboratory model for simulated electrocardiography

This chapter sought to develop a suitable laboratory model of skin which could be used for simulated ECG measurements by adapting a pre-existing skin model, normally used for drug delivery studies (Ng et al. 2009) and incorporating methods of signal generation and acquisition. The first stage of development aimed to obtain a realistic waveform, and several methods were considered. Traces captured from patients, by clinicians can be downloaded from physiological signal databases such as PhysioNet (Goldberger et al. 2000). Physiological data contained within this database has been used by several research groups. For instance, Almutairi and colleagues proposed a deep learning model to classify obstructive sleep apnoea using the PhysioNet Apnoea-ECG database (Almutairi et al. 2021). Whilst Hegarty-Craver et al. (2021) used the PhysioNet database to evaluate an approach to detect seizures lacking in motor activity. An alternative approach to PhysioNet which was considered was the creation of a waveform using mathematical software such as MATLAB. For example, Manju and Akshaya (2020) used MATLAB to simulate abnormal ECG traces resulting from conditions such as angina, hypo- and hyperkalaemia. Conversely, ECG simulated code has been developed by MATLAB users such as Raviprakash (2021), which can generate both healthy and abnormal ECG traces depending upon criteria set by the user. Whilst both the aforementioned options have merits, using an AWG with a pre-programmed cardiac waveform was simpler and did not require advanced coding expertise.

Although signal generation was an essential element of the model, a method of signal acquisition was also required. The acquisition system used throughout this chapter was the OpenBCI Cyton biosensing board, introduced in Chapter 3. This board was an off-the-shelf product using the ADS-1299 chip to capture low noise (1µVpp) and lower power signals (5mW/channel) (Texas Instruments 2012). Different physiological signals vary in their amplitude and therefore this board was developed to address challenges facing EEG recordings (Uktveris and Jusas 2018). For 10-100µV EEG signals, Uktveris and Jusas (2018) demonstrated an SNR range from 12db to 35dB. This system has also been used to record cardiac signals which are known to be larger in amplitude than EEGs (Zhang et al. 2018; Burma et al. 2021). When recording cardiac signals, the electrocardiograph must meet or exceed the requirements of the International Electrotechnical Commission standards IEC 60601-2-25:205, which documents the requirements for the performance of recording and analysing single channel and multichannel electrocardiographs (Young 2019). The first consideration when recording signals was sampling frequency. This is of vital importance and the minimum sample frequency can depend on the ECG feature being measured. Low sample

rates may reduce the accuracy of the acquired signals and a wide variety of sample rates have been proposed throughout the literature. Kligfield et al. (2007) highlighted sample rates of new analogue to digital converters as high as 15kHz. Whilst Kligfield et al. (2007) documents that ordinary signal processing techniques of 500 to 1000Hz cannot reliably detect pacemaker stimulus outputs it does not clearly define a minimum sample rate for ECG devices. The International Electrotechnical Commission standards IEC 60601-2-25:205 state that '*if uniform sampling of ECG signals is employed, the ECG signals shall be sampled with at least 500 samples/s per channel*'. The Cyton board has a fixed sample rate of 250Hz when communicating data via Bluetooth. Whilst a 250Hz sampling rate is lower than Kligfield et al. (2007) recommends, studies have shown that lower sample rates could be used. Mahdiani et al. (2015) investigated if a sampling frequency of 50Hz was high enough for accurate heart rate variability (HRV) analysis. After sampling cardiac signals at 5kHz, they were down sampled to between 40 to 500Hz where it was concluded that a 50Hz sampling rate could be used for HRV analysis (Mahdiani et al. 2015). Kwon et al. (2018) also investigated the acceptability of sampling frequency for HRV analysis by down sampling an original 1000Hz ECG signal. Sample rates of 500 or 250Hz resulted in excellent concordance, whilst a sample rate of 100Hz was considered acceptable (Kwon et al. 2018). Further work would be required to evaluate the suitability of these sample rates in patients with cardiovascular conditions or could be trialled using the ex vivo skin model. Alternative devices such as the Bio-Pac system used by Arquilla et al. (2020) and O'Mahony et al. (2016) captured cardiac signals from volunteers using higher sampling rates and amplification. However due to cost and convenience, a Wi-Fi shield was attached to the Cyton board allowing for an increased sample rate of 500Hz, meeting the criteria stipulated by the IEC standard. This add-on component was in beta testing mode at the time this study was conducted. In addition to the sampling frequency, ECGs can be recorded using multiple channels or 'leads' to generate a full picture of the electrical activity of the heart. Whilst 12-lead ECGs are the gold standard, 2, 3 and 5 lead systems have been used to monitor ECGs in newer wearable ECG devices (Halcox et al. 2017). Therefore the 8-channel Cyton board was suitable and allowed for simultaneous signal acquisition at multiple stages of the model.

The pre-existing skin model was combined with components of an electrical model described by O'Sullivan et al. (2019). Similarly, to O'Sullivan and colleagues, signals recorded from the AWG, resistor divider and conductive fabric achieved near perfect correlation before and after filtering. Whilst the signal of interest differed, SNR values for the initial three stages were of slightly higher fidelity than O'Sullivan et al. (2019). As cardiac signals progressed through to the electrodes, a decrease in both correlation and SNR was observed. Similarly, to O'Sullivan et al. (2019) the electrode-skin interface was investigated. Electrode-skin

impedance or, contact impedance, is a parameter used to assess the electrical properties of the interaction between the electrode and skin. At lower frequencies, the electrode-skin impedance is high due to the presence of the SC (Grimnes and Martinsen 2014; Ventrelli et al. 2015; O'Mahony et al. 2016). It has been shown that MNs can pierce the SC and directly contact underlying epidermal layers which have a higher water content, thereby reducing the overall contact impedance (Griss et al. 2001; Griss et al. 2002; Forvi et al. 2012). Instability between the electrode and skin can increase impedance resulting in the acquisition of low quality biopotential signals. Therefore, the electrode-skin impedance of wet, MN and dry disc electrodes were assessed within this chapter over a frequency range of 0.1 to 100kHz. In summary, it was observed that as frequency increased, contact impedance decreased for all electrode types which is consistent with other publications (Rahal et al. 2009; Chlaihawi et al. 2018). Overall, wet electrodes resulted in the lowest electrode-skin impedance which is similar to other publications including Li et al. (2017) and part of the reason behind their established use in clinical practice. Impedance was highest for the 9mm disc electrodes which is likely due to the reduced surface area and lack of electrolytic gel. When the diameter of the disc electrode was increased to 18mm, a reduction in impedance was observed due to the increased surface area in contact with skin. A similar effect was observed for MN electrodes. Arrays measuring 9mm in diameter resulted in a higher contact impedance than the 18mm MN array. The larger MN electrode is likely to have reduced impedance due to a greater contact area with skin, increased number of MNs per array and potentially increased penetration. When comparing disc and MN electrodes with the same diameter, MN electrodes achieved lower impedances than the disc electrodes demonstrating that the needles had penetrated the SC and potentially contacted viable layers (Forvi et al. 2012). At 0.1kHz, a larger difference in impedance existed between the 9mm and 18mm disc electrodes (82.39 kΩ) than between the 9mm and 18mm MN electrodes (45.82kΩ), again suggesting that the presence of MNs could reduce contact impedance. It is well known that several parameters affect contact impedance. Investigations conducted by Mayotte et al. (1994) and McAdams et al. (1996) demonstrated that the electrode gel, gel properties and electrode size can affect the electrode-skin interface impedance and therefore the quality of recordings. As changes in contact impedance due to contact area are likely to impact the quality of recorded signals, a future study could investigate the effects of several electrode diameters on impedance to optimise electrode size. However, a balance must exist between signal quality, electrode size and number of MNs. The mean number of MNs per 18mm array was approximately 85, and similarly to needle length, if the number of MNs per array increased a higher quality signal may be recorded due to the greater surface area. However, increased MNs and electrode size is likely to impact device wearability and subsequent use by users. These differences in electrode-skin impedance were reflected when assessing signal loss using the model.

Simulated cardiac signals recorded using wet electrodes resulted in the highest SNR initially, and after filtering. They were closely followed by MN electrodes, whilst the disc electrodes recorded cardiac signals with the lowest SNR. Despite steps taken to reduce the susceptibility of the model to PLI, a notch filter was included during data analysis to remove this artifact from recordings. Overall, SNR values for wet and MN electrodes reported during this chapter are similar to O'Sullivan et al. (2019) and demonstrated that this adapted model could be used for simulated ECG measurements.

4.5.2 Characterisation of electrode technologies

Direct comparisons between wet, MN and disc electrodes with other publications prove challenging. Several electrodes have been proposed throughout the literature, each with different materials, fabrication methods and methods of assessment. When characterising electrode contact impedance during this Chapter, wet electrodes resulted in the lowest contact impedance overall, however, impedance was measured over a short time interval of 10 seconds. When investigating the effects of electrode design on contact impedance over 20 minutes, Searle and Kirkup (2000) demonstrated that the wet Ag/AgCl electrode demonstrated a considerably lower contact impedance. In comparison, the dry electrodes resulted in a higher initial contact impedance however, this reduced and resulted in similar endpoints. In all instances, time was required for the impedance to settle (Searle and Kirkup 2000). With respect to this chapter, Searle and Kirkup (2000) compared wet, dry and insulated electrodes. No MN electrodes were included. In recent years however, O'Mahony et al. (2016) investigated temporal variations in skin-electrode impedance over 2 hours. Using the same electrodes as this study, wet electrodes initially had a lower contact impedance than the MN electrode which supports the findings in this chapter. Within an hour however, the electrode impedances were approximately equal (O'Mahony et al. 2016). Unlike many of the aforementioned publications, a notable limitation of the impedance experimental setup refers to the small sample size (n=1) which resulted from limited access to recording equipment. The impedance analyser used was based at Tyndall National Institute, in Ireland, therefore, the study resulted in n=1. Whilst this study provides some information regarding the interface between the skin and electrode types, it is important not to draw too many conclusions from this limited sample size. Despite this limitation, the results help support the simulated signal results.

The susceptibility of wet, MN and dry disc electrodes to PLI was also assessed. Overall, this study found that disc electrodes were the most susceptible, recording signals containing a greater magnitude of 50Hz noise due to a lack of conductive gels (Searle and Kirkup 2000; Puurtinen et al. 2006; Meziane et al. 2013; Halford et al. 2016). Within this study, the electrode

contact area measured approximately 18mm, however electrode noise can depend upon area, electrolytic gel, patient and placement site (Fernández and Pallás-Areny 2000). Whilst PLI is present in all ECG recordings, both in this thesis and in practice, steps can be taken during device development to reduce the susceptibility to PLI, for instance cable components within ECG recording equipment could contain a layer of braided or spiral shielding to protect against external electrical interference or noise, including triboelectric noise caused by vibration, or materials rubbing inside the cable (Crawford and Doherty 2012).

Conductive gels are incorporated within electrodes to create a conductive path between the skin's surface and electrode. Whilst wet electrodes resulted in the overall lowest electrode-skin impedance, conductive gels are not without limitations. It is documented that standard Ag/AgCl electrodes dry out over a few days resulting in increased noise and measurement errors (Lagow et al. 1971; David and Portnoy 1972; Padmadinata et al. 1990; Searle and Kirkup 2000). Several of these publications refer to the use of an electrolytic paste or jelly, rather than the newer type of electrodes which are pre-gelled. However, to the best of our knowledge, there are limited, up-to-date studies investigating this limitation on current ECG monitoring wet electrodes. Throughout this thesis, 3M Red Dot 2239 ECG monitoring electrodes were used which were supplied pre-gelled with a built-in abrader disc marketed to improve trace quality. Indicated for ambulatory cardiac monitoring in adult patients, the electrolytic gel used in these electrodes contained a low chloride concentration and had a quoted wear time of up to 3 days (3M 2021). To investigate the extent of gel dehydration, a study was conducted which aimed to weigh gel-soaked foam pads removed from wet electrodes over 2 days. The study showed that over time, there was a loss in weight when the gel-soaked foam pads were left exposed to the surrounding environment and when covered. Covering the pads with the remaining portion of the electrode was included to make the study more representative of clinical conditions as the full electrode is applied to skin. It is, however, still not directly comparable to the use of electrodes in practice as the effects of the skin on the gel-soaked foam pad were not examined as moisture and sweat can build up beneath the electrode. Furthermore, this study measured weight loss, not moisture. However, as imaging revealed that the foam pads appeared noticeably dryer after 2 days it is likely that the weight loss was due to moisture. These results build upon the existing evidence that wet electrodes are susceptible to gel dehydration. Future studies however could investigate how the effects of gel dehydration impact signal quality and measurements. Furthermore, this study was conducted under controlled temperature conditions. Temperature, however, can fluctuate widely within healthcare settings, particularly on ward environments. Therefore, a study could be conducted investigating the rate of moisture loss at changing temperatures, and relative humidity.

4.5.3 Influence of changing parameters on electrode performance

When investigating the effect of MN length on electrode performance, this study determined that SNR was comparable between the three electrodes, despite both length MNs piercing the skin. Identifying a suitable length MN is important as they need to contact conductive layers to acquire high quality recordings without stimulating pain receptors. There are, however, several considerations when interpreting these results. In the context of the literature, the 100μm difference between the MN electrodes may not have been large enough to observe a significant improvement in SNR. For instance, Patel et al. (2016) characterised a MN cuff electrode using needles ranging from 75 to 200μm in height. As MN length increased, the electrode-tissue interface impedance decreased whilst SNR increased, with 200μm MNs achieving the highest SNR of approximately 20dB. Unlike this chapter which used ex vivo skin, the authors performed the study on the sciatic nerves of anaesthetised Lewis rats. Furthermore, other publications have demonstrated that circumvention of the SC is more reliable when applying MNs using a high velocity insertion method (Verbaan et al. 2008; van der Maaden et al. 2014). MN electrodes within this study were pressed into ex vivo skin by the operators' thumb. Further studies could investigate the effects of application technique, to identify the most efficient option which can subsequently inform the development of a device with a built-in applicator. Regarding the effects of application technique, Lozano and Stoeber (2021), characterised a flexible MN electrode using porcine skin explants under thumb pressure and using a high velocity applicator. The authors demonstrated that when pressed into in vivo skin, impedance was higher, but comparable to wet electrodes without preparing skin. When inserting MNs using a higher velocity, the electrode-skin impedance interface was considerably lower. Similarly, to this thesis, Lozano and Stoeber (2021) used an OpenBCI acquisition board to capture biopotentials from volunteers. They found that MN electrodes inserted using a higher velocity resulted in the greatest SNR of 7.9dB compared to the 1.4dB achieved with pressing force. Whilst the SNR values for changing MN length presented in this chapter ranged between 24 and 25dB, they were greater than Patel et al. (2016) and Lozano and Stoeber (2021). These values however were acquired using an ex vivo model rather than healthy volunteers. Whilst this model affords benefits regarding electrode optimisation and testing of wearability parameters prior to human testing, the model could not provide information regarding pain or level of discomfort. In addition to signal quality, microchannel width and depth were measured using OCT to assess the effects of MN length and electrode design on channel dimensions. Unlike Chapter 2, MNs used throughout this, and the previous chapter, were coated with Ti/Au enabling the MNs to conduct signals. Therefore, microchannel measurements could also indicate if the metallised coating affected insertion and subsequent channel dimensions. Overall, microchannels were deeper and wider than those shown in

Chapter 2. However, dimensions were comparable between 500µm and 600µm length MNs as well as both MN electrode designs. Studies conducted in this chapter involved pressing MN electrodes into prepared porcine skin explants by the operators' thumb. As 10N is considered moderate thumb pressure (Sharma et al. 2017), the increased microchannel dimensions shown suggests that MN electrodes were inserted at forces exceeding 10-15N. With this increased force the MNs are likely to pierce deeper into skin therefore, increasing microchannel depth. Moreover, a greater proportion of the MN structure would enter skin thereby increasing channel width as MNs are wider at the baseplate than the needle tip. Attributing microchannel changes to the conductive coating is challenging, as application force and method were not consistent. Therefore, a future study directly comparing coated and uncoated epoxy MNs using a controlled force and application method could better inform the effects of the 220nm conductive coating on microchannel dimensions.

A parameter known to affect devices interfacing with biological fluids is biofouling. Regarding sensing, biofouling is the accumulation of substances such as cells and proteins on the surface of the sensor which subsequently impedes performance (Minnikanti et al. 2010; Meijs et al. 2016). Non-invasive wet electrodes are unlikely to biofoul as they are non-invasive and do not breach the skins barrier. Unlike wet electrodes, MNs can be considered minimally invasive. Whilst MNs are associated with reduced pain, tissue trauma and skin irritation, in the form of a sensor they would penetrate the SC and, depending upon length, would reside within skin. The trauma elicited by the implantation of MN electrodes could trigger the immune system to start the healing process (Minnikanti et al. 2010; Anderson and McNally 2011). In comparison to invasive devices, minimally invasive devices such as the MN are suggested to possess reduced biofouling effects due to the reduced trauma upon application (El-Laboudi et al. 2013). However, studies investigating the effects of biofouling using MN sensors in physiological signal monitoring are limited, therefore a study was conducted to compare the performance of wet and MN electrodes over an extended time period, as this thesis currently, has only presented comparisons based on electrode performance immediately following application. Over the duration of the study SNR values for both wet and MN electrodes were comparable, and no signal deterioration occurred. MN electrodes appeared to stabilise after 1 hour before producing more consistent readings. This could be due to the needles settling within the skin following application or moisture accumulating beneath the electrode. Studies investigating the effects of biofouling for MN ECG measurements are lacking, making comparisons challenging. The reduced number of studies investigating the MN biofouling could be related to the fact that AECG monitoring using the Holter can last up to 48 hours whilst resting ECGs conducted in primary care take approximately 10 seconds. For instance, Ren at al. (2016) described the use of their MN electrode in the acquisition of physiological

signals. Whilst they do not explicitly state the total recording duration, results show only a few seconds. The biofouling effects of these MN sensors were not explored. Some research groups developing MN-based electrochemical sensors have observed MN biofouling. Chinnadayyala et al. (2021) fabricated a MN electrode for continuous glucose monitoring. MNs used within this sensor measured 650µm in height and exhibited good stability in vivo. Device functionality was lost after 7 days due to biofouling. Bollella et al. (2019) also observed a decline in signal when their MN-based lactate sensor was conducted in human serum. Whilst the MN sensors discussed in the aforementioned studies were fabricated for different indications, these publications highlight the need to conduct further experiments whereby cardiac signals are captured over a prolonged duration. Biofouling at the tissue device interface remains a challenge, particularly for AECG monitoring where devices could be worn for longer durations up to 14 days. Future studies involving MN electrodes for cardiac signal monitoring would require a minimum recording duration of 24 hours to compare with the current Holter monitor alongside the monitoring of electrode-skin impedance. Furthermore, it would be prudent to conduct these in vivo. Whilst the model uses porcine skin explants which, whilst considered anatomically relevant, is not representative of in vivo conditions. Similarly, to Bollella et al. (2019), testing MN electrodes in human serum could provide useful insights into potential fouling effects. Whilst it is known that lower levels of protein exist within interstitial fluid, the extent of biofouling could also depend upon the contacting material (Voskerician et al. 2003). For instance, silicon-based microelectrodes perform well in vitro but show significant biofouling in vivo over time (Dario et al. 2000). Should future studies identify when these metallised epoxy MN electrodes lose functionality due to biofouling, steps could be taken to during device development to incorporate antifouling surfaces. For example, Song and colleagues explored the antifouling properties of the conductive polymer PEDOT, doped with an ionic liquid. Although the electrodes and indication discussed in this publication were not related to MN-based ECG electrode, this electrochemical sensor was shown to resist biofouling when immersed in a complex media (Song et al. 2019).

If a device is to be worn on the body for extended periods of time, there must be a balance between functionality and wearability. For instance, AECG monitoring is migrating from bulky Holter monitors to PEMs which have improved wearability and patient compliance (Martinez-Tabares et al. 2014). As discussed previously, limitations were identified with the original MN electrode design. Therefore, a bespoke MN electrode was designed to start addressing these drawbacks. As stated in Chapter 3, application force and method were not consistent between volunteers, therefore MNs may not have truly pierced the skin. The new, bespoke MN electrode incorporated a button which, when deployed, pressed MNs into the skin at an approximate force of 15N. The incorporation of notches allowed the button to remain

deployed thereby retaining the MNs in place. Additionally, the original snap connection was located directly above the arrays allowing ECG leads to potentially pull MNs out of skin during movement. For this reason, the snap connection was moved away from the array. Using the laboratory ex vivo model described above, comparisons between the three types of electrodes were made. No statistical significance was observed between the designs suggesting that both MN electrode types were similar in performance to wet electrodes. When evaluating signal quality for each electrode, it was observed that the SNR was lower than presented elsewhere within this chapter. When acquiring simulated signals from the MN electrodes, in some cases the system 'railed'. A railed system occurs when microvolt magnitudes for the channels exceed the top end of the scale. This means that there was a problem with the differential voltage measured between the channel and the reference resulting from a poor connection. In the case of a railed system and as per the manufacturer's instructions, wires, electrodes, electrode contacts and connectors were checked. Poor electrode connections could result in a higher skin-electrode impedance which are associated with a lower SNR and increased susceptibility to artifacts. Whilst all the aforementioned points were intact, the amplification was reduced from x24 to x12 which de-railed the system. Furthermore, one porcine skin specimen used had been frozen twice which may have impacted the quality and hydration of the sample. Future ex vivo studies could benefit from assessing the interface between each electrode type with the excised porcine skin by measuring impedance prior to the acquisition of cardiac signals to compare electrode-skin contact with signal quality.

Comparisons between the data presented in this chapter regarding electrode design and other published work is challenging as each publication presents their own unique electrode. Unlike this study several publications for instance Chlaihawi et al. (2018), Shahandashti et al. (2019) and Dong et al. (2021) have assessed and compared their novel dry electrodes with wet electrodes using healthy volunteers. Whilst comparing the designs using the ex vivo skin model provides information regarding device functionality, it does not however, provide information regarding device wearability. The bespoke MN electrode is bulkier than the previous design, therefore further studies involving human volunteers are required to capture user feedback regarding wearability aspects such as comfort, pain, and discretion. It is however challenging when testing in volunteers since the wearable devices would be constantly exposed to uncontrolled conditions during wear including varying temperature, pressure, humidity, and foreign body response. These conditions, however, could demonstrate the durability of the electrode.

The development of an ex vivo model offers several advantages and could now be used to assess the functionality of novel devices and any associated algorithms in their targeted

disease states as the signal could be adapted to better reflect a particular cardiovascular condition.

4.6 Conclusion

The work presented in this chapter achieved its primary aim of developing a laboratory model for simulated cardiac measurements. An AWG included a pre-programmed cardiac waveform which was optimised in terms of HR and amplitude to better reflect the characteristics of a human ECG. This optimised waveform was successfully generated and acquired through ex vivo porcine skin using three types of electrodes. Simulated signals were recorded at multiple locations of the model to account for signal loss. As signals progressed from the AWG to the individual electrodes, correlation and SNR declined. Upon removal of PLI, correlation and SNR values improved. This laboratory model was used to assess the effects of MN length, duration, and design on electrode performance. Electrode performance was comparable between wet electrodes, 500µm and 600µm MN electrodes. No decline in signal quality was observed when assessing SNR over 6 hours. A bespoke electrode design was developed to address the limitations identified in Chapter 3. Signal quality was comparable between wet electrodes, initial and bespoke MN electrodes. Having assessed the bespoke design ex vivo, further work is required to assess this design in vivo and gather feedback regarding device wearability. Characterising electrodes revealed that wet electrodes resulted in the lowest overall electrode-skin impedance, but when exposed to the environment were found to lose weight, potentially indicating moisture loss. Regarding PLI susceptibility, wet and MN electrodes performed comparably, whilst the dry, disc electrodes were the most sensitive.

CHAPTER 5

WEARABILITY AND PERFORMANCE OF POLYMERIC MICRONEEDLE ELECTRODES IN VIVO

5.1 Introduction to wearable devices

The terms wearable device, wearables and wearable technology refer to smart, electronic devices which are incorporated into gadgets (Lubitz et al. 2021) or clothing (Fink et al. 2021) to monitor human health. The technology and collection of personal data is becoming increasingly popular and consumer wearables for instance the Fitbit®, allow users to collect various forms of health data including HR, step count and weight (Maher et al. 2017). Within healthcare, wearables can be used in the management of chronic disease (Ozanne et al. 2018), diagnosis and treatment (Halcox et al. 2017) and rehabilitation (Jayaraman et al. 2018). Within the field of cardiology, the 24-hour Holter monitor is the current gold standard of ambulatory ECG monitoring. Three key challenges posed by this system include i) discomfort due to adhesive electrodes being attached to skin for extended periods, ii) poor concealment, therefore, the device is noticeable to others, and iii) dehydration of conductive gels which impacts signal quality (Yokus and Jur 2016). In recent years, patch electrode monitors (PEM) for AECG are becoming more widespread. Numerous recreational devices are now capable of recording cardiac activity. Although clinical experience with these new generation devices remains limited, they are addressing the shortcomings of traditional methods.

'Wearability' encompasses many parameters including discretion, aesthetic, location, and comfort. Evaluating device wearability, however, is a multifaceted problem as this can depend on how the device is viewed by the wearer. Numerous devices have been developed

to address the aforementioned challenges with one approach being the MN. Since their conception, the effects of MNs as transdermal drug delivery devices have long been established ex vivo and in vivo (Bal et al. 2008; Gill et al. 2008; Haq et al. 2009; Arya et al. 2017; Jeong et al. 2017). Despite increasing progress, few groups have assessed the wearability of MN devices, particularly in cardiac monitoring. Alternative devices have been proposed and their wearability assessed using multiple approaches. One such developing area is 'smart' textiles which involves the integration of advanced monitoring technologies into everyday items (Mestrovic et al. 2007). Smart textiles are considered to have improved wearability with several groups having assessed various concepts of wearability which are described below.

5.1.1 Flexibility and conformability

To enable health monitoring, sensors should ideally be worn continuously to facilitate data collection. However, suitable contact between electronics and skin is essential for detecting vital signs and intricate movements during activities (Seo et al. 2018). To produce a wearable system that is suitable for extended monitoring, devices are required to conform to the skin. Traditional real-time monitoring equipment suffers from several defects which inconvenience daily life and limit medical applications. Flexible devices are ideal candidates for wearable sensors and several concepts have been investigated including the development of ultra-thin, light weight and flexible epidermal patches (Son et al. 2014; Yamamoto et al. 2016; Wang et al. 2018b). Yamamoto et al. (2016) demonstrated a screen-printed Ag electrode capable of capturing ECG signals. Whilst specific flexibility studies were not conducted, the authors state that the device was printed with a unique kirigami structure (Shyu et al. 2015) allowing it to stretch comfortably on the body (Yamamoto et al. 2016). In 2020, Arquilla and colleagues assessed the wearability of a sewn textile electrode and investigated if the device could perform to the same fidelity as conventional wet electrodes. The electrodes themselves were not flexible, however they were mounted onto fabric thereby creating a tight-fitting garment. The authors subsequently exposed the garment to stretch testing by assessing changes in resistance when the fabric was stretched to two different extents. The textile electrode was also exposed to bend and wash testing to assess performance during use. No changes in resistance during stretch, bending or wash testing were exhibited (Arquilla et al. 2020).

With respect to MN sensors, flexible and stretchable patches have been reported (Yu et al. 2015; Lee et al. 2016; Rajabi et al. 2016). Many MN arrays are fabricated as monolithic components in which both the supporting substrate and needles are comprised of the same material. Whilst MNs are required to be mechanically robust to avoid fracturing, the baseplate

should be flexible to conform to the curvature and deformations of human skin. Polymer-based arrays can provide a degree of flexibility; however, the use of a polymer could compromise mechanical strength and sharpness of the MN tips thereby affecting insertion (Yung et al. 2011). Research groups such as Rajabi et al. (2016) have investigated the combination of rigid MNs with flexible base substrates. The authors fabricated a patch comprised of an elastomeric polymer base combined with solid, stainless steel MNs. To assess flexibility and stretchability of the base substrate the flexural modulus, Young's modulus and maximum elongation at the point of breakage were evaluated. Whilst the patches displayed full functional integrity, the authors found that the attachment between the substrate and MNs required further investigation (Rajabi et al. 2016).

5.1.2 Biocompatibility and functionality

Medical devices are heavily regulated by agencies such as the FDA and Medicines and Healthcare products Regulatory Agency (MHRA) as biocompatibility between the body and wearable device is crucial to avoid triggering an immune response (Kvist et al. 2006). This technology should not induce skin irritation which is a known barrier to compliance. In the development of wearable technology, several groups have investigated the effects of their devices using a variety of methods. Ackermans et al. (2012) assessed the effects of a proposed patch device on human skin daily, using a questionnaire. The extent of erythema was evaluated using a validated rating scale. Images were captured of the volunteers' skin prior to device application to determine a baseline and 24 to 72 hours after patch removal. Furthermore, the Skindex-19 quality of life questionnaire was completed by volunteers to determine the overall effect of the study on the participants quality of life. The device proposed by Ackermans, and colleagues was considered comfortable with minimal skin irritation. Liu and colleagues assessed skin irritation using an 8-point scale. However, skin irritation scores were not compared between the 24-hour Holter and 14-day ECG patch as scores were only recorded following the removal of the devices (Liu et al. 2021). Many publications have fabricated devices consisting of biocompatible materials. Boutry et al. (2015) constructed a pressure sensor for cardiovascular monitoring. During the development of this sensor, several biocompatible and biodegradable materials were used to reduce the risk of irritation and waste. Research however is still required to improve the biocompatibility of wearables particularly for prolonged measurements. Functionality of wearable technology can be assessed using several methods; however, the majority of studies involve the application of wearables to volunteers (Perez et al. 2019; Shahandashti et al. 2019; Liu et al. 2021). For instance, Shahandashti et al. (2019) assessed the performance of their stretchable electrode by measuring the skin-electrode impedance which plays a key role in the quality of the

recorded signal. The authors also assessed device functionality by applying their prototype electrode to human volunteers and recording physiological signals.

5.1.3 Comfort and compliance

The term comfort is broad and can depend upon how the device is perceived by the user. Key objectives in the development of novel acquisition systems revolve around the construction of devices which cause the least amount of aggravation for the patient and ease of use for the clinician. In recent years, patch-based ambulatory monitoring is becoming more widespread. The ease of application of the PEM have resulted in high study completion rates (Shinbane et al. 2013; Fung et al. 2015), suggesting a high acceptance rate which could translate into improved compliance when compared to other devices (Barrett et al. 2014; Halcox et al. 2017). When assessing new wearables such as PEM, user experience and comfort are often assessed using observation and questionnaire-based methods (Cancela et al. 2014; Maher et al. 2017; Rho et al. 2018). When evaluating the comfort of a device, questionnaires typically focus on areas including sensations such as erythema, pruritis, burning or stinging and ease of application. For instance, Bolourchi et al. (2020) compared the traditional Holter monitor with the Zio XT patch in children. Patients and parents were asked to complete a satisfaction survey after the 48-hour monitoring period. Overall, 75% of patients and parents preferred the Zio XT, whilst 13% preferred the Holter. The Zio XT patch was often preferred over the Holter for reasons including increased comfort, less noticeable and reduced skin irritation (Bolourchi et al. 2020).

During use, wearables must maintain structural and functional integrity when encountering environmental stimuli for instance humidity, sweating or exposure to rain, as devices could undergo performance deterioration due to interference from moisture. Therefore, during the fabrication of flexible electronics, developing substrate materials with breathability is important in ensuring device comfort. Erythema, pruritis and inflammation are key challenges for user comfort and could be induced when applying electrodes with poor gas permeability to skin (Wang et al. 2018a; Gong et al. 2019; Zhang et al. 2021). Several devices with improved breathability have been reported (Dong et al. 2016; Qiu et al. 2019; Wang et al. 2020; Zhang et al. 2021). Whilst Qiu and colleagues did not specifically test for breathability in their wearable device, a breathable conductive fabric was employed during device fabrication (Qiu et al. 2019). Zhang et al. (2021) assessed the breathability of a proposed paper-based device by attaching various substrate materials to rabbit skin for 24 hours. The degree of inflammation induced by these patches was then compared. Device breathability was demonstrated with only the control group inducing visible skin inflammation. The authors

state that the adverse effects of inflammation could be alleviated by the patches as they did not block sebum and sweat section during wear (Zhang et al. 2021).

Although there are many advantages of increased ECG monitoring durations, several challenges, including wearability, still hinder the widespread adoption of wearable technology in clinical practice. This final results chapter will seek to compare the performance and wearability of a bespoke MN electrode, introduced in Chapter 4, with two alternative designs, in vivo. Using the three challenges and wearability themes discussed previously, the discretion, discomfort and signal quality of this bespoke electrode will be assessed following immediate application to skin and after prolonged wear.

5.1.4 Aims and objectives of the chapter

This chapter aimed to assess the quality of cardiac signals recorded from a commercially available wet electrode, initial MN electrode prototype and novel bespoke MN electrode design in healthy, adult volunteers under resting and active conditions immediately following electrode application, and after 6 hours of prolonged wear. This chapter also aims to compare the wearability of both MN electrode designs with wet electrodes by capturing volunteer feedback both initially and following prolonged wear using a two-part questionnaire. The objectives were to:

- To write, develop and obtain ethical approval from the School of Pharmacy and Pharmaceutical Sciences ethics committee to record cardiac activity from up to ten healthy, adult volunteers.

- To record cardiac signals from volunteers under resting conditions using a commercially available wet electrode, initial MN electrode prototype and novel bespoke MN electrode design immediately following application and following 6 hours of wear.

- To record cardiac signals from volunteers during active conditions using a commercially available wet electrode, initial MN electrode prototype and novel bespoke MN electrode design immediately following application and following 6 hours of wear.

- To confirm MN penetration using OCT to capture sub-surface images of the volunteer's skin immediately following electrode removal.

- To assess the effects of each electrode type on skin by capturing images of the volunteers' skin immediately following electrode removal.

- To conduct a two-part exploratory questionnaire to capture user feedback regarding the wearability of the different electrode designs.

- To compare and assess the performance of three electrode designs by calculating the SNR of recorded ECG traces at rest, during active conditions and following 6 hours of prolonged wear.

5.2 Materials

Details of equipment and reagents used in the studies described below are listed in the equipment and reagents tables. Cardiac data was acquired using the OpenBCI GUI version 5.0.6 (OpenBCI, USA). Questionnaires were developed using Microsoft Forms (Microsoft Corporation, USA). Data processing was conducted using Microsoft Excel version 16.46 (Microsoft Corporation, USA) and MATLAB 2018a (The MathWorks Inc., Natick, MA). Image processing was conducted using ImageJ software (NIH, USA) and Microsoft PowerPoint version 16.37 (Microsoft Corporation, USA).

5.3 Methods

This clinical study was conducted during the COVID-19 pandemic. All relevant University and Welsh Assembly Government guidelines relevant at the time of the study were followed.

5.3.1 Eligibility and recruitment

To be eligible for this new study, the original inclusion criteria of $\geq$18 years of age and no known cardiovascular conditions were updated. No known skin conditions were included due to the enhanced erythema observed in previous participants with dermatological conditions such as eczema. Furthermore, participants were required to have no known allergies to any of the materials used in the fabrication of the electrodes.

Similarly, to Chapter 3, volunteers were again recruited using word of mouth, existing contacts and via recruitment email. The previous email, shown in Appendix II, was updated to include information relevant to this study and highlighted the safety precautions associated with the ongoing COVID-19 pandemic (Appendix XI). Unlike the previous study, detailed in Chapter 3, volunteers in this case were recruited only from Cardiff School of Pharmacy and Pharmaceutical Sciences. Volunteers therefore had received and completed the mandatory training provided by the school ensuring that they were able to work in a COVID-safe environment. This ensured that all COVID-19 safe practices were followed and adhered to. The previous participant information leaflet (Appendix IV) and consent form (Appendix III) were amended to include updated information regarding study procedure and safety considerations regarding the pandemic. The updated consent form also included new statements regarding the sharing of data with our collaborators, SymlConnect Ltd and Professor Julian Halcox. Prospective volunteers were provided with the updated electronic consent form (Appendix XII) and participant information sheet (Appendix XIII). Upon registration of interest, participants were given 72 hours to decide whether they wished to be involved. Participants were also supplied with a training video, developed by the research team to provide more information regarding study protocol. Recruitment of up to ten volunteers occurred once the study received

ethical approval from Cardiff School of Pharmacy and Pharmaceutical Sciences Ethics Committee (Ref: 2021-11).

5.3.2 Study design and COVID-19 considerations

Due to the pandemic, aspects of the study design were adapted to follow university and government guidelines. Prior to face-to-face data collection, COVID-19 status of both the researcher and volunteer required clarification. Initially, volunteers were asked three questions prior to the start to the start of the study and on the day of recording which included:

- Are you, your child, or anyone in your household a confirmed case of COVID-19?
- Do you, your child, or anyone in your household have symptoms of COVID-19 which include a new continuous cough, elevated temperature/fever and/or loss of smell or taste?
- Are you, your child, or anyone in your household in self-isolation?

Due to the expansion of COVID-19 symptoms during the pandemic, participants were advised that if, on the day they felt unwell, to contact the research team, isolate and follow advice provided by contact tracers. Upon completion of the required isolation period, a new date and time were re-scheduled. On the day of recordings, the researcher completed a lateral flow test to confirm COVID-19 status. Should a positive COVID-19 result occur, the researcher would contact the volunteer to re-schedule, isolate and follow advice provided by contact tracers.

All ECG recordings were conducted within consultation rooms in Cardiff School of Pharmacy and Pharmaceutical Sciences. The largest of these consultation rooms was used, as this allowed for a maximum room occupancy of three individuals, therefore 2m social distancing was maintained. Prior to volunteer arrival, contact areas including door handles, medical bed, chairs, and table surfaces were cleaned using an appropriate disinfectant containing a minimum of 70% ethanol. On the day of recording and following confirmation of a negative COVID-19 status, volunteers were asked to sanitise their hands with either alcohol or non-alcohol-based hand sanitiser as they would be handling the biosensing board during signal acquisition. In total, three electrode designs were used throughout this clinical study. A commercially available wet electrode was used as a positive control as this is the current gold standard. The initial MN electrode prototype, introduced and assessed in Chapter 3, was included in order to compare with the bespoke MN electrode fabricated by Maddison Product Design Ltd (West Sussex, UK), introduced in Chapter 4, to determine if the modifications made improved signal quality. Volunteers applied these electrodes to their torso in the locations shown in Figure 5.1. No skin preparation was conducted prior to electrode application to skin.
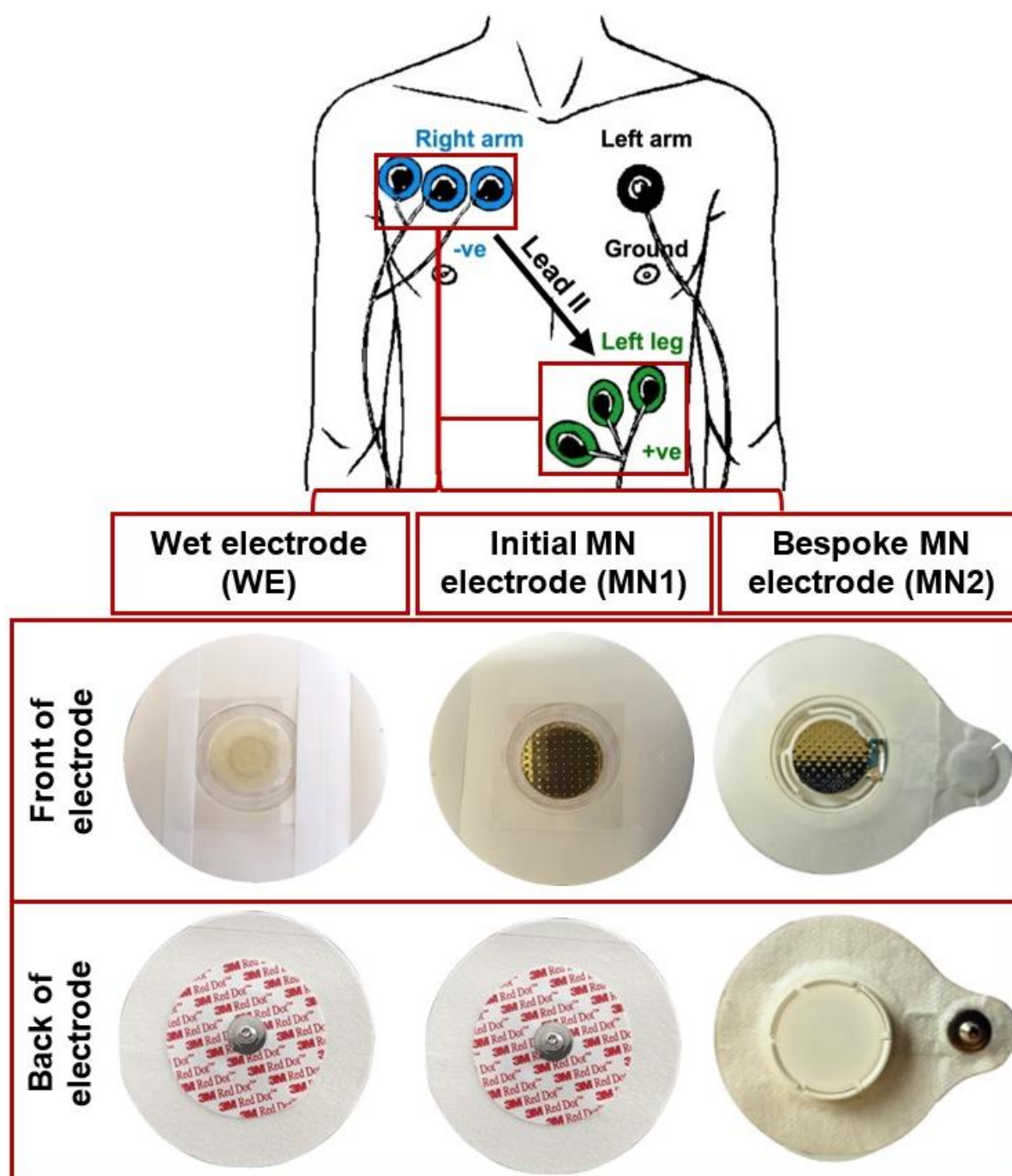
Figure 5.1: Positioning of the three electrodes on the torso of volunteers. Electrodes were placed to achieve a lead II configuration which measures the potential difference between the right arm and left leg. An electrode of each type was applied below the right (negative) and left (ground) clavicle as well as left of the umbilicus (positive). Data was simultaneously acquired from each type of electrode.

The ground electrode was placed beneath the left clavicle whilst the negative electrodes were placed underneath the right clavicle ensuring that the electrodes were not directly applied on top of bone. Positive electrodes were attached left of, but near to the umbilicus. The order in

which volunteers applied each type of electrode was randomised. Each electrode type was assigned a number (wet = 1, MN1 = 2 and MN2 = 3). Using a number generator, the type of electrode applied first, second and third was randomly generated. Each single-use electrode was connected to a separate channel on a Cyton biosensing board shown in Figure 5.2.
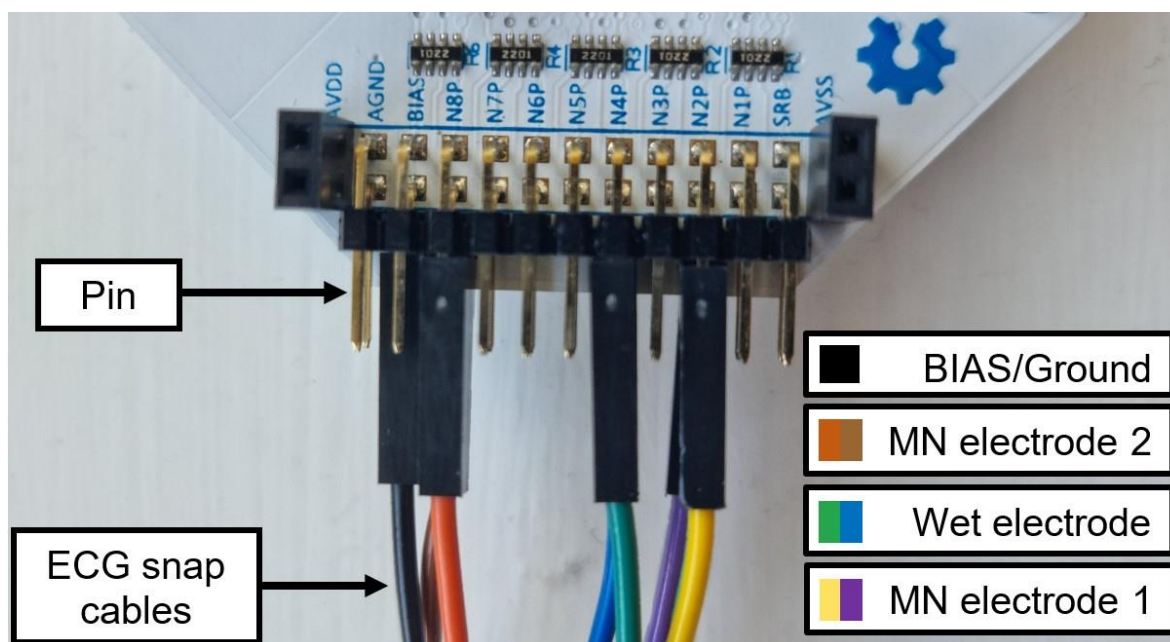
Figure 5.2: Connection of snap cables to the OpenBCI Cyton biosensing board. Black lead is connected to the BIAS pin which acts as the ground. Green/blue leads are connected to the N4P and N4N pins which act as the positive and negative for the wet electrodes. Yellow/purple leads are connected to the N2P and N2N which act as the positive and negative for the original microneedle electrode design. Orange/brown leads are connected to the N8P and N8N which act as the positive and negative for the new microneedle electrode design.

To capture data at rest, volunteers were placed in a semi-recumbent position at an approximate 45° angle to minimise movement. When comfortable, volunteers were asked to press firmly down on the MN electrode and deploy the push button applicator. After a 5-minute rest period to allow the electrodes to stabilise, three, 60-second recordings of cardiac data were simultaneously captured from each electrode type. Data were communicated wirelessly to the OpenBCI GUI, via Bluetooth. Cardiac activity was recorded using a sampling frequency of 250Hz, gains of x12 or x24 in a lead II configuration. Upon conclusion of the resting ECG, cardiac signals were then recorded during simple movement. Volunteers were placed in a chair where they stood up and sat down a total of three times per minute (every 15-seconds) when instructed to do so by the researcher. This was repeated a total of three times using the same lead configuration, sampling, and amplification criteria. Leads were subsequently disconnected to allow for movement, and volunteers were asked to wear all the electrodes for a total of 6 hours. Following this period, volunteers returned to the consultation room where

resting and active ECGs were re-recorded. Upon completion of these recordings, four electrodes were removed leaving one of each electrode type beneath the right clavicle. Volunteers were asked to wear these electrodes for the remaining 24 hours. During this time, they were asked to refrain from bathing, showering, and exercising as the electrodes were not waterproof and these activities would have affected the adhesive. If at any point during the 24 hours the electrodes caused any discomfort, the volunteer was informed to remove the offending electrode. Where possible the volunteer was also asked to take a photograph of their skin should they remove any electrodes. Following 24 hours, volunteers returned to the School of Pharmacy where the remaining electrodes were removed. All recorded data was anonymised using a numerical identifier to maintain subject confidentiality. The anonymised data was stored in its unprocessed state on an encrypted external hard drive to further protect the confidentiality of data.

5.3.3 Questionnaire development

A two-part questionnaire was developed using Microsoft Forms for completion by the volunteer at certain stages of the study. This was an exploratory questionnaire to capture initial views and feedback regarding the wearability of the electrode designs. Volunteers completed part I of the questionnaire (Appendix XV) following the initial recording of the resting and active ECGs and part II following the 24 hours of wear (Appendix XVI). Part I focused on capturing information pertaining to volunteer demographics in addition to sensations felt upon initial application of the electrodes. Part II focused on capturing feedback after 24 hours of wearing the devices. This part of the questionnaire assessed themes including sensations, comfort, and device preference. A variety of open and closed questions were used including types of responses (e.g., multiple choice, open-ended). Questions were posed to the volunteer by the researcher to capture immediate feedback and allow for higher response rates. Responses were recorded by the researcher using an electronic version of the questionnaire on Microsoft Forms.

5.3.4 Effect of electrodes on human skin

Prior to the application of each electrode, photographs of the volunteers' skin were taken to function as a reference. This was the only instance where 2m social distancing was not maintained. However, both volunteer and researcher would have confirmed their negative COVID-19 status and the maximum duration in which both would be in close proximity was less than 5 minutes. Furthermore, both volunteers and researcher were wearing appropriate PPE consisting of face coverings and gloves. Upon conclusion of cardiac signal data acquisition, electrodes near the umbilicus and under the left clavicle were removed. Images

of the skin were captured using a DSLR camera with zoom lens immediately following electrode removal to observe the effects of the electrodes on skin. Additionally, OCT imaging was conducted to capture sub-surface images of skin to confirm MN penetration. Scans were acquired using the method documented in Chapter 2.

After 24 hours, the remaining three electrodes beneath the right clavicle were removed. Images and scans were captured immediately following their removal. Electrode sites from the previous day were re-imaged and re-scanned to observe if any signs of irritation had resolved and microchannels resealed. All images and scans captured the area of skin in direct contact with the electrode and did not contain any identifying features. Data were anonymised and stored on an encrypted external hard drive to further protect the confidentiality of data.

5.3.5 Ethical approval

An initial application (Appendix IX) and subsequent amendment (Appendix X) with supplementary materials were submitted to and approved by the Cardiff School of Pharmacy and Pharmaceutical Sciences Ethics Committee (Ref: 2021-11).

5.3.6 Quantitative comparisons of electrode performance

Quantitative comparisons between the three electrode designs were made by calculating the SNR of recorded traces. Code documented in Appendix V which was developed and discussed during Chapter 3 was again used to calculate this measure of signal quality.

Data were imported into the MATLAB workspace for analysis and converted from µV to mV. The data were filtered offline using a digital high-pass filter with cut-off frequency of 0.5Hz to remove BW and DC offset. Cardiac signals were isolated using a digital lowpass filter with 40Hz cut-off frequency. Using the equation documented in Figure 3.11, signal power was determined by taking the maximum and minimum values of the ECG which were found within the QRS complex of filtered signals. As maximum and minimum values varied with each heartbeat, six individual QRS complexes were selected through the 60-second trace and mean maximum and minimum values were calculated. To isolate noise, a second digital high-pass filter was applied to the data using a cut-off of 40Hz. Noise power was calculated by determining the standard deviation of the noise and multiplying this number by four to obtain a 95% confidence interval. SNR values were calculated for each of the three, 60-second recordings acquired from every volunteer and averaged. Mean SNR values were calculated for each individual electrode in addition to an overall SNR for each type of electrode.

5.3.7 Qualitative comparisons of electrode performance

Visual comparisons of ECG traces were made to qualitatively compare between the three types of electrodes. Traces were plotted using MATLAB following the implementation of a 0.5Hz digital high-pass filter to remove artifacts. FFT of cardiac signals were plotted to identify the peak frequency of PLI. A digital notch filter was subsequently used to remove this frequency.

5.3.8 Statistical analysis

Where appropriate, statistical significance was calculated using SPSS. A one-way ANOVA was used to determine significance which was defined as $p < 0.05$.

5.4 Results

5.4.1 Participant demographics

In total, nine subjects were included in the present study. Volunteers were aged 18 years and older with all subjects completing the research study in its entirety. Demographic data including biological sex, age, ethnicity, and BMI were captured for each participant following the initial recording of cardiac signals during resting and active conditions. Table 5.1 displays the biological sex, age ranges and ethnicities of the volunteers.

Table 5.1: Demographics of recruited volunteers were captured using an online questionnaire following the initial resting and active ECGs.

Demographic		Numbers (n=9)	Percentage (%)
Biological sex	Male	5	56
	Female	4	44
Age category (years)	25-34	2	22
	35-44	4	45
	45-54	2	22
	55-64	1	11
Ethnicity	White (Welsh, Scottish, Northern Irish, English, British)	8	89
	Any other mixed/multiple ethnic background	1	11

Out of the nine volunteers, five were male and four were female with participants ranging in age from 25 to 64 years. In terms of ethnicity, eight volunteers identified themselves as Caucasian (Welsh, Scottish, Northern Irish, English or British) and one as any other mixed or multiple ethnic background. In addition, the BMI of participants were calculated. If the volunteer did not know their BMI, height and weight were recorded to allow the researcher to calculate this information. Table 5.2 displays the maximum, minimum and mean BMI measurements of the nine volunteers in addition to the BMI equation used to calculate these values. The mean BMI was 24.9kg/m^2 with a maximum of 34kg/m^2 and a minimum of 20kg/m^2.

Using the BMI calculation, one participant would be considered obese, whilst three were overweight and five had a normal BMI.

Table 5.2: Maximum, minimum and mean body mass index of volunteers. As part of the initial questionnaire volunteers were asked to state their BMI or provide their height and weight. Data presented as the mean ±SD (*n=9*).

	Maximum	Minimum	Mean
BMI (kg/m^2)	34	20	24.9 ±4.67

*BMI = $\dfrac{\text{Weight (kilograms)}}{\text{Height (metres)}^2}$

5.4.2 Quantitative comparison of electrode performance

5.4.2.1 Electrode performance under resting conditions

Table 5.3 and Figure 5.3 display SNR comparisons of signals recorded using three electrodes immediately following application to skin, and after 6 hours of wear, under resting conditions. Overall, wet electrodes recorded signals of higher fidelity than both MN electrodes, however standard deviation indicated comparable performance between the designs. No statistical significance was determined between the designs both initially (p=0.725) and following prolonged wear (p=0.966).

Table 5.3: Signal-to-noise ratio comparison between three electrode designs in healthy adult volunteers under resting conditions. Overall mean signal-to-noise ratio (dB) for wet (WE), microneedle electrode 1 (MN1) and microneedle electrode 2 (MN2) are highlighted. The black cross indicates that cardiac data was not recorded from volunteer five as microneedle electrode 2 had detached prior to prolonged recordings. For each volunteer, data presented as the mean ±SD (*n=3*). For the overall average, data presented as the mean ±SD (*n=9*).

Volunteer Number	Signal to noise ratio (dB)					
	Signal acquisition at 0hrs (initial)			Signal acquisition at 6hrs (prolonged)		
	WE	MN1	MN2	WE	MN1	MN2
1	31.2 ±0.50	27.8 ±0.35	29.2 ±0.16	30.8 ±0.69	29.6 ±0.16	28.9 ±0.52
2	28.3 ±1.22	26.0 ±1.89	28.5 ±1.91	25.0 ±3.78	24.4 ±3.68	27.4 ±5.31
3	22.8 ±1.54	21.2 ±1.86	22.2 ±2.76	20.5 ±0.61	20.0 ±1.42	20.0 ±1.42
4	21.9 ±6.99	20.9 ±7.19	13.7 ±2.29	16.2 ±8.11	16.8 ±7.66	14.0 ±7.36
5	25.4 ±3.12	22.7 ±4.53	27.0 ±3.28	22.0 ±5.96	21.8 ±8.16	**X**
6	29.4 ±0.43	22.0 ±3.27	28.5 ±0.31	30.4 ±0.56	29.2 ±0.73	19.7 ±0.53
7	9.8 ±7.52	11.3 ±9.41	12.7 ±6.92	9.2 ±1.83	4.1 ±1.63	16.6 ±2.20
8	27.5 ±0.23	32.3 ±0.37	28.9 ±0.30	33.4 ±0.32	32.6 ±0.13	32.6 ±0.04
9	28.4 ±0.33	24.4 ±0.29	12.1 ±4.93	29.7 ±0.18	29.7 ±0.24	29.8 ±0.39
Mean	24.9 ±6.44	23.2 ±5.79	22.5 ±7.57	24.1 ±7.96	23.1 ±8.83	23.7 ±6.88

Whilst the bespoke MN electrode resulted in no significant improvement in performance, it remained comparable to the previous MN electrode and, importantly, the wet electrode. Throughout the present study, SNR ranged from 4dB to 33dB and varied between volunteers, electrode type and time of recording (0hrs vs 6hrs). All electrodes remained attached to the skin in eight volunteers when cardiac activity was re-recorded after 6 hours of wear. In the

remaining volunteer, the bespoke MN electrode at the umbilicus had dislodged prior to the prolonged recordings. Therefore, cardiac activity was not recorded from this electrode type in volunteer five as a pair of electrodes are required to capture cardiac signals. This is represented in Figure 5.3 by a black cross. Out of the nine subjects, SNR values were lowest for volunteer seven both initially, and following prolonged wear.
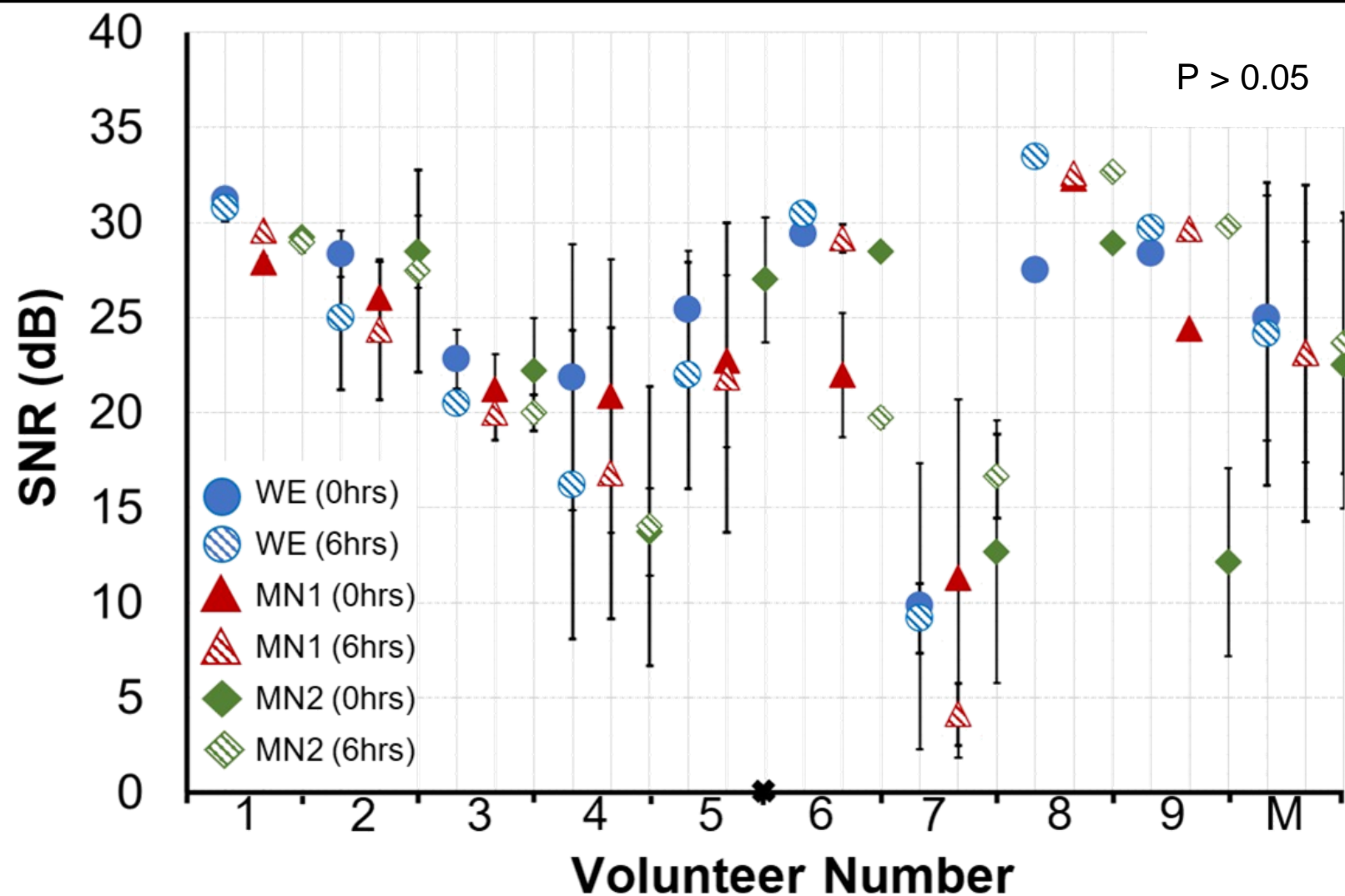
Figure 5.3: Signal-to-noise ratio comparison between three electrode designs in healthy adult volunteers under resting conditions. Overall mean signal-to-noise ratio (dB) for wet (WE), microneedle electrode 1 (MN1) and microneedle electrode 2 (MN2) are highlighted by the blue box. Black cross indicates that cardiac data was not recorded from volunteer five as microneedle electrode 2 had detached prior to prolonged recordings. For each volunteer, data presented as the mean ±SD (*n=3*). For the overall average, data presented as the mean ±SD (*n=9*).

5.4.2.2 Electrode performance during active conditions

Table 5.4 and Figure 5.4 display SNR comparisons of signals recorded using three electrodes immediately following application to skin and after 6 hours of wear, during movement. Overall, a decline in performance was observed for all electrodes. Whilst wet electrodes again recorded signals of higher fidelity than both MN electrodes, comparable performance between the designs was observed. No statistically significant difference was observed between the designs both initially (p=0.598) and following a 6-hour wear-time (p=0.675).

Table 5.4: Signal-to-noise ratio comparison between three electrode designs in healthy adult volunteers during active conditions. Overall mean signal-to-noise ratio (dB) for wet (WE), microneedle electrode 1 (MN1) and microneedle electrode 2 (MN2) are highlighted. The black cross indicates that cardiac data was not recorded from volunteer five as microneedle electrode 2 had detached prior to prolonged recordings. For each volunteer, data presented as the mean ±SD (*n=3*). For the overall average, data presented as the mean ±SD (*n=9*).

| Volunteer Number | Signal to noise ratio (dB) | | | | | |
| | Signal acquisition at 0hrs (initial) | | | Signal acquisition at 6hrs (prolonged) | | |
	WE	MN1	MN2	WE	MN1	MN2
1	26.2 ±1.86	21.0 ±1.06	27.8 ±0.41	27.1 ±0.59	26.0 ±0.86	24.8 ±2.55
2	22.7 ±2.89	18.2 ±2.35	20.1 ±4.07	25.5 ±0.62	22.2 ±0.62	19.0 ±2.83
3	21.1 ±1.64	16.9 ±0.29	20.0 ±2.57	18.0 ±4.20	14.8 ±3.16	15.0 ±3.08
4	17.1 ±5.69	15.8 ±5.48	15.2 ±4.61	8.23 ±9.52	13.7 ±1.90	13.0 ±3.14
5	16.0 ±9.54	17.8 ±8.58	16.4 ±8.86	22.2 ±1.10	22.4 ±2.10	**X**
6	28.5 ±0.47	23.8 ±0.06	27.5 ±0.31	28.7 ±1.16	27.2 ±2.75	11.5 ±2.70
7	11.6 ±7.82	13.0 ±9.45	13.2 ±10.31	10.6 ±4.64	12.1 ±2.62	13.8 ±2.70
8	25.7 ±0.23	24.9 ±1.95	27.3 ±0.36	22.6 ±11.96	21.6 ±13.07	23.2 ±12.36
9	27.4 ±0.61	26.1 ±0.71	9.8 ±4.03	14.4 ±9.19	14.2 ±9.45	14.7 ±9.91
Mean	21.8 ±5.83	19.7 ±4.48	19.7 ±6.67	19.7 ±7.34	19.4 ±5.69	16.9 ±4.91

During active conditions SNR ranged from approximately 8dB to 28dB and again varied between volunteers, electrode type and time of recording. Cardiac activity was not recorded using the bespoke electrode from volunteer five due to this electrode becoming dislodged prior to the 6-hour recordings. This is again represented in Figure 5.4 by a black cross.
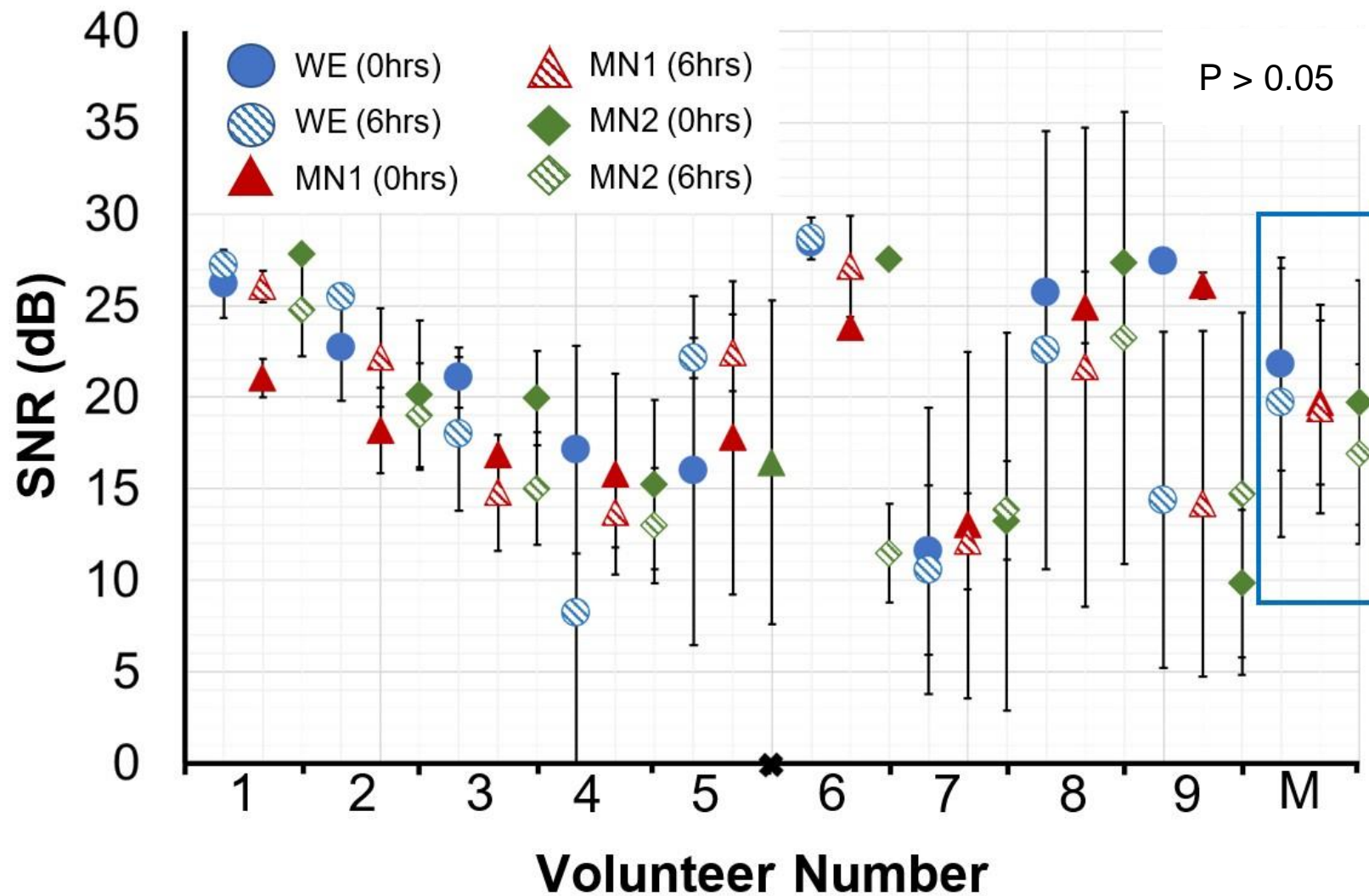
Figure 5.4: Signal-to-noise ratio comparison between three electrode designs in healthy adult volunteers during active conditions. Overall mean signal-to-noise ratio (dB) for wet (WE), microneedle electrode 1 (MN1) and microneedle electrode 2 (MN2) are highlighted by the blue box. Black cross indicates that cardiac data was not recorded from volunteer five as microneedle electrode 2 had detached prior to prolonged recordings. For each volunteer, data presented as the mean ±SD (*n=3*). For the overall average, data presented as the mean ±SD (*n=9*).

5.4.3 Magnitude of powerline interference in cardiac signals

5.4.3.1 Powerline interference under resting conditions

Using FFT, the frequency domain of cardiac signals recorded using all electrode types were plotted. Table 5.5 displays the magnitude of PLI for each volunteer and overall, both initially and following prolonged wear at rest. Signals acquired immediately after electrode application to skin resulted in a mean noise frequency of 49.98Hz ±0.08. When signals were re-acquired 6 hours later, a similar noise frequency of 49.94Hz ±0.08 was determined. Overall mean results for both the initial and prolonged recordings demonstrate that bespoke MN electrodes were the most susceptible to noise measuring 25.7µV ±48.78 and 37.8µV ±40.43, respectively. Furthermore, they were the most variable. However, the magnitude of PLI in signals acquired using this type of electrode from volunteer nine differs from the rest of the data and could be considered an outlier. Immediately after application to skin, wet electrodes and original MN electrodes acquired signals with the similar magnitudes of noise measuring 5.6µV ±5.88 and 8.8µV ±6.94, respectively. After 6 hours, signals contained 7.3µV ±14.52 of interference for wet electrodes and 9.8 ±4.69 for the original MN electrodes.

Table 5.5: 50Hz powerline interference comparison between three electrode designs in healthy adult volunteers at rest. Individual powerline interference results and overall mean calculated for each of the nine adult volunteers. For each volunteer data presented as the mean ±SD (*n=3*). For the overall mean data presented as the mean ±SD *(n=9)*. Microneedle electrode 2 (MN2) on volunteer five became dislodged prior to the reacquisition of cardiac activity.

Volunteer Number	Magnitude of powerline interference (µV)					
	Signal acquisition at 0hrs (initial)			Signal acquisition at 6hrs (prolonged)		
	WE	MN1	MN2	WE	MN1	MN2
1	0.2 ±0.04	2.0 ±0.2	0.23 ±0.09	0.6 ±0.65	0.9 ±0.58	1.3 ±0.55
2	1.7 ±0.49	4.0 ±1.22	3.1 ±1.75	0.8 ±0.37	1.1 ±0.58	1.2 ±0.42
3	6.7 ±1.71	14.1 ±3.90	20.4 ±9.84	5.4 ±0.77	5.5 ±0.87	3.6 ±0.65
4	1.0 ±1.02	9.0 ±6.23	25.4 ±14.11	6.9 ±6.20	10.1 ±6.07	40.6 ±15.29
5	0.8 ±0.50	8.0 ±0.57	4.1 ±3.89	1.4 ±0.22	2.7 ±2.41	X
6	1.8 ±1.28	4.7 ±3.15	1.9 ±0.97	0.3 ±0.05	0.2 ±0.03	9.1 ±2.57
7	15.6 ±4.52	11.6 ±2.33	9.6 ±3.07	45.5 ±11.93	60.2 ±14.03	18.5 ±7.64
8	13.9 ±1.32	4.2 ±1.07	12.9 ±1.37	0.9 ±0.17	4.8 ±0.16	0.8 ±0.41
9	7.7 ±1.75	24.4 ±3.66	153.7 ±88.26	3.8 ±1.1	2.7 ±0.68	227.2 ±117.34
Mean	5.6 ±5.88	8.8 ±6.94	25.7 ±48.78	7.3 ±14.51	9.8 ±4.69	37.8 ±40.43

5.4.3.2 Powerline interference during active conditions

Table 5.6 displays the magnitude of PLI for each volunteer and overall, both initially and following prolonged wear during movement. Signals acquired following electrode application to skin resulted in a mean noise frequency of 49.94Hz ±0.11. When signals were re-acquired 6 hours later, approximately the same noise frequency of 49.94Hz ±0.17 was determined. Bespoke MN electrodes were considered the most susceptible to powerline interference measuring 24.7µV ±50.09 initially and 36.5µV ±48.80 after 6 hours. The magnitude of interference acquired from volunteer nine using this electrode type differed considerably from the rest of the data and again could be considered an outlier. Immediately following application, wet electrodes and the original MN electrode acquired signals with magnitudes of noise measuring 8.4µV ±9.77 and 17.4µV ±31.48, respectively. Interference, however, became increasingly variable after 6 hours measuring 14.2µV ±19.53 for wet electrodes and 16.7µV ±23.21 for the original MN electrodes.

Table 5.6: 50Hz powerline interference comparison between three electrode designs in healthy adult volunteers during simple movement. Individual powerline interference results and overall mean calculated for each of the nine adult volunteers. For each volunteer data presented as the mean ±SD (*n=3*). For the overall mean data presented as the mean ±SD *(n=9).* Microneedle electrode 2 (MN2) on volunteer five became dislodged prior to the reacquisition of cardiac activity.

Volunteer Number	Magnitude of powerline interference (µV)					
	Signal acquisition at 0hrs (initial)			Signal acquisition at 6hrs (prolonged)		
	WE	MN1	MN2	WE	MN1	MN2
1	0.4 ±0.01	4.9 ±1.11	0.8 ±0.23	0.5 ±0.11	0.6 ±0.11	1.0 ±0.29
2	13.9 ±14.62	100.4 ±42.87	14.0 ±12.21	5.2 ±1.63	6.5 ±3.67	18.8 ±5.86
3	29.0 ±21.35	14.0 ±5.52	27.6 ±5.43	19.3 ±1.62	21.7 ±1.93	18.3 ±2.47
4	2.1 ±0.89	7.9 ±1.54	2.8 ±1.93	9.4 ±0.31	8.7 ±5.12	56.1 ±4.57
5	1.6 ±0.54	1.2 ±0.86	1.5 ±0.52	1.0 ±0.44	3.3 ±4.40	X
6	0.6 ±0.09	0.5 ±0.39	1.0 ±0.19	0.5 ±0.16	0.2 ±0.05	12.7 ±0.58
7	17.3 ±3.95	10.4 ±10.87	13.9 ±10.40	34.2 ±13.02	29.2 ±9.74	28.4 ±11.31
8	4.4 ±0.92	4.7 ±0.75	4.3 ±0.59	1.2 ±0.96	8.2 ±10.38	0.8 ±0.41
9	6.4 ±2.09	13.0 ±6.80	156.1 ±26.74	56.7 ±26.62	73.3 ±23.97	149.8 ±57.66
Mean	8.4 ±9.77	17.4 ±31.48	26.4 ±50.09	14.2 ±19.53	16.7 ±23.21	36.5 ±48.80

5.4.4 Qualitative comparison of ECG traces

5.4.4.1 Visual comparison of performance under resting conditions

A visual comparison of ECG traces was undertaken to support the quantitative data. Figure 5.5 displays 5-second segments of cardiac activity recorded using the three types of electrodes whilst volunteer two was at rest in the supine position. A selection of ECG traces was chosen based upon the SNR results to demonstrate differences in signal quality between the electrodes, volunteers, and time of recording. All the ECG traces captured during the present study are shown in Appendix XVI. The data shown in Figure 5.5 was filtered offline in MATLAB using a 0.5Hz high-pass filter to remove BW and DC offset. A digital notch filter was not applied to show waveforms with minimal DSP. Figure 5.5 was included to reflect an example where initial recordings (Figure 5.5a-c) were superior to prolonged recordings (Figure 5.5d-f). Bespoke MN electrodes achieved an initial SNR of 28.4dB ±1.91, followed by an SNR of 28.4dB ±1.22 for wet electrodes and 26.0dB ±1.89 for original MN electrodes. Whilst, numerically, the original MN electrode recorded signals of slightly lower quality, Figure 5.5a-c highlights that the traces follow each other closely with few extraneous deviations from the baseline. After 6 hours of wear, signal quality from all three electrode types decreased. Bespoke MN, original MN, and wet electrodes achieved SNRs of 27.4dB ±5.31, 24.4dB ±3.68 and 25.0dB ±3.87, respectively. This decline in signal fidelity is observed on the subsequent ECG traces (Figure 5.5d-f) particularly for the original MN electrode where spurious waves were present in the baseline. In both recordings however, all relevant waves (PQRST) were visible. Whilst it is difficult to observe the individual R-peaks recorded by each electrode, bespoke MN electrodes recorded R-peaks of greater amplitude.
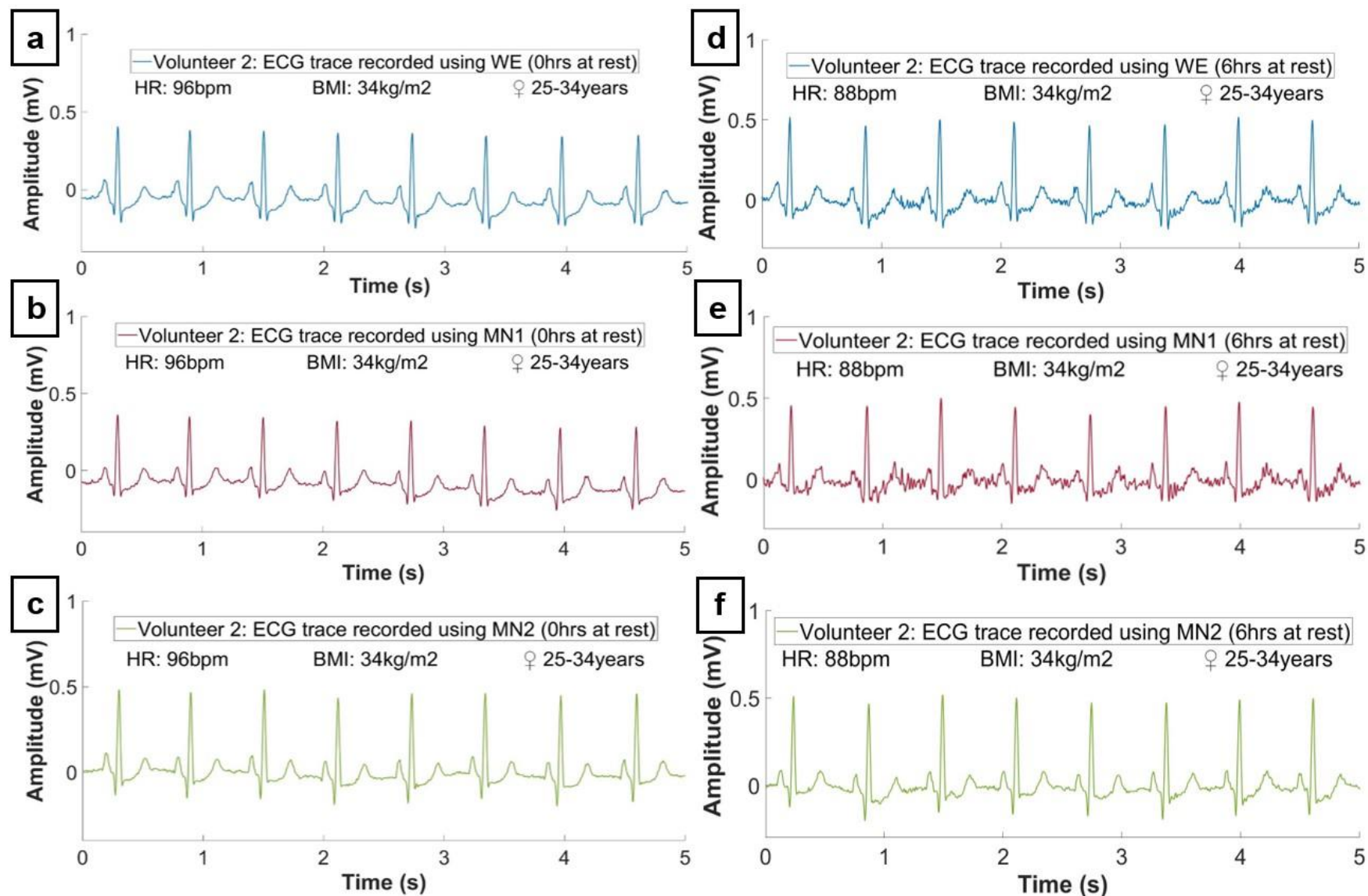
Figure 5.5: Segments of cardiac activity obtained using three types of electrodes at rest from volunteer two. Data filtered with a high-pass filter to adjust the baseline. Wet electrode (WE) traces are shown in blue, original microneedle electrode (MN1) in red and bespoke microneedle electrode (MN2) in green at 0 hours (**a-c**) and 6 hours (**d-f**) Data acquired with x12 gain and 250Hz sampling frequency.

Similarly, to Figure 5.5, traces shown in Figure 5.6 were filtered using a high-pass filter to remove artifacts. Whilst Figure 5.6 also demonstrates a case where the initial recordings were of higher fidelity in comparison to those taken at 6 hours, Figure 5.6 was included as signals recorded from this volunteer were of the lowest signal quality overall. Initially following application, wet, original MN and bespoke MN electrode achieved SNRs of 9.8dB ±7.52, 11.3dB ±9.41 and 12.7dB ±6.92, respectively. Whilst spurious waves can be observed in the baseline, indicating the presence of PLI, key ECG waves are identifiable. When cardiac activity was re-recorded after 6 hours of wear, SNR values for wet and original MN electrodes further declined to 9.2dB ±1.83 and 4.1dB ±1.63, respectively. Signals recorded by the bespoke design however, improved to 16.6dB ±2.20. These changes in signal fidelity can be observed in the subsequent ECG trace as increased PLI is present due to the increased spikes in the baseline. Plotting the FFT of these traces revealed that PLI for wet and original MN electrodes measured 45.5μV ±11.94 and 60.2μV ±14.03, respectively. Bespoke MN electrodes however resulted in 18.5μV ±7.64 of 'noise'. Discernible ECG characteristics (PQRS) remained for traces recorded with the bespoke design, however PQRS waves were slightly obscured for the wet and original MN electrodes.
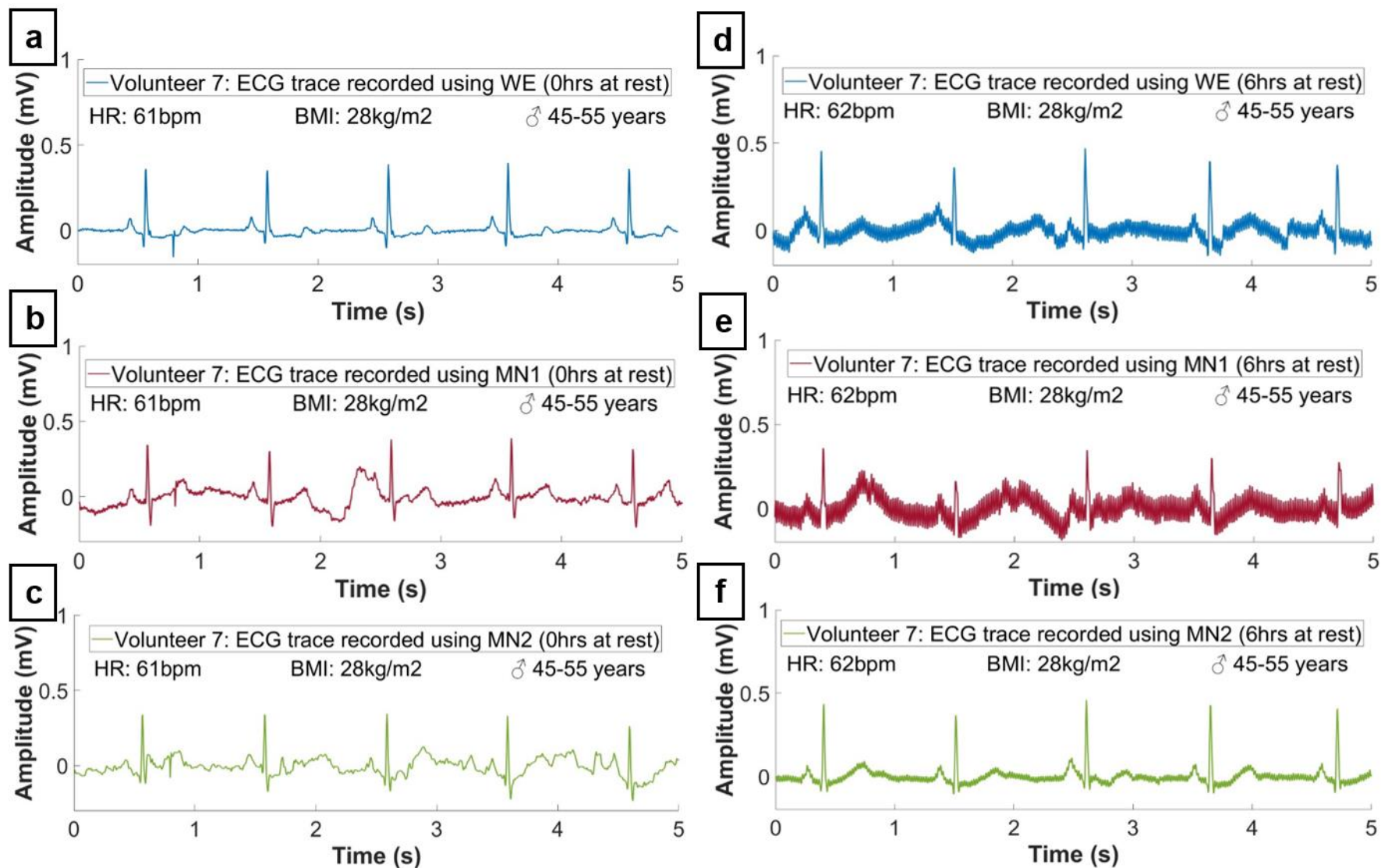
Figure 5.6: Segment of cardiac activity obtained using three types of electrodes at rest from volunteer seven. Data filtered with a high-pass filter to adjust the baseline. Wet electrode (WE) traces are shown in blue, original microneedle electrode (MN1) in red and bespoke microneedle electrode (MN2) in green at 0 hours (**a-c**) and 6 hours (**d-f**) Data acquired with x12 gain and 250Hz sampling frequency.

5.4.4.2 Visual comparison of performance during active conditions

Volunteers were asked to perform the simple movement of sitting to standing three times, over 1 minute. Overall, electrode performance was more variable during active conditions than at rest. No consistent trend was identified within the data sets as signal quality declined in some participants following 6 hours for instance, volunteers three, four and eight. Conversely, performance between electrodes within the same volunteer also varied. For example, in volunteers seven and nine the performance of both the wet and original MN electrodes declined after 6 hours whilst bespoke electrode performance improved. The alternative was observed for volunteers one, two, five and six. It was observed that upon moving from a sedentary to standing position a clear change in the ECG trace was identified in all volunteers, as highlighted in Figure 5.7. As shown in Figure 5.7a-c electrodes follow a similar pattern during the movement however, the original MN electrode resulted in the largest deviation. When visually assessing the traces, P and T waves were challenging to identify, however R peaks can be easily identified. When cardiac activity was re-acquired after 6 hours (Figure 5.7d-f), periods of volunteer movement can be identified from the trace, however the deviations were less pronounced.
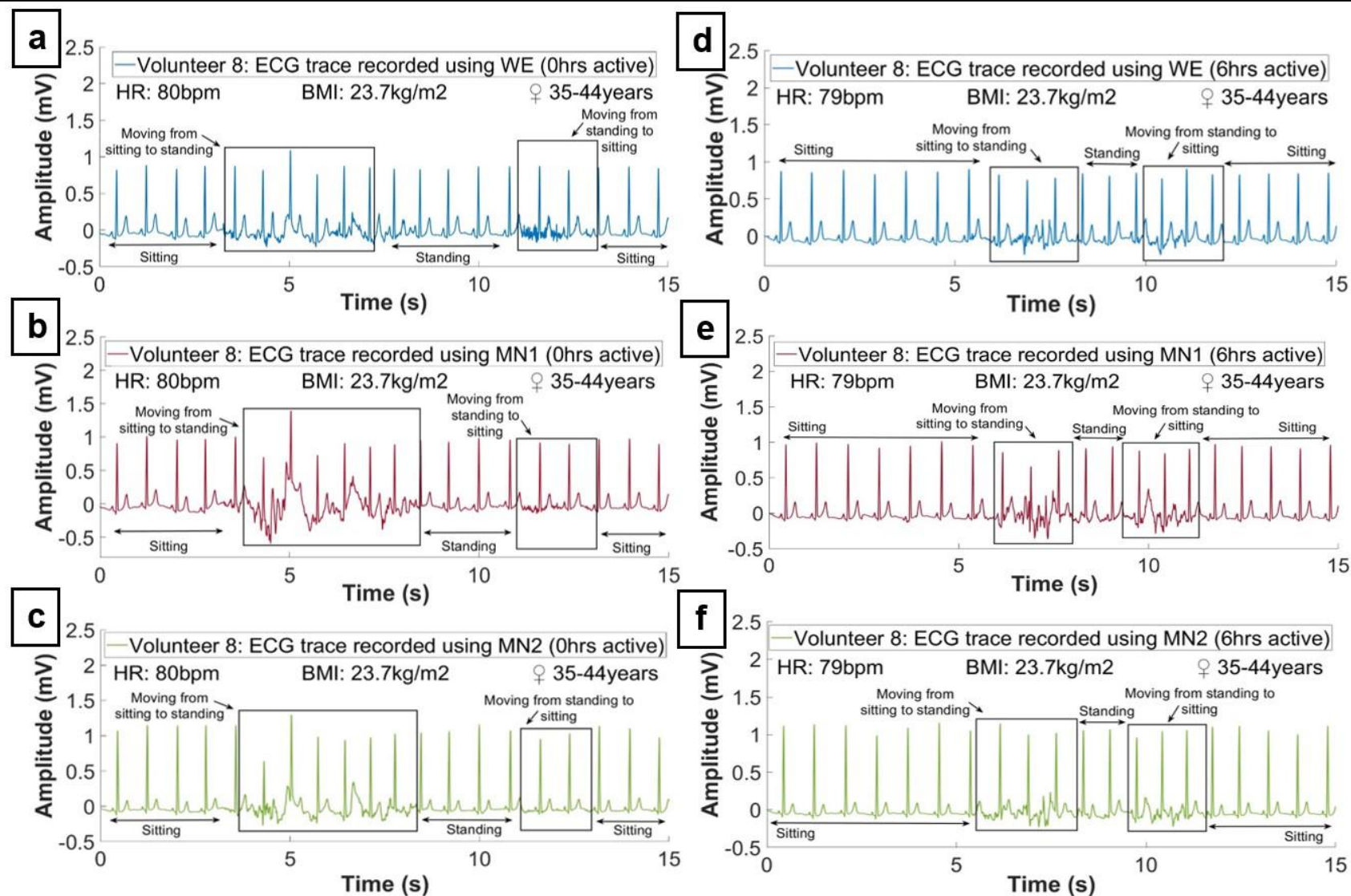
Figure 5.7: Segment of cardiac activity obtained using three types of electrodes during movement from volunteer eight. Data filtered with a high-pass filter to adjust the baseline. Wet electrode (WE) traces are shown in blue, original microneedle electrode (MN1) in red and bespoke microneedle electrode (MN2) in green at 0 hours (**a-c**) and 6 hours (**d-f**) Data acquired with x24 gain and 250Hz sampling frequency. Areas of movement highlighted by the black box.

Figure 5.8 is a further example ECG trace acquired from volunteer one. Volunteer movement was again evident from the traces due to fluctuations in the baseline as highlighted in Figure 5.8. Overall, traces recorded by wet electrodes were the most stable during periods of movement both initially and after 6 hours. As highlighted in Figure 5.8a, wet electrodes produced less visible deviations in the baseline during movement when compared with both MN electrodes. When comparing MN electrodes, the original design initially recorded signals with the lowest SNR which was apparent from the trace shown in Figure 5.8b. Upon movement it was evident that this MN electrode was more susceptible to movement as the subsequent trace deviates from the baseline more than the wet and bespoke designs during activity. After prolonged wear, signal quality for the original MN electrodes increased which was evidenced by Figure 5.8e which displays smaller baseline fluctuations during periods of movement. For the bespoke design however, the reverse was observed. SNR decreased following 6 hours of wear and increased baseline fluctuations were observed in the corresponding traces during activity (Figure 5.8f). This is likely due to the push button dislodging during wear. During movement, P and T waves were obscured in some traces, however the R peak remained visible for all recordings.
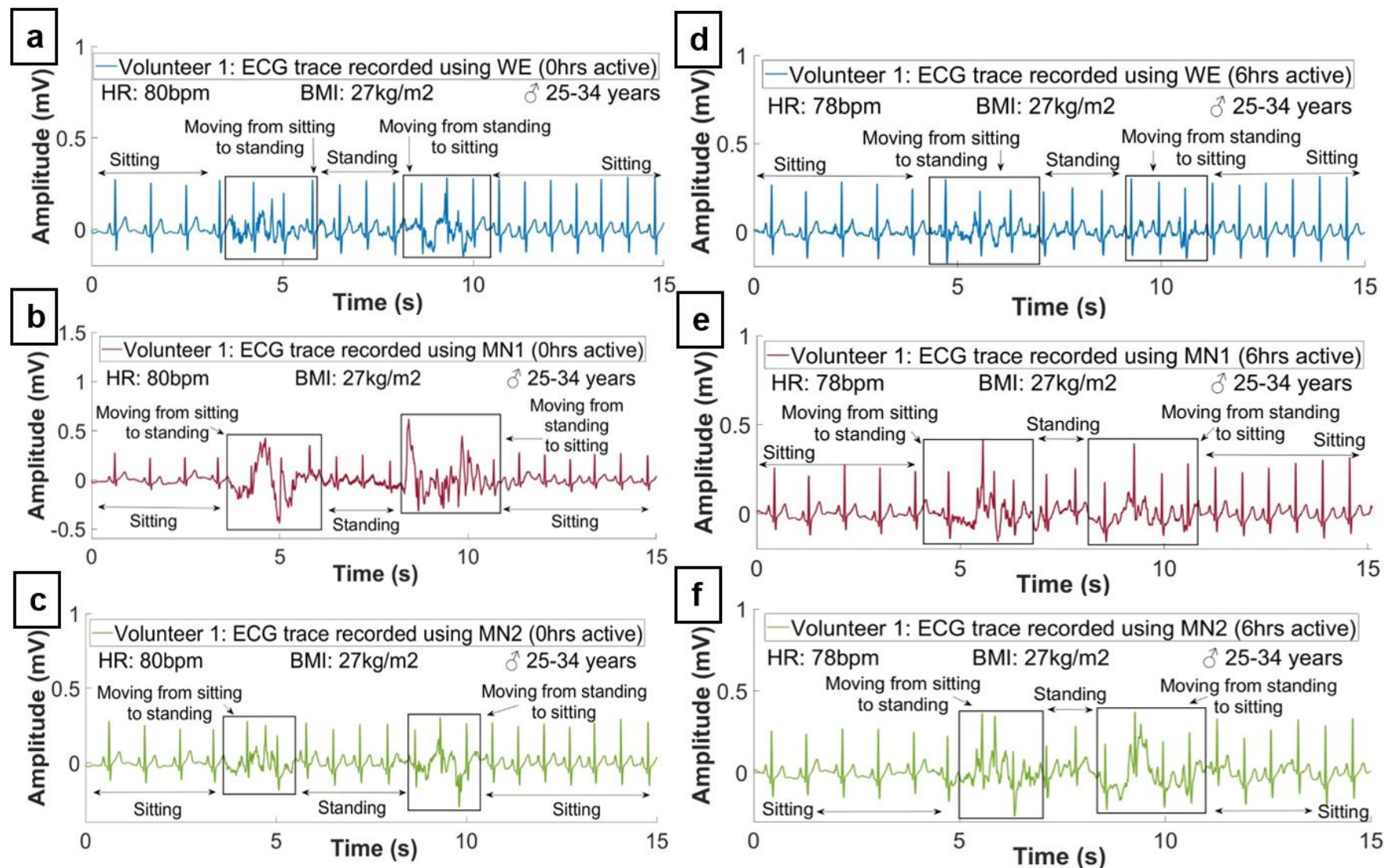
Figure 5.8: Segment of cardiac activity obtained using three types of electrodes during movement from volunteer one. Data filtered with a high-pass filter to adjust the baseline. Wet electrode (WE) traces are shown in blue, original microneedle electrode (MN1) in red and bespoke microneedle electrode (MN2) in green at 0 hours (**a-c**) and 6 hours (**d-f**) Data acquired with x24 gain and 250Hz sampling frequency. Areas of movement highlighted by the black box.

5.4.5 Effect of electrodes on human skin

To assess the effects of the three electrode designs on human skin, images were captured at specific stages of the study. Figure 5.9 displays a selection of images captured from volunteer two, three and six prior to the application of each electrode to the abdomen. These images functioned as a reference for all subsequent images. As shown by Figure 5.9, the skin selected for electrode application was visibly intact with no erythema.
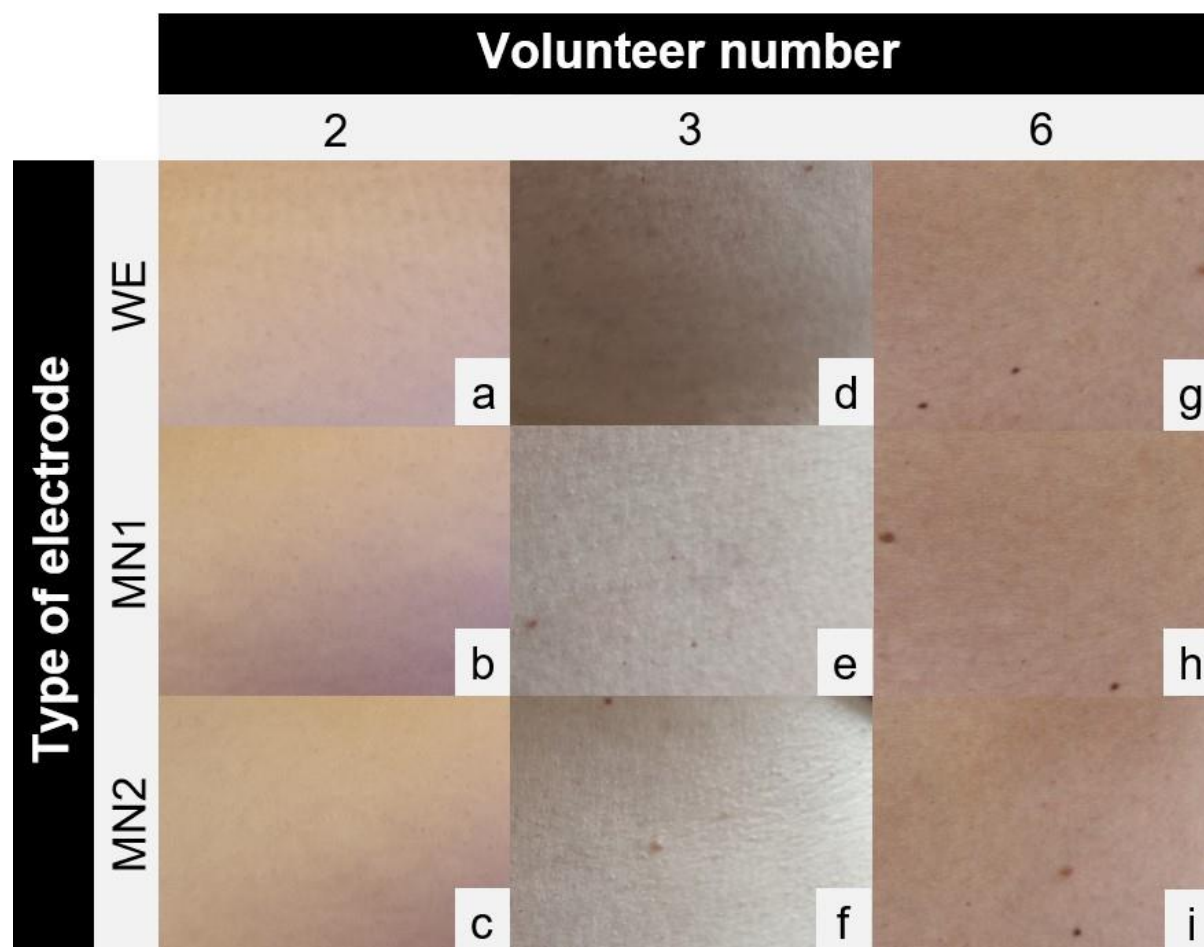
Figure 5.9: Selection of reference images of human skin prior to electrode application (0 hours). Images were captured prior to the application of wet electrodes (WE), original microneedle electrodes (MN1) and bespoke microneedle electrodes with push button applicator (MN2). Images shown in the Figure were from volunteer two aged (**a-c**), three (**d-f**) and six (**g-i**). Skin sites were located on the lower abdomen, left of the umbilicus.

After prolonged wear, electrodes located on the abdomen and beneath the left collarbone were removed. The skin beneath these electrodes was subsequently imaged. Figure 5.10 displays a selection of images captured from volunteer two, three and six after 6 hours of wear. As shown by Figure 5.10, each type of electrode affected the skin in a specific way. Wet electrodes contained conductive gels which is reported to induced skin irritation. Visible

erythema was not observed following the removal of wet electrodes in seven of the volunteers after 6 hours. In the remaining volunteers' minor erythema was observed, particularly on the lower abdomen. Unlike the smooth skin shown in Figure 5.9, creases in the skin were observed in the area in direct contact with the adhesive. Changes in the hydration of the skin was observed in the areas contacting the gel-soaked foam pad and sensing element. As highlighted in Figure 5.10, the surface of the skin appeared uneven and slightly raised compared to the surrounding skin.
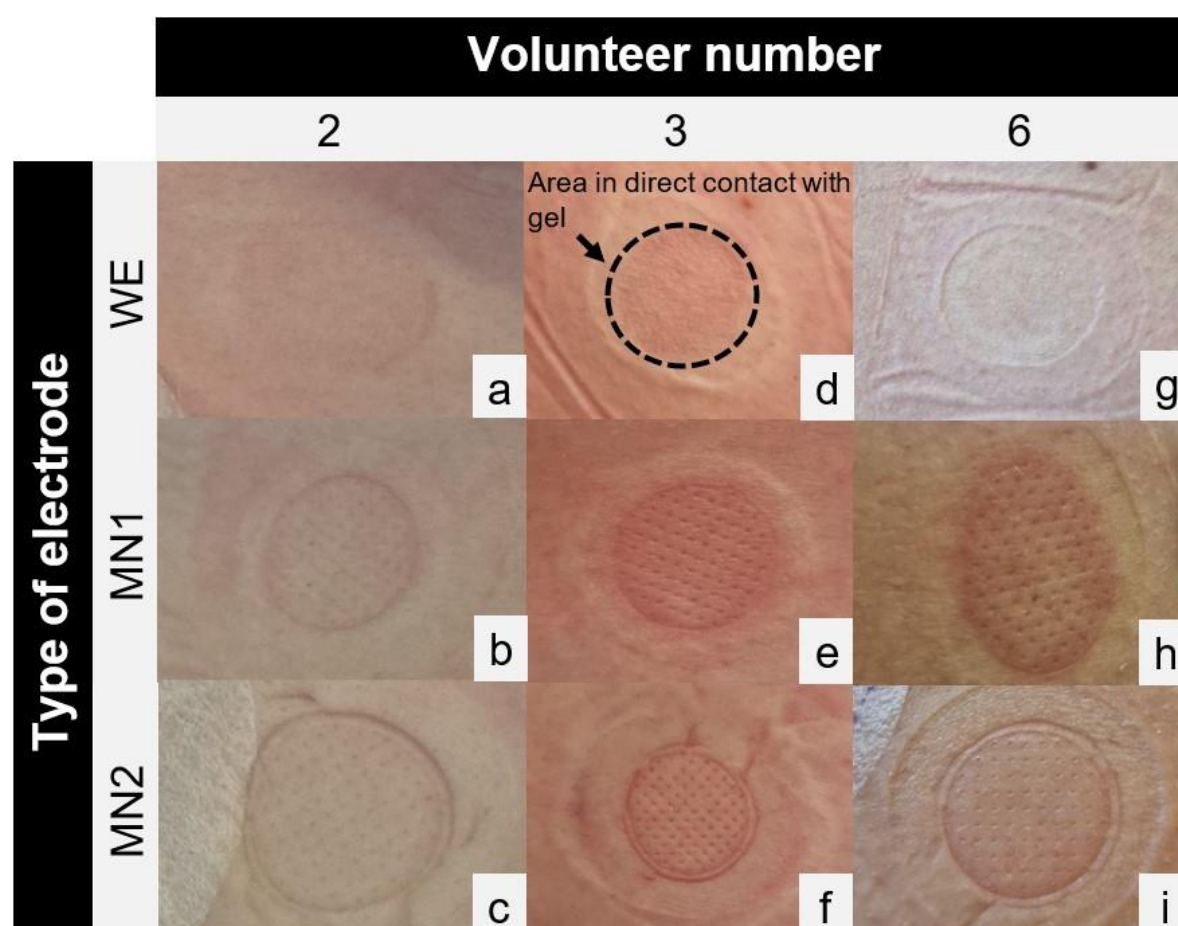
Figure 5.10: Selection of images of human skin following electrode removal from the lower abdomen after 6 hours of wear. Images were captured immediately following the removal of wet electrodes (WE), original microneedle electrodes (MN1) and bespoke microneedle electrodes with push button applicator (MN2). Images shown in the Figure were from volunteer two (**a-c**), three (**d-f**) and six (**g-i**). Skin sites were located on the lower abdomen, left of the umbilicus.

The removal of both the original MN electrode and bespoke MN design revealed a well-defined skin erythema in the shape of a circular array which was present in all volunteers. Visible indentations were present indicating where each individual needle was in contact with the skin. In some instances, the bespoke design produced more discernible indentations and less

erythema than the original MN electrode. Unlike the wet electrode, both MN designs did not appear to induce changes in skin hydration.

Volunteers wore one of each electrode beneath the right clavicle for the remaining 24 hours. Following this time, the electrodes were removed and the skin imaged. Follow-up images of electrode sites from the previous day (left clavicle and lower abdomen) were captured to document if any electrode induced skin changes had resolved. Figure 5.11 shows a selection of follow-up images captured from the abdomen of volunteer two, three and six after completion of the remaining 24 hours.
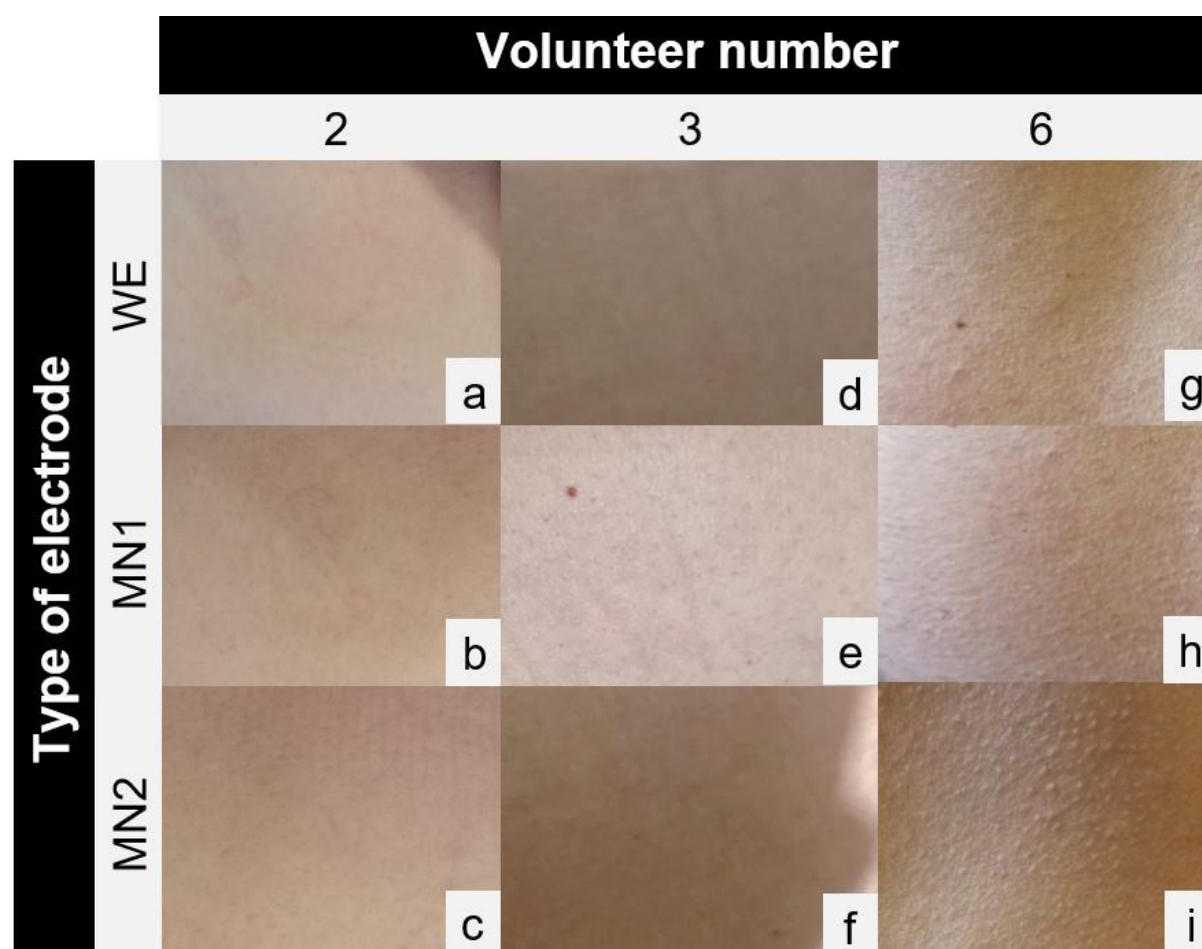
Figure 5.11: Selection of follow-up images of human abdominal skin taken 24 hours after removal of each type of electrode. Images were captured the next day when the volunteer returned after wearing one of each electrode design for the remaining 24 hours. Photos shown in the Figure were from volunteer two (**a-c**), three (**d-f**) and six (**g-i**). Skin sites were located on the lower abdomen, left of the umbilicus.

Skin erythema and additional effects resulting from the wet, original, and bespoke MN electrodes had resolved within 24 hours in all volunteers (Figure 5.11). No bleeding was observed for any of the MN electrode application sites in eight volunteers. However, a spot of blood was identified in one volunteer following the removal of the initial MN electrode prototype located beneath the right collarbone. Markings induced by this MN electrode were present for a further two days after removal.

The circular markings resulting from the adhesive pad were also transient and had resolved in all volunteers. Figure 5.12 displays images captured from the electrodes located beneath the right collarbone of volunteer two, three and six after completion of the remaining 24 hours. Overall, circular markings resulting from the adhesive pad were increasingly noticeable following 24 hours of wear. Similarly, to Figure 5.10, skin erythema and visible indentations were present indicating the location of individual needles for both the original and bespoke MN electrodes.
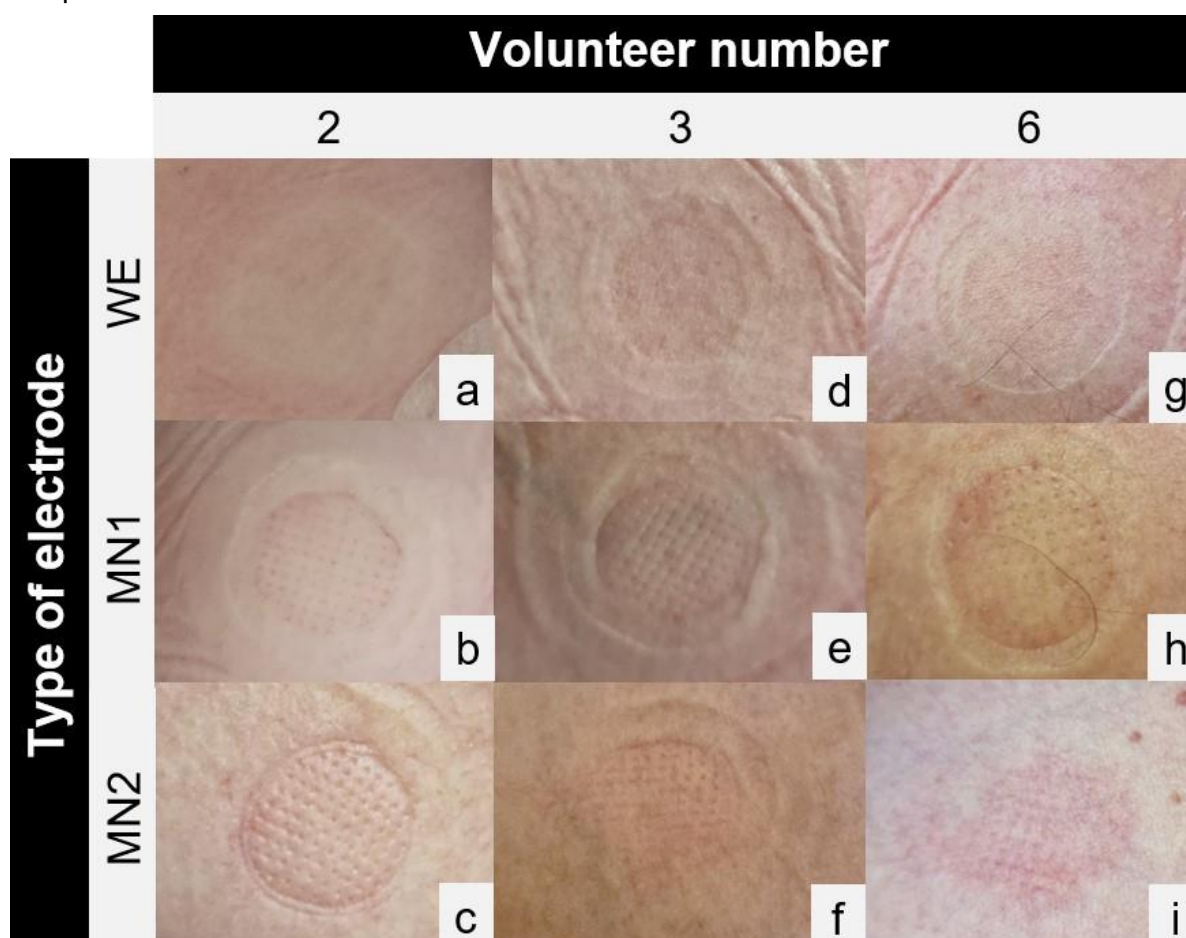
Figure 5.12: Selection of images of human skin following the removal of electrodes beneath the right clavicle after 24 hours of wear. Images were captured immediately following the removal of wet electrodes, original microneedle electrodes and bespoke microneedle electrodes with push button applicator. Images shown were from volunteer two (**a-c**), three (**d-f**) and six (**g-i**). Skin sites were below the right collarbone.

5.4.6 Microneedle penetration analysis

In addition to en face imaging, OCT was conducted immediately following the removal of each electrode for all volunteers. Figure 5.13 shows a selection of cross-sectional images of volunteer nine's skin following the removal of a wet electrode (Figure 5.13a), original MN electrode (Figure 5.13b) and bespoke MN electrode (Figure 5.13c).
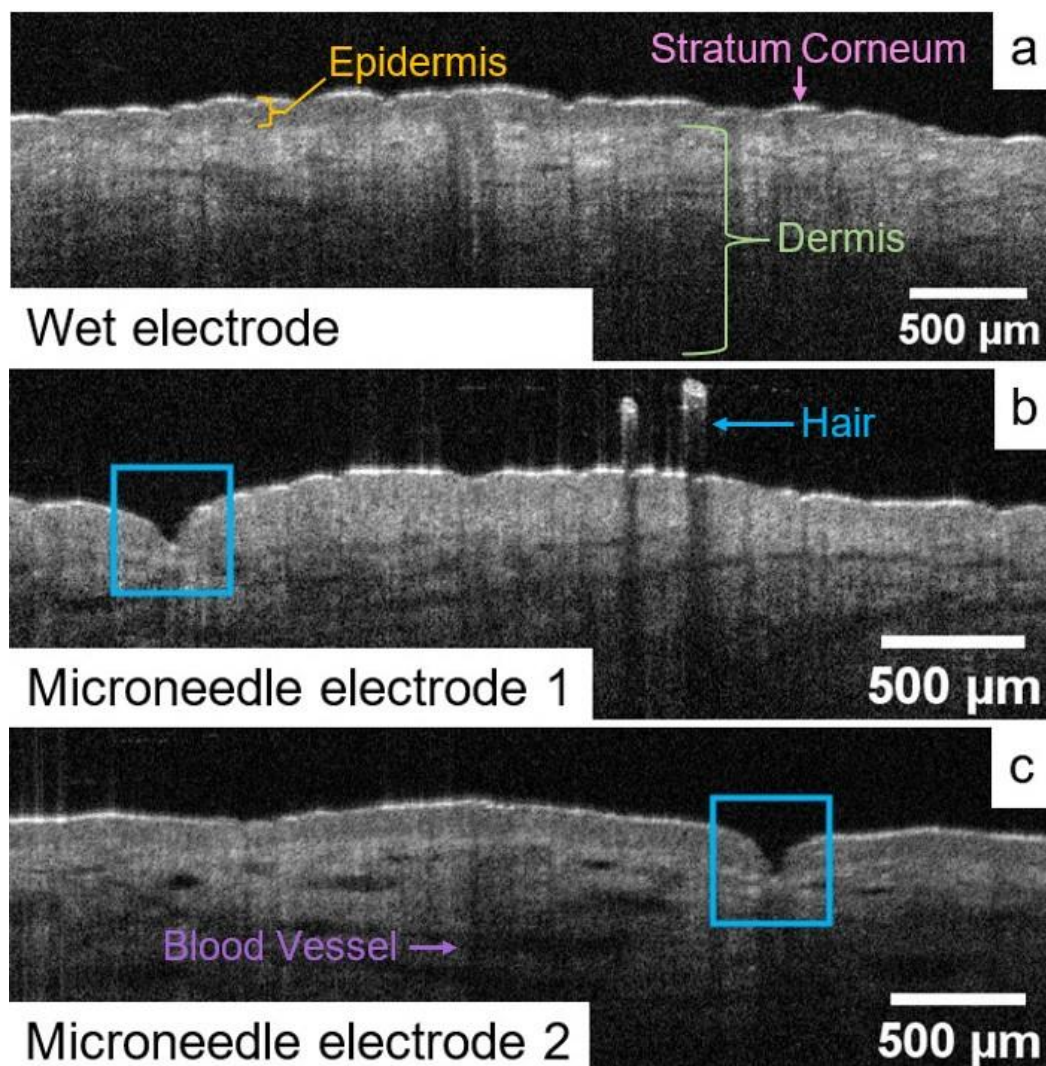
Figure 5.13: Sub-surface OCT images comparing the effects of three types of electrodes on human skin. Scans containing 500 frames were acquired following the removal of wet electrodes (WE) (**a**), original microneedle electrode (MN1) (**b**) and bespoke microneedle electrode (MN2) with push-button applicator (**c**). Skin sites shown in the Figure were from the abdomen, just left of the umbilicus. Scan area of 6x2mm (width x length). Images were analysed using Fiji. Blue box highlights a microchannel.

Similarly, to the ex vivo OCT scans shown in Chapter 2, the regular morphology of human skin was observed. As highlighted in Figure 5.13, the SC was represented by a distinct, grey line. A slightly darker section below corresponded to the VE. The dermis was not as well defined

by the scans, however additional features including hair and blood vessels were observed when scanning the skin of all volunteers.

Wet electrodes are non-invasive and therefore do not breach the SC. This was corroborated using OCT as no disruption within the epidermis was observed for all volunteer skin sites after both 6 hours and 24 hours of wear. Imaging of the lower abdominal skin beneath the original MN electrode at 6 hours resulted in the observation of both indentations and microchannels. As shown by Figure 5.13b a clear microchannel was observed. However, in at least three volunteers' identification of microchannels proved inconclusive. Following the removal of the remaining MN electrode located beneath the right collarbone after 24 hours, microchannels were observed in seven of the volunteers. Similarly, to the previously discussed MN electrode, the bespoke design also resulted in the observation of both indentations and microchannels on the lower abdominal sites at 6 hours (Figure 5.13c). Again, identification of microchannels was inconclusive in some volunteers. Following the removal of the remaining MN electrode located beneath the right collarbone after 24 hours, microchannels were observed in five of the volunteers.

5.4.7 User feedback regarding device wearability

5.4.7.1 Electrode-induced sensations

To capture information regarding electrode-induced 'sensations,' volunteers were asked two questions. Following the conclusion of the initial acquisition of cardiac signals volunteers were asked 'Did you experience any 'sensations' when the devices were initially applied to your skin?' As shown in Appendix XV, these questions were asked for each specific device to ensure information was captured for all electrodes. Device one referred to wet electrodes. Device two corresponded to the original MN electrodes, whilst Device three related to the bespoke MN electrodes. Figure 5.14 reveals the percentage response from volunteers when posed these questions. In total, five volunteers reported experiencing sensations following the initial application of bespoke MN electrodes. Sensations were reported in two volunteers when the original MN electrodes were initially applied to their skin. Wet electrodes caused the least sensations with only one volunteer reporting 'slight tingling.' When asked to further explain the types of sensation experienced when wearing MN electrode's common statements included 'stinging,' 'itching,' 'tingling' and 'prickly.' Following the application of the bespoke design it was reported to cause a feeling of pressure on the skin.
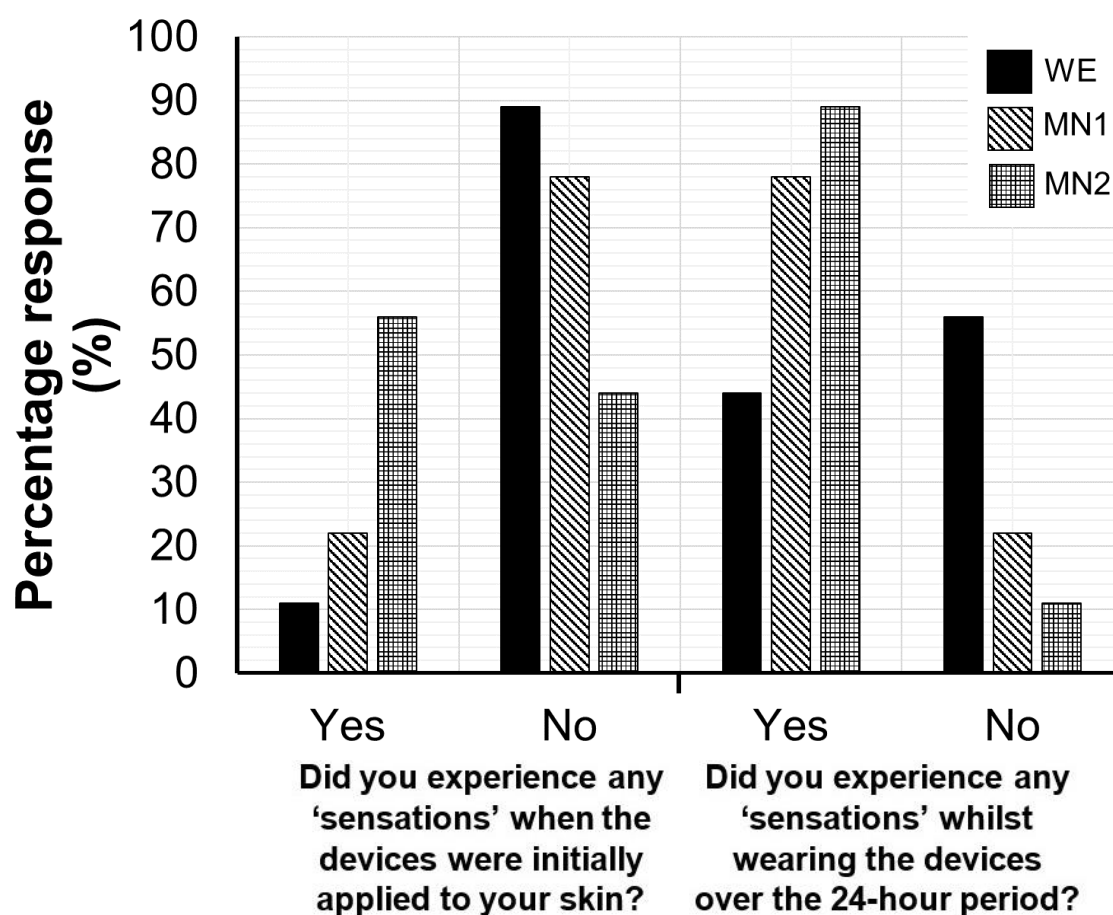
Figure 5.14: Percentage response of volunteers when asked if the experienced electrode-induced sensations immediately following application and after 24 hours of prolonged wear.

The following day, volunteers were then asked, 'Did you experience any 'sensations' whilst wearing the devices over the 24-hour period?'. Sensations reported by volunteers increased for all electrode types. When describing the sensations experienced for wet electrodes, terms including 'noticeable,' 'sticky,' and 'tugging' were used. One such volunteer reported experiencing discomfort due to the electrode pulling on hair. Similarly, to the terms used after the initial application of MN electrodes, phrases including 'stinging,' 'itching,' 'prickly' and 'scratchy' were reported. Volunteers noted that the devices became more noticeable and uncomfortable the longer the devices were worn with the bespoke MN electrodes reported to cause more discomfort particularly when moving or pressing down on the electrode site. Whilst this information was not captured on the questionnaire, volunteers verbally reported that they experienced the most discomfort from electrodes placed underneath the right clavicle rather than those situated on the lower abdomen.

5.4.7.2 Ease of application

In addition to electrode-induced sensations, the questionnaire also investigated ease of device application. Volunteers were faced with a statement and asked to provide their level of agreement which ranged from strongly disagree to strongly agree (Figure 5.15). 'Prefer not to say' was included, although no volunteer selected this option. Similarly, to sensations, the statement was adapted to capture feedback for each specific device. When asked 'Device one was easy to apply,' four volunteers agreed with the statement and another four strongly agreed with the statement. In total, one volunteer strongly disagreed. The same results were observed for the original MN electrodes. However, when asked if 'Device three was easy to apply,' one volunteer strongly disagreed with the statement, another volunteer neither agree nor disagreed, two volunteers agreed and five strongly agreed with the statement. No further information was provided by the volunteers to explain their reasoning.
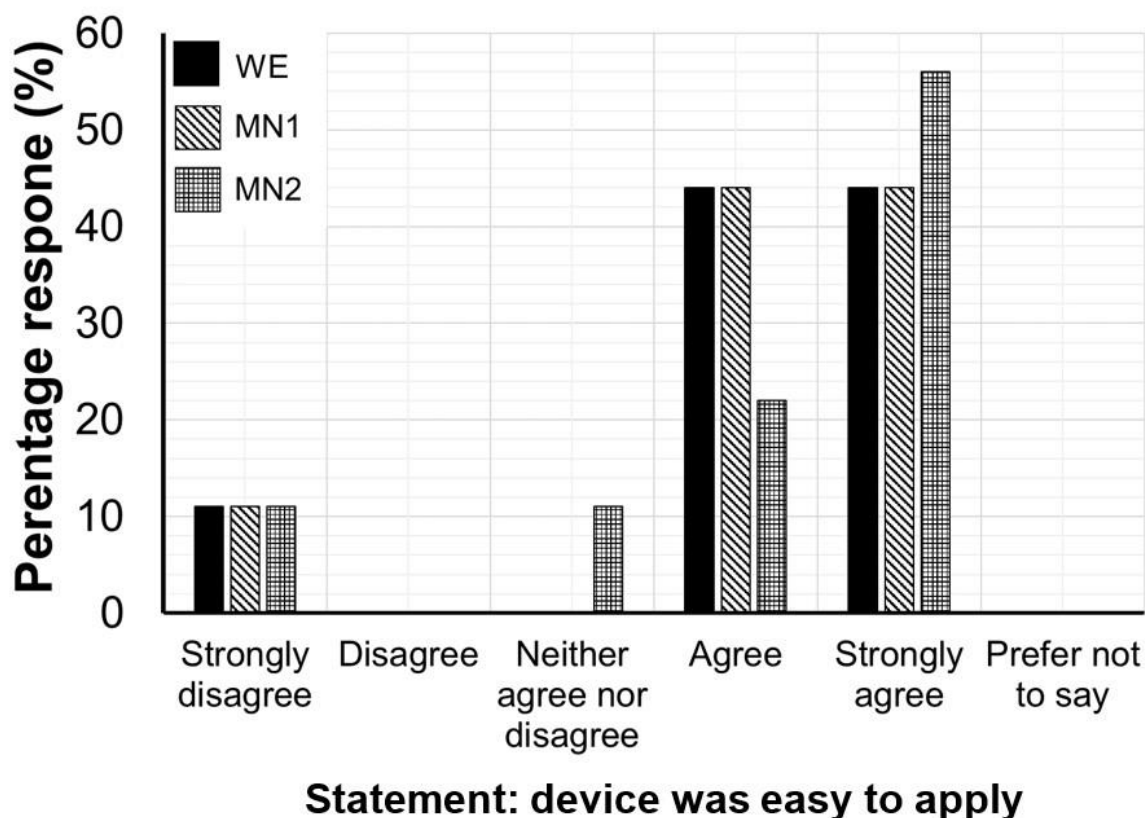
Figure 5.15: Percentage response of volunteers when asked about ease of device application. Volunteers were asked to state their level of agreement with the statements: device one (wet electrode) was easy to apply, device two (original microneedle electrode) was easy to apply and device three (bespoke microneedle electrode) was easy to apply.

5.4.7.3 Removal of electrode devices

When asked the following the day 'Did you remove any of the devices over the 24-hour period?', five volunteers stated they had removed at least one device, whilst four wore all three electrodes for the remaining 24 hours (Figure 5.16). Out of the five volunteers who stated that a device was removed during the 24-hour four reported that only device three, the bespoke MN electrode, had been removed. The remaining volunteer reported removing device two, the original MN electrode, first around 7.30pm in the evening, followed by the removal of device three at approximately 11pm at night. In total, three of the volunteers did not actively remove device three, the device 'fell off' or 'came unstuck' highlighting potential issues with the adhesive used in these electrodes. The remaining two volunteers decided to remove specific devices. Volunteer one initially removed device two citing that it was 'uncomfortable and couldn't relax with it on.' Later, in the night this volunteer also removed device three because it was 'uncomfortable when sleeping.' Volunteer two removed device three only, stating that it was 'uncomfortable and impacted sleep due to position.' This volunteer also stated that the device became increasingly 'prickly, like a stingy nettle.'
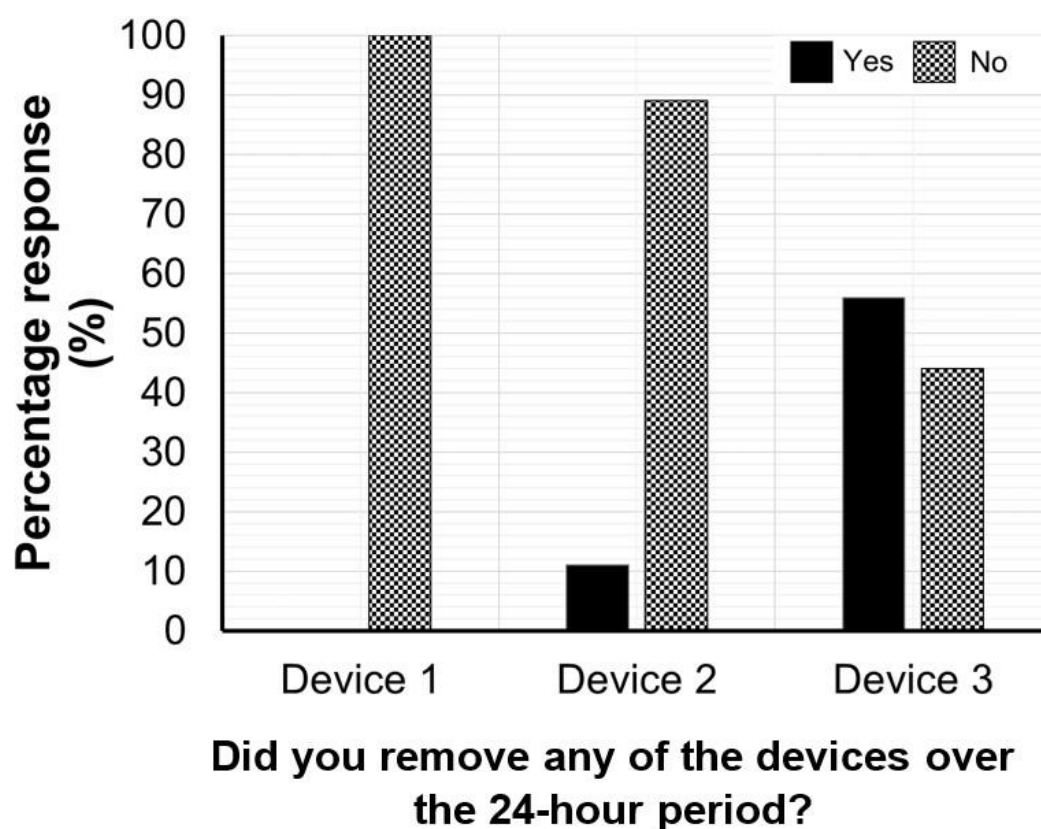
Figure 5.16: Percentage response of volunteers when asked about device removal. After 24 hours volunteers were asked if they removed any devices and if so which device(s) were removed.

5.4.7.4 Device visibility and discretion

Following 24 hours of prolonged wear, volunteers were asked to provide their level of agreement with the statement 'I felt self-conscious whilst wearing the device'. Similarly, to previous sections, the question was tailored to capture information for the specific electrodes. Figure 5.17 displays the percentage volunteer response to this statement for devices one, two and three. Regarding device one, five volunteers disagreed with the statement, whilst three strongly disagreed. The remaining volunteer indicated that they felt self-conscious whilst wearing the wet electrode. A similar response was observed with respect to device two. Many volunteers indicated that they disagreed with the statement highlighting that they did not feel self-conscious whilst wearing the original MN electrode. Again, one volunteer agreed with the statement and indicated that they were increasingly aware of this device. Out of the electrodes, the bespoke design was considered the most visible with four volunteers indicating that they felt self-conscious wearing this device. Conversely, two volunteers disagreed and another two strongly disagreed with the statement. The remaining volunteer neither agreed nor disagreed suggesting no preference.
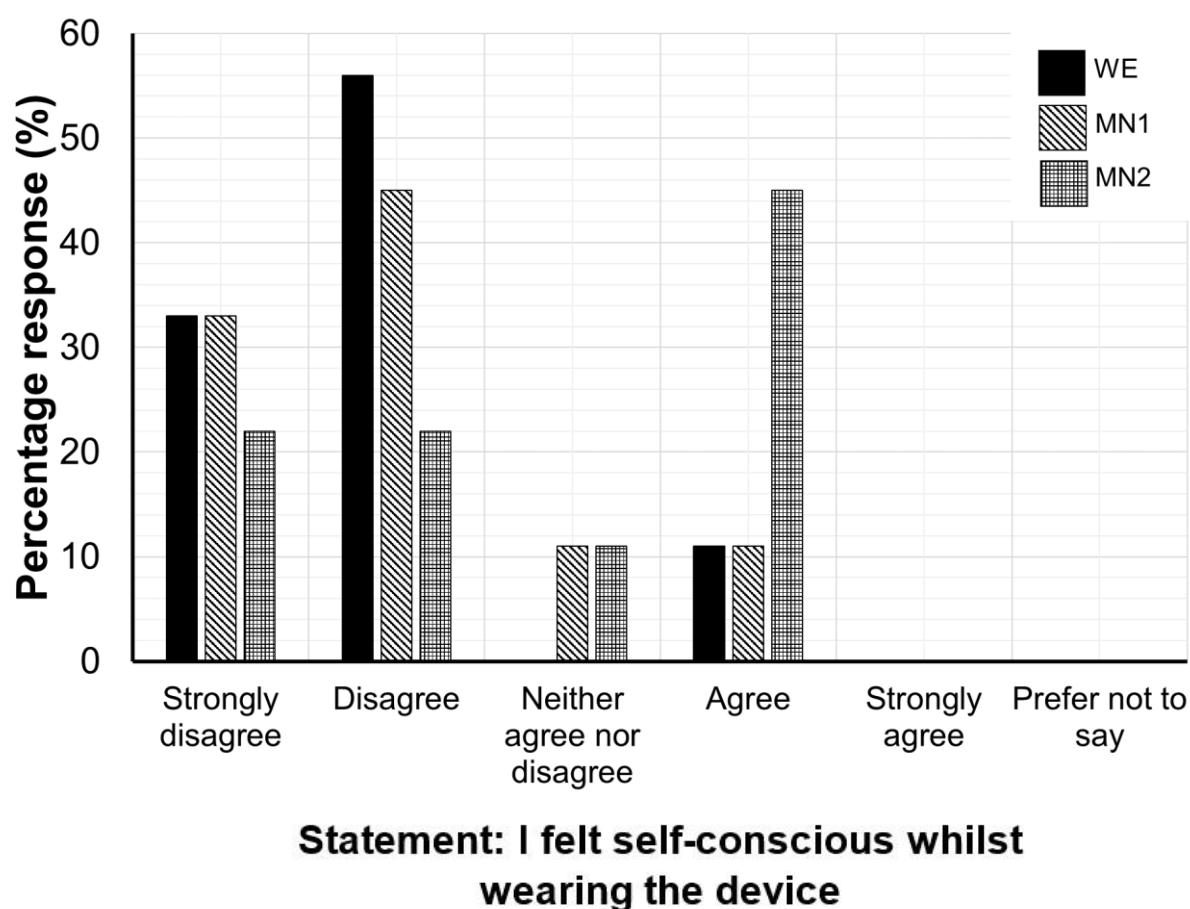
Figure 5.17: Percentage response of volunteers when asked if they felt conscious whilst wearing the devices over the 24-hour period.

5.4.7.5 Volunteer perception of device comfort

For prolonged wear, devices must be comfortable to wear. For each device volunteers were asked to provide their level of agreement with the statement 'Device was comfortable to wear.' As shown by Figure 5.18, device one (wet electrode) was found to be the electrode considered the most comfortable with three individuals strongly agreeing and four agreeing with the statement 'Device one was comfortable to wear.' The remaining two volunteers neither agreed nor disagreed indicating no clear preference. When asked if device two (original MN electrode) was comfortable, volunteer responses were mixed. The bespoke design was reported to be the most uncomfortable with six volunteers disagreeing with the statement 'Device three was comfortable to wear.' Only one volunteer agreed with the statement whilst the remaining volunteers neither agreed nor disagreed.
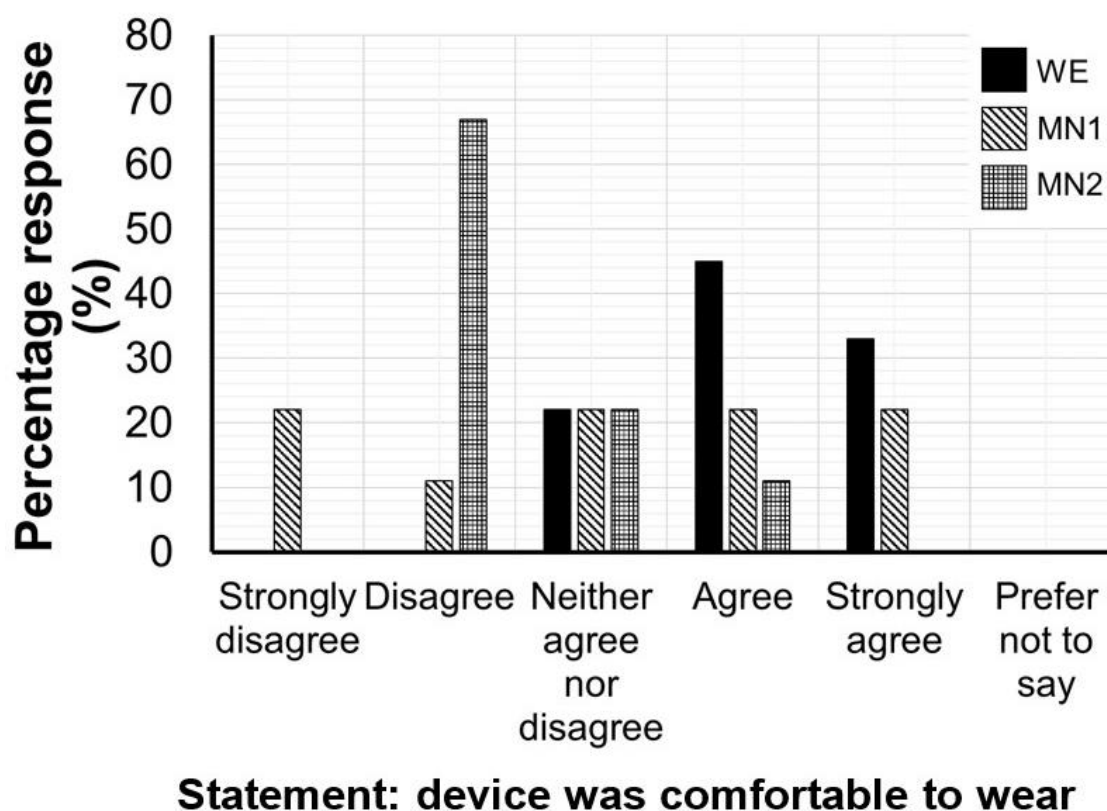
Figure 5.18: Percentage response of volunteers when asked if devices were comfortable to wear over 24 hours. Device one (wet electrode), device two (original microneedle electrode) and device three (bespoke microneedle electrode).

5.4.7.6 Device duration

To assess how long each of the volunteers would be willing to wear the devices, they were asked 'Would you be prepared to wear the devices for 1 day, 7 days and 28 days?'. This question was posed for all three devices (Figure 5.19). All participants stated that they would

be prepared to wear device's one and two for 24-hours. Only seven however, would be prepared to wear device three for 24-hours. When the duration of wear increased to 7 days the overall number of volunteers stating that they would be prepared to wear the devices reduced. In total, seven volunteers would be prepared to wear device one however, one volunteer stated no, and a further volunteer stated that they did not know. For the initial MN electrode prototype, six volunteers would be prepared to wear this device for 7 days, whilst only three would wear device three. When asked if they would be prepared to wear the devices for a duration of 28 days, four volunteers stated that would wear device one and two for this duration. Most volunteers (n=8) however, stated that they would not be prepared to wear device three for a month.
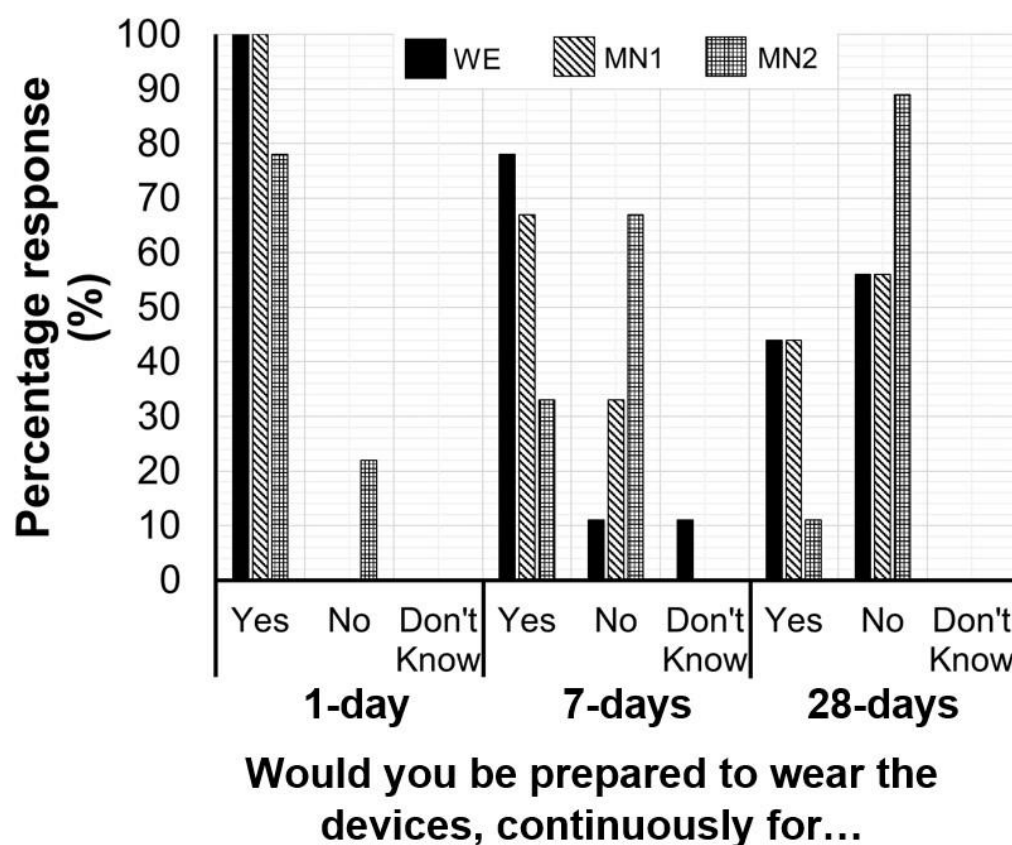
Figure 5.19: Percentage response of volunteers when asked how long they would be prepared to wear each device. Device one (wet electrode), device two (original microneedle electrode) and device three (bespoke microneedle electrode).

When asked to explain their selection, volunteers cited several reasons, a selection of which are shown in Figure 5.20. The bespoke electrodes elicited the greatest number of comments particularly surrounding the size and visibility of the device. Volunteers were concerned that if they wore this device for longer durations, they would be concerned about damaging the electrode as it protruded more so than the other electrodes. Concerns were raised about the

wearability of MN electrodes particularly if the skin would be damaged if MNs were worn for extended periods. During the study participants refrained from showering, bathing, or vigorous exercise. Therefore, a recurrent theme encountered across all devices was water repulsion. Furthermore, the adhesion of the bespoke electrodes to skin was poor with several volunteers reporting that the device fell-off after prolonged wear.

'Personally a month is too long. However, if a doctor told me that I had to wear it for a month, then I might'.

'I need to be able to shower'.

'I wouldn't like to wear any device for that long'.

'I imagine it would get very annoying after a few days. It also needs to be kept dry so washing would be a significant issue'.

Device 1

'I am concerned about the damage device 2 would do to my skin. Due to the discomfort I experienced, I couldn't tolerate 7 or 28 days'.

'It was irritating after 24-hours, anything longer than a couple of days would probably be unbearable'.

'Too uncomfortable to wear. Under seat-belt strap it became really itchy. Not waterproof'.

'I'm not sure I'd like to wear any device for that long'.

Device 2

'Feel it is restrictive and it would get in the way of my daily activities. I would be worried that I would hit the device e.g. seatbelt in car. Would have to consider loose-fit clothing whilst wearing device 3, because it caught on my trousers/t-shirt'.

'It would hamper washing significantly and the extra bulk would become very annoying after a couple of days'.

'Just too uncomfortable and also came unstuck. Not waterproof'.

'Would become more of a burden over prolonged time due to visibility of device'.

'Irritating, adhesive coming undone, uncomfortable and 'spiky'.'

'Comfortable to wear but more aware of it because of the large plastic clip which is visible through clothing on a daily basis'.

Device 3

Figure 5.20: Selection of volunteer responses when asked to elaborate why they would wear the devices for either 1, 7 and 28 days. Images of device one, two and three located alongside direct quotes taken from questionnaire responses. Device one (wet electrode), device two (original microneedle electrode) and device three (bespoke microneedle electrode).

5.4.7.7 Volunteer device preference

Participants were asked to list the devices in order of preference. Table 5.7 displays the order of preference for the three devices used in the present study for each volunteer. Overall, the wet electrode was listed as the most preferred option in most volunteers (n=7). Reasons stipulated included lack of sensations, most comfortable and many volunteers 'didn't notice it was on.' No volunteer listed device one as their least preferred option. The remaining volunteers (n=2) listed either device two or three as their most preferred option. Device three was the least preferred option with volunteers stating that skin adhesion was poor resulting in partial or complete detachment of the electrode. Furthermore, due to the increased size of the device, it frequently caught on clothing and was more visible when compared to the other devices. Volunteer nine was the only individual to list device three as their most preferred option. The initial MN electrode prototype (device two) was listed as the least preferred by three volunteers mainly due to the presence of sensations which were described as 'prickly' and 'itchy.' Volunteer eight was the only individual to select device two as their most preferred option.

CHAPTER 5

Table 5.7: Volunteer order of preference when asked to order the devices from their most preferred to least preferred option. Responses provided by the volunteers explaining their selection are also shown in the table.

Volunteer Number	Order of preference			Reasons for most preferred option	Reasons for least preferred option
	1 = Most preferred	2	3 = Least preferred		
1	Device 1	Device 3	Device 2	Lack of pain and irritation associated with device 1. Didn't notice it was on.	Device which caused the most discomfort/pain. Didn't want to move my shoulder/chest.
2	Device 1	Device 2	Device 3	Didn't notice or feel it on my skin and didn't impact my movement.	Device 3 fell off. Became more noticeable towards the end of the day.
3	Device 1	Device 2	Device 3	Didn't know it was attached to my skin for the 24-hours.	Uncomfortable. Plastic caught on my clothing. Pain (like pressing a bruise) when told to activate.
4	Device 1	Device 3	Device 2	Least irritating.	Most itchy. No protection from plastic insertion device.
5	Device 1	Device 2	Device 3	No sensation whilst wearing.	Most uncomfortable and came unstuck.
6	Device 1	Device 2	Device 3	More flat, didn't catch on clothing. Flat MN device was similar.	Comfortable when wearing no shirt, however clothes rubbed on the device.
7	Device 1	Device 2	Device 3	Most comfortable.	Push button made for bulkier and more visible attachment.
8	Device 2	Device 1	Device 3	No sensations and comfortable to wear.	Uncomfortable for long periods. Adhesive coming undone.
9	Device 3	Device 1	Device 2	Most comfortable and less restrictive.	Prickly to the skin and a little irritation at first, although this settled down.

5.5 Discussion

5.5.1 Influence of design on electrode performance

As discussed in Chapter 3, two limitations of the original MN electrode design were identified. Firstly, electrode application force and velocity were not measured or controlled resulting in inter- and intravariability. Data gleaned from Chapter 2 was used to inform the subsequent development of a bespoke MN electrode. As skin puncture was greatest when MNs were pressed into skin at 15N, the new electrode incorporated a push-button applicator which, when deployed, continuously pressed MNs against skin at approximately 15N. The second limitation suggested that MNs could have pierced human skin, however due to volunteer movement needles could have dislodged. Alternatively, due to wired connections located directly above MN arrays, needles could have been pulled out of the skin. During device development and similarly to additional ECG monitoring electrodes including the Ambu® Blue Sensor (Ambu 2013), the snap connection was placed at an alternative location situated away from the MN array. Furthermore, following activation of the push-button, the applicator remained deployed due to the presence of notches which aimed to prevent movement of the MN array against skin.

The present study investigated the performance of three electrode designs under resting, active and prolonged conditions. Overall, signal quality was comparable between all electrode designs under each condition. Whilst the fabrication of a bespoke MN electrode with push-button applicator did not significantly improve signal quality, it did provide insight into device wearability without resulting in signal deterioration. Comparisons between the present study and published work is challenging. To the best of our knowledge a lack of guidance exists detailing standardised methods of quantitatively assessing physiological signals acquired from wearable devices. Multiple research groups use SNR as a marker of signal quality which is useful when comparing electrode performance (O'Sullivan et al. 2019; Zahed et al. 2020; Dong et al. 2021). However, standardised information regarding SNR as a measure of signal quality is lacking. Whilst mean SNR ranged from 16dB to 24dB in the present study, no guidance exists regarding physiological signal monitoring to determine if these values are considered acceptable for interpretation in clinical practice. It is acknowledged that publications such as Dong et al. (2021) used different electrodes and analytical methods, however the authors considered an SNR of 17.5dB to be suitable for signal recordings. When comparing fabricated electrodes with Ag/AgCl electrodes Zahed et al. (2020) calculated the SNR as 12.9dB and 13.3dB, respectively. In the aforementioned publications, clinical interpretation and opinion was not sought. Collaborating with clinicians

would be beneficial in developing a device which suits both the need of practitioner and patient.

SNR values achieved for wet and original MN electrodes in the present study were also comparable to data presented in Chapter 3. However, unlike Chapter 3, signal gain was reduced from x 24 to x12 as system railing or near-railing was encountered in most volunteers, specifically for channel eight which was used to connect the bespoke MN electrodes to the biosensing board. Railing was not encountered for wet and initial MN electrodes. During signal acquisition the system 'railed' when microvolt magnitudes exceeded the limits of the channel. This had significant implications, as a railed system resulted in no data acquisition. System railing was again encountered when the bespoke MN electrodes were connected to a different channel. Railing could, therefore, be the result of poor electrode connections. Due to cost the number of bespoke electrodes provided by Maddison Product Design Ltd. was limited to twenty which equated to two electrodes per volunteer. Therefore, electrodes could not be exchanged. To counteract or prevent the system from railing, signal gain was reduced from x24 to x12, particularly during active conditions where large amplitude changes were introduced resulting from movement. A reduction in amplification resulted in lower amplitude cardiac signals compared to the previous study. Subsequent device optimisation is required to address the connection between MN arrays and the remaining electrode as railing was not observed when recording signals using wet electrodes nor with the original MN electrodes. Railing was not encountered or discussed by Burma et al. (2021) who also used an OpenBCI biosensing board to record cardiac signals.

The present study found that signals recorded at rest were of higher fidelity than those recorded during active conditions. During development of the study protocol, moving from a sedentary position to standing was identified as the activity of choice similarly to Dong et al. (2021). Whilst the recruitment process ensured that volunteers had no known cardiovascular conditions, participants may be suffering from other medical conditions. Therefore, a simple movement was selected. Alternative potential activities would include arm swing, talking (Fink et al. 2021), cycling (Chareonthaitawee and Askew 2020) and walking (Dong et al. 2021). A conscious decision was made not to include walking due to the differences in gait. Furthermore, vigorous activities such as running were also not included due to COVID-19 and the risk of aerosol generation. As expected, increased motion artifacts were present in active traces where large signal deviations were observed under dynamic conditions which is similar to other published work for instance Tong et al. (2018). Whilst the authors did not use a MN-based electrode they demonstrated that ECG signals captured when walking were contaminated by noise resulting in the generation of false R peaks (Tong et al. 2018). During

bespoke electrode development, it was expected that MNs would be less likely to move resulting in less distortion in the ECG trace due to the increased pressure exerted by the push button applicator which remained deployed. However, motion artifacts were present in traces recorded by both MN electrodes. It is documented that dry electrodes are more susceptible to motion artifacts due to changes in charge distribution at the electrode interface developing on movement. In some volunteers the original MN design demonstrated greater motion artifacts. In volunteers who encountered problems with the bespoke design including damage to the push button or adhesive problems, increased artifacts were observed. Flexible baseplates could be considered in future devices to enable conformal contact with the skin and reduce the impact of motion artifact. For instance, Zahed et al. (2020) proposed a flexible dry electrode comprised of a biocompatible polymer. The authors observed fewer motion artifacts when electrodes were exposed activities such as swinging of the arms (Zahed et al. 2020).

A previous comparison of wet, original, and bespoke MN electrodes was conducted in Chapter 4 using a developed laboratory skin model over 6 hours. No decline in performance between the three electrodes was observed. During the development of the study protocol used in the current chapter it was decided, similarly, to Chapter 4, to include a prolonged wear-time of 6 hours. This duration allowed volunteers to complete the signal acquisition section during their working day. However, unlike the experiment discussed in Chapter 4, the present study involved recording cardiac activity at 0 hours following electrode application to skin, and after 6 hours of wear as opposed to designated time intervals which can inconvenience volunteers. As the ex vivo study was conducted with wet electrodes and the original MN electrodes, conclusions comparing the bespoke MN electrode used in this chapter with results from the ex vivo model cannot be made. Overall, SNR of signals recorded using wet and the original MN electrode ex vivo were comparable with those acquired in vivo. Signal quality was less variable using the laboratory model, although a lower sample number (n=3) was used. SNR comparisons at 6 hours demonstrated that ex vivo SNR results were slightly higher and less variable than those at the same time, in vivo. During device development, durations of wear vary between publications. For instance, in the development of their prototype, Fink et al. (2021) trialed their ECG shirt on a single volunteer for 30 seconds under a variety of conditions. Longer durations have been used for instance Dong et al. (2021) evaluated their recording patch by taking measurements on days 1, 4 and 7 to verify stability. Unlike Dong and colleagues whose volunteer wore one patch for the whole duration, the present study involved applying seven electrodes to the torso of volunteers. All the devices were worn for 6 hours, it was decided during study development to remove four electrodes leaving one of each type beneath the right clavicle to ensure the volunteers did not experience significant

discomfort and aid in completion of the study. The development of future MN patch devices could follow examples such as the Zio® XT and designs similar to Dong et. al (2021) which involve a single patch located on the left pectoral region. Longer usability and wearability studies could subsequently be conducted as these devices may not interfere as much with participants daily lives.

5.5.2 Volunteer demographics and perceptions of device wearability

5.5.2.1 Influence of volunteer demographics

Whilst signal quality was found to be comparable between devices, user feedback was captured at specific stages of the study to document information regarding the wearability of each electrode type. Similarly, to other publications including Karaoğuz et al. (2019) and Peck et al. (2021), an initial questionnaire was administered by the researcher following the initial acquisition of cardiac signals at 0hrs. This questionnaire captured data pertaining to biological sex, age, ethnicity, and BMI as studies have indicated that these demographics can result in ECG changes (Santhanakrishnan et al. 2016; Vaidean et al. 2016; Macfarlane 2018). Historically, reference ranges for ECGs have been derived from Western White populations. Whilst limited studies have reported ECG changes in different ethnicities, the effects of this demographic were not assessed as the researcher is not an electrophysiologist and does not have experience in interpreting ECG traces. Furthermore, the cohort of volunteers recruited was not ethnically diverse and the overall majority identified as Caucasian.

BMI is used as a standard screening measure to assess body fat (Nuttall 2015). Increased BMI is known to result in several electrocardiographic changes for instance, increased P wave duration and dispersion (Magnani et al. 2012; Vaidean et al. 2016), low QRS voltage in the limb leads (Frank et al. 1986; Fraley et al. 2005) and QT-interval prolongation (Fraley et al. 2005). Overall, three of the volunteers would be considered overweight or obese based on their BMI. Similarly, to ethnicity, the effects of BMI on subsequent ECG traces was not assessed. During study development clinicians working in the specialty of cardiovascular were involved to capture their opinions regarding the traces and to identify any ECG changes as a result of biological sex, age, ethnicity and BMI. However, due to the impact of COVID-19, clinicians were unavailable due to increased NHS pressure and lack of timing due to the delay in starting the present study. Whilst the BMI data shown in this Chapter does provide an idea of the values calculated across the nine volunteers, BMI should be used with caution. For example, BMI is unable to distinguish between lean and fat mass. Therefore, a muscular athlete may result in a higher BMI resulting from extra muscle mass and could be mischaracterised as obese. BMI may not be equally valid across the sexes,

ethnicities, and age groups. Asians have a higher percentage of body fat at lower BMIs (Deurenberg-Yap et al. 2002). Men also have a lower body fat percentage and higher lean mass in comparison to women (Schorr et al. 2018). Although this simple calculation is widely used, results should be interpreted with care.

5.5.2.2 User feedback and device wearability

A second questionnaire was administered following completion of the 24-hour period of wear. Evaluating device wearability is a multifaceted problem as wearables can affect users in diverse ways. Therefore, the second questionnaire explored and gathered user feedback regarding different wearability issues. Overall, seven key wearability themes were highlighted by volunteers. These included, ease of application, wireless connectivity, adhesion to skin, visibility, robustness, comfort, and water repulsion. These themes are important as they could inform the development of future devices.

Electrode application to skin emphasised several challenges. Multiple publications have involved the researcher directly applying prototypes to their subjects (Chlaihawi et al. 2018; Karunadas and Mathew 2020; Liu et al. 2021). Due to COVID-19 considerations however, the present study required participants to apply the electrodes directly to their skin. Volunteers found accessing the adhesive section of the electrode difficult, with several participants nearly tearing the electrodes. Future devices could include directions, for instance 'peel here' with a tab to aid in device application. Alternatively, if used in clinical environments, healthcare professionals could apply devices directly to users or provide detailed instructions (Benjamin et al. 2021). After applying the electrodes to skin, volunteers were asked to deploy the push-button applicator on the bespoke MN device. Several volunteers stated that this button was simple to use. Furthermore, volunteers also highlighted that the audible 'click' helped inform them that they had correctly deployed the device. However, some volunteers stated that when pressing the push-button applicator, they experienced discomfort and it '*felt like pressing on a bruise.*' Furthermore, deploying the bespoke device was an additional step in the application process compared to the alternative electrodes. Optimisation of application force and velocity is required to ensure that device application is not painful without hindering performance.

Self-application of device prototypes highlighted another key wearability theme, namely wireless connectivity. Volunteers considered the presence of leads restrictive for a normal everyday routine. During signal acquisition volunteers were connected to a biosensing board using leads as the electrodes were not able to communicate data wirelessly. Volunteers were directed by the researcher regarding the specific electrode locations and corresponding leads. Leads were disconnected between recording sessions to avoid interfering with daily activities.

Current methods of ambulatory monitoring e.g., Holter monitor still utilise a lead connection between the electrodes and recording device. Whilst leads are necessary for Holter monitors, they can impede wearability as patients must refrain from bathing during the monitoring period. For longer monitoring durations i.e., >48 hours, this is impractical as patients would need to remove electrodes and re-apply following bathing. This could introduce errors as patients would be required to apply the electrodes at the same location and connect them to the relevant leads. Therefore, it would be prudent for future MN electrodes to communicate data wirelessly which would also facilitate telemonitoring, allowing practitioners to monitor patients at home, which is of particular importance under the current pandemic conditions. Within the literature, cardiac data has been acquired using several communication protocols for instance Wi-Fi (Marsili et al. 2020), Bluetooth (Dong et al. 2021), ZigBee (Ehnesh et al. 2020) and near-field communication (NFC) (Zulqarnain et al. 2020). Each of these different solutions can be adopted to enable wireless data transmission in real time. Depending upon the indication, the type of data communication requires careful consideration. For instance, Dong et al. (2021) developed an ECG patch capable of acquiring cardiac activity and communicating this data wirelessly using Bluetooth. The use of Bluetooth Low Energy (LE) is advantageous in terms of power consumption (Poliks et al. 2016) which will have a direct effect on the duration of device wear. However, if the device is to communicate continuous transmission of data, this may impose impractical traffic loads of existing wireless technology such as Bluetooth and ZigBee (Rault et al. 2017).

Compared to the wet and original MN electrodes, the adhesion of the bespoke device to skin was inadequate as several participants experienced problems. During fabrication, the adhesive backing used in the bespoke electrode consisted of a double-sided medical tape which has been used by Maddison Product Design Ltd for healthcare-related medical devices. Overall, the bespoke electrode either dislodged completely or loosened from the skin's surface. In one volunteer the device completely detached before the repeat recordings thereby preventing the re-acquisition of cardiac activity using this electrode. It remains unknown whether the adhesive itself was unsuitable. Alternatively, the 15N force exerted on deployment and maintained by the device may have resulted in a high equal, but opposite force on the skin adhesive. This may have resulted in the adhesive ring loosening and subsequently dislodging completely. Increasing the size of the adhesive ring could provide less pressure on the surrounding adhesive interface. Nevertheless, further work is required to develop the adhesion between the skin and electrode to ensure the electrodes remain in contact with skin for the total monitoring duration and during periods of activity. The implications of poor patch adhesion would be poor or incomplete signal acquisition which would further impede

diagnoses. Many transdermal patches for example Reletrans (Sandoz Ltd 2021) remain attached to skin for 7 days. The properties of these patches could be adapted to suit a patch-based monitoring system. Adhesive performance could then be evaluated by assessing the key features of patch adhesion which include tack, shear adhesion and peel adhesion (Cilurzo et al. 2012). Despite previous use of the adhesive in medical devices, biocompatibility testing and suitability over longer durations under changing conditions was not investigated during this study. If the device is to remain attached for extended periods, it is essential that the device is breathable to prevent user discomfort and prevent skin irritation. To assess the breathability of the current bespoke electrode and future designs, studies like Zhang et al. (2021) could be conducted whereby substrate materials could be tested on skin explants for a minimum of 24 hours.

Further wearability themes related to device visibility and robustness. It was reported by several volunteers that due to size and shape, bespoke electrodes frequently caught on clothing. When asked for any additional comments, wet and original MN electrodes were considered '*smoother*' and more '*curved*' resulting in less interference with clothing. Furthermore, volunteers stated that the bespoke device was more visible than the other electrode types used in the study. Compared to alternative adhesive patch monitors such as the Zio® XT (Yenikomshian et al. 2019), the bespoke design is smaller but contained a single electrode. The applicator within the device was housed in rigid plastic and was raised to allow for the inclusion of applicator components e.g., springs. Further development is required to reduce the bulk and subsequent visibility of the device particularly if additional components relating to wireless capability are included. Similarly, to the Zio® XT patch, further designs could include rounded edges to avoid interference with clothing. Furthermore, volunteer handling of the device demonstrated reduced robustness. The handling of bespoke devices in a few volunteers resulted in the breakage of the push button mechanism, which in turn could have contributed to the system railing as the MNs were not in direct contact with the skin. The main source of artifacts observed in the recordings were motion artifact and PLI. Compared to the magnitude of PLI documented in the previous clinical study, noise values were lower for wet and the original MN electrodes. However, the use of a lower amplification setting could have contributed to the reduced PLI. Overall, the magnitude of PLI was greatest in signals recorded from volunteer nine using the bespoke design. This is likely due to the volunteer damaging the internal applicator design upon application therefore MN contact with skin would have been variable. This study found that noise levels were considerably variable and increased with wear. Whilst PLI can distort signals, it is easily removed using digital signal processing techniques such as notch filters (Kher 2019). Filters, however, can also distort

signals and therefore must be optimised to avoid altering signals significantly. Unlike PLI, removal of motion artifact from ECG traces is a challenge particularly in frequencies below 5Hz as this unfilterable to due to P and T waves occurring at a similar bandwidth (Fink et al. 2021). Techniques such as empirical mode decomposition have been used by groups such as Fink et al. (2021) to remove low frequency motion artifacts.

Whilst the electrode design requires further development to improve the quality of acquired signals, device comfort is a theme of paramount importance to users. During electrode construction, MN arrays adhered to the sensing element were comprised of a rigid polymer. As skin is both viscoelastic and anisotropic it is unlikely that suitable conformal contact was achieved during wear. This could have contributed to the 'noticeable' nature of the MNs which were often described as '*prickly*' or '*spiky.*' It was mentioned by users however that compared with the original MN electrode, the bespoke design did not irritate the skin as much. This was observed following device removal where images of the skin beneath the original MN electrode appeared more inflamed. Drawing a balance between user comfort and performance is key in designing ECG wearables. Within this field electrodes have been incorporated into garments which lend themselves to improved wearability (Qiu et al. 2019; Arquilla et al. 2020; Fink et al. 2021). Soft electronics are a further area of interest in the next generation of wearable technology. Rigid materials including metals and certain polymers can result in irritation and poor contact leading to a high electrode-skin impedance, which was reflected in this Chapter. The ability of soft or stretchable electrodes enables conformal contact on irregular surfaces of the body and during movement (Chen et al. 2014; Shay et al. 2018; Shahandashti et al. 2019). For instance, Chen et al. (2014) fabricated soft, flexible polymeric based dry electrodes which subjects reported did not cause discomfort. Despite improved comfort this study did not evaluate comfort over prolonged wear. Whilst the interface of electronics with the body remains a challenge, future MN device development could adopt a multi-substrate whereby hard and soft components are combined within a device similarly to Rajabi et al. (2016) who fabricated a MN patch which combined a soft flexible base substrate with stainless steel MNs.

An overwhelming theme which many volunteers highlighted related to water resistance. In the present study, volunteers refrained from showering or bathing when wearing the electrodes. Whilst no further recording sessions were conducted after 6 hours of wear, excessive moisture is likely to have interfered with the adhesive. If ambulatory devices are to be worn for greater than 24 hours, users must be able to shower or bathe with the devices attached. Furthermore, if users are to conduct their daily routine whilst being monitored, this may include physical activity such as swimming. Many of the commercial devices e.g.,

smartwatches and ambulatory patches such as Zio® XT and BodyGuardian® are designed to be waterproof. Up to 28 days of wear are possible with some ambulatory patch monitors (Tian et al. 2019). If MN device functionality is to be assessed over extended time periods, further development is needed to make the electrodes resistant to water.

5.5.3 Limitations and future recommendations

During participant recruitment, the study aimed to enroll a total of ten volunteers. However, due to the presence of COVID-19 and resultant social distancing measures, nine volunteers were recruited. In addition to the increased number of staff and students working from home, the time of year at which the study was conducted resulted in a reduced number of individuals to recruit due to additional commitments such as school holidays and annual leave. Regardless, the sample size achieved for the present study was too small to make definitive statistical conclusions. Furthermore, all volunteers recruited were healthy individuals. Whilst this is beneficial when testing initial designs, further studies must be tested in the target population once a suitable prototype has been developed and optimised. In addition, this study was unable to account for additional factors which could impact the ECG namely co-morbidities and medication which are likely present in the target population.

Overall, the present study recorded 12 minutes of cardiac activity over 6 hours under different conditions. Unlike studies including Marozas et al. (2011) who collected cardiac activity over 30 minutes, the short recording durations used in this Chapter could produce less consistent results and have an increased likelihood for anomalies. Contrariwise, short recording durations were deliberately chosen to reduce the contact time between volunteer and researcher due to COVID-19. Additionally, it may not have been appropriate to ask volunteers to remain under resting condition for 30 minutes due to prior commitments. Moreover, whilst participants had no pre-existing cardiac conditions, they may have other medical conditions which would have prevented them from performing an activity for 30 minutes whilst cardiac activity was simultaneously captured. Cardiac activity was recorded after electrode application to skin and following 6 hours of wear. A conscious decision was made to remove the electrodes located on the lower abdomen after 6 hours as it would have been unreasonable to ask participants to wear a total of seven electrodes for a full 24-hour period. Future studies need to evaluate MN electrode performance over an extended timeframe to firstly compare against the current gold standard Holter monitor over 24 hours, and secondly to investigate the effects of biofouling which could determine how long a MN electrode could remain attached to skin before signal deterioration is observed.

As highlighted previously, skin preparation is routinely used as a method of improving signal quality. Whilst the wet electrodes used in this study contained a built-in abrader disc, a deliberate decision was made to avoid the use of additional skin preparation methods including abrasive sandpaper prior to electrode application to skin. It was observed however, that in volunteers with increased body hair electrodes did not fully adhere to skin and resulted in poor signal quality. It is therefore recommended that for future studies, hair located on the torso could be trimmed using hair clippers to improve electrode attachment to skin. The use of shaving or depilatory creams is not recommended as they could damage the skin's surface and affect skin hydration.

A topic unrelated to the aforementioned wearability themes is cost. Compared with the previous MN electrode, the bespoke design incurred increased cost due to the development and testing of previous prototypes. Furthermore, the specific cost of MN fabrication by Tyndall National Institute was unknown, therefore comments on price to performance cannot be made. Compared to wet electrodes, MNs can be considered more fragile. The transportation and manufacturing of such devices make it unlikely that costs will be lower or at least comparable to wet electrodes. In contrast, significant efforts are likely to have been made to produce and market cost effective wet electrodes. At present, the same cost-saving efforts have not been applied to MN electrodes and therefore, their cost may not be represented in the existing literature.

5.6 Conclusion

Chapter 5 aimed to capture cardiac activity in up to ten further healthy adults using three electrode designs under three conditions. In total, nine volunteers were recruited for the study resulting in a slight unequal distribution of males to females. All electrodes recorded cardiac signals, however differences in performance and magnitude of PLI were observed. Under resting, active, and prolonged conditions calculation of SNR demonstrated a comparable performance between the three electrode designs. When visually assessing ECG traces, increased motion artifacts were observed during active conditions when volunteers were asked to stand up from a seated position. The presence of motion artifacts resulted in a decline in signal quality. Following the re-acquisition of cardiac signals after 6 hours of wear, no significant decline in performance was observed. After device removal, imaging techniques demonstrated the presence of indentations and microchannels confirming microneedle penetration. Re-imaging after 24 hours demonstrated resolution of electrode site effects. At specific points of the study, user feedback and demographics were captured using an online questionnaire. In total, seven key themes relating to wearability were identified. These included ease of application, comfort, wireless connectivity, adhesion, visibility, robustness,

and water repulsion. Overall, increased sensations were felt when wearing both MN electrodes with volunteers using words such as 'spiky,' 'prickly' and 'like Velcro' to describe the effects of MNs on their skin. Most volunteers chose wet electrodes are their most preferred device, therefore further work is required to improve the wearability of MN electrodes.

CHAPTER 6

GENERAL DISCUSSION

MN arrays were initially developed as a means of enhancing the penetration and transportation of therapeutics across the skin through the creation of MN-induced channels. With the growth in the microelectronics industry, the applications of this versatile device have expanded. Over the past decade, a synergism between MNs and wearable technology has gained increasing attention due to the potential for longer-term monitoring in a minimally invasive manner. Hence the aim of this thesis was to define, develop and test key parameters relating to a wearable and functional MN-based electrode for the longer-term monitoring of cardiac patients.

6.1 Significance and discussion of findings

MN systems are an emerging technology in the fields of medical devices and pharmaceutics. Different types of MNs exist and are produced using a variety of technologies. Therefore, guidelines are required to establish manufacturing procedures, evaluation methods and tests required for approval and quality control. In 2017, the FDA published guidance entitled 'Regulatory Considerations for Microneedling Devices' to facilitate the development of MNs as medical devices. According to FDA guidelines, whether a MN system can be classified as a medical device depends upon its intended indication. If MNs are used '*in the diagnosis of disease or other conditions, or in the cure, mitigation, treatment, or prevention of disease'* they can be regarded as medical devices.

The first step in this postgraduate research involved investigating the geometry and penetration efficiency of epoxy MNs. This work provided the researcher with practical experience of MN systems, use and an understanding of the specific insertion profile of the 500μm length, out-of-plane, epoxy MNs prior to their use as electrodes. In the early days of MN research, silicon was used to develop the first MN device (Henry et al. 1998) and has subsequently been used to fabricate MNs with multiple shapes, heights, and densities. MNs

used throughout this thesis were produced using two methods of fabrication. Initially, silicon MN templates were etched in 29%w/v aqueous KOH solution to produce 500µm length MNs with an aspect ratio of 3:2 (O'Mahony et al. 2016). The many physical properties of silicon make it an attractive option however, it is costly and concerns regarding biocompatibility have been reported (Runyan and Bean 1990; Braybrook 1997). Due to various drawbacks associated with silicon which include expensive raw materials, complicated manufacturing and fragility, many researchers are drawn to the use of polymers. Due to their low manufacturing costs, flexibility and ease of production, polymers have been used to create MNs for both transdermal drug delivery and sensing (Forvi et al. 2012; Srivastava et al. 2015). Therefore, to replicate these silicon MNs in polymeric materials, PDMS moulds of the silicon master templates were created. Whilst the use of a biocompatible epoxy is considered more cost-effective, particularly when considering scale up, it has been reported that polymer MNs have a lower Young's Modulus compared to silicon (O'Mahony 2014; O'Mahony et al. 2016). Post-insertion imaging, discussed in Chapter 2, revealed that the epoxy MN tips had either remained intact, blunted or in some instances bent, indicating an area of weakness within the structure. Therefore, maintaining needle integrity during insertion is crucial and can be achieved using sharper needles or materials of suitable mechanical strength.

As introduced in Chapter 2, application force and method influenced the extent of MN penetration. The optimal force of MN application to both ex vivo skin models from the range of forces tested was 15N. It was found that applying MNs to both skin explants with a greater velocity improved the overall mean penetration efficiency. Therefore, the way MNs are applied to skin is an important consideration in preparation for clinical trials. Several parameters including force and application are known to influence MN penetration (Verbaan et al. 2008; Khanna et al. 2010; Kim et al. 2018; Leone et al. 2018). These parameters can affect the consistency and reproducibility of MN application, and therefore, performance. If wearable devices are to be used in healthcare rather than by consumers, an option could involve the healthcare professional manually applying the device to the patient. Alternatively, the patient could be provided with verbal and/or written instructions detailing the method of application. Patients could also be trained to use devices including a force gauge to apply MNs at an optimal force. For instance, in response to the COVID-19 pandemic, Benjamin et al. (2021) designed a protocol for mail-out ambulatory ECG monitoring devices and educational materials developed to teach patients how to install the device for 14 days of continuous AECG monitoring. Whilst the authors found that a mail-delivered home-based recording platform could be used reliably to acquire cardiac data, this process may not be practical or simple for users (Benjamin et al. 2021). Variability in MN application could also be minimised using applicator systems. Various applicators have been shown to result in MNs piercing human

(Leone et al. 2018), animal (Park et al. 2013) and artificial skin (Sakamoto et al. 2021). These devices can apply MNs at a consistent force and velocity therefore, improving the reliability and reproducibility of skin puncture and thereby enhancing device performance (Singh et al. 2011; Prausnitz 2017). If an applicator is simple to use, healthcare professionals may not be required to apply MN devices and patients would not have to follow detailed instructions. This, therefore, results in an application process which is not user dependent. Conversely, increased cost, complexity and product size are known disadvantages of applicators (Prausnitz 2017). These factors require consideration during MN device development.

After assessing MN insertion, metallised, polymeric MN arrays were fabricated into electrodes and subsequently used to record cardiac activity from healthy volunteers. This study discussed in Chapter 3, demonstrated MN electrode functionality yet identified limitations in its design. Moreover, this study did not include methods confirming MN penetration nor did it capture user feedback regarding wearability. Building upon these shortcomings, Chapter 5 sought to investigate a bespoke electrode which was designed with the aim of improving MN application to, and retention of MNs within skin. Using the data captured during Chapter 2, this design involved a push-button applicator which pressed MNs into skin using an approximate downward force of 15N. The button remained deployed to retain the MNs within the skin and minimise movement. Whilst this custom-built electrode resulted in a more consistent application, there are still several adaptations that could be made to both the MN and surrounding applicator to improve device wearability and functionality. Epoxy MNs used throughout this thesis were not conductive, therefore metallisation was required to functionalise this integral component. Alternative polymers which are conductive could be trialled thereby removing this additional metallisation step. Whilst conductive polymers have been explored as alternatives to metallic interfaces within biomedical devices, mechanical stability (Hassarati et al. 2014; Green and Goding 2016) and biocompatibility (Venkatraman et al. 2011; Green and Goding 2016) prevent them from performing well in biological environments. Many publications exploring the potential of MN electrodes in physiological signal monitoring use similar methods of applying a conductive coating. Griss et al. (2001) recorded low amplitude EEG signals using Ag/AgCl coated MNs. Similarly, to O'Mahony et al. (2016), Ren et al. (2016) coated polymeric MNs with titanium and gold. More recently, Satti et al. (2020) captured cardiac signals using parylene coated MN arrays. Promising conductive polymers for biomedical applications include poly(3,4-ethylenedioxythiophene) (PEDOT) and polypyrrole (Kaur et al. 2015). For instance, Chen et al. (2013) investigated the electrochemical performance of MN based dry electrodes which were coated with electropolymerized PEDOT. These electrodes were shown to successfully capture biopotentials in both humans and rats (Chen et al. 2013). Similarly, to metals and

silicon, polymers can be stiff and friable. The viscoelastic, anisotropic, and non-linear nature of skin, coupled with rigid, fragile wafer-based electronics presents a major challenge to maintaining adequate sensor-skin contact. To continuously monitor physiological signals, wearable devices are required to conform to the shape of the body to improve the quality of signal monitoring whilst ensuring maximum comfort for the wearer. Many proposed MN devices for both drug delivery and sensing are based upon rigid substrates which do not conform to the curvature of the skin (Wang et al. 2011; Arai et al. 2015; Mohan et al. 2017; Zhao et al. 2017; Pere et al. 2018; Ellison et al. 2020). Regarding sensing, MNs are unlikely to conform to areas of skin with concavity or convexity. Loss of contact with skin, particularly on areas which undergo frequent movement could result in increased contact impedance, PLI and motion artifact (Chen et al. 2016) resulting in signal degradation and potentially hindering clinical interpretations. For acute, short-term applications where MN electrodes are applied to areas of the body, for instance on the chest, flexible substrates may not be required. As shown in Chapter 5, when asked about the duration of wear, 100% (n=9) of volunteers stated they would be prepared to wear the initial MN electrode for 24 hours. The percentage of volunteers prepared to wear any of the electrode designs for 7 days and 28 days decreased. Many volunteers reported experiencing sensations with wearing the three electrode types. On areas of skin with frequent movement, rigid MNs could dislodge and cause increased indentations, pain, and discomfort. Therefore, for longer term monitoring, flexible arrays could offer a more effective approach. As well as new materials, advancements in fabrication techniques make it possible to construct flexible and conformal electronics. For instance, Nishinaka and colleagues produced flexible polymer based MNs using photolithography, micro-moulding, and vapour deposition methods (Nishinaka et al. 2013). In 2015, this group recognised that the use of PDMS may not be sufficiently stiff to penetrate through the SC and subsequently fabricated MNs consisting of SU-8 (Arai et al. 2015). These MN electrodes were verified to possess sufficient sharpness to penetrate through the SC and produced a low skin-electrode contact impedance. Epidermal electronics, termed e-tattoos, are another emerging candidate which are addressing the limitations regarding comfort and wearability (Lee et al. 2018). Compared with conventional sensors, the conformability of e-tattoos can follow skin displacement reducing motion artefacts. Wang et al. (2018b) demonstrated the ability of e-tattoos to simultaneously measure temperature, hydration, and ECG during perspiration without any signal degradation. These systems, however, are ultra-thin which may limit their reusability. Alternatively, textile-based systems have been developed which improves the overall wearability. However, as the electrodes do not directly contact the skin, textile-based sensors suffer from reduced signal quality and increased noise when compared to commercial wet electrodes (Puurtinen et al. 2006; Marozas et al. 2011).

An important consideration regarding device development is the target market. Whilst wearables can enable the diagnosis and monitoring of specific diseases in healthcare, wearables including the Apple Watch and Pebble smartwatch (Kalantari 2017) provide feedback to consumers on different physical performance variables and 'wellness'. Therefore, it is important to understand the specific requirements and challenges faced by each area. In the consumer world, many individuals are interested in wearable devices. Whilst small numbers have adopted this technology, the market is predicted to grow (Jayathilaka et al. 2019). Understanding what influences an individual's adoption of a device is important for success. For instance, Basoglu et al. (2017) explored factors which influenced the use of smart glasses. The authors concluded that product characteristics (features of the design, price, and display resolution) and user intention characteristics (utility, ease of use and attitude) affected product usage. Devices such as smart glasses are not as popular as smartwatches. Little, however, is known why some consumers are more likely to use smartwatches than other wearable devices (Chuah et al. 2016). Key attributes of wearables include size, shape, standalone communication, brand, and price (Jung et al. 2016). These themes were also highlighted by participants following 24 hours of wearing the three electrode designs. Users in Chapter 5 discussed wearability aspects including device colour, shape, size, and ease of application. Commercial devices such as the smartwatch cover both mobile computing and fashion characteristics. Whilst this combination of features is new, there is a growing importance in the aesthetics and recognition of smartwatches as a fashion accessory. Wearables in the context of this thesis refer to ECG monitoring devices used for medical purposes. While consumers may not need to frequently monitor their ECG, wearability aspects important to this target market could be equally as important for the sustainability of wearable medical devices. For instance, a known limitation of Holter monitors is the wired connection, for consumer wearable devices standalone communication is prioritised (Jung et al. 2016). Currently smartwatches are connected indirectly to wireless networks by means of a smartphone using short-distance communication such as Bluetooth. At present this makes smartwatches an accessory to smart phones. If they were capable of standalone communication, they could become more independent and serve more diverse functions. Whilst wearables in general offer user's numerous benefits, several challenges remain. New consumer wearables are expanding their capability including functions such as ECG and oxygen saturation. ECG trace interpretation typically requires medical expertise; however, algorithms have been and continue to be developed to assess this type of physiological data. Problems could arise relating to the accuracy of these algorithms resulting in inaccurate physiological estimates which in turn could affect health-related decisions. A further key challenge faced by the consumer sector is ensuring sustainable usage of wearable technology. Lee et al. (2016) highlighted that a third of American consumers cease using

wearable devices within 6 months of purchase. Despite the effectiveness of fitness trackers in motivating individuals to increase their activity level, similarly to Lee et al. (2016), Rupp et al. (2018) found that consumers abandoned the technology soon after purchase. Wearable products can empower people to take responsibility for their health. However, the current 'fad' view of wearables needs to change, and the benefits will only materialise if consumers use, and continue to use these products rather than abandon them after purchase.

In the health sector wearables allow for the ambulatory acquisition and monitoring of vital signs and health status over time, outside clinical environments. Within the human body, there are numerous physiological parameters that could be monitored using this technology e.g., ECG, HR, glucose, and perspiration. With respect to cardiac monitoring there are three main types of devices namely chest straps, adhesive patches and clothing containing embedded electronics (Dias and Cunha 2018). Many of these devices are developed with the aim of acquiring one type of measurement and its design adapted to suit that specific use. Conversely, when combining several physiological signals and acquisition methods, extracting the required information from all the data could be challenging. Adhesive patches such as the ZIO® XT patch (Barrett et al. 2014; Bolourchi et al. 2020) and EZYPRO® (Dilaveris and Tsioufis 2021) have been shown to be equal or superior to the current Holter monitor. These devices lend themselves to improved wearability and are considered more patient-friendly. User feedback from the in vivo study in Chapter 5 highlighted that water resistance was an important wearability consideration as volunteers stated that they would not wear the devices unless they could shower or bathe. Unlike the Holter monitor and electrodes used during this thesis, patches such as the ZIO® XT are waterproof allowing patients to exercise and bathe during use (Lobodzinski 2013). Most PEM are adhered to the skin on the left pectoral region. Devices, therefore, can be worn underneath clothing allowing for improved discretion. Furthermore, these newer devices allow for significantly longer durations of monitoring than the current Holter, resulting in improved detection of cardiac anomalies and meaningful changes in clinical management. Whilst these devices are leadless, they do not automatically transmit data. At the end of the monitoring period however, the patch must be mailed to a central monitoring processing centre. This process may delay a patient's diagnosis as physicians are required to wait until a report is produced. As PEM become more popular within the field of cardiology, improvements in device functionality and capabilities can be expected. The adoption of digital technologies in clinical practice, including electronic health records and wearable devices, has occurred at a faster pace than the ability of healthcare to evaluate these products (Coravos et al. 2020). Caution must therefore be exercised as inaccurate data is more harmful than no data at all. To determine the appropriateness of a particular wearable device, the question of validity is often posed. The term validation, however, often carries

different meanings for different stakeholders. Regarding wearables, several validation studies have questioned the accuracy of the raw data acquired from various devices (Shcherbina et al. 2017; Herkert et al. 2019; Vetrovsky et al. 2019). Medical grade sensors which can monitor physiological parameters such as ECG are usually regulated by agencies such as the FDA and are often labelled as class I or class II medical devices. However, traditional consumer-facing companies such as Apple and Fitbit are now approaching the FDA as they develop products to be used in a clinical setting (Turakhia et al. 2013; Daligadu et al. 2018; Bayoumy et al. 2021). There are, however, a lack of clear regulatory policies governing commercial wearable devices. In 2020, Coravos and colleagues outlined a framework to assess the validity and accuracy of sensor technologies, including wearables, across biomedical research and clinical care. This comprehensive framework covered both the hardware and software components of wearable technologies (Coravos et al. 2020). Within the publication, potential resources, evaluation criteria and target thresholds for five dimensions are highlighted. These dimensions include validation (1), security practices (2), data rights and governance (3), utility and usability (4) and economic feasibility (5) (Coravos et al. 2020). With respect to the process of validation, the authors recommend a three-stage approach. Firstly, verification, which evaluates and demonstrates the performance of a sensor technology against as pre-defined set of criteria (Coravos et al. 2020). Secondly, analytical validation to evaluate the performance and ability of the algorithm to detect, measure or predict physiological metrics (Coravos et al. 2020). Finally, clinical validation to evaluate where a device identifies, measures, or predicts meaningful data in the specific patient population (Coravos et al. 2020).

Unlike many wearable devices, electrodes used in this thesis did not contain any form of wireless communication. Data were captured directly from the electrodes using leads which were connected to a biosensing board. This wired connection is unsuitable for longer monitoring periods as leads will interfere with the day-to-day activity of users and could pose problems if patients need to reconnect leads following showering. Different solutions are available to facilitate wireless data transmission in real time. For instance, Bluetooth Low Energy is advantageous in terms of power consumption (Poliks et al. 2016). Radio frequency (RF) is suitable for short-range transmissions but can suffer from instability and packet loss during transmission (Sylvester et al. 2017). Wi-Fi can also be used for the realisation of local area networks (Kang et al. 2011). During the development of a wireless MN electrode, data transmission methods will need to be considered carefully. For instance, the method of data transmission can impact battery life. Power consumption should be limited with the dual purpose of extending battery life and easing the miniaturisation of the sensor, as the battery can be considered the most cumbersome component (Cosoli et al. 2021). A balance should be achieved between power consumption and efficiency of the hardware to ensure that system

performance is not compromised (Pin et al. 2014). One such instance of an efficient solution is rechargeable LiPo batteries which represent a viable compromise between size and lifetime (Mittal et al. 2020). In 2008, the IEEE issued guidance to address the use of RF wireless technology for the communication of medical data, both to, and from point-of-care medical devices (IEEE 2008). This guidance established the foundations for adopting off the shelf RF technologies for data transmission. When communicating data using these wireless techniques, a major concern faced by both consumer and healthcare wearables relates to the privacy and security of sensitive medical and user information. To ensure the security and privacy of data during the in vivo studies conducted in this thesis, each participant was assigned a unique numerical identifier in place of their personal identifiable information. This number was used to label all data pertaining to the specific volunteer. Any anonymised data collected throughout this thesis will be retained in accordance with the University's research records retention scheme. Furthermore, cardiac data shared with SymlConnect Ltd was anonymised, password protected and stored on their secure server. In this era of big data and the internet of things (IoT), wearable devices can collect data regardless of time, place, and occasion. This data is subsequently transferred using various forms of wireless communication which introduces risk. An attack could occur allowing remote access of the device and thereby resulting in a data breach. Data breaches unfortunately are an eventuality, rather than a mere possibility, for instance, in 2017, NHS services in Scotland and England faced a cyber-attack that resulted in severe disruption (BBC 2017). Data security during transmission is a significant requirement. A secure communication channel employing strong encryption, authorisation and authentication technology is needed to safeguard personal medical information (Ameen et al. 2012). De-identification is a possibility, this however, may not be sufficient and next-generation cybersecurity technology such as blockchain could be considered (Hasselgren et al. 2020). Security in sensor network applications used in healthcare cannot be compromised as wearables can collect the user's private and sensitive information during usage. Traditional user authentication techniques such as entry of a Personal Identification Number (PIN) can be vulnerable to attack. Therefore, during development and use, a product's security risk must be reviewed continuously as new attack methods become available (Coravos et al. 2020). In addition to cybersecurity, unrealistic patient expectations regarding data handling can prove challenging. From a patient's perspective regular reports regarding the function of their device and access to their data following clinical review is desirable (Slotwiner et al. 2019). However, clear expectations between patients and their clinicians need to be established through next-generation data user agreements. These agreements, however, should be transparent to address concerns about patient privacy and be presented in a way that is comprehensible (Slotwiner et al. 2019). Agreements should detail the nature of data transmission, regularity of data review, personnel

reviewing the data and contact details should urgent communication be required (Bayoumy et al. 2021). The use of wireless, wearable technology within healthcare is expected to become more prominent, therefore it can be beneficial if individuals are educated regarding security and privacy issues associated with the use of wearables (Ameen et al. 2012).

In vivo and simulated cardiac studies conducted throughout this thesis were acquired over 30 to 60 seconds. A future consideration of AECG monitoring devices relates to how the data is monitored. Continuous or intermittent monitoring have their own benefits and limitations. Continuous data acquisition in any field of sensing is beneficial as asymptomatic episodes such as AF, or trends in glucose over time for example, can be captured and inform therapeutic interventions. Challenges, however, can arise during data interpretation. Whilst continuous ECG monitoring provides comprehensive data regarding a patient's health status, data collected by various devices must be evaluated by a physiologist which requires time and expertise despite automation. Furthermore, clinicians and other members of the healthcare team have additional clinical commitments and are therefore, unable to continuously monitor ECG data whilst the patient goes about their daily activities. In addition, continuous monitoring captures a significant amount of data, therefore, devices such as the Holter monitor are used for short periods. However newer patches have the potential to increase this duration to 14 days (Cheung et al. 2014). When recording 3 minutes of cardiac activity from volunteers in this thesis, MATLAB was required to handle the large data sets. Acquired biopotential data requires processing by a digital signal processing (DSP) unit to obtain valuable health information. Processing can occur in real-time using an onboard microcontroller. This method of DSP requires fast algorithms which are completed onboard for noise reduction and to determine fundamental ECG parameters e.g., detection of QRS complex and HR calculations. Alternatively, processing can occur after data acquisition. This form of DSP allows for more in-depth analysis in a more relaxed time frame. Computing devices can also improve the SNR of signals using filters (Akhbari et al. 2016) and decomposition techniques (Kabir and Shahnaz 2012; Pin et al. 2014; García et al. 2018). Many wearable devices use software algorithms which deploy artificial intelligence (AI) to analyse recordings and allow for the processing of substantial amounts of health data. The US National Academy of Medicine published a reference document providing guidance for the responsible development and maintenance of AI in clinical settings (Matheny et al. 2019). The performance of AI algorithms in medical tasks still faces considerable ethical and technical challenges. The FDA's new digital health innovation plan promises a risk-based approach that aims to initially look at the software developer rather than the product (FDA 2019; Bayoumy et al. 2021). It is hoped that providing healthcare with a framework or creating standards by which medical societies can evaluate

these devices will aid in the recruitment of high-quality wearable technologies whilst slowing the adoption of substandard devices.

Intermittent monitoring conversely can be used for longer monitoring periods and do not record the large quantities of data as the continuous method however, studies such as Ziegler et al. (2006) concluded that intermittent monitoring is inaccurate for identifying patients with long-duration AF. A study by Downey et al. (2018) evaluated whether continuous monitoring of vital signs via a wireless patch was an acceptable method of monitoring surgical patients. Whilst this method was determined to be practical and acceptable to patients, the authors concluded that more research was required to determine if there was significant benefit for continuous over intermittent monitoring (Downey et al. 2018). Whilst the decision to start patients on continuous or intermittent monitoring is up to the clinician, this factor will influence the development of a device and its corresponding software.

Sterilisation is a further important consideration during the development of future MN systems. MNs can be considered minimally invasive, however their ability to pierce the skin could introduce microbes. The target tissue, duration of application, penetration depth and target population are factors used to determine whether a MN is required to be sterile (Lee et al. 2020). Whilst there has been little research investigating sterilisation processes for MN electrode systems, a study conducted by Donnelly et al. (2009) found that *C. albicans*, *P. aeruginosa* and *S. epidermidis* were able to penetrate the skin through MN-induced channels. Whilst the magnitude of microorganisms in MN induced channels were significantly lower compared to hypodermic needles, MNs are required to be completely sterile or at least have a low bioburden as they can penetrate the deeper layers of skin (Prausnitz 2017; Tarbox et al. 2018). If a product needs to be sterile, processes such as terminal sterilisation, for example gamma irradiation, aseptic manufacturing or ultraviolet (UV) sterilisation need to be incorporated during the initial stages of development (FDA 2016; AAMI 2019; Lee et al. 2020). Aseptic processing involves the sterilisation of individual components comprising the device e.g., MN arrays and holder followed by assembly of the final system in a sterile environment. This process however can be expensive and can be dependent on the manual dexterity of the operator. In comparison, terminal sterilisation can be considered a cost-effective option (Prausnitz 2017). Whilst there are some concerns regarding the detrimental effects that terminal sterilisation can have on the stability of therapeutics such as proteins and peptides (Prausnitz 2017; Tarbox et al. 2018), the process could still be used for MN-based sensing systems. For instance, Sharma et al. (2016), Rawson et al. (2019) and Gowers et al. (2019) sterilised their MN arrays using gamma irradiation with 25kGy cobalt-60 irradiation. In this thesis, fabrication of MN electrodes for use in clinical studies, involved sterilising individual MN arrays using 70% ethanol and assembly within a GMP suite. Alternative methods such as

autoclaving were unsuitable as heat would affect the adhesive ring. Material selection during device development, therefore, would be essential to allow for MN systems which are cost-effective, biocompatible, conductive and remain unaffected by the sterilisation process.

Several additional factors also need to be considered at later stages of development including packaging, disposal, and user acceptance. Once sterilised, the device's packaging needs to maintain this sterility, protect MNs from damage and remain cost-effective (Prausnitz 2017). As healthcare professionals and users are unfamiliar with MN-based systems and their disposal, unexpected problems may occur (Prausnitz 2017). The near invisibility of MNs is often publicised as a factor in countering needle phobia (Birchall et al. 2011; Mooney et al. 2014). It is this feature however, that could constitute a safety issue. Since MNs directly contact biological fluids upon penetration, they can be considered biohazardous. The absence of an intimidating sharps hazard could have the potential to create a false perception of the device possessing little to no danger (Martin et al. 2017). Furthermore, MNs are needles and hence constitute a sharps risk. These devices therefore should be disposed of in appropriate, designated sharps waste containers. Since needle-stick injuries still occur in practice, during development a safety mechanism e.g., a safety guard or a safety indicator for visual confirmation could be incorporated within the device to prevent MN-based injuries. For example, the Ateria® SafeControl® is a needle used for insulin administration. This device contains a safety guard which, when pushed covers both ends of the needle. Moreover, the device contains visual confirmation that the needle has been used (Mumford 2021). Since current methods of physiological signal monitoring and glucose measurements are single use, re-using or re-loading of MNs within future devices could prove challenging for users. Regarding user acceptance, studies have reported a general acceptance of MN devices amongst patients, however reservations about self-administration of MN patches remain. Indicators of successful puncture/application would be beneficial to the user administration. For example, the bespoke electrode design showcased in Chapter 5 resulted in audible click when the MN array had been deployed. Whilst these factors have been discussed briefly, they will need to be considered once the functionality of the MN system has been demonstrated and when clinical trials are in progress.

To date and to the best of our knowledge, no commercially available MN product exists for physiological signal monitoring. Whilst MN electrodes have been shown to record biopotentials with benefits including reduced impedance and removal of electrolytic gels, competitors such as epidermal electronics and PEM which are non-invasive with improved electrode-skin contact may have the advantage. Furthermore, the cost, convenience and long clinical experience with wet electrodes could pose a challenge for MN-based biopotential electrodes. The ability of MNs to pierce the skin may better suit the monitoring of analytes and

biomarkers including glucose which represents the major target within the field of transdermal sensing (Ventrelli et al. 2015). For commercialisation, MN electrode designs need to consider many of the factors discussed in this Chapter. For the future development of MN sensors, it is essential for academia, industry, and governing bodies to work closely to help transform the innovations within the research field into commercial products.

6.2 Limitations and further work

This postgraduate research was subject to various limitations. There are still several areas of work which could reduce these constraints and develop both the study and MN device further. Due to restrictions in the supply of ex vivo human skin and presence of COVID-19, this research presented preliminary findings relating to a small number of donor skin samples and recruited volunteers. Regarding the ex vivo work presented, this limitation was addressed through the incorporation of excised porcine skin which is considered the next appropriate alternative to human skin explants. However, when recording ECGs, electrodes are placed at specific locations on the human body. Throughout this research, MN insertion and simulated ECG studies were conducted using excised human and porcine skin. Human breast skin was acquired from mastectomies whilst porcine skin was acquired from different anatomical locations. It is known that skin thickness can vary with anatomical location and due to sample availability and other users of the skin specimens, skin location was not kept consistent. Therefore, it may be beneficial to assess and compare the quality of the recorded ECG at several locations on the body, particularly with respect to MN insertion and in areas with increased hair. Future studies could also be developed with increased sample sizes alongside the recruitment of a more heterogeneous group of subjects to increase the robustness and validity of results.

When recording cardiac activity from healthy adult volunteers, the acquired data were manually analysed offline using MATLAB. Despite recording cardiac activity for a short period of time, large volumes of data were acquired. Therefore, a small number of individual waveforms were selected from each trace and analysed further. To improve the efficiency of data analysis, code could be developed in MATLAB to analyse the whole trace compared to a small number of individual waveforms. Furthermore, filters including notch, high-pass and low-pass were created in MATLAB and used for data processing. Work is required to optimise these filters to avoid introducing unwanted artifacts to data or finding alternative methods to their use. Moreover, this research relied upon manual data analysis and did not investigate the use of cardiac-specific algorithms. Further studies could be conducted to investigate how different algorithms on the acquired cardiac data compared with clinician interpretation.

This postgraduate research was funded by CALIN and exploited complementary expertise between Cardiff University, Tyndall National Institute and SymlConnect. Our partnered SME, SymlConnect, creates digital health solutions and was created to bridge the communication gap between patients and clinicians. Throughout this thesis, raw cardiac data acquired from in vivo studies were supplied to SymlConnect to help them in achieving their aim of developing a remote cardiovascular monitoring platform with user alerts based upon a traffic light system. Whilst this data provides SymlConnect with real-world, healthy cardiac examples, further work is required to help inform colleagues at SymlConnect regarding specific ECG parameters for instance durations and amplitudes of normal PQRST values. This would help SymlConnect in developing thresholds for their remote monitoring system.

6.3 Influence of COVID-19

In March of 2022, the ongoing COVID-19 pandemic began. With the uncertainty surrounding COVID-19 most laboratory research came to a halt. This subsequently delayed the progression of the research discussed throughout this thesis, particularly regarding the in vivo study conducted in Chapter 5. Acquiring ethical approval was challenging as COVID-related considerations including social distancing and face coverings required attention. Furthermore, this study aimed to recruit a total of ten volunteers, however potentially because of the pandemic, only nine were recruited. This resulted in an even smaller sample size and uneven distribution of biological males to females. Whilst this clinical study provided preliminary results about the performance and wearability of the bespoke MN electrode, the current situation is uncertain. Further studies could increase the number of volunteers to capture more views surrounding the wearability and performance of the design. Moreover, cardiac activity recorded throughout this thesis was from healthy adult volunteers with no known cardiovascular problems. The ex vivo model also utilised a healthy ECG waveform which was emitted to produce a normal HR. As the ability of MN electrodes at recording abnormal ECG traces was not assessed, future work could focus on adapting the model to generate abnormal traces representing various cardiac conditions such as AF or supraventricular tachycardias. Utilisation of the model would also be beneficial under the current climate as volunteers would not be required thereby reducing potential COVID-19 implications.

6.4 Impact of research

Since the start of this postgraduate research, the world is now in a different position because of COVID-19. The pandemic has brought numerous challenges and highlighted the importance and benefits of scientific research. In the early stages of the pandemic thousands of patients were considered vulnerable and were required to shield. Healthcare had to evolve and adapt to the imposed restrictions whilst still monitoring and caring for patients. This has

highlighted the need for remote systems to enable both patients and practitioners to monitor and manage health conditions during these challenging times.

Within the field of cardiology, ECG is a fundamental tool which is used for patient monitoring. Conductive gels used in monitoring electrodes are associated with dehydration, thereby impacting signal quality. As an alternative, MNs can directly contact the underlying epidermis removing the requirement for electrolytic gels. This research, therefore, set out to assess the wearability and performance of MN electrodes using ECG as an exemplar. In the development of wearable technology there are several steps in achieving a fully functional and wearable device. Initially, MN insertion studies and a clinical study aided the first stage of MN electrode optimisation where the original design, developed by Tyndall National Institute, was adapted. At present, the novel MN electrode design does require further optimisation. However, the alterations made will aid patients in the application of MNs through a simple push button applicator with audible confirmation when deployed. Furthermore, a model was developed to allow for the testing of various parameters and novel devices prior to their application in vivo and in the desired target population. Whilst this model requires further adjustments, it has the potential to allow for the optimisation of uncertified devices prior to their use in human volunteers.

Remote health monitoring is a rapidly expanding field aided by user-friendly technology to monitor patients in non-clinical environments. With an aging population and increased prevalence of chronic conditions, these remote monitoring systems make it possible for patients to live more independent and active lives. Simulated and clinical cardiac data collected from healthy adult volunteers were shared with SymlConnect. The provision of this data helped support a local company allowing them to access university facilities, skills, and knowledge. The data were provided to help in the development of a remote clinical monitoring platform. This would be a simple, cost-effective system where data could be automatically transferred to a remote platform such as a mobile phone and generate threshold alerts to family or medical staff regarding cardiac activity. This dynamic sharing of critical information would allow for smarter communication between healthcare professionals and patients thereby reducing delays in the appropriate clinical action taken.

6.5 Concluding remarks

This thesis aimed to define, develop, and test key parameters relating to a wearable and functional relating to a wearable and functional MN-based electrode for the longer-term monitoring of cardiac patients. The objectives originally introduced in Chapter 1 were met as follows:

i.   Prior to their conversion to electrodes, epoxy MNs were inserted into two established skin models to assess the effects of changing MN parameters, application force and method on skin penetration. Pressing MNs into ex vivo porcine and human skin using a downward force of 15N or using greater impact energy resulted in the greatest mean penetration efficiency. Information gleaned from these studies aided the development and use of an initial MN electrode and a further bespoke design.

ii. An initial MN electrode prototype was fabricated by adapting a commercially available wet electrode and adhering a metallised, epoxy MN array to the sensing element. This initial design successfully recorded cardiac signals in vivo under resting conditions. SNR comparisons revealed that current gold standard wet electrodes recorded signals of higher fidelity than initial MN electrodes. Overall, a 1.6dB difference existed between the designs, however the clinical impact of these traces was not assessed, and this difference may be negligible in practice.

iii. A laboratory model was developed by combining a pre-existing ex vivo porcine skin model with suitable methods of signal generation and acquisition. Traces acquired from in vivo studies were used to optimise the pre-programmed simulated cardiac waveform to reflect a healthy, resting, adult ECG. The laboratory model was optimised to reduce the magnitude of PLI acquired alongside the simulated waveform. This ex vivo model would allow for the optimisation of electrode designs prior to their testing on human volunteers.

iv. Following optimisation, the laboratory model was used to assess the effects of MN length, duration, and design on electrode performance. No statistical significance was determined when comparing 500μm and 600μm length MNs. This 100μm may not be large enough to observe a significant difference in SNR. No decline in performance was observed when simulated signals were recorded using wet and MN electrodes over 6 hours. Comparisons between wet, initial MN and bespoke MN electrodes yielded no statistical difference demonstrating that both MN electrodes were comparable to wet electrodes.

v.   Further comparisons between wet electrodes, initial MN electrodes and the bespoke design were conducted in nine healthy volunteers. Each electrode type could record cardiac activity at rest, during simple movement and after 6 hours of wear. Under each condition, SNR comparisons revealed comparable performance between the three electrode designs, however visual assessment of traces highlighted increased motion artifact during activity.

vi. Alongside demographics, volunteer feedback regarding electrode wearability was captured online, using questionnaires. Overall, seven wearability themes were identified. These included ease of application, comfort, wireless connectivity, adhesion, visibility, robustness, and water repulsion. Increased sensations were felt when wearing both MN electrodes with volunteers using words such as 'spiky' and 'prickly' to describe the effects of MNs on their skin. Whilst the performance of both MN electrodes was found to be comparable to the current gold standard, wet electrodes remained the current preference of many volunteers. Therefore, further optimisation of MN electrodes for physiological signal monitoring is warranted.

vii. As part of CALIN, this postgraduate research was partnered with SymlConnect Ltd. In vivo cardiac data acquired throughout this project were shared with SymlConnect Ltd to aid them in the development of a remote clinical system which could be used to monitor cardiovascular health.

APPENDICES

Appendix I: Cardiff School of Pharmacy and Pharmaceutical Sciences Research Ethics Approval

(ref: 1819-15)

SPPS Ethics Approval Notification (EAN)   8/9/14 v12

Cardiff School of Pharmacy and Pharmaceutical Sciences, Research Ethics Approval

This form has been signed by the School Research Ethics Officer as evidence that approval has been granted by the Cardiff School of Pharmacy and Pharmaceutical Sciences Research Ethics Committee for the following study:

Project title:	1819-15: Comparing gel and microneedle electrodes for recording ECGs in human volunteers

This is a/an:	Undergraduate project	
	ERASMUS project	
	Postgraduate project	X
	Staff project	

Name of researcher: (PG/Staff projects only)	Emma Baczkowski
Name of supervisor(s):	James Birchall & Sion Coulman

STATEMENT OF ETHICS APPROVAL

This project has been considered and has been approved by the Cardiff School of Pharmacy and Pharmaceutical Sciences Research Ethics Committee

Signed ███████   Name _M Ivory_   Date _28/05/19__
(Deputy Chair, School Research Ethics Committee)

Appendix II: Recruitment email (ref: 1819-15)

School of Pharmacy and Pharmaceutical Sciences
Redwood Building
Cardiff University
King Edward VII Avenue
Cardiff
CF10 3NB

Recruitment Email

Dear colleague,

I am a PhD student at Cardiff School of Pharmacy and Pharmaceutical Sciences. I am assessing the performance of commercially available wet electrodes with a novel alternative when recording an electrocardiogram (ECG). An ECG is a quick and painless test that records the electrical activity of the heart. The quality of the ECG signal is important and our research wants to improve the way that ECGs are recorded.

Therefore, we would like to test the way that current ECG equipment performs against a novel alternative and so we are looking for healthy volunteers to test this. If you decide to participate then electrodes will be attached to your skin and three, one-minute recordings will be taken using both types of electrode. This will be conducted in a private consultation room and will take approximately forty-five minutes of your time. If you are interested in taking part in this study then please reply to this email, but please note that this does not commit you to taking part.

A participant information leaflet and consent form are attached if you require further information and if you have any questions, then please do not hesitate to contact me.

Best wishes,
Emma Baczkowski
PhD student at Cardiff School of Pharmacy and Pharmaceutical Sciences

Email: BaczkowskiEL@cardiff.ac.uk
Supervised by: Professor James Birchall (BirchallJC@cardiff.ac.uk) and Dr Sion Coulman (CoulmanSA@cardiff.ac.uk).

Appendix III: Consent form (ref: 1819-15)

School of Pharmacy and Pharmaceutical Sciences
Redwood Building
Cardiff University
King Edward VII Avenue
Cardiff
CF10 3NB

Consent Form

You are being asked to participate in a research study. To decide if you want to be a part of this study, you should understand enough information about its risks and benefits to make an informed choice. Once you have read the information leaflet you will be asked to sign this form if you wish to participate. Please read the following statements and circle the boxes next to the statements for which you give consent.

Participant Consent	
1. I confirm that I have read and understood the information sheet dated 16/05/2019 (version 2.0) for the above study. I have had the opportunity to consider the information, ask questions and have had these answered satisfactorily.	Yes / No
2. I understand that my participation is voluntary and that I am free to withdraw at any time, without giving a reason, and without my medical care or legal rights being affected.	Yes / No
3. I consent to the recording of data for research purposes.	Yes / No
4. I consent to localised images being taken of my skin before and after the application of electrodes for research purposes.	Yes / No
5. I understand that if the data are used for research presentations, posters or journal publications, my identity will not be disclosed.	Yes / No
6. I understand that the information collected about me will be used to support other research and I consent to my anonymised data being shared with SymlConnect Ltd. for the purpose of developing a method for assessing heart signals.	Yes / No
7. I understand that the ECG recording will be reviewed by a clinician, Dr Peter O'Callaghan, within 28 days and I will be contacted should a problem be identified.	Yes / No
8. I have informed the researcher about allergies and that I do not have any known skin or heart related conditions.	Yes / No
9. I agree to take part in the above study.	Yes / No
Please provide one method of directly contacting you. You will only be contacted if an unexpected abnormality is detected. You will not be contact if your ECG is normal. **Contact email/number**……………………………………………………………………………………..	

Please sign and date the consent form below	
Name of Participant:	Date:
Signature:	

Name of Researcher:	Date:
Signature:	

Appendix IV: Participant information leaflet (ref: 1819-15)

School of Pharmacy and Pharmaceutical Sciences
Redwood Building
Cardiff University
King Edward VII Avenue
Cardiff
CF10 3NB

Participant Information Sheet

You are invited to partake in a research study. Before you decide whether or not to participate it is important for you to understand why the research is being done and what is involved. We would appreciate it if you could take the time to read the following information. You can then decide whether you would like to take part?

What is the purpose of the study?

An electrocardiogram (ECG) is a simple test which records the electrical activity of your heart. It is often used alongside other tests to help clinicians such as doctors diagnose and monitor conditions affecting the heart. The quality of the ECG recording is important because additional signals could result in misinterpretation. These sorts of additional signals can occur from movement and different methods of recording have different signal qualities. This project aims to record the electrical activity of your heart using commercially available sticky pad electrodes and a novel alternative electrode using microneedles. We will then compare the quality of the signal we get from these different electrodes.

What are microneedle electrodes?

Microneedles are tiny needles which are grouped together in a large number and are designed to be applied to the skin like a patch. They were originally developed to help deliver medicines across the skin. Microneedles are considered painless because they do not go deep enough to touch nerves or damage blood vessels. When the microneedles are covered in a conductive metal such as gold, they can pick up signals from your body such as the electrical activity of your heart. When pressed onto the skin's surface, the needles can cross the outer layer of the skin and reach underlying layers which are considered more conductive. This means that there is the potential to improve the ECG signal that we record.

Do I have to take part?

No, the decision to take part is up to you. If you decide to participate you will be asked to sign a consent form at the start of the project and you will have three days to complete and return it if you wish to be involved. You will also be provided with a copy of this information sheet for your records.

Your participation in this study is entirely voluntary, and you are free to withdraw from the study at any time without giving a reason. Your decision will not affect any future treatment or care in any way. The decision to participate will not negatively affect employment, or (if you are a student), student status or grades.

What will happen to me if I take part?

Before the test, you will be asked to declare if you suffer from any KNOWN allergies, skin or heart related conditions. You will also be asked to sign a consent form and provide one method of directly contacting you.

The entire procedure will be conducted in a private consultation room and will take approximately forty-five minutes. On the day of recording, please wear loose fitting clothing to allow the electrodes to be easily applied. You will be asked to apply three electrodes to your chest. The type of electrode you apply first will be decided randomly. The researcher will be in the room with you to ensure that the electrodes are applied correctly. You will then be asked to lie horizontally on a medical bed to reduce movement.

Each electrode will be connected to a recording device and three 1-minute recordings of your heat will be taken. Following this, the electrodes will be removed, and three further electrodes will be applied, and three additional 1-minute recordings will be taken. If at any point you become uncomfortable, let the researcher know and the electrodes will be removed immediately.

We would also like to take images of your skin both before and after the electrodes have been applied. These images will only capture the small area of skin directly in contact with the ECG pad and will not contain any identifying features. You will be asked for consent for this imaging. All images will be stored securely, and no images will reveal your identity.

Will my taking part in this study be kept confidential?

All personal identifiable information will be kept confidential. Consent forms will be stored within a lockable room at Cardiff School of Pharmacy and Pharmaceutical Sciences.

Only the researcher will have access to this information. Any report or publication arising from this study will not reveal your identity. All handling and processing of your data will comply with the Data Protection Act, 2018.

Cardiff University is the Data Controller and is committed to respecting and protecting your personal data in accordance with your expectations and Data Protection legislation. The University has a Data Protection Officer who can be contacted at **inforequest@cardiff.ac.uk**. Further information about Data Protection, including your rights and details about how to contact the Information Commissioner's Office should you wish to complain, can be found at the following: **https://www.cardiff.ac.uk/public-information/policies-and-procedures/data-protection**.

Under data protection law we have to specify the legal basis that we are relying on to process your personal data. In providing your personal data for this research we will process it on the basis that doing so is necessary for our public task for scientific and historical research purposes in accordance with the necessary safeguards and is in the public interest. The University is a public research institution established by royal charter to advance knowledge and education through its teaching and research activities. The charter can be found on the Cardiff University website. Cardiff University will need to share your anonymised ECG data with Dr Peter O'Callaghan and SymlConnect Ltd for the purposes of this research. Your ECG recording will be reviewed within 28 days by cardiologist, Dr Peter O'Callaghan. After 28 days, your personal data will be anonymised meaning we will remove any identifiers that can identify you from the data you have provided. This anonymous information may be kept indefinitely or published in support of the research. Other personal data we may have collected such as your consent to participate in the study will be kept in accordance with the University Records Retention Schedules.

You have a number of rights under data protection law and can find out more about these on the Cardiff University website. Note that your rights to access, change or move your personal data are limited, as we need to manage your personal information in specific ways in order for the research to be reliable and accurate. If you withdraw from the study, we will keep the information about you that we have already obtained. To safeguard your rights, we will use the minimum personally identifiable information possible.

What are the possible risks?

The microneedles are minimally-invasive so there is very little risk to you. The needles are very small and do not reach nerves or blood vessels that are found in the skin. Therefore, the application of the microneedle patch is unlikely to result in any pain or bleeding. When the patch is applied you will feel pressure on you skin similar to when a plaster is applied. Patches covered with microneedles have been described as feeling similar to a cat's tongue or Velcro when touched. Before the microneedle patches are applied to your skin, they will have been sterilised. These microneedles only pierce the outmost layer of your skin, so the risk of infection is minimal. If at any point you feel uncomfortable, the electrodes will be removed immediately.

An ECG is a quick and painless test. The commercial sticky pad electrodes are non-invasive and are widely used in hospitals to monitor conditions of the heart, brain and muscle. You may experience some slight discomfort when the electrodes are removed from you skin. It is quite similar to removing a plaster. If you are sensitive to some of the materials contained in the adhesives in the electrodes, then some reddening or irritation may occur. It is a rare possibility to observe an allergic reaction. If at any time you become uncomfortable the electrodes will be removed immediately.

Each ECG recording will be reviewed by a cardiologist within 28 days. In the event of detecting an unexpected abnormality, you will be contact by the researcher via the contact method you provide and advised regarding what action you should take. We will be assessing the quality of the recorded signals from each type of electrode. We will not be interpreting the ECGs therefore should a cardiac abnormality be identified you ECG data will still be used in the study. If your ECG is normal, you will not be contacted. Your data will then be anonymised, and identifiable information will be deleted.

What will happen to the results of this research study?

Once reviewed by a clinical cardiologist, Dr Peter O'Callaghan, your <u>anonymised</u> data will be shared with our collaborating partner, SymlConnect Ltd. This partner specialises in developing software for healthcare monitoring and your anonymised numerical data will be used to help contribute to the development of software that is able to assess and monitor heart signals. The results of this project will be written in a thesis and may be put forward in peer-reviewed journals. All information will be anonymised. This means that you will not be identified in the report.

Where will the study take place?

All measurements will be carried out in a private consultation room at Cardiff School of Pharmacy and Pharmaceutical Sciences.

What benefits are there?

There are no direct benefits to you but the results from the study may help contribute towards the goal of creating an alternative to monitoring electrodes with an improve performance?

What will happen if I don't want to carry on with the study?

Please get in touch with us if you no longer wish to be involved with this project. We will make sure that information you have provided will be disposed of securely. This information will also be removed from the results.

What if I have any questions?

If you have any questions about the study, the research or the rights of research subjects, you can contact Emma Baczkowski (BaczkowskiEL@cardiff.ac.uk).

Who has reviewed this study?

This study has been reviewed, and accepted by Cardiff School of Pharmacy and Pharmaceutical Sciences Research Ethics Committee.

Who can I contact to raise concerns or complaints?

If you have any concerns or complaints during the course of this research project, please contact Professor James Birchall (**BirchallJC@cardiff.ac.uk**) who will address the issue. If you remain unhappy and wish to complain formally, you can so this by contacting the Director of Research, Cardiff School of Pharmacy and Pharmaceutical Sciences, Redwood Building, King Edward VII Avenue, Cardiff, CF10 3NB, **phrmyresoffice@cardiff.ac.uk**.

Who to contact to participate in, or further information?

If you have any queries or concerns about the study, please contact Emma Baczkowski (**BaczkowskiEL@cardiff.ac.uk**) at Cardiff School of Pharmacy and Pharmaceutical Sciences.

This is an academic study organised within the pharmacy department. None of the researchers are receiving payment from commercial sources for their work on this project.

Appendix V: MATLAB code for the management of ECG traces obtained from healthy volunteers and subsequent SNR calculation

%% Management of cardiac data recorded from healthy adult volunteers
% Script written by Emma Baczkowski on 16/10/2019.
% Import data prior to using this code.

%% Rename variables, removal of unnecessary rows and data conversion
WE = VarName5 (7:end,:);
% VarName5 renamed as WE (wet electrode) and rows 1-6 have been removed.
MN = VarName3(7:end,:);
% VarName7 renamed as MN (microneedle electrode) and rows 1-6 have been removed.
Time = VarName13(7:end,:);
% VarName13 renamed as Time and rows 1-6 have been removed.
WE = WE/1000;
MN = MN/1000;
% Converts the data from µV to mV.

%% Recreation of the time domain
Fs = 2.5e2;
% When transferring data over Bluetooth, Cyton board samples data at 250Hz.
Num_secs = size(Time,1)/Fs;
% Divide the number of measurements by the sample rate for the total number of seconds.
T = linspace(0,Num_secs, size(Time,1));
% Linear array from 0 to the total number of seconds taken divided into the number of measurements.
T(1:5)
% View what the data looks like.
T=T.';
% Transpose the data from rows to columns.

%%Plotting the initial data
figure
% Creates a new figure.
plot (T,WE,'LineWidth',1,'color',[0 0 1])
% Plots wet electrode with time.
% Seconds (x-axis) and amplitude in mV (y-axis).
hold on
% Allows you to plot cardiac data recorded with microneedle electrodes on the same graph as cardiac data recorded with wet electrodes.

```matlab
plot (T,MN,'LineWidth',1,'color',[1 0 0])
% Plots wet electrode with time.
% Seconds (x-axis) and amplitude in mV (y-axis).

box off
% Removes the box outlining the plot

ylabel ('Amplitude (mV)', 'FontSize', 40, 'FontWeight', 'bold')
% Labels the y-axis with size 40 and bold font.

xlabel ('Time (s)', 'FontSize', 40, 'FontWeight', 'bold');
% Labels the x-axis with size 40 and bold font.

set (gca, 'FontSize', 30);
% Sets size of the aces to 30.

legend('Wet electrode', 'Microneedle electrode');
% Creates a legend which describes the plotted data.
% Write the legend in the order in which you plotted the data.


%%% Removing baseline wander from cardiac signals
% Script written by Emma Baczkowski on 13/03/2019.
% Complete initial management of data prior to filtering.


fWE = highpass(WE, 0.5, Fs);
% Implement a highpass filter with a 0.5Hz cut-off on data recorded using wet electrodes.
fMN = highpass(MN, 0.5, Fs);
% Implement a highpass filter with a 0.5Hz cut-off on data recorded using microneedle electrodes.


%%% Plotting Fast Fourier Transform (FFT)
function [f, P1] = do_FFT(X, Fs, Fmax)
% Simple FFT function originally written by Stephen Grigg and amended by Emma Baczkowski.
% A plot is created with the waveform and the FFT.
T = 1/Fs;
Y = fft(X);
L = length(X);
% Length of signal.


P2 = abs(Y/L);
P1 = P2(1:l/2+1);
P1(2:end-1) = 2*P1(2:end-1);
f = Fs*(0:(L/2))/L;
figure();
X1 = linspace(0,L*T,L).';
```

```
%% Plot FFT
% subplot(2,2,2);
Subplot(2,1,1);
hold;
plot(f,P1)
axis([0 500000 0 max(P1)+0.1*max(P1)]);
ylabel('Magnitude','FontSize',16, 'FontWeight', 'bold');
xlabel('Frequency (Hz)', 'FontSize', 16, 'FontWeight', 'bold');
set(gca, 'FontSize', 16);
box off
axis([0 Fmax 0 max(P1)+0.1*max(P1)]);


%% Plot waveform
Subplot(2,1,2);
Plot(X1,X);
xlabel('Time (s)', 'FontSize', 16, 'FontWeight', 'bold');
ylabel('Amplitude (mV)', 'FontSize', 16, 'FontWeight', 'bold');
set(gca, 'FontSize', 16);
box off
axis([0 max(X1) min(X)+0.1*min(X)+0.1*max(X)]);


end


%% Removing powerline interference from cardiac signals
% Notch filter to remove 50Hz PLI from data - to be used when required.
% Notch filter pre-designed using Filter Designer.

NFWE = filter(IIR, fWE);
% Implement a digital notch filter to remove PLI from data recorded with wet electrodes.
NFMN = filter(IIR, fMN;);
% Implement a digital notch filter to remove PLI from data recorded with microneedle electrodes.


%% Calculating the signal-to-noise ratio (SNR) of cardiac signals
LPWE = lowpass(fWE, 40, Fs);
% Implement a lowpass filter with a 40Hz cut-off to isolate signal (wet electrode).
HPWE = highpass(fWE, 40, Fs);
% Implement a highpass filter with a 40Hz cut-off to isolate noise (wet electrode).
```

```
LPMN = lowpass(fMN, 40, Fs);
```

% Implement a lowpass filter with a 40Hz cut-off to isolate signal (microneedle electrode).

```
HPMN = highpass(fMN, 40, Fs);
```

% Implement a highpass filter with a 40Hz cut-off to isolate noise (microneedle electrode).

% SPWE = signal power of data recorded using wet electrode (manually calculated).

% SPMN = signal power of data recorded using microneedle electrode (manually calculated).

% Six QRS complexes selected and average maximum/minimum values were determined.

% SPWE = maximum(QRS) – (minimum(QRS))

% SPMN = maximum(QRS) – (minimum(QRS))


```
SDWE = std(HPWE);
```

% Calculate the standard deviation (std) of noise (wet electrode).

```
SDMN = std(HPMN);
```

% Calculate the standard deviation (std) of noise (microneedle electrode).

```
NPWE = 4*SDWE;
```

% NPWE = noise power of signals recorded using wet electrodes.

```
NPMN = 4*SDMN;
```

% NPMN = noise power of signals recorded using microneedle electrodes.

```
SPNPWE = SPWE/NPWE;
```

% Signal power divided by the power of noise (wet electrode).

```
SPNPMN = SPMN/NPMN;
```

% Signal power divided by the power of noise (microneedle electrode).

```
SNRWE = 20*log10(SPNPWE);
```

% Calculates the SNR of the signal recorded using wet electrodes.

% SNR(db) = 20log10*(signal power/noise power).

```
SNRMN = 20*log10(SPNPMN);
```

% Calculates the SNR of the signal recorded using microneedle electrodes.

Appendix VI: ECG traces acquired from the baseline comparative study in Chapter 3

Note: all traces have been filtered offline with a 0.5Hz digital high-pass and notch filter.

Volunteer 1: 21-year-old female
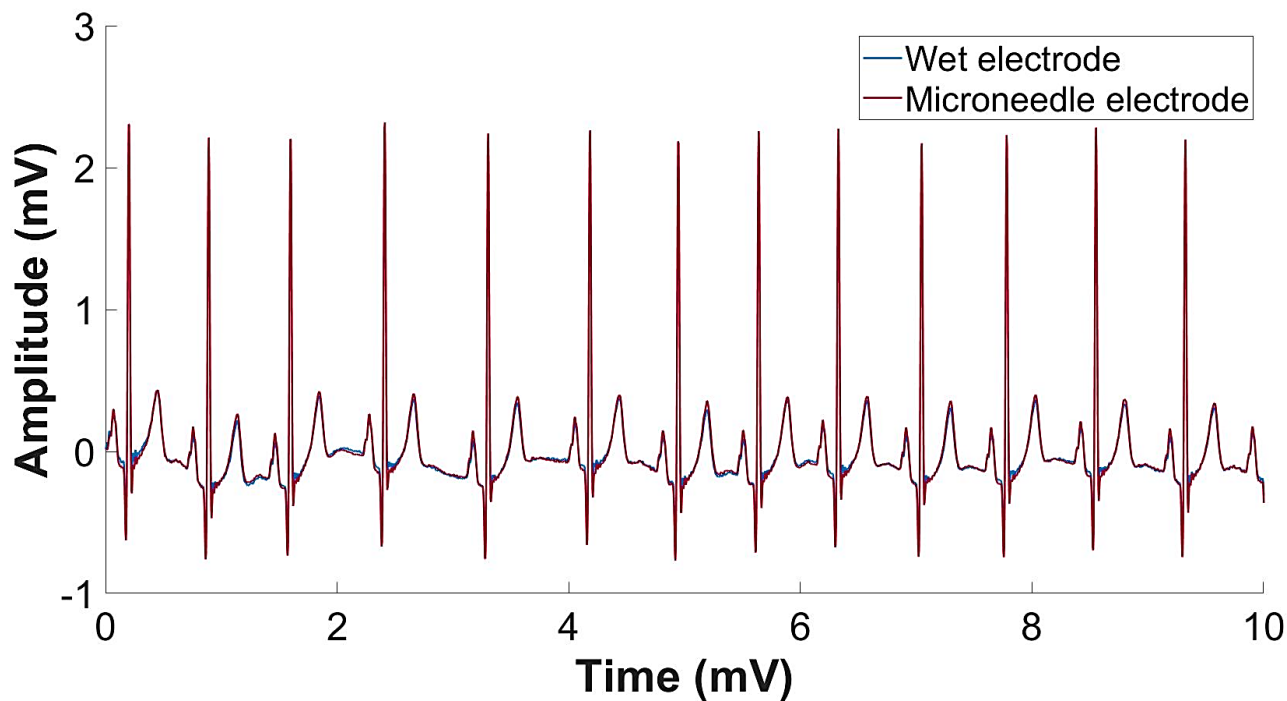
Volunteer 2: 25-year-old male
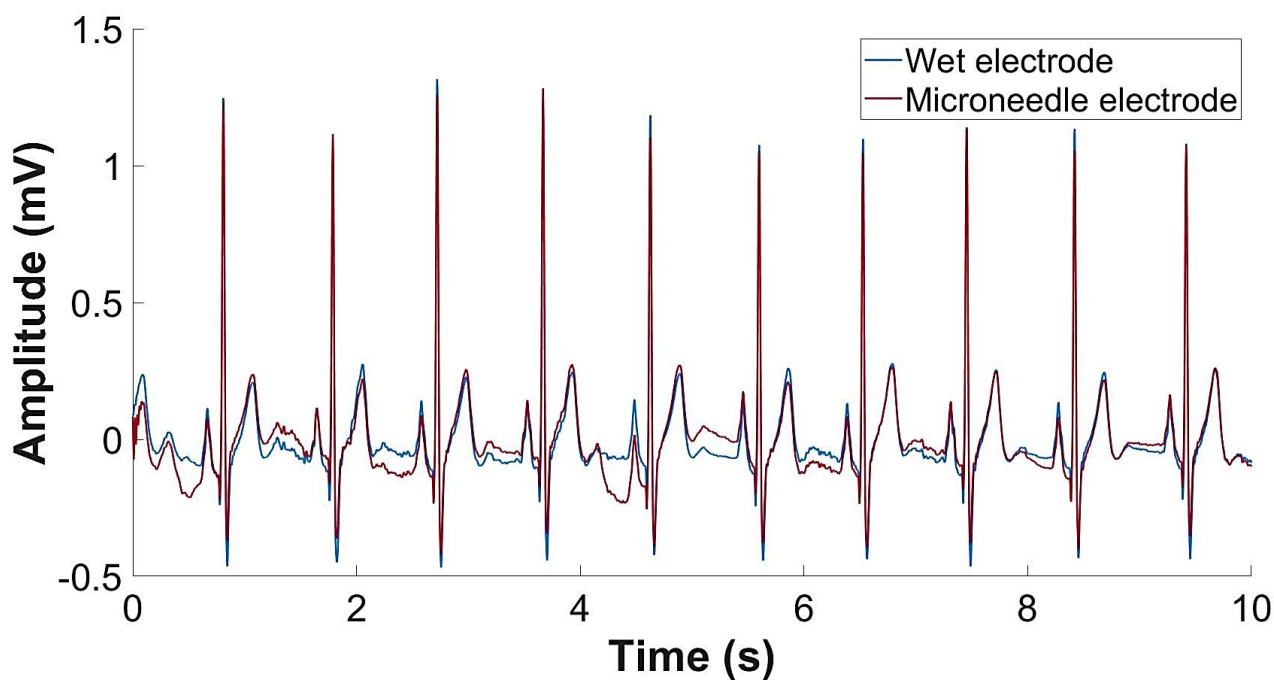
Volunteer 3: 25-year-old male
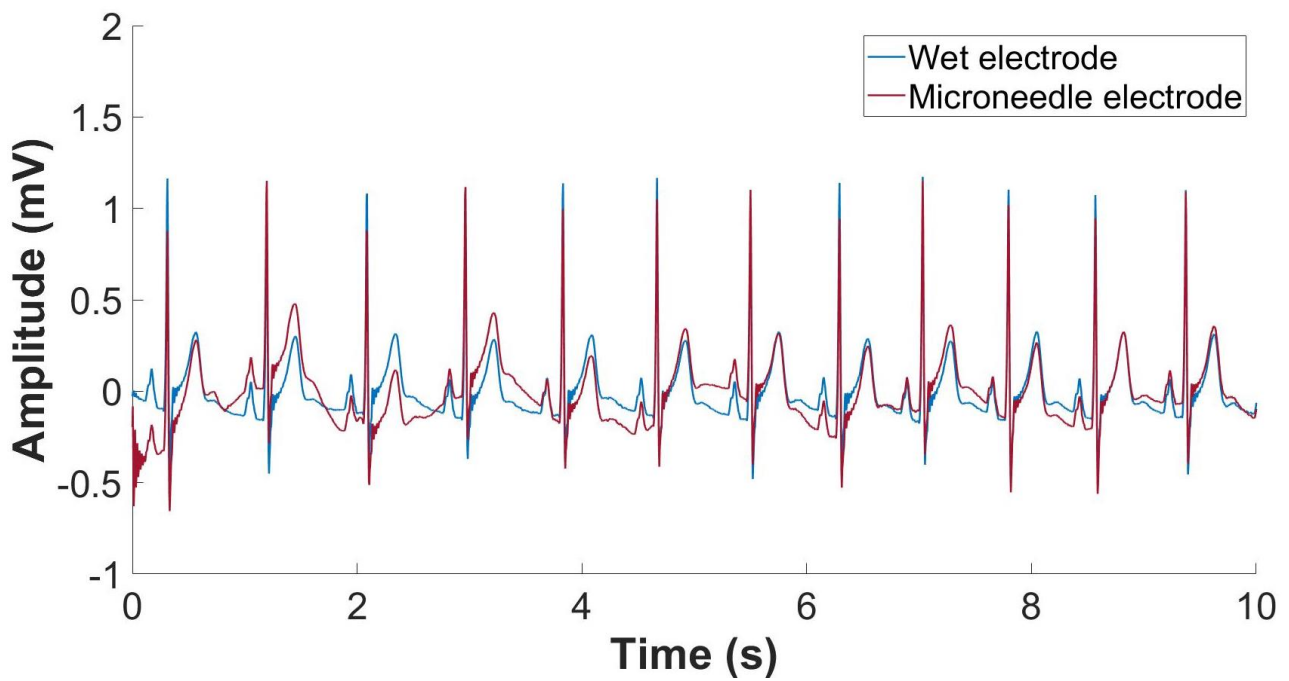
Volunteer 4: 25-year-old female
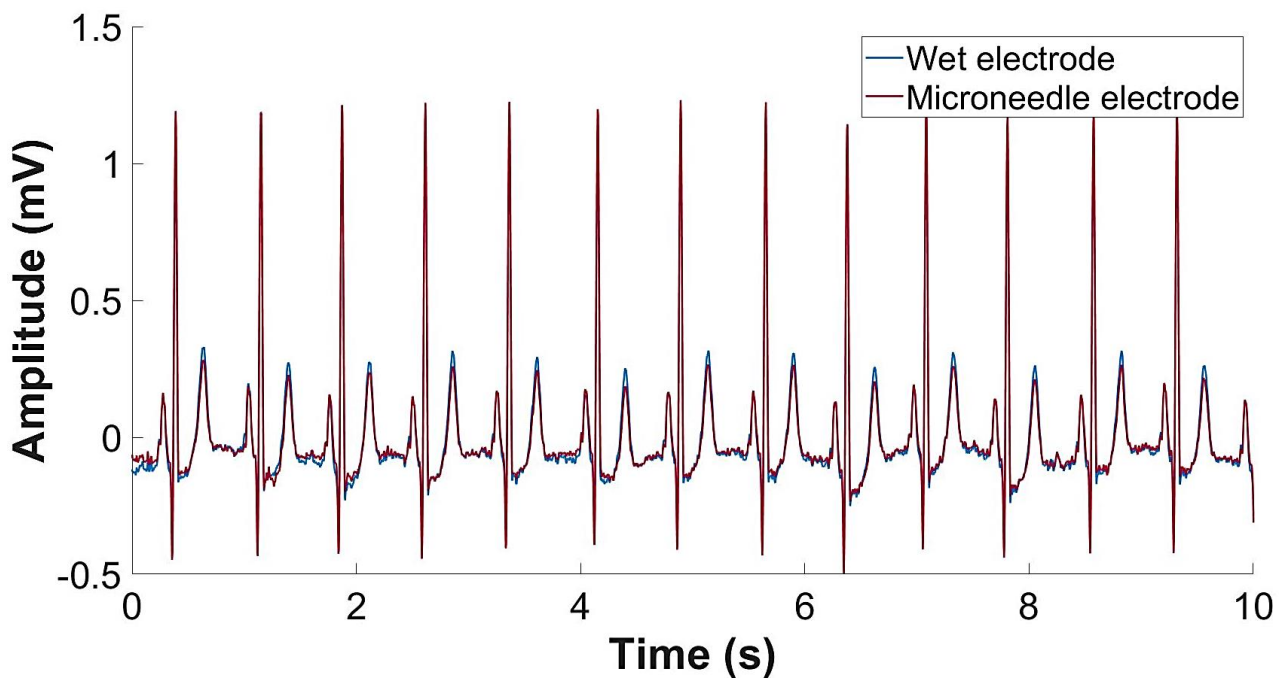
Volunteer 5: 21-year-old female
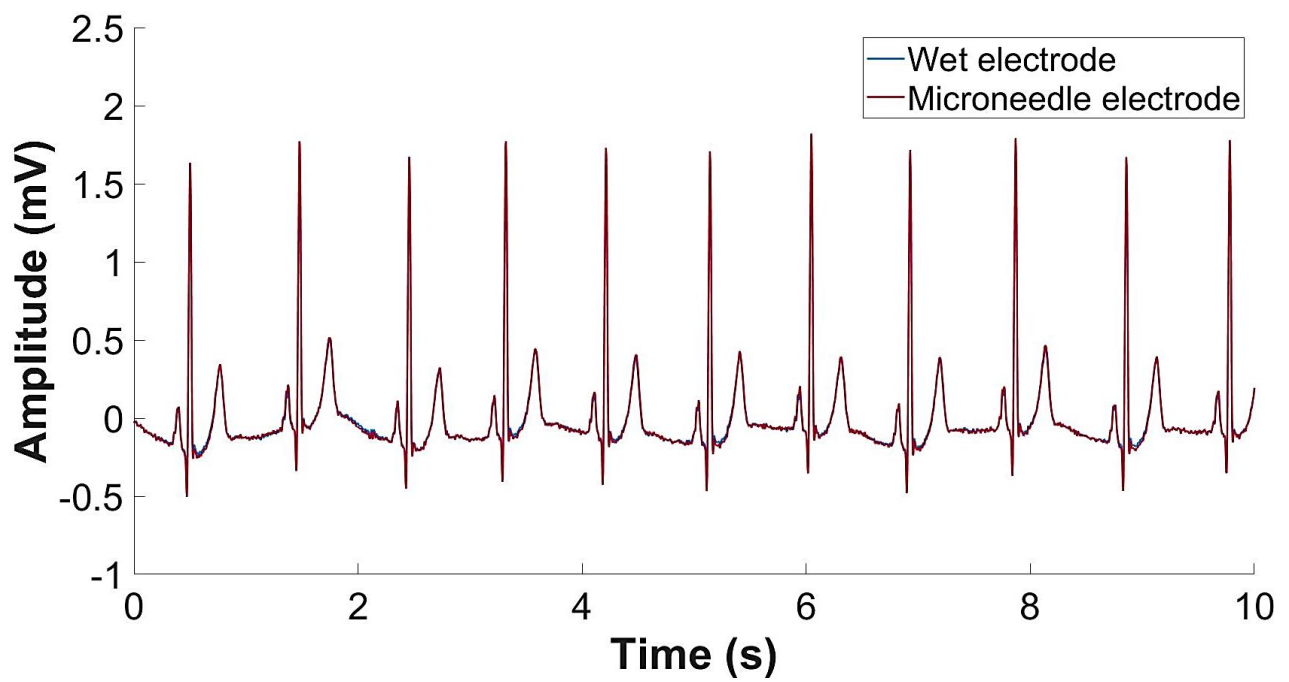
Volunteer 6: 23-year-old male
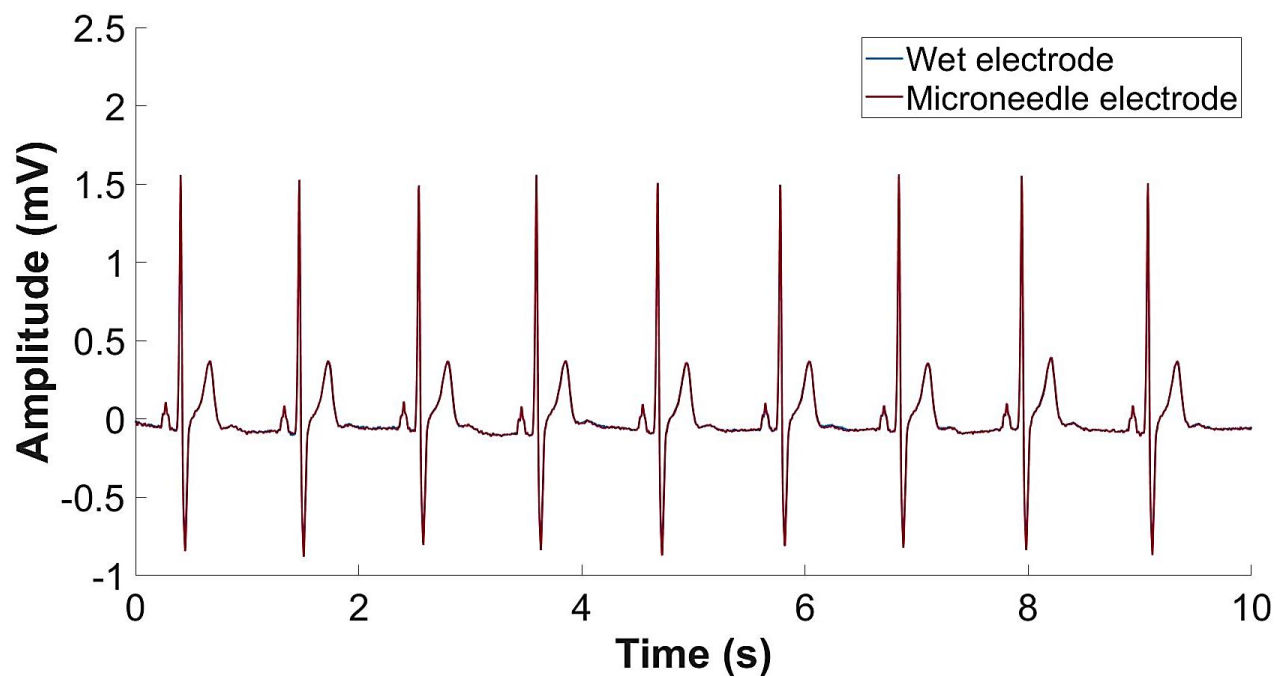
Volunteer 7: 21-year-old male
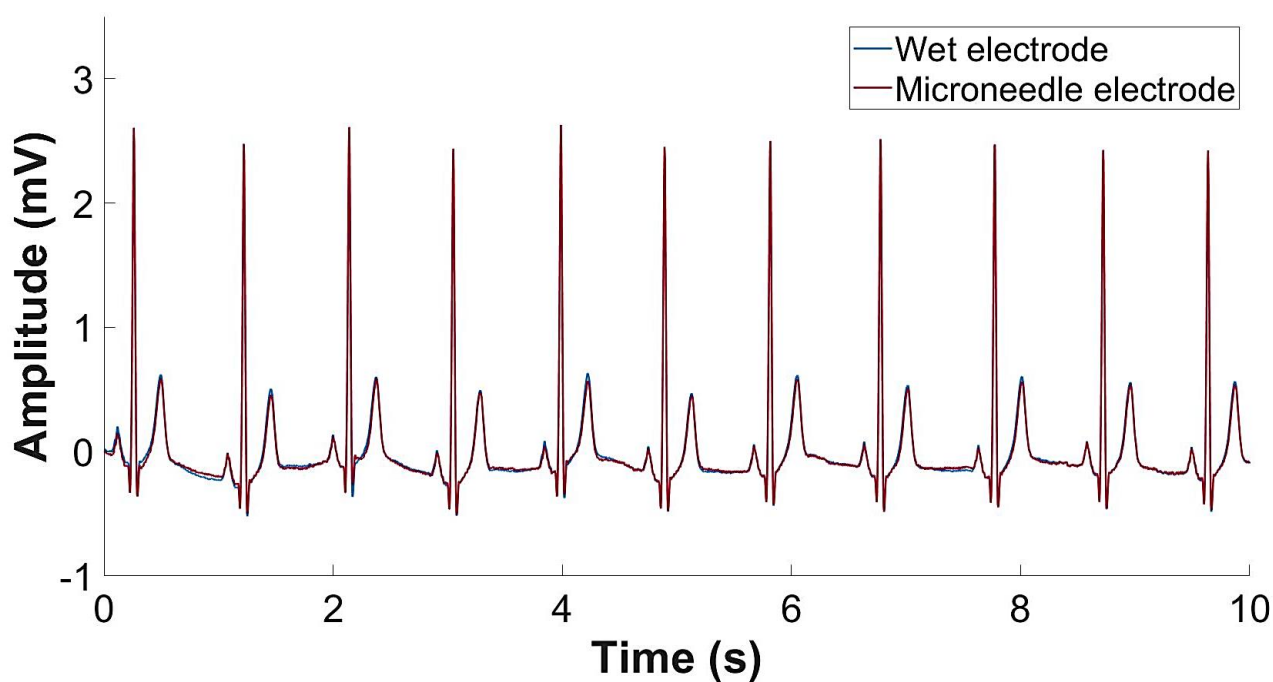
Volunteer 8: 22-year-old female
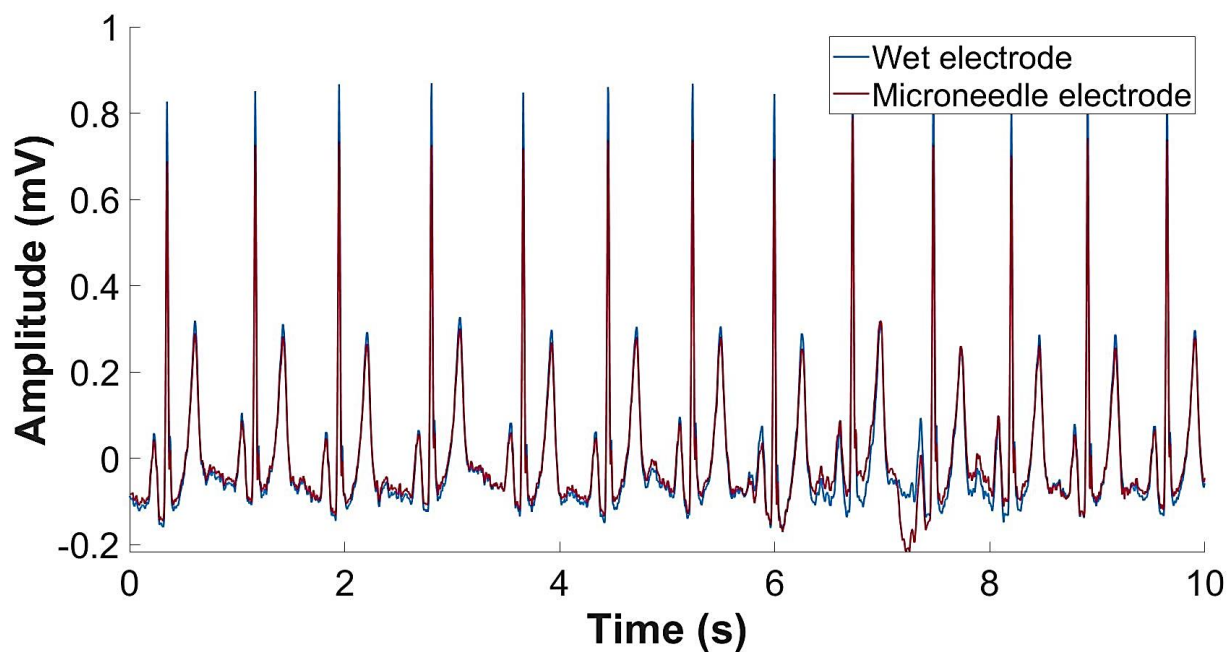
Volunteer 9: 21-year-old female
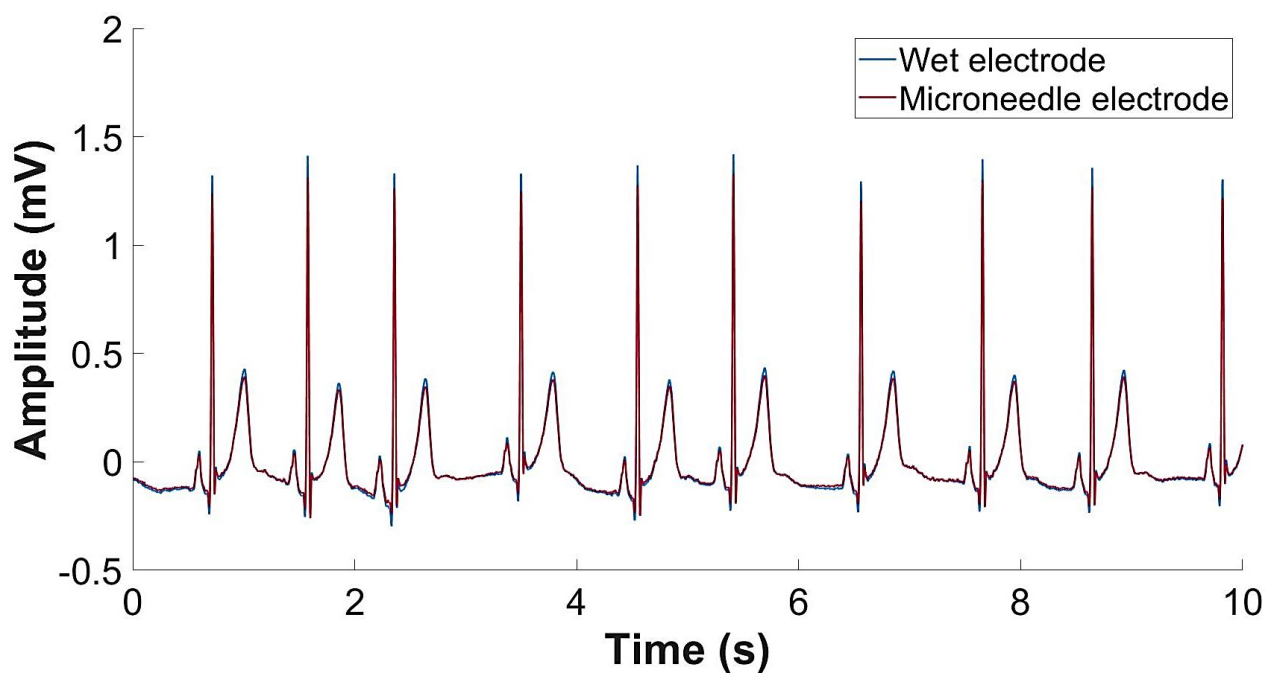
Volunteer 10: 24-year-old male
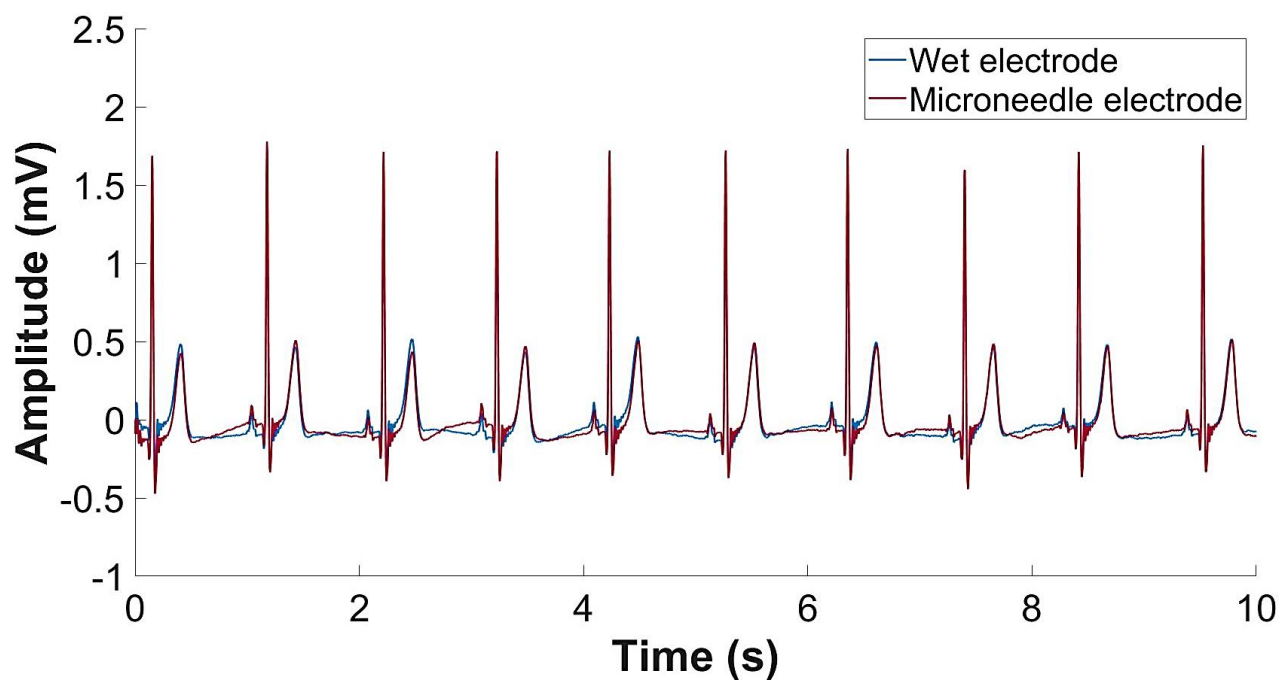
Appendix VII: MATLAB code for the management of <u>simulated</u> ECG traces and calculation of Pearson's correlation coefficient and SNR

```
%% Management and analysis of simulated cardiac data
% Script written by Emma Baczkowski on 13/03/2019 and amended on 16/10/2019.
% Import data prior to using this code.


%% Rename variables, removal of unnecessary rows and data conversion
we = VarName2 (8:end,:);
% VarName2 renamed as we (wet electrode) and rows 1-7 have been removed.
mn = VarName3 (8:end,:);
% VarName3 renamed as mn (microneedle electrode) and rows 1-7 have been removed.
be = VarName4 (8:end,:);
% VarName4 renamed as be (blank electrode) and rows 1-7 have been removed.
cf = VarName5 (8:end,:);
% VarName5 renamed as cf (conductive fabric) and rows 1-7 have been removed.
rd = VarName6 (8:end,:);
% VarName6 renamed as rd (resistor divider) and rows 1-7 have been removed.
wgen = VarName7 (8:end,:);
% VarName7 renamed as wgen (waveform generator) and rows 1-7 have been removed.
Time = VarName13 (8:end,:);
% VarName13 renamed as Time and rows 1-7 have been removed.


%% Converting data from microvolts to millivolts
we = we/1000;
mn = mn/1000;
cf = cf/1000;
rd = rd/1000;
wgen = wgen/1000;


%% Recreation of the time domain
fs = 2.5e2;
% When transferring data over Bluetooth, Cyton board samples data at 250Hz.
Num_secs = size(Time,1)/fs;
% Divide the number of measurements by the sample rate for the total number of seconds.
t = linspace(0,Num_secs, size(Time,1));
% Linear array from 0 to the total number of seconds taken divided into the number of
measurements.
```

```matlab
t(1:5)
% View what the data looks like.
t=t.';
% Transpose the data from rows to columns.

%% Removing unnecessary variables
clear VarName2 VarName3 VarName4 VarName5 VarName6 VarName7 VarName13
clear Time ans Num_secs

%% Plotting Fast Fourier Transform of simulated signals
% Simple FFT function written by Stephen Grigg and amended by Emma Baczkowski.
% A plot is created with the waveform and the FFT.
% FFT = converts a signal from the time domain into a signal in the frequency domain.
% Code used to find peak frequency of powerline interference.

function [f, P1] = do_FFT(X, Fs, Fmax)
T = 1/Fs;
Y = fft(X);
L = length(X);
% Length of signal.

P2 = abs(Y/L);
P1 = P2(1:l/2+1);
P1(2:end-1) = 2*P1(2:end-1);
f = Fs*(0:(L/2))/L;
figure();
X1 = linspace(0,L*T,L).';
%% Plot FFT
% subplot(2,2,2);
Subplot(2,1,1);
hold;
plot(f,P1)
axis([0 500000 0 max(P1)+0.1*max(P1)]);
ylabel('Magnitude','FontSize',16, 'FontWeight', 'bold');
xlabel('Frequency (Hz)', 'FontSize', 16, 'FontWeight', 'bold');
set(gca, 'FontSize', 16);
box off
axis([0 Fmax 0 max(P1)+0.1*max(P1)]);
```

```
%% Plot waveform
Subplot(2,1,2);
Plot(X1,X);
xlabel('Time (s)', 'FontSize', 16, 'FontWeight', 'bold');
ylabel('Amplitude (mV)', 'FontSize', 16, 'FontWeight', 'bold');
set(gca, 'FontSize', 16);
box off
axis([0 max(X1) min(X)+0.1*min(X)+0.1*max(X)]);


end


%%  Normalising signal amplitude
 % Script written by Emma Baczkowski on 13/03/2019.
% Normalisation ensures all elements of the input vector are transformed into the output vector
whose mean is approximately 0 whilst the standard deviation is in a range close to 1.


% Step 1: calculating the standard deviation and mean of the emitted signal.
% Import the file entitled 'Emitted Signal' from the file entitled 'MATLAB Code'.
 x=AmplitudemV(2:end,:);
% Rename variable as x whilst removing the first row which contains a NaN.
stdES=std(x); % Calculates the standard deviation of the emitted signal.
uES=mean(x); % Calculates the mean of the emitted signal.
clear AmplitudemV Times


% Step 2: calculating the standard deviation and mean of the recorded signal
y=n1;
% Rename variable as 'y' as this is the received signal.
stdy = std(y); % Calculates the standard deviation of the recorded signal.
uy = mean(y); % Calculates the mean of the recorded signal.


% Step 3: Normalise and plot the signals (z-score)
% Zy = ((y-uy)/stdy)*stdx+ux (where Z (normalised signal), y (received signal), x (emitted signal), u
(mean) and std (standard deviation)).
% Equation taken from 'System Level Framework for Assessing the Accuracy of Neonatal EEG
Acquisition' (2018).
NRS=(((((y-uy)/stdy)*stdES)+uES);
```

```matlab
figure
% Creates a new figure.
plot(T, NRS)
% Plots a graph of the normalised received signal (millivolts) against time (seconds).
hold on
% Allows you to plot another graph on top of the previous one.
plot(T, x)
% Plots a graph of the emitted signal (millivolts) against time (seconds).
ylabel ('Amplitude (mV)','FontWeight','bold','FontSize',16,'FontName','Arial');
% Labels the y-axis.
xlabel ('Time (Secs)','FontWeight','bold','FontSize',16,'FontName','Arial');
% Labels the x-axis.
Title ('Normalised versus Emitted ECG Trace','FontSize',16,'FontName','Arial');
% Creates a title for the graph.
legend('Normalised Received ECG', 'Emitted ECG');
% Creates a legend which describes the plotted data.
% Write the legend in the order in which you plotted the data.


%%  Calculating signal-to-noise ratio of simulated signal
% x = emitted, original signal
% y = received/recorded signal
noise = x-NRS;
% removes signal and leaves noise
r = snr(x, noise);
% MATLAB function: snr(X, Y) computes the signal to noise ratio (snr) in dB, by computing the
% ratio of the summed squared magnitude of the signal, X, to the summed squared magnitude of the
% noise, Y, where Y has the same dimensions as X.  Use this form of snr when your input signal is
% not sinusoidal and you have an estimate of the noise.
% Code is repeated for remaining n numbers and an average is taken.
```

Appendix VIII: Cardiff School of Pharmacy and Pharmaceutical Sciences Research Ethics
Approval (ref: 2021-11)

Cardiff School of Pharmacy and Pharmaceutical Sciences, Research Ethics Approval

This form has been signed by the School Research Ethics Officer as evidence that approval
has been granted by the Cardiff School of Pharmacy and Pharmaceutical Sciences
Research Ethics Committee for the following study:

Project title:	2021-11: Comparing standard wet electrodes with two novel microneedle electrode designs when recording cardiac signals from healthy volunteers

This is a/an:	Undergraduate project	
	ERASMUS project	
	Postgraduate project	X
	Staff project	

Name of researcher: (PG/Staff projects only)	Emma Baczkowski
Name of supervisor(s):	James Birchall and Sion Coulman

STATEMENT OF ETHICS APPROVAL

**This project has been considered and has been approved by the Cardiff
School of Pharmacy and Pharmaceutical Sciences Research Ethics
Committee**

Signed ████████████   Name R Deslandes   Date 27/04/21
(Chair, School Research Ethics Committee)

Appendix IX: Cardiff School of Pharmacy and Pharmaceutical Sciences Research Ethics Approval
(ref: 2021-11) - Amendment

SPPS Amendment Approval Notification (AAN)   11/10/14 v1

Cardiff School of Pharmacy and Pharmaceutical Sciences, Research Ethics Approval

AMENDMENT APPROVAL
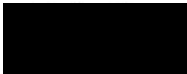
This form has been signed by the School Research Ethics Officer as evidence that approval has been granted by the Cardiff School of Pharmacy and Pharmaceutical Sciences Research Ethics Committee for amendment(s) to the following study:

Project ref and title:	2021-11: Comparing standard wet electrodes with two novel microneedle electrode designs when recording cardiac signals from healthy volunteers.

Name of researcher: (PG/Staff projects only)	Emma Baczkowski
Name of supervisor(s):	James Birchall, Sion Coulman

The amendment(s) dated 21st June 2021 have been reviewed and approved.

Any further amendments will require approval.

STATEMENT OF ETHICS APPROVAL
The proposed amendment(s) have been considered and approved by the Cardiff School of Pharmacy and Pharmaceutical Sciences Research Ethics Committee Signed ███████   Name _M Ivory_   Date _27/07/2021_ (Deputy Chair, School Research Ethics Committee)

Appendix X: Recruitment email (ref: 2021-11)

School of Pharmacy and Pharmaceutical Sciences
Redwood Building
Cardiff University
King Edward VII Avenue
Cardiff
CF10 3NB

Recruitment Email

Dear colleague,

I am a PhD student at Cardiff School of Pharmacy and Pharmaceutical Sciences. I am assessing the performance of commercially available wet electrodes with a novel alternative when recording an electrocardiogram (ECG). An ECG is a quick and painless test that records the electrical activity of the heart. The quality of the ECG signal is important, and our research wants to improve the way that ECGs are recorded.

Therefore, we would like to test the way current ECG equipment performs against two novel alternatives and so are looking for healthy volunteers to test this. Taking part in this study is voluntary. If you do decide to participate then, you will be asked to meet me (socially distanced) in a private consultation room in the Redwood Building and apply three types of electrode to your skin. You will wear the electrodes for up to 24 hours. At the start of this 24-hour period initial recordings of your heart will be taken when you are at rest and during a simple movement. You will also be asked to return to the consultation room after six hours of wear for another recording. The following day (after 24 hours of wear) you will make a third, and final visit to the consultation room. At this time we will you to complete a questionnaire regarding your experience of wearing the electrodes. All ECG recordings will be conducted in a private consultation room.

We would like to reassure you that all COVID-safe practices will be followed, in line with the Welsh Government and University guidelines that you are currently adhering to (Phase 3 guidance for return to the Redwood Building). If you decide to take part in this study, we will ask that you wear a face covering at all times and if you are unwell or need to self-isolate on the day of the study then you should inform us by email and not attend. A participant information sheet and consent form are attached if you require further information.

If you are interested in taking part in this study then please reply to this e-mail, but please note that this does not commit you to taking part. In the meantime, if you have any questions, please do not hesitate in contacting me.

School of Pharmacy and Pharmaceutical Sciences
Redwood Building
Cardiff University
King Edward VII Avenue
Cardiff
CF10 3NB

Best wishes,

Emma Baczkowski

PhD student at Cardiff School of Pharmacy and Pharmaceutical Sciences

Email: BaczkowskiEL@cardiff.ac.uk

Supervised by: Professor James Birchall (BirchallJC@cardiff.ac.uk) and Dr Sion Coulman (CoulmanSA@cardiff.ac.uk).

Appendix XI: Consent form (ref: 2021-11)

School of Pharmacy and Pharmaceutical Sciences
Redwood Building
Cardiff University
King Edward VII Avenue
Cardiff
CF10 3NB

Consent Form

Title: Comparing the wearability and performance of three cardiac monitoring devices.

SREC reference and committee: Cardiff School of Pharmacy and Pharmaceutical Sciences Ethics Committee (Ref: 2021-11).

Name of Principal Investigator(s): Professor James Birchall/Dr Sion Coulman

You are being asked to participate in a research study. To decide if you want to be a part of this study, you should understand enough information about its risks and benefits to make an informed choice. Once you have read the information sheet, you will be asked to sign this form if you wish to participate. Please read the following statements and initial next to the statements for which you give consent.

Statement	Please initial box
I confirm that I have read the information sheet dated 21st June 2021, version 3.0 for the above research project.	
I confirm that I have understood the information sheet dated21st April 2021, version 2.0 for the above research project and that I have had the opportunity to ask questions and that these have been answered satisfactorily.	
I understand that my participation in voluntary, and I am free to withdraw at any time without giving a reason and without my medical care, legal rights, student status or grades being affected. I understand that if I withdraw, information about me that has already been obtained may be kept by Cardiff University.	
I understand that data collected during the research project may be looked at by individuals from Cardiff University or from regulatory authorities, where it is relevant to my taking part in the research project. I give permission for these individuals to have access to my data.	
I consent to the processing of my cardiac data, images and questionnaire responses for the purposes explained to me. I understand that such information will be held in accordance with all applicable data protection legislation and in strict confidence, unless disclosure is required by law or professional obligation.	
I understand who will access to the personal information will have I provide, how the data will be stored and what will happen to the data at the end of the research project.	

CARDIFF UNIVERSITY
PRIFYSGOL CAERDYD

School of Pharmacy and Pharmaceutical Sciences
Redwood Building
Cardiff University
King Edward VII Avenue
Cardiff
CF10 3NB

I consent to having localised photographs and scans taken of my skin for the purposes of the research project and I understand how it will be used in the research.	
I understand that the information collected about me will be used to support other research and I consent to my anonymised data being shared with SymlConnect Ltd for the purpose of developing a method of assessing heart signals. I understand that it will not be possible to identify me from this data.	
I understand that my ECG trace will be reviewed by a clinician, Professor Julian Halcox, within 28 days. I understand that my ECG trace will not be used to provide a clinical diagnosis however should an abnormal trace be identified, I will be contacted using the contact method I provide at the start of the study.	
I consent to my anonymised data being shared with clinicians for the purpose of developing a method of assessing heart signals. I understand that it will not be possible to identify me from this data.	
I have informed the researcher about any allergies and that I do not have any KNOWN skin or heart related health conditions.	
I understand how the findings and results of this research project will be written up and published.	
I agree to take part in this research project.	

Please sign and date the consent form below	
Participant name:	Date:
Signature:	

Name of person taking consent:
Role of person taking consent:
Date:
Signature:

PLEASE KEEP A COPY OF THIS CONSENT FORM FOR YOUR RECORDS

Appendix XII: Participant information leaflet (ref: 2021-11)

School of Pharmacy and Pharmaceutical Sciences
Redwood Building
Cardiff University
King Edward VII Avenue
Cardiff
CF10 3NB

Participant Information Sheet

Title: Comparing the wearability and performance of three cardiac monitoring devices.

You are being invited to take part in a research project. Before you decide whether or not to take part, it is important for you to understand why the research is being undertaken and what it will involve. Please take time to read the following information carefully and discuss it with others, if you wish. Thank you for taking the time to read this information leaflet.

1. What is the purpose of this research project?

An electrocardiogram (ECG) is a simple test which records the electrical activity of your heart. It is often used alongside other tests to help clinicians, such as doctors, diagnose and monitor heart conditions. The quality of the ECG recording is important because additional signals could result in misinterpretation. These sorts of additional signals can occur from movement, and different methods of recording have different signal qualities. This research project aims to record the electrical activity of your heart using commercially available sticky pad devices and two alternative designs using microneedles. We will then compare the quality of the signal that we get from these different devices under different conditions.

2. What are microneedles?

Microneedles are tiny needles which are grouped together in a large number and are designed to be applied to the skin like a patch. They were originally developed to help deliver medicines across the skin. Microneedles are considered painless because they do not go deep enough to touch nerves or damage blood vessels. When the microneedles are covered in a metal such as gold, they can pick up signals from your body such as your heartbeat. When pressed onto the surface of the skin the needles can cross the outer layer of your skin and reach the underlying layers which are considered more conductive. This means that there is the potential to improve the signal that we record.

School of Pharmacy and Pharmaceutical Sciences
Redwood Building
Cardiff University
King Edward VII Avenue
Cardiff
CF10 3NB
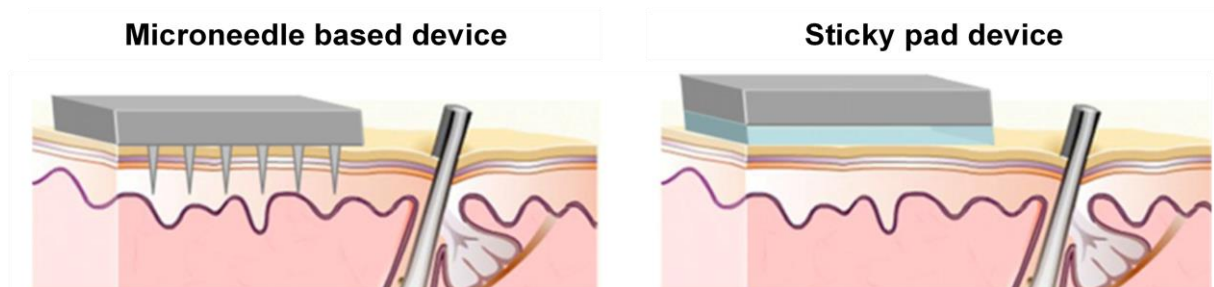
Figure 1: Comparison between a microneedle device which is in close contact with the conductive layers of skin and a sticky pad device which contains a layer of gel to improve the transfer of cardiac signals. Image adapted from Forvi et al. (2012).

3. Why have I been invited to take part?

We are looking for participants, currently working in the Redwood Building (on the Phase 3 rota), to take part in our study to allow us to compare the performance of different types of cardiac monitoring devices.

4. Do I have to take part?

No. Your participation in this research project is entirely voluntary and it is up to you to decide whether or not to take part. If you decide to take part, we will discuss the research project with you and ask you to sign an electronic consent form. If you decide not to take part, you do not have to explain your reasons and it will not affect your legal rights, employment, or if you are a student, student status or grades. You are free to withdraw your consent to participate in the research project at any time, without giving a reason, even after signing the consent form.

School of Pharmacy and Pharmaceutical Sciences
Redwood Building
Cardiff University
King Edward VII Avenue
Cardiff
CF10 3NB

5. What will taking part involve?

Prior to data collection

Before any face-to-face data collection, you will be asked to sign an electronic consent form and email a copy to the researcher. You will be asked to declare if you suffer from any known allergies, skin, or heart related conditions. You will also be asked to provide one contact method. This can be your university email address.

A few days before the study you will receive an email asking you to confirm your COVID-19 status. You will be asked these questions again on the day of recording. We will ask that you wear a face covering at all times. If you are unwell or need to self-isolate on the day of the study then you should inform us by email and not attend. On the day of recording we would ask that you **wear loose fitting** clothing to allow you to easily apply the monitoring devices to your chest. The entire procedure will be conducted in a private consultation room in the Redwood Building.

Day One

You will be asked to meet the researcher (socially distanced) in a private consultation room in the Redwood Building. The first part of this project will take approximately 45 minutes of your time. You will again be asked to confirm your COVID-19 status by answering three questions. Prior to your arrival, all contact areas will have been disinfected. Gloves and handwashing facilities will be available for you to use.

School of Pharmacy and Pharmaceutical Sciences
Redwood Building
Cardiff University
King Edward VII Avenue
Cardiff
CF10 3NB

Day One Continued

Before we ask you to apply the monitoring devices we would like to take photos of your skin to act as a reference. These images will be of the areas of your skin where the monitoring devices will be applied. They will not contain any identifying features. When the researcher is taking photos of your skin, 2m social distancing **will not** be possible. The researcher will be wearing appropriate protective equipment (face covering, visor and gloves) whilst capturing the photos and will not remain in close proximity for long (<5 minutes).

You will then be asked to clean areas of your skin with a non-alcoholic wipe and apply three different types of monitoring device as shown in Figure 2 to your chest. We would ask that you wear loose fitting clothing to allow you to easily apply the monitoring devices. The researcher will be present in the room to provide advice and answer any questions that you may have. If you require further privacy during the process of applying the monitoring devices, please ask, and the researcher will leave the room. Alternatively screens will be made available. Other than when the researcher is taking photographs of your skin, 2m social distancing will be maintained.
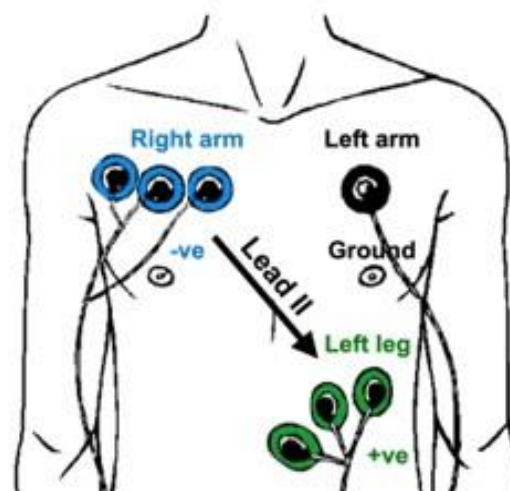
Figure 2: Placement of the three types of cardiac monitoring device used during this project to record the heart's activity whilst at rest, during movement and following a 6-hour wear time.

You will be asked to lie down on a medical bed to help reduce movement. You will then be asked to press down on each device and hold for 30 seconds to make sure that they have attached to your skin. Each monitoring device will be connected to a recording system which will record the activity of your heart whilst you are at rest for a total of 3 minutes.

School of Pharmacy and Pharmaceutical Sciences
Redwood Building
Cardiff University
King Edward VII Avenue
Cardiff
CF10 3NB

Day One Continued

After this, you will be asked to move to a chair where a further 3 minutes of your heart's activity will be recorded whilst you perform the simple movement of sitting to standing. Following this part of the study, the researcher will ask you several questions which will focus on your demographics and initial impression of the cardiac monitoring devices. Upon completion of this part of the questionnaire, you will then be asked to wear all of the devices for six hours, after which we would ask you to return to the consultation room and we will re-record your heart's activity at rest and during simple movement.

After this, you will be able to remove four of the monitoring devices from you skin. Again, we would like to take photos of your skin following the removal of the devices using a camera and device which is similar to ultrasound.

One of each monitoring device will remain attached your chest. We will then ask you to wear these devices to complete a 24-hour period of wear. During this time we would ask if you could avoid showering, bathing or exercising as these devices are not waterproof and heat may affect their ability to stick to your skin. You will be provided with the researcher's contact details should you experience any problems whilst wearing the monitoring devices during this time.

If, at any point you become uncomfortable, let the researcher know and the monitoring devices can be removed immediately. If any of the monitoring devices fall off your skin during the remaining 24-hour period, please do not re-apply them and let the researcher know.

Day Two

The following day we would ask that you return to the consultation room at the same time as the previous day. The remaining 3 monitoring devices can be removed from your skin at this time. The second part of this study will take approximately 30 minutes of your time. Similarly to day one, we would like to take photos of your skin following the removal of the monitoring devices using a camera and a device which is similar to ultrasound. They will not contain any identifying features. When the researcher is taking photos of your skin with a camera, 2m social distancing **will not** be possible. These images will again only capture the small area of skin directly in contact with the device and will not contain any identifying features. All images will be stored securely, and no images will reveal your identity.

The final part of the study will involve the researcher asking you several questions regarding your opinions of wearing the devices for a 24-hour period.

School of Pharmacy and Pharmaceutical Sciences
Redwood Building
Cardiff University
King Edward VII Avenue
Cardiff
CF10 3NB

6. Will I be paid for taking part?

No, you will not be paid for taking part. Taking part in this study is voluntary. You should understand that any data you give will be as a gift and you will not benefit financially in the future should this research project lead to the development of a new device which monitors heart signals.

7. What are the possible benefits of taking part?

There will be no direct advantages or benefits to you from taking part, but your contribution may help contribute towards the goal of creating an alternative cardiac monitoring device with improved performance.

8. What are the possible risks of taking part?

An ECG is a quick and painless test. The commercial sticky pad devices are non-invasive and are widely used in hospitals. You may experience some slight discomfort when the monitoring devices are removed from your skin. It is similar to removing a plaster. If you are sensitive to some of the materials contained in the adhesives in the devices, then reddening or irritation may occur. It is a rare possibility to observe an allergic reaction and we do not anticipate this happening. Should you experience any discomfort or signs of an allergic reaction at any point during the study, including the prolonged wear time of up to 24-hours, please remove the monitoring devices immediately and seek medical attention if treatment is required. Please inform the researcher using the contact details provided to you.

The microneedles used during this research project are minimally invasive, so there is very little risk to you. The needles are very small and do not reach nerves or blood vessels that are found in the skin. Therefore, the application of the microneedle patch is unlikely to result in any pain or bleeding. When you apply the patch, you may feel some pressure on your skin, similar to when a plastic is applied. Patches covered with microneedles have been described as feeling similar to a cat's tongue or Velcro when touched.

School of Pharmacy and Pharmaceutical Sciences
Redwood Building
Cardiff University
King Edward VII Avenue
Cardiff
CF10 3NB

Before the microneedle devices are applied to your skin, they will have been sterilised. You will also be asked to wash your hands prior to their application and clean your skin with a non-alcoholic wipe. These microneedles only pierce the outermost layer of your skin, so the risk of infection is minimal. The microneedles used are made from and coated with material that are compatible with your skin.

If at any point you feel uncomfortable, please let the researcher know and the monitoring devices can be removed immediately.

9. What are the possible risks of taking part?

All information collected from (or about) you during the research project will be kept confidential and any personal information that you provide will be managed in accordance with data protection legislation. Please see below 'What will happen to my Personal Data?' for further information.

Within 28 days of recording, your cardiac data will be reviewed by a consultant cardiologist, Professor Julian Halcox. Your ECG trace will not be used to provide a clinical diagnosis, however, should an abnormal trace be identified, the research team will contact you, using the method you provide at the start of the research project. If an abnormal trace is not clearly identified, you will not be contacted, and your data will be anonymised meaning that we will remove any information that can identify you from the data you have provided.

10. What will happen to my Personal Data?

During this research project we will collect some Personal Data which will be accessed by the researcher. To safeguard your rights, we will use the minimum personally identifiable information possible. Cardiff University is the Data Controller and is committed to respecting and protecting your personal data in accordance with your expectations and Data Protection legislation. Further information about Data Protection including the following may be found at https://www.cardiff.ac.uk/public-information/policies-and-procedures/data-protection.

School of Pharmacy and Pharmaceutical Sciences
Redwood Building
Cardiff University
King Edward VII Avenue
Cardiff
CF10 3NB

Your rights

- The legal basis under which Cardiff University processes your personal data for research
- Cardiff University's Data Protection Policy.
- How to contact the Cardiff University Data Protection Officer.
- How to contact the Information Commissioner's Office.

If you do not have access to the aforementioned information, please contact the researcher and printed or pdf copies will be made readily available.

Under the Data Protection Act we must specify the legal basis that we are relying on to process your personal data. In providing your personal data for this research we will process it on the basis that doing so is necessary for our public task for scientific and historical research purposes in accordance with the necessary safeguards and is in the public interest. The University is a public research institution established by the royal charter to advance knowledge and education through its teaching and research activities. The charter can be found on the Cardiff University website.

Cardiff University will need to share your <u>anonymised</u> ECG data with Professor Julian Halcox and SymlConnect Ltd for the purposes of this research. Your ECG recording will be reviewed within 28 days by consultant cardiologist, Professor Julian Halcox. After 28 days, the research team will anonymise all the personal data it has collected from, or about you, in connection with this research project, with the exception of your consent form. Your consent form will be retained in accordance with the University Records Retention Schedules and may be accessed by members of the research team and, where necessary, by members of the University's governance and audit teams, or by regulatory authorities. Your anonymised data will also be shared with our collaborating partner, SymlConnect Ltd, who will receive the anonymised, password protected data. This data will be stored on their secure server and only accessed by the research team.

School of Pharmacy and Pharmaceutical Sciences
Redwood Building
Cardiff University
King Edward VII Avenue
Cardiff
CF10 3NB

Anonymised information will be kept for the appropriate timeframe in accordance with the University Records Retention Schedules but may be published in support of the research project and/or retained indefinitely, where it is likely to have continuing value for research purposes.

You have a number of rights under data protection law and can find out more about these on the Cardiff University website. Note that your rights to access, change or move your personal data are limited, as we need to manage your personal information in specific ways in order for the research to be reliable and accurate. If you withdraw from the study, we will keep the information about you that we have already obtained. Please note that it will not be possible to withdraw any anonymised data that has already been published or in some cases, where identifiers are irreversibly removed during the course of a research project, from the point at which it has been anonymised.

11. What happens to the data at the end of the research project?
Once reviewed by a consultant cardiologist, Professor Julian Halcox, your anonymised data will be shared with our collaborating partner, SymlConnect Ltd. This partner specialises in the development of software for healthcare monitoring. Your anonymised numerical data will be used to help contribute to the development of software that is able to assess and monitor heart signals. Your data will be stored using their secured sever and only accessed by members of the research team. We will share your anonymised cardiac data with clinicians to receive their input regarding the quality of the traces that we record using the three types of monitor. Please be reassured that any personal data will be removed before any form of sharing takes place.

12. What will happen to the results of the research project?
It is our intention to publish the results of this research project in a PhD thesis, academic journals and present our findings at scientific conferences. Participants will not be identified in any report, publication or presentation.

School of Pharmacy and Pharmaceutical Sciences
Redwood Building
Cardiff University
King Edward VII Avenue
Cardiff
CF10 3NB

13. What if there is a problem?

If you have any concerns or complaints during the course of this research project, please contact Professor James Birchall (BirchallJC@cardiff.ac.uk) who will address the issue. If your complaint is not managed to your satisfaction, please contact the Director of Research, School of Pharmacy and Pharmaceutical Sciences, Cardiff University, Redwood Building, King Edward VII Avenue, Cardiff, CF10 3NB, Wales or via phrmyresoffice@cardiff.ac.uk.

If you are harmed by taking part in this research project, there are no special compensation arrangements. If you are harmed due to someone's negligence, you may have grounds for legal action, but you may have to pay for it.

14. Who is organizing and funding this research project?

This research is organised and led by Professor James Birchall, Dr Sion Coulman and Emma Baczkowski (PhD student) in Cardiff University. The research is currently funded by the Celtic Advanced Life Science Innovation Network (CALIN).

15. Who has reviewed this research project?

This research project has been reviewed and given a favourable opinion by the School of Pharmacy and Pharmaceutical Sciences Research Ethics Committee (SREC), Cardiff University.

16. Further information and contact details

Should you have any questions relating to this research project, you may contact us during normal working hours:

Principal researcher: Emma Baczkowski (PhD Student)

Email: BaczkowskiEL@cardiff.ac.uk

School of Pharmacy and Pharmaceutical Sciences
Redwood Building
Cardiff University
King Edward VII Avenue
Cardiff
CF10 3NB

Address: School of Pharmacy and Pharmaceutical Sciences,

Cardiff University,

Redwood Building,

King Edward VII Avenue,

Cardiff,

CF10 3NB,

Wales.

THANK YOU FOR CONSIDERING TO TAKE PART IN THIS RESEARCH PROJECT. IF YOU DECIDE TO PARTICIPATE, YOU WILL BE GIVEN A COPY OF THIS INFORMATION SHEET AND A SIGNED CONSENT FORM TO KEEP FOR YOUR RECORDS.

User Feedback: Comparing the Wearability of Three Cardiac Monitoring Devices Part I

Title: Comparing standard gel electrodes with two novel microneedle electrode designs when recording cardiac signals from healthy volunteers.

SREC reference and committee: Cardiff School of Pharmacy and Pharmaceutical Sciences Ethics Committee (Ref: to be inserted upon approval)

To be completed on day ONE following the initial recording of the resting and active ECGs

This section will focus on capturing participant demographics which can influence the ECG trace we record in addition to sensations i.e. itching/tingling/discomfort and ease of application of the three cardiac monitoring devices.

Key
Device 1: Gel Electrode
Device 2: Flat Microneedle Electrode
Device 3: Push Button Microneedle Electrode

1. What is your biological sex?

○ Biological female

○ Biological male

○ Prefer not to say

2. What is your current age?

○ 18-24 years

○ 25-34 years

○ 35-44 years

○ 45-54 years

○ 55-64 years

○ 65 years +

○ Prefer not to say

3. What is your ethnic group?

(Please choose one option that best describes your ethnic group or background)

○ White (Welsh/Scottish/Northern Irish/English/British)

○ White (Irish)

○ White (Gypsy or Irish Traveller)

○ Any other White background, please describe

○ Mixed/Multiple ethnic groups (White and Black Caribbean)

○ Mixed/Multiple ethnic groups (White and Black African)

○ Mixed/Multiple ethnic groups (White and Asian)

○ Any other Mixed/Multiple ethnic background

○ Asian/Asian British (Indian)

○ Asian/Asian British (Pakistani)

○ Asian/Asian British (Bangladeshi)

○ Asian/Asian British (Chinese)

○ Any other Asian background, please describe

○ Black/African/Caribbean/Black British (African)

○ Black/African/Caribbean/Black British (Caribbean)

○ Any other Black/African/Caribbean background, please describe

○ Arab

○ Any other ethnic group, please describe.

○ Prefer not to say

4. Do you know your current BMI?

○ Yes

○ No

○ Prefer not to say

5. What is your current BMI?

(Question to be used only if the participant knows their BMI or has calculated it themselves on the day using the scales/stadiometer provided)

6. What is your current height? (Please specify units)

(This question will only be asked if the participant does not know their BMI and consents to the researcher calculating their BMI on their behalf. The value provided will only be used to calculate BMI.)

7. What is your current weight? (Please specify units)

(This question will only be asked if the participant does not know their BMI and consents to the researcher calculating their BMI on their behalf. The value provided will only be used to calculate BMI.)

8. Did you experience any sensations when device number 1 was INITIALLY applied to your skin?

○ Yes

○ No

○ Prefer not to say

9. Please use up to THREE terms to describe any sensations that you felt when device number 1 was INITIALLY applied to you skin.

10. Did you experience any sensations when device number 2 was INITIALLY applied to your skin?

○ Yes

○ No

○ Prefer not to say

11. Please use up to THREE terms to describe any sensations that you felt when device number 2 was INITIALLY applied to you skin.

12. Did you experience any sensations when device number 3 was INITIALLY applied to your skin?

    ○ Yes

    ○ No

    ○ Prefer not to say

13. Please use up to THREE terms to describe any sensations that you felt when device number 3 was INITIALLY applied to you skin.

14. What is your level of agreement with the following statements?

	Strongly disagree	Disagree	Neither agree nor disagree	Agree	Strongly Agree	Prefer not to say
Device 1 was easy to apply.	○	○	○	○	○	○
Device 2 was easy to apply.	○	○	○	○	○	○
Device 3 was easy to apply.	○	○	○	○	○	○

Appendix XIV: Questionnaire Part II

User Feedback: Comparing the Wearability of Three Cardiac Monitoring Devices Part II

Title: Comparing standard gel electrodes with two novel microneedle electrode designs when recording cardiac signals from healthy volunteers.

SREC reference and committee: Cardiff School of Pharmacy and Pharmaceutical Sciences Ethics Committee (Ref: to be inserted upon approval).

To be completed on day TWO following a prolonged wear time of 24 hours

This section will focus on capturing user feedback regarding sensations, device removal, visibility, comfort and acceptability following 24 hours of wearing the three cardiac monitoring devices.

Key
Device 1: Gel Electrode
Device 2: Flat Microneedle Electrode
Device 3: Push Button Microneedle Electrode

1. Did you experience any sensations whilst wearing device number 1 over the 24-hour period?

   ○ Yes

   ○ No

   ○ Prefer not to say

APPENDICES

2. Please use up to THREE terms to describe any sensations that you felt whilst wearing device number 1 over the 24-hour period.

3. Did you experience any sensations whilst wearing device number 2 over the 24-hour period?

○ Yes

○ No

○ Prefer not to say

4. Please use up to THREE terms to describe any sensations that you felt whilst wearing device number 2 over the 24-hour period.

5. Did you experience any sensations whilst wearing device number 3 over the 24-hour period?

   ○ Yes

   ○ No

   ○ Prefer not to say

6. Please use up to THREE terms to describe any sensations that you felt whilst wearing device number 3 over the 24-hour period.

7. Did you remove any of the devices over the 24-hour period?

   ○ Yes

   ○ No

   ○ Prefer not to say

8. Which device or devices did you remove over the 24-hour period?

   (Please select all that apply)

   ☐ Device 1

   ☐ Device 2

   ☐ Device 3

9. Why did you remove this device/these devices?

10. What is your level of agreement with the following statements?

	Strongly disagree	Disagree	Neither agree nor disagree	Agree	Strongly agree	Prefer not to say
I felt self-conscious whist wearing device 1.	○	○	○	○	○	○
I felt self-conscious whist wearing device 2.	○	○	○	○	○	○
I felt self-conscious whist wearing device 3.	○	○	○	○	○	○
Device 1 was comfortable to wear.	○	○	○	○	○	○
Device 2 was comfortable to wear.	○	○	○	○	○	○
Device 3 was comfortable to wear.	○	○	○	○	○	○

APPENDICES

11. Please rank the devices in order of preference.

    (1=most preferred and 3=least preferred)
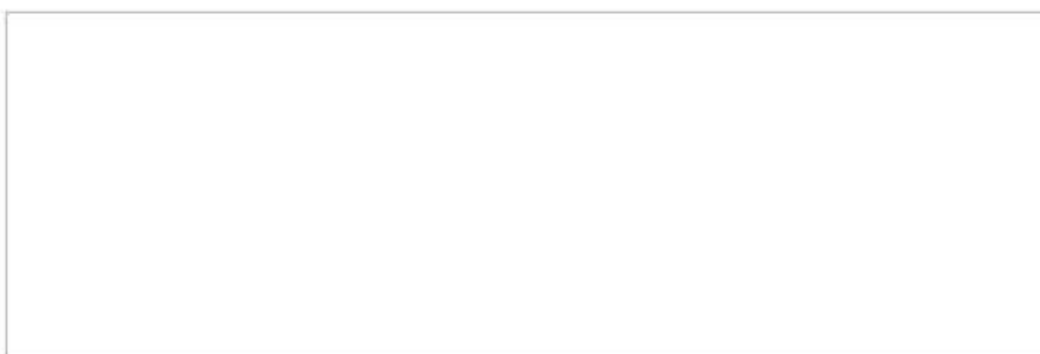
        Device 1

        Device 2
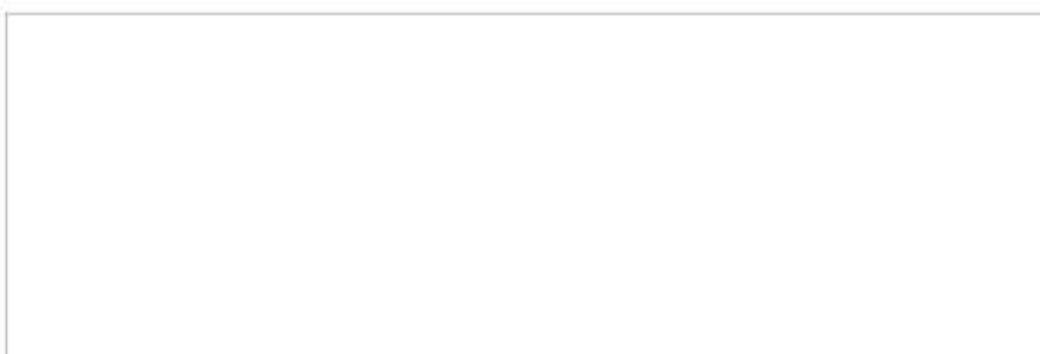
        No clear preference

        Device 3

12. Please explain why you have chosen this device as your most preferred.

13. Please explain why you have chosen this device as your least preferred.

299

14. Would you be prepared to wear device 1 continuously for...

	Yes	No	Don't know	Prefer not to say
1 day	○	○	○	○
1 week	○	○	○	○
1 month	○	○	○	○

15. If you answered no to any of the options in question 14, please explain why.

16. Would you be prepared to wear device 2 continuously for...

	Yes	No	Don't know	Prefer not to say
1 day	○	○	○	○
1 week	○	○	○	○
1 month	○	○	○	○

17. If you answered no to any of the options in question 16, please explain why.

18. Would you be prepared to wear device 3 continuously for...

	Yes	No	Don't know	Prefer not to say
1 day	○	○	○	○
1 week	○	○	○	○
1 month	○	○	○	○

19. If you answered no to any of the options in question 18, please explain why.

20. If you any additional comments regarding the devices, please write them here.

Appendix XV: ECG traces acquired from the electrode comparison study in Chapter 5

Note: all traces have been filtered offline with a 0.5Hz digital high-pass and notch filter.

Volunteer 1: Male (25-34 years)

Resting (0hrs) – x12 gain

Active (0hrs) – x12 gain

Volunteer 1: Male (25-34 years)
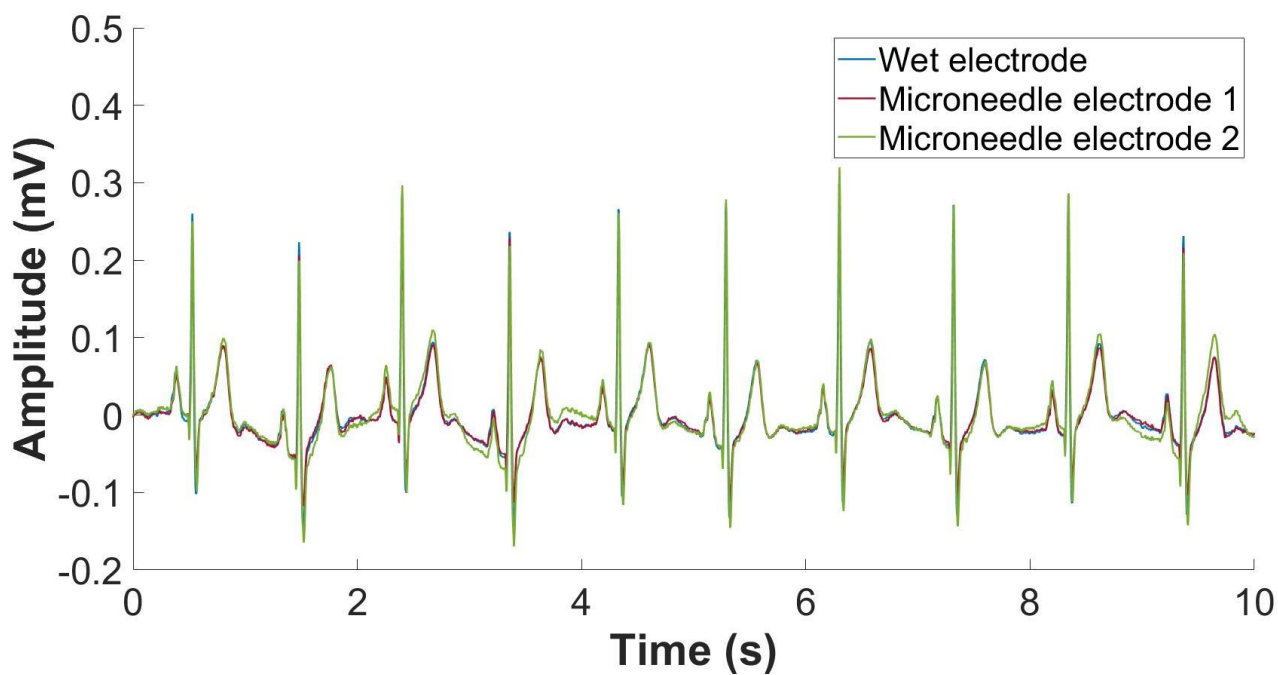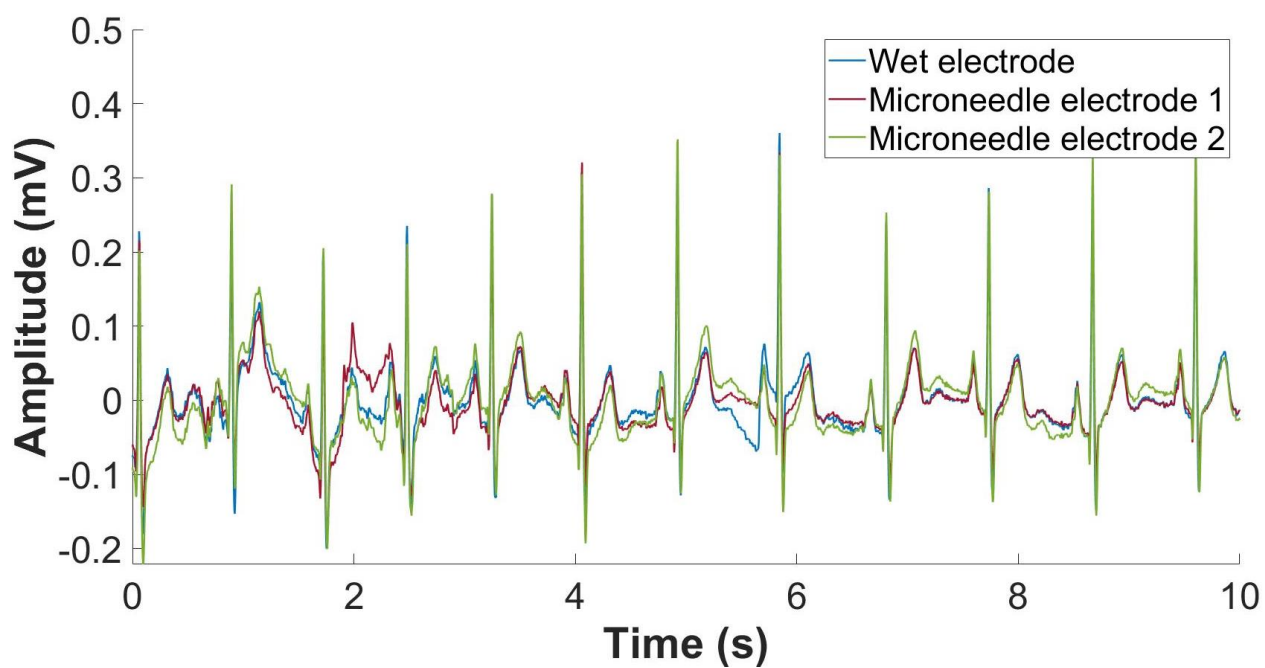
Resting (6hrs) – x12 gain

Active (6hrs) – x12 gain

Volunteer 2: Female (25-34 years)

Resting (0hrs) – x12 gain
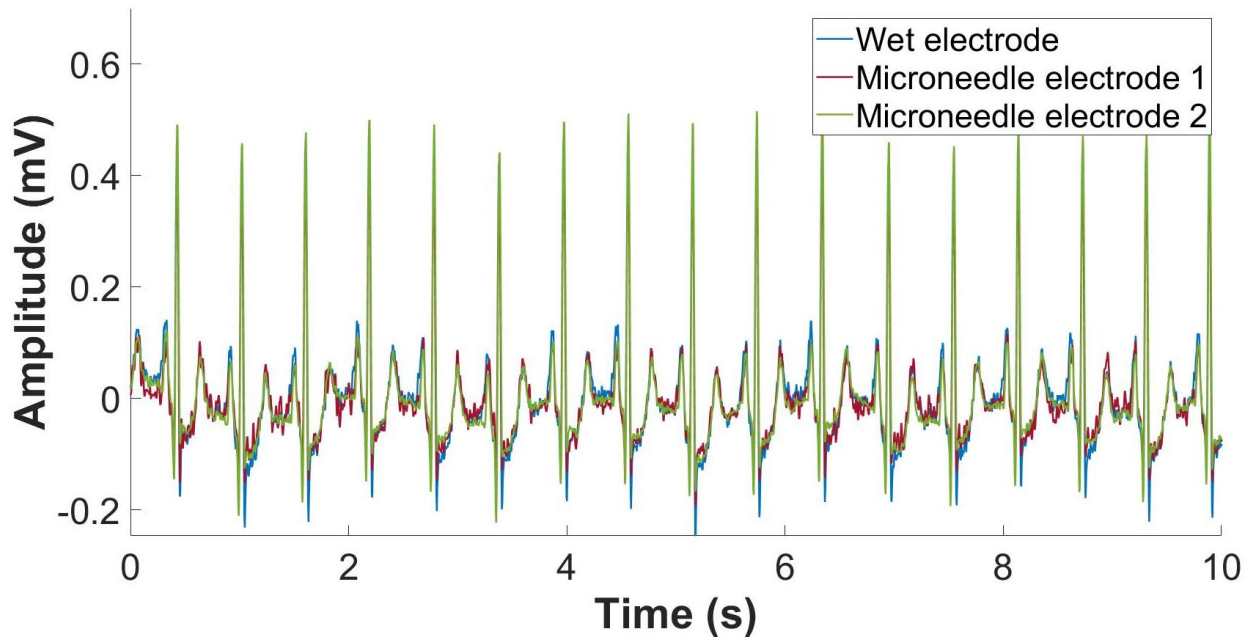
Active (0hrs) – x12 gain
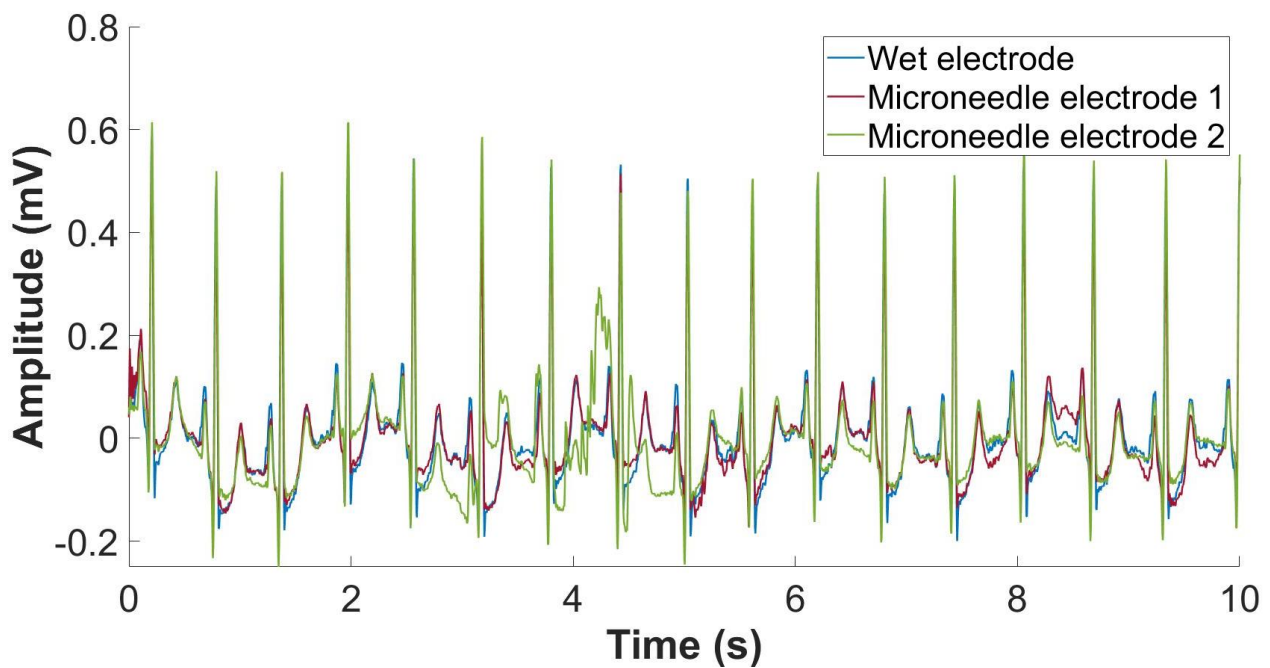
Volunteer 2: Female (25-34 years)

Resting (6hrs) – x12 gain
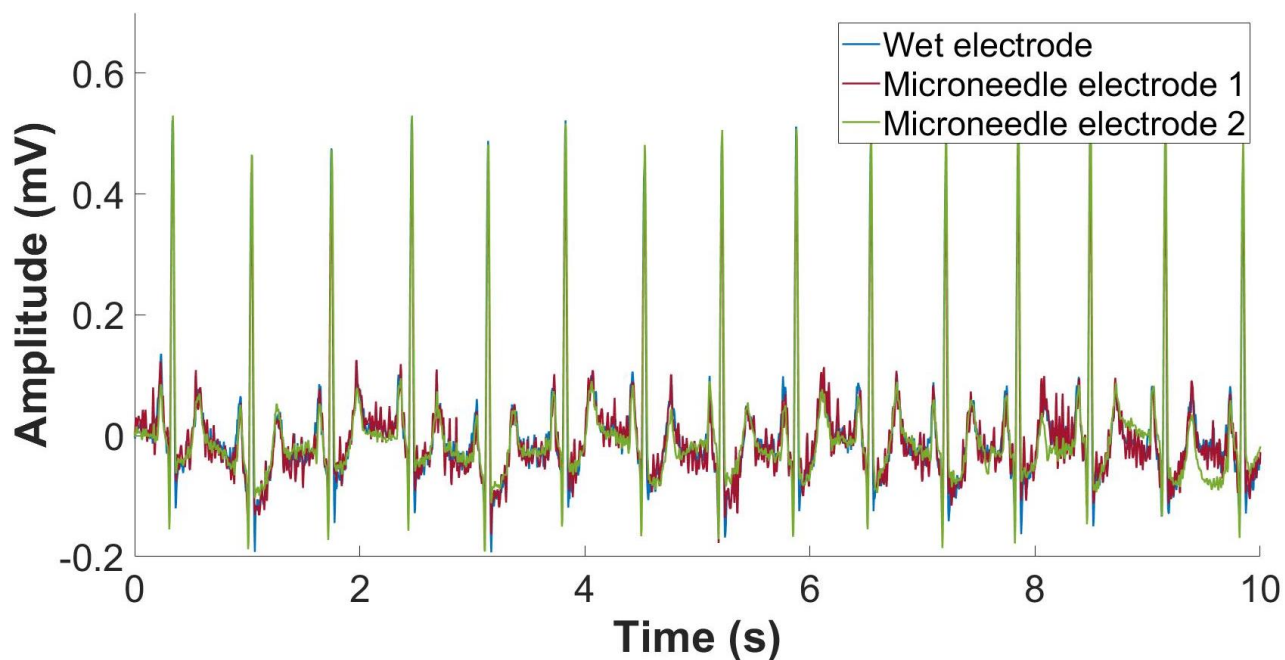
Active (6hrs) – x12 gain
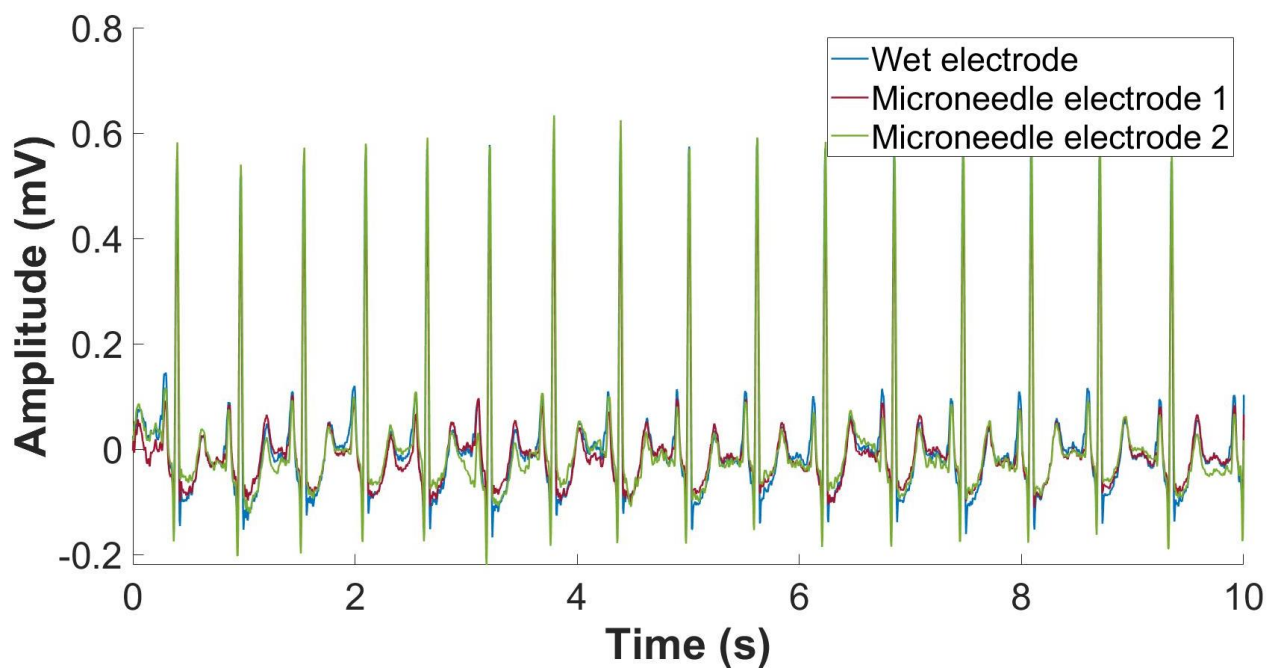
Volunteer 3: Female (55-64 years)

Resting (0hrs) – x12 gain
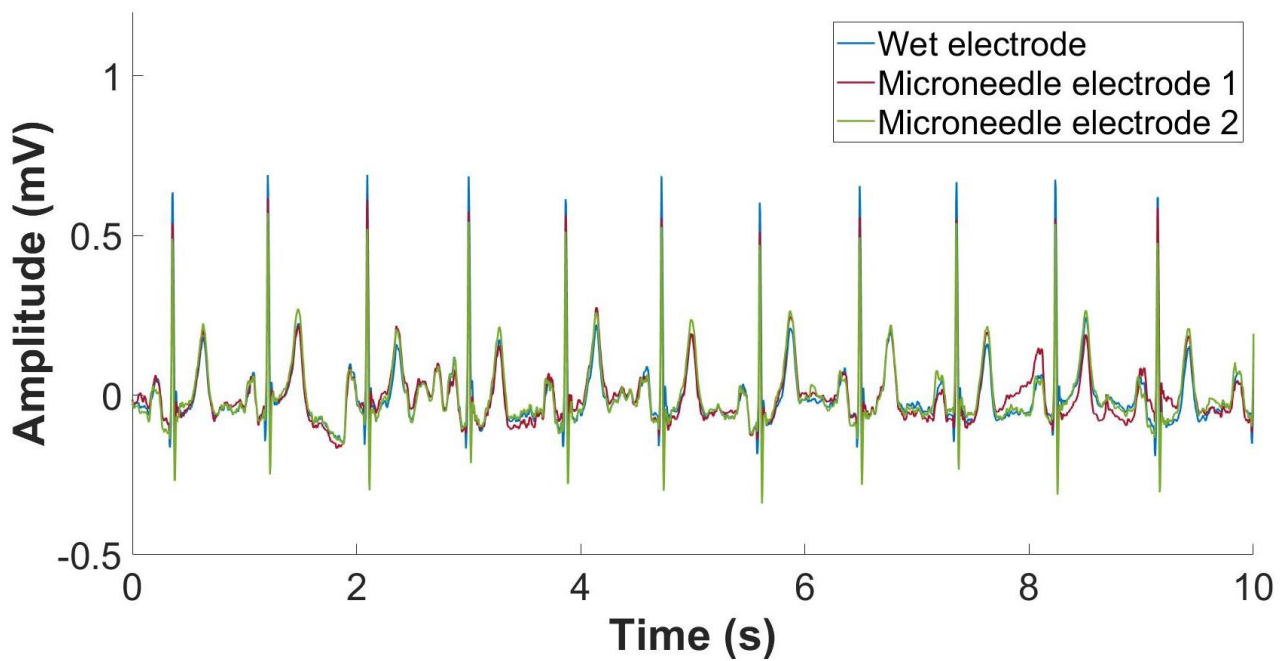
Active (0hrs) – x12 gain
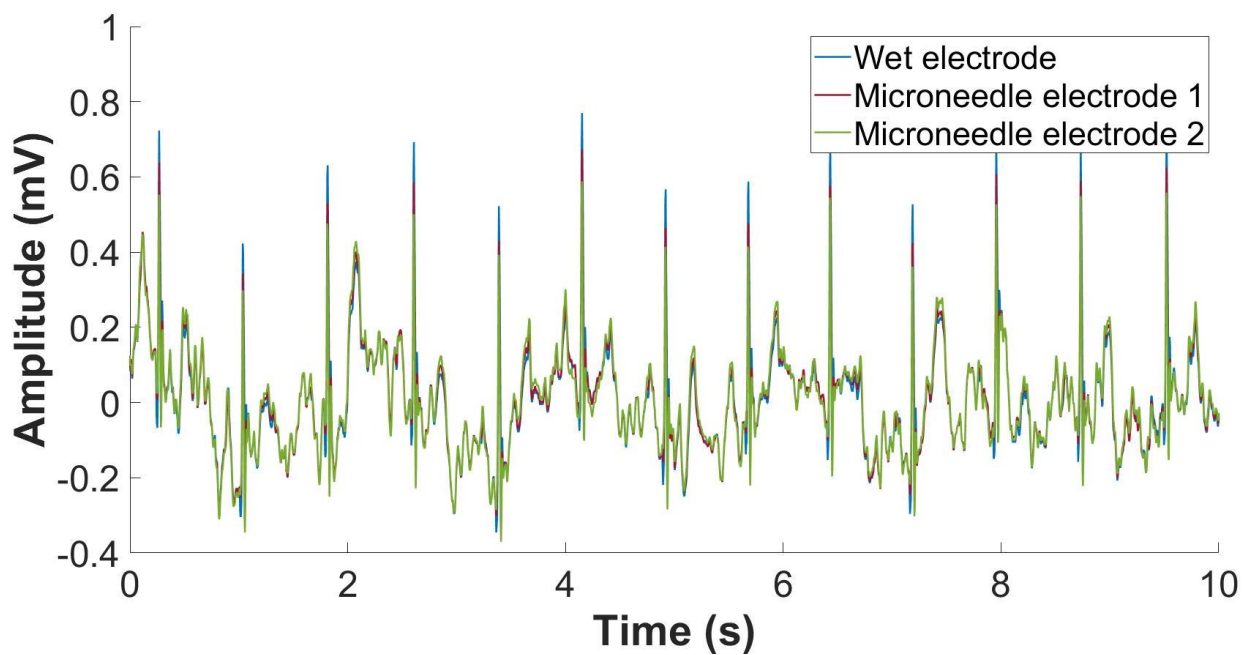
Volunteer 3: Female (55-64 years)

Resting (6hrs) – x12 gain
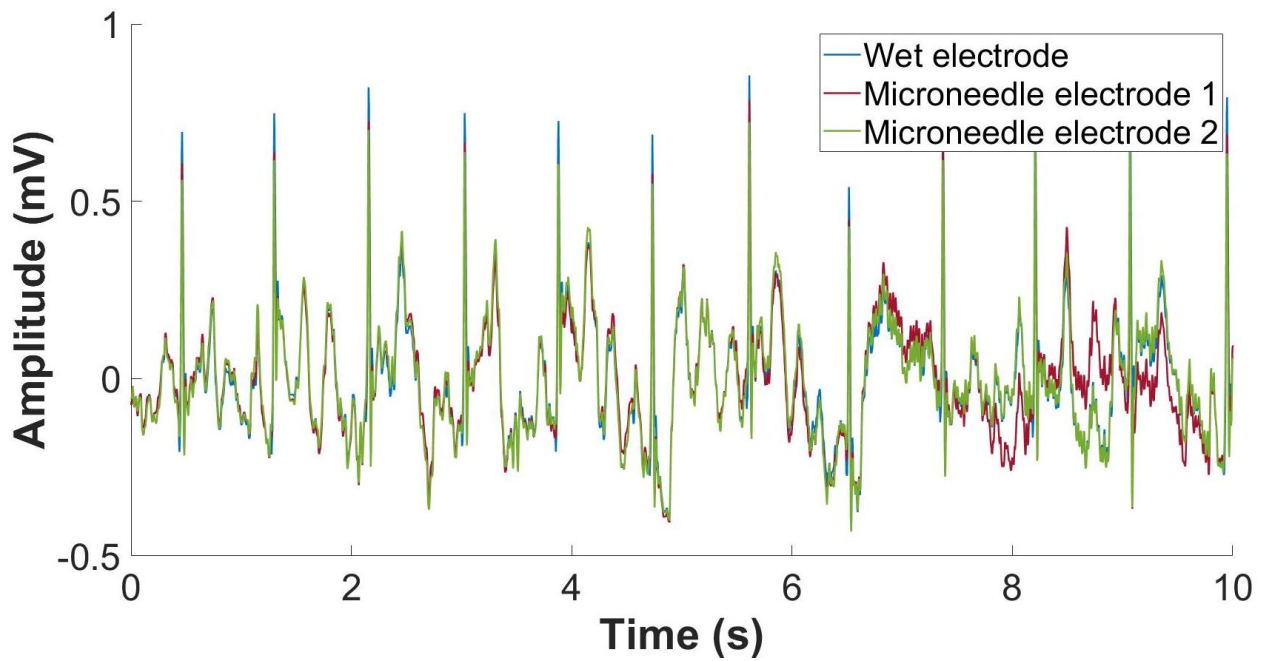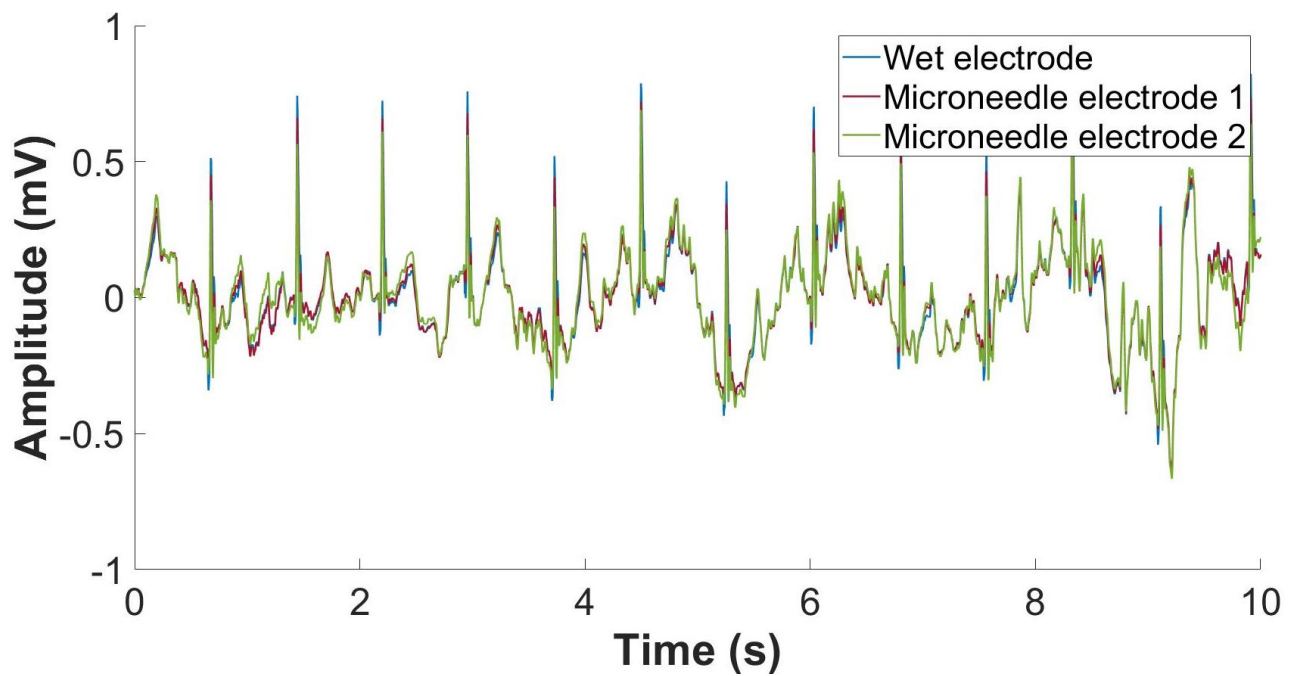
Active (6hrs) – x12 gain

Volunteer 4: Male (35-44 years)

Resting (0hrs) – x12 gain
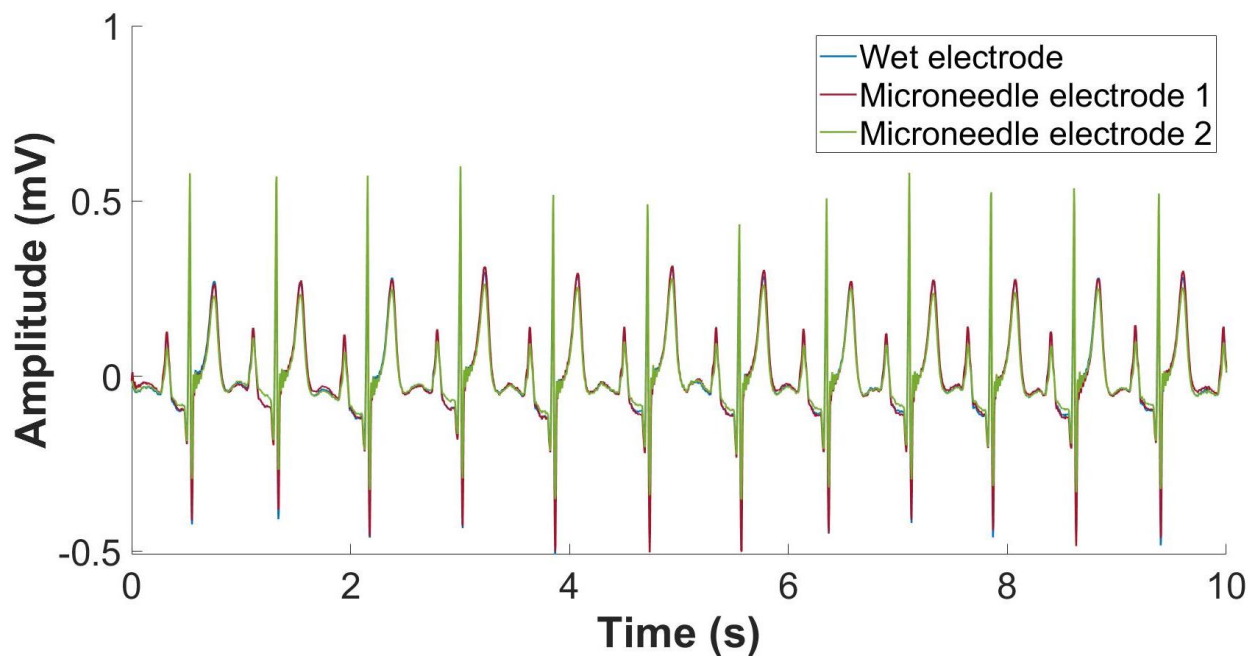
Active (0hrs) – x12 gain
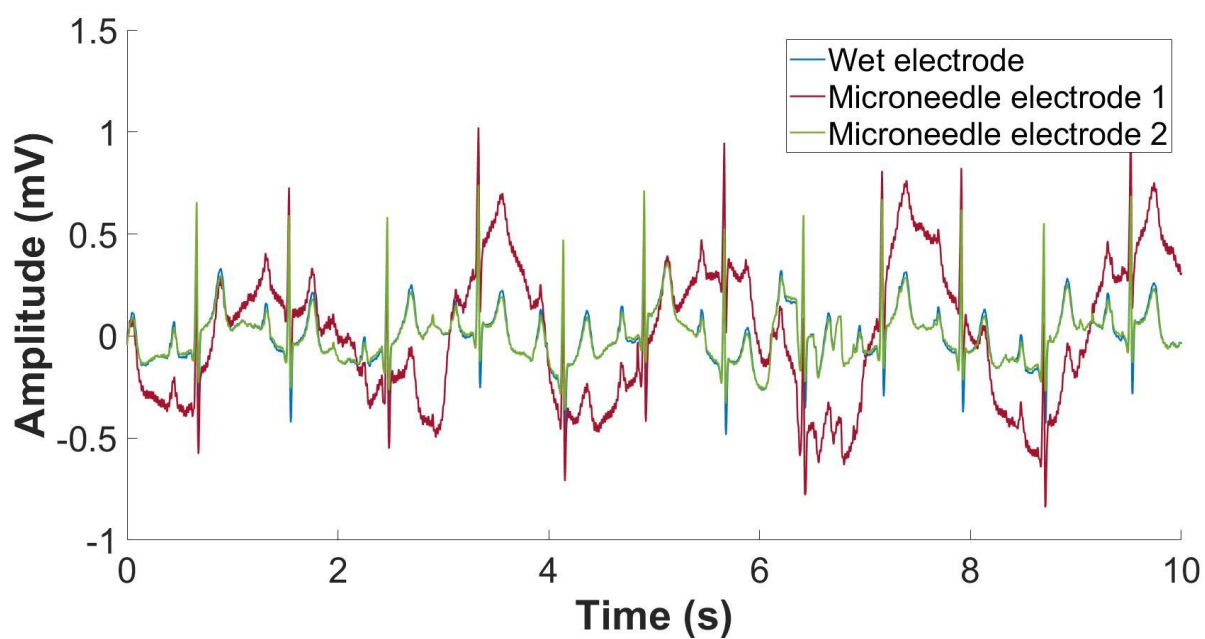
Volunteer 4: Male (35-44 years)

Resting (6hrs) – x12 gain
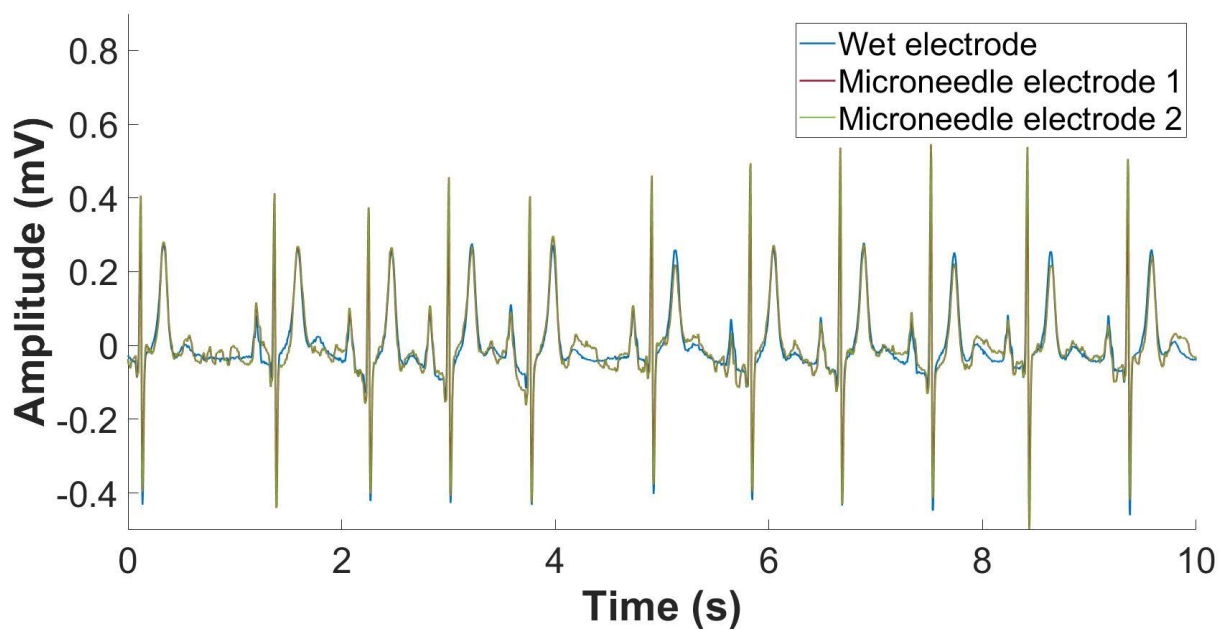
Active (6hrs) – x12 gain
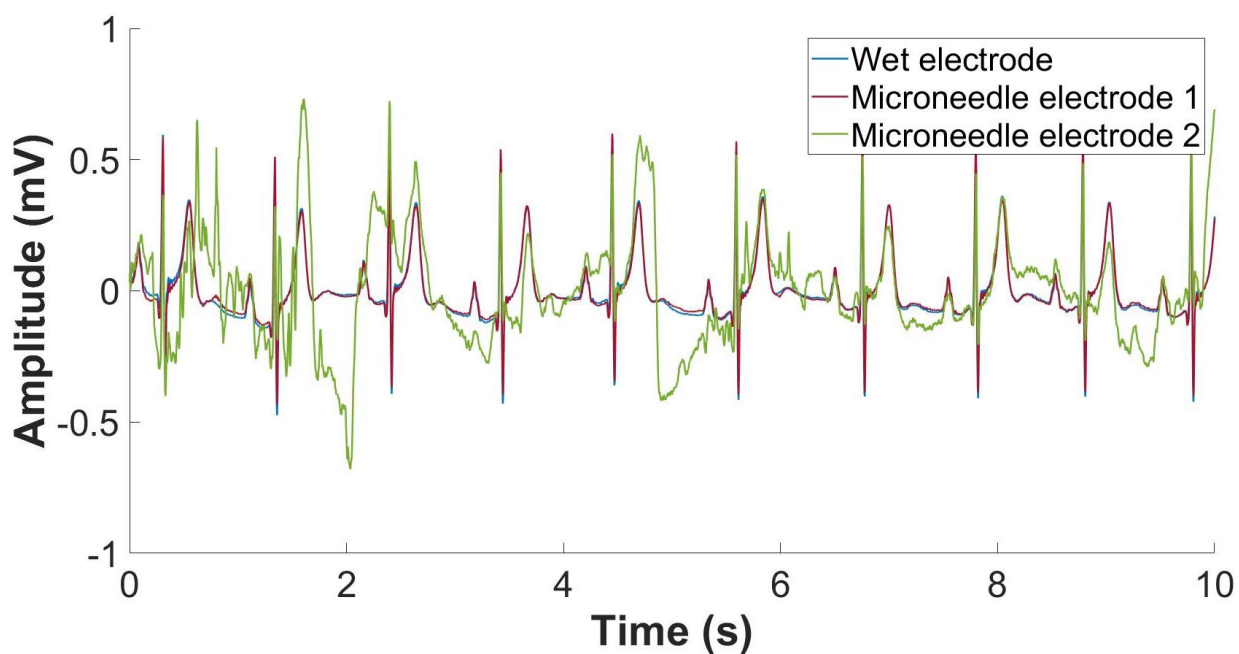
Volunteer 5: Female (45-54 years)

Resting (0hrs) – x12 gain
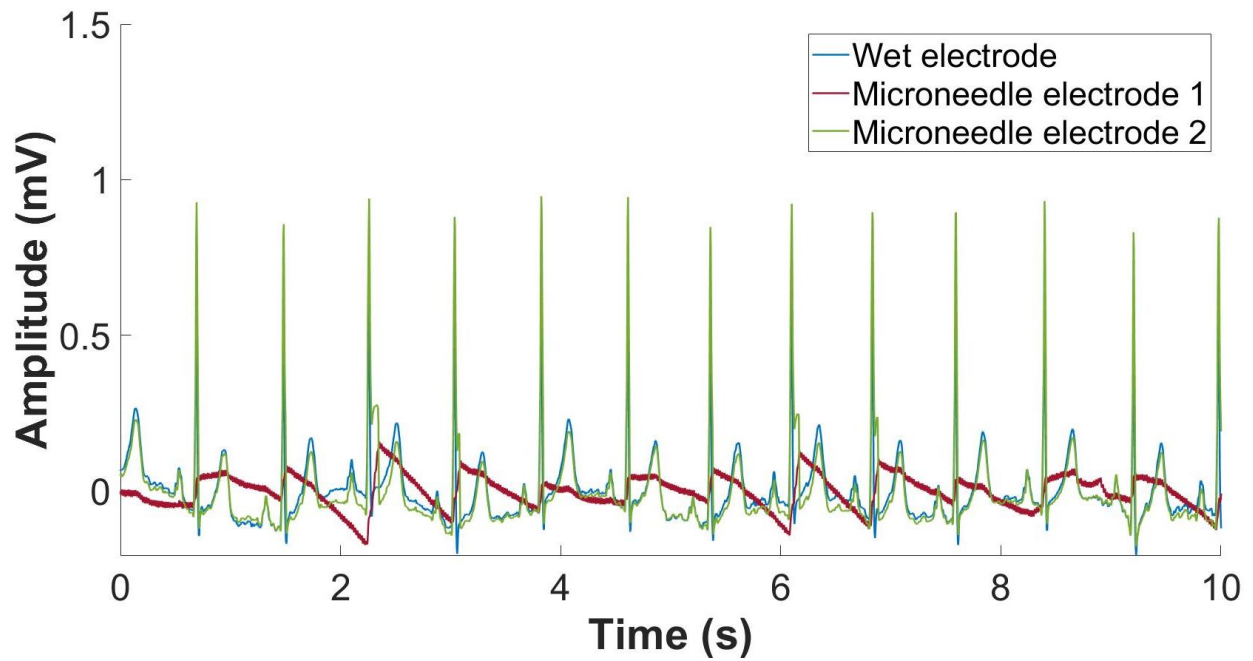
Active (0hrs) – x12 gain
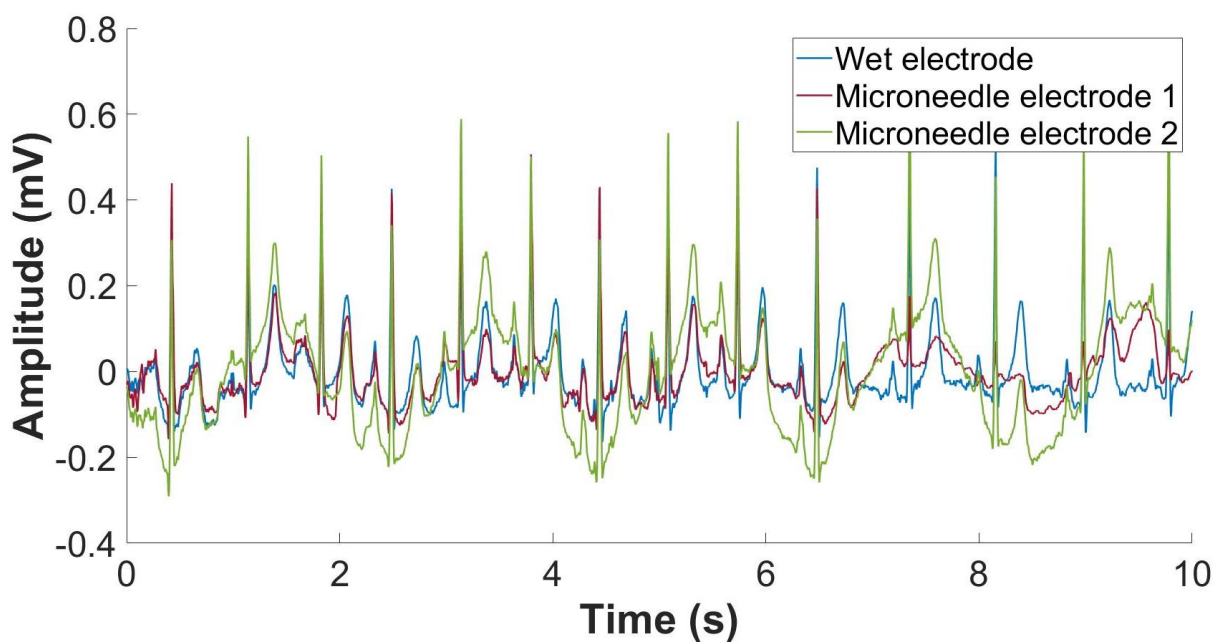
Volunteer 5: Female (45-54 years)

(Microneedle electrode 2 dislodged prior the re-acquisition of cardiac activity)

Resting (6hrs) – x12 gain
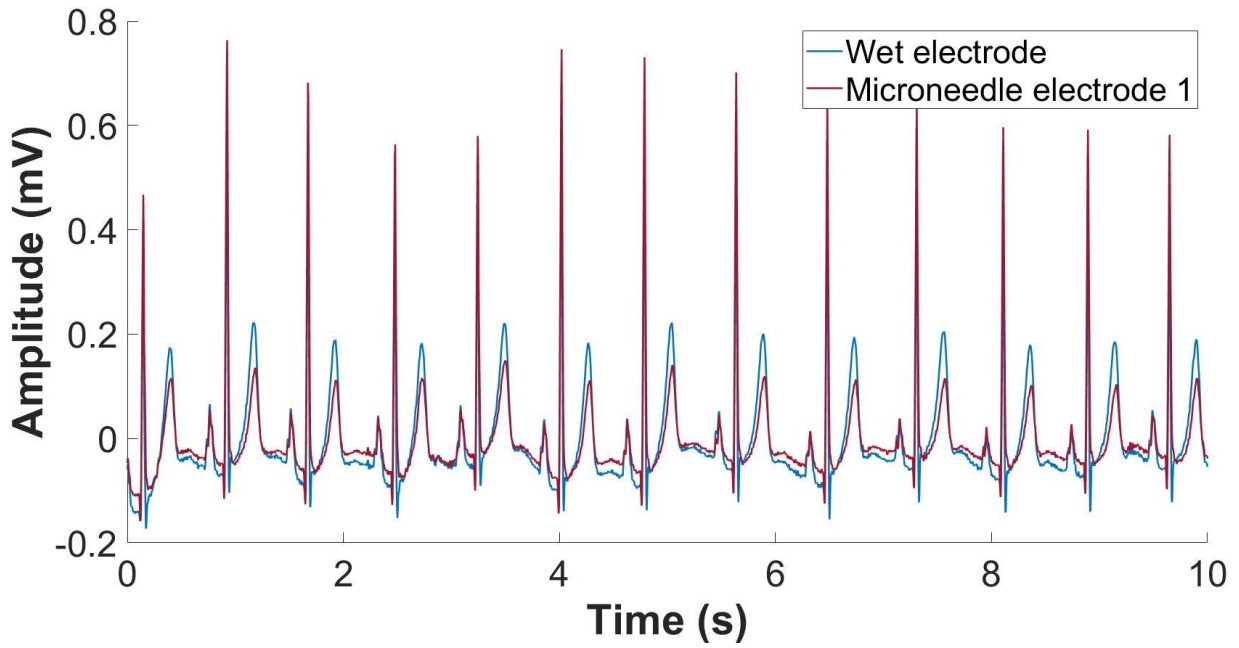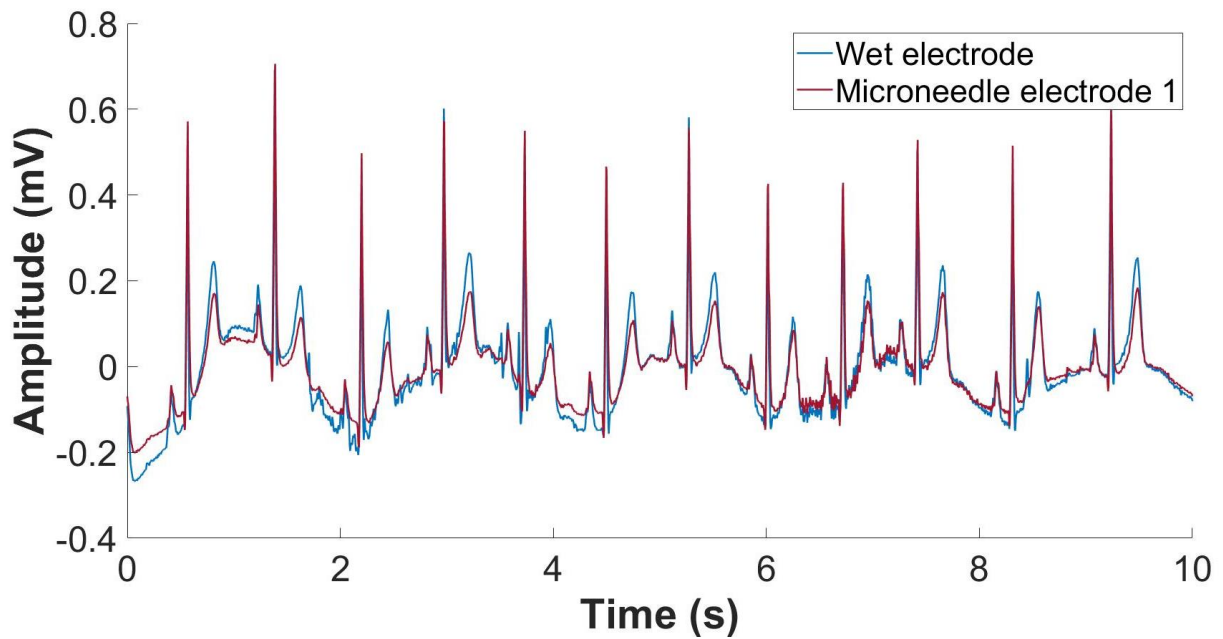
Active (6hrs) – x12 gain

Volunteer 6: Male (35-44 years)

Resting (0hrs) – x12 gain
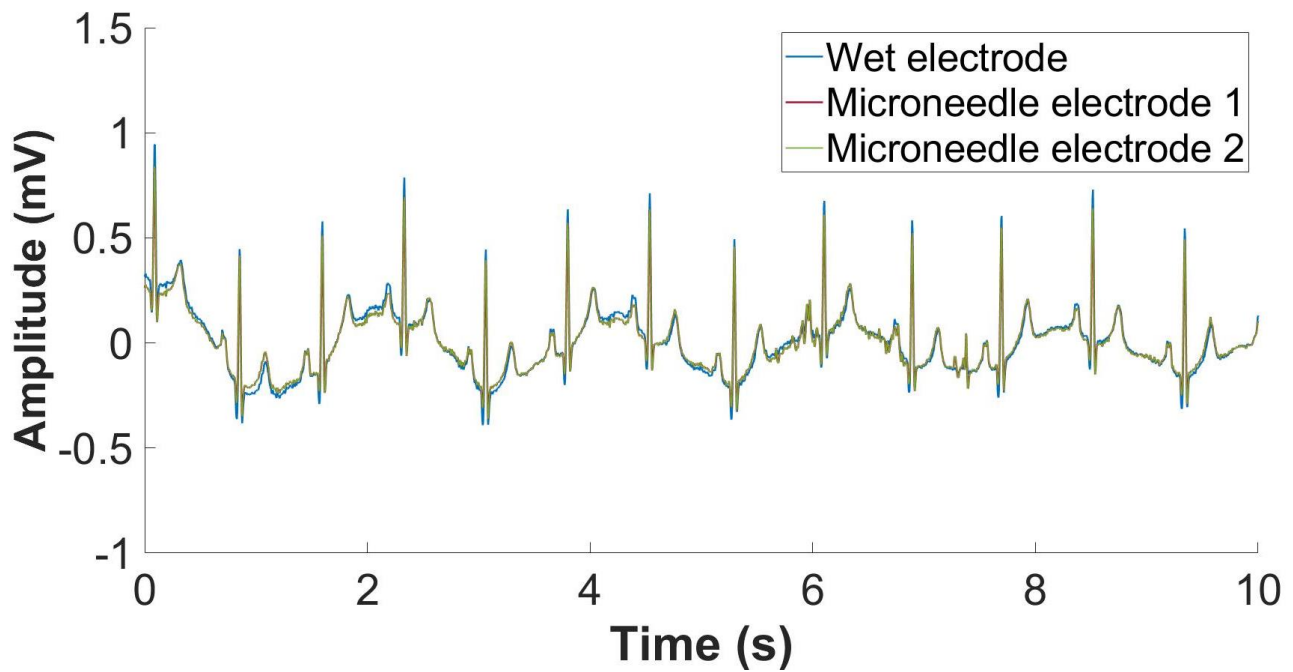
Active (0hrs) – x12 gain
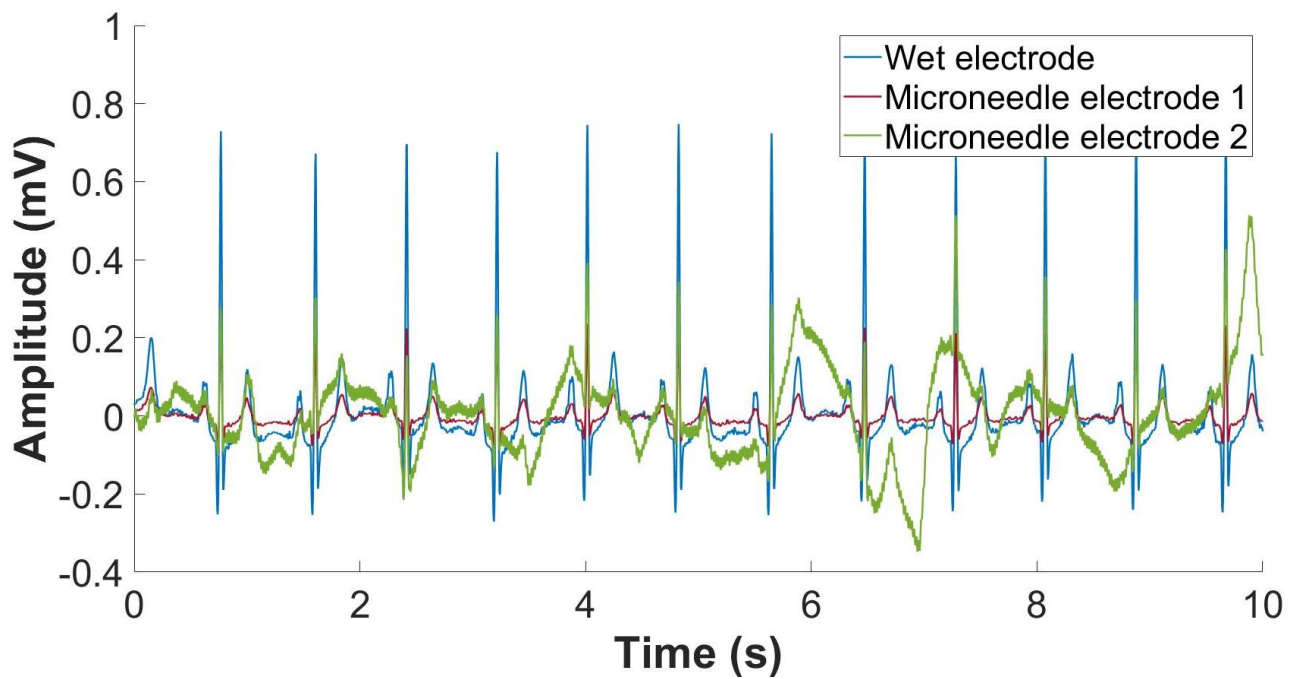
Volunteer 6: Male (35-44 years)

Resting (6hrs) – x12 gain
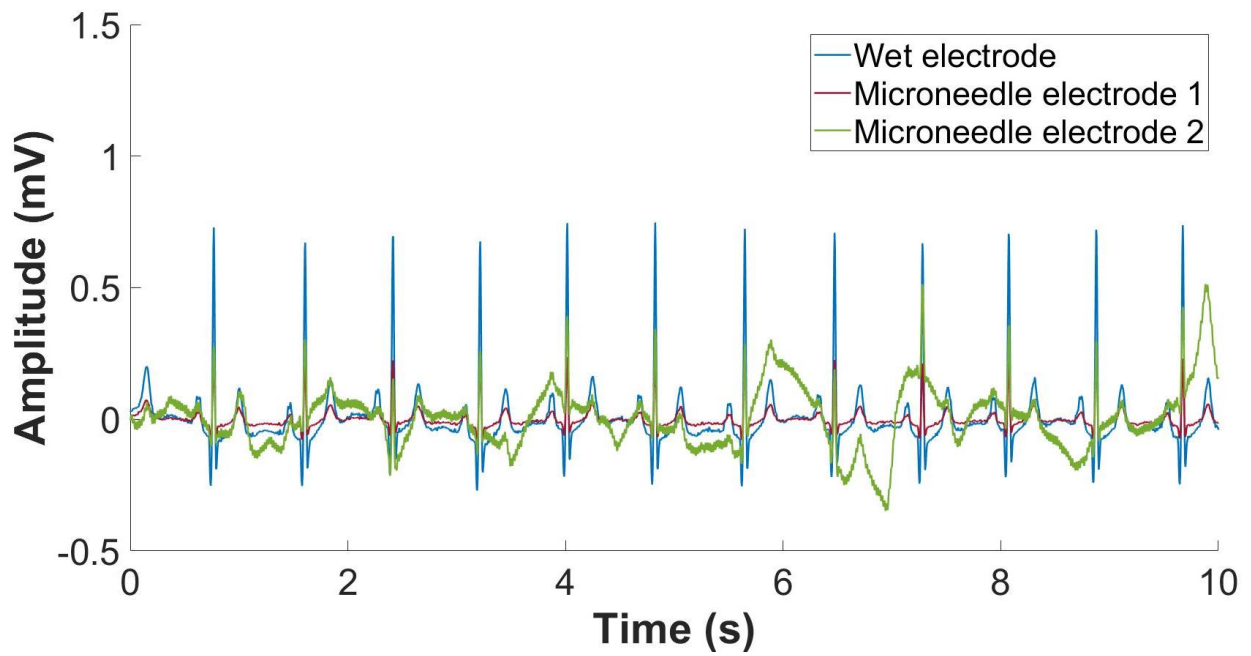
Active (6hrs) – x12 gain
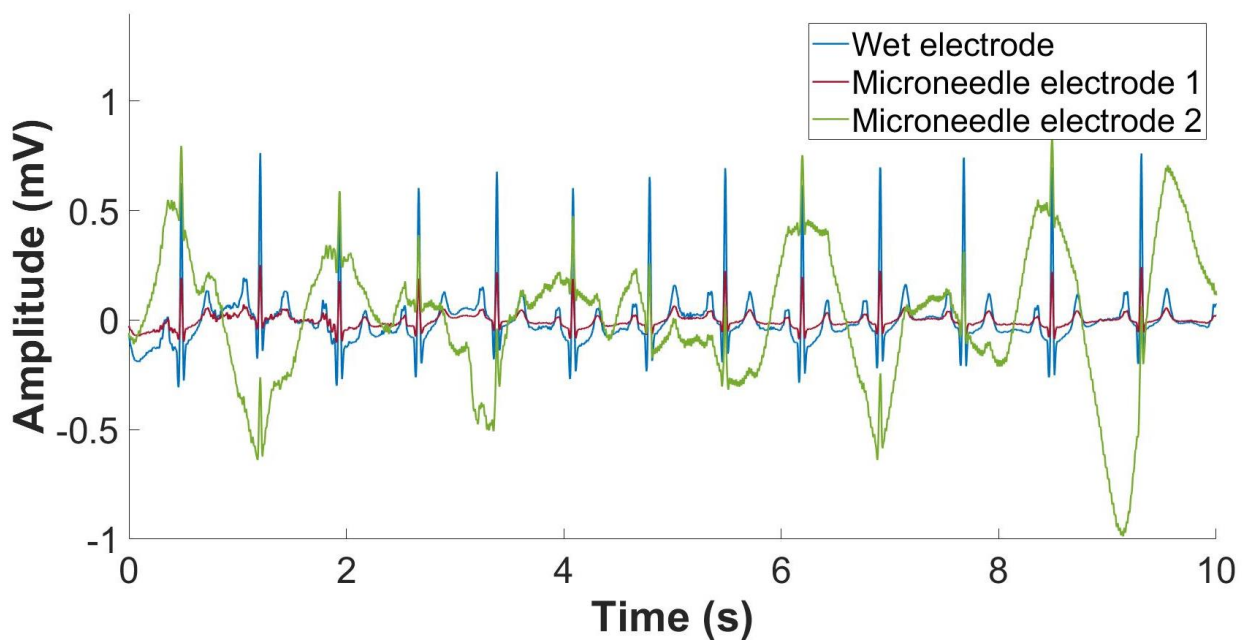
Volunteer 7: Male (45-54 years)

Resting (0hrs) – x12 gain
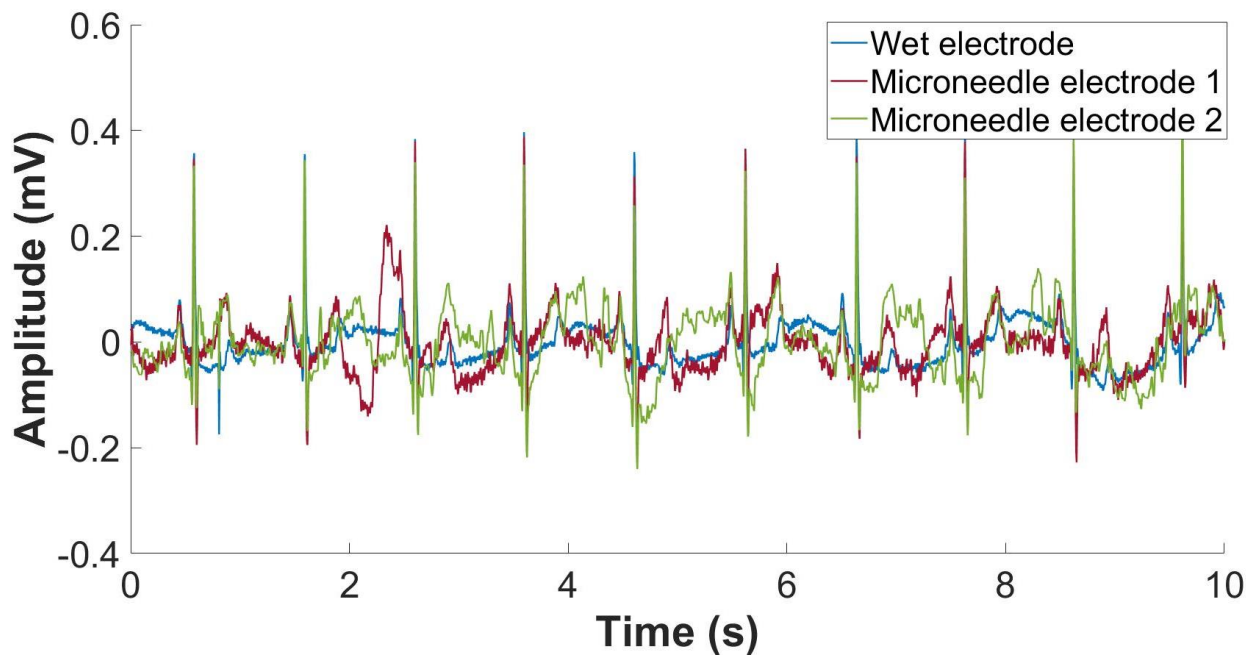
Active (0hrs) – x12 gain
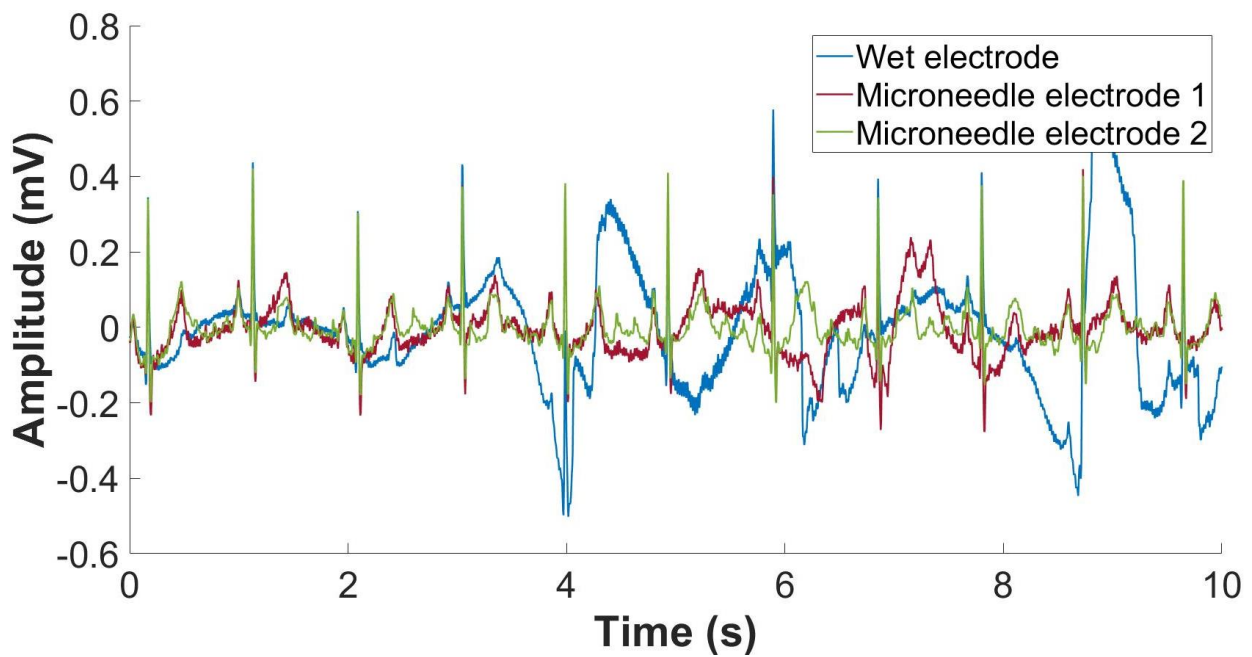
Volunteer 7: Male (45-54 years)

Resting (6hrs) – x12 gain
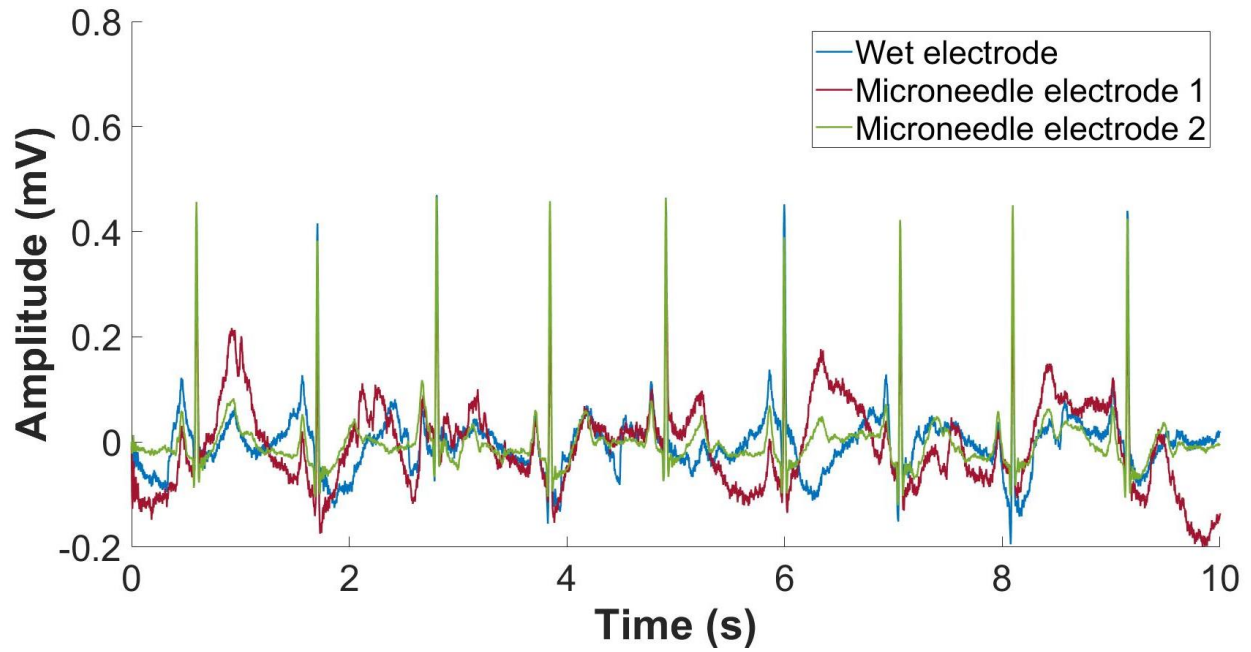
Active (6hrs) – x12 gain
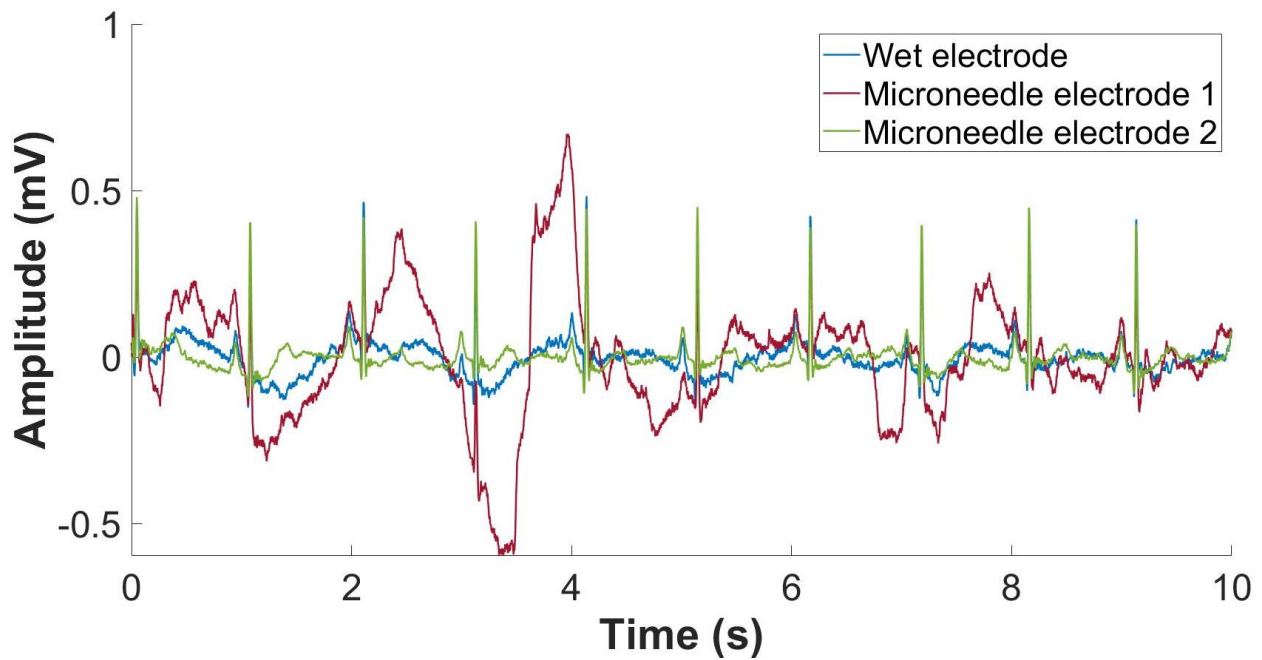
Volunteer 8: Female (35-44 years)

Resting (0hrs) – x24 gain
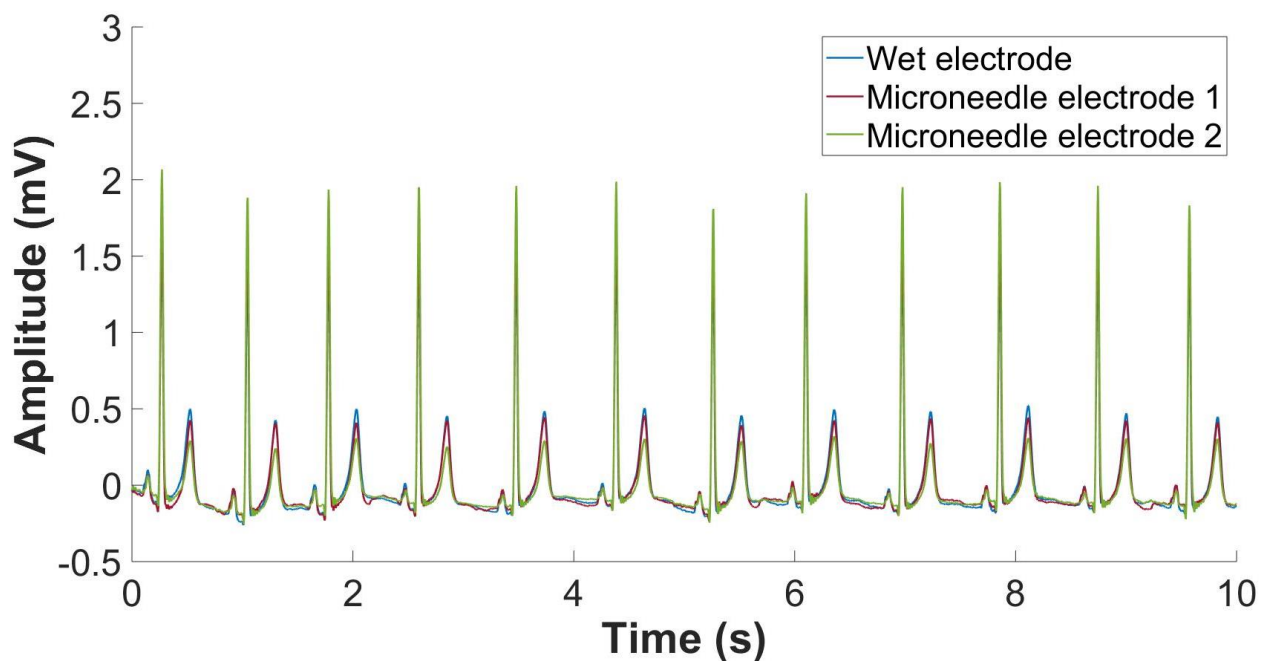
Active (0hrs) – x24 gain
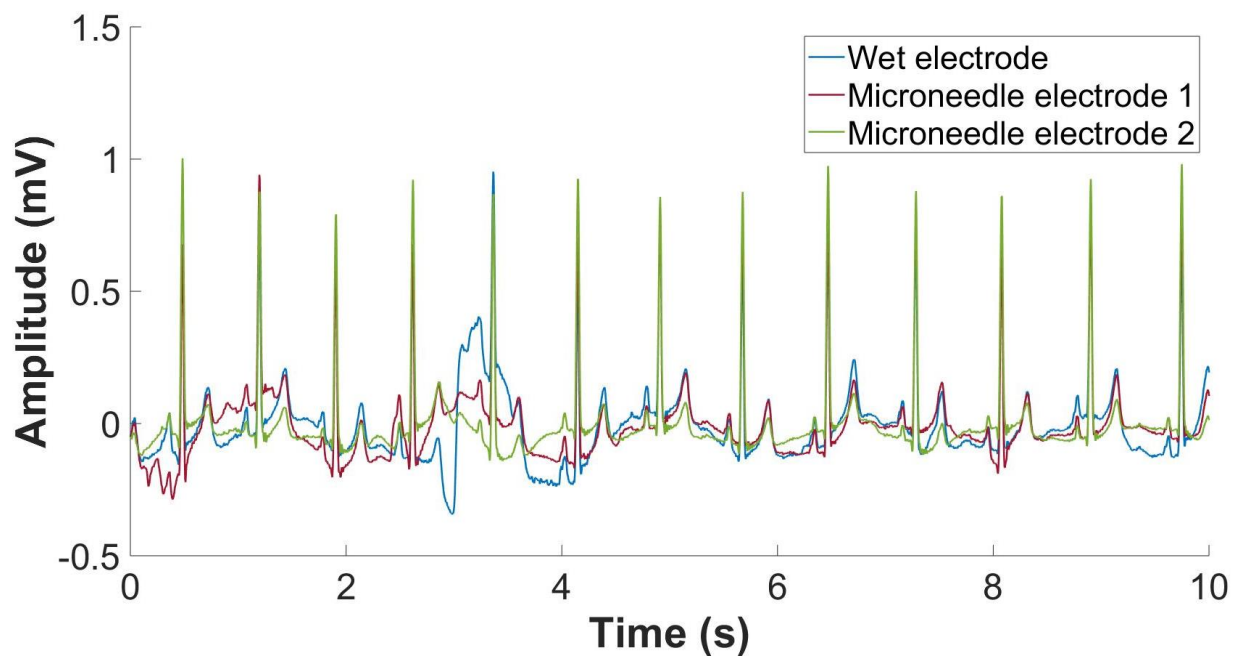
Volunteer 8: Female (35-44 years)
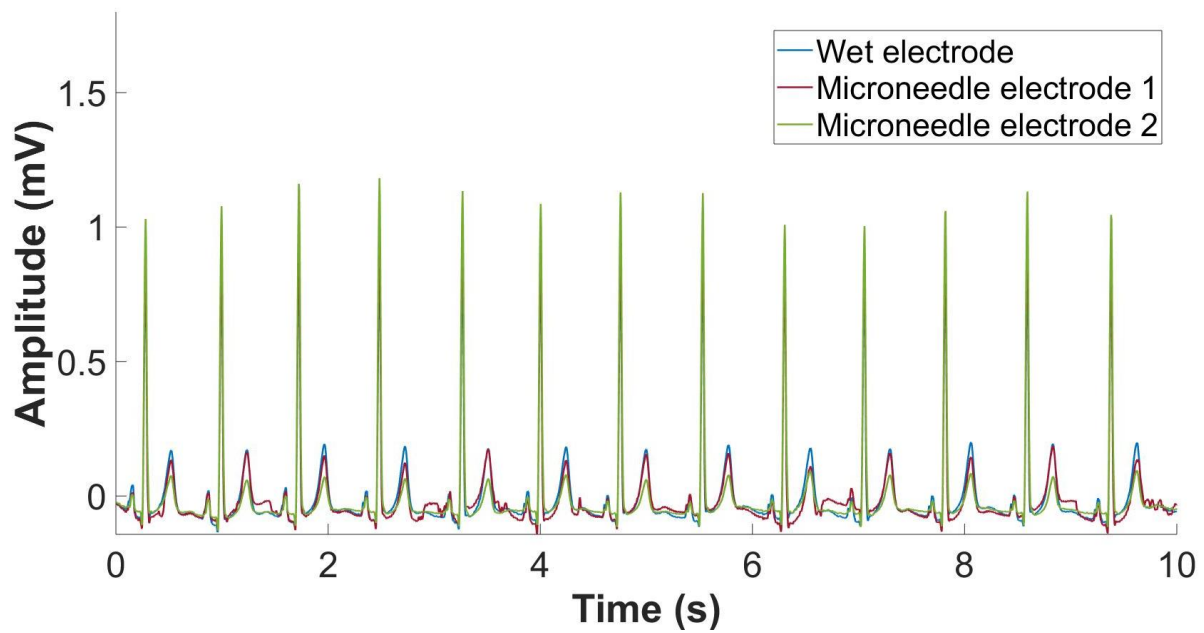
Resting (6hrs) – x24 gain

Active (6hrs) – x24 gain

Volunteer 9: Male (35-44 years)

Resting (0hrs) – x24 gain
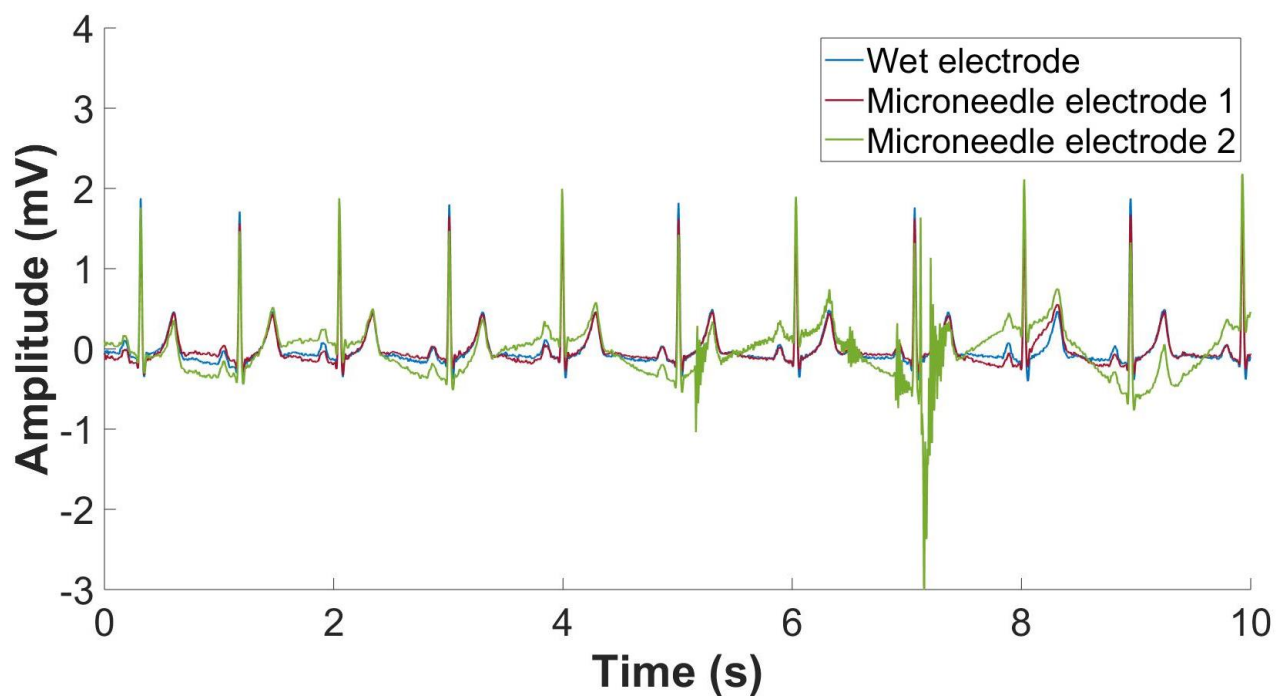
Active (0hrs) – x24 gain
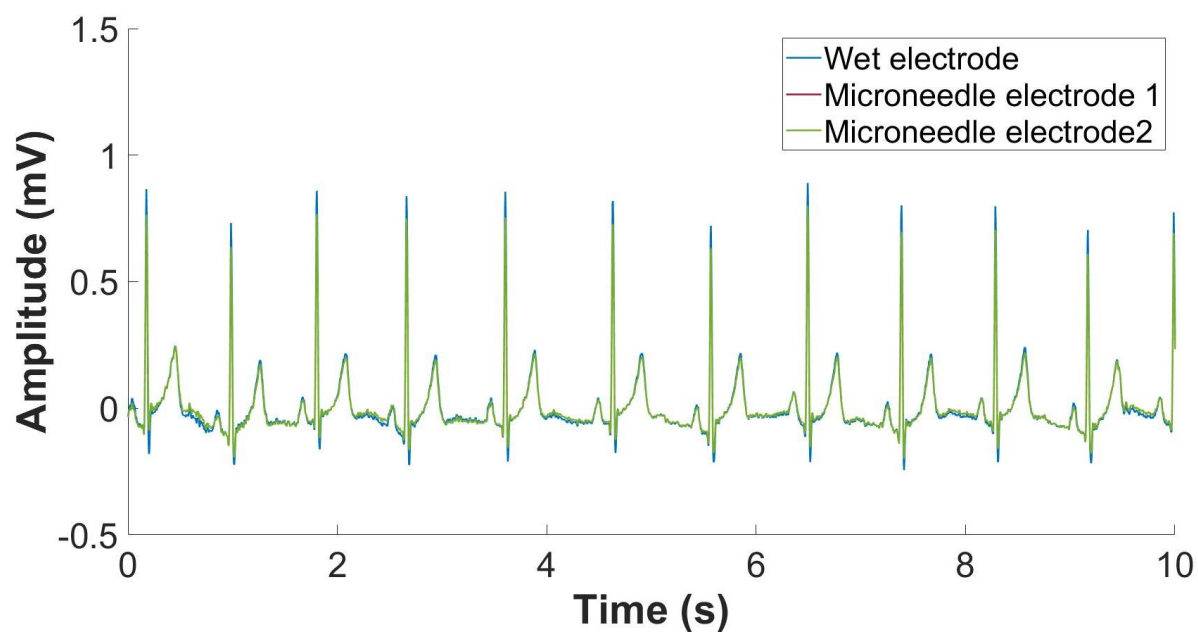
Volunteer 9: Male (35-44 years)

Resting (6hrs) – x24 gain
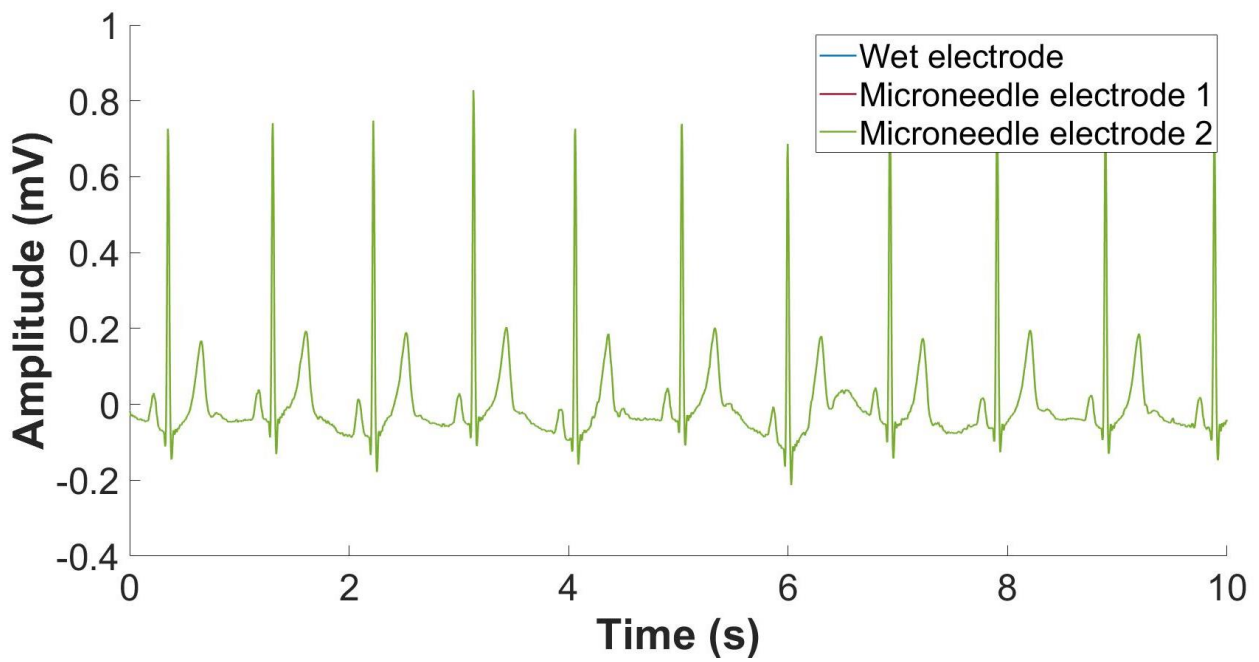
Active (6hrs) – x24 gain
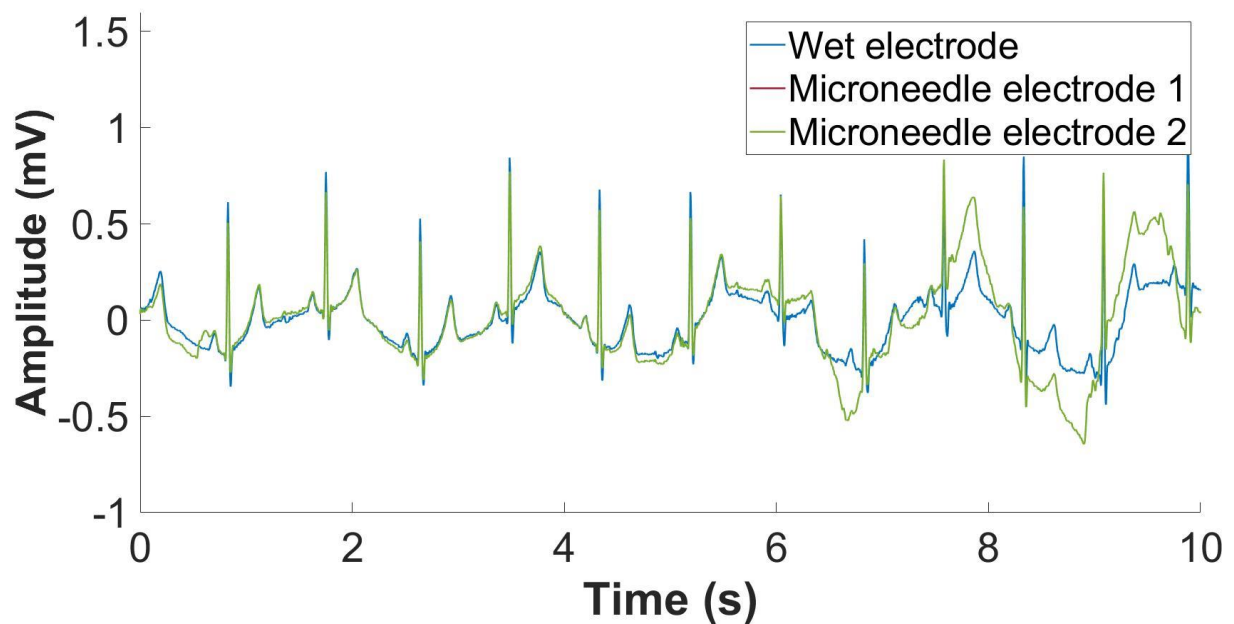
REFERENCES

AAMI. 2005. Disposable ECG electrodes. Association for the Advancement of Medical Instrumentation.

Abd, E. et al. 2016. Skin models for the testing of transdermal drugs. *Clinical Pharmacology: Advances and Applications*, pp. 163-176. doi: 10.2147/cpaa.s64788

Ackermans, P. A. J. et al. 2012. A user-friendly integrated monitor-adhesive patch for long-term ambulatory electrocardiogram monitoring. *Journal of Electrocardiology* 45(2), pp. 148-153. doi: 10.1016/j.electrocard.2011.10.007

Afonso, V. 1993. ECG QRS detection. *Computer Science*.

Afra, T. P., Muhammed T. R., Narang, T., Dogra, S. and Kumar, A. 2019. Topical tazarotene gel, 0.1%, as a novel treatment approach for atrophic postacne scars: a randomized active-controlled clinical trial. *JAMA Facial Plastic Surgery* 21(2), pp. 125-132. doi: 10.1001/jamafacial.2018.1404

Ajmal, M. and Marcus, F. 2021. Standardization in Performing and Interpreting Electrocardiograms. *The American Journal of Medicine* 134(4), pp. 430-434. doi: 10.1016/j.amjmed.2020.10.042

Alarcon, J., Hartley, A., Harvey, N. and Mikszta, J. 2007. Preclinical evaluation of microneedle technology for intradermal delivery of influenza vaccines. *Clinical and Vaccine Immunology* 14(4), pp. 375-381. doi: 10.1128/CVI.00387-06

Alba, N. A., Sclabassi, R. J., Sun, M. and Cui, X. T. 2010. Novel hydrogel-based preparation-free EEG electrode. *IEEE Transactions on Neural Systems and Rehabilitation Engineering* 18(4), doi: 10.1109/TNSRE.2010.2048579

Albulbul, A. 2016. Evaluating major electrode types for idle biological signal measurements for modern medical technology. *Bioengineering* 3(3), p. 20. doi: 10.3390/bioengineering3030020

AliveCor. 2018. *User manual for Kardia^{TM} Mobile by AliveCor*. AliverCor Inc. Available at: www.alivecor.com/previous-labeling/kardiamobile/00LB17.4.pdf [Accessed: 17 May 2021].

AliveCor. 2020. *KardiaMobile*. AliveCor Inc. Available at: www.alivecor.co.uk [Accessed: 17 May 2021].

Almutairi, H., Hassan, G. M. and Datta, A. 2021. Classification of obstructive sleep apnoea from single-lead ECG signals using convolutional neural and long short term memory networks. *Biomedical Signal Processing and Control* 69, p. 102906. doi: 10.1016/j.bspc.2021.102906

Alonso, A., Meirelles, N. C., Yushmanov, V. E. and Tabak, M. 1996. Water increases the fluidity of intercellular membranes of stratum corneum: correlation with water permeability, elastic, and electrical resistance properties. *Journal of Investigative Dermatology* 106(5), pp. 1058-1063. doi: 10.1111/1523-1747.ep12338682

322

Alpert, M. A., Terry, B. E., Hamm, C. R., Fan, T. M., Cohen, M. V., Massey, C. V. and Painter, J. A. 2001. Effect of weight loss on the ECG of normotensive morbidly obese patients. *Chest* 119(2), pp. 507-510. doi: 10.1378/chest.119.2.507

Ambu. 2013. *Ambu BlueSensor R*. Copenhagen, Denmark: AmBu A/S. Available at: https://www.ambu.co.uk/cardiology/ecg-electrodes/product/ambu-bluesensor-r [Accessed: 4 May 2021].

Ameen, M. A., Liu, J. and Kwak, K. 2012. Security and privacy issues in wireless sensor networks for healthcare applications. *Journal of Medical Systems* 36(1). doi: 10.1007/s10916-010-9449-4

An, X. and Stylios, G. K. 2018. A hybrid textile electrode for electrocardiogram (ECG) measurement and motion tracking. *Materials (Basel)* 11(10), doi: 10.3390/ma11101887

An, Y., Ji, C., Li, Y., Wang, J., Zhang, X. and Huang, Y. 2017. In vivo measurements of human neck skin elasticity using MRI and finite element modeling. *Medical Physics* 44(4), pp. 1402-1407. doi: 10.1002/mp.12154

Anderson, S. I., Anderson, P. G. and Lowe, J. S. 2018. *Stevens & Lowe's human histology*. Fifth ed. Elsevier.

Anderson, J. M. and McNally, A. K. 2011. Biocompatibility of implants: lymphocyte/macrophage interactions. *Seminars in Immunopathology* 33(3), pp. 221-233. doi: 10.1007/s00281-011-0244-1

Annaidh, A. N., Bruyère, K., Destrade, M., Gilchrist, M. D. and Otténio, M. 2012. Characterization of the anisotropic mechanical properties of excised human skin. *Journal of the Mechanical Behavior of Biomaterials (JMBBM)* 5(1), pp. 139-148. doi: 10.1016/j.jmbbm.2011.08.016

Apple. 2020. *Using apple watch for arrhythmia detection*. Apple Inc. Available at: www.apple.com/healthcare/docs/site/Apple_Watch_Arrhythmia_Detection.pdf [Accessed: 18 May 2021].

Arai, M., Nishinaka, Y. and Norihisa, N. 2015. Electroencephalogram measurement using polymer-based dry microneedle electrode. *Japanese Journal of Applied Physics* 54, doi: 10.7567/JJAP.54.06FP14

Arda, O., Göksügür, N. and Tüzün, Y. 2014. Basic histological structure and functions of facial skin. *Clinics in Dermatology* 32(1), pp. 3-13. doi: 10.1016/j.clindermatol.2013.05.021

Arikat, F. 2019. *Microneedle delivery of antigen-specific immunotherapy for type 1 diabetes.* PhD Thesis, Cardiff University.

Arikat, F. et al. 2020. Targeting proinsulin to local immune cells using an intradermal microneedle delivery system; a potential antigen-specific immunotherapy for type 1 diabetes. *Journal of Controlled Release* 322, pp. 593-601. doi: 10.1016/j.jconrel.2020.02.031

Arquilla, K., Webb, A. K. and Anderson, A. P. 2020. Textile electrocardiogram (ECG) electrodes for wearable health monitoring. *Sensors* 20(4), doi: 10.3390/s20041013

Arya, J., Henry, S., Kalluri, H., McAllister, D. V., Pewin, W. P. and Prausnitz, M. R. 2017. Tolerability, usability and acceptability of dissolving microneedle patch administration in human subjects. *Biomaterials* 128, pp. 1-7. doi: 10.1016/j.biomaterials.2017.02.040

Ashcroft, G. S., Mills, S. J. and Ashworth, J. J. 2002. Ageing and wound healing. *Biogerontology* 3(6), pp. 337-345. doi: 10.1023/a:1021399228395

Asher, M. I., Montefort, S., Björkstén, B., Lai, C. K., Strachan, D. P., Weiland, S. K. and Williams, H. 2006. Worldwide time trends in the prevalence of symptoms of asthma, allergic rhinoconjunctivitis, and eczema in childhood: ISAAC Phases One and Three repeat multicountry cross-sectional surveys. *Lancet* 368(9537), pp. 733-743. doi: 10.1016/s0140-6736(06)69283-0

Avenel-Audran, M., Goossens, A., Zimerson, E. and Bruze, M. 2003. Contact dermatitis from electrocardiograph-monitoring electrodes: role of *p-tert*-butylphenol-formaldehyde resin. *Contact Dermatitis* 48(2), pp. 108-111. doi: 10.1034/j.1600-0536.2003.480210.x

Avon, S. L. and Wood, R. E. 2005. Porcine skin as an in-vivo model for ageing of human bite marks. *Journal of Forensic Odonto-Stomatology* 23(2), pp. 30-39.

Babu, R. J. et al. 2003. The influence of various methods of cold storage of skin on the permeation of melatonin and nimesulide. *Journal of Controlled Release* 86(1), pp. 49-57. doi: 10.1016/S0168-3659(02)00368-1

Baevsky, R. H., Haber, M. D., Blank, F. S. and Smithline, H. 2007. Supine vs semirecumbent and upright 12-lead electrocardiogram: does change in body position alter the electrocardiographic interpretation for ischemia? *The American Journal of Emergency Medicine* 25(7), pp. 753-756. doi: 10.1016/j.ajem.2006.12.005

Bal, S. M., Caussin, J., Pavel, S. and Bouwstra, J. A. 2008. In vivo assessment of safety of microneedle arrays in human skin. *European Journal of Pharmaceutical Sciences* 35(3), pp. 193-202. doi: 10.1016/j.ejps.2008.06.016

Barbero, A. M. and Frasch, H. F. 2016. Effect of frozen human epidermis storage duration and cryoprotectant on barrier function using two model compounds. *Skin Pharmacology and Physiology* 29(1), pp. 31-40. doi: 10.1159/000441038

Bariya, S. H., Gohel, M. C., Mehta, T. A. and Sharma, O. P. 2012. Microneedles: an emerging transdermal drug delivery system. *Journal of Pharmacy and Pharmacology* 64(1), pp. 11-29. doi: 10.1111/j.2042-7158.2011.01369.x

Barrett, C., Dawson, K. and O'Riordan, A. 2015. Development of low cost rapid fabrication of sharp polymer microneedles for in vivo glucose biosensing applications. *ECS Journal of Solid State Science and Technology* 4(10), doi: 10.1149/2.0141510JSS

Barrett, P. M. et al. 2014. Comparison of 24-hour Holter monitoring with 14-day novel adhesive patch electrocardiographic monitoring. *The American Journal of Medicine* 127(1), pp. 95-97. doi: 10.1016/j.amjmed.2013.10.003

Barry, D. M. and Nerbonne, J. M. 1996. Myocardial potassium channels: electrophysiological and molecular diversity. *Annual review of physiology* 58, pp. 363-394. doi: 10.1146/annurev.ph.58.030196.002051

Basoglu, N., Ok, A. E. and Daim, T. U. 2017. What will it take to adopt smart glasses: A consumer choice based review? *Technology in Society* 50, pp. 50-56. doi: 10.1016/j.techsoc.2017.04.005

Bayoumy, K. et al. 2021. Smart wearable devices in cardiovascular care: where we are and how to move forward. *Nature Reviews Cardiology*, pp. 1-19. doi: 10.1038/s41569-021-00522-7

Bazett, H. C. 1920. An analysis of the time-relations of electrocardiograms. *Heart* 7, pp. 353-370.

BBC. 2017. *NHS cyber-attack: GPs and hospitals hit by ransomware*. London: British Broadcasting Corporation [BBC]. Available at: www.bbc.co.uk/news/health-39899646 [Accessed: 19 May 2021].

Beck, T. W., DeFreitas, J. M., Cramer, J. T. and Stout, J. R. 2009. A comparison of adaptive and notch filtering for removing electromagnetic noise from monopolar surface electromyographic signals. *Physiological Measurement* 30(4), pp. 353-361. doi: 10.1088/0967-3334/30/4/001

Benjamin, H., Bischof, M., Goldshtein, D., Fecteau, P. and Newman, D. 2021. A pandemic response to home delivery for ambulatory ECG monitoring: Development and validation. *Journal of Electrocardiology* 64, pp. 72-75. doi: 10.1016/j.jelectrocard.2020.11.003

Bennett, D. H. 2013. *Bennett's cardiac arrhythmias: practical notes on interpretation and treatment*. Eighth ed. London: Hodder Arnold.

Benson, H. A. E. and Watkinson, A. C. 2012. *Transdermal and topical drug delivery: principles and practice*. Wiley-Blackwell.

Bergey, G. E., Squires, R. D. and Sipple, W. C. 1971. Electrocardiogram recording with pasteless electrodes. *IEEE Transactions on Biomedical Engineering* BME-18(3), pp. 206-211. doi: 10.1109/TBME.1971.4502833

Bhatnagar, S., Kumari, P., Pattarabhiran, S. P. and Venuganti, V. V. K. 2018. Zein microneedles for localized delivery of chemotherapeutic agents to treat breast cancer: drug loading, release behavior, and skin permeation studies. *The American Association of Pharmaceutical Scientists* 19(4), pp. 1818-1826. doi: 10.1208/s12249-018-1004-5

BHF. 2021. *UK Factsheet.* British Heart Foundation. Available at: bhf-cvd-statistics-uk-factsheet.pdf [Accessed: 10 May 2021].

Birchall, J. et al. 2005. Cutaneous DNA delivery and gene expression in ex vivo human skin explants via wet-etch micro-fabricated micro-needles. *Journal of Drug Targeting* 13(7), pp. 415-421. doi: 10.1080/10611860500383705

Birchall, J. C., Clemo, R. N., Anstey, A. V. and John, D. N. 2011. Microneedles in clinical practice-an exploratory study into the opinions of healthcare professionals and the public. *Pharmaceutical Research* 28(1), pp. 95-106. doi: 10.1007/s11095-010-0101-2

Björklund, S., Ruzgas, T., Nowacka, A., Dahi, I., Topgaard, D., Sparr, E. and Engblom, J. 2013. Skin membrane electrical impedance properties under the influence of a varying water gradient. *Biophysical Journal* 104(12), pp. 2639-2650. doi: 10.1016/j.bpj.2013.05.008

Blair, M. J., Jones, J. D., Woessner, A. E. and Quinn, K. P. 2020. Skin structure-function relationships and the wound healing response to intrinsic aging. *Advances in Wound Care* 9(3), pp. 127-143. doi: 10.1089/wound.2019.1021

Blanco-Velasco, M., Weng, B. and Barner, K. E. 2008. ECG signal denoising and baseline wander correction based on the empirical mode decomposition. *Computers in Biology and Medicine* 38(1), pp. 1-13. doi: 10.1016/j.compbiomed.2007.06.003

Blank, I. H. 1952. Factors which influence the water content of the stratum corneum. *Journal of Investigative Dermatology* 18(6), pp. 433-440. doi: 10.1038/jid.1952.52

Blank, I. H., Moloney, J., Emslie, A. G., Simon, I. and Apt, C. 1984. The diffusion of water across the stratum corneum as a function of its water content. *Journal of Investigative Dermatology* 82(2), pp. 188-194. doi: 10.1111/1523-1747.ep12259835

Bock, M., Gerth, C. and Lorenz, B. 2000. Impact of notch filter use on waveforms of First- and Second-Order-Kernel responses from multifocal ERGs. *Documenta Ophthalmologica* 101(3), pp. 195-210. doi: 10.1023/a:1002720819696

Bollella, P., Sharma, S., Cass, A. E. G., Tasca, F. and Antiochia, R. 2019. Minimally invasive glucose monitoring using a highly porous gold microneedles-based biosensor: characterization and application in artificial interstitial fluid. *Catalysts* 9(7). doi: 10.3390/catal9070580

Bollella, P., Sharma, S., Cass, A. E. G. and Antiochia, R. 2019. Microneedle-based biosensor for minimally-invasive lactate detection. *Biosensors and Bioelectronics* 123, pp. 152-159. doi: 10.1016/j.bios.2018.08.010

Bolourchi, M., Silver, E. S., Muwanga, D., Mendez, E. and Liberman, L. 2020. Comparison of Holter With Zio Patch Electrocardiography Monitoring in Children. *The American Journal of Cardiology* 125(5), pp. 767-771. doi: 10.1016/j.amjcard.2019.11.028

Boudoulas, H., Schaal, S. F., Lewis, R. P. and Robinson, J. L. 1979. Superiority of 24-hour outpatient monitoring over multi-stage exercise testing for the evaluation of syncope. *Journal of Electrocardiology* 12(1), pp. 103-108. doi: 10.1016/s0022-0736(79)80052-7

Boutry, C. M., Nguyen, A., Lawal, Q. O., Chortos, A., Rondeau-Gagné, S. and Bao, Z. 2015. A Sensitive and Biodegradable Pressure Sensor Array for Cardiovascular Monitoring. *Advanced Materials* 27(43), pp. 6954-6961. doi: 10.1002/adma.201502535

Braybrook, J. H. 1997. *Biocompatibility : assessment of medical devices and materials.* New York: Wiley.

Brown, I. A. 1973. A scanning electron microscope study of the effects of uniaxial tension on human skin. *The British Journal of Dermatology* 89(4), pp. 383-393.

Buendía-Fuentes, F. et al. 2012. High-bandpass filters in electrocardiography: source of error in the interpretation of the ST segment. *International Scholarly Research Notices* 2012. doi: 10.5402/2012/706217

Burma, J. S., Lapointe, A. P., Soroush, A., Oni, I. K., Smirl, J. D. and Dunn, J. F. 2021. The validity and reliability of an open source biosensing board to quantify heart rate variability. *Heliyon* 7(6). doi: 10.1016/j.heliyon.2021.e07148

Burns, T. and Rook, A. 2010. *Rook's textbook of dermatology*. 8th ed. Oxford: Oxford : Wiley-Blackwell.

Burton, S. A. et al. 2011. Rapid intradermal delivery of liquid formulations using a hollow microstructured array. *Pharmaceutical Research* 28(1), pp. 31-40. doi: 10.1007/s11095-010-0177-8

Caliò, A., Dardano, P., Di Palma, V., Bevilacqua, M. F., Di Matteo, A., Iuele, H. and De Stefano, L. 2016. Polymeric microneedles based enzymatic electrodes for electrochemical biosensing of glucose and lactic acid. *Sensors and Actuators B: Chemical* 236, pp. 343-349. doi: 10.1016/j.snb.2016.05.156

Campbell, B., Richley, D., Ross, C. and Eggett, C. J. 2017. *Clinical Guidelines by Consensus: Recording a standard 12-lead electrocardiogram. An approved method by the Society for Cardiological Science and Technology (SCST).* Available at: http://www.scst.org.uk/resources/SCST_ECG_Recording_Guidelines_2017 [Accessed: 02 March 2021].

Cancela, J., Pastorino, M., Tzallas, A. T., Tsipouras, M. G., Rigas, G., Arredondo, M. T. and Fotiadis, D. I. 2014. Wearability assessment of a wearable system for Parkinson's Disease remote monitoring based on a body area network of sensors. *Sensors* 14(9), pp. 17235-17255. doi: 10.3390/s140917235

Carim, H. M. and Hawkinson, R. W. 1982. EKG electrode electrolyte-skin AC impedance studies. *Proceedings of the 4th Annual International Conference of the IEEE Engineering in Medicine and Biology Society (EMBC)*, pp. 503-504.

Castelletti, S., Dagradi, F., Goulene, K., Danza, A. I., Baldi, E., Stramba-Badiale, M. and Schwartz, P. J. 2018. A wearable remote monitoring system for the identification of subjects with a prolonged QT interval or at risk for drug-induced long QT syndrome. *International Journal of Cardiology* 266, pp. 89-94. doi: 10.1016/j.ijcard.2018.03.097

Censi, F., Calcagnini, G., Triventi, M., Mattei, E., Bartolini, P., Corazza, I. and Boriani, G. 2009. Effect of high-pass filtering on ECG signal on the analysis of patients prone to atrial fibrillation. *Annali dell'Istituto Superiore di Sanità* 45(4), pp. 427-431. doi: 10.1590/s0021-25712009000400012

Chareonthaitawee, P. and Askew, J. W. 2020. *Exercise ECG testing: performing the test and interpreting the ECG results*. UpToDate. Available at: www.uptodate.com/contents/exercise-ecg-testing-performing-the-test-and-interpreting-the-ecg-results?search=exercise%20ECG&source=search_result&selectedTitle=1~150&usage_type=default&display_rank=1 [Accessed: 20 May 2021].

Chase, C. and Brady, W. J. 2000. Artifactual electrocardiographic change mimicking clinical abnormality on the ECG. *American Journal of Emergency Medicine* 18(3), pp. 312-316. doi: 10.1016/s0735-6757(00)90126-8

Chen, C-Y., Chang, C-L., Chien, T-F. and Luo, C-H. 2013a. Flexible PDMS electrode for one-point wearable wireless bio-potential acquisition. *Sensors and Actuators A: Physical* 203, pp. 20-28. doi: 10.1016/j.sna.2013.08.010

Chen, K., Ren, L., Chen, Z., Pan, C., Zhou, W. and Jiang, L. 2016. Fabrication of micro-needle electrodes for bio-signal recording by a magnetization-induced self-assembly method. *Sensors* 16 (9). doi: 10.3390/s16091533

Chen, X. et al. 2010. Improved DNA vaccination by skin-targeted delivery using dry-coated densely-packed microprojection arrays. *Journal of Controlled Release* 148(3), pp. 327-333. doi: 10.1016/j.jconrel.2010.09.001

Chen, Y., Pei, W., Chen, S., Wu, X., Zhao, S., Wang, H. and Chen, H. 2013. Poly(3,4-ethylenedioxythiophene) (PEDOT) as interface material for improving electrochemical performance

of microneedles array-based dry electrode. *Sensors and Actuators B: Chemical* 188, pp. 747-756. 10.1016/j.snb.2013.07.075

Chen, Y-H. et al. 2014. Soft, comfortable polymer dry electrodes for high quality ECG and EEG recording. *Sensors* 14(12), pp. 23758–23780. doi: 10.3390/s141223758

Chen, Z., Ren, L., Li, J., Yao, L., Chen, Y., Liu, B. and Jiang, L. 2018. Rapid fabrication of microneedles using magnetorheological drawing lithography. *Acta Biomaterialia* 65, pp. 283-291. doi: 10.1016/j.actbio.2017.10.030

Cheung, C. C., Kerr, C. R. and Krahn, A. D. 2014. Comparing 14-day adhesive patch with 24-hour Holter monitoring. *Future Cardiology* 10(3), pp. 319-322. doi: 10.2217/fca.14.24

Cheung, K., Han, T. and Das, D. B. 2014. Effect of force of microneedle insertion on the permeability of insulin in skin. *Journal of Diabetes Science and Technology* 8(3), pp. 444-452. doi: 10.1177/1932296813519720

Chinnadayyala, S. R., Park, J., Satti, A. T., Kim, D. and Cho, S. 2021. Minimally invasive and continuous glucose monitoring sensor based on non-enzymatic porous platinum black-coated gold microneedles. *Electrochimica Acta* 369, p. 137691. doi: 10.1016/j.electacta.2020.137691

Chlaihawi, A. A., Narakathu, B. B., Emamian, S., Bazuin, B. J. and Atashbar, M. Z. 2018. Development of printed and flexible dry ECG electrodes. *Sensing and Bio-Sensing Research* 20, pp. 9-15. doi: 10.1016/j.sbsr.2018.05.001

Choi, H. R., Kim, S. K., Kwon, S. B. and Park, K. C. 2006. The fixation of living skin equivalents. *Applied Immunohistochemistry & Molecular Morphology* 14(1), pp. 122-125. doi: 10.1097/01.pai.0000142159.75540.e0

Chu, L. Y. and Prausnitz, M. R. 2011. Separable arrowhead microneedles. *Journal of Controlled Release* 149(3), pp. 242-249. doi: 10.1016/j.jconrel.2010.10.033

Chuah, S. H.-W., Rauschnabel, P. A., Krey, N., Nguyen, B., Ramayah, T. and Lade, S. 2016. Wearable technologies: The role of usefulness and visibility in smartwatch adoption. *Computers in Human Behavior* 65, pp. 276-284. doi: 10.1016/j.chb.2016.07.047

Cilurzo, F., Gennari, C. G. and Minghetti, P. 2012. Adhesive properties: a critical issue in transdermal patch development. *Expert Opinion on Drug Delivery* 9(1), pp. 33-45. doi: 10.1517/17425247.2012.637107

Clark, L. and Lyons, C. 1962. Electrode systems for continuous monitoring in cardiovascular surgery. *Annals of the New York Academy of Sciences* 102(1), pp. 29-45. doi: 10.1111/j.1749-6632.1962.tb13623.x

Collet, J. P. et al. 2021. 2020 ESC Guidelines for the management of acute coronary syndromes in patients presenting without persistent ST-segment elevation. *European Heart Journal* 42(14), pp. 1289-1367. doi: 10.1093/eurheartj/ehaa575

Cömert, A. and Hyttinen, J. 2015. Investigating the possible effect of electrode support structure on motion artifact in wearable bioelectric signal monitoring. *BioMedical Engineering OnLine* 14, p. 44. doi: 10.1186/s12938-015-0044-2

Coravos, A., Doerr, M., Goldsack, J., Manta, C., Shervey, M., Woods, B. and Wood, W. A. 2020. Modernizing and designing evaluation frameworks for connected sensor technologies in medicine. *NPJ Digital Medicine* 3(37). doi: 10.1038/s41746-020-0237-3

Corbett, H. J., Fernando, G. J., Chen, X., Frazer, I. H. and Kendall, M. A. 2010. Skin vaccination against cervical cancer associated human papillomavirus with a novel micro-projection array in a mouse model. *PLOS ONE* 5(10), p. e13460. doi: 10.1371/journal.pone.0013460

Cosoli, G., Spinsante, S., Scardulla, F., D'Acquisto, L. and Scalise, L. 2021. Wireless ECG and cardiac monitoring systems: State of the art, available commercial devices and useful electronic components. *Measurement* 177, p. 109243. doi: 10.1016/j.measurement.2021.109243

Coulman, S. A., Anstey, A., Gateley, C., Morrissey, A., McLoughlin, P., Allender, C. and Birchall, J. C. 2009. Microneedle mediated delivery of nanoparticles into human skin. *International Journal of Pharmaceutics* 366(1), pp. 190-200. doi: 10.1016/j.ijpharm.2008.08.040

Coulman, S. A. et al. 2011. In vivo, in situ imaging of microneedle insertion into the skin of human volunteers using optical coherence tomography. *Pharmaceutical Research* 28(1), pp. 66-81. doi: 10.1007/s11095-010-0167-x

Crawford, J. and Doherty, L. 2012. *Practical aspects of ECG recording*. Cumbria, UK: M&K Update Ltd.

Crawford, J. and Doherty, L. 2013. Recording a standard 12-lead ECG: filling in gaps in knowledge. *Journal of Paramedic Practice* 2(3), doi: 10.12968/jpar.2010.2.3.47285

Crawford, M. H. et al. 1999. ACC/AHA guidelines for ambulatory electrocardiography: executive summary and recommendations. A report of the American College of Cardiology/American Heart Association task force on practice guidelines (committee to revise the guidelines for ambulatory electrocardiography). *Circulation* 100(8), pp. 886-893. doi: 10.1161/01.cir.100.8.886

Cua, A. B., Wilhelm, K. P. and Maibach, H. I. 1990. Elastic properties of human skin: relation to age, sex, and anatomical region. *Archives of Dermatological Research* 282(5), pp. 283-288. doi: 10.1007/bf00375720

Curtis, H. J. 1949. Action potential of heart muscle. *The American Journal of Physiology* 159(3), pp. 499-504. doi: 10.1152/ajplegacy.1949.159.3.499.

Daggumati, P., Matharu, Z., Wang, L. and Seker, E. 2015. Biofouling-resilient nanoporous gold electrodes for DNA sensing. *Analytical Chemistry* 87(18), pp. 8618-8622. doi: 10.1021/acs.analchem.5b02969

Daligadu, J. et al. 2018. Validation of the Fitbit Flex in an Acute Post-Cardiac Surgery Patient Population. *Physiotherapy Canada* 70(4), pp. 314-320. doi: 10.3138/ptc.2017-34

Dario, P., Carrozza, M. C., Benvenuto, A. and Menciassi, A. 2000. Micro-systems in biomedical applications. *Journal of Micromechanics and Microengineering* 10(2). doi: 10.1088/0960-1317/10/2/322.

Danso, M. O., Berkers, T., Mieremet, A., Hausil, F. and Bouwstra, J. A. 2015. An ex vivo human skin model for studying skin barrier repair. *Experimental Dermatology* 24(1), pp. 48-54. doi: 10.1111/exd.12579

David, R. M. and Portnoy, W. M. 1972. Insulated electrocardiogram electrodes. *Medical & Biological Engineering & Computing* 10(6), pp. 742-751. doi: 10.1007/bf02477385

Davies, L., Gateley, C., Holland, P., Coulman, S. and Birchall, J. 2017. Accelerating topical anaesthesia using microneedles. *Skin Pharmacology and Physiology* 30, pp. 277-283. doi: 10.1159/000479530

Davis, D. A. 2012. Optimize oxidation for the fastest hematoxylin staining. *Dermatologic Surgery* 38(8), pp. 1331-1335. doi: 10.1111/j.1524-4725.2012.02428.x

Davis, S. P., Landis, B. J., Adams, Z. H., Allen, M. G. and Prausnitz, M. R. 2004. Insertion of microneedles into skin: measurement and prediction of insertion force and needle fracture force. *Journal of Biomechanics* 37(8), pp. 1155-1163. doi: 10.1016/j.jbiomech.2003.12.010

Davis-Smith, C. 2000. Skin preparation to reduce ECG artifact. *Biomedical Instrumentation & Technology* 34(4).

Debeer, S., Le Luduec, J. B., Kaiserlian, D., Laurent, P., Nicolas, J. F., Dubois, B. and Kanitakis, J. 2013. Comparative histology and immunohistochemistry of porcine versus human skin. *European Journal of Dermatology* 23(4), pp. 456-466. doi: 10.1684/ejd.2013.2060

De Luca, C. J., Le Fever, R. S. and Stulen, F. B. 1979. Pasteless electrode for clinical use. *Medical & Biological Engineering & Computing* 17(3), pp. 387-390. doi: 10.1007/bf02443828

Deurenberg-Yap, M., Chew, S. K. and Deurenberg, P. 2002. Elevated body fat percentage and cardiovascular risks at low body mass index levels among Singaporean Chinese, Malays and

Indians. *Obesity reviews: an official journal of the International Association for the Study of Obesity* 3(3), pp. 209-215. doi: 10.1046/j.1467-789x.2002.00069.x

Dias, D. and Paulo Silva Cunha, J. 2018. Wearable Health Devices-Vital Sign Monitoring, Systems and Technologies. *Sensors (Basel, Switzerland)* 18(8), p. 2414. doi: 10.3390/s18082414

Dias, N. S., Carmo, J. P., da Silva, A. F., Mendes, P. M. and Correia, J. H. 2010. New dry electrodes based on iridium oxide (IrO) for non-invasive biopotential recordings and stimulation. *Sensors and Actuators A: Physical* 164(1), pp. 28-34. doi: 10.1016/j.sna.2010.09.016

Dilaveris, P. and Tsioufis, C. 2021. The single-lead 14-day ECG patch EZYPRO®: a new kid in the block. *International Journal of Cardiology* 332, pp. 89-90. doi: 10.1016/j.ijcard.2021.03.069

DiLibero, J., DeSanto-Madyea, S. and O'Dongohue, S. 2016. Improving accuracy of cardiac electrode placement: outcomes of clinical nurse specialist practice. *Clinical Nurse Specialist CNS* 30(1), pp. 45-50. doi: 10.1097/nur.0000000000000172

Dong, L. et al. 2016. Breathable and wearable energy storage based on highly flexible paper electrodes. *Advanced Materials* 28(42), pp. 9313-9319. doi: 10.1002/adma.201602541

Dong, L. et al. 2021. Fully integrated flexible long-term electrocardiogram recording patch with gel-less adhesive electrodes for arrhythmia detection. *Sensors and Actuators A: Physical* 332, p. 113063. doi: 10.1016/j.sna.2021.113063

Donnelly, R. F., Garland, M. J., Morrow, D. I. J., Migalska, K., Singh, T. R. R., Majithiya, R. and Woolfson, A. D. 2010a. Optical coherence tomography is a valuable tool in the study of the effects of microneedle geometry on skin penetration characteristics and in-skin dissolution. *Journal of Controlled Release* 147(3), doi: 10.1016/j.jconrel.2010.08.008

Donnelly, R. F., Singh, T. R. R. and Woolfson, A. D. 2010b. Microneedle-based drug delivery systems: microfabrication, drug delivery, and safety. *Drug Delivery* 17(4), pp. 187-207. doi: 10.3109/10717541003667798

Donnelly, R. F., Singh, T. R., Tunney, M. M., Morrow, D. I., McCarron, P. A., O'Mahony, C. and Woolfson, A. D. 2009. Microneedle arrays allow lower microbial penetration than hypodermic needles in vitro. *Pharmaceutical Research* 26(11), pp. 2513-2522. doi: 10.1007/s11095-009-9967-2

Eckardt, L., Breithardt, G. and Haverkamp, W. 2002. Electrophysiologic Characterization of the Antipsychotic Drug Sertindole in a Rabbit Heart Model of Torsade de Pointes: Low Torsadogenic Potential Despite QT Prolongation. *Journal of Pharmacology and Experimental Therapeutics* 300(1), p. 64. doi: 10.1124/jpet.300.1.64

Edens, C., Dybdahl-Sissoko, N. C., Weldon, W. C., Oberste, M. S. and Prausnitz, M. R. 2015. Inactivated polio vaccination using a microneedle patch is immunogenic in the rhesus macaque. *Vaccine* 33(37), pp. 4683-4690. doi: 10.1016/j.vaccine.2015.01.089

Ehnesh, M., Abatis, P. and Schlindwein, F. S. 2020. A portable electrocardiogram for real-time monitoring of cardiac signals. *SN Applied Sciences* 2(8), p. 1419. doi: 10.1007/s42452-020-3065-9

Einthoven, W. 1895. Ueber die Form des menschlichen Electrocardiogramms. *Archiv für die gesamte Physiologie des Menschen und der Tiere* 60, pp. 101-123.

El-Laboudi, A., Oliver, N. S., Cass, A. and Johnston, D. 2013. Use of microneedle array devices for continuous glucose monitoring: a review. *Diabetes Technology & Therapeutics* 15(1), pp. 101-115. doi: 10.1089/dia.2012.0188

Elias, P. M. 1983. Epidermal lipids, barrier function, and desquamation. *Journal of Investigative Dermatology* 80, pp. 44-49. doi: 10.1038/jid.1983.12

Elias, P. M. 1988. Structure and function of the stratum corneum permeability barrier. *Drug Development Research* 13(2-3), pp. 97-105. doi: 10.1002/ddr.430130203

Enfield, J., O'Connell, M. L., Lawlor, K., Jonathan, E., O'Mahony, C. and Leahy, M. 2010. In-vivo dynamic characterization of microneedle skin penetration using optical coherence tomography. *Journal of Biomedical Optics* 15(4), p. 046001. doi: 10.1117/1.3463002

Engel, J. M., Chakravarthy, B. L., Rothwell, D. and Chavan, A. 2015. SEEQ™ MCT wearable sensor performance correlated to skin irritation and temperature. *Annual International Conference of the IEEE Engineering in Medicine and Biology Society (EMBC)* 2015, pp. 2030-2033. doi: 10.1109/embc.2015.7318785

Fatoorechi, M., Parkinson, J., Prance, R. J., Prance, H., Seth, A. K. and Schwartzman, D. J. 2015. A comparative study of electrical potential sensors and Ag/AgCl electrodes for characterising spontaneous and event related electroencephalagram signals. *Journal of Neuroscience Methods* 251, pp. 7-16. doi: 10.1016/j.jneumeth.2015.04.013

Fayyaz Shahandashti, P., Pourkheyrollah, H., Jahanshahi, A. and Ghafoorifard, H. 2019. Highly conformable stretchable dry electrodes based on inexpensive flex substrate for long-term biopotential (EMG/ECG) monitoring. *Sensors and Actuators A: Physical* 295, pp. 678-686. doi: 10.1016/j.sna.2019.06.041

Federici, A., Rizzo, A. and Cevese, A. 1985. Role of the autonomic nervous system in the control of heart rate and blood pressure in the defence reaction in conscious dogs. *Journal of the Autonomic Nervous System* 12(4), pp. 333-345. doi: 10.1016/0165-1838(85)90048-7

Feinstein, B. 1946. The application of electromyography to affections of the facial and the intrinsic laryngeal muscles. *Proceedings of the Royal Society of Medicine* 39(12), pp. 817-819.

Fercher, A. F. 2010. Optical coherence tomography - development, principles, applications. *Zeitschrift für Medizinische Physik* 20(4), pp. 251-276. doi: 10.1016/j.zemedi.2009.11.002

Fernández, M. and Pallás-Areny, R. 2000. Ag-AgCl electrode noise in high-resolution ECG measurements. *Biomedical Instrumentation & Technology* 34(2), pp. 125-130.

Ferree, T. C., Luu, P., Russell, G. S. and Tucker, D. M. 2001. Scalp electrode impedance, infection risk, and EEG data quality. *Clinical Neurophysiology* 112(3), pp. 536-544. doi: 10.1016/S1388-2457(00)00533-2

Fink, P. L., Muhammad Sayem, A. S., Teay, S. H., Ahmad, F., Shahariar, H. and Albarbar, A. 2021. Development and wearer trial of ECG-garment with textile-based dry electrodes. *Sensors and Actuators A: Physical* 328, p. 112784. doi: 10.1016/j.sna.2021.112784

Finlay, D. D., Nugent, C. D., Nelwan, S. P., Bond, R. R., Donnelly, M. P. and Guldenring, D. 2010. Effects of electrode placement errors in the EASI-derived 12-lead electrocardiogram. *Journal of Electrocardiology* 43(6), pp. 606-611. doi: 10.1016/j.jelectrocard.2010.07.004

Firooz, A., Rajabi-Estarabadi, A., Zartab, H., Pazhohi, N., Fanian, F. and Janani, L. 2017. The influence of gender and age on the thickness and echo-density of skin. *Skin Research and Technology* 23(1), pp. 13-20. doi: 10.1111/srt.12294

Fischer, A. H., Jacobson, K. A., Rose, J. and Zeller, R. 2008a. Hematoxylin and eosin staining of tissue and cell sections. *Cold Spring Harbor Protocols* 2008. doi: 10.1101/pdb.prot4986

Fish, R. M. and Geddes, L. A. 2009. Conduction of electrical current to and through the human body: a review. *Eplasty* 9, p. e44.

Fluhr, J. W. et al. 2003. Glycerol regulates stratum corneum hydration in sebaceous gland deficient (asebia) mice. *Journal of Investigative Dermatology* 120(5), pp. 728-737. doi: 10.1046/j.1523-1747.2003.12134.x

Fong, E.-M. and Chung, W.-Y. 2015. A hygroscopic sensor electrode for fast stabilized non-contact ECG signal acquisition. *Sensors* 15(8), pp. 19237-19250. doi: 10.3390/s150819237

Fore, J. 2006. A review of skin and the effects of aging on skin structure and function. *Ostomy Wound Management* 52(9), pp. 24-35.

Forvi, E. et al. 2012. Preliminary technological assessment of microneedles-based dry electrodes for biopotential monitoring in clinical examinations. *Sensors & Actuators: A. Physical* 180, pp. 177-186. doi: 10.1016/j.sna.2012.04.019

Foutz, T. L., Stone, E. A. and Abrams, C. F., Jr. 1992. Effects of freezing on mechanical properties of rat skin. *American Journal of Veterinary Research* 53(5), pp. 788-792.

Fraley, M. A., Birchem, J. A., Senkottaiyan, N. and Alpert, M. A. 2005. Obesity and the electrocardiogram. *Obesity Reviews* 6(4), pp. 275-281. doi: 10.1111/j.1467-789X.2005.00199.x

Frank, S., Colliver, J. A. and Frank, A. 1986. The electrocardiogram in obesity: statistical analysis of 1,029 patients. *Journal of the American College of Cardiology* 7(2), pp. 295-299. doi: 10.1016/s0735-1097(86)80494-6

Friesen, G. M., Jannett, T.C., Jadallah, M. A., Yates, S. L., Quint, S. R. and Nagle, H. T. 1990. A comparison of the noise sensitivity of nine QRS detection algorithms. *IEEE Transactions on Biomedical Engineering*, pp. 85-98. doi: 10.1109/10.43620

Froning, J. N., Olson, M. D. and Froelicher, V. F. 1988. Problems and limitations of ECG baseline estimation and removal using a cubic spline technique during exercise ECG testing: recommendations for proper implementation. *Journal of Electrocardiology* 21 Suppl, pp. 149-157. doi: 10.1016/0022-0736(88)90083-0

Fukushima, K., Ise, A., Morita, H., Hasegawa, R., Ito, Y., Sugioka, N. and Takada, K. 2011. Two-layered dissolving microneedles for percutaneous delivery of peptide/protein drugs in rats. *Pharmaceutical Research* 28(1), pp. 7-21. doi: 10.1007/s11095-010-0097-7

Fung, E. et al. 2015. Electrocardiographic patch devices and contemporary wireless cardiac monitoring. *Frontiers in Physiology* 6(149), doi: 10.3389/fphys.2015.00149

Funk, M., Fennie, K. P., Stephens, K. E., May, J. L., Winkler, C. G. and Drew, B. J. 2017. Association of Implementation of Practice Standards for Electrocardiographic Monitoring With Nurses' Knowledge, Quality of Care, and Patient Outcomes: Findings From the Practical Use of the Latest Standards of Electrocardiography (PULSE) Trial. *Circulation* 10(2), doi: 10.1161/circoutcomes.116.003132

Gambichler, T., Matip, R., Moussa, G., Altmeyer, P. and Hoffmann, K. 2006. In vivo data of epidermal thickness evaluated by optical coherence tomography: Effects of age, gender, skin type, and anatomic site. *Journal of Dermatological Science* 44(3), pp. 145-152. doi: 10.1016/j.jdermsci.2006.09.008

Gargiulo, G., Bifulco, P., Calvo, R. A., Cesarelli, M., Jin, C. and van Schaik, A. 2008. Mobile biomedical sensing with dry electrodes. *International Conference on Intelligent Sensors, Sensor Networks and Information Processing.* Sydney, Australia, IEEE, pp. 261-266. doi: 10.1109/ISSNIP.2008.4761997.

Gawkrodger, D. J. and Arden-Jones, M. R. 2017. *Dermatology: an illustrated colour text.* Sixth ed. Amsterdam: Elsevier.

Gerstel, M. S. and Place, V. A. 1976. *Drug delivery device.* [Patent].

Giannetta, N., Campagna, G., Di Muzio, F., Di Simone, E., Dionisi, S. and Di Muzio, M. 2020. Accuracy and knowledge in 12-lead ECG placement among nursing students and nurses: a web-based Italian study. *Acta Biomaterialia* 91(12-s), p. e2020004. doi: 10.23750/abm.v91i12-S.10349

Gibbons, W. R. and Fozzard, H. A. 1975. Slow inward currect and contraction of sheep cardiac Purkinje fibers. *The Journal of General Physiology* 65(3), pp. 367-384. doi: 10.1085/jgp.65.3.367

Gill, H. S., Denson, D. D., Burris, B. A. and Prausnitz, M. R. 2008. Effect of microneedle design on pain in human subjects. *The Clinical Journal of Pain* 24(7), pp. 585-594. doi: 10.1097/AJP.0b013e31816778f9

Gill, H. S. and Prausnitz, M. R. 2007. Coated microneedles for transdermal delivery. *Journal of Controlled Release* 117(2), pp. 227-237. doi: 10.1016/j.jconrel.2006.10.017

Gittard, S. D., Chen, B., Xu, H., Ovsianikov, A., Chichkov, B. N., Monteiro-Riviere, N. A. and Narayan, R. J. 2013. The effects of geometry on skin penetration and failure of polymer microneedles. *Journal of Adhesion Science and Technology* 27(3), pp. 227-243. doi: 10.1080/01694243.2012.705101

Gladstone, D. J. et al. 2014. Atrial fibrillation in patients with cryptogenic stroke. *The New England Journal of Medicine* 370(26), pp. 2467-2477. doi: 10.1056/NEJMoa1311376

Goldberger, A. L. et al. 2000. PhysioBank, PhysioToolkit, and PhysioNet: components of a new research resource for complex physiologic signals. *Circulation* 101(23), pp. 215-220. doi: 10.1161/01.cir.101.23.e215.

Goldberger, A. L., Goldberger, Z. D. and Shvilkin, A. 2017. *Goldberger's clinical electrocardiography: a simplified approach*. Ninth ed. Philadelphia, PA: Elsevier.

Gomaa, Y. A., Morrow, D. I. J., Garland, M. J., Donnelly, R. F., El-Khordagui, L. K. and Meidan, V. M. 2010. Effects of microneedle length, density, insertion time and multiple applications on human skin barrier function: assessments by transepidermal water loss. *Toxicology in Vitro* 24(7), pp. 1971-1978. doi: 10.1016/j.tiv.2010.08.012

Gong, M. et al. 2019. Flexible breathable nanomesh electronic devices for on-demand therapy. *Advanced Functional Materials* 29(26). doi: 10.1002/adfm.201902127

González-González, E. et al. 2011. Visualization of plasmid delivery to keratinocytes in mouse and human epidermis. *Scientific Reports* 1, p. 158. doi: 10.1038/srep00158

Gralinski, M. R. 2003. The Dog's Role in the Preclinical Assessment of QT Interval Prolongation. *Toxicologic Pathology* 31(1_suppl), pp. 11-16. doi: 10.1080/01926230390174887

Green, M., Ohlsson, M., Lundager Forberg, J., Björk, J., Edenbrandt, L. and Ekelund, U. 2007. Best leads in the standard electrocardiogram for the emergency detection of acute coronary syndrome. *Journal of Electrocardiology* 40(3), pp. 251-256. doi: 10.1016/j.jelectrocard.2006.12.011

Green, R. A. and Goding, J. A. 2016. Biosynthetic conductive polymer composites for tissue-engineering biomedical devices. In: Poole-Warren, L., Martens, P. and Green, R. eds. *Biosynthetic Polymers for Medical Applications*. Woodhead Publishing, pp. 277-298.

Grimnes, S. and Martinsen, O. G. 2014. *Bioimpedance and bioelectricity basics*. 3rd ed. Amsterdam: Elsevier Science.

Griss, P., Enoksson, P., Tolvanen-Laakso, H., Merilainen, P., Ollmar, S. and Stemme, G. 2000. Spiked biopotential electrodes. *Proceedings IEEE Thirteenth Annual International Conference on Micro Electro Mechanical Systems.* Miyazaki; Japan, 23-27 Jan, 2000. IEEE, pp. 323-328. doi: 10.1109/MEMSYS.2000.838537

Griss, P., Enoksson, P., Tolvanen-Laakso, H. K., Merilainen, P., Ollmar, S. and Stemme, G. 2001. Micromachined electrodes for biopotential measurements. *Journal of Microelectromechanical Systems* 10(1), pp. 10-16. doi: 10.1109/84.911086

Griss, P., Tolvanen-Laakso, H. K., Merilainen, P. and Stemme, G. 2002. Characterization of micromachined spiked biopotential electrodes. *IEEE Transactions on Biomedical Engineering* 49(6), pp. 597-604. doi: 10.1109/TBME.2002.1001974

Grond, M. et al. 2013. Improved detection of silent atrial fibrillation using 72-hour Holter ECG in patients with ischemic stroke: a prospective multicenter cohort study. *Stroke* 44(12), pp. 3357-3364. doi: 10.1161/strokeaha.113.001884

Groves, R. B., Coulman, S. A., Birchall, J. C. and Evans, S. L. 2013. An anisotropic, hyperelastic model for skin: Experimental measurements, finite element modelling and identification of parameters for human and murine skin. *Journal of the Mechanical Behavior of Biomedical Materials* 18, pp. 167-180. doi: 10.1016/j.jmbbm.2012.10.021

Gruetzmann, A., Hansen, S. and Müller, J. 2007. Novel dry electrodes for ECG monitoring. *Physiological Measurement* 28(11), pp. 1375-1390. doi: 10.1088/0967-3334/28/11/005

Gula, L. J., Krahn, A. D., Massel, D., Skanes, A., Yee, R. and Klein, G. J. 2004. External loop recorders: determinants of diagnostic yield in patients with syncope. *American Heart Journal* 147(4), pp. 644-648. doi: 10.1016/j.ahj.2003.10.036

Gunda, S. et al. 2015. Initial real world experience with a novel insertable (Reveal LinQ™@Medtronic) compared to the conventional (Reveal XT™@Medtronic) implantable loop recorder at a tertiary care center — Points to ponder! *International Journal of Cardiology* 191, pp. 58-63. doi: 10.1016/j.ijcard.2015.04.241

Gupta, J., Felner, E. and Prausnitz, M. 2009. Minimally invasive insulin delivery in subjects with type 1 diabetes using hollow microneedles. *Diabetes Technology & Therapeutics* 11(6), pp. 329-337. doi: 10.1089/dia.2008.0103.

Gupta, J., Gill, H. S., Andrews, S. N. and Prausnitz, M. R. 2011. Kinetics of skin resealing after insertion of microneedles in human subjects. *Journal of Controlled Release* 154(2), pp. 148-155. doi: 10.1016/j.jconrel.2011.05.021

Gupta, P., Sharma, K. K. and Joshi, S. D. 2015. Baseline wander removal of electrocardiogram signals using multivariate empirical mode decomposition. *Healthcare Technology Letters* 2(6), pp. 164-166. doi: 10.1049/htl.2015.0029

Ha, S., Kim, C., Chi, Y. M., Cauwenberghs, G., Sazonov, E. and Neuman, M. R. 2014. Chapter 4.3 - Low-Power Integrated Circuit Design for Wearable Biopotential Sensing.*Wearable Sensors*. Oxford: Academic Press, pp. 323-352.

Halcox, P. J. J., Wareham, P. K., Cardew, B. A., Gilmore, B. M., Barry, B. J., Phillips, B. C. and Gravenor, B. M. 2017. Assessment of remote heart rhythm sampling using the alivecor heart monitor to screen for atrial fibrillation: the rehearse-af study. *Circulation* 136(19), pp. 1784-1794. doi: 10.1161/CIRCULATIONAHA.117.030583

Halford, J. J., Schalkoff, R. J., Satterfield, K. E., Martz, G. U., Kutluay, E., Waters, C. G. and Dean, B. C. 2016. Comparison of a Novel Dry Electrode Headset to Standard Routine EEG in Veterans. *Journal of Clinical Neurophysiology* 33(6), pp. 530-537. doi: 10.1097/wnp.0000000000000284

Hamdy, D. A. and Brocks, D. R. 2009. Experimental hyperlipidemia causes an increase in the electrocardiographic changes associated with amiodarone. *Journal of Cardiovascular Pharmacology* 53(1), pp. 1-8. doi: 10.1097/FJC.0b013e31819359d1

Hamilton, P. S., Curley, M. and Aimi, R. 2000. Effect of adaptive motion-artifact reduction on QRS detection. *Biomedical Instrumentation & Technology* 34(3), pp. 197-202.

Hancock, E. W. et al. 2009. AHA/ACCF/HRS recommendations for the standardization and interpretation of the electrocardiogram: part V: electrocardiogram changes associated with cardiac chamber hypertrophy: a scientific statement from the American Heart Association Electrocardiography and Arrhythmias Committee, Council on Clinical Cardiology; the American College of Cardiology Foundation; and the Heart Rhythm Society: endorsed by the International Society for Computerized Electrocardiology. *Circulation* 119(10), pp. e251-261. doi: 10.1161/circulationaha.108.191097

Haq, M. et al. 2009. Clinical administration of microneedles: skin puncture, pain and sensation. *Biomedical Microdevices* 11(1), pp. 35-47. doi: 10.1007/s10544-008-9208-1

Hassarati, R. T., Goding, J. A., Baek, S., Patton, A. J., Poole-Warren, L. A. and Green, R. A. 2014. Stiffness quantification of conductive polymers for bioelectrodes. *Journal of Polymer Science, Part B: Polymer Physics* 52(9), pp. 666-675. doi: 10.1002/polb.23465

Hasselgren, A., Kralevska, K., Gligoroski, D., Pedersen, S. A. and Faxvaag, A. 2020. Blockchain in healthcare and health sciences - A scoping review. *International Journal of Medical Informatics* 134, p. 104040. doi: 10.1016/j.ijmedinf.2019.104040

Hegarty-Craver, M., Kroner, B. L., Bumbut, A., DeFilipp, S. J., Gaillard, W. D. and Gilchrist, K. H. 2021. Cardiac-based detection of seizures in children with epilepsy. *Epilepsy & Behavior* 122, p. 108129. doi: 10.1016/j.yebeh.2021.108129

Henry, S., McAllister, D. V., Allen, M. G. and Prausnitz, M. R. 1998. Microfabricated microneedles: a novel approach to transdermal drug delivery. *Journal of Pharmaceutical Sciences* 87(8), pp. 922-925. doi: 10.1021/js980042+

Herkert, C., Kraal, J. J., van Loon, E. M. A., van Hooff, M. and Kemps, H. M. C. 2019. Usefulness of Modern Activity Trackers for Monitoring Exercise Behavior in Chronic Cardiac Patients: Validation Study. *JMIR mHealth and uHealth* 7(12), p. e15045. doi: 10.2196/15045

Hille, B. 2001. *Ion channels of excitable membranes*. Massachusetts: Sinauear Associates.

Hindricks, G. et al. 2021. 2020 ESC Guidelines for the diagnosis and management of atrial fibrillation developed in collaboration with the European Association for Cardio-Thoracic Surgery (EACTS). *European Heart Journal* 42(5), pp. 373-498. doi: 10.1093/eurheartj/ehaa612

Hodgkin, A. L. and Huxley, A. F. 1939. Action potentials recorded from inside a nerve fibre. *Nature* 144, pp. 710-711.

Holter, N. J. 1961. New method for heart studies: continuous electrocardiography of active subjects over long periods is now practical. *Science* 134, pp. 1214-1220.

Holter, N. J. and Generelli, J. A. 1949. Remote recording of physiological data by radio. *Rocky Mountain Medical Journal* 46(9), pp. 747-751.

Hopenfeld, B. and Ashikaga, H. 2010. Origin of the electrocardiographic U wave: effects of M cells and dynamic gap junction coupling. *Annals of Biomedical Engineering* 38(3), pp. 1060-1070. doi: 10.1007/s10439-010-9941-5

Houben, E., De Paepe, K. and Rogiers, V. 2007. A keratinocyte's course of life. *Skin Pharmacology and Physiology* 20(3), pp. 122-132. doi: 10.1159/000098163

Houghton, A. R. 2019. *Making sense of the ECG: a hands-on guide.* Fifth ed. Boca Raton; London: CRC Press.

Hsu, L., Tung, S., Kuo, C. and Yang, Y. 2014. Developing barbed microtip-based electrode arrays for biopotential measurement. *Sensors* 14(7), pp. 12370-12386. doi: 10.3390/s140712370.

Hua, H., Tang, W., Xu, X., Feng, D. D. and Shu, L. 2019. Flexible multi-layer semi-dry electrode for scalp EEG measurements at hairy sites. *Micromachines* 10(8), doi: 10.3390/mi10080518

Huelsman, L. P. 2003. Analog electrical filters. In: Meyers, R.A. ed. *Encyclopedia of Physical Science and Technology (Third Edition).* New YorkL Academic press, pp. 519-530.

Huszar, R. J. and Wesley, K. 2017. *Huszar's ECG and 12- lead interpretation.* Fifth ed. St. Louis, Missouri: Elsevier.

Ibanez, B. et al. 2018. 2017 ESC Guidelines for the management of acute myocardial infarction in patients presenting with ST-segment elevation: The Task Force for the management of acute myocardial infarction in patients presenting with ST-segment elevation of the European Society of Cardiology (ESC). *European Heart Journal* 39(2), pp. 119-177. doi: 10.1093/eurheartj/ehx393

IEEE. 2008. *IEEE 11073-00101-2008 - IEEE Health informatics - PoC medical device communication Part 00101: Guide -- Guidelines for the use of RF wireless technology.* IEEE. Available at: [Accessed: 19 October 2021].

iRhythm. 2019. *Zio® by iRhythm UK - Uninterrupted Cardiac Monitoring Service.* iRhythm Technologies Limited. Available at: https://irhythmtech.co.uk [Accessed: 17 May 2021].

Isaksen, J., Leber, R., Schmid, R., Schmid, H-J., Generali, G. and Abächerli, R. 2017. Quantification of the first-order high-pass filter's influence on the automatic measurements of the electrocardiogram. *Computer Methods and Programs in Biomedicine* 139, pp. 163-169. doi: 10.1016/j.cmpb.2016.11.003

Isbister, G. K. and Page, C. B. 2013. Drug induced QT prolongation: the measurement and assessment of the QT interval in clinical practice. *British Journal of Clinical Pharmacology* 76(1), pp. 48-57. doi: 10.1111/bcp.12040

Jacobi, U. et al. 2007. Porcine ear skin: an in vitro model for human skin. *Skin Research and Technology* 13(1), pp. 19-24. doi: 10.1111/j.1600-0846.2006.00179.x

Jayaraman, C., Mummidisetty, C. K., Mannix-Slobig, A., McGee Koch, L. and Jayaraman, A. 2018. Variables influencing wearable sensor outcome estimates in individuals with stroke and incomplete spinal cord injury: a pilot investigation validating two research grade sensors. *Journal of NeuroEngineering and Rehabilitation* 15(1), p. 19. doi: 10.1186/s12984-018-0358-y

Jayathilaka, W. et al. 2019. Significance of Nanomaterials in Wearables: A Review on Wearable Actuators and Sensors. *Advanced Materials* 31(7), p. e1805921. doi: 10.1002/adma.201805921

Jemec, G. B., Selvaag, E., Agren, M. and Wulf, H. C. 2001. Measurement of the mechanical properties of skin with ballistometer and suction cup. *Skin Research and Technology* 7(2), pp. 122-126. doi: 10.1034/j.1600-0846.2001.70211.x

Jeong, H. R., Lee, H. S., Choi, I. J. and Park, J. H. 2017. Considerations in the use of microneedles: pain, convenience, anxiety and safety. *Journal of Drug Targeting* 25(1), pp. 29-40. doi: 10.1080/1061186x.2016.1200589

Johnsen, G. K., Martinsen, O. G. and Grimnes, S. 2009. Estimation of in vivo water content of the stratum corneum from electrical measurements. *The Open Biomedical Engineering Journal* 3, pp. 8-12. doi: 10.2174/1874120700903010008

Jung, Y., Son, D., Kwon, S., Kim, J. and Han, K. 2013. Experimental pig model of clinically relevant wound healing delay by intrinsic factors. *International Wound Journal* 10(3), pp. 295-305. doi: 10.1111/j.1742-481X.2012.00976.x

Jung, Y., Kim, S. and Choi, B. 2016. Consumer valuation of the wearables: The case of smartwatches. *Computers in Human Behavior* 63, pp. 899-905. doi: 10.1016/j.chb.2016.06.040

Kaese, S., Frommeyer, G., Verheule, S., van Loon, G., Gehrmann, J., Breithardt, G. and Eckardt, L. 2013. The ECG in cardiovascular-relevant animal models of electrophysiology. *Herzschrittmachertherapie & Elektrophysiologie* 24(2), pp. 84-91. doi: 10.1007/s00399-013-0260-z

Kaese, S. and Verheule, S. 2012. Cardiac electrophysiology in mice: a matter of size. *Frontiers in Physiology* 3, p. 345. doi: 10.3389/fphys.2012.00345

Kalantari, M. 2017. Consumers' adoption of wearable technologies: literature review, synthesis, and future research agenda. *International Journal of Technology Marketing* 12(3), doi: 10.1504/IJTMKT.2017.089665

Kaleschke, G. et al. 2009. Prospective, multicentre validation of a simple, patient-operated electrocardiographic system for the detection of arrhythmias and electrocardiographic changes. *Europace* 11(10), pp. 1362-1368. doi: 10.1093/europace/eup262

Kalluri, H., Kolli, C. and Banga, A. 2011. Characterisation of microchannels created by metal microneedles: formation and closure. *The American Association of Pharmaceutical Scientists* 13(3), pp. 473-481. doi: 10.1208/s12248-011-9288-3

Kalra, A., Lowe, A. and Al-Jumaily, A. M. 2016. Mechanical behaviour of skin: a review. *Journal of Material Science & Engineering* 5(4), doi: 10.4172/2169-0022.1000254

Kang, K., Park, K.-J., Song, J.-J., Yoon, C.-H. and Sha, L. 2011. A medical-grade wireless architecture for remote electrocardiography. *IEEE Transactions on Information Technology in Biomedicine* 15(2), pp. 260-267.

Kant, V., Srivastava, A. K., Verma, P. K., Raina, R. and Pankaj, N. K. 2010. Alterations in Electrocardiographic Parameters after Subacute Exposure of Fluoride and Ameliorative Action of Aluminium Sulphate in Goats. *Biological Trace Element Research* 134(2), pp. 188-194. doi: 10.1007/s12011-009-8460-4

Karaoğuz, M. R. et al. 2019. The quality of ECG data acquisition, and diagnostic performance of a novel adhesive patch for ambulatory cardiac rhythm monitoring in arrhythmia detection. *Journal of Electrocardiology* 54, pp. 28-35. doi: 10.1016/j.jelectrocard.2019.02.012

Karlsson, J. O. and Toner, M. 1996. Long-term storage of tissues by cryopreservation: critical issues. *Biomaterials* 17(3), pp. 243-256. doi: 10.1016/0142-9612(96)85562-1

Karunadas, C. P. and Mathew, C. 2020. Comparison of arrhythmia detection by conventional Holter and a novel ambulatory ECG system using patch and Android App, over 24 h period. *Indian Pacing and Electrophysiology Journal* 20(2), pp. 49-53. doi: 10.1016/j.ipej.2019.12.013

Kaur, G., Adhikari, R., Cass, P., Bown, M. and Gunatillake, P. 2015. Electrically conductive polymers and composites for biomedical applications. *RSC Advances* 5, pp. 37553-37567. doi: 10.1039/C5RA01851J

Kaushik, S., Hord, A., Denson, D., McAllister, D., Smitra, S., Allen, M. and Prausnitz, M. 2001. Lack of pain associated with micro fabricated microneedles. *Anesthesia & Analgesia* 92(2), pp. 502-504. doi: 10.1097/00000539-200102000-00041

Kennedy, H. L. 2013. The evolution of ambulatory ECG monitoring. *Progress in Cardiovascular Diseases* 56(2), pp. 127-132. doi: 10.1016/j.pcad.2013.08.005

Keysight. 2014. *E4980A/AL precision LCR meter users guide*. Keysight Technologies. Available at: www.keysight.com/gb/en/assets/9018-05655/user-manuals/9018-05655.pdf [Accessed: 01 June 2021].

Khalil, C. A., Haddad, F. and Suwaidi, J. A. 2017. Investigating palpitations: the role of Holter monitoring and loop recorders. *British Medical Journal* 358, doi: 10.1136/bmj.j3123

Khanna, P., Luongo, K., Strom, J. A. and Bhansali, S. 2010. Sharpening of hollow silicon microneedles to reduce skin penetration force. *Journal of Micromechanics and Microengineering* 20(4), doi: 10.1088/0960-1317/20/4/045011

Kharabsheh, S. M., Al-Sugair, A., Al-Buraiki, J. and Al-Farhan, J. 2006. Overview of exercise stress testing. *Annals of Saudi Medicine* 26(1), pp. 1-6. doi: 10.5144/0256-4947.2006.1

Kher, R. 2019. Signal processing techniques for removing noise from ECG signals. *Journal of Biomedical Engineering and Research* 3(101).

Kim, H. M., Lim, Y. Y., An, J. H., Kim, M. N. and Kim, B. J. 2012. Transdermal drug delivery using disk microneedle rollers in a hairless rat model. *International Journal of Dermatology* 51(7), pp. 859-863. doi: 10.1111/j.1365-4632.2011.05343.x

Kim, J., Park, S., Nam, G., Choi, Y., Woo, S. and Yoon, S.-H. 2018. Bioinspired microneedle insertion for deep and precise skin penetration with low force: Why the application of mechanophysical stimuli should be considered. *Journal of the Mechanical Behavior of Biomedical Materials* 78, pp. 480-490. doi: 10.1016/j.jmbbm.2017.12.006

Kirchhof, P. et al. 2016. Guidelines for the management of atrial fibrillation developed in collaboration with eacts. *European Heart Journal* 37(38), pp. 2893-2962. doi: 10.1093/eurheartj/ehw210

Kishore, A., Vail, A., Majid, A., Dawson, J., Lees, K. R., Tyrrell, P. J. and Smith, C. J. 2014. Detection of atrial fibrillation after ischemic stroke or transient ischemic attack: a systematic review and meta-analysis. *Stroke* 45(2), pp. 520-526. doi: 10.1161/strokeaha.113.003433

Kitoko, V., Nguyen, T. N., Nguyen, J. S., Tran, Y. and Nguyen, H. T. 2011. Performance of dry electrode with bristle in recording EEG rhythms across brain state changes. *Annual International Conference of the IEEE Engineering in Medicine and Biology Society (EMBC)* 2011, pp. 59-62. doi: 10.1109/iembs.2011.6089896

Kligfield, P. et al. 2007. Recommendations for the standardization and interpretation of the electrocardiogram: part I: The electrocardiogram and its technology: a scientific statement from the American Heart Association Electrocardiography and Arrhythmias Committee, Council on Clinical Cardiology; the American College of Cardiology Foundation; and the Heart Rhythm Society: endorsed by the International Society for Computerized Electrocardiology. *Circulation* 115(10), pp. 1306-1324. doi: 10.1161/circulationaha.106.180200

Kochhar, J., Quek, T., Soon, W., Choi, J., Zou, S. and Kang, L. 2013. Effect of microneedle geometry and supporting substrate on microneedle array penetration into skin. *Journal of Pharmaceutical Sciences* 102(11), pp. 4100-4108. doi: /10.1002/jps.23724

Kohlhardt, M., Figulla, H. R. and Tripathi, O. 1976. The slow membrane channel as the predominant mediator of the excitation process of the sinoatrial pacemaker cell. *Basic Research in Cardiology* 71(1), pp. 17-26. doi: 10.1007/BF01907779

Kohno, R., Abe, H. and Benditt, D. G. 2017. Ambulatory electrocardiogram monitoring devices for evaluating transient loss of consciousness or other related symptoms. *Journal of Arrhythmia* 33(6), pp. 583-589. doi: 10.1016/j.joa.2017.04.012

Kong, R. and Bhargava, R. 2011. Characterization of porcine skin as a model for human skin studies using infrared spectroscopic imaging. *Analyst* 136(11), pp. 2359-2366. doi: 10.1039/c1an15111h

Konopelski, P. and Ufnal, M. 2016. Electrocardiography in rats: a comparison to human. *Physiological Research* 65(5), pp. 717-725. doi: 10.33549/physiolres.933270

Kottner, J., Lichterfeld, A. and Blume-Peytavi, U. 2013. Transepidermal water loss in young and aged healthy humans: a systematic review and meta-analysis. *Archives of Dermatological Research* 305(4), pp. 315-323. doi: 10.1007/s00403-012-1313-6

Koutsonanos, D. G. et al. 2012. Delivery of subunit influenza vaccine to skin with microneedles improves immunogenicity and long-lived protection. *Scientific Reports* 2(357). doi: 10.1038/srep00357

Kvist, P. H., Iburg, T., Bielecki, M., Gerstenberg, M., Buch-Rasmussen, T., Hasselager, E. and Jensen, H. E. 2006. Biocompatibility of electrochemical glucose sensors implanted in the subcutis of pigs. *Diabetes Technology & Therapeutics* 8(4), pp. 463-475. doi: 10.1089/dia.2006.8.463

Kwon, O., Jeong, J., Kim, H. B., Kwon, I. H., Park, S. Y., Kim, J. E. and Choi, Y. 2018. Electrocardiogram sampling frequency range acceptable for heart rate variability analysis. *Healthcare Informatics Research* 24(3), pp. 198-206. doi: 10.4258/hir.2018.24.3.198

Lagow, C. H., Sladek, K. J. and Richardson, P. C. 1971. Anodic insulated tantalum oxide electrocardiograph electrodes. *IEEE Transactions on Biomedical Engineering* 18(2), pp. 162-164. doi: 10.1109/tbme.1971.4502820

Larrañeta, E., Moore, J., Vicente-Pérez, E. M., González-Vázquez, P., Lutton, R., Woolfson, A. D. and Donnelly, R. F. 2014. A proposed model membrane and test method for microneedle insertion studies. *International Journal of Pharmaceutics* 472(1-2), pp. 65-73. doi: 10.1016/j.ijpharm.2014.05.042

Laurent, P., Bonnet , S., Alchas , P., Regolini , P., Mikszta , J., Pettis , R. and Harvey, N. 2007. Evaluation of the clinical performance of a new intradermal vaccine administration technique and associated delivery system. *Vaccine* 25(52), pp. 8833-8842. doi: 10.1016/j.vaccine.2007.10.020

Lavker, R. M., Dong, G., Zheng, P. S. and Murphy, G. F. 1991. Hairless micropig skin. A novel model for studies of cutaneous biology. *The American Journal of Pathology* 138(3), pp. 687-697.

Lee, J. S., Su, Y. W. and Shen, C. C. eds. 2007. *A comparative study of wireless protocols: Bluetooth, UWB, ZigBee, and Wi-Fi. 33rd Annual Conference of the IEEE Industrial Electronics Society.* Taipei, 5-8 November, 2007. IEEE.

Lee, J. S., Heo, J., Lee, W. K., Lim, Y. G., Kim, Y. H. and Park, K. S. 2014. Flexible capacitive electrodes for minimizing motion artifacts in ambulatory electrocardiograms. *Sensors* 14, pp. 14732-14743. doi: 10.3390/s140814732

REFERENCES

Lee, H. et al. 2016. A graphene-based electrochemical device with thermoresponsive microneedles for diabetes monitoring and therapy. *Nature Nanotechnology* 11(6), pp. 566-572. doi: 10.1038/nnano.2016.38

Lee, J., Kim, D., Ryoo, H-Y. and Shin, B-S. 2016. Sustainable wearables: wearable technology for enhancing the quality of human life. *Sustainability* 8(5), p. 466. doi: 10.3390/su8050466

Lenis, G., Pilia, N., Loewe, A., Schulze, W. H. and Dössel, O. 2017. Comparison of Baseline Wander Removal Techniques considering the Preservation of ST Changes in the Ischemic ECG: A Simulation Study. *Computational and Mathematical Methods in Medicine* 2017, p. 9295029. doi: 10.1155/2017/9295029

Leone, M. et al. 2018. Universal applicator for digitally-controlled pressing force and impact velocity insertion of microneedles into skin. *Pharmaceutics* 10(4), doi: 10.3390/pharmaceutics10040211

Levick, J. R. 2010. *An introduction to cardiovascular physiology.* London: Hodder Arnold.

Levin, Y., Kochba, E., Shukarev, G., Rusch, S., Herrera-Taracena, G. and van Damme, P. 2016. A phase 1, open-label, randomized study to compare the immunogenicity and safety of different administration routes and doses of virosomal influenza vaccine in elderly. *Vaccine* 34(44), pp. 5262-5272. doi: 10.1016/j.vaccine.2016.09.008

Levin, Y., Kochba, F. and Kenney, R. 2014. Clinical evaluation of a novel microneedle device for Intradermal delivery of an influenza vaccine: are all delivery methods the same? *Vaccine* 32(34), pp. 4249-4252. doi: 10.1016/j.vaccine.2014.03.024

Levkov, C., Mihov, G., Ivanov, R., Daskalov, I., Christov, I. and Dotsinsky, I. 2005. Removal of power-line interference from the ECG: a review of the subtraction procedure. *BioMedical Engineering OnLine* 4, p. 50. doi: 10.1186/1475-925x-4-50

Lewis, T. 1912. Electro-cardiography and its importance in the clinical examination of heart affections. *British Medical Journal* 2(2689), pp. 65-67. doi: 10.1136/bmj.2.2689.65

Lhernould, M. S., Deleers, M. and Delchambre, A. 2015. Hollow polymer microneedles array resistance and insertion tests. *International Journal of Pharmaceutics* 480(1), pp. 152-157. doi: 10.1016/j.ijpharm.2015.01.019

Li, G., Badkar, A., Nema, S., Kolli, C. and Banga, A. 2009. In vitro transdermal delivery of therapeutic antibodies using maltose microneedles. *International Journal of Pharmaceutics* 368(1-2), pp. 109-115. doi: 10.1016/j.ijpharm.2008.10.008

Li, G., Wang, S. and Duan, Y. Y. 2018. Towards conductive-gel-free electrodes: Understanding the wet electrode, semi-dry electrode and dry electrode-skin interface impedance using electrochemical

impedance spectroscopy fitting. *Sensors and Actuators B: Chemical* 277, pp. 250-260. doi: 10.1016/j.snb.2018.08.155

Li, L. et al. 2006. Age-related changes in skin topography and microcirculation. *Archives of Dermatological Research* 297(9), pp. 412-416. doi: 10.1007/s00403-005-0628-y

Li, W. Z., Huo, M. R., Zhou, J. P., Zhou, Y. Q., Hao, B. H., Liu, T. and Zhang, Y. 2010. Super-short solid silicon microneedles for transdermal drug delivery applications. *International Journal of Pharmaceutics* 389(1-2), pp. 122-129. doi: 10.1016/j.ijpharm.2010.01.024

Li, W., Li, S., Fan, X. and Prausnitz, M. R. 2021. Microneedle patch designs to increase dose administered to human subjects. *Journal of Controlled Release* 339, pp. 350-360. doi: 10.1016/j.jconrel.2021.09.036

Liang, X. and Boppart, S. A. 2010. Biomechanical properties of in vivo human skin from dynamic optical coherence elastography. *IEEE Transactions on Biomedical Engineering* 57(4), pp. 953-959. doi: 10.1109/tbme.2009.2033464

Lim, H., Ha, S., Bae, M. and Yoon, S.-H. 2021. A highly robust approach to fabricate the mass-customizable mold of sharp-tipped biodegradable polymer microneedles for drug delivery. *International Journal of Pharmaceutics* 600, p. 120475. doi: 10.1016/j.ijpharm.2021.120475

Limaye, H. and Deshmukh, V. V. 2016. ECG noise sources and various noise removal techniques: a survey. *International Journal of Application or Innovation in Engineering and Management* 5(2), pp. 86-92.

Liu, C. M. et al. 2021. Enhanced detection of cardiac arrhythmias utilizing 14-day continuous ECG patch monitoring. *International Journal of Cardiology* 332, pp. 78-84. doi: 10.1016/j.ijcard.2021.03.015

Liu, S. et al. 2014. Transdermal delivery of relatively high molecular weight drugs using novel self-dissolving microneedle arrays fabricated from hyaluronic acid and their characteristics and safety after application to the skin. *European Journal of Pharmaceutics and Biopharmaceutics* 86(2), pp. 267-276. doi: 10.1016/j.ejpb.2013.10.001

Liu, W., Zhou, W., Liu, S., Zhang, C., Huang, S., Li, Y. and Hui, K. 2018. Electrical impedance performance of metal dry bioelectrode with different surface coatings. *Sensors and Actuators A: Physical* 269, pp. 515-523. doi: 10.1016/j.sna.2017.12.006

Liu, Z. and Yeung, K. 2008. The preconditioning and stress relaxation of skin tissue. *Journal of Biomedical and Pharmaceutical Engineering* 2(1), pp. 22-28.

Lobodzinski, S. S. 2013. ECG Patch Monitors for Assessment of Cardiac Rhythm Abnormalities. *Progress in Cardiovascular Diseases* 56(2), pp. 224-229. doi: 10.1016/j.pcad.2013.08.006

Loizidou, E. Z., Inoue, N. T., Ashton-Barnett, J., Barrow, D. A. and Allender, C. J. 2016. Evaluation of geometrical effects of microneedles on skin penetration by CT scan and finite element analysis. *European Journal of Pharmaceutics and Biopharmaceutics* 107, pp. 1-6. doi: 10.1016/j.ejpb.2016.06.023

Loizidou, E. Z., Williams, N. A., Barrow, D. A., Eaton, M. J., McCrory, J., Evans, S. L. and Allender, C. J. 2015. Structural characterisation and transdermal delivery studies on sugar microneedles: experimental and finite element modelling analyses. *European Journal of Pharmaceutics and Biopharmaceutics* 89, pp. 224-231. doi: 10.1016/j.ejpb.2014.11.023

Lozano, J. and Stoeber, B. 2021. Fabrication and characterization of a microneedle array electrode with flexible backing for biosignal monitoring. *Biomedical Microdevices* 23(4), p. 53. doi: 10.1007/s10544-021-00583-y

Lubitz, S. A. et al. 2021. Rationale and design of a large population study to validate software for the assessment of atrial fibrillation from data acquired by a consumer tracker or smartwatch: The Fitbit heart study. *American Heart Journal* 238, pp. 16-26. doi: 10.1016/j.ahj.2021.04.003

Lutton, R., Moore, J., Larrañeta, E., Ligett, S., Woolfson, A. and Donnelly, R. 2015. Microneedle characterisation: the need for universal acceptance criteria and GMP specifications when moving towards commercialisation. *Drug Delivery and Translational Research* 5(4), pp. 313-331. doi: 10.1007/s13346-015-0237-z

Macfarlane, P. W. et al. 2014. Racial differences in the ECG-selected aspects. *Journal of Electrocardiology* 47(6), pp. 809-814. doi: 10.1016/j.jelectrocard.2014.08.003

Macfarlane, P. W. 2018. The Influence of Age and Sex on the Electrocardiogram. *Advances in Experimental Medicine and Biology* 1065, pp. 93-106. doi: 10.1007/978-3-319-77932-4_6

Machekposhti, S. A., Soltani, M., Najafizadeh, P., Ebrahimi, S. A. and Chen, P. 2017. Biocompatible polymer microneedle for topical/dermal delivery of tranexamic acid. *Journal of Controlled Release* 261, pp. 87-92. doi: 10.1016/j.jconrel.2017.06.016

Mackiewicz, U., Gerges, J. Y., Chu, S., Duda, M., Dobrzynski, H., Lewartowski, B. and Mączewski, M. 2014. Ivabradine protects against ventricular arrhythmias in acute myocardial infarction in the rat. *Journal of Cellular Physiology* 229(6), pp. 813-823. doi: 10.1002/jcp.24507

Madden, J., O'Mahony, C., Thompson, M., O'Riordan, A. and Galvin, P. 2020. Biosensing in dermal interstitial fluid using microneedle based electrochemical devices. *Sensing and Bio-Sensing Research* 29, p. 100348. doi: 10.1016/j.sbsr.2020.100348

Madias, C. 2019. *Ambulatory ECG monitoring.* UpToDate. Available at: https://www.uptodate.com/contents/ambulatory-ecg-monitoring?source=history_widget [Accessed: 4th July 2019].

Maeda, K. 2017. New method of measurement of epidermal turnover in humans. *Cosmetics* 4(4), doi: 10.3390/cosmetics4040047

Magnani, J. W., Lopez, F. L., Soliman, E. Z., Maclehose, R. F., Crow, R. S. and Alonso, A. 2012. P wave indices, obesity, and the metabolic syndrome: the atherosclerosis risk in communities study. *Obesity (Silver Spring)* 20(3), pp. 666-672. doi: 10.1038/oby.2011.53

Mahdiani, S., Jeyhani, V., Peltokangas, M. and Vehkaoja, A. 2015. Is 50 Hz high enough ECG sampling frequency for accurate HRV analysis? *37th Annual International Conference of the IEEE Engineering in Medicine and Biology Society (EMBC).* Milan, Italy, pp. 5948-5951. doi: 10.1109/embc.2015.7319746

Maher, C., Ryan, J., Ambrosi, C. and Edney, S. 2017. Users' experiences of wearable activity trackers: a cross-sectional study. *BMC Public Health* 17(1), p. 880. doi: 10.1186/s12889-017-4888-1

Maiti, R., Duan, M., Danby, S. G., Lewis, R., Matcher, S. J. and Carré, M. J. 2020. Morphological parametric mapping of 21 skin sites throughout the body using optical coherence tomography. *Journal of the Mechanical Behavior of Biomedical Materials* 102, p. 103501. doi: 10.1016/j.jmbbm.2019.103501

Manju, B. R. and Akshaya, B. 2020. Simulation of pathological ECG signal using transform method. *Procedia Computer Science* 171, pp. 2121-2127. doi: 10.1016/j.procs.2020.04.229

Majumder, S., Mondal, T. and Deen, M. J. 2017. Wearable sensors for remote health monitoring. *Sensors* 17(1). doi: 10.3390/s17010130

Makrantonaki, E. and Zouboulis, C. C. 2008. Skin alterations and diseases in advanced age. *Drug Discovery Today: Disease Mechanisms* 5(2), pp. 153-162. doi: 10.1016/j.ddmec.2008.05.008

Makvandi, P. et al. 2021a. Stimuli-responsive transdermal microneedle patches. *Materials Today* 47, pp. 206-222. doi: 10.1016/j.mattod.2021.03.012

Makvandi, P. et al. 2021b. Engineering Microneedle Patches for Improved Penetration: Analysis, Skin Models and Factors Affecting Needle Insertion. *Nanomicro Lett* 13(1), p. 93. doi: 10.1007/s40820-021-00611-9

Mansoor, I. et al. 2015. A microneedle-based method for the characterization of diffusion in skin tissue using doxorubicin as a model drug. *Biomedical Microdevices* 17(3), p. 9967. doi: 10.1007/s10544-015-9967-4

Mansoor, I., Liu, Y., Häfeli, U. O. and Stoeber, B. 2013. Arrays of hollow out-of-plane microneedles made by metal electrodeposition onto solvent cast conductive polymer structures. *Journal of Micromechanics and Microengineering* 23(8), doi: 10.1088/0960-1317/23/8/085011

Marozas, V., Petrenas, A., Daukantas, S. and Lukosevicius, A. 2011. A comparison of conductive textile-based and silver/silver chloride gel electrodes in exercise electrocardiogram recordings. *Journal of Electrocardiology* 44(2), pp. 189-194. doi: 10.1016/j.jelectrocard.2010.12.004

Marsili, I. A., Biasiolli, L., Masè, M., Adami, A., Andrighetti, A. O., Ravelli, F. and Nollo, G. 2020. Implementation and validation of real-time algorithms for atrial fibrillation detection on a wearable ECG device. *Computers in Biology and Medicine* 116, p. 103540. doi: 10.1016/j.compbiomed.2019.103540

Martanto, W., Davis, S. P., Holiday, N. R., Wang, J., Gill, H. S. and Prausnitz, M. R. 2004. Transdermal delivery of insulin using microneedles in vivo. *Pharmaceutical Research* 21(6), pp. 947-952. doi: 10.1023/b:pham.0000029282.44140.2e

Martin, A., McConville, A., Anderson, A., McLister, A. and Davis, J. 2017. Microneedle manufacture: assessing hazards and control measure. *Safety* 3(4). doi: 10.3390/safety3040025

Martin, C. J., Allender, C. J., Brain, K. R., Morrissey, A. and Birchall, J. C. 2012. Low temperature fabrication of biodegradable sugar glass microneedles for transdermal drug delivery applications. *Journal of Controlled Release* 158(1), pp. 93-101. doi: 10.1016/j.jconrel.2011.10.024

Martinez-Tabares, F. J., Gaviria-Gomez, N. and Castellanos-Dominguez, G. 2014. Very long-term ECG monitoring patch with improved functionality and wearability. *Annual International Conference of the IEEE Engineering in Medicine and Biology Society (EMBC)* 2014, pp. 5964-5967. doi: 10.1109/embc.2014.6944987

Matteucci, M. et al. 2007. Micropatterned dry electrodes for brain–computer interface. *Microelectronic Engineering* 84(5), pp. 1737-1740. doi: 10.1016/j.mee.2007.01.243

Mayer-Davis, E., Dabelea, D. and Lawrence, J. 2017. Incidence Trends of Type 1 and Type 2 Diabetes among Youths, 2002-2012. *New England Journal of Medicine* 377(3), p. 301. doi: 10.1056/NEJMc1706291

Mayotte, M. J., Webster, J. G. and Tompkins, W. J. 1996. Reduction of motion artefacts during paediatric/infant apnoea monitoring. *Medical and Biological Engineering and Computing* 34, pp. 93-96.

McAdams, E. T., Jossinet, J., Lackermeier, A. and Risacher, F. 1996. Factors affecting electrode-gel-skin interface impedance in electrical impedance tomography. *Medical and Biological Engineering and Computing* 34(6), pp. 397-408. doi: 10.1007/bf02523842

McAllister, D., Wang, P., Davis, S., Park, J., Canatella, J., Allen, M. and Prausnitz, M. 2003. Microfabricated needles for transdermal delivery of macromolecules and nanoparticles: fabrication methods and transport studies. *Proceedings of the National Academy of Sciences of the United States of America* 100(24), pp. 13755-13760. doi: doi:10.1073/pnas.2331316100

Medina, V., Clochesy, J. M. and Omery, A. 1989. Comparison of electrode site preparation techniques. *Heart and Lung* 18(5), pp. 456-460.

Medtronic. 2020. *Reveal LINQ ICM system*. Medtronic. Available at: www.medtronic.com/uk-en/patients/treatments-therapies/heart-monitors/our-monitors/reveal-linq-icm.html [Accessed: 18 May 2021].

Meijs, S. et al. 2016. Biofouling resistance of boron-doped diamond neural stimulation electrodes is superior to titanium nitride electrodes in vivo. *Journal of Neural Engineering* 13(5), p. 056011. doi: 10.1088/1741-2560/13/5/056011

Mestrovic, M. A., Helmer, R. J. N., Kyratzis, L. and Kumar, D. 2007. Preliminary study of dry knitted fabric electrodes for physiological monitoring. *3rd International Conference on Intelligent Sensors, Sensor Networks and Information.* Melbourne, Australia, IEEE, pp. 601-606. doi: 10.1109/ISSNIP.2007.4496911

Meyer, W., Schwarz, R. and Neurand, K. 1978. The skin of domestic mammals as a model for the human skin, with special reference to the domestic pig. *Current Problems in Dermatology* 7, pp. 39-52. doi: 10.1159/000401274

Meziane, N., Webster, J. G., Attari, M. and Nimunkar, A. J. 2013. Dry electrodes for electrocardiography. 34(9), pp. 47-69. doi: 10.1088/0967-3334/34/9/R47

Mikszta, J. A., Alarcon, J. B., Brittingham, J. M., Sutter, D. E., Pettis, R. J. and Harvey, N. G. 2002. Improved genetic immunization via micromechanical disruption of skin-barrier function and targeted epidermal delivery. *Nature Medicine* 8, pp. 415-419. doi: 10.1038/nm0402-415

Milliez, P. et al. 2005. Spironolactone reduces fibrosis of dilated atria during heart failure in rats with myocardial infarction. *European Heart Journal* 26(20), pp. 2193-2209.

Minnikanti, S., Pereira, M. G. A. G., Jaraiedi, S., Jackson, K., Costa-Neto, C. M., Li, Q. and Peixoto, N. 2010. In vivo electrochemical characterization and inflammatory response of multiwalled carbon nano-tube-based electrodes in rat hippocampus. *Journal of Neural Engineering* 7(1), p. 016002.

Mirza, K., Zuliani, C., Hou, B., Ng, F., Peters, N. and Toumazou, C. eds. 2017. *Injection moulded microneedle sensor for real-time wireless pH monitoring. Proceedings of the 39th Annual International Conference of the IEEE Engineering in Medicine and Biology Society (EMBC).* Seogwipo, South Korea, 11-15 July. IEEE.

Mittal, S., Rogers, J., Sarkar, S., Koehler, J., Warman, E. N., Tomson, T. T. and Passman, R. S. 2016. Real-world performance of an enhanced atrial fibrillation detection algorithm in an insertable cardiac monitor. *Heart Rhythm* 13(8), pp. 1624-1630. doi: 10.1016/j.hrthm.2016.05.010

Mittal, S. S., Zabran, M., Ghose, K. and Turner, J. N. 2020. Low-power discreetly-wearable smart ECG patch with on-board analytics. *2020 IEEE International Symposium on Medical Measurements and Applications.* Bari, Italy, 1 June -1 July 2020. IEEE. doi: 10.1109/MeMeA49120.2020.9137284

Moga, K. A. et al. 2013. Rapidly-dissolvable microneedle patches via a highly scalable and reproducible soft lithography approach. *Advanced Materials* 25(36), pp. 5060-5066. doi: 10.1002/adma.201300526

Mohammed, Y. H. et al. 2014. Microneedle enhanced delivery of cosmeceutically relevant peptides in human skin. *PLoS One* 9(7). doi: 10.1371/journal.pone.0101956

Molander, U., Dey, D. K., Sundh, V. and Steen, B. 2003. ECG abnormalities in the elderly: prevalence, time and generation trends and association with mortality. *Aging Clinical and Experimental Research* 15(6), pp. 488-493. doi: 10.1007/bf03327371

Moronkeji, K., Todd, S., Dawidowska, I., Barrett, S. and Akhta r, R. 2017. The role of subcutaneous tissue stiffness on microneedle performance in a representative in vitro model of skin. *Journal of Controlled Release* 265, pp. 102-112. doi: 10.1016/j.jconrel.2016.11.004

Moruzzi, G. and Magoun, H. W. 1949. Brain stem reticular formation and activation of the EEG. *Electroencephalography and Clinical Neurophysiology* 1(4), pp. 455-473.

Moss, A. J. 2010. Gender differences in ECG parameters and their clinical implications *Annals of Noninvasive Electrocardiology* 15(1), doi: 10.1111/j.1542-474X.2009.00345.x

Mota, A. R. et al. 2013. Development of a quasi-dry electrode for EEG recording. *Sensors and Actuators A: Physical* 199, pp. 310-317. doi: 10.1016/j.sna.2013.06.013

Murray, C. J. L. et al. 2020. Global burden of 87 risk factors in 204 countries and territories, 1990–2019: a systematic analysis for the Global Burden of Disease Study 2019. *The Lancet* 396(10258), pp. 1223-1249. doi: 10.1016/S0140-6736(20)30752-2

National Society for Histotechnology [NSH]. 2001. *Guidelines for hematoxylin & eosin staining*. Available at: http://nsh.org/sites/default/files/Guidelines_For_Hematoxylin_and_Eosin_Staining.pdf [Accessed: 08 May 2019].

Neuman, M. R. 2000. Biopotential electrodes. In: Bronzino, J.D. and Peterson, D.R. eds. *The biomedical engineering handbook*. Boca Raton: London: CRC Press LLC.

Ng, K. W. et al. 2009. Development of an ex vivo human skin model for intradermal vaccination: tissue viability and Langerhans cell behaviour. *Vaccine* 27(43), pp. 5948-5955. doi: 10.1016/j.vaccine.2009.07.088

NHS. 2018. Clinical review: adult ECG electrodes. NHS Supply Chain.

NICE. 2012. *Epilepsies: diagnosis and management*. London: National Institute for Health and Care Excellence [NICE]. Available at: https://www.nice.org.uk/guidance/CG137 [Accessed: 15 March 2021].

NICE. 2014. *Acute coronary syndromes in adults*. London: National Institute for Health and Care Excellence [NICE]. Available at: https://www.nice.org.uk/guidance/qs68 [Accessed: 09 March 2021].

NICE. 2020a. *Implantable cardiac monitors to detect atrial fibrillation after cryptogenic stroke*. National Institute of Health and Care Excellence [NICE]. Available at: www.nice.org.uk/guidance/DG41 [Accessed: 18 May 2021].

NICE. 2020b. *Transcranial magnetic stimulation for obsessive-compulsive disorder*. London: National Institute of Health and Care Excellence [NICE]. Available at: https://www.nice.org.uk/guidance/ipg676 [Accessed: 15 March 2021].

NICE. 2020c. *Zio XT for detecting cardiac arrhythmias*. National Institute for Health and Care Excellence [NICE]. Available at: www.nice.org.uk/guidance/mtg52 [Accessed: 17 May 2021].

Nicholas, D. et al. 2018. Rapid paper based colorimetric detection of glucose using a hollow microneedle device. *International Journal of Pharmaceutics* 547(1), pp. 244-249. doi: 10.1016/j.ijpharm.2018.06.002

Nielsen, J. B., Plasencia, I., Sørensen, J. A. and Bagatolli, L. A. 2011. Storage conditions of skin affect tissue structure and subsequent in vitro percutaneous penetration. *Skin Pharmacology and Physiology* 24(2), pp. 93-102. doi: 10.1159/000322304

Nimi, N., Paul, W. and Sharma, C. P. 2011. Blood protein adsorption and compatibility studies of gold nanoparticles. *Gold Bulletin* 44, pp. 15-20.

Nishinaka, Y., Jun , R., Prihandana, G. S. and Miki, N. 2013. Fabrication of polymer microneedle electrodes coated with nanoporous parylene. *Japanese Journal of Applied Physics* 52, doi: 10.7567/JJAP.52.06GL10

Nordquist, L., Roxhed, N., Griss, P. and Stemme, G. 2007. Novel microneedle patches for active insulin delivery are efficient in maintaining glycaemic control: an initial comparison with subcutaneous administration. *Pharmaceutical Research* 24(7), pp. 1381-1388. doi: 10.1007/s11095-007-9256-x

Norman, J. J., Arya, J. M., McClain, M. A., Frew, P. M., Meltzer, M. I. and Prausnitz, M. R. 2014. Microneedle patches: usability and acceptability for self-vaccination against influenza. *Vaccine* 32(16), pp. 1856-1862. doi: 10.1016/j.vaccine.2014.01.076

Novacor. 2018. *R.test evolution 4*. Novacor UK Ltd. Available at: www.novacor.co.uk/item-rtest_4.html [Accessed: 18 May 2021].

Nuttall, F. Q. 2015. Body Mass Index: Obesity, BMI, and Health: A Critical Review. *Nutrition today* 50(3), pp. 117-128. doi: 10.1097/NT.0000000000000092

Ödman, S. and Åke Öberg, P. 1982. Movement-induced potentials in surface electrodes. *Medical and Biological Engineering and Computing* 20(2), pp. 159-166. doi: 10.1007/bf02441351

Olatunji, O., Das, D. B., Garland, M. J., Belaid, L. and Donnelly, R. F. 2013. Influence of array interspacing on the force required for successful microneedle skin penetration: theoretical and practical approaches. *Journal of Pharmaceutical Sciences* 102(4), pp. 1209-1221. doi: 10.1002/jps.23439

Olshansky, B., Sabbah, H. N., Hauptman, P. J. and Colucci, W. S. 2008. Parasympathetic nervous system and heart failure: pathophysiology and potential implications for therapy. *Circulation* 118(8), pp. 863-871. doi: 10.1161/circulationaha.107.760405

O'Mahony, C., Pini, F., Blake, A., Webster, C., O'brien, J. and McCarthy, K. G. 2012. Microneedle-based electrodes with integrated through-silicon via for biopotential recording. *Sensors & Actuators: A. Physical* 186, pp. 130-136. doi: 10.1016/j.sna.2012.04.037

O'Mahony, C. et al. 2013. Skin insertion mechanisms of microneedle-based dry electrodes for physiological signal monitoring. *IEEE Biomedical Circuits and Systems Conference.* Rotterdam; Netherlands, 21 Oct - 2 Nov, 2013. IEEE, pp. 69-72. doi: 10.1109/BioCAS.2013.6679642

O'Mahony, C. 2014. Structural characterization and in-vivo reliability evaluation of silicon microneedles. *Biomedical Microdevices* 16(3), pp. 333-343. doi: 10.1007/s10544-014-9836-6

O'Mahony, C., Grygoryev, K., Ciarlone, A., Giannoni, G., Kenthao, A. and Galvin, P. 2016. Design, fabrication and skin-electrode contact analysis of polymer microneedle-based ECG electrodes. *Journal of Micromechanics and Microengineering* 26(8), doi: 10.1088/0960-1317/26/8/084005

Oster, C. D. 2005. *Proper skin prep helps ensure ECG trace quality*. 3M. Available at: https://multimedia.3m.com/mws/media/358372O/proper-skin-prep-ecg-trace-quality-white-paper.pdf [Accessed: 19 April 2021].

O'Sullivan, M., Temko, A., Bocchino, A., O'Mahony, C., Boylan, G. and Popovici, E. 2019. Analysis of a low-cost EEG monitoring system and dry electrodes toward clinical use in the neonatal icu. *Sensors* 19(11), doi: 10.3390/s19112637

Ozanne, A., Johansson, D., Hällgren Graneheim, U., Malmgren, K., Bergquist, F. and Alt Murphy, M. 2018. Wearables in epilepsy and Parkinson's disease - A focus group study. *Acta Neurologica Scandinavica* 137(2), pp. 188-194. doi: 10.1111/ane.12798

Padmadinata, F. Z., Veerhoek, J. J., van Dijk, G. J. A. and Huijsing, J. H. 1990. Microelectronic skin electrode. *Sensors and Actuators B: Chemical* 1(1), pp. 491-494. doi: 10.1016/0925-4005(90)80257-Z

Pailler-Mattei, C., Bec, S. and Zahouani, H. 2008. In vivo measurements of the elastic mechanical properties of human skin by indentation tests. *Medical Engineering & Physics* 30(5), pp. 599-606. doi: 10.1016/j.medengphy.2007.06.011

Park, J. H., Allen, M. G. and Prausnitz, M. R. 2005. Biodegradable polymer microneedles: fabrication, mechanics and transdermal drug delivery. *Journal of Controlled Release* 104(1), pp. 51-66. doi: 10.1016/j.jconrel.2005.02.002

Park, J.-H., Choi, S.-O., Seo, S., Choy, Y. B. and Prausnitz, M. R. 2010. A microneedle roller for transdermal drug delivery. *European Journal of Pharmaceutics and Biopharmaceutics* 76(2), pp. 282-289. doi: 10.1016/j.ejpb.2010.07.001

Park, K. Y. et al. 2013. Safety evaluation of stamp type digital microneedle devices in hairless mice. *Annals of Dermatology* 25(1), pp. 46-53. doi: 10.5021/ad.2013.25.1.46

Park, H. Y. L., Lee, N. Y., Choi, J. A. and Park, C. K. 2014. Measurement of scleral thickness using swept-source optical coherence tomography in patients with open-angle glaucoma and myopia. *American Journal of Ophthalmology* 157(4), pp. 876-884. doi: 10.1016/j.ajo.2014.01.007

Patel, Y. A., Willsie, A., Clements, I. P., Aguilar, R., Rajaraman, S. and Butera, R. J. 2016. Microneedle cuff electrodes for extrafascicular peripheral nerve interfacing. *Annual International Conference of the IEEE Engineering in Medicine and Biology.* 2016, pp. 1741-1744. doi: 10.1109/embc.2016.7591053

Pattani, A. et al. 2012. Microneedle mediated intradermal delivery of adjuvanted recombinant HIV-1 CN54gp140 effectively primes mucosal boost inoculations. *Journal of Controlled Release* 162(3), pp. 529–537. doi: 10.1016/j.jconrel.2012.07.039

Pearton, M. et al. 2010. Influenza virus-like particles coated onto microneedles can elicit stimulatory effects on Langerhans cells in human skin. *Vaccine* 28(37), pp. 6104-6113. doi: 10.1016/j.vaccine.2010.05.055

Pearton, M., Saller, V., Coulman, S. A., Gateley, C., Anstey, A. V., Zarnitsyn, V. and Birchall, J. C. 2012. Microneedle delivery of plasmid DNA to living human skin: Formulation coating, skin insertion and gene expression. *Journal of Controlled Release* 160(3), pp. 561-569. doi: 10.1016/j.jconrel.2012.04.005

Peck, J., Wishon, M. J., Wittels, H., Lee, S. J., Hendricks, S., Davila, H. and Wittels, S. H. 2021. Single limb electrocardiogram using vector mapping: Evaluation and validation of a novel medical device. *Journal of Electrocardiology* 67, pp. 136-141. doi: 10.1016/j.jelectrocard.2021.06.003

Pelliccia, A. et al. 2021. 2020 ESC Guidelines on sports cardiology and exercise in patients with cardiovascular disease. *European Heart Journal* 42(1), pp. 17-96. doi: 10.1093/eurheartj/ehaa605

Peng, K., Vora, L. K., Domínguez-Robles, J., Naser, Y. A., Li, M., Larrañeta, E. and Donnelly, R. F. 2021. Hydrogel-forming microneedles for rapid and efficient skin deposition of controlled release tip-implants. *Materials Science and Engineering: C* 127, p. 112226. doi: 10.1016/j.msec.2021.112226

Perez, M. V. et al. 2019. Large-Scale Assessment of a Smartwatch to Identify Atrial Fibrillation. *The New England Journal of Medicine* 381(20), pp. 1909-1917. doi: 10.1056/NEJMoa1901183

Pérez-Riera, A. R., Barbosa-Barros, R., Daminello-Raimundo, R. and de Abreu, L. C. 2018. Main artifacts in electrocardiography. *Annals of noninvasive electrocardiology* 23(2). doi: 10.1111/anec.12494

Philips. 2008. *Improving ECG quality*. USA: Koninklijke Philips Electronics N.V. Available at: https://philipsproductcontent.blob.core.windows.net/assets/20170523/f2fc03ac224d4d5bb6aaa77c0151ac70.pdf [Accessed: 11 March 2021].

Pierleoni, P. et al. 2019. Simultaneously acquired data from contactless and wearable devices for direct and indirect heart-rate measurement. *Data in Brief* 26, p. 104436. doi: 10.1016/j.dib.2019.104436

Pin, O. C., Jambek, A. B. and Yaacob, S. 2014. Circuit architectures reviews for portable ECG signal analyzer. *2nd International Conference on Electronic Design.* Penang, Malaysia, 19-21 August. IEEE. doi: 10.1109/ICED.2014.7015810

Pini, F., O'Mahony, C. and McCarthy, K. G. 2012. Electrical characterisation of dry microneedle electrodes for portable bio-potential recording applications. *IEEE International Conference on Microelectronic Test Structures.* San Diego; USA, 19-22 March, 2012. IEEE, pp. 87-90. doi: 10.1109/ICMTS.2012.6190624

Pliquett, U., Langer, R. and Weaver, J. C. 1995. Changes in the passive electrical properties of human stratum corneum due to electroporation. *Biochimica et Biophysica Acta* 1239(2), pp. 111-121. doi: 10.1016/0005-2736(95)00139-t

Poblete, P. F., Kennedy, H. L. and Caralis, D. G. 1978. Detection of ventricular ectopy in patients with coronary heart disease and normal subjects by exercise testing and ambulatory electrocardiography. *Chest* 74(4), pp. 402-407. doi: 10.1378/chest.74.4.402

Pocock, G. and Richards, C. D. 2018. *Human Physiology (Fifth edition).* Oxford, UK: Oxford University Press.

Poliks, M. et al. 2016. A wearable flexible hybrid electronics ECG monitor. *2016 IEEE 66th Electronic Components and Technology Conference.* Las Vegas, USA, 31 May - 3 June 2016. IEEE, pp. 1623-1631.

Ponikowski, P. et al. 2016. 2016 ESC Guidelines for the Diagnosis and Treatment of Acute and Chronic Heart Failure. *Revista Española de Cardiología (English Edition)* 69(12), p. 1167. doi: 10.1016/j.rec.2016.11.005

Prasad, B. V. P. and Parthasarathy, V. 2018. Detection and classification of cardiovascular abnormalities using FFT based multi-objective genetic algorithm. *Biotechnology & Biotechnological Equipment* 32(1), pp. 183-193.

Prausnitz, M. R. and Langer, R. 2008. Transdermal drug delivery. *Nature Biotechnology* 26(11), pp. 1261-1268. doi: 10.1038/nbt.1504

Prausnitz, M. R. 2017. Engineering microneedle patches for vaccination and drug delivery to skin. *Annual Review of Chemical and Biomolecular Engineering* 8, pp. 177-200. doi: 10.1146/annurev-chembioeng-060816-101514

Prineas, R. J., Crow, R. S. and Zhang, Z-M. 2010. *The Minnesota code of manual electrocardiographic findings*. London: Springer London.

Prutkin, J. M. 2019. *ECG tutorial: basic principles of ECG analysis*. UpToDate. Available at: https://www.uptodate.com/contents/ecg-tutorial-basic-principles-of-ecg-analysis?source=history_widget [Accessed: 4th July 2019].

Pürerfellner, H., Sanders, P., Pokushalov, E., Di Bacco, M., Bergemann, T. and Dekker, L. R. C. 2015. Miniaturized Reveal LINQ insertable cardiac monitoring system: First-in-human experience. *Heart Rhythm* 12(6), pp. 1113-1119. Doi:10.1016/j.hrthm.2015.02.030

Puurtinen, M. M., Komulainen, S. M., Kauppinen, P. K., Malmivuo, J. A. and Hyttinen, J. A. K. 2006. Measurement of noise and impedance of dry and wet textile electrodes, and textile electrodes with hydrogel. *International Conference of the IEEE Engineering in Medicine and Biology Society (EMBC).* New York, USA, 30 August - 3 September 2006. IEEE. doi: 10.1109/IEMBS.2006.260155

Qiu, Q., Zhu, M., Li, Z., Qiu, K., Liu, X., Yu, J. and Ding, B. 2019. Highly flexible, breathable, tailorable and washable power generation fabrics for wearable electronics. *Nano Energy* 58, pp. 750-758. doi: 10.1016/j.nanoen.2019.02.010

Quinn, H. L., Hughes, C. M. and Donnelly, R. F. 2018. In vivo and qualitative studies investigating the translational potential of microneedles for use in the older population. *Drug Delivery and Translational Research* 8(2), pp. 307-316. doi: 10.1007/s13346-017-0393-4

Rahal, M., Khor, J. M., Demosthenous, A., Tizzard, A. and Bayford, R. 2009. A comparison study of electrodes for neonate electrical impedance tomography. *Physiological Measurement* 30(6). doi: 10.1088/0967-3334/30/6/S05

Rajabi, M. et al. 2016. Flexible and stretchable microneedle patches with integrated rigid stainless steel microneedles for transdermal biointerfacing. *PLoS One* 11(12). doi: 10.1371/journal.pone.0166330

Rajakariar, K., Koshy, A. N., Sajeev, J. K., Nair, S., Roberts, L. and Teh, A. W. 2018. Modified positioning of a smartphone based single-lead electrocardiogram device improves detection of atrial flutter. *Journal of Electrocardiology* 51(5), pp. 884-888. doi: 10.1016/j.jelectrocard.2018.07.008

Rampton, M. et al. 2013. Antibody responses to Sarcoptes scabiei apolipoprotein in a porcine model: relevance to immunodiagnosis of recent infection. *PLoS One* 8(6), p. e65354. doi: 10.1371/journal.pone.0065354

Ramöller, I. K., McAlister, E., Bogan, A., Cordeiro, A. S. and Donnelly, R. F. 2020. Novel design approaches in the fabrication of polymeric microarray patches via micromoulding. *Micromachines (Basel)* 11(6), p. 554. doi: 10.3390/mi11060554

Ranamukhaarachchi, S. A. et al. 2016. A micromechanical comparison of human and porcine skin before and after preservation by freezing for medical device development. *Scientific Reports* 6, p. 32074. doi: 10.1038/srep32074

Ranamukhaarachchi, S. A. et al. 2015. Development and validation of an artificial mechanical skin model for the study of interactions between skin and microneedles. *Macromolecular Materials and Engineering* 301(3), pp. 306-314. doi: 10.1002/mame.201500320

Raphisak, P., Schuckers, S. C. and de Jongh Curry, A. 2004. An algorithm for EMG noise detection in large ECG data. *Computers in Cardiology.* Chicago, IL, USA, 19-22 Sept. 2004. IEEE. doi: 10.1109/CIC.2004.1442949

Rault, T., Bouabdallah, A., Challal, Y. and Marin, F. 2017. A survey of energy-efficient context recognition systems using wearable sensors for healthcare applications. *Pervasive and Mobile Computing* 37, pp. 23-44. doi: 10.1016/j.pmcj.2016.08.003

Rautaharju, P. M., Zhou, S. H., Wong, S., Calhoun, H. P., Berenson, G. S., Prineas, R. and Davignon, A. 1992. Sex differences in the evolution of the electrocardiographic QT interval with age. *Canadian Journal of Cardiology* 8(7), pp. 690-695.

Reeder, G. S., Awtry, E. and Mahler, S. A. 2021. *Initial evaluation and management of suspected acute coronary syndrome (myocardial infarction, unstable angina) in the emergency room.* UpToDate. Available at: www.uptodate.com/contents/initial-evaluation-and-management-of-suspected-acute-coronary-syndrome-myocardial-infarction-unstable-angina-in-the-emergency-

department?search=resting%20ECG&source=search_result&selectedTitle=3~150&usage_type=d efault&display_rank=3 [Accessed: 20 May 2021].

Reiffel, J. A., Schwarzberg, R. and Murry, M. 2005. Comparison of autotriggered memory loop recorders versus standard loop recorders versus 24-hour Holter monitors for arrhythmia detection. *American Journal of Cardiology* 95(9), pp. 1055-1059. doi: 10.1016/j.amjcard.2005.01.025

Reilly, R. B. and Lee, T. C. 2010. Electrograms (ECG, EEG, EMG, EOG). *Technology and Health Care* 18(6), pp. 443-458. doi: 10.3233/THC-2010-0604

Ren, L., Jiang, Q., Chen, K., Chen, Z., Pan, C. and Jiang, L. 2016. Fabrication of a micro-needle array electrode by thermal drawing for bio-signals monitoring. *Sensors* 16 (6). doi: 10.3390/s16060908

Ren, L., Jiang, Q., Chen, Z., Chen, K., Xu, S., Gao, J. and Jiang, L. 2017. Flexible microneedle array electrode using magnetorheological drawing lithography for bio-signal monitoring. *Sensors and Actuators A: Physical* 268, pp. 38-45. doi: 10.1016/j.sna.2017.10.042

Ren, L. et al. 2018. Fabrication of flexible microneedle array electrodes for wearable bio-signal recording. *Sensors (Basel)* 18(4). doi: 10.3390/s18041191

Resnik, D., Možek, M., Pečar, B., Dolžan, T., Janež, A., Urbančič, V. and Vrtačnik, D. 2015. Characterization of skin penetration efficacy by Au-coated Si microneedle array electrode. *Sensors and Actuators A: Physical* 232, pp. 299-309. doi: 10.1016/j.sna.2015.05.020

Rho, R., Vossler, M., Blancher, S. and Poole, J. E. 2018. Comparison of 2 ambulatory patch ECG monitors: The benefit of the P-wave and signal clarity. *American Heart Journal* 203, pp. 109-117. doi: 10.1016/j.ahj.2018.03.022

Ribet, F., Stemme, G. and Roxhed, N. 2018. Real-time intradermal continuous glucose monitoring using a minimally invasive microneedle-based system. *Biomedical Microdevices* 20(101), doi: 10.1007/s10544-018-0349-6

Rizos, T. et al. 2012. Continuous stroke unit electrocardiographic monitoring versus 24-hour Holter electrocardiography for detection of paroxysmal atrial fibrillation after stroke. *Stroke* 43(10), pp. 2689-2694. doi: 10.1161/strokeaha.112.654954

Robinson, B. F., Epstein, S. E., Beiser, G. D. and Braunwald, E. 1966. Control of heart rate by autonomic nervous system. Studies in man on the interrelation between baroreceptor mechanisms. *Circulation Research* 19(2), pp. 400-411. doi: 10.1161/01.res.19.2.400

Roccia, H., Argaud, L., Le Goic, M., Guérin, C. and Cour, M. 2021. Electrocardiogram monitoring in the prone position in coronavirus disease 2019 acute respiratory distress syndrome. *European Journal of Cardiovascular Nursing* 20(8), pp. 792-796. doi: 10.1093/eurjcn/zvab094

Roffi, M. et al. 2015. 2015 ESC Guidelines for the Management of Acute Coronary Syndromes in Patients Presenting Without Persistent ST-segment Elevation. *Revista Española de Cardiología (English Edition)* 68(12), p. 1125. doi: 10.1016/j.rec.2015.10.009

Romanovsky, A. A. 2014. Skin temperature: its role in thermoregulation. *Acta Physiologica* 210(3), pp. 498-507. doi: 10.1111/apha.12231

Römgens, A. M., Bader, D. L., Bouwstra, J. A., Baaijens, F. P. T. and Oomens, C. W. J. 2014. Monitoring the penetration process of single microneedles with varying tip diameters. *Journal of the Mechanical Behavior of Biomedical Materials* 40, pp. 397-405. doi: 10.1016/j.jmbbm.2014.09.015

Rood, A. and Sparks, K. 2006. Comparison of ECG signal quality between a novel dry electrode and a standard gel electrode. *Medicine and Science in Sports and Exercise* 38(11).

Rothman, S. A. et al. 2006. The diagnosis of cardiac arrhythmias: a prospective multi-center randomized study comparing mobile cardiac outpatient telemetry versus standard loop event monitoring. *Journal of Cardiovascular Electrophysiology* 18(3), pp. 241-247. doi: 10.1111/j.1540-8167.2006.00729.x

Rouphael, N. G. et al. 2017. The safety, immunogenicity, and acceptability of inactivated influenza vaccine delivered by microneedle patch (TIV-MNP 2015): a randomised, partly blinded, placebo-controlled, phase 1 trial. *Lancet* 390(10095), pp. 649-658. doi: 10.1016/s0140-6736(17)30575-5

Roxhed, N., Gasser, T., Griss, P., Holzapfel, G. and Stemme, G. 2007. Penetration-enhanced ultrasharp microneedles and prediction on skin interaction for efficient transdermal drug delivery. *Journal of Mircoelectromechanical Systems* 16(6), pp. 1429 - 1440. doi: 10.1109/JMEMS.2007.907461

Ruffini, G. et al. 2006. A dry electrophysiology electrode using CNT arrays. *Sensors & Actuators: A. Physical* 132(1), pp. 34-41. doi: 10.1016/j.sna.2006.06.013

Runyan, W. R. and Bean, K. E. 1990. *Semiconductor Integrated Circuit Processing Technology*. New York: Addison-Wesley Longman, Incorporated.

Rupp, M. A., Michaelis, J. R., McConnell, D. S. and Smither, J. A. 2018. The role of individual differences on perceptions of wearable fitness device trust, usability, and motivational impact. *Applied Ergonomics* 70, pp. 77-87. doi: 10.1016/j.apergo.2018.02.005

Ruwald, M. H. and Zareba, W. 2013. ECG Monitoring in Syncope. *Progress in Cardiovascular Diseases* 56(2), pp. 203-210. doi: 10.1016/j.pcad.2013.08.007

Sadikoglu, F., Kavalcioglu, C. and Dagman, B. 2017. Electromyogram (EMG) signal detection, classification of EMG signals and diagnosis of neuropathy muscle disease. *Procedia Computer Science* 120, pp. 422-429. doi: 10.1016/j.procs.2017.11.259

Sakamoto, M., Hasegawa, Y. and Shikida, M. 2021. Development of spear-shaped microneedle and applicator for tip insertion into artificial skin. *Microsystem Technologies* 163. doi: 10.10007/s00542-020-05195-9

Salerno, S. M., Alguire, P. C. and Waxman, H. S. 2003a. Competency in interpretation of 12-lead electrocardiograms: a summary and appraisal of published evidence. *Annals of Internal Medicine* 138(9), pp. 751-760. doi: 10.7326/0003-4819-138-9-200305060-00013

Salerno, S. M., Alguire, P. C. and Waxman, H. S. 2003b. Training and competency evaluation for interpretation of 12-lead electrocardiograms: recommendations from the American College of Physicians. *Annals of Internal Medicine* 138(9), pp. 747-750. doi: 10.7326/0003-4819-138-9-200305060-00012

Sampson, M. 2019. Ambulatory electrocardiography: indications and devices. *British Journal of Cardiac Nursing* 14(3). doi: 10.12968/bjca.2019.14.3.114

Sandby-Møller, J., Poulsen, T. and Wulf, H. C. 2003. Epidermal thickness at different body sites: relationship to age, gender, pigmentation, blood content, skin type and smoking habits. *Acta Dermato-Venereologica* 83(6), pp. 410-413. doi: 10.1080/00015550310015419

Sanders, R. 1973. Torsional elasticity of human skin in vivo. *Pflügers Archiv: European Journal of Physiology* 342(3), pp. 255-260. doi: 10.1007/bf00591373

Sandoz Ltd. 2021. *Reletrans 5 microgram/hour transdermal patch SmPC*. Electronic Medicines Compendium (emc). Available at: www.medicines.org.uk/emc/product/7335/smpc [Accessed: 01 January 2022].

Sanna, T. et al. 2014. Cryptogenic stroke and underlying atrial fibrillation. *The New England Journal of Medicine* 370, pp. 2478-2486. doi: 10.1056/NEJMoa1313600

Santhanakrishnan, R. et al. 2016. Racial Differences in Electrocardiographic Characteristics and Prognostic Significance in Whites Versus Asians. *Journal of the American Heart Association* 5(3). doi: 10.1161/jaha.115.002956

Sareen, S., Nayyar, M., Wheeler, B., Skelton, M. and Khouzam, R. N. 2018. Electrocardiographic artifact potentially misleading to the wrong management. *Annals of Translational Medicine*. Vol. 6(1). doi: 10.21037/atm.2017.11.33

Sasaki, G. H. 2017. Micro-needling depth penetration, presence of pigment particles, and fluorescein-stained platelets: clinical usage for aesthetic concerns. *Aesthetic Surgery Journal* 37(1), pp. 71-83. doi: 10.1093/asj/sjw120

Satti, A. T., Park, J., Park, J., Kim, H. and Cho, S. 2020. Fabrication of parylene-coated microneedle array electrode for wearable ECG device. *Sensors* 20(18). doi: 10.3390/s20185183

Schmook, F. P., Meingassner, J. G. and Billich, A. 2001. Comparison of human skin or epidermis models with human and animal skin in in-vitro percutaneous absorption. *International Journal of Pharmaceutics* 215(1), pp. 51-56. doi: 10.1016/S0378-5173(00)00665-7

Schnabel, R. B. et al. 2015. 50 year trends in atrial fibrillation prevalence, incidence, risk factors, and mortality in the Framingham Heart Study: a cohort study. *The Lancet* 386(9989), pp. 154-162. doi: 10.1016/S0140-6736(14)61774-8

Schorr, M., Dichtel, L. E., Gerweck, A. V., Valera, R. D., Torriani, M., Miller, K. K. and Bredella, M. A. 2018. Sex differences in body composition and association with cardiometabolic risk. *Biology of sex differences* 9(1), p. 28. doi: 10.1186/s13293-018-0189-3

Searle, A. and Kirkup, L. 2000. A direct comparison of wet, dry and insulating bioelectric recording electrodes. *Physiological Measurement* 21(2), pp. 271-283. doi: 10.1088/0967-3334/21/2/307

Seo, J.-W., Kim, H., Kim, K., Choi, S. Q. and Lee, H. J. 2018. Calcium-modified silk as a biocompatible and strong adhesive for epidermal electronics. *Advanced Functional Materials* 28(36). doi: 10.1002/adfm.201800802

Serhani, M. A., H, T. E. K., Ismail, H. and Nujum Navaz, A. 2020. ECG monitoring systems: review, architecture, processes, and key challenges. *Sensors (Basel)* 20(6). doi: 10.3390/s20061796

Seshadri, D. R., Bittel, B., Browsky, D., Houghtaling, P., Drummond, C. K., Desai, M. Y. and Gillinov, A. M. 2020. Accuracy of Apple Watch for Detection of Atrial Fibrillation. *Circulation* 141(8), pp. 702-703. doi: 10.1161/circulationaha.119.044126

Sgarbossa, E. B., Birnbaum, Y. and Parrillo, J. E. 2001. Electrocardiographic diagnosis of acute myocardial infarction: Current concepts for the clinician. *American Heart Journal* 141(4), pp. 507-517. doi: 10.1067/mhj.2001.113571

Shahandashti, P. F., Pourkheyrollah, H., Jahanshahi, A. and Ghafoorifard, H. 2019. Highly conformable stretchable dry electrodes based on inexpensive flex substrate for long-term biopotential (EMG/ECG) monitoring. *Sensors and Actuators A: Physical* 295, pp. 678-686. doi: 10.1016/j.sna.2019.06.041

Sharma, S., Saeed, A., Johnson, C., Gadegaard, N. and Cass, A. E. 2017. Rapid, low cost prototyping of transdermal devices for personal healthcare monitoring. *Sens Biosensing Res* 13, pp. 104-108. doi: 10.1016/j.sbsr.2016.10.004

Saraf, S., Neal, C. J., Park, S., Das, S., Barkam, S., Cho, H. J. and Seal, S. 2015. Electrochemical study of nanoporous gold revealing anti-biofouling properties. *RSC Advances* 58. doi: 10.1039/C5RA05043J

Shay, T., Velev, O. D. and Dickey, M. D. 2018. Soft electrodes combining hydrogel and liquid metal. *Soft Matter* 14(17), pp. 3296-3303. doi: 10.1039/c8sm00337h

Shcherbina, A. et al. 2017. Accuracy in Wrist-Worn, Sensor-Based Measurements of Heart Rate and Energy Expenditure in a Diverse Cohort. *Journal of Personalized Medicine* 7(2), doi: 10.3390/jpm7020003

Sheu, S. Y. et al. 2014. The pig as an experimental model for mid-dermal burns research. *Burns* 40(8), pp. 1679-1688. doi: 10.1016/j.burns.2014.04.023

Shinbane, J. S., Merkert, M., Fogoros, R., Mehta, V., Cao, M. and Saxon, L. A. 2013. Wearable wireless arrhythmia detection patches: diagnostic arrhythmia yield, time to first arrhythmia, and patient compliance. *Heart Rhythm* 10, p. 5S:S305.

Shyu, T. C. et al. 2015. A kirigami approach to engineering elasticity in nanocomposites through patterned defects. *Nature Materials* 14(8), pp. 785-789. doi: 10.1038/nmat4327

Silver, F. H., Siperko, L. M. and Seehra, G. P. 2003. Mechanobiology of force transduction in dermal tissue. *Skin Research and Technology* 9(1), pp. 3-23. doi: 10.1034/j.1600-0846.2003.00358.x

Singh, B. N. and Tiwari, A. K. 2006. Optimal selection of wavelet basis function applied to ECG signal denoising. *Digital Signal Processing* 16(3), pp. 275-287. doi: 10.1016/j.dsp.2005.12.003

Singh, T. R., Dunne, N. J., Cunningham, E. and Donnelly, R. F. 2011. Review of patents on microneedle applicators. *Recent Pat Drug Deliv Formul* 5(1), pp. 11-23. doi: 10.2174/187221111794109484

Singh, T. R., Tekko, I., McAvoy, K., McMillan, H., Jones, D. and Donnelly, R. F. 2017. Minimally invasive microneedles for ocular drug delivery. *Expert Opinion on Drug Delivery* 14(4), pp. 525-537. doi: 10.1080/17425247.2016.1218460

Sivamani, R., Stoeber, B., Wu, G., Zhai, H., Liepmann, D. and Maibach, H. 2005. Clinical microneedle injection of methyl nicotinate: stratum corneum penetration. *Skin Research and Technology* 11(2), pp. 152-156. doi: 10.1111/j.1600-0846.2005.00107.x

Slotwiner, D. J. et al. 2019. Transparent sharing of digital health data: A call to action. *Heart Rhythm* 16(9), pp. e95-e106. doi: 10.1016/j.hrthm.2019.04.042

Smalls, L. K., Randall Wickett, R. and Visscher, M. O. 2006. Effect of dermal thickness, tissue composition, and body site on skin biomechanical properties. *Skin Research and Technology* 12(1), pp. 43-49. doi: 10.1111/j.0909-725X.2006.00135.x

Solbiati, M. et al. 2017. The diagnostic yield of implantable loop recorders in unexplained syncope: A systematic review and meta-analysis. *International Journal of Cardiology* 231, pp. 170-176. doi: 10.1016/j.ijcard.2016.12.128

Son, D. et al. 2014. Multifunctional wearable devices for diagnosis and therapy of movement disorders. *Nature Nanotechnology* 9(5), pp. 397-404. doi: 10.1038/nnano.2014.38

Song, Z., Sheng, G., Cui, Y., Li, M., Ding, C. and Luo, X. 2019. Low fouling electrochemical sensing in complex biological media by using the ionic liquid-doped conducting polymer PEDOT: application to voltammetric determination of dopamine. *Mikrochimica Acta* 186(4), p. 220. doi: 10.1007/s00604-019-3340-x

Sörnmo, L. and Laguna, P. 2005. *Bioelectrical signal processing in cardiac and neurological applications*. Elsevier Academic Press.

Srikureja, W., Darbar, D. and Reeder, G. S. 2000. Tremor-induced ECG artifact mimicking ventricular tachycardia. *Circulation* 102(11), pp. 1337-1338. doi: 10.1161/01.cir.102.11.1337

Srivastava, A. K., Bhartia, B., Mukhopadhyay, K. and Sharma, A. 2015. Long term biopotential recording by body conformable photolithography fabricated low cost polymeric microneedle arrays. *Sensors and Actuators A: Physical* 236, pp. 164-172. doi: 10.1016/j.sna.2015.10.041

Stahl, J., Wohlert, M. and Kietzmann, M. 2012. Microneedle pretreatment enhances the percutaneous permeation of hydrophilic compounds with high melting points. *BMC Pharmacology and Toxicology* 13, doi: 10.1186/2050-6511-13-5.

Stavrinidis, G. et al. 2016. SU-8 microneedles based dry electrodes for Electroencephalogram. *Microelectronic Engineering* 159, pp. 114-120. doi: 10.1016/j.mee.2016.02.062

Steinberg, J. S. et al. 2017. 2017 ISHNE-HRS expert consensus statement on ambulatory ECG and external cardiac monitoring/telemetry. *Heart Rhythm* 14(7), pp. 55-96. doi: 10.1016/j.hrthm.2017.03.038

Stephen, P. L. et al. 2018. Highly flexible, wearable, and disposable cardiac biosensors for remote and ambulatory monitoring. *npj Digital Medicine* 1(1), pp. 1-8. doi: 10.1038/s41746-017-0009-x

Strambini, L. M. et al. 2015. Self-powered microneedle-based biosensors for pain-free high-accuracy measurement of glycaemia in interstitial fluid. *Biosensors and Bioelectronics* 66, pp. 162-168. doi: 10.1016/j.bios.2014.11.010

Stroobandt, R. X., Barold, S. S. and Sinnaeve, A. F. 2016. *ECG from basics to essentials: step by step*. First ed. Chichester, England: Wiley Blackwell.

Stubhan, M., Markert, M., Mayer, K., Trautmann, T., Klumpp, A., Henke, J. and Guth, B. 2008. Evaluation of cardiovascular and ECG parameters in the normal, freely moving Göttingen Minipig. *Journal of Pharmacological and Toxicological Methods* 57(3), pp. 202-211. doi: 10.1016/j.vascn.2008.02.001

Summerfield, A., Meurens, F. and Ricklin, M. E. 2015. The immunology of the porcine skin and its value as a model for human skin. *Molecular Immunology* 66(1), pp. 14-21. doi: 10.1016/j.molimm.2014.10.023

Sutton, R., Mears, R., Kohno, R. and Benditt, D. 2018. Ambulatory electrocardiogram monitoring for syncope and collapse: a comparative assessment of clinical practice in UK and Germany. *Europace* 20(12), pp. 2021-2027. doi: 10.1093/europace/euy178

Sylvester, S., Yeong, C. F. and Harun, F. 2017. Miniaturized and wearable electrocardiogram (ECG) device with wireless transmission. *Journal of Telecommunication, Electronic and Computer Engineering* 9, pp. 15-19.

Taheri, B. A., Knight, R. T. and Smith, R. L. 1994. A dry electrode for EEG recording. *Electroencephalography and Clinical Neurophysiology* 90(5), pp. 376-383. doi: 10.1016/0013-4694(94)90053-1

Tallgren, P., Vanhatalo, S., Kaila, K. and Voipio, J. 2005. Evaluation of commercially available electrodes and gels for recording of slow EEG potentials. *Clinical Neurophysiology* 116(4), pp. 799-806. doi: 10.1016/j.clinph.2004.10.001

Tam, H. W. and Webster, J. G. 1977. Minimizing electrode motion artifact by skin abrasion. *IEEE Transactions on Biomedical Engineering* 24(2), pp. 134-139. doi: 10.1109/tbme.1977.326117

Tamborlane, W. et al. 2008. Continuous glucose monitoring and intensive treatment of type 1 diabetes. *New England Journal of Medicine* 359(14), pp. 1464-1476. doi: 10.1056/NEJMoa0805017

Tatarenko, L. 1975. The problem of skin-electrode processes during medical electrography. *Biotelemetry* 2(6), pp. 324-328.

Tepper, S., Dodick, D., Schmidt, P. and Kellerman, D. 2019. Efficacy of adam zolmitriptan for the acute treatment of difficult-to-treat migraine headaches. *Headache* 59(4), pp. 509-517. doi: 10.1111/head.13482

Tereshchenko, L. G. and Josephson, M. E. 2015. Frequency content and characteristics of ventricular conduction. *Journal of Electrocardiology* 48(6), pp. 933-937. doi: 10.1016/j.jelectrocard.2015.08.034

Texas Instruments. 2012. *ADS1299-x Low-Noise, 4-, 6-, 8-Channel, 24-Bit, Analog-to-Digital Converter for EEG and Biopotential Measurements*. Dallas, Texas: Texas Instruments. Available at: [Accessed: 27 April 2021].

Tfaili, S., Gobinet, C., Josse, G., Angiboust, J. F., Manfait, M. and Piot, O. 2012. Confocal Raman microspectroscopy for skin characterization: a comparative study between human skin and pig skin. *Analyst* 137(16), pp. 3673-3682. doi: 10.1039/c2an16292j

Thakur, R. R. S., Fallows, S. J., McMillan, H. L., Donnelly, R. F. and Jones, D. S. 2014. Microneedle-mediated intrascleral delivery of *in situ* forming thermoresponsive implants for sustained ocular drug delivery. *Journal of Pharmacy and Pharmacology* 66(4), pp. 584-595. doi: 10.1111/jphp.12152

Tian, Y. et al. 2019. Utility of 30-Day Continuous Ambulatory Monitoring to Identify Patients With Delayed Occurrence of Atrioventricular Block After Transcatheter Aortic Valve Replacement. *Circulation: Cardiovascular Interventions* 12(12), p. e007635. doi: 10.1161/circinterventions.118.007635

Tieleman, R. G. et al. 2014. Validation and clinical use of a novel diagnostic device for screening of atrial fibrillation. *Europace* 16(9), pp. 1291-1295. doi: 10.1093/europace/euu057

Tobin, D. J. 2006. Biochemistry of human skin - our brain on the outside *Chemistry Society Reviews* 35, pp. 52-67. doi: 10.1039/B505793K

Tsai, M. T. et al. 2016. In vivo investigation of temporal effects and drug delivery induced by transdermal microneedles with optical coherence tomography. *Biomedical Optics Express* 7(5), pp. 1865-1876. doi: 10.1364/boe.7.001865

Tsugita, T., Nishijima, T., Kitahara, T. and Takema, Y. 2013. Positional differences and aging changes in Japanese woman epidermal thickness and corneous thickness determined by OCT (optical coherence tomography). *Skin Research and Technology* 19(3), pp. 242-250. doi: 10.1111/srt.12021

Tsukada, Y. T. et al. 2019. Validation of wearable textile electrodes for ECG monitoring. *Heart Vessels* 34(7), pp. 1203-1211. doi: 10.1007/s00380-019-01347-8

Turakhia, M. P. et al. 2013. Diagnostic utility of a novel leadless arrhythmia monitoring device. *American Journal of Cardiology* 112(4), pp. 520-524. doi: 10.1016/j.amjcard.2013.04.017

Turner, N. J., Pezzone, D. and Badylak, S. F. 2014. Regional variations in the histology of porcine skin. *Tissue Engineering Part C: Methods* 21(4), doi: 10.1089/ten.tec.2014.0246

Uktveris, T. and Jusas, V. 2018. Development of a modular board for EEG signal acquisition. *2018 5th International Conference on Mathematics and Computers in Sciences and Industry (MCSI).* Corfu, Greece, 25-27 August 2018. IEEE.

Ullas Pradhan, U., Reddy, N., Chandrashekar, K. and Mohan, C. B. 2021. Titanium dioxide based bioelectric sensor for the acquisition of electrocardiogram signals. *Microchemical Journal* 160, p. 105656. doi: 10.1016/j.microc.2020.105656

Uter, W. and Schwanitz, H. J. 1996. Contact dermatitis from propylene glycol in ECG electrode gel. *Contact Dermatitis* 34(3), pp. 230-231. doi: 10.1111/j.1600-0536.1996.tb02190.x

Vaidean, G. D., Manczuk, M. and Magnani, J. W. 2016. Atrial electrocardiography in obesity and hypertension: Clinical insights from the Polish-Norwegian Study (PONS). *Obesity (Silver Spring)* 24(12), pp. 2608-2614. doi: 10.1002/oby.21678

Vale-Cardoso, A. S. and Guimarães, H. N. 2010. The effect of 50/60 Hz notch filter application on human and rat ECG recordings. *Physiological Measurement* 31(1), pp. 45-58. doi: 10.1088/0967-3334/31/1/004

Van Alsté, J. A. and Schilder, T. S. 1985. Removal of base-line wander and power-line interference from the ECG by an efficient FIR filter with a reduced number of taps. *IEEE Transactions on Biomedical Engineering* 32(12), pp. 1052-1060. doi: 10.1109/tbme.1985.325514

Van der Maaden, K., Sekerdag, E., Jiskoot, W. and Bouwstra, J. 2014. Impact-insertion applicator improves reliability of skin penetration by solid microneedle arrays. *The American Association of Pharmaceutical Scientists* 16(4), pp. 681-684. doi: 10.1208/s12248-014-9606-7

Vashi, N. A., de Castro Maymone, M. B. and Kundu, R. V. 2016. Aging differences in ethnic skin. *The Journal of Clinical and Asthetic Dermatology* 9(1), pp. 31-38.

Venkatachalam, K. L., Herbrandson, J. E. and Asirvatham, S. J. 2011. Signals and signal processing for the electrophysiologist: part I: electrogram acquisition. *Circulation: Arrhythmia and Electrophysiology* 4(6), pp. 965-973. doi: 10.1161/circep.111.964304

Venkatraman, S., Hendricks, J., King, Z. A., Sereno, A. J., Richardson-Burns, S., Martin, D. and Carmena, J. M. 2011. In vitro and in vivo evaluation of PEDOT microelectrodes for neural stimulation and recording. *IEEE Transactions on Neural Systems and Rehabilitation Engineering* 19(3), pp. 307-316. doi: 10.1109/tnsre.2011.2109399

Ventrelli, L., Marsilio Strambini, L. and Barillaro, G. 2015. Microneedles for transdermal biosensing: current picture and future direction. *Advanced Healthcare Materials* 4(17), pp. 2606-2640. doi: 10.1002/adhm.201500450

Verbaan, F. J. et al. 2008. Improved piercing of microneedle arrays in dermatomed human skin by an impact insertion method. *Journal of Controlled Release* 128(1), pp. 80-88. doi: 10.1016/j.jconrel.2008.02.009

Verbaan, F. J., Bal, S. M., van den Berg, D. J., Groenink, W. H., Verpoorten, H., Lüttge, R. and Bouwstra, J. A. 2007. Assembled microneedle arrays enhance the transport of compounds varying over a large range of molecular weight across human dermatomed skin. *Journal of Controlled Release* 117(2), pp. 238-245. doi: 10.1016/j.jconrel.2006.11.009

Vetrovsky, T., Siranec, M., Marencakova, J., Tufano, J. J., Capek, V., Bunc, V. and Belohlavek, J. 2019. Validity of six consumer-level activity monitors for measuring steps in patients with chronic heart failure. pp. 1-14. doi: 10.1371/journal.pone.0222569

Voskerician, G., Shive, M. S., Shawgo, R. S., von Recum, H., Anderson, J. M., Cima, M. J. and Langer, R. 2003. Biocompatibility and biofouling of MEMS drug delivery devices. *Biomaterials* 24(11), pp. 1959-1967. doi: 10.1016/s0142-9612(02)00565-3

Vrdoljak, A., Allen, E. A., Ferrara, F., Temperton, N. J., Crean, A. M. and Moore, A. C. 2016. Induction of broad immunity by thermostabilised vaccines incorporated in dissolvable microneedles using novel fabrication methods. *Journal of Controlled Release* 225, pp. 192-204. doi: 10.1016/j.jconrel.2016.01.019

Wang, L. et al. 2020. A CNT-PDMS wearable device for simultaneous measurement of wrist pulse pressure and cardiac electrical activity. *Materials Science and Engineering: C* 117, p. 111345. doi: 10.1016/j.msec.2020.111345

Wang, W. et al. 2020. Association of Life's Simple 7 with Atrial Fibrillation Burden (From the Atherosclerosis Risk in Communities Study). *The American Journal of Cardiology* 137, pp. 31-38. doi: 10.1016/j.amjcard.2020.09.033

Wang, L. et al. 2018a. Weaving sensing fibres into electrochemical fabric for real-time health monitoring. *Advanced Functional Materials* 28(42). doi: 10.1002/adfm.201804456

Wang, L. F., Liu, J. Q., Yan, X. X., Yang, B. and Yang, C. S. 2013. A MEMS-based pyramid micro-needle electrode for long-term EEG measurement. *Microsystem Technologies* 19(2), pp. 269-276. doi: 10.1007/s00542-012-1638-2

Wang , P., Cornwell, M., Hill, J. and Prausnitz, M. 2006. Precise microinjection into skin using hollow microneedles. *Journal of Investigative Dermatology* 126(5), pp. 1080-1087. doi: 10.1038/sj.jid.5700150

Wang, Q., Yao, G., Dong, P., Gong, Z., Li, G., Zhang, K. and Wu, C. 2015. Investigation on fabrication process of dissolving microneedle arrays to improve effective needle drug distribution. *European Journal of Pharmaceutical Sciences* 66, pp. 148-156. doi: 10.1016/j.ejps.2014.09.011

Wang, R., Jiang, X., Wang, W. and Li, Z. 2017. A microneedle electrode array on flexible substrate for long-term EEG monitoring. *Sensors and Actuators B: Chemical* 244, pp. 750-758. doi: 10.1016/j.snb.2017.01.052

Wang, Y., Chao, M., Wan, P. and Zhang, L. 2020. A wearable breathable pressure sensor from metal-organic framework derived nanocomposites for highly sensitive broad-range healthcare monitoring. *Nano Energy* 70, p. 104560. doi: 10.1016/j.nanoen.2020.104560

Wang , Y., Pei, W., Guo , K., Gui , Q., Li , X., Chen, H. and Yang, J. 2011. Dry electrode for the measurement of biopotential signals. *Science China Information Sciences* 54(11), pp. 2435–2442. doi: 10.1007/s11432-011-4354-0

Wang, Y., Qiu, Y., Ameri, S. K., Jang, H., Dai, Z., Huang, Y. and Lu, N. 2018b. Low-cost μm- thick, tape-free electronic tattoo sensors with minimized motion and sweat artifacts. *npj Flexible Electronics* 2(6). doi: 10/1038/s41528-017-0019-4

Weder, M. et al. 2015. Embroidered electrode with silver/titanium coating for long-term ECG monitoring. *Sensors* 15(1), pp. 1750-1759. doi: 10.3390/s150101750

Wegner, F. K. et al. 2020. Prospective blinded evaluation of the smartphone-based AliveCor Kardia ECG monitor for atrial fibrillation detection: The PEAK-AF study. *European Journal of Internal Medicine* 73, pp. 72-75. doi: 10.1016/j.ejim.2019.11.018

Wei-Ze, L., Mei-Rong, H., Jian-Ping, Z., Yong-Qiang, Z., Bao-Hua, H., Ting, L. and Yong, Z. 2010. Super-short solid silicon microneedles for transdermal drug delivery applications. *International Journal of Pharmaceutics* 389(1), pp. 122-129. doi: 10.1016/j.ijpharm.2010.01.024

Widera, G., Johnson, J., Kim, L., Libiran, L., Nyam, K., Daddona, P. E. and Cormier, M. 2006. Effect of delivery parameters on immunization to ovalbumin following intracutaneous administration by a coated microneedle array patch system. *Vaccine* 24(10), pp. 1653-1664. doi: 10.1016/j.vaccine.2005.09.049

Weidmann, S. 1955. The effect of the cardiac membrane potential on the rapid availability of the sodium-carrying system. *The Journal of Physiology* 127(1), pp. 213-224. doi: 10.1113/jphysiol.1955.sp005250

Wilke, N. and Morrissey, A. 2007. Silicon microneedle formation using modified mask designs based on convex corner undercut. *Journal of Micromechanics and Microengineering* 17(2). doi: 10.1088/0960-1317/17/2/008

Willems, J. L. et al. 1991. The diagnostic performance of computer programs for the interpretation of electrocardiograms. *The New England Journal of Medicine* 325(25), pp. 1767-1773. doi: 10.1056/nejm199112193252503

William, A. D. et al. 2018. Assessing the accuracy of an automated atrial fibrillation detection algorithm using smartphone technology: The iREAD Study. *Heart Rhythm* 15(10), pp. 1561-1565. doi: 10.1016/j.hrthm.2018.06.037

Willigenburg, N. W., Daffertshofer, A., Kingma, I. and van Dieën, J. H. 2012. Removing ECG contamination from EMG recordings: a comparison of ICA-based and other filtering procedures. *Journal of Electromyography and Kinesiology* 22(3), pp. 485-493. doi: 10.1016/j.jelekin.2012.01.001

Wu, K. S., Van Osdol, W. W. and Dauskardt, R. H. 2006. Mechanical properties of human stratum corneum: effects of temperature, hydration, and chemical treatment. *Biomaterials* 27(5), pp. 785-795.

Wu, W., Pirbhulal, S., Sangaiah, A. K., Mukhopadhyay, S. C. and Li, G. 2018. Optimization of signal quality over comfortability of textile electrodes for ECG monitoring in fog computing based medical applications. *Future Generation Computer Systems* 86, pp. 515-526. doi: 10.1016/j.future.2018.04.024

Wu, Y., Gao, Y., Qin, G., Zhang, S., Qiu, Y., Li, F. and Xu, B. 2010. Sustained release of insulin through skin by intradermal microdelivery system. *Biomedical Microdevices* 12(4), pp. 665-671. doi: 10.1007/s10544-010-9419-0

Xenikakis, I. et al. 2021. Transdermal delivery of insulin across human skin in vitro with 3D printed hollow microneedles. *Journal of Drug Delivery Science and Technology*, p. 102891. doi: 10.1016/j.jddst.2021.102891

Xiao, N., Yu, W. and Han, X. 2020. Wearable heart rate monitoring intelligent sports bracelet based on Internet of things. *Measurement* 164, p. 108102. doi: 10.1016/j.measurement.2020.108102

Xie, L., Li, Z., Zhou, Y., He, Y. and Zhu, J. 2020. Computational diagnostic techniques for electrocardiogram signal analysis. *Sensors (Basel)* 20(21), doi: 10.3390/s20216318

Xing, X. et al. 2018. Assessing a novel micro-seepage electrode with flexible and elastic tips for wearable EEG acquisition. *Sensors and Actuators A: Physical* 270, pp. 262-270. doi: 10.1016/j.sna.2017.12.048

Yamamoto, Y., Harada, S., Yamamoto, D., Honda, W., Arie, T., Akita, S. and Takei, K. 2016. Printed multifunctional flexible device with an integrated motion sensor for health care monitoring. *Science Advances* 2(11). doi: 10.1126/sciadv.1601473

Yamamoto, T. and Yamamoto, Y. 1976. Electrical properties of the epidermal stratum corneum. *Medical and Biological Engineering and Computing* 14(2), pp. 151-158. doi: 10.1007/bf02478741

Yan, G., Warner, K. S., Zhang, J., Sharma, S. and Gale, B. K. 2010. Evaluation needle length and density of microneedle arrays in the pretreatment of skin for transdermal drug delivery. *International Journal of Pharmaceutics* 391(1-2), pp. 7-12. doi: 10.1016/j.ijpharm.2010.02.007

Yang, M. and Zahn, J. D. 2004. Microneedle insertion force reduction using vibratory actuation. *Biomedical Microdevices* 6(3), pp. 177-182. doi: 10.1023/B:BMMD.0000042046.07678.2e

Yenikomshian, M., Jarvis, J., Patton, C., Yee, C., Mortimer, R., Birnbaum, H. and Topash, M. 2019. Cardiac arrhythmia detection outcomes among patients monitored with the Zio patch system: a systematic literature review. *Current Medical Research and Opinion*, pp. 1-12. doi: 10.1080/03007995.2019.1610370

Yokus, A. M. and Jur, J. 2016. Fabric-based wearable dry electrodes for body surface biopotential recording. *IEEE Transactions on Biomedical Engineering* 63(2), pp. 423 - 430. doi: 10.1109/TBME.2015.2462312

Young, B. 2019. New standards for ECG equipment. *Journal of Electrocardiology* 57, pp. S1-S4. doi: 10.1016/j.jelectrocard.2019.07.013

Yu, J. et al. 2015. Microneedle-array patches loaded with hypoxia-sensitive vesicles provide fast glucose-responsive insulin delivery. *Proceedings of the National Academy of Sciences of the United States of America* 112(27), pp. 8260-8265. doi: 10.1073/pnas.1505405112

Yu, L. M., Tay, F. E. H., Guo, D. G., Xu, L. and Yap, K. L. 2009. A microfabricated electrode with hollow microneedles for ECG measurement. *Sensors and Actuators A: Physical* 151(1), pp. 17-22. doi: 10.1016/j.sna.2009.01.020

Yu, M., Lu, Z., Shi, Y., Du, Y., Chen, X. and Kong, M. 2021. Systematic comparisons of dissolving and swelling hyaluronic acid microneedles in transdermal drug delivery. *International Journal of Biological Macromolecules* 191, pp. 783-791. doi: 10.1016/j.ijbiomac.2021.09.161

Yung, K. L. et al. 2011. Sharp tipped plastic hollow microneedle array by microinjection moulding. *Journal of Micromechanics and Microengineering* 22. doi: 10.1088/0960-1317/22/1/015016

Zahed, M. A., Das, P. S., Maharjan, P., Barman, S. C., Sharifuzzaman, M., Yoon, S. H. and Park, J. Y. 2020. Flexible and robust dry electrodes based on electroconductive polymer spray-coated 3D porous graphene for long-term electrocardiogram signal monitoring system. *Carbon* 165, pp. 26-36. doi: 10.1016/j.carbon.2020.04.031

Zhang, G. 2020. A wearable device for health management detection of multiple physiological parameters based on ZigBee wireless networks. *Measurement* 165, p. 108168. doi: 10.1016/j.measurement.2020.108168

Zhang, H. et al. 2021. A fully integrated wearable electronic device with breathable and washable properties for long-term health monitoring. *Sensors and Actuators A: Physical* 322, p. 112611. doi: 10.1016/j.sna.2021.112611

Zhang, J. X. J. and Hoshino, K. 2019. Chapter 8 - Implantable and wearable sensors. *Molecular Sensors and Nanodevices (Second Edition)*. Academic Press, pp. 489-545.

Zhang, N., Stauffer, F., Simona, B. R., Zhang, F., Zhang, Z.-M., Huang, N.-P. and Vörös, J. 2018. Multifunctional 3D electrode platform for real-time in situ monitoring and stimulation of cardiac tissues. *Biosensors and Bioelectronics* 112, pp. 149-155. doi: 10.1016/j.bios.2018.04.037

Zhao, X., Coulman, S. A., Hanna, S. J., Wong, F. S., Dayan, C. M. and Birchall, J. C. 2017. Formulation of hydrophobic peptides for skin delivery via coated microneedles. *Journal of Controlled Release* 265, pp. 2-13. doi: 10.1016/j.jconrel.2017.03.015

Zhou, W., Liu, S., Liu, W., Zhang, C., Li, Y., Xu, W. and Hui, K. 2017. Novel dry metal electrode with tilted microstructure fabricated with last micromilling process. *Sensors and Actuators A: Physical* 264, pp. 76-83. doi: 10.1016/j.sna.2017.07.028

Zimetbaum, P. and Goldman, A. 2010. Ambulatory arrhythmia monitoring: choosing the right device. *Circulation* 122(16), pp. 1629-1636. doi: 10.1161/CIRCULATIONAHA.109.925610

Zipes, D. P. et al. 2006. ACC/AHA/ESC 2006 guidelines for management of patients with ventricular arrhythmias and the prevention of sudden cardiac death: a report of the American College of Cardiology/American Heart Association Task Force and the European Society of Cardiology Committee for Practice Guidelines (Writing Committee to Develop Guidelines for Management of Patients With Ventricular Arrhythmias and the Prevention of Sudden Cardiac Death). *Journal of the American College of Cardiology* 48(5), pp. 247-346. doi: 10.1016/j.jacc.2006.07.010

Zorniak, M., Mitrega, K., Bialka, S., Porc, M. and Krzeminski, T. F. 2010. Comparison of thiopental, urethane, and pentobarbital in the study of experimental cardiology in rats in vivo. *Journal of Cardiovascular Pharmacology* 56(1), pp. 38-44. doi: 10.1097/FJC.0b013e3181dd502c

Zouboulis, C. C. and Makrantonaki, E. 2011. Clinical aspects and molecular diagnostics of skin aging. *Clinics in Dermatology* 29(1), pp. 3-14. doi: 10.1016/j.clindermatol.2010.07.001

Zulkifly, H., Lip, G. Y. H. and Lane, D. A. 2018. Epidemiology of atrial fibrillation. *International Journal of Clinical Practice* 72(3). doi: 10.1111/ijcp.13070

Zulqarnain, M., Stanzione, S., Rathinavel, G., Smout, S., Willegems, M., Myny, K. and Cantatore, E. 2020. A flexible ECG patch compatible with NFC RF communication. *npj Flexible Electronics* 4(1), p. 13. doi: 10.1038/s41528-020-0077-x

Zywietz, C. and Willems, J. L. 1987. Stability of ECG amplitude measurements in systematic noise tests. Results and recommendations from the CSE project. *Journal of Electrocardiology* 20, pp. 61-67.

3M. 2021. *3M™ red dot™ monitoring electrodes with 3M™ micropore™ tape backing 2239, with solid gel and lift tab*. 3M. Available at: https://www.3m.co.uk/3M/en_GB/company-uk/3m-products/~/3M-Red-Dot-Monitoring-Electrodes-with-3M-Micropore-Tape-Backing-2239-with-Solid-Gel-and-Lift-Tab-6-cm/?N=5002385+8711096+3288983426&rt=rud [Accessed: 09 March 2021].